NCHRP Project 15-61

Applying Climate Change Information to Hydrologic and Coastal Design of Transportation Infrastructure

Final Report

PREPARED FOR

THE NATIONAL COOPERATIVE HIGHWAY RESEARCH PROGRAM

TRANSPORTATION RESEARCH BOARD

Roger Kilgore, Kilgore Consulting and Management, Denver, CO

Wilbert O. Thomas, Jr. and Sabu Paul, Michael Baker International, Cary, NC

Scott Douglass and Bret Webb, South Coast Engineers, Fairhope, AL

Katharine Hayhoe and Anne Stoner, Atmos Research and Consulting, Lubbock, TX

Jennifer M. Jacobs, Jennifer M. Jacobs and Associates, Portsmouth, NH

David B. Thompson, Thompson Hydrologics, Carson City, NV

George R. Herrmann, Desert Sky Engineering and Hydrology, Lubbock, TX

Ellen Douglas, Fremont, NH

Chris Anderson, SkyDoc, LLC, Ames, IA

March 22, 2019

ACKNOWLEDGMENT

This work was sponsored by the American Association of State Highway and Transportation Officials, in cooperation with the Federal Highway Administration, and was conducted in the National Cooperative Highway Research Program**,** which is administered by the Transportation Research Board of the National Academies of Sciences, Engineering, and Medicine.

Applying Climate Change Information to Hydrologic and Coastal Design of Transportation Infrastructure

Final Report

PREPARED FOR

THE NATIONAL COOPERATIVE HIGHWAY RESEARCH PROGRAM

TRANSPORTATION RESEARCH BOARD

Roger Kilgore, Kilgore Consulting and Management, Denver, CO
Wilbert O. Thomas, Jr. and Sabu Paul, Michael Baker International, Cary, NC
Scott Douglass and Bret Webb, South Coast Engineers, Fairhope, AL
Katharine Hayhoe and Anne Stoner, Atmos Research and Consulting, Lubbock, TX
Jennifer M. Jacobs, Jennifer M. Jacobs and Associates, Portsmouth, NH
David B. Thompson, Thompson Hydrologics, Carson City, NV
George R. Herrmann, Desert Sky Engineering and Hydrology, Lubbock, TX
Ellen Douglas, Fremont, NH
Chris Anderson, SkyDoc, LLC, Ames, IA

March 22, 2019

Table of Contents

CHAPTER 1. BACKGROUND 1
1.1. Problem Statement 1
1.2. Research Objectives and Scope 1
1.3. What Does it Mean to Design for Climate Change? 2

CHAPTER 2. RESEARCH APPROACH 1
2.1. Work Plan 1
2.1.1 Phase I: Literature Review and Opportunities Assessment 1
2.1.2 Phase II: Implementation of Study Scope 1
2.2. Literature Review Summary 2

CHAPTER 3. DECISION-MAKING FRAMEWORKS 1
3.1. Traditional (Top-Down) Framework 2
3.1.1 Inland Hydrology 3
3.1.2 Coastal Applications 3
3.2. Threshold (Bottom-Up) Framework 4
3.3. Selecting a Decision-Making Framework 5

CHAPTER 4. CLIMATE MODELING OUTPUTS FOR HYDROLOGIC DESIGN 1
4.1. Terminology 2
4.1.1 Climate Extremes in Climate Science 2
4.1.2 Climate Extremes in Engineering 3
4.1.3 Comparing Extremes in Climate Science and Hydrologic Engineering 4
4.1.4 Detecting and Projecting Changes in Extremes 5
4.2. Suitability of Climate Model Outputs 7
4.2.1 Objectives 7
4.2.2 Overview 7
4.2.3 Actionable Climate Projections for No-Regrets Hydrological Analyses 9
4.2.4 Observations 11
4.2.5 Climate Information: Trends and Projections 14
4.2.6 Sources of Uncertainty in Future Projections 19
4.2.7 Global Climate Models 24
4.2.8 Global Climate Projections 31
4.2.9 High-Resolution Climate Projections 32
4.2.10 Evaluating Climate Projections for Specific Applications 37
4.3. Guidance for Selecting Climate Modeling Outputs 39
4.3.1 Selection of Climate Inputs by Level of Analysis 40
4.3.2 Model Selection 43
4.3.3 Future Scenarios – Description and Guidance 47
4.4. Incorporating New High-Resolution Climate Projections into Guidance 51
4.4.1 Future Advances in Climate Modeling 52
4.4.2 WMO Climatological Standard Normal Updates and Guidance 55

CHAPTER 5. TEMPORAL AND SPATIAL ADAPTATION OF PROJECTED PRECIPITATION FOR RAINFALL/RUNOFF MODELING 1
5.1. Projected 24-Hour Precipitation 2
5.1.1. Method 2
5.1.2. Example 8
5.1.3. Applicability and Limitations 14

5.1.4. Discussion and Other Resources 15
5.2. Sub-Daily Precipitation/IDF Curves 21
5.2.1. General Description of IDF Relations 21
5.2.2. Sub-Daily Precipitation from the Climate Science Community 25
5.2.3. Sub-Daily Precipitation and Development of IDF Curves 29
5.2.4. Adaptation of the Simonovic Approach to the United States 40
5.3. Spatial Scale Compatibility 47
5.3.1. Background and Development 48
5.3.2. Identification of Projected Point Precipitation Data 50
5.3.3. Application of an Areal Reduction Factor 50

CHAPTER 6. STATISTICAL AND INDEX METHODS FOR PROJECTING DISCHARGES 53
6.1. Trend Projection Based on Historical Discharges 53
6.1.1. Trends and Nonstationarity in Historical Peak Discharges 53
6.1.2. Time-Varying Statistical Distribution Parameters 54
6.1.3. Adjusting Historical Discharge Records for Land Use or Climate Change 63
6.1.4. Analyzing Recent Homogeneous Sub-Periods of Record 64
6.1.5. Summary and Recommendations 65
6.2. Regression Approaches for Projecting Discharges 65
6.2.1. Traditional Multiple Linear Regression Hydrologic Equations 66
6.2.2. Panel Regression Techniques for Projecting Flood Discharges 73
6.2.3. Summary and Recommendations 82
6.3. Index Flood Methods for Accommodating Climate Change 84
6.3.1. The Index Flood Method 84
6.3.2. Application of the Index Flood Method for Climate Change 91
6.3.3. Estimation of Uncertainty 94

CHAPTER 7. ADAPTATION OF PROJECTED PRECIPITATION TIME SERIES FOR CONTINUOUS SIMULATION 95
7.1. Modeling Framework 95
7.1.1. Available Modeling Tools 95
7.1.2. Levels of Analysis 98
7.1.3. Generalized Modeling Approach for Climate Change 99
7.2. Change Factor Methodology 100
7.2.1. Additive and Multiplicative Change Factors. 100
7.2.2. Single and Multiple Change Factors 101
7.2.3. Customized Change Factors 102
7.3. Projected Time Series 104
7.3.1. Precipitation Time Series 104
7.3.2. Time Series for Other Climate Variables 107
7.4. Autocorrelation Structure of Climatic Time Series Data 110
7.5. Obtaining Projected Data for Continuous Simulation 112
7.5.1. Mapping Climate Stations to Downscaled GCM Grid Data for Change Factors 112
7.5.2. The Climate Resilience Evaluation and Analysis Tool Database 113

CHAPTER 8. EVALUATION OF CLIMATE OUTPUTS AND DESIGN FOR COASTAL TRANSPORTATION ASSETS 116
8.1. Selecting Sea Level Rise for Design 116
8.1.1. Current Understanding of Sea Level Rise and Variations 117
8.1.2. Sea Level Rise Projections 122
8.1.3. Selecting Sea Level Rise Scenarios for Design 131

8.1.4. Recommendations 135
8.2. Combining Coastal Hazard and Climate Change Information 142
8.2.1. Sources of Coastal Hazard Data 143
8.2.2. Modifying Coastal Hazards to Account for Sea Level Rise 146
8.2.3. Incorporating Climate Change Information into Hydrodynamic Modeling 160
8.2.4. Case Study: Climate Change Impacts on a Coastal Roadway – Brookhaven, NY 162
8.2.5. Case Study: Climate Change Effects on an Interstate Bridge –Pensacola, FL 166
8.3. Selected Coastal Issues 170
8.3.1. Watershed Contributions to the Coast 170
8.3.2. Evaluating the Effects of Sea level Rise on Coastal Geomorphology 171

REFERENCES 173

ABBREVIATIONS 192

GLOSSARY 195

APPENDIX A. LITERATURE REVIEW A-1

APPENDIX B. DETAILED INFORMATION ON ESDM AND RCM DATASETS B-1

APPENDIX C. CONTINUOUS SIMULATION WATERSHED MODELS FOR CLIMATE CHANGE STUDIES C-1

APPENDIX D. FLOOD FREQUENCY CURVES D-1

List of Figures

Figure 3.1. Levels of analysis, effort, and climate information. 2
Figure 3.2. Considerations for choosing a decision-making framework. 5
Figure 3.3. Relationship between headwater and discharge for structure 02423 (Connecticut Department of Transportation 2014). 7
Figure 4.1. Decision matrix and definitions of Type I and Type II errors for regrets analysis (from Rosner et al. 2014). 10
Figure 4.2. Observed changes (left) in the 20-year return value of seasonal daily precipitation totals over the period 1948 to 2015, calculated by determining the exceedance probability from historical climate observations from the GHCN dataset (Source: Easterling et al. 2017) and (right) four metrics of extreme precipitation where numerical value is the percent change over the entire period, either 1901-2016 or 1958-2016 (Source: Easterling et al. 2017) 15
Figure 4.3. Trends in annual flood magnitude and direction from the 1920s through 2008 (Source: NCA3 Chapter 2). Most significant changes are located where consistency between precipitation and flood trends are evident: an increasing trend for floods in the Midwest and Northeast, and a decreasing trend in the Southwest. 15
Figure 4.4. Projected change (left) in the 20-year return period amount for daily precipitation for mid- and late-21st century for a lower scenario (top, RCP4.5) and a higher scenario (bottom, RCP8.5) calculated from the LOCA downscaled dataset (Source: USGCRP 2017) and (right) the number of days exceeding the historical (1971-2000) 2-percent most extreme or heaviest daily 24h precipitation for the Great Plains region where by mid-century (2041-2070), the projected change in days exceeding those precipitation amounts remains greatest in the northern area (Source: NCA3 Chapter 19). 16
Figure 4.5. (Left) The CMIP5 2081–2100 multi-model ensemble median percent change in 20-year return values (RV) of annual maximum daily precipitation per 1°C of local warming relative to the 1986–2005 reference period. (Right) The average 2081–2100 CMIP5 multi-model ensemble median of the return periods (RP, years) of 1986–2005 20-year return values of annual maximum daily precipitation corresponding to 1°C of local warming. Regions of no change would have return periods of 20 years. Regions identified as most significant changes also are regions for which increase in rainfall extremes is projected to continue. (Source: IPCC AR5 WG1 Chapter 12). 17
Figure 4.6. Sample plot of projected changes in a fixed threshold indicator of heavy precipitation: here, 2” in 24 hours, for the city of San Angelo, TX under the higher RCP8.5 and lower RCP4.5 scenarios as simulated by climate projections from 9 GCMs statistically downscaled to the local airport weather station. The bars indicate the multi-model mean values while the whiskers show the range resulting from the 9 different CMIP5 GCMs (Source: figure and data, K. Hayhoe.). 18
Figure 4.7. Observed annual June-August cumulative precipitation (green) and long-term trend (blue) for Baltimore, MD. (Source: NOAA’s Climate at a Glance). 19
Figure 4.8. Proportion of the total uncertainty in future annual mean precipitation projections corresponding to the internal natural variability of the climate system (orange), scientific or model uncertainty (blue) and human or scenario uncertainty (green). (Source: Hawkins and Sutton 2011). 21

Figure 4.9. Percent increases in the amount of precipitation falling in very heavy events (defined as the heaviest 1% of all daily events) from 1958 to 2012 for each region of the continental United States. These trends are larger than natural variations for the Northeast, Midwest, Puerto Rico, Southeast, Great Plains, and Alaska. The trends are not larger than natural variations for the Southwest, Hawai'i, and the Northwest. (Source: NCA3 2014)..... 26
Figure 4.10. Comparing observed (black) with historical model simulated total forcing (pink) and natural forcing (blue) scenarios shows that GCMs are able to reproduce observed long-term temperature trends over every major continent of the world. (IPCC AR4 2007)..... 28
Figure 4.11. Decision tree for identifying appropriate climate projection information by level of analysis. 41
Figure 4.12. Comparison of projected carbon emissions (top) and resulting global mean temperature change that would result from the central estimate (lines) and the likely range (shaded areas) of climate sensitivity (bottom) for the 2000 SRES (left) with the 2010 RCPs (right). (Source: Hayhoe et al. 2017). 49
Figure 5.1. Recommended procedure for projecting 24-hour precipitation quantiles. 4
Figure 5.2. Projected (2050-2099) estimates of the 24-hour precipitation for Denver, Colorado. 14
Figure 5.3. Baseline and future (RCP8.5) model estimates for 24-hour precipitation for Baltimore from the CSIRO GCM. 16
Figure 5.4. Baseline and future (RCP8.5) model estimates for 24-hour precipitation for Philadelphia from the MIROC5 GCM. 17
Figure 5.5. Baseline and future (RCP8.5) model estimates for 24-hour precipitation for Pittsburgh from the CCSM4 GCM. 17
Figure 5.6. Future (RCP8.5) model estimates for 24-hour precipitation for Baltimore (2050-2099) from an ensemble of the three CCMs. 19
Figure 5.7. Future (RCP8.5) model estimates for 24-hour precipitation for Philadelphia (2050-2099) from an ensemble of the three CCMs. 19
Figure 5.8. Future (RCP8.5) model estimates for 24-hour precipitation for Pittsburgh (2000-2049) from an ensemble of the three CCMs. 20
Figure 5.9. Depth-duration curve for an AEP of 0.01 for Roxboro, NC (data from NOAA Atlas 14). 22
Figure 5.10- Intensity-duration curve for an AEP of 0.01 for Roxboro, NC (NOAA Atlas 14). 23
Figure 5.11. 24-h depth-duration-frequency curves for AEP values of 0.5 and 0.01 for five randomly selected stations reduced to non-dimensional shapes by normalizing on the largest value (d_{24}). 24
Figure 5.12. DDF curves (0.5, 0.04, and 0.01 AEP) for Roxboro, NC, normalized to the largest value (d_{24}) augmented by the 90th percentile curves for the 25-year curve, also normalized by dividing all values by the 25-year 24-h depth. 25
Figure 5.13. Projected increases in precipitation measures with changes in temperature [Kharin et al. 2013] Top left: Relative changes (%) in globally averaged 20-year return values of annual daily precipitation extremes versus globally averaged changes in annual mean near surface temperature simulated by the CMIP5 models for the RCP2.6, RCP4.5 and RCP8.5 in 2046–2065 and 2081–2100. Top right: Histograms of the ratio of globally averaged 20-year return values of annual daily precipitation extremes to the globally averaged changes in annual mean near surface temperature. Bottom figures same as top except for mean annual precipitation. 27
Figure 5.14. Four regional 24-hour rainfall distributions from Volume 2 of NOAA Atlas 14 (Ohio Valley and neighboring states). 37

Figure 5.15. Map of the synthetic rainfall distributions used by NRCS as of January 2016 (NRCS 2015). . 38
Figure 5.16. Relation between observed 60-minute duration quantiles and baseline GCM 24-hour quantiles for the example application to Philadelphia, PA. 43
Figure 5.17. Relation between the GCM future and baseline 24-hour quantiles for the example application to Philadelphia, PA. 44
Figure 5.18. IDF curves for historical and future conditions for the 0.01 AEP for Philadelphia, PA. 46
Figure 5.19. Areal reduction factor graph for 0.5, 0.1, and 0.01 AEP and 1-, 6-, and 24-hour durations (NWS-24). 49
Figure 6.1. Watershed map for the Northeast Branch of the Anacostia River upstream of East Riverdale, Maryland. 56
Figure 6.2. Time series of annual maximum peak discharges from 1933 to 2016 for the Northeast Branch of the Anacostia River at Riverdale, Maryland. 57
Figure 6.3. Time series of annual maximum peak discharges from 1939 to 2016 for the Northeast Branch of the Anacostia River at Riverdale, Maryland. 58
Figure 6.4. Impervious area since 1939 for the Northeast Branch of the Anacostia River at Riverdale, Maryland. 60
Figure 6.5. The 24-hour annual maximum precipitation at Beltsville, Maryland from 1941 to 2016. 61
Figure 6.6. Annual peak discharges for Stockley Branch at Stockley, Delaware from 1943 to 2004. 63
Figure 6.7. Urban fraction coefficients from temporal regression analysis of 117 stream gauges in northeastern Illinois and adjacent states as a function of exceedance probability (Over et al., 2016b). 80
Figure 6.8. Observed and adjusted annual peak discharges for the Skokie River at Lake Forest, IL (05535000). 81
Figure 6.9. Flood ratios for 677 Texas watersheds using the 0.1 AEP (10-year) flood discharge as the index flood. Ratios are plotted with the median, 25th, and 75th percentile values. 86
Figure 6.10. Five counties in Texas selected for DDF analyses. 87
Figure 6.11. Comparison of the middle 50 percent of flood ratios to rainfall ratios for 40 rainfall ratio curves for Texas. 91
Figure 7.1. Schematic representation of VIC model components (University of Washington 2017). 98
Figure 7.2. Flow chart showing the general approach for incorporating Downscaled GCM precipitation data into continuous simulation. 99
Figure 7.3. Comparison of average monthly future (2000-2049) and baseline (1950-1999) precipitation for the CCSM4 model and the RCP8.5 scenario in Philadelphia, PA. 106
Figure 7.4. Monthly average temperature for future (2000-2049) and baseline (1950-1999) periods and the corresponding monthly change factor for a location in Fairfax, VA (CCSM4 model and RCP8.5). 109
Figure 7.5. Example partial autocorrelation function values for a baseline precipitation time series and three future precipitation series using single, seasonal, and threshold CFs. 111
Figure 7.6. Example partial autocorrelation function values for baseline and projected future precipitation time series. 112
Figure 8.1. Relative sea level rise trend for New York City based on tide gauge data (downloaded from www.tidesandcurrents.noaa.gov/sltrends Sept. 30, 2017). 118

Figure 8.2. RSL trends based on tide gauges around the US (Adapted from www.tidesandcurrents.noaa.gov/sltrends, downloaded September 30, 2017) 119
Figure 8.3. Annual average RSL at Dauphin Island, Alabama. 120
Figure 8.4. Global mean sea level rise projection (from NRC 2012). 123
Figure 8.5. General relationship between the central estimate and probabilistic range of sea level rise and the relationship between RCP-based scenarios (from Sweet et al. 2017a). 123
Figure 8.6. Global mean sea level rise (GMSLR) projections with probabilities (from Kopp et al. 2014; solid lines = median, dashed = 5th-95th percentile, dotted = 0.5th-99.5th percentile). 124
Figure 8.7. Example of sea level rise projections (baseline 2005) using linear extrapolation of historical sea level trend (green), lower and higher emissions estimates from process-based models (yellow and red; from IPCC 2007) and higher emissions estimates a semi-empirical model (blue; from Vermeer and Rahmstorf 2009). Source: unpublished figure from Frumhoff et al. 2007. 125
Figure 8.8. Range of global mean sea level rise (GMSLR) projections for the 21st century (adapted from Nicholls et al. 2014; used with permission). Sources listed in Table 8.1. 127
Figure 8.9. GMSLR data and projections from NCA3 (Melillo et al. 2014). 128
Figure 8.10. GMSLR data and projections from Sweet et al. (2017a) with central probability ranges and extremes of RCP-based projections, as used in NCA4 (Sweet et al. 2017b). 129
Figure 8.11. RSLR, scenario projections at four US locations (from Sweet et al. 2017a). 130
Figure 8.12. Selection of GMSLR projections for vulnerability assessment and adaptation strategies for the Central Artery/Tunnel system in Boston, MA Source; Bosma et al. (2015), Douglas et al. (2016a). Used with permission. 133
Figure 8.13. Recommended minimum (solid blue line) projection of GMSLR with the NOAA scenarios (dashed lines) from Sweet et al. (2017a). 138
Figure 8.14. Recommended alternative RCP8.5 (solid blue line) projection of GMSLR with the NOAA scenarios (dashed lines) from Sweet et al. (2017a). 139
Figure 8.15. Water level, wave height, and wave period AEP values near San Luis Pass, Texas. 144
Figure 8.16. Return period (spectrally) significant wave heights in 19 m depth offshore of Hatteras Island, NC. 145
Figure 8.17. Water level exceedance probabilities for Sandy Hook, NJ above the MHHW tidal datum. The thick black line is the GEV fit and the thin black lines above and below are the 95-percent confidence intervals. 146
Figure 8.18. Comparison of simulated (hydrodynamic models) maximum still water level (SWL) and predicted (Equation 8.2) maximum still water level. The color of each point (N=278255) represents the depth, relative to mean sea level, at that location under non-storm conditions. 148
Figure 8.19. The variation of amplification ratio with depth for each model node colored by its maximum SWL in 1970 (top two panels) along with the means and standard deviations by depth range (lower panel). 150
Figure 8.20. Comparison of actual *AR* value statistics (relative and cumulative frequency) to those fit by a normal probability distribution (normal CDF, normal PMF). 151
Figure 8.21. Comparison of simulated (modeled) and predicted maximum zero moment wave height. Each point (*N*=278255) is colored by its depth relative to the given scale. 153

Figure 8.22. Direct comparison of simulated (modeled) and predicted peak wave periods. Each point (N=278255) is colored by its depth relative to the given scale. 154
Figure 8.23. Comparison of simulated (model) and predicted maximum water velocity magnitude for all non-zero velocity values in the model simulation (*N*=278079). 156
Figure 8.24. Estimated 100-year and 50-year maximum still water level at San Luis Pass, TX for three sea level rise scenarios adjusted for regional effects. The black dashed line shows the baseline 100-year still water level. 158
Figure 8.25. Estimated 100-year and 50-year maximum significant wave height (Hmo) at San Luis Pass, TX for three sea level rise scenarios adjusted for regional effects. The black dashed line shows the baseline 100-year wave height. 159
Figure 8.26. Estimated 100-year and 50-year maximum water velocity at San Luis Pass, TX for three sea level rise scenarios adjusted for regional effects. The black dashed line shows the baseline 50-year velocity. 159
Figure 8.27. Case study: Shore Road, Brookhaven, NY location overview map. 162
Figure 8.28. Projections of mean sea level, tidal datums (MLLW, MHHW), storm water levels, and wave overtopping elevations (WOT) for the intermediate-low scenario at Shore Road, NY. 164
Figure 8.29. Projections of mean sea level, tidal datums (MLLW, MHHW), storm water levels, and wave overtopping (WOT) elevations for the intermediate-high scenario at Shore Road, NY. 164
Figure 8.30. Projections of mean sea level, tidal datums (MLLW, MHHW), storm water levels, and wave overtopping (WOT) elevations for the extreme scenario at Shore Road, NY. 165
Figure 8.31. Location map and damage overview for the I-10 Escambia Bay Bridge in Florida. 167
Figure 8.32. Mean sea level data, trend, and confidence intervals for Pensacola, FL. 168
Figure 8.33. Time-series results from the 1970 and 2004 hydrodynamic model simulations of Hurricane Ivan at location Damage W. 168
Figure 8.34. Time-series results from the 1970 and 2004 hydrodynamic model simulations of Hurricane Ivan at location Damage W, shown for a shorter time period during the storm event. 169

List of Tables

Table 4.1. Examples of extreme precipitation indices used in climate science literature and assessments. 3
Table 4.2. Examples of extreme precipitation and hydrological indices used for engineered structures; actual definitions are project-specific. 4
Table 4.3. Comparing the definition and calculation of “extremes” in climate science and engineering. ..5
Table 4.4. Archives of historical observations. 13
Table 4.5. Performance evaluation for global climate models. 29
Table 4.6. List of empirical-statistical downscaling methods and available datasets. 36
Table 4.7. Performance evaluation standards for downscaled global climate model output. 38
Table 4.8. Evaluation tool for US climate projection dataset suitability. 39
Table 4.9. Potential climate resources for a range of levels of analysis. 42
Table 4.10. Group 1 GCMs from the ICNet analysis and corresponding climate sensitivity (Randall et al. 2007; Flato et al. 2013). 46
Table 5.1. Example matrix of future/baseline ratios by grid cell and model for a future scenario. 6
Table 5.2. NOAA Atlas 14 24-hour precipitation quantiles for Denver, Colorado, example. 8
Table 5.3. Estimated moments and quantiles for the baseline period (1950-1999). 10
Table 5.4. Estimated moments and quantiles for the future period (2000-2049). 10
Table 5.5. Estimated moments and quantiles for the future period (2050-2099). 11
Table 5.6. Estimated quantile ratios future period (2000-2049) to baseline. 11
Table 5.7. Estimated quantile ratios future period (2050-2099) to baseline. 11
Table 5.8. Ensemble summary of ratios and projections for 2000-2049. 13
Table 5.9. Ensemble summary of ratios and projections for 2050-2099. 13
Table 5.10. Precipitation depth (inches) from NOAA Atlas 14 for AEP 0.5 to 0.01 and durations from 5 min. to 24 h for Roxboro, NC. 24
Table 5.11. Methods and examples of sub-daily disaggregation. 29
Table 5.12. Factors for adjusting daily values. 32
Table 5.13. Confidence intervals based on hydrologic service life. 39
Table 5.14. Summary of observed sub-daily AEPs for selected durations from NOAA Atlas 14 for Philadelphia, PA. 42
Table 5.15. Summary of model-based (GCM) 24-hour quantiles for the example. 42
Table 5.16. Summary of historical and future 60-minute quantiles for Philadelphia, PA. 45
Table 5.17. Summary of historical and future (2000-2049, RCP8.5) quantiles for the 5- and 15-minute and 6- and 24-hour durations for Philadelphia, PA. 45
Table 5.18. Summary of historical and future (2000-2049) precipitation depths for the 0.01 AEP for Philadelphia, PA for the CSIRO model and the RCP8.5 scenario. 45
Table 6.1. Summary of AEP discharges using different periods of record and the time-varying mean approach for the Northeast Branch of the Anacostia River at Riverdale, Maryland. 58
Table 6.2. Largest floods of record for the Northeast Branch of the Anacostia River at Riverdale, Maryland (station 01649500). 64

Table 6.3. MAP results for hypothetical example. 69
Table 6.4. Depths of rainfall for various durations and return periods for five Texas counties. 89
Table 6.5. Depth Ratios to 10-year for various durations and return periods for Texas. 90
Table 7.1. Percentile thresholds of baseline precipitation and total precipitation above the threshold calculated based on observed period (1950-1999) and future period (2000-2049) for the CCSM4 model for RCP8.5 in Philadelphia, PA. 103
Table 7.2. Percentile values of baseline precipitation and the total precipitations below the percentile calculated based on observed period 1950-1999 and future period 2000-2049 for the CCSM4 model for RCP8.5 in the Philadelphia, PA area. 104
Table 7.3. Downscaled GCM monthly average values based on a baseline period 1950-1999 and a future period 2000-2049. 105
Table 7.4. Monthly average temperatures based on baseline period 1950-1999 and future period 2000-2049 for the CCSM4 model for RCP8.5 scenario in Fairfax, VA. 109
Table 8.1. Comparison of global mean sea level rise (GMSLR) projections for the 21st century. (Source: modified from Table 3 in Nicholls et al. 2014; used with permission). 127
Table 8.2. RSLR projections (in feet above year 2000 sea level) by exceedance probability and representative concentration pathway (RCP) for Boston Harbor, following Kopp et al. (2014). (Modified from Table 1-1 in Douglas et al. 2016b). 134
Table 8.3. Recommended minimum GMSLR estimates for use in planning and design. 137
Table 8.4. Analysis of velocity magnitude error associated with Equation 8.10. 155
Table 8.5. Relative sea level by year for three scenarios from Sweet et al. (2017a). Values are relative to the MSL tidal datum of 1983-2001 for Port Jefferson, NY. 163
Table 8.6. Return period storm water levels and significant wave heights at a location near Shore Road obtained from the USACE ERDC Coastal Hazards System. 163

Chapter 1. Background

1.1. Problem Statement

Transportation hydraulic engineers are being asked to account for global climate change within hydrologic and hydraulic (H&H) and coastal design practice. Current H&H and coastal design procedures use historical data that are assumed to represent a stationary process (McCuen et al. 2002, Douglass and Krolak 2008). Climate change introduces nonstationary risks such as sea level and temperature rise, and changes in timing and distribution of precipitation, snowpack, and snowmelt (USGCRP 2017, 2018). Failure to account for such nonstationary risks may compromise the operational characteristics of existing and future transportation infrastructure.

Climate scientists employ outputs from a suite of models to develop scenarios representing these nonstationary phenomena that are not associated with specific probabilities. Existing guidance for H&H design does not provide methods to incorporate such information. Collaborative efforts and a common set of terms and definitions between climate change scientists, hydrologists, hydraulic engineers, and coastal engineers are essential to harmonize climate change inputs and H&H design practice.

Incorporating the results of climate models and assessments may have large cost implications for future infrastructure. For example, overestimates of the magnitude of peak flows can result in costly oversizing of drainage infrastructure, while underestimates might leave infrastructure vulnerable and the resultant flooding impacts on surrounding lands and structures inadequately addressed. It is often questioned if the magnitude of change in hydrologic and hydraulic inputs resulting from climate change is within the range of uncertainties accounted for in the current state of practice. Furthermore, accounting for climate change in hydrologic design is complicated by additional nonstationary processes arising from urbanization and other land cover changes.

Similarly, designing for higher estimates of sea level rise might also result in unnecessary costs, while designing for lower estimates might leave infrastructure and the public vulnerable. The timing of a given rise in sea level may also be a question. Will it take 50 years, 100 years, or 200 years for a particular sea level to be experienced, and how does that affect planning and design?

1.2. Research Objectives and Scope

Research is needed to provide H&H and coastal engineers with practical tools to: 1) account for the effects of climate change in hydrologic design and coastal applications where appropriate and 2) justify when such changes are not warranted for a project of a particular type or scale. To address this need, the National Cooperative Highway Research Program (NCHRP) initiated this study, number 15-61 "Applying Climate Change Information to Hydrologic and Hydraulic Design of Transportation Infrastructure."

The objectives of this research were to review the literature for tools and techniques that represent the state of the art for actionable hydrologic design of transportation infrastructure accounting for the potential effects of climate change. In addition to this final report, the study produced a *Design Practices* manual of national scope to provide H&H and coastal engineers with the tools needed to amend practice to account for climate change.

The emphasis in this report and the companion *Design Practices* manual is on practices applicable to inland hydrology. In addition, attention is applied to the coastal environment, particularly as it relates to sea level rise and coastal hazards.

Chapter 2 provides a description of the research approach. This includes a brief description of the project work plan followed by a summary of the literature review. Chapter 3 provides an overview of various decision-making frameworks. Within these frameworks, the concept of levels of analysis is introduced.

Chapter 4 summarizes concepts and themes related to climate science and modeling relevant for use of these resources for hydrologic design and coastal assessment. Evaluation and guidance on the appropriate selection and use climate models, scenarios, and other topics is provided.

Chapters 5 through 7 provide detailed discussion of technical topics related to the need for incorporation of climate science projections into inland hydrology design and analysis. Chapter 5 addresses issues related to the gaps between spatial and temporal resolution of climate modeling products and hydrologic engineering requirements. Chapter 6 outlines a range of statistical approaches for incorporating climate projection in hydrologic analyses. Chapter 7 focuses on climate considerations for continuous simulation modeling.

Chapter 8 addresses the coastal environment. Issues and guidance related to sea level rise is the focus. Other climate-related issues related to the coasts are also presented.

1.3. What Does it Mean to Design for Climate Change?

Before even considering climate change, planners and engineers strive to create transportation infrastructure components and systems that are ***resilient***, that is, are capable of maintaining or rapidly recovering functionality in response to changing conditions or disruptions. Planning and designing for climate change means recognizing that the future may not look like the past. It means using climate information from the past along with projections about the future to design resilient transportation infrastructure. Resilient design principles include reducing vulnerability of infrastructure through lowering the probability of failure, experiencing less severe consequences when failure occurs, and enabling faster recovery times from failure or damage.

Traditionally, H&H engineers have used various data and techniques to characterize the historical patterns of storm and flood events ranging from the frequent to the extreme in order to understand and design for the probability that such events may occur in the future. Similarly, coastal engineers characterize historical patterns of water levels, winds, waves, and sediment transport in order to understand and design for the probability that those events may also occur in the future. In both contexts, engineers have traditionally relied on historical conditions to be reasonable predictors of future conditions; that is, they rely on ***stationarity***. However, a changing climate undermines this assumption so that precipitation patterns, water levels, and other climate driven parameters of the future may not be estimated as reliably from the past. This is known as ***nonstationarity***.

In both inland hydrology and along the coast, designing for climate change means augmenting what is known about the historical occurrence of extreme events with changes in the magnitude and frequency of these events associated with climate change. This means adapting existing tools and techniques to incorporate information from the climate science community.

This report describes the current state of knowledge and understanding of possible future conditions developed by the climate science community. However, climate science and modeling is a dynamic field that is continually advancing and changing.

BOTTOM LINE: Planning and designing for climate change means recognizing that the future may not look like the past and using information from the past along with future projections to design resilient transportation infrastructure.

Chapter 2. Research Approach

To meet the project objectives, the research was divided into two phases. In the first phase, the consultant team performed a literature review as well as an opportunities assessment of what may be included in a design practices manual. Phase I closed with a presentation to - and conversation with the panel - about the direction of Phase II. In Phase II, the consultant team implemented the remaining work plan under the guidance of the panel.

2.1. Work Plan

2.1.1 Phase I: Literature Review and Opportunities Assessment

Phase I comprised three tasks culminating in a Phase I report and presentation to the panel. Improving the quality of the design of hydraulic features including bridges, culverts, stormwater management facilities (e.g., storm drains and detention), and water quality facilities was the focus.

Task 1. Amplified Work Plan and Literature Review. Task 1 was divided into two activities: 1) an amplified work plan and 2) a literature review. The amplified work plan integrated the original proposed work with the panel comments. The consultant team completed an extensive literature search for recent and relevant projects.

Task 2. Opportunities Assessment and Report. In this task, opportunities for better integrating climate science outputs into hydrologic design were assessed. The results of these assessments provided a foundation for Phase II and guided the refinement of the Phase II work plan.

Task 3. Phase I Panel Presentation.

The consultant team prepared and delivered a presentation for the panel based on the Phase I work. Considering the feedback from the panel, the Phase II work plan was revised to guide the Phase II work.

2.1.2 Phase II: Implementation of Study Scope

Phase II was composed of nine tasks addressing topics intended for the design practices manual and includes collaboration with the project panel through presentations and feedback. The first four tasks of Phase II represented in-depth work developing key components for the anticipated design practices. These tasks were oriented to guidance and tools as they relate to: 1) potential modifications to climate modeling outputs for hydrologic design, 2) frameworks for incorporating uncertainty into hydrologic design, 3) development of a hydrologic design framework for inland transportation assets, and 4) evaluation of climate outputs and design techniques for coastal transportation assets. Following a panel meeting, the remaining tasks focused on synthesizing the concepts and procedures into a design practices manual and this final report.

Task 4. Evaluate Potential Modifications to Climate Modeling Outputs for Hydrologic Design. The consultant team of climate scientists, statisticians, and hydrologists evaluated how climate modeling outputs can be modified to enhance their utility in H&H design processes.

Task 5. Develop Approaches for Incorporating Climate Change and Uncertainty: Temporal and Spatial Precipitation Data. This task focused on issues related to the temporal and spatial incompatibility between climate modeling outputs and hydrologic design inputs. These included: 1) development of projected sub-daily precipitation estimates and Intensity Duration Frequency (IDF) curves, 2) addressing spatial scale compatibility of spatially-averaged precipitation, and 3) the use of point versus spatially-averaged precipitation.

Task 6. Develop Approaches for Incorporating Climate Change and Uncertainty: Precipitation Time Series and Statistical Methods. This task focused on issues related to the time series hydrology applications and the use of various statistical methods. These included: 1) proper used of continuous simulation data, 2) trend projections from historical discharges, 3) regression approaches for projecting discharges, and 4) ratio or index-based approaches.

Task 7. Evaluation of Climate Outputs and Design for Coastal Transportation Assets. This task focused on the unique issues related to the coastal environment with emphasis on sea level rise. A secondary focus addressed combining coastal hazard and climate change information.

Task 8. Interim Progress Meeting. The consultant team reported on the research progress to the panel based on the first four tasks of Phase II.

Task 9. Synthesis of Approaches for Nonstationarity in Hydrologic Design. The consultant team synthesized the components of the study into a framework for design guidance for incorporating climate change into hydrologic and hydraulic design. As part of the synthesis alternative decision-making frameworks were assessed to develop a decision framework for engineers to incorporate uncertainty in their designs while improving the adaptability of the design to climate change.

Task 10. Draft Final Report and Design Practices. The consultant team prepared two complementary documents: 1) a draft final report and 2) a draft final design practices manual. The draft final report documented the cumulative findings of both Phase I and Phase II. The draft design practices manual is national in scope to provide H&H and coastal engineers with the tools needed to amend current practice to account for nonstationarity, including climate change.

Task 11. Phase II Panel Presentation and Progress Meeting. The consultant team prepared and delivered a presentation for the panel based on the draft final report and draft final design practices manual.

Task 12. Final Report and Design Guide. The consultant team prepared the final versions of the two complementary documents, incorporating the feedback and guidance from the panel from Task 11: 1) final report and 2) design practices manual.

2.2. Literature Review Summary

The literature review was completed as part of Task 1. The primary purpose of the literature review was to support the project objective to "develop a design guide of national scope to provide hydraulic engineers with the tools needed to amend practice to account for climate change."

It is divided into four major sections. Because design is essentially a decision-making process, the first section describes literature on decision-making frameworks.

Next, the literature review discusses high-resolution climate projections, including global climate model simulations, future scenarios, and downscaling models, and their application to quantify future trends and distributions.

The third major section reviews the literature applicable to integrating climate inputs into hydrologic design for inland applications. Topics include nonstationarity, climate inputs for hydrologic design, sub-daily rainfall, and confidence limits.

The final major section reviews the literature related to the effects of climate change on coastal processes, with an emphasis on those topics with potential for immediate integration into coastal design applications. Topics include sea level rise, increasing ground water levels, changes in tropical and extratropical cyclones, watershed contributions to total water level at the coast, storm surges and wave hazards, and changes to coastal morphology.

The literature review is provided in this report as Appendix A as it was on completion of Task 1. Throughout the project the consultant team continued to find additional resources and new publications became available. As appropriate, these have been incorporated into this final report and the design practices manual.

Chapter 3. Decision-Making Frameworks

This report considers two decision-making frameworks within which planning and design of transportation infrastructure may be conducted: 1) traditional (top-down) and 2) threshold (bottom-up). As suggested by its name, traditional (top-down) design is the dominant approach for designing transportation infrastructure projects today. Threshold (bottom-up) design has been more frequently used in larger system design and vulnerability assessment and is increasingly being considered for infrastructure design when future uncertainties, such as climate change, are important.

Traditional (top-down) design is a process where designers apply a defined set of information, design procedures, and design criteria to determine an appropriate plan or design for a new project or to evaluate an existing project plan or design. The process is typically sequential, and uncertainty in the inputs may be considered. A factor of safety is sometimes incorporated as an acknowledgement of uncertainty. In the context of climate change, traditional (top-down) design can be characterized as a "predict, then act" approach. A relevant question is "what is likely to happen under the future design conditions?" The goal, then, is to design the infrastructure to perform for those future conditions. In the context of climate change, traditional design seeks to predict the future, or at least a likely range of futures, and then plan or design infrastructure to perform according to standards for those future conditions. Section 3.1 provides a more detailed description of the traditional (top-down) decision-making framework.

Threshold (bottom-up) design is a process where the vulnerabilities of existing or proposed infrastructure are identified so that potential conditions that expose those vulnerabilities can be quantified. The conditions under which the infrastructure becomes vulnerable are called "thresholds." In threshold design, the process is to assess vulnerabilities and develop plans or designs that address those vulnerabilities. The evaluation seeks to identify the greatest vulnerabilities across a range of possible future conditions, and then planners and designers select from alternative approaches those that perform reasonably well under those futures. The goal is to assess vulnerabilities, to seek robust solutions that minimize regret in decision making. Relevant questions under this paradigm are, "how does my system work?" and "under what circumstances might it fail?" In the context of climate change, threshold design identifies vulnerabilities first and then examines how alternative future scenarios expose those vulnerabilities. Planning and design choices are focused on what outcomes are acceptable or unacceptable, rather than defining and relying on a likely range of futures. Section 3.2 provides a more detailed description of the threshold (bottom-up) decision-making framework.

Decision makers may experience ***regret*** in one of two forms. One is regret associated with insufficiently investing in infrastructure to prepare for changes in climate. In this case, the results are excessive damages and negative effects on the public health, safety, and welfare. The second form is regret associated from overinvesting and consuming resources that could be better used elsewhere. Since the future is unknown, planners and designers cannot objectively "minimize" regret. However, this report provides tools and procedures that promote an understanding of the uncertainty associated with projecting future conditions and integrating that with the uncertainty associated with existing data, tools, and models for hydrologic and coastal design.

A probabilistic risk framework can be applied within either traditional or threshold decision frameworks to evaluate consequences and potential regret. A probabilistic risk framework is one in which the joint probabilities of different types of events (e.g., hurricane) and their responses (e.g., storm surge) are determined, and where those results are used to make risk-based decisions.

With the context of these design-making frameworks, this report describes how planners and engineers can adapt existing tools for analysis and design to address the potential effects of a changing climate. The remainder of this chapter provides additional description of the decision-making frameworks and introduces the concept of levels of analysis. Guidance for selecting a decision-making framework is provided in Section 3.3

3.1. Traditional (Top-Down) Framework

Transportation infrastructure design teams typically follow a traditional (top-down) design approach with varying ***levels of analysis*** depending on the nature of the project. The project design team bases the selection of an appropriate level of analysis on the criticality of the project, expected service life, the vulnerability of the project to climate change, the functional classification of the project (roadway, bridge, or tunnel), regulatory requirements, and the resources available for the project. These factors are not independent. For example, available project resources are usually linked to, and often dictated by, the type of environmental review process required for the project. The environmental review process is often closely tied to a particular funding program.

A higher level of analysis requires more effort (resources) to conduct and also incorporates more information about historical and possible future climate as shown in Figure 3.1. The goal of using higher levels of analysis is a more informed basis for decision making for those projects for which the investment is justified. The following sections provide an overview of levels of analysis for inland hydrology and coastal projects, respectively.

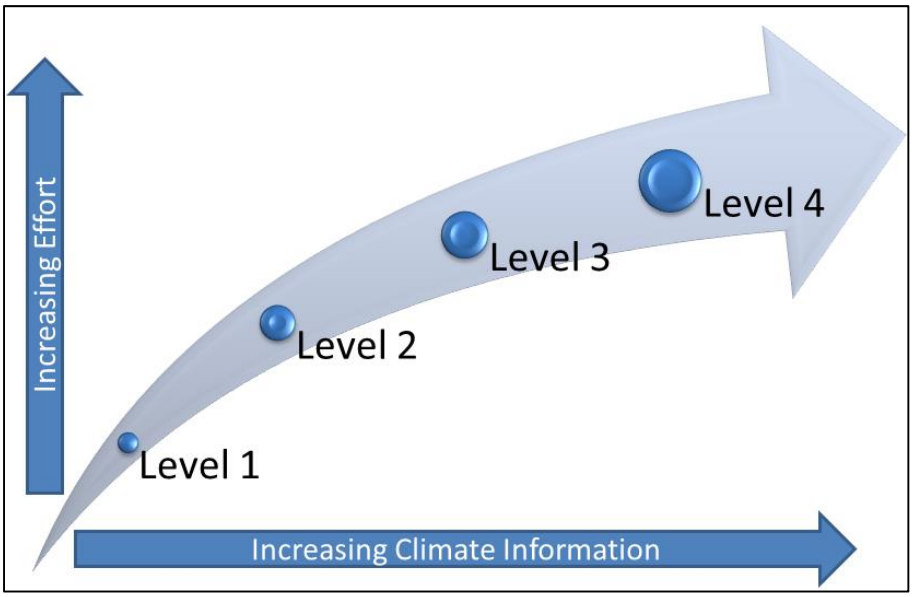

Figure 3.1. Levels of analysis, effort, and climate information.

3.1.1 Inland Hydrology

HEC-17 describes a generalized hierarchy of traditional (top-down) analyses for inland hydrology (Kilgore et al. 2016). These levels, ordered from least to most intensive, not only apply to specific bridges, culverts, or other hydraulic structure projects, but also to plans that may include multiple hydraulic structures or other natural or constructed features.

At each level of analysis, the design team chooses the hydrologic tools and methods appropriate for the project and site conditions given the governing guidance and appropriate design practice. Beginning at Level 2, the concept of ***confidence limits*** for estimating discharge is employed. Confidence limits define a range in which the true value of discharge is expected to lie with a given probability. The levels of analysis for inland hydrology are summarized as follows:

Level 1 – Design discharge based on historical data. The design team applies the appropriate hydrologic design techniques based on historical data to estimate the design discharge. In addition, the design team qualitatively considers possible changes in the estimated design discharge based on future changes in land use and climate, e.g., precipitation.

Level 2 – Design discharge based on historical data/confidence limits. The design team performs all Level 1 analyses. In addition, the design team quantitatively estimates a range of discharges (confidence limits) based on historical data to evaluate plan/project performance.

Level 3 – Design discharge based on projected information/confidence limits. The design team performs all Level 2 analyses. In addition, the design team obtains and applies existing quantitative projections of changes in land use and climate, where feasible. The design team performs hydrologic analyses using land use and climate projections, as applicable, to estimate projected design discharges and their associated confidence limits.

Level 4 – Design discharge based on projected information/confidence limits/custom evaluation. The design team performs the equivalent of the Level 3 analyses, but augments the analyses with customized projections of land use and climate and/or customized hydrologic modeling techniques. Customization usually requires augmenting the typical design team to include appropriate expertise in climate science and/or land use planning to secure site-specific projections and/or expertise in advanced hydrologic modeling techniques.

Each level of analysis represents increasingly involved project processes and builds on the information developed at lower levels of analysis. At Levels 1 and 2, the design team conducts analyses with general skills and expertise that are characteristic of existing project design and planning teams. Moving to a Level 3 analysis requires the retrieval and analysis of projected climate information, which may require the addition of expertise to the project team. By definition, a Level 4 analysis will require additional tools and expertise.

3.1.2 Coastal Applications

HEC-25 Volume 2 describes a generalized hierarchy of traditional (top-down) analyses for coastal applications (Douglass et al. 2014). These levels, ordered from least to most intensive, not only apply to specific tunnel, bridge, and road projects, but also to plans or projects that may include multiple structures or other natural or constructed features.

Coastal vulnerability assessments and design activities may range from broad planning overviews to highly detailed investigations employing state-of-the-art modeling tools. This

report presents techniques for different levels of analysis for these assessments. As with inland hydrology, the detail and degree of complexity grow with each subsequent level of analysis, with the intention that the quality and comprehensiveness of the assessment also increases. Suggested levels of analysis for coastal applications are as follows:

Level 1 - Use of existing data and resources. The design team uses existing inundation, e.g., Federal Emergency Management Agency (FEMA) or tsunami hazard maps, to determine the exposure of infrastructure under selected sea (lake) level change scenarios, and sensitivity to depth-limited wave or wave run-up processes.

Level 2 - Original modeling of storm surge and waves. The design team performs all Level 1 analyses for the initial assessment. The design team also performs original modeling of surge and wave fields for specified storm and climate change scenarios, or modeling of tsunami inundation under climate change scenarios, to provide more detailed information on water levels, waves, etc. for the specified conditions.

Level 3 - Modeling in a probabilistic risk framework. The design team performs original modeling of surge, sea levels, currents, and waves or tsunamis, including the potential effects of climate change, in a probabilistic risk framework. The specified storm and climate change scenarios are expanded from Level 2.

Each level of analysis represents increasingly involved project processes and builds on the information developed in the lower levels of analysis.

3.2. Threshold (Bottom-Up) Framework

The numerous sources of uncertainty involved in climate modeling and sea level rise projections, inland hydrologic analyses, and coastal hydrodynamic analyses represent a significant challenge for traditional (top-down) approaches. For that reason, planners and designers are increasingly considering alternative ***threshold (bottom-up)*** decision-making frameworks for inland and coastal applications. In such a framework, the goal can be summarized as "assess vulnerabilities and seek robust solutions to minimize regret." In the threshold (bottom-up) paradigm, the relevant questions are, "how does my system work?" and "under what circumstances might it fail?"

In a threshold (bottom-up) framework, the first step is to identify the vulnerabilities or thresholds of a location or system. For example, in the case of a tunnel, the planning/design team identifies at what elevation a coastal or riverine flood would begin to enter the tunnel, affecting its performance. Other potential vulnerabilities are also identified.

Next, the planning/design team evaluates the possibilities of those conditions occurring. This process could include the development of "climate narratives" that capture projected future conditions. These narratives are evaluated to see which of the vulnerabilities identified are exposed by the climate narrative and to identify the consequences of that exposure.

Finally, the planning/design team considers the vulnerabilities and the exposure consequences from various climate narratives to evaluate or design infrastructure intended to serve its function for a certain service life. The team identifies a range of policies, plans, or designs that perform reasonably well across that range of climate narratives, minimizing expected regret in decision making. Regret may be in the form of not preparing for climate change and bearing the

consequences if projected conditions occur or, alternatively, in the form of over preparing for climate change if projected conditions do not occur.

The threshold (bottom-up) approach can be used for:

- Evaluating existing transportation infrastructure such as roads, bridges, and tunnels, and their associated hydraulic structures, to assess which possible future outcomes may unacceptably threaten the transportation infrastructure.
- Designing new elements of the transportation infrastructure to assess which possible future outcomes may unacceptably threaten the transportation infrastructure.
- Evaluating the value of the threshold (bottom-up) approach itself, in contrast to traditional (top-down) approaches, in the form of pilot studies.

3.3. Selecting a Decision-Making Framework

Both traditional and threshold frameworks have advantages and limitations. The choice depends on many factors including the project goal, the perspective of the project team, project context, and potential adaptability of the project. Figure 3.2 summarizes these factors and illustrates that they exist on a continuum with one side favoring traditional decision making and the other favoring threshold decision making. However, planners and designers should recognize that these are general characterizations only.

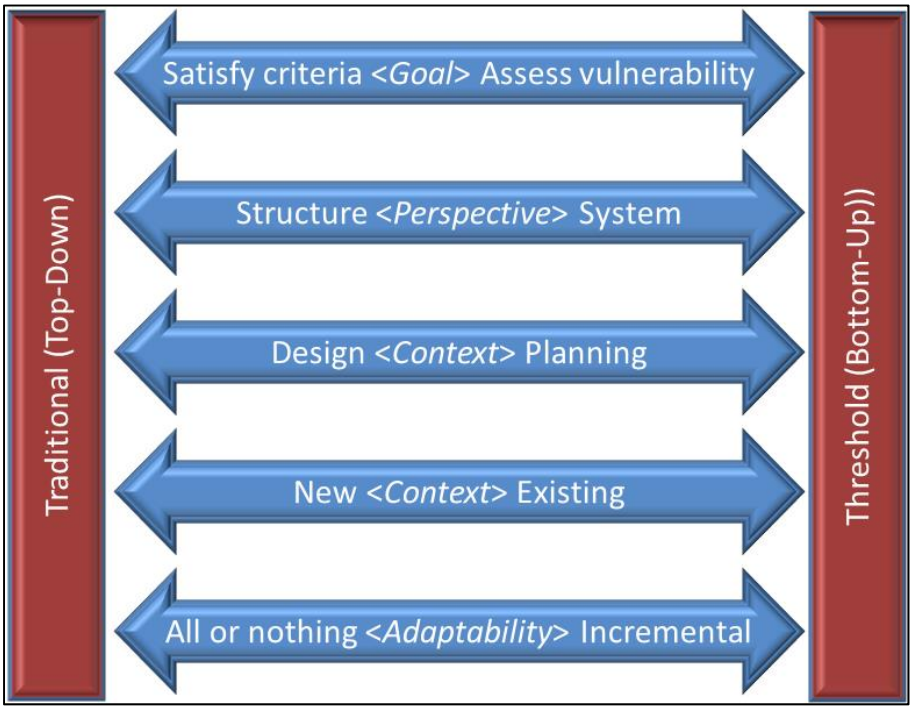

Figure 3.2. Considerations for choosing a decision-making framework.

If the objective of a project is to design a new individual structure with fixed design criteria, traditional (top-down) decision making is often the preferred choice. However, if the objective is to plan possible options for enhancing an existing system of infrastructure by identifying its

vulnerabilities, threshold decision making is likely to be a more valuable approach. Beyond these two extremes, the relative importance of each of the factors shown in Figure 3.2 will influence the choice of a decision-making framework.

Figure 3.2 also refers to the potential for project adaptability for selecting the decision-making framework. Can the project be implemented in an incremental manner over time as conditions change or is the project such that it must all be built at one time to serve its function? While many types of infrastructure may have adaptable features, such as building in additional bridge width to add lanes later, design choices are often fixed and are not easily incrementally expanded or modified. For example, a culvert installed in a roadway embankment cannot easily be expanded to accommodate future increases in discharge.

To illustrate the differences in the two decision-making frameworks, consider a vulnerability pilot project performed by the Connecticut Department of Transportation (CTDOT) of its bridges and culverts in the northwest part of the state (Connecticut Department of Transportation 2014). Furthermore, consider one of the culverts included in the study, known as structure number 02423, which was built in 1950 over an unnamed waterway. This structure was designed using the traditional decision-making framework to satisfy applicable design criteria related to the 1-percent AEP and 0.2-percent AEP (100-year and 500-year return periods) including providing adequate freeboard and maintaining an allowable headwater to diameter ratio (HW/D). Headwater is the depth of water at the upstream end of a culvert measured from the bottom of the culvert at that location.

CTDOT computed the relationship between headwater and discharge for the culvert shown in Figure 3.3. As discharge increases, the headwater also increases. The figure shows that the headwater at both the 100-year and 500-year design discharges are lower than relevant thresholds including the HW/D and freeboard criteria. Therefore, the culvert design more than satisfied these criteria suggesting that other considerations led to the size and type of culvert built.

In the pilot study, CTDOT considered the vulnerability of this culvert to current (higher) estimates of design discharge as well as to potentially higher discharges in the future that might occur because of a changing climate. Continuing with the traditional decision-making framework, the next task would be to estimate a future design discharge or discharges and evaluate the culvert with those estimated discharge(s).

A threshold decision-making framework could also be applied for this purpose. Referring to Figure 3.3 one can determine that the HW/D and freeboard criteria are reached at discharges of 2,330 cubic feet per second (cfs) and 2,700 cfs, respectively. Water would begin to flow over the road (referred to as overtopping) at a discharge of 2,900 cfs.

As described in Section 3.2, the threshold decision-making framework begins by defining the vulnerabilities and then evaluating the possibilities of such conditions occurring. For the first step, the planning/design team evaluates whether violation of the criteria (in this case HW/D or freeboard) represents a problem. At these levels, is there flooding of property or are there threats to the public safety? Are velocities at the culvert exit a threat downstream or do they present an erosion threat that could cause failure of the roadway? Similarly, at the threshold of overtopping, what are the answers to these same types of questions?

Once the thresholds of concern are identified, then the possibility of such events occurring are evaluated. In the example, if it was determined that threshold of concern is overtopping, under what possible scenarios could a discharge of greater than 2,900 cfs occur? For this culvert, a 2,900 cfs discharge would be a very large increase over the existing design discharge suggesting that the vulnerability of this culvert to climate change may be low.

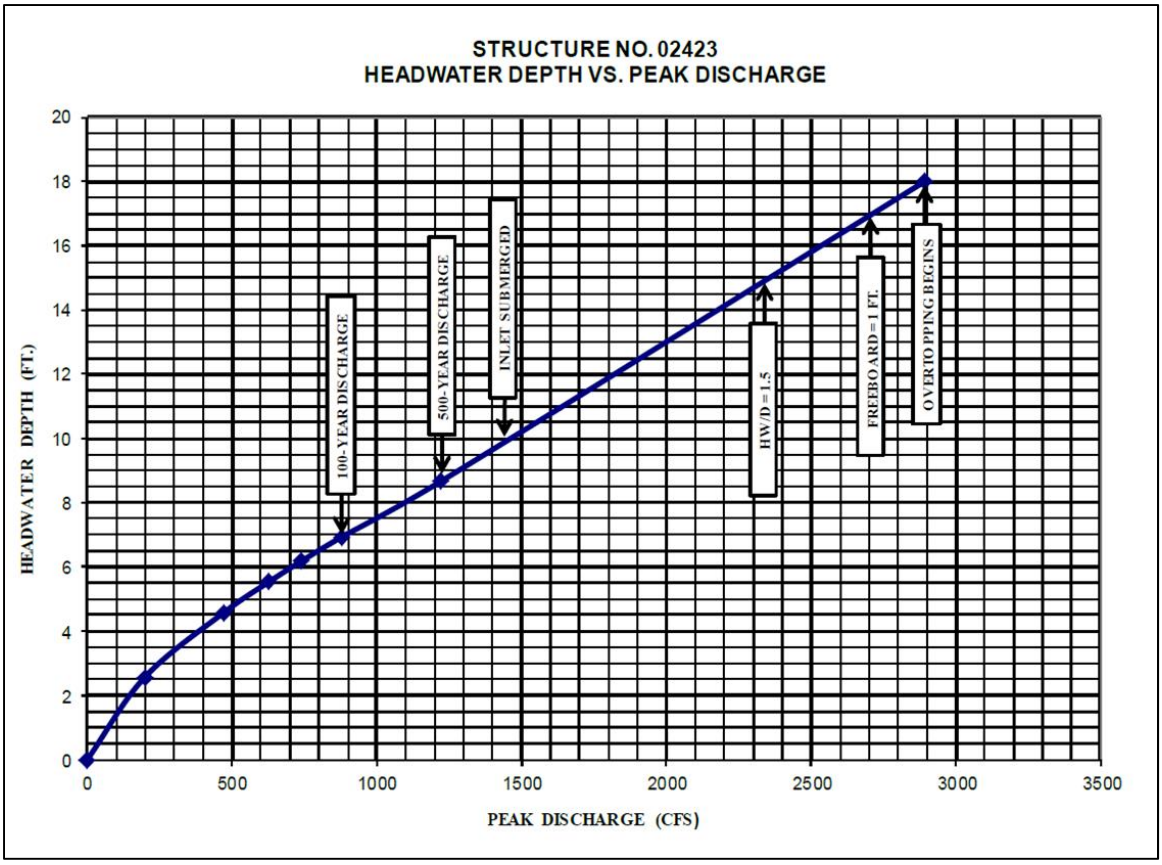

Figure 3.3. Relationship between headwater and discharge for structure 02423 (Connecticut Department of Transportation 2014).

The threshold decision-making approach can be extended beyond the assessment of a particular structure to a larger system or collection of structures. In the pilot study, CTDOT evaluated numerous culverts in the state to identify those that were the most vulnerable. In this way, resources available to address vulnerabilities could be prioritized to those locations with the greatest threats. Referring to Figure 3.2, CTDOT approached their pilot study with the threshold approach because they were interested in assessing vulnerabilities, it was within a planning context to evaluate their resource allocation, and they were evaluating existing structures. Each of these point toward the threshold decision-making framework. Their study did not address responses to identified vulnerabilities, which leads to the questions about whether corrective action would require an "all or nothing" type replacement or if there are incremental changes available to address vulnerabilities.

The tools provided in this report can be used to support either traditional or threshold decision making. As this example demonstrates, traditional and threshold decision-making frameworks

should not be considered mutually exclusive. They can be blended so that the advantages of each are brought to the decision-making and design processes.

Chapter 4. Climate Modeling Outputs for Hydrologic Design

Historical weather records typically form the basis for quantifying the risk of weather-related effects on the design, maintenance, and longevity of transportation infrastructure. Implicit to these calculations is the assumption that these risks are not changing over time, so historical records can be used to accurately assess future risk. As climate changes, however, historical return periods may no longer describe conditions over the lifetime of some structures. Even if a trend is not yet statistically significant in the historical data, future flood risks may still change. In a changing climate, assessing climate projections and, if they show the possibility of change, integrating them into the design is essential to ensuring a structure will remain resilient throughout its lifetime.

Climate projections are based on a range of plausible future scenarios that might result from human choices. These scenarios quantify how the human influence on climate could evolve in the future if, for example, we continued to depend on fossil fuels, or if we are able to transition -- slowly or quickly -- to zero-carbon sources of energy. Scenarios are then input to global climate models (GCMs), which simulate the physical processes of the climate system to calculate resulting changes in the Earth's climate system. GCM outputs can be used to quantify regional changes in temperature, precipitation, humidity, winds, and other relevant variables at horizontal resolutions currently ranging from 25 to 300 km (30 to 200 miles) per side, which is much coarser than gauge data or other sources used by engineers. Furthermore, analysis of sub-daily GCM output is very recent and its suitability for use in engineering applications has not been determined.

As GCM outputs are much coarser than gauge data or other sources used by engineers, GCM outputs are typically *downscaled* (a procedure that can include spatial disaggregation or higher-resolution deterministic physics process models or both) to higher spatial and/or temporal resolutions and *adjusted for systematic error* (e.g., bias corrected) before being used in quantitative analyses at the local to regional scale. To ensure a robust design, engineering analyses must use multiple GCMs and – for projects with timelines greater than 20 to 30 years, the time horizon over which projected changes under the different scenarios begin to diverge – an envelope of multiple scenarios.

A very accessible summary of the scientific understanding of past and future climate is available from the Third US National Climate Assessment (NCA3) Appendix 3: Climate Science Supplement (Walsh et al. 2014b), and Appendix 4: Climate Science Frequently Asked Questions (Walsh et al. 2014c). More information on the scenarios and models used to develop future projections is provided by the Fourth US National Climate Assessment (NCA4) Volume 1, Chapter 4: Models, Scenarios, and Future Projections (Hayhoe et al. 2017).

The purpose of this chapter is to evaluate the limitations and potential application of climate model outputs for hydrologic design. GCMs, scenarios, and downscaling methods are constantly being evaluated, tested, and improved, but GCM intercomparison and evaluation projects are primarily designed by scientists to increase scientific understanding of Earth system processes, rather than to support the applications community. Because climate modeler objectives are not always directly aligned with the needs of engineers, it is important to assess the available climate science information that is relevant and appropriate for hydrologic analyses and the design needs

of the transportation infrastructure. To that end, Section 4.1 provides an overview of the terminology used in climate projections that is relevant to hydrologic applications. Section 4.2 discusses the relevance of downscaled climate model output to hydrologic analyses for transportation infrastructure design. Section 4.3 addresses the selection and use of global climate models and scenarios. Finally, Section 4.4 provides guidance on how future high-resolution climate projections should be considered in engineering analyses.

4.1. Terminology

Although both the climate science and engineering communities use the word 'extreme,' there are important differences in analytical context, technical definitions, and quantitative methods. This section describes the distinctions between concepts of extreme in the two communities, including a list of relevant terms and their definitions. A *Glossary* provides definitions for terms that are relevant to engineering design and climate science.

4.1.1 Climate Extremes in Climate Science

The Intergovernmental Panel on Climate Change (IPCC) defines an extreme event as "the occurrence of a value of a weather or climate variable above (or below) a threshold value near the upper (or lower) ends of the range of observed values of the variable" (IPCC 2012a). Extremes are commonly defined in terms of thresholds, percentiles, or return periods relative to a historical period of 30 years or longer. (A climatological standard normal is defined as a consecutive 30-year period of observations.) Climate extremes include, but are not limited to, heat waves, cold waves, heavy precipitation, drought, flood, and storms. Yet even these definitions can be highly subjective; the quantitative definition of *rare* can differ by event and by location, and the societal impact can vary even more, depending on the intersection of the event with evolving landscapes and demographic characteristics. For that reason, the most detailed report on climate extremes, the IPCC Special Report on Managing the Risks of Extreme Events and Disasters to Advance Climate Change Adaptation (IPCC 2012b) concludes that "there is no precise definition of an extreme" (Seneviratne et al. 2012); rather, extremes tend to be location and application specific.

One way to identify extremes is to combine historical weather records with corresponding socioeconomic damages or costs to identify impactful events such as precipitation deficits that have historically led to widespread crop losses or heavy precipitation events that have resulted in significant flooding and damages. Such comparisons enable scientists to develop regionally and sectorally relevant metrics of extremes, from the drought of record used in state planning, to the maximum annual daily precipitation metric used in NCA4 (Easterling et al. 2017).

As the IPCC states, "because climates are so diverse across different parts of the world, it is difficult to provide a single definition of extreme or heavy precipitation. In general, two different approaches have been used: (1) relative thresholds such as percentiles (typically the 95th percentile) and return values; and (2) absolute thresholds [e.g., 50.8 mm (2 inches) per day of rain in the United States, and 100 mm per day of rain in China]" (Seneviratne et al. 2012).

Table 4.1 provides examples of extreme precipitation indices that have been used in IPCC reports, National Climate Assessments, and the climate science literature. It is important to note that these indices all represent precipitation extremes occurring over timescales of 24 hours or

longer. The majority of GCM outputs are archived at the daily scale, and the generation and evaluation of reliable sub-daily outputs is still in its infancy.

Table 4.1. Examples of extreme precipitation indices used in climate science literature and assessments.

Indicator Name (ID)	Indicator Definition	Units
Max 1-day, 5-day, 7-day, 14-day precipitation amount[1,2,3,4,7]	Monthly, seasonal, or annual maximum cumulative precipitation falling in a given number of consecutive days or weeks	mm or in
Frequency of exceedance (10 mm, 50 mm, 100 mm)[6]	Average number of days per year with cumulative precipitation exceeding a given threshold	number of days
10-, 20-, or 50-year return interval amount from annual or seasonal maximum of 1- or 2-day precipitation[1,3,4,5,6,7]	General extreme value distribution fit to annual maximum of cumulative precipitation for a given number of days (e.g., 1 day, 2 days, 1 week)	mm or in
Amount of precipitation falling in the 90th, 95th or 99th percentile of all non-zero precipitation days[5,6,7]	Empirical distribution	mm or in

1. Kharin et al. 2005, 2013; 2. Zhang et al. 2007, 2013; 3. Wuebbles et al. 2014; 4. Walsh et al. 2014; 5. USGCRP 2017; 6. IPCC 2012b; 7. Easterling et al. 2017.

4.1.2 Climate Extremes in Engineering

H&H engineers commonly define an extreme as an exceedance threshold within the tail of a probability distribution for hydrological measurements (e.g., American Association of State Highway Officials (AASHTO) Highway Drainage Guidelines (HDG) and the Federal Highway Administration Hydraulic Design Series No. 2 (McCuen et al. 2002). A precipitation extreme is expressed as either the percent chance of annual occurrence (i.e., 1-percent annual exceedance probability [AEP]) or as the average period between occurrences (i.e., 100-year flood), and it is estimated from a hypothetical probability distribution fit to the observations under the assumption of stationary distribution parameters.

For a given engineering project, the relevant threshold is specific to a structure in a given place. It informs cost-benefit analysis that includes construction and maintenance cost, as well as human safety consequences when exceedance occurs. In H&H engineering planning and design, commonly-used thresholds are 25-, 50-, 100-, and 500-year return periods and 4-percent, 2-percent, 1-percent, and 0.2-percent AEPs, respectively. The threshold value is estimated using extreme value statistics applied to the entire period of measurement record, so it is possible the threshold is not exceeded in the measurement record that may span as few as 10 years (e.g., from a specialized urban rain gauge network) to more than 100 years (e.g., a stream gauge network established by the United States Geological Society). Examples of extreme indices used in engineering for design of hydraulic structures are provided in Table 4.2.

Table 4.2. Examples of extreme precipitation and hydrological indices used for engineered structures; actual definitions are project-specific.

Structure	Indicator Name	Indicator Definition	Units
Bridge	100-yr peak streamflow	Log Pearson Type III fit to logarithm of annual instantaneous peak flow	$ft^3\ s^{-1}$
Culvert	25-yr 24-hour design rainfall intensity	Intensity-Duration-Frequency curve or rainfall atlases; instantaneous peak flow	inch hr^{-1} $ft^3\ s^{-1}$
Storm Drains	10-yr x-hour design rainfall intensity (x is less than 24 hours	Intensity-Duration-Frequency curve or rainfall atlases	inch hr^{-1}

4.1.3 Comparing Extremes in Climate Science and Hydrologic Engineering

How do the indicators listed in Table 4.1 and Table 4.2 compare? A comprehensive comparison does not yet exist in the peer-reviewed literature, but the most obvious differences can still be seen by comparing the illustrative examples in these tables.

First, though some of the indicators overlap, the majority of extreme indices used in hydrologic engineering, while similar in definition, tend to be rarer than those commonly used in climate science. Table 4.1 primarily contains daily maxima and 20-year intervals or shorter, for example, while Table 4.2 contains sub-daily maxima or daily maxima with 25-year intervals or longer. Though climate science and hydrologic engineering definitions overlap on 25- to 50-year return intervals of daily precipitation, Table 4.1 shows that the number of climate analyses that have calculated 50-year return interval metrics are so limited that this information is best used to indicate the directionality of the trend rather than quantifying the magnitude of the trend.

Second, as climate science typically uses "less extreme" extremes, it can rely on shorter observational time periods. Its metrics are nearly always empirical, derived directly from the data. In contrast, engineering applications typically not only use the entire period of record, but also fit theoretical distributions to the record, to estimate events that may be more extreme than those observed in the historic record.

Third, the two fields can also differ on temporal and spatial resolutions and aggregations. Engineering typically relies on gauge measurements and observations, while climate studies can use gauge measurements that are either station-based or interpolated onto regular grids, reanalysis (gridded output from historical data assimilation using weather models), historical model simulations, and future projections.

A fourth important difference is that the climate products traditionally used by engineers include rainfall depth and intensity values for a comprehensive range of return periods (2-, 5-, 10-, 25-, 50- and 100-year) and durations that are generated in a consistent manner. In contrast, climate science assessments (e.g., NCA3, NCA4) typically calculate precipitation indices for a limited and more illustrative subset of periods and durations in any given analyses. These and other key differences between climate science and H&H engineering, in terms of how each characterizes extremes, are summarized in Table 4.3.

However, there are also important similarities in how both fields define extremes. Both climate science and H&H engineering require a minimum number of years to define the statistics of climate at a given location. Both use measurements or observations from weather stations and stream gauges. And both climate scientists and H&H engineers consider similar and often identical variables: precipitation, including both rain and snow; streamflow; temperature; etc. While precipitation is the most frequently mentioned hydrological metric in both historical climate analyses and future projections, most global models explicitly model runoff as part of their land surface module and some models (particularly high-resolution regional models) explicitly model streamflow routing processes as well. In addition, climate scientists with relevant research interests often work with streamflow observations, projections, and output from hydrological models.

Table 4.3. Comparing the definition and calculation of "extremes" in climate science and engineering.

Variable	Climate Science	Engineering
Data Series Length	Minimum 20 to 30 years; can use entire period of record or occasionally a theoretical distribution fit to the record	Minimum 10 years; typically requires entire measurement record to fit distributional parameters
Data Source	Observations, reanalysis, historical model simulations, future model projections	Observations and synthesis of observations
Variables	Precipitation (rain, snow), temperature, streamflow	Precipitation (rain, snow), temperature, streamflow
Temporal Resolution	Monthly, daily, 3-hourly[1]	Daily, hourly, 15-minute, 5-minute, continuous
Spatial Resolution	Point values; averages over regular grids ranging 4 km^2 to 150 km^2	Point values; scaling relationships for larger scales (e.g., areal reduction factors)
Analytical Basis	Primarily empirical, with some theoretical distributions	Primarily theoretical distributions
Thresholds	90th to 99th percentile of empirical distribution	10% to 0.2% annual exceedance probability of theoretical distribution

[1]Climate scientists currently assign low confidence to simulations of sub-daily precipitation, but this is an area of active research that is expected to evolve in the future.

4.1.4 Detecting and Projecting Changes in Extremes

A changing climate – which can affect both mean and extreme conditions in a given location – is the motivation for incorporating climate projections into engineering design. However, one confusing consequence of the two fields using different definitions and indices for extremes is that a statistically significant change may be detected in the "not-as-extreme" indices used in climate science, but not the "more extreme" indices used in H&H engineering – or vice versa (see Table 4.3). Similarly, a change might be detected in one type of index, such as extreme precipitation, but not in a different type of index, such as flood risk.

With respect to extreme precipitation and flood risk, for example, NCA4 states that "detectable changes in some classes of flood frequency have occurred in parts of the United States and are a mix of increases and decreases. Extreme precipitation, one of the controlling factors in flood statistics, is observed to have generally increased and is projected to continue to do so across the United States in a warming atmosphere. However, formal attribution approaches have not established "a significant connection of increased riverine flooding to human-induced climate change and the timing of any emergence of a future detectable anthropogenic change in flooding is unclear" (Wehner et al. 2017).

For a given type of extreme in a given region, this can lead to a situation where analysis of observed trends or climate projections for relevant variable(s) such as precipitation statistics may suggest changes relevant to engineering design even though engineers may not see evidence of changes in historical streamflow statistics. This may create the perception of conflicting information regarding the relevance of accounting for a changing climate in a given H&H application, despite the fact that there are explanations for this apparent inconsistency.

The first explanation is that observed and projected changes in extreme precipitation may not be occurring at the same rate in every location throughout a given region. Extreme precipitation at daily and sub-daily time scales in some regions, particularly away from mountainous areas, can be a spatially isolated phenomenon resulting from local weather conditions such as thunderstorms and other small-scale convective activity that can in turn be influenced by local topography, land use and cover, and even small-scale activities such as irrigation. In addition, the response of heavy downpours to climate trends can only be reliably detected over time scales of decades rather than years. This means trends in rainfall extremes may not be spatially coherent (Pryor et al. 2009), and it is possible for a climatological analysis of regional observations to show a statistically significant change for a majority of gauge locations within that region, while at the same time the analysis for a single study site within the region might find that trends in rainfall extremes are not statistically significant at that location.

Second, a statistically significant increase in extreme precipitation does not necessarily imply a corresponding increase in riverine flooding because there are multiple factors that influence flooding. In addition to precipitation extremes, these include land use, topography, and even flood control, all of which may act to mitigate or amplify flood risk. For example, landscape processes that transform precipitation into streamflow do not necessarily dictate that rare precipitation will result in rare streamflow or that rare streamflow results only from rare precipitation. For runoff extremes, the consequence of precipitation that immediately precedes the event can be significantly moderated by more localized conditions such as soil moisture, snowpack, and the spatiotemporal characteristics of rainfall systems that affect the relationship between a rainfall event and the subsequent runoff.

Third, linear mapping between precipitation and streamflow extremes may be reasonable for small, impervious basins. But for large basins with internal storage, there is a potential disconnect between precipitation and flood. This disconnect is illustrated by the 2008 June flood in eastern Iowa, in which a period of record flood that was five times the average annual peak flow was caused by a sequence of rainfall systems that were not equally rare (Krajewski and Mantilla 2008). This is just one of many case studies that demonstrate how basin size and slope characteristics, soil moisture, and the spatiotemporal sequence of spatially correlated rainfall systems can lead to a disconnect between the rarity of the rainfall versus the streamflow.

Finally, a change in flood risk may occur in the future even if a statistically significant change for a specific flood risk at a given location is not yet evident in the historical data. This possibility underscores the need for engineers to incorporate climate projections into the planning and design for a given structure, as the evidence for anticipated change in heavy precipitation and/or flood risk may come from: 1) historical data, 2) climate projections, or 3) both.

4.2. Suitability of Climate Model Outputs

The section discusses the relevance of downscaled climate model output to hydrologic analyses for transportation infrastructure design.

4.2.1 Objectives

The first objective of this section is to describe criteria for evaluating the relevance and suitability of climate information for the types of hydrologic analyses required for transportation infrastructure design. Assessment criteria include the information on past and future trends available in the literature; scientific confidence in model ability to generally simulate relevant variable(s) over the region(s) of interest; the ability of climate models to accurately reproduce the specific types of statistical distributions and extremes (e.g., 100-year precipitation event); and the accessibility, availability, and relevance of data and model outputs to hydrologic engineers. This section describes appropriate sources of climate information for engineering analysis of varying complexity, spatial resolution (e.g., large compared to small watersheds), and analysis approaches. It also discusses the limitations of existing data in providing the information required for these various types of analyses.

The second objective of this section is to provide background for design guidance that assists in the selection and integration of appropriate dataset(s) of projected changes in precipitation, temperature, and other relevant climate variables into engineering design. This background information:

- Provides recommendations consistent with tiered levels of analysis (Chapter 3) to weigh project risks and costs in selecting tools and methods for evaluating climate change.
- Focuses on currently available information and data, as well as discussing ways to incorporate future datasets so as to remain robust over time.
- Highlights the conditions under which climate projections should not be extrapolated beyond their confidence levels, which could result in misleading design guidance.

4.2.2 Overview

In assessing potential future climate effects, the first step is to understand the overall performance of the infrastructure component or system under a range of plausible environmental conditions, from present to future, over the lifetime of the structure. The second step is to identify and apply appropriate climate information, with the goal of reasonably bounding future conditions and hence accounting for future vulnerabilities.

Some states and cities have already developed specific guidance for the use of climate projections in transportation engineering. For those that have not, selection of appropriate

datasets, methods, and models can be a daunting task. It is complicated by the sheer volume of observations and climate model simulations available, as well as by the fact that climate projections are subject to important uncertainties (described further in Section 4.3) arising from natural variability within the climate system, scientific or model uncertainty, and future human activities and emissions. The most important implication of these uncertainties is that the reliance on a single future climate simulation is more likely than not to result in either over-spending or under-spending on a project, as discussed in Section 4.2.4. To avoid these errors, multiple future simulations should be used.

In addition, climate model development and preparation of simulations is an expensive and time-consuming process. It is generally undertaken at national research laboratories supported by federal governments, where the focus is on basic research to expand scientific understanding of the Earth's climate system, rather than generating inputs specifically for H&H transportation engineering design. This mismatch between the primary motivation for conducting climate model simulations and their applicability to hydrologic engineering is apparent in at least three important ways: in the spatial resolution, the temporal resolution, and the statistical resolution of the tails of the climate model projections.

Hydrologic engineering design covers a range of temporal and spatial scales, including runoff from small watersheds that depend on rainfall that occurs over periods from sub-daily to multi-day, often focusing on extremely rare events. Climate projections, whether output from global climate models or downscaled with empirical-statistical or regional climate models, are used to study weather and climate processes and analyses of extremes tend to focus on weather events that have societal impact but, as discussed in Section 4.1, may not necessarily be extremely rare events of concern to engineers.

Unless engineers are aware of the characteristics and limitations of climate model output, there is a risk that climate projections could be selected and/or applied in inappropriate ways. For example, the spatial scale of gridded output from regional climate models available to engineers from public archives is 25 km per side. (Individual scientists, including the authors, have produced regional climate model output with finer resolution, but the many individual experiments of this type have not been compiled into a public archive.) If this relatively coarse information were used in the analysis of a small watershed or a culvert design, the gridded projections will underestimate extreme precipitation events as the precipitation from a localized, heavy storm event will be distributed over the entire grid cell. This could have important consequences for the hydrologic design, leading planners to underestimate the heaviest of events.

In addition, climate projections are not hindcasts. While the variability in climate model output over 20 to 30 years are intended to be similar to that of the real world, the day-to-day values are not. Therefore, evaluating climate models based on their ability to, for example, reproduce record-breaking rain that occurred in the observational record at a given time such as April 2008 would actually tell the user nothing at all about the performance of one climate model relative to another. Whether there is a record-breaking rain in 2008 or 2018 is primarily a function of natural, chaotic variability rather than specific model ability to reproduce observed conditions.

BOTTOM LINE: Climate model simulations are not designed specifically for use in H&H engineering applications, but they can be used in these applications if the engineer is aware of how to apply and interpret them appropriately.

4.2.3 Actionable Climate Projections for No-Regrets Hydrological Analyses

Actionable climate information, data, and projections are defined those that are suitable inputs to hydrologic design procedures. Climate information, including both historical trends and future projections, can be used to inform design procedures and help the engineer reach one of three conclusions: 1) that the variability in relevant climate indicator(s) is too great to identify any statistically significant trends and enable risk assessment at that location; 2) that projected climate trends do not materially alter the risk for that structure at that location; or 3) that projected climate trends do materially alter the risk. If the first or second conclusions are reached, no further climate information is necessary. If the last conclusion is reached, then climate projections do need to be incorporated into robust future planning.

To be used in the design process, climate information, data, and projections should ideally be:

- Generated by procedures deemed reasonable, reliable, and defensible by the climate science community.
- Consistent with or able to be transformed by acceptable tools or methods into the temporal and spatial scale of historical data already used in design procedures.
- Able to reproduce key features of natural variability and long-term trends over the region and for the variable(s) of interest.
- Representative of the range of scientific uncertainty in reproducing the response of the climate system to human forcing.
- For analyses with time horizons longer than 30 years, able to adequately capture future uncertainty due to human scenarios and, given a scenario, provide a reasonable sample of the population of rainfall and temperature events in the scenario.
- Be accessible and available appropriate for use by hydrologic design engineers.

Actionable climate projections should also be sufficient to enable engineers to expand on their initial conclusion to determine whether the risk mitigated by the team's engineering design is likely to be significantly or notably altered under future climate conditions compared to historical data, or whether evaluation of future risk mitigation is not possible because of the large uncertainty in the direction and/or magnitude of trend in risk from climate projections for that given location and/or variable. They should also be sufficient to avoid two types of regrets as summarized in Figure 4.1: 1) Type I, the cost of over-investment when an increase in floods from climate change is predicted, but does not occur, or 2) Type II, the loss from under-preparing when an increase in floods is not predicted, but does occur.

Floods in this framework refer to the annual maximum streamflow values and the trend is a linear trend in the annual maximum streamflow values over a period of interest. The trend could be diagnosed from either historical data or projected data or a combination of both. The null hypothesis, H_O, is that there is no statistically significant linear trend in the annual maximums. The alternative hypothesis, H_A, is that there is a statistically significant linear trend. The probability of rejecting H_O when it is true is α. The probability of not rejecting H_O (i.e., accepting H_A) when it is false is β. The choice for α is project dependent and depends on the acceptable level of risk for the project.

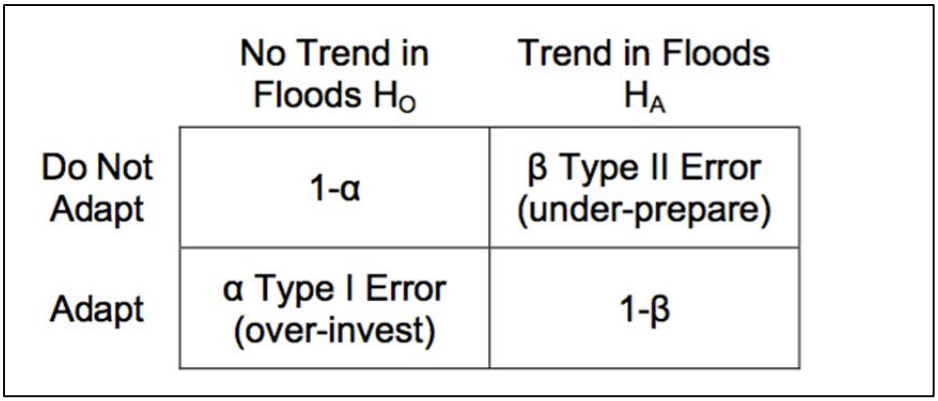

Figure 4.1. Decision matrix and definitions of Type I and Type II errors for regrets analysis (from Rosner et al. 2014).

The matrix in Figure 4.1 illustrates several of the requirements for actionable information listed above. For most projects with service lifetimes exceeding 30 years, the projections should contain a range of future scenarios to reduce the possibility of either type of regret. Projections based solely on one or more lower scenarios run the risk of Type II regrets, underpreparing if change is greater than projected, while projections based solely on a higher scenario run the risk of Type I regrets, over-preparation.

Even if a hypothetically perfect scenario were able to predict precisely the path of future emissions from human activities and their resulting effects on climate (see Section 4.2.6.1 for further discussion of scenario uncertainty), the likelihood of either a Type I or a Type II regret will still be greater than zero. This results from the inherent internal variability of the climate system, which is chaotic, and the fact that extremely rare rainfall events tend to occur in isolation. Realistic weather variability provides accurate assessment of *likelihood* of temporary and isolated events, but it is still a likelihood rather than a certainty. For a given future scenario or pathway, a climate model with realistic weather variability is able to provide reasonable probabilities for extreme rainfall conditioned upon the scenario. This enables quantification for Type I and II errors in regrets analysis.

Realistic weather variability is foundational for gaining confidence in estimating the likelihood of either regret. Climate projections can be expected to realistically represent weather variability over periods of 20 to 30 years or longer. Too small a set of simulations may provide an incomplete representation of uncertainty from natural weather variability and/or scientific modeling. A larger number of simulations increases the "power" of the analysis and potentially allows changes to be detected when one is present. Specifically, the use of a large ensemble of simulations generally increases the skill, reliability, and consistency of model forecasts (Tebaldi and Knutti 2007), as well as increasing the sample size of the information from which conclusions can be drawn regarding possible changes in variability and extremes. In contrast, by relying on a small set of projections, one is at risk of placing weight on a projection that is unreliable, and might misjudge the likelihood of change in a design storm resulting in either over- or under-preparation. More information on the importance of large ensembles of simulations to capture changes in extremes, as well as guidance regarding how to select a suitable subset of climate models and scenarios to generate those simulations, is given in Section 4.3.3.3.

Regrets analysis can also inform how much time and effort should be invested in developing appropriate climate projections. For example, for structures with lifetime of 30 years or less, a structure insensitive to under-preparing (Type II error) or highly sensitive to over-investing (Type I error) would have little reason to include additional funding for climate projections unless the projected change was for a very sizeable directional change. Such a change would be evident from only a small set of climate projections, or even from a cursory review of pre-existing information on observed and projected changes, such as would be available in a regional or national assessment (e.g., Mellilo et al. 2014). On the other hand, for a structure insensitive to over-preparing (Type I error), an engineer may be highly motivated to seek additional funding for climate information even if the directionality of change were inconclusive, and this directionality can also be obtained from pre-existing assessments and reports. Finally, a structure highly sensitive to under-preparing (Type II error) would require the most precise assessment of change; this would require a substantial investment in relevant, quantitative projections. More information on selection of climate models and projections to include based on the needs and characteristics of a given analysis is provided in Section 4.3.

BOTTOM LINE: The type of climate information required for a given analysis can also be informed by regrets analysis, weighing the relative costs of over- versus under-preparing.

4.2.4 Observations

Observations provide the basis for defining historical climatological normals, quantifying historical trends, and building products derived from observations, such as the National Oceanic and Atmospheric Administration (NOAA) Atlas 14. These activities rely on at least three types of observations or products: 1) point-based measurements, 2) gridded observational data, and 3) reanalysis data.

The first type of observations is the traditional **station, gauge, radiosonde (balloon), or other type of point-based observations**, such as the Global Historical Climatology Network (GHCN) (Menne et al. 2012). Daily station, gauge, radiosonde, and other point-based measurements are widely available, but in their raw form are generally considered to be less reliable than their aggregates at monthly and longer periods. Once a vigorous quality-check has been done, as is common for most datasets, point-based measurements are the most accurate product for describing historical weather and climate, particularly in a specific location. As spatial or temporal smoothing is performed, these types of datasets provide the most accurate values of actual conditions experienced during extreme rainfall events, without altering the output. The density of these observations is typically high over well-populated areas, but sparse over less densely populated regions. Examples of locations with sparse point-based data range can include individual locations, such as Big Bend National Park in southwest Texas; large parts of states or entire regions, such as Alaska, the Rocky Mountains, and northern Canada; and many developing countries.

The National Centers for Environmental Information (NCEI) formerly known as the National Climatic Data Center (NCDC) provides public access to multiple collections of surface-based station data for a broad range of variables and of varying levels of quality and spatial and temporal coverage. A comprehensive list of the collections of surface-based station data available for the United States and globally are summarized on NCEI's Land-Based Datasets and

Products page, available online at: http://www.ncdc.noaa.gov/data-access/land-based-station-data/land-based-datasets/. Local Climatological Data (LCD) summarizes hourly, daily, and monthly data from automated observing systems at 1,600 locations in the United States as well as from a limited sub-set of weather stations, typically located at airports. Daily data from the Cooperative Observer Network (CON) are collected by more than 10,000 volunteer observers across the United States. The US Historical Climatology Network (USHCN) is a subset of monthly data from the CON that has been quality-controlled. And finally, the GHCN is the most comprehensive and carefully quality-controlled station-based dataset in the world. It provides daily and monthly station observations from around the world and is the gold standard for long-term daily temperature and precipitation observations.

In addition to NCEI resources, hourly and five-minute observations from mesonet stations are available from individual networks, such as the West Texas Mesonet, some of which have been collated and incorporated into NCEI's US Climate Reference Network (USCRN). These observations are unique in that they characterize historical sub-daily variability for the locations for which they are available, and in the future may contribute to efforts to generate sub-daily projections.

The second type of dataset is **gridded observations** (e.g., Livneh et al. 2013). Gridded observational datasets are typically the result of a spatial interpolation of point-based observations. As satellite records become long enough to provide climatological data, however, they are increasingly being incorporated into gridded datasets as well, such as the Global Precipitation Climatology Projection (GPCP) (Adler et al. 2003). They provide consistent coverage of larger areas for which point-based observations may not be representative; however, they also run the risk of underestimating extremes due to the fact that observations are typically averaged over the spatial and temporal scale of the dataset. Some datasets, such as the 1/16th degree assimilated daily temperature and precipitation dataset developed by Livneh et al. (2013), the PRISM dataset, and others listed in Table 4.4, are derived from point-based observations alone. Others, such as the GPCP, combine data from rain gauge stations, radiosondes, and satellites to provide gridded global monthly rainfall estimates from 1979 to present.

Gridded datasets are often used in regional trend analyses, for regional analyses requiring geographic coverage, and for training empirical statistical downscaling methods and models (ESDMs), as the spatial correlation of aggregate data is more stable than daily point-based data. When daily data are missing, however, the lack of spatial correlation means measurement error can be large because neighboring stations may not be useful for estimating measurements at the missing location. For gridded observations, individual values within the dataset are the average value for the area within a grid cell. For example, for a gridded dataset at 1/8th degree (~12 km) resolution, the precipitation value for a particular day within one grid cell is the average precipitation amount for a 144 km^2 area. In mountainous regions, extreme precipitation events occur in winter and areal coverage much larger than 144 km^2; in other regions, the events are usually associated with summer thunderstorms, which generally occur at much smaller areal coverage than 144 km^2. This means that the most extreme precipitation events are smoothed out and hence down-weighted in gridded datasets. Higher resolution datasets have less smoothing per grid cell, but more spatial interpolation is required to generate values where point-based observations are sparse.

Table 4.4. Archives of historical observations.

Dataset[1]	Temporal Resolution	Spatial Resolution	Availability
GHCN	Daily, hourly, 15-minute	Point-based weather stations	Public data archives
Maurer, Livneh, PRISM, Daymet, NOAA CPC	Daily, hourly	30 arcsec to 1/4th degree	Public data archives
NCEP NARR	3-hourly, daily, monthly	25 km	Authorization required
NEXRAD	5-minute	Point-based radar installations	Amazon Web Services

[1]GHCN: Global Historical Climatology Network; Maurer: Maurer gridded meteorological data, Livneh: Livneh daily near-surface gridded meteorological dataset, PRISM: Parameter-elevation Regressions on Independent Slopes Model, Daymet: Daily surface weather and climatological summaries, NOAA CPC: National Oceanic and Atmospheric Administration Climate Prediction Center gridded precipitation, NARR: National Center for Environmental Prediction North American Regional Reanalysis, NEXRAD: Next Generation Weather Radar Level II historical analysis.

The third type of datasets consists of **reanalysis** (www.reanalyses.org). Reanalysis is a composite product resulting from assimilation of observations into a weather model to produce gridded fields consistent with available observations for each day. Reanalysis provides gridded data at both daily and sub-daily (3-, 6-hour) resolution for a broad range of surface and atmospheric variables, similar to those generated by GCMs and regional climate models (RCMs). Reanalysis output is not a dataset of "observations," but rather a form of quasi-observations. It is the result weather model simulations run retrospectively, regularly updated to incorporate available observations from stations, gauges, radiosondes, and even satellites at regular intervals, to produce gridded near-surface and vertical output fields consistent with observations over the period of record. In this sense, reanalysis is perhaps best understood as an intelligent form of spatial and temporal interpolation that relies primarily on physical modeling rather than statistics to "fill in the dots" between the observations of different spatial and temporal resolutions, as well as at different times of measurement.

There are multiple sets of reanalysis covering different geographic regions and time periods, with different spatial resolutions (reanalyses.org). For example, the North American Regional Reanalysis provides daily and sub-daily data from 1979 to 2008 at a spatial resolution of 25 km. NASA's global Modern-Era Retrospective Analysis for Research and Applications (MERRA) reanalysis incorporates satellite observations from 1980 to present at a 50-km resolution. Coarser-scale National Centers for Environmental Prediction (NCEP) and European Centre for Medium-Range Weather Forecasts (ECMWF) reanalysis provides daily and sub-daily data from 1948 to present on a 2.5-degree grid, while NOAA's Cooperative Institute for Research in Environmental Sciences (NOAA-CIRES) reanalysis goes from 1851 to 2012 at temporal resolutions of 6 hours and daily, and a 2-degree spatial resolution.

BOTTOM LINE: Observational datasets used in climate science analysis of historical normal and trends, and which form the basis for derived products such as NOAA Atlas 14, include point-based observations, gridded observations, and reanalysis. Point-based data provide the most realistic source for extreme precipitation, but typically require quality control to remove potentially erroneous points. Gridded data are more consistent, but may underestimate magnitude of extremes and their trends, particularly for larger grid sizes and in regions with sparse point-based inputs.

4.2.5 Climate Information: Trends and Projections

Existing products that document the direction and approximate magnitude of observed trends and future projections at the regional scale may provide insight for design and planning of transportation infrastructure including:

- Regularly-updated national and international assessments such as the NCA (www.usgcrp.gov) and the IPCC (www.ipcc.ch).
- Region- or city-specific assessments such as the Chicago Climate Action Plan (CCAP) (http://www.chicagoclimateaction.org/) or the California Climate Impact Assessments (CCIAs) (http://climatechange.ca.gov/climate_action_team/reports/climate_assessments.html).
- Federal, regional, state, and academic pre-packaged, web-based products that allow users to choose from and plot a variety of maps and/or time series for regions, states, and/or the entire United States.

The U.S. Global Change Research Program (USGCRP) is mandated to produce a comprehensive NCA every four years that documents global and regional trends across the United States, as well as detailed analyses of trends in indicators and impacts relevant to individual regions and sectors including hydrology, transportation, and infrastructure. NCA3 was published in 2013. Volume 1 of the Fourth NCA was published in November 2017.

Examples of the types of products and information available from these assessments are provided in Figure 4.2, Figure 4.3, and Figure 4.4. Figure 4.2 shows the regional 1948-2015 change in 20-year return value of seasonal daily precipitation totals (calculated directly from annual maximum series observations, not from a statistical fit to the data), and the observed change in several other metrics of heavy precipitation, including the 5-year maximum daily precipitation, the 99th percentile precipitation event, and the 5-year, 2-day heaviest rainfall events, from NCA4. Figure 4.3 shows observed trends in flood risk at individual gauge locations across the contiguous United States from NCA3. These regional changes are all calculated from GHCN station-based observations, aggregated to the regional scale. They show how observed trends vary in magnitude across the United States.

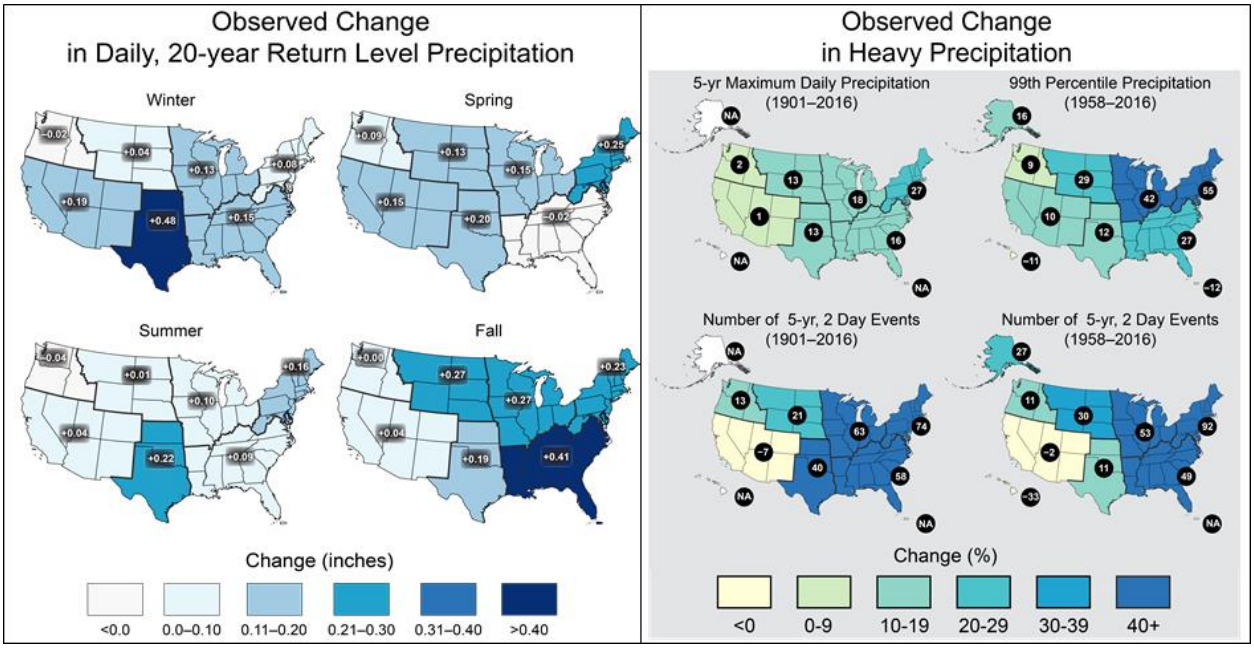

Figure 4.2. Observed changes (left) in the 20-year return value of seasonal daily precipitation totals over the period 1948 to 2015, calculated by determining the exceedance probability from historical climate observations from the GHCN dataset (Source: Easterling et al. 2017) and (right) four metrics of extreme precipitation where numerical value is the percent change over the entire period, either 1901-2016 or 1958-2016 (Source: Easterling et al. 2017)

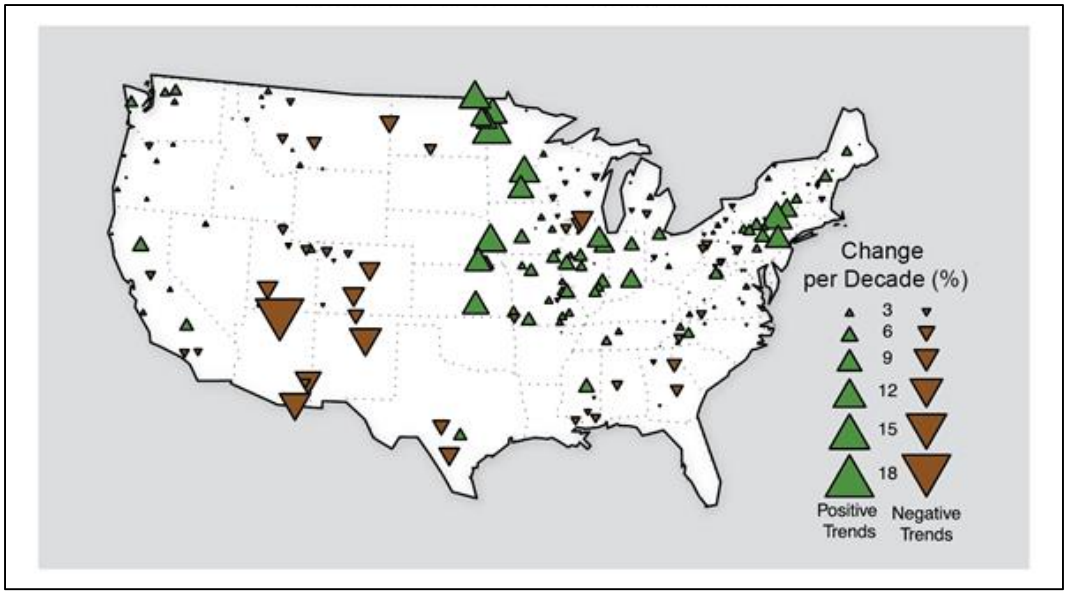

Figure 4.3. Trends in annual flood magnitude and direction from the 1920s through 2008 (Source: NCA3 Chapter 2). Most significant changes are located where consistency between precipitation and flood trends are evident: an increasing trend for floods in the Midwest and Northeast, and a decreasing trend in the Southwest.

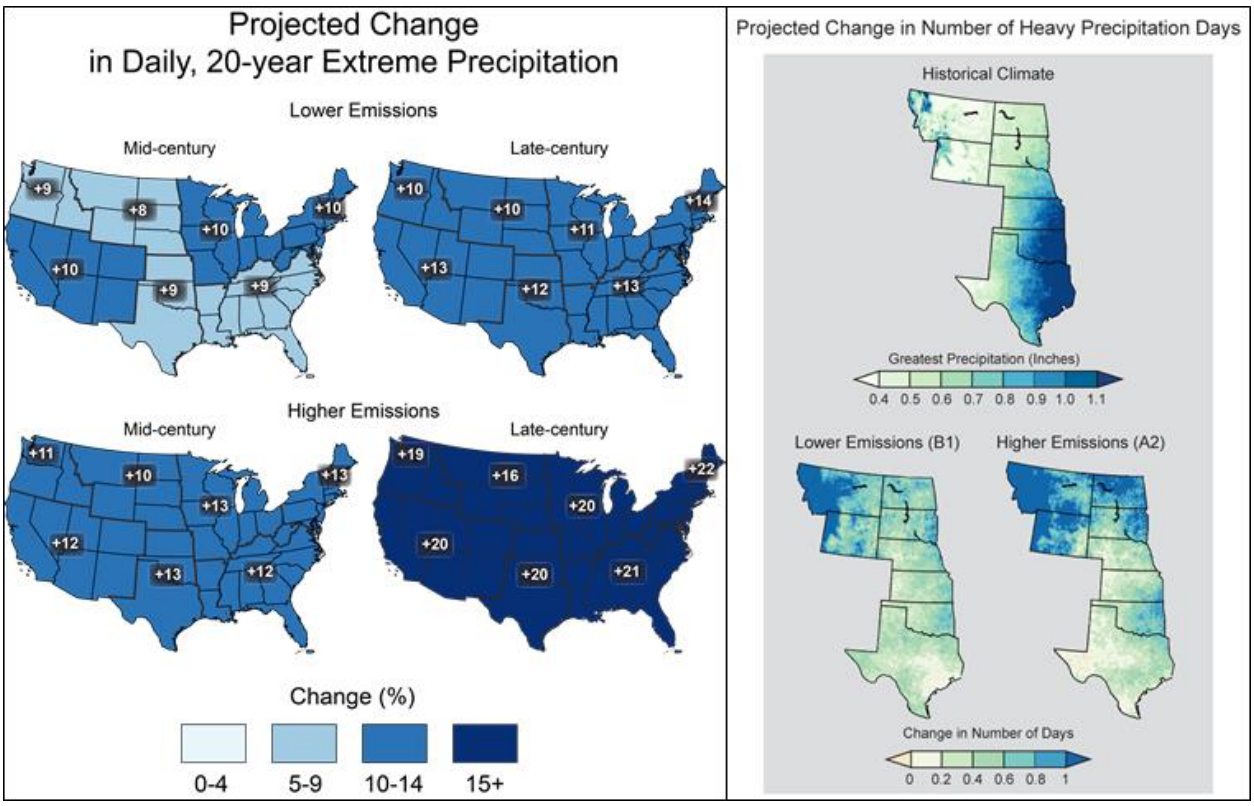

Figure 4.4. Projected change (left) in the 20-year return period amount for daily precipitation for mid- and late-21st century for a lower scenario (top, RCP4.5) and a higher scenario (bottom, RCP8.5) calculated from the LOCA downscaled dataset (Source: USGCRP 2017) and (right) the number of days exceeding the historical (1971-2000) 2-percent most extreme or heaviest daily 24h precipitation for the Great Plains region where by mid-century (2041-2070), the projected change in days exceeding those precipitation amounts remains greatest in the northern area (Source: NCA3 Chapter 19).

In terms of future projections, Figure 4.4 shows two examples of projected changes in extreme precipitation from NCA3 and NCA4. On the left is the projected change in the 20-year event for a lower future scenario (top) and a higher future scenario (bottom) for the middle (left) and late (right) 21st century from NCA4. (See Section 4.3 for more information on future scenarios). These figures were calculated using statistically downscaled output from the LOCA dataset (see Section 4.2.9), and values are averaged over all the GCMs in the Coupled Model Intercomparison Project phase 5 (CMIP5). On the right is the projected change in the 2-percent most extreme 24-hour precipitation events over the Great Plains region for a lower and a higher scenario from NCA3. These figures show how projected future trends vary across the United States and how these trends also depend on the metric used.

In terms of international assessments, the IPCC publishes a comprehensive Assessment Report every 5 to 10 years that documents primarily global trends, though with some regional differentiation. The assessment reports cover climate science and trends (Working Group 1), sectoral and regional impacts (Working Group 2), and technology, emissions, and mitigation (Working Group 3). The most recent is the Fifth Assessment Report (IPCC AR5), published in 2013. The sixth report is scheduled to be published after 2020.

The most recent IPCC AR5 concludes that "it is likely that since about 1950 the number of heavy precipitation events over land has increased … it is very likely that there have been trends towards heavier precipitation events in central North America." It also contains information on observed and projected changes in extreme precipitation, typically at the global scale. An example of the type of information available from IPCC reports is provided in Figure 4.5, which compares the change in the amount of precipitation associated with the 20-year daily event with the change in the 20-year return value. This figure shows the changes in the multi-model mean values projected to occur per 1°C increase in global mean temperature.

Many regions, states, and even cities have conducted their own one-time assessments. Depending on how recent these assessments are, they can be extremely useful in providing location-specific information. There are assessments for regions, such as the US Northeast Climate Impacts Assessment (Frumhoff et al. 2007); for individual states, such as the California Climate Change Assessments (http://resources.ca.gov/climate/safeguarding/research/); and for cities, such as the Chicago Climate Action Plan (http://www.chicagoclimateaction.org/) and the Washington DC Climate Projections and Scenarios Project (https://doee.dc.gov/publication/climate-projections-scenario-development). Many contain location-specific climate projections, and often contain analyses of extreme precipitation metrics relevant to that location. A typical product for extreme precipitation at the city level is shown in Figure 4.6**,** where the average number of days per year with more than two inches of rain for a given weather station are compared for five different climatological (30-year) time periods. Each bar represents the multi-model mean, while the "whiskers" on each bar illustrate the range spanned by all the climate models used.

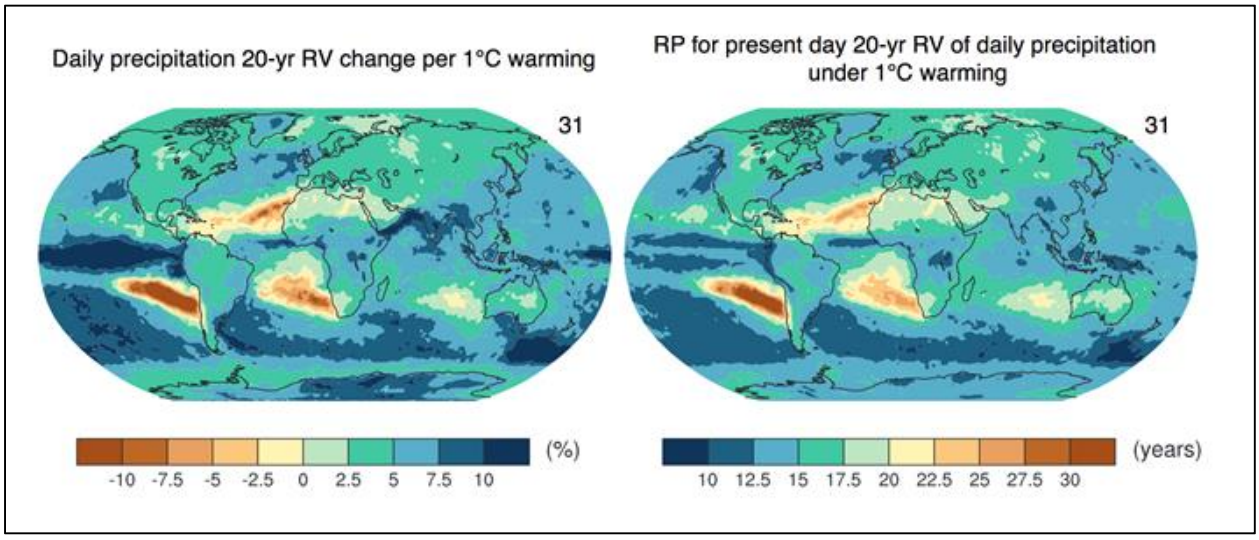

Figure 4.5. (Left) The CMIP5 2081–2100 multi-model ensemble median percent change in 20-year return values (RV) of annual maximum daily precipitation per 1°C of local warming relative to the 1986–2005 reference period. (Right) The average 2081–2100 CMIP5 multi-model ensemble median of the return periods (RP, years) of 1986–2005 20-year return values of annual maximum daily precipitation corresponding to 1°C of local warming. Regions of no change would have return periods of 20 years. Regions identified as most significant changes also are regions for which increase in rainfall extremes is projected to continue. (Source: IPCC AR5 WG1 Chapter 12).

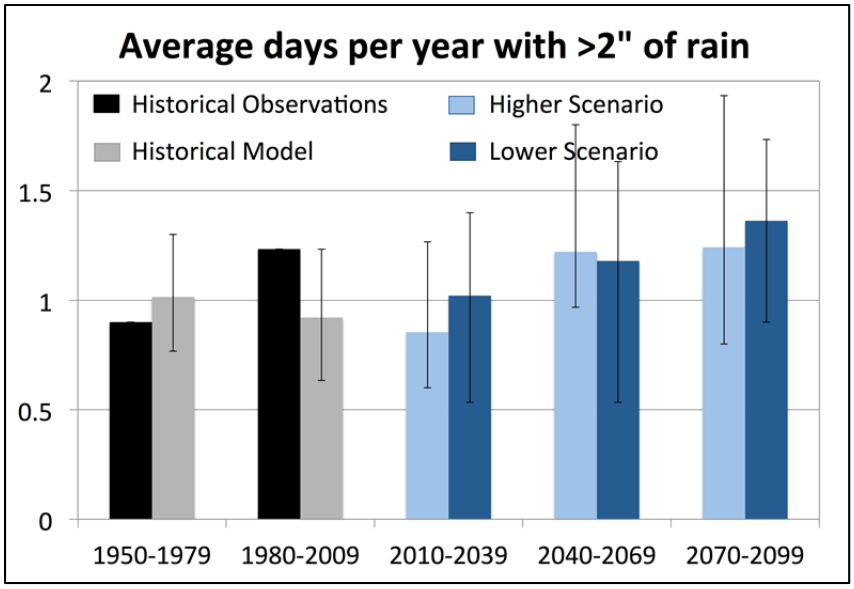

Figure 4.6. Sample plot of projected changes in a fixed threshold indicator of heavy precipitation: here, 2" in 24 hours, for the city of San Angelo, TX under the higher RCP8.5 and lower RCP4.5 scenarios as simulated by climate projections from 9 GCMs statistically downscaled to the local airport weather station. The bars indicate the multi-model mean values while the whiskers show the range resulting from the 9 different CMIP5 GCMs (Source: figure and data, K. Hayhoe.).

Finally, several interactive websites are available that allow users to plot a variety of maps and/or time series from pre-packaged, web-based products in order to analyze historical trends and/or future projections. In terms of observational data, NOAA's Climate at a Glance (CAG) website (https://www.ncdc.noaa.gov/cag/) is an easily-accessible resource that can be used to plot time series and observed trends in monthly, seasonal, and annual temperature, precipitation, and drought indices for continents, states, climate regions, climate divisions within a state, and even some individual cities. Figure 4.7 shows an example of a typical CAG plot – here, average summer precipitation for the city of Baltimore, Maryland for the period of record. In terms of future projections, the Climate Wizard website (http://www.climatewizard.org/) allows users to generate maps of projected changes in temperature and precipitation across the United States, based on high-resolution projections.

Resources and tools such as these can be useful in determining observed and projected future trends at the regional scale for specific indicators. While figures from NCA and IPCC assessments appropriately consider projections from all available GCMs and a range of future scenarios, the metadata for similar maps in individual publications or regional studies should be examined carefully to understand what kind of data went into making them, how many GCMs were used to create the figure (the more the better), and whether a spectrum of scenarios are represented (at least two) to show the lower and higher ends of future change. It is important to be aware of the source of information and data used as well as to determine whether they meet the standards discussed in Sections 4.2.7 and 4.2.9.

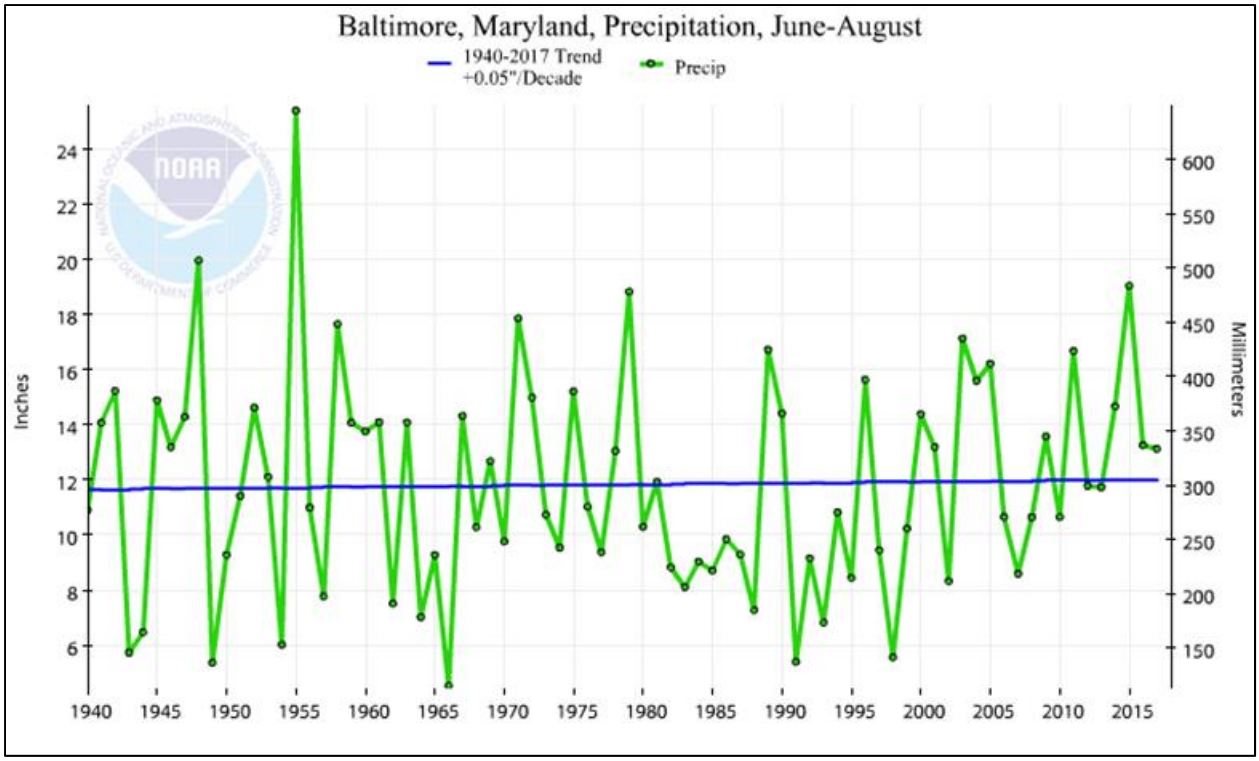

Figure 4.7. Observed annual June-August cumulative precipitation (green) and long-term trend (blue) for Baltimore, MD. (Source: NOAA's Climate at a Glance).

4.2.6 Sources of Uncertainty in Future Projections

Future projections are inherently uncertain. As climate changes, however, one thing is clear: in many locations and for many applications, information on historical conditions alone is becoming increasingly insufficient to serve as a reliable guide to the future. To ensure that current and future infrastructure is resilient to the range of environmental conditions it will face over its lifetime, climate projections are often needed to quantify how conditions may change over time.

Understanding how and why climate projections are uncertain is critical to appropriately selecting and correctly interpreting projections. Over time scales of several decades, natural variability and scientific uncertainty play important roles in determining the range of likely outcomes for a given region and variable. The further into the future the projections extend, however, the more important the role of human forcing becomes and hence the use of multiple future scenarios, such as the Special Report on Emission Scenarios (SRES) and Representative Concentration Pathways (RCPs) described in Section 4.3.3.

In general, projected increases in extreme precipitation events are consistent with basic physics and observed trends across the United States. There is less certainty in projected changes in seasonal and annual mean precipitation. Precipitation projections vary regionally, with a general pattern of increases expected at higher latitudes and decreases in subtropical regions, moderated by local and regional topography.

An additional source of uncertainty in future projections at the regional to local scale is introduced by the many factors that interact to determine how the climate of a specific location will respond to global-scale change over the coming century. To address this source of uncertainty, global climate model simulations can be downscaled to individual weather stations as well as to fine scale grids covering the region of interest (as discussed in Section 4.2.9).

4.2.6.1 Sources of Uncertainty in Decadal to Century-Scale Projections

There are three primary sources of uncertainty in projections of both global and regional climate through the end of the century (Hayhoe et al. 2017, Hawkins and Sutton 2009 and 2011). These sources consist of:

- **Natural variability**, which causes temperature, precipitation, and other aspects of climate to vary from year to year and even decade to decade.
- **Scientific uncertainty**, as it is still uncertain exactly how much the Earth will warm in response to human emissions, and global climate models cannot perfectly represent every aspect of Earth's climate.
- **Scenario or human uncertainty**, as future climate change will occur largely in response to emissions from human activities that have not yet occurred.

As shown in Figure 4.8, the relative importance of each of these sources varies over the time horizon of the projections. **Natural variability** is an important source of uncertainty in both average conditions and the magnitude and timing of extreme events, particularly over shorter time scales. Averaged over longer time scales of multiple decades, however, the contribution of natural variability to overall uncertainty in both mean conditions and the statistics of variability decreases in importance (Hawkins and Sutton 2011). To address the uncertainty in future projections resulting from natural variability, climate projections, including both mean conditions as well as the magnitude or frequency of extreme events, should be calculated for the type of climatological periods of 20 to 30 years shown above in Figure 4.6 or other periods, for example, such as historical (1971-2000), near-term (2011-2040), mid-century (2041-2070) and/or end-of-century (2071-2100).

The more rare the event(s) being considered, the more important is the role of natural variability in determining the likely occurrence and magnitude of the event(s). Each individual climate model simulation – even simulation ensembles generated by the same GCM but initialized with different conditions – will have a different pattern of natural variability. The initial conditions used to begin a GCM simulation represent the state of the climate at a certain point in time, within the range of observational error (a range that is typically quite large, as most GCMs are initialized to pre-industrial conditions). Small changes to the initial conditions create a slightly different climate state, resulting in slightly different patterns of day-to-day and even year-to-year variability. Large ensembles of GCM simulations can be created that encapsulate a broad range of natural variability, just by varying the initial conditions slightly. Over climate time scales of 20 to 30 years, however, long-term trends in every simulation will respond to the same forcing: natural factors, such as changes in energy from the Sun and volcanic eruptions; and human factors, such as observed and projected emissions of heat-trapping gases, dust, soot, and other relevant substances.

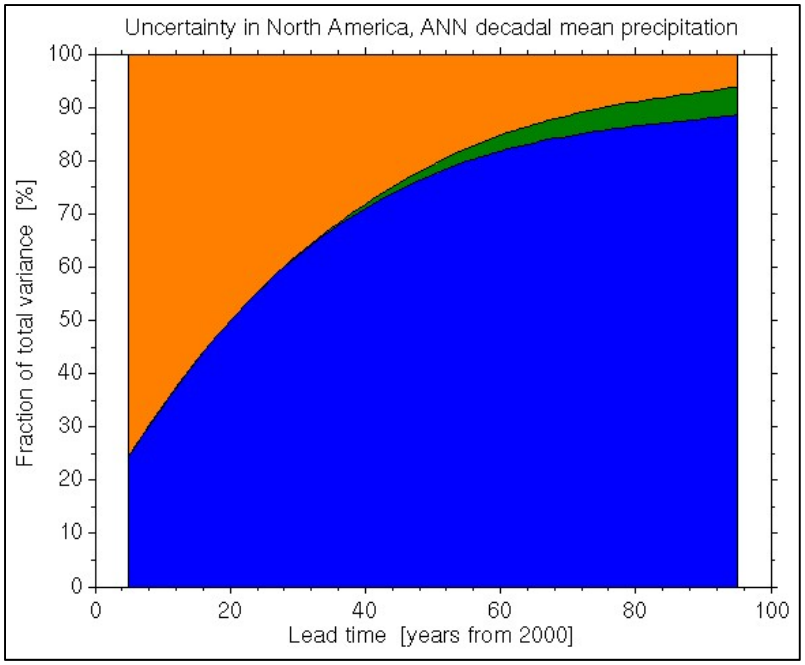

Figure 4.8. Proportion of the total uncertainty in future annual mean precipitation projections corresponding to the internal natural variability of the climate system (orange), scientific or model uncertainty (blue) and human or scenario uncertainty (green). (Source: Hawkins and Sutton 2011).

The more ensemble members used in a given analysis, the more comprehensive the range of possible outcomes over time scales from days to years, due to natural variability. Therefore, analyses that require a robust range of uncertainty in extremely rare events should take advantage of this feature of climate projections, using as many simulations as possible to capture the broadest possible range in variability over the time period of interest, including large ensembles of multiple simulations from the same GCM. GCMs are discussed in more detail in Section 4.2.8.

When using multiple simulations from multiple models, however, care should be taken to avoid treating each individual simulation as independent. Rather, multiple simulations from one GCM should be used to construct a representative range of projections for that GCM first, then that representative range can be averaged with other GCMs. This accounts for the fact that not all GCMs will have the same number of ensembles available: one might have 10 simulations in its ensemble for a given future scenario, while another has only 3. These should not be treated as 13 independent simulations, but rather as two groups of simulations that should be equally weighted for the same future scenario (Knutti et al. 2013, Sanderson et al. 2015 and 2017). The rarer the event(s) being considered, the more important it is to consider using large ensembles of simulations from multiple models.

Scientific uncertainty is an important source of uncertainty in determining the magnitude and sometimes even the direction of projected changes in average precipitation, as well as dry days and extreme precipitation, over medium to longer ranges. Scientific uncertainty arises from two sources. The first source is climate sensitivity (see Collins et al. 2013) – how will the planet respond to the large stores of carbon being moved from the lithosphere into the atmosphere through combustion of fossil fuels, on time scales orders of magnitude faster than natural

processes? The direct effect of increasing carbon dioxide concentration can be calculated relatively precisely; uncertainty in climate sensitivity arises primarily due to the feedbacks or self-reinforcing cycles that occur as a result of a warming planet. Such processes include increasing emissions of carbon and methane from permafrost, and changes in the physical properties of many important elements of the climate system, from ocean circulation patterns to clouds. The second source of scientific uncertainty arises from the challenges of attempting to model a system as complex as the earth's climate system (Flato et al. 2013). Are the key processes relevant to determining regional climate conditions included in a given GCM? Are they correctly represented? If they occur at spatial and/or temporal scales below, what can be directly resolved by the GCM, and are these parameterizations accurate?

To address the uncertainty in future projections due to scientific uncertainty, analyses should use projections from as many global climate models as possible (Hayhoe et al. 2017). In contrast to the recommendation above, where multiple simulations from a single or a limited number of GCMs can be used to capture a more robust range of natural variability, here a more robust range of likely outcomes for a given future scenario will be obtained from a larger ensemble of GCMs, where differences between the models represent the limitations of scientific ability to simulate the climate system. Many GCMs share code, parameterizations, and other aspects of their design. Therefore, if an analysis is required to select a subset of GCMs for logistical reasons, these GCMs should be chosen such that they cover a range of climate sensitivities and are relatively independent of each other. Model selection is discussed in Section 4.3.2.

Scenario uncertainty is an important source of uncertainty in temperature-related projections, particularly over the second half of the century as the scenarios diverge (Hawkins and Sutton, 2009, Hayhoe et al. 2017). This uncertainty is not scientific, but rather socioeconomic: how will the population, technology, and economy of the world evolve over coming decades? And what impact will these changes have on emissions of carbon dioxide and the other heat-trapping gases that are primarily responsible for the observed warming and future change?

A certain amount of future change is already nearly inevitable because of past emissions and current energy infrastructure. This is the result of inertia in both the physical climate system, in responding to emissions that have already occurred, and in the energy sector, due to the time required to transition from traditional fossil-based energy to low or zero-carbon energy. A substantial amount of future change, however, may be avoided by following a lower future scenario with large reductions in and eventual elimination of net carbon emissions from human activities, as opposed to continuing on a higher, carbon-intensive future pathway in which the world continues to rely on fossil fuels for the majority of its energy. The difference between these two futures is the motivation of international efforts such as the Paris Agreement, which aims to hold "the increase in the global average temperature to well below 2°C above pre-industrial levels and to pursue efforts to limit the temperature increase to 1.5°C above pre-industrial levels, recognizing that this would significantly reduce the risks and impacts of climate change."

To address scenario uncertainty, future projections rely on a range of scenarios described in Section 4.3.3. These encompass a range of futures, from pathways where carbon emissions continue to grow throughout the century, to those where emissions are reduced consistent with global targets such as the Paris Agreement. Over relatively short time scales there is no significant difference between scenarios. However, for analyses with time horizons past 30 years

and with a focus on temperature and/or extreme precipitation, using projections based on a higher and a lower scenario will span the range of projected changes.

BOTTOM LINE: Future projections are uncertain due to natural variability, scientific uncertainty, and human choices. The relative importance of each of these sources varies over the time horizon considered and the variable of interest.

4.2.6.2 Abrupt Climate Change and the Potential for Surprise

While the transportation community has used the term "abrupt climate change" to differentiate discrete climate events such a hurricane or a storm from longer-term incremental changes traditionally associated with global warming (Lindquist 2011), this report uses the CCSP (2008) definition of abrupt climate change, as follows: "a large-scale change in the climate system that takes place over a few decades or less, persists (or is anticipated to persist) for at least a few decades, and causes substantial disruptions in human and natural systems."

Based on the paleoclimate record, at least four significant types of abrupt climate change have been identified that, if they were to recur, would pose a significant risk to society and its infrastructure (Kopp et al. 2017). These include: 1) rapid disintegration of glaciers and ice sheets leading to rapid sea level rise that would endanger coastal areas; 2) widespread and sustained changes to the hydrologic cycle that could significantly alter the hydroclimate of large regions of the world; 3) abrupt change in the northward flow of warm, salty water in the upper layers of the Atlantic Ocean associated with the Atlantic Meridional Overturning Circulation (AMOC) that would affect the distribution of heat around the world and thus the temperature and other average conditions of most locations on the planet; and 4) rapid release to the atmosphere of methane trapped in permafrost and on continental shelves in the Arctic that would accelerate the rate of global change. The first two types of abrupt change are directly relevant to the H&H design of transportation infrastructure, while the second two types would be likely to have the potential for indirect, but nonetheless substantial impacts.

The likelihood of rapid change in glaciers, ice sheets, and hence sea level is dependent on a number of physical factors that are not presently considered in sea level rise models. For example, the fact that large ice masses that are grounded below sea level (e.g., the West Antarctic Ice Sheet) have potential for rapid ice-sheet changes is known, "but is not yet well enough understood to be modeled accurately" (Sweet et al. 2017b). If this potential is realized, sea level rise could increase substantially. Over the last decade, growing scientific understanding of the mechanisms that determine the response of ice sheets to warming temperatures has already substantially increased the projected range of sea level rise over this century, moving it up from the range of 7 inches to 2 feet given by the 2007 IPCC Fourth Assessment Report to projections of "1–4 feet by 2100, but a rise of as much as 8 feet by 2100 cannot be ruled out," according to Sweet et al. (2017b) in NCA4.

The likelihood of widespread and sustained changes to the hydrologic cycle is already well documented in existing projections from GCMs, and well-established based on the fundamental physics governing evaporation rates and atmospheric water vapor content in a warmer world. Projections indicate that, broadly, current wet areas are likely to get wetter and current dry areas are likely to get drier over periods of years to decades. To date, the focus of these abrupt changes has been on dry conditions/drought rather than wet conditions, because floods tend to be more

localized in space and time than droughts. However, large climate anomalies can result in major flooding at the regional scale. Though there is considerable uncertainty regarding the likelihood of abrupt changes in the flood regime due to limitations in large-scale hydrological modeling, datasets for documenting past hydrological changes, and knowledge of the physical processes that generate floods, the possibility of changes beyond what are simulated by GCMs cannot be discounted, particularly over longer time horizons past mid-century (Kopp et al. 2017).

While the likelihood of abrupt climate change is a subject of active research, little is known about specific effects on transportation and adaptation strategies if abrupt climate change were to occur. Although referring to ecosystems, Alley et al. (2003) indicate that abrupt climate changes are particularly harmful where the systems have long lifetimes or are relatively immobile. They also indicate that damage is likely to scale with the abruptness and unpredictability of the climate change. These findings imply that infrastructure with 50- or 100-year design lifetimes may be particularly vulnerable. However, assets with shorter lifetimes could also be affected by abrupt climate change even though they may be relatively less sensitive to gradual hydrologic changes.

If it were to occur, abrupt climate change would likely require a "transformational adaption" approach. According to Kates et al. (2012), there are three types of transformational adaptations: 1) those that are applied at a much larger scale than previously, 2) those that are new to a region or sector, and 3) those that transform places or shift locations. The Thames Estuary 2100 Plan (Environment Agency 2009) is an example of the first type of adaptation; the city of Miami Beach's ambitious plan to install pumps and raise the level of key roads and infrastructure is an example of the second type, and the Netherlands coastal defense and riverine flooding abatement (Deltacommissie 2008) an example of the latter type.

BOTTOM LINE: Most global climate model simulations do not include the mechanisms responsible for many of the abrupt climate changes or "surprises" that have been observed in the paleoclimate record. It is important to be aware that GCM-based projections do not encompass the entire range of possible outcomes, and may underestimate future change, particularly under higher scenarios and over longer time horizons.

4.2.7 Global Climate Models

Global climate models (GCMs) are complex, three-dimensional models that are continually evolving to incorporate the latest scientific understanding of the atmosphere, oceans, and Earth's surface. Originally, "GCM" stood for General Circulation Model, since these models were originally designed to simulate the circulation of the atmosphere and ocean. Today, however, "GCM" is more commonly used to refer to global climate models, as they incorporate many other facets of the Earth's climate system, including chemistry, biospheric processes, vegetation, soils, and more (Hayhoe et al. 2017); and GCMs that explicitly include a carbon cycle component are often referred to as Earth System Models (ESMs).

Using historical conditions for the past and scenarios for the future, GCMs calculate grid-based projections of temperature, precipitation, and other important aspects of the climate system. Their output is available from the global to regional scale, on timescales typically ranging from daily to annual. Because of the important role climate model projections play in informing policy decisions at every level, from the individual city to international negotiations, GCMs are

subjected to comprehensive and continuous scrutiny and testing in the scientific literature and through the Coupled Model Intercomparison Projects (CMIPs). Determining the accuracy and reliability of climate model projections is a unique challenge, however, as these models produce *projections,* not *predictions (*forecasts*).*

Climate scientists use the term *prediction* to refer to the evolution of specific weather events and *forecast* for future weather events under known forcing factors. Even though GCMs produce daily outputs, climate model projections cannot be used as a long-term weather forecast model, to predict the chances of rain on July 18, 2064, or by how much the average temperature in January 2032 will exceed the long-term average. Rather, GCM simulations generate *projections* (aggregate weather conditions over 20 to 30 years) under plausible future forcing factors. The response of the Earth's climate system to future emissions from human activities is evaluated with projections, rather than predictions, because human activities cannot be predicted with certainty. These projections are intended to describe the behavior of the climate system averaged over climate timescales of 20 to 30 years, and the most likely response of the climate system to the specific scenario used as input to that specific climate model simulation.

BOTTOM LINE: GCMs are complex representations of the physics and chemistry of the earth's climate system that produce climate projections intended to accurately simulate the statistics of weather over climatological timescales of 20 to 30 years.

4.2.7.1 Coupled Model Intercomparison Project Simulations

The Coupled Model Intercomparison Project (CMIP) is a series of simulation experiments to assess climate model reliability. CMIP phase 3 (CMIP3) produced the first reliable datasets for climate impacts analysis, using the SRES scenarios and more than 20 GCMs. The most recent CMIP phase 5 (CMIP5) includes simulations from over 50 GCMs using the RCP scenarios (see Section 4.3.3 for a description of the scenarios). CMIP phase 6 experiments are currently underway, with the new archive scheduled for completion by 2020.

With a new research emphasis on regional climate change impacts, CMIP3 was the first dataset of climate projections for which reliability of daily and extreme precipitation was evaluated. Kharin et al. (2005) evaluated 24-hour and 5-day precipitation of 12 CMIP3 models. They began with data from the companion historical simulations produced by the Atmospheric Model Intercomparison Project (AMIP) for 1979 to 1995, diagnosing the 20-year return period value of daily precipitation with a generalized extreme value distribution provided annual maximum daily precipitation, and then averaging the results over broad latitudinal regions such as the tropics and extra-tropics. They found the majority of the CMIP models underestimate the amplitude of 20-year return period values of annual precipitation extremes and the amplitude of their spatial variations, as would be expected from gridded fields where the amount of precipitation that falls each time step is the average of the entire area covered by the grid. They also concluded the spatial pattern of extreme precipitation rates in the multi-model mean matches the observations reasonably well in the extratropical but not tropical regions, a foundational result for establishing confidence in GCM projections of extreme precipitation.

Historical climate model simulations have also been used to diagnose the human influence on observed increases in extreme precipitation, including those seen across the United States, as

shown in Figure 4.9. Zhang et al. (2007) used output from CMIP3 simulations to detect latitudinal changes in average precipitation that cannot be explained by climate variability or natural forcing, and Zhang et al. (2013) updated these findings using CMIP5 simulations to estimate the human contribution to continental-scale change in 1-day and 5-day "extreme" or heavy precipitation. For North America, they concluded that human-induced climate change has increased annual maximum 1-day and 5-day precipitation, respectively, by 3.3 percent and 3.8 percent, during 1951 to 2005. They also estimated that the 20-year return period for extreme precipitation had decreased to 15-year for 1-day and 14-year for 5-day annual maximum precipitation. However, an analysis of trend in 1-day annual maximum precipitation in 15 CMIP5 models for 1901 to 2010 reveals the trend is underestimated (Krakauer and Fekete 2014, Asadieh and Krakauer 2015). This means that future projections produce a climate change signal in daily and extreme precipitation that is consistent with, but likely underestimates, observed trends; in other words, climate model reliability is sufficiently established to conclude that changes in both mean and extreme precipitation have already occurred, and – particularly for US regions that have experienced the greatest changes, such as the Northeast and Midwest – they are already affecting the reliability of engineering design precipitation metrics, based on historical data.

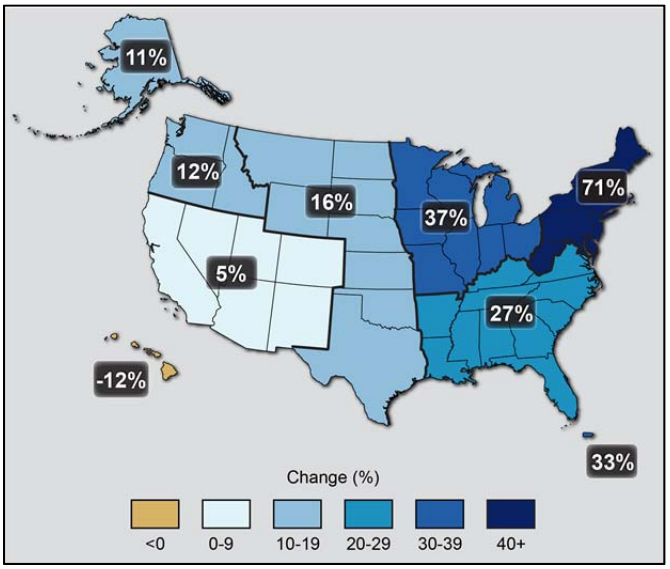

Figure 4.9. Percent increases in the amount of precipitation falling in very heavy events (defined as the heaviest 1% of all daily events) from 1958 to 2012 for each region of the continental United States. These trends are larger than natural variations for the Northeast, Midwest, Puerto Rico, Southeast, Great Plains, and Alaska. The trends are not larger than natural variations for the Southwest, Hawai'i, and the Northwest. (Source: NCA3 2014).

With each new CMIP, some new GCMs are created and many older GCMs are updated to a new generation. Most large modeling groups and national laboratories that develop and run GCMs for the CMIP assessments create a new generation of their previous model for each new CMIP. For example, the National Center for Atmospheric Research in Boulder, CO first released the Coupled Climate System Model (CCSM1) in 1996. Today, the most recent version is CCSM4. However, the same group also included simulations from some newer experimental models for CMIP5, such as CESM1-CAM5, which includes an advanced chemistry module.

Typically, the spatial resolution and the range of physical processes included in the CMIP GCMs increase from one generation to the next. In general, it is best to select GCMs from the most recent CMIP ensemble (currently, CMIP5; by 2020, CMIP6). However, from CMIP3 to CMIP5, Hayhoe et al. (2017) conclude that, "the overall improvement in performance [in the entire multi-model ensemble] is relatively minor. For certain variables, regions, and seasons, there is some improvement; for others, there is little difference or even sometimes degradation in performance, as greater complexity does not necessarily imply improved performance. CMIP5 simulations do show modest improvement in model ability to simulate ENSO … and the rate of Arctic sea ice loss, as well as greater consensus regarding projected drying in the southwestern United States and Mexico." This suggests that analyses related to the southwest may benefit by prioritizing CMIP5 over CMIP3, as well as analyses in geographic regions with rapidly varying topography where spatial resolution can improve model ability to resolve a range of climate conditions – but in other areas, while it is true that CMIP5 provides a greater range of GCM simulations, analyses that use CMIP3 simulations can still produce useful results.

In terms of extreme precipitation, differences in CMIP3 and CMIP5 extreme precipitation across the United States are also found to be minimal. Comparison of extreme precipitation indices in CMIP3 and CMIP5 reveals overlap in model distributions in every region of the United States (Kharin et al. 2013). Wuebbles et al. (2014) compare the 5-year return value of 2-day precipitation and find no appreciable difference between CMIP3 and CMIP5 across the United States. Conversely, Koutroulis et al. (2016) found that CMIP5 models were better able to simulate intense precipitation and wet day fractions than CMIP3 models, particularly over central and eastern North America.

BOTTOM LINE: GCM simulations from the most recent CMIP archive represent the latest standard collection of global climate model simulations for the historical period and a range of future scenarios. While CMIP5 model output is generally at a higher spatial resolution than CMIP3, projected changes in extreme precipitation from CMIP3 and CMIP5 are broadly comparable.

4.2.7.2 Assessing Global Climate Model Performance

Climate model simulations cannot be validated like weather forecast models can, by comparing multiple short-term forecasts with observations for the same period. To use future projections for validation purposes, it would be necessary to: 1) have the entire world adopt a specific scenario exactly as forecast, including associated changes in population, demographics, technological development, and energy use; 2) follow this pathway precisely for multiple decades, to mid-century or beyond; then 3) look backwards to assess the accuracy of projections made today. This process is clearly impossible from a logistical perspective, as it would require an unprecedented level of international and national coordination. It is also futile from a utilitarian perspective, as it precludes the primary use of climate models today, which is to quantify the impacts of a *range* of future scenarios on human society and infrastructure in order to select the most viable pathway forward that minimizes the costs of both adaptation and mitigation. By the time the projection was validated, that amount of climate change would be inevitable due to the emissions that had occurred while the pathway was being followed.

Instead, GCM simulations are evaluated against satellite observations and reanalysis (see Section 4.2.4) from the last few decades, against instrumental records from the last few centuries, against

paleoclimate records for past conditions very different than today, and are even used to simulate atmospheric conditions on other planets such as Venus and Mars (Flato et al. 2013). Comparing observed annual temperature change to that simulated by CMIP5 total forcing historical simulations (IPCC AR4 2007), which include all known natural and human factors that affect climate, demonstrates that GCMs are able to reproduce the observed increase in temperature over every continent and that projected future changes are significantly different than what would be expected under natural forcing alone as illustrated in Figure 4.10.

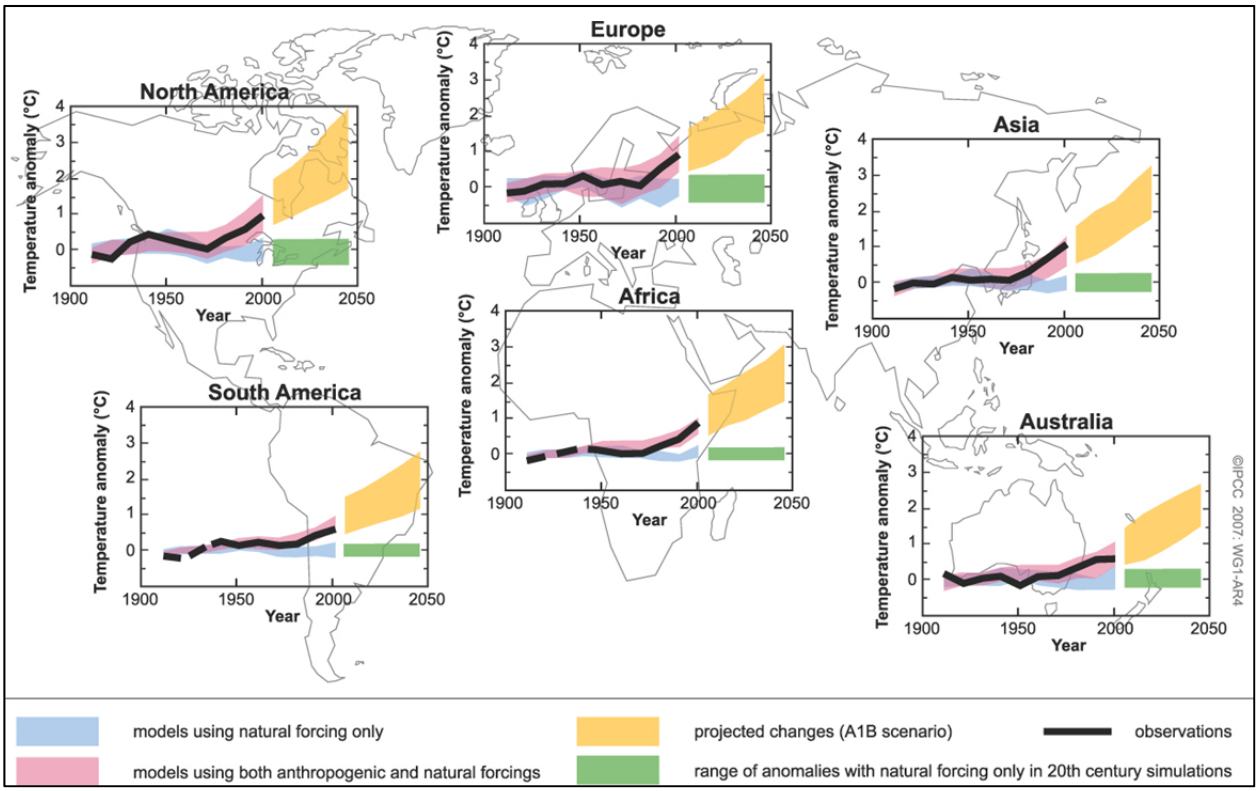

Figure 4.10. Comparing observed (black) with historical model simulated total forcing (pink) and natural forcing (blue) scenarios shows that GCMs are able to reproduce observed long-term temperature trends over every major continent of the world. (IPCC AR4 2007).

In terms of their regional performance, model reliability is demonstrated when climate models are able to generate dynamical weather and precipitation patterns that: 1) occur due to known and observed processes and are consistent with historical observations; 2) have shifted or changed (in terms of both temporal and/or spatial distribution) in a manner consistent with known physics and/or observed trends; and 3) project future changes that are consistent with known physics and/or observed trends (Table 4.5). Future changes are *significant* when their magnitude exceeds that of historical observed and internal model variability.

Table 4.5. Performance evaluation for global climate models.

Performance Attribute	Description	Rationale
Process Realism	Agreement with forcing mechanisms for precipitation.	Do climate models recreate historical dynamical processes that bring dry and wet conditions to the region of interest?
Short-range Forecast	Agreement with 5 - 15 years of measurements (e.g., 2001 – 2015).	Have climate models accurately forecasted observed trends over the last 20 to 30 years?
Internal Variability	Agreement with range of measurements over a time period.	Do climate models replicate the range of historical variability in the region?
Model Variability	Agreement among models.	Do climate model results depend upon the climate model?
Signal Variability	Agreement among different future scenarios.	Do climate model projections of variables that basic physics indicates should differ depending on the amount of forcing applied to the system vary by scenarios of future conditions? Do projections of other variables, such as mean annual or seasonal precipitation, that are not expected to differ broadly between future scenarios, diverge?
Signal-to-Noise	Ratio of mean to variability.	Does the combination of model and internal variability exceed differences in mean change between scenarios?

Model reliability *cannot* be demonstrated by assessing whether the model reproduces a specific historical event in the year in which it occurred, such as the Midwestern heat wave of 1995, or the South-Central drought of 2011. Climate model projections are initialized with conditions from the 1800s and then allowed to generate their own chaotic patterns of internal natural variability that evolve over time into a different temporal sequence than experienced in the real world. This means that, while models should be able to (and in fact, most do) simulate a heatwave of the magnitude and geographic location observed in 1995 sometime in the 30-year climatological period surrounding 1995, there is no reason *per se* to expect that event to occur in 1995.

In addition, model reliability *cannot* be demonstrated by calculating *model bias*: comparing, for example, the absolute value of seasonal or annual mean precipitation for a given region with the observed value – either for an individual year or even for a 30-year climatological period. The absolute value of modeled precipitation over a region is frequently biased or offset from the observed value due to both the limited spatial resolution of the model as well as the limited geographic coverage of the observations. This bias is commonly removed through bias correction and/or full empirical-statistical downscaling before applying climate simulations to quantify impacts at the local to regional scale. Biases in absolute values are not indicative of overall model reliability.

Climate scientists typically address uncertainty in future projections by using an ensemble of models for which all projections are considered as possible and equally credible outcomes of

future climate. However, given the similarities in source code among some models, they cannot all be treated as independent realizations. For this reason, NCA4 (USGCRP 2018) uses a weighting scheme that accounts for interdependence among GCMs as proposed by Sanderson et al. (2015 and 2017).

For some regions and variables, there may be a benefit to removing GCMs from the ensemble if there is literature demonstrating that they are unable to reproduce relevant aspects of regional climate for the geographic region of interest. As discussed in more detail in Section 4.3.2, however, a number of studies have concluded that model selection based on historical performance adds little if anything to the accuracy of the multi-model ensemble. Specifically, Mehran et al. (2014) compared CMIP5 GCMs to gauge-based observations to show that the majority of simulations agreed with the spatial pattern of observed precipitation across North America, including up to the 75th and 90th quantiles of the distribution of daily wet-day values. They noted, however, a general tendency for models to overestimate precipitation over mountainous areas and underestimate it over arid regions. Evaluating the processes that bring precipitation to a region, Ryu and Hayhoe (2015) found that it was possible to identify which CMIP3 and CMIP5 GCMs were and were not able to reproduce the large-scale weather patterns associated with precipitation over the Caribbean and Gulf of Mexico regions. They concluded that "systematic biases in model structure may be responsible for biases in observed precipitation variability over the Caribbean, and more confidence may be placed in the precipitation simulated by the GCMs that are able to correctly simulate seasonal cycles of sea surface temperature and the North Atlantic Subtropical High."

Finally, a detailed analysis by Sheffield et al. (2013) examining CMIP5 performance across North America found that, "no single model stands out as being particularly better or worse across all analyses, although some models consistently outperform the others for certain variables across most regions and seasons and higher-resolution models tend to perform better for regional processes." In particular, they highlight differences in model abilities to simulate the North American monsoon.

If the engineering team is concerned with a very specific phenomenon, such as precipitation associated with the North American Monsoon in the US Southwest, or the influence of the North Atlantic Subtropical High on drought risk on the South-Central United States, where studies have shown that models do differ in their ability to reproduce these specific phenomena, then based on the existing literature it may be possible *not to identify the best, but rather to eliminate the worst* models based on regional performance. To that end, analysis investigating previous work for the study region is recommended to determine whether the literature or reports show some models to perform notably more poorly than others for the atmospheric phenomena relevant to precipitation and for the seasons of interest. Further discussion on selecting GCMs is given in Section 4.3.2.

BOTTOM LINE: Global climate models are evaluated on their ability to reproduce the physics and dynamics of precipitation and other core climate variables. In general, the multi-model mean is often more accurate than simulations from a single model. GCMs should not be evaluated on their bias or ability to reproduce specific historical events.

4.2.8 Global Climate Projections

The first criterion for actionable climate information is that it be generated by procedures deemed reasonable, reliable, and defensible by the climate science community (Section 4.2.3). For global climate models (GCMs), the minimum standard for their non-experimental use in the climate community is to have contributed to and participated in CMIP. In order to contribute to a CMIP, models must first be endorsed by the members of the CMIP Panel, their development and evaluation must be published in the peer-reviewed literature, their simulations must be conducted according to the guidelines laid out by the most recent CMIP experiment, and their output must be submitted in the required format.

Each of the GCMs that provide output to CMIP has its own unique name, which is typically an acronym that reflects its provenance and the institution that created it, as well as the generation of the current model. For example, HadCM3 stands for the U.K. Hadley Centre Climate Model version 3; CCSM4, the acronym for the US National Center for Atmospheric Research model, stands for Coupled Climate System Model version 4. Collectively, GCMs that have submitted output to a CMIP experiment are referred to as "CMIP models" or "CMIP GCMs". These models also form the basis for the analyses and projections in the IPCC assessment reports as well as the US NCAs. However, it is not correct to refer to these as "IPCC models" or "NCA models," since both the IPCC and the NCA simply use the simulations conducted for and made available under CMIP.

CMIP Phase 3 (CMIP3) was the first phase to include both historical and transient (year-by-year) future simulations for a range of different future scenarios. The CMIP3 archive, completed in 2006, includes contributions from 17 research groups from 12 countries and a total of 24 GCMs (Meehl et al. 2007). The most recent CMIP5 archive was completed in 2016. It provides output from over 50 GCMs with spatial resolutions ranging from about 50 to 300 km (30 to 200 miles) per horizontal side, corresponding to four future scenarios called Representative Concentrations Pathways (RCPs) that are discussed in more detail in Section 4.3.3. Simulations for CMIP6 are currently underway, with the majority of simulations expected to be complete by 2020. This new archive will include even higher-resolution simulations as fine as 25 km (15 miles).

Through the CMIP process as well as in the larger body of scientific literature, GCMs are subjected to vast, comprehensive, and continuous scrutiny and testing. Determining the accuracy and reliability of climate model projections is a unique challenge, however, for at least two reasons. First, as discussed previously, GCM simulations are allowed to establish their own temporal patterns of natural variability. These patterns include everything from daily weather systems to long-term natural cycles such as El Nino. Because the temporal patterns of natural variability in GCM simulations are allowed to develop independently, and are not constrained to match the real world, the resulting simulations are referred to as projections, not predictions or forecasts as they would be if they were generated by a weather model whose initial conditions are constrained to match observed variability. This means that there is no one-to-one correspondence between individual days or years in the real world and those simulated by the GCM. The statistics of climate over 20 to 30 years simulated by the GCM should match those of the real world, in terms of their means, averages, percentiles and/or moments of distributions. If a heavy precipitation event occurred in the real world on, for example, June 18, 1998, there is no reason to expect that the climate model simulation will show a similar event on the same day; however, it is reasonable to evaluate the simulation based on whether a similarly extreme event occurred over that region sometime in the 20- to 30-year period surrounding 1998.

Second, the relatively coarse spatial resolution of GCMs (and even the higher-resolution regional climate models, Section 4.2.9.1) compared to the physical processes that determine local conditions means that model simulations are typically biased or offset from the observed value. While this is true for both the absolute value as well as the shape of the probability distribution or density function of modeled temperature or precipitation over a region, the magnitude of this bias, which is largely stationary over time, does not necessarily translate to an assessment of GCM performance. For extreme precipitation, for example, it is largely a function of spatial resolution. When the small-scale features that typically produce heavy precipitation are smoothed out over a large grid, the precipitation becomes less extreme. An analysis of CMIP3 model output confirmed this, finding that the value of 20-year and 30-year return period values for daily precipitation are more severely underestimated as grid spacing increases (Kharin et al. 2005). Model performance is also related to the physical representation of important small-scale processes, such as rainfall and cloud formation that occurs at spatial scales far smaller than the model is able to resolve.

BOTTOM LINE: CMIP GCM simulations form the basis for future climate projections used in local, regional, national and international assessments. GCM precipitation output is typically generated at relatively coarse spatial scales and is subject to biases due to limitations in the GCMs. Thus, few engineering applications use GCM output directly, though it can be useful for identifying trends and is required to generate high-resolution projections.

4.2.9 High-Resolution Climate Projections

When using climate projections to quantify potential changes at the local to regional scale, GCM output is typically downscaled and bias-corrected, using a physics-based dynamical regional climate model (RCM), or an empirical-statistical downscaling method or model (ESDM), or an RCM followed by an ESDM for bias correction.

In climate science, downscaling and bias-correction incorporates new information – either high-resolution modeling of physical processes via an RCM, or historical observations at the location of interest via an ESDM – in combination with GCM projections to produce locally-relevant projections of variables such as temperature, precipitation, and relative humidity at a given location or region. Many ESDMs are comprised of a two-step approach, spatial disaggregation, which increases the spatial resolution and bias correction that adjusts for errors in the GCM. These two steps can also be done independently of one another and often use different techniques, such as quantile mapping for bias correction and an analog approach for disaggregation.

When ESDMs are used to downscale historical GCM simulations and the results are compared with observational data not used in training the ESDM, downscaling is found to reduce and, in the case of a good ESDM, virtually eliminate biases as well as improve the variance of both historical climate simulations and future projections at the local to regional scale relative to the original GCM simulation. The sections below describe the important issues to consider when selecting output from RCMs and ESDMs. For more background information on downscaling and a detailed discussion surrounding the issues related to downscaling and its application to assessing impacts at the local to regional scale, readers are directed to the comprehensive US

Department of Defense report, "Use of Climate Information for Decision-Making and Impact Research: State of Our Understanding" (Kotamarthi et al. 2016).

4.2.9.1 Regional Climate Modeling

RCMs simulate physical processes of regional climate at finer spatial and temporal scales than can be resolved by global models, using global model simulation data as boundary conditions. RCMs are sometimes referred to as "nested models," as they essentially operate as a higher-resolution limited-area grid embedded into the coarser global grid of a GCM. However, the term "nested" is most commonly used to refer to a specific type of experiment where RCMs are run interactively within a GCM framework, with information being exchanged back and forth between the GCM and RCM at regular time intervals throughout the simulation. The majority of RCM simulations are non-interactive – i.e., they use inputs from GCM simulations that have already been completed, and the flow of information is in one direction only, from the GCM to the RCM.

RCMs usually cover a rectangular domain with a grid size that typically ranges from about 5 to 50 km per side, depending on the model used and the geographic extent of the domain. Like GCMs, RCMs generate output on a three-dimensional grid. Vertical levels include the surface, two meters above the ground (the standard height for temperature observations), and specified vertical pressure levels in the atmosphere. In addition to precipitation and air temperature, RCMs also calculate humidity, solar radiation, wind, pressure, soil temperature, heat fluxes, and a host of other variables. Output is typically available at three-hourly, six-hourly, and/or daily increments.

RCMs have the benefit of directly calculating the physical processes that determine regional climate as well as, to a certain extent, how these relationships might be altered by a changing climate. RCMs are challenged, on the other hand, by their need to cope with the introduction of GCM information as boundary conditions, as well as by the computational demand of conducting simulations at such high temporal and spatial resolutions. In addition, like GCMs, their output should not be directly compared to observations, but must still be bias corrected to remove offsets in both mean values and the shape of the modeled distribution relative to observed before being used as input to hydrological models or other types of quantitative impact analyses. As part of a European RCM inter-comparison project called ENSEMBLES, Themeßl et al. (2011) (http://ensembles-eu.metoffice.com) showed that when empirical quantile mapping (a type of ESDM) was applied to RCM output, it substantially reduced model error; although Maruan (2013) qualifies this by noting that some types of bias correction, such as quantile mapping, may over-correct model biases, leading to overestimation of extremes.

Since RCM simulations are computationally intensive, most impacts analyses draw from existing, publicly available simulations rather than generating new ones. For North America, RCM simulations are currently available from two databases. The first is the North American Regional Climate Change Assessment Project (NARCCAP, Mearns et al. 2013) (http://www.narccap.ucar.edu). The NARCCAP archive contains output fields from six RCMs at a spatial resolution of 50 km and a temporal resolution of three hours, based on simulations from four previous-generation CMIP3 global climate models for one mid-high future scenario (SRES A2) for one historic time period (1971-2000) and one future time period (2041-2070). The second is the North American COordinated Regional Downscaling EXperiment (CORDEX,

Jacob et al. 2014) (https://na-cordex.org). The NA-CORDEX archive contains output fields from seven RCMs at spatial resolutions ranging from 25 to 50 km based on simulations from six CMIP5 GCMs for the higher (RCP8.5) and lower (RCP4.5) scenarios. Though these RCM outputs have not been corrected for bias, plans are underway to bias-adjust both NARCCAP and CORDEX-NA output using a type of ESDM, Kernel Density Distribution Mapping (KDDM) (McGinnis et al. 2015).

One of the most active research questions in RCM development today is the extent to which models are able to simulate sub-daily precipitation at finer grid spacing. In principal, RCMs could provide output at each model time step, typically 30 seconds to a few minutes. In practice, however, writing out model output every time step is very time consuming, as well as increasing the storage needed by an order of magnitude or more. Even more importantly, just because the information can be generated does not mean it is accurate. At 50 km grid spacing, three-hourly precipitation results are inconsistent from model to model (Anderson et al. 2003, Cook et al. 2016). Similar results were also found for extreme daily precipitation by Wehner (2013) who used GEV to estimate 20-year return period values of season-dependent daily rainfall.

Inconsistencies in simulated precipitation are related to an RCM's inability to consistently relate convective precipitation to moisture flux divergence. The working hypothesis is that with finer grid spacing (4 km or less), the explicit simulation of convective rainstorms will improve consistency among models, and hence the accuracy of spatial correlation and sub-daily rainfall. But such ultra-high resolution modeling efforts are still highly experimental, involving only a few simulations with a single model, and are not intended for application to impacts analyses. They are additionally complicated by the lack of sub-daily gridded observational datasets that make it difficult to evaluate the model's ability to reproduce observed characteristics of precipitation at sub-daily increments. Preliminary results from simulations over the United Kingdom show substantial improvements in one RCM's ability to simulate rainfall duration and hourly extremes during the summer season (Kendon et al. 2017). Similar simulations for the United States (Liu et al. 2016) find that a higher resolution RCM better resolves snowpack in the intermountain west; their analysis of warm-season rainfall in the rest of the United States is pending.

BOTTOM LINE: RCMs produce three-hourly and daily outputs on a regular grid for a host of variables including temperature, precipitation, humidity, solar radiation, and winds. Simulations for North America are available from NARCCAP and NA-CORDEX. Before applying to impact analyses, their output must be bias-corrected to remove offsets in both mean values and the shape of the distribution of a given variable relative to observations.

4.2.9.2 Empirical-Statistical Downscaling Methods and Models

Empirical-statistical downscaling methods and models (ESDMs) use different statistical methods to combine historical observations with GCM output to reduce or remove the bias in GCM output. As noted above, they can be used to remove biases from RCM output. ESDMs can be very simple. The delta approach, for example, that is used in the WorldClim dataset, calculates a "delta" by subtracting the average for a historical GCM time period (e.g., 1970-1999) from a future one (e.g., 2070-2099) and adding that delta to historical observations for the same time period. ESDMs can also be very complex, with computational demand rivaling that of an RCM.

For example, the method of Vrac et al. (2007), which combines hierarchical clustering with a non-homogeneous Markov model to define daily precipitation states and simulate the transitions between them, is able to accurately simulate precipitation intensity at individual weather stations, as well as the occurrence and duration of wet spells, but is extremely computationally intensive. Other approaches such as ARRM and LOCA use different statistical methods to remap the quantiles of the distribution to match that of observations or identify "analog" weather patterns (e.g., Wood et al. 2004, Stoner et al. 2012, Pierce et al. 2014).

ESDMs can generate output at the spatial scale of nearly any observations, from a gridded dataset to an individual station, provided that relevant and reliable observations at that scale have been collected over a climatologically relevant period of record. They can be applied to a single weather station, or a grid covering an area up to and including the entire globe, if observations of the desired variable are available for that area. In terms of the temporal resolution of the output, it depends on the GCM output and the observations used as input, as well as on the nature of the statistical model used. Some methods, such as the delta approach, produce monthly output. Others use monthly input from the GCM and combine this with daily observations or a stochastic weather simulator to generate daily projections. It is more common now for ESDMs to use daily GCM input to generate daily projections, and there are some experimental efforts that combine daily GCM input with hourly temperature observations to generate sub-daily temperature projections.

One of the most important benefits of ESDM output is that it is bias-corrected. In other words, for the historical training period, the statistical properties of ESDM output (such as climatological seasonal precipitation, or the climatological frequency of days per year with more than 2 inches of precipitation in 24 hours) should be virtually identical to that of the observations in the historical period, over climatological time scales of at least 20 to 30 years. In addition, ESDMs are commonly relatively computationally efficient, flexible, and able to process a large number of global climate scenarios in a limited amount of time.

In contrast to global climate model output, it *is* appropriate to compare the climatological mean absolute values from an ESDM for the historical period with observations. However, it is important to emphasize that comparisons of means and variability may only be done over climatological periods of 20 to 30 years or more, since day-to-day correspondence between observations and downscaled output cannot be expected due to the fact that each GCM simulation establishes its own internally consistent patterns of natural variability.

ESDMs are typically trained on a multi-decadal period of historical data, such as 1950-1999 or 1981-2010. The time period over which the ESDM is trained will vary by location and the length of the data record available. For the purposes of application, ESDM records encompassing the entire historical and future period (e.g., 1950-2100) can be used for analysis. For the purposes of evaluation, however, when ESDM simulations or output for the training period are compared to observations for that same time period, any differences that result are simply a measure of the goodness-of-fit of the ESDM. To determine transferability, or how well the ESDM is able to reproduce values outside the calibration period, its output must be compared to observational data not used to train the model. In the first example above, comparing ESDM output with observations for the period 1950-1999 would yield a measure of goodness-of-fit; comparing ESDM output with observations for, say, 2000 to present would yield a measure of transferability. During evaluation, under no circumstances should ESDM simulations from a period of time that combines both training and independent observations be compared to

observations as this conflates a measure of goodness-of-fit with a measure of transferability. Similarly, ESDM output should not be compared with observations from a dataset not used to train the ESDM, because any differences will be dominated by differences between the observational datasets themselves, and these differences can be more appropriately resolved by directly comparing the two sets of observations.

ESDMs can be sensitive to errors in the observational data, requiring extensive quality control and error-checking before the observations are used. They also assume that the relationship between local climate and large-scale weather patterns that can be resolved by GCM output remains stationary both now and in the future. This assumption is difficult to evaluate since there are no observations for the future. However, experiments using an independent set of high-resolution climate projections as "future observations" can test whether the bias in long-range projections is within an acceptable range. This so-called "Perfect Model" approach has shown that for even simple ESDMs the stationarity assumption generally is valid in the central part of the distribution for temperature, but more complex methods are needed when downscaling the more extreme tails. For all ESDMs tested to date, the stationarity assumption is violated more often in areas of rapidly varying topography (Dixon et al. 2016, Stoner et al. 2017).

The stationarity issue has important implications for the ability of ESDMs to simulate projected changes in extremes. Simpler ESDMs (e.g., Bias Corrected Spatial Disaggregation (BCSD) (Wood et al. 2004) and Bias Corrected Constructed Analogue (BCCA) (Hidalgo et al. 2008)) have been shown to perform adequately for long-term means near the center of the distribution, such as seasonal and annual means of temperature and precipitation. However, more complex ESDMs (e.g., Multivariate Adaptive Constructed Analogs (MACA) (Abatzoglou and Brown 2011), Asynchronous Regional Regression Model (ARRM) (Stoner et al. 2013), Kernel Density Distribution Mapping (KDDM) (McGinnis et al. 2015), or Localized Constructed Analogs (LOCA) (Pierce et al. 2014)) are required to resolve extremes at the tails of the distributions, such as 50-year precipitation events and days per year with temperature above 95°F.

In contrast to the two publicly available RCM datasets, a wide variety of ESDM datasets are available. Table 4.6 lists the ESDM datasets currently available for contiguous United States. In general, analysts can use any method that meets their project needs. However, the needs of the analysis are critical to identifying the most appropriate dataset to use.

Table 4.6. List of empirical-statistical downscaling methods and available datasets.

Downscaling Technique	Available Datasets
Parametric Quantile Mapping and Linear Spatial Disaggregation	ARRM
Empirical Quantile Mapping and Constructed Analogs	BCCA[1]
Empirical Quantile Mapping and Linear Spatial Disaggregation	BCSD, NEX-DCP30[2], NEX-GDDP
Empirical Quantile Mapping with Adjustment and Multivariate Adaptive Constructed Analogs	MACAv2-METDATA MACAv2-Livneh
Equidistant Empirical Quantile Mapping with Adjustments and Localized Constructed Analogs	LOCA
Delta	WorldClim

[1] A dry bias affecting much of the contiguous United States has been identified in BCCA precipitation; see Appendix B.

For analysis concerned with **monthly, seasonal, or annual values**, the simplest approaches that bias correct only the mean of the distribution are often adequate. These methods are transparent and understandable, and can be easily obtained or calculated in-house. The output from these methods is accurate for assessing seasonal and monthly precipitation, but not for sub-monthly indices (e.g., wettest week of the year, 25-year rainfall event).

For analyses that focus on the **extreme events**, simpler methods that do not produce daily outputs and/or do not use statistical methods that resolve the shape of the distribution of daily variables are not recommended. Instead, it is necessary to use datasets with daily output, where the output is at least theoretically accurate to indices down to the individual day. For hydrologic assessments, it is recommended to use datasets with proven ability to simulate extreme events (ARRM or LOCA). Newer kernel density techniques are showing promising results, especially for extreme event simulation (McGinnis, personal communication; Hayhoe and Stoner, personal communication); downscaled climate projections created with ARRM that uses KDDM techniques are scheduled to be released in 2019 (Hayhoe and Stoner, personal communication).

Where extreme precipitation displays **spatial correlation**, weather mapping techniques such as MACA and LOCA that incorporate spatial weather maps into the downscaling process are preferable over methods that use a grid cell-by-grid cell technique. However, simulation of extreme events can be compromised due to averaging of weather patterns, forcing users to weigh the importance of spatial structure versus extreme event simulation.

The ESDM datasets listed in Table 4.6 differ in temporal resolution, with the BCSD methods having monthly output (with the exception of NEX-GDDP, which is daily), the two MACA datasets having both monthly and daily output, and ARRM, LOCA, and BCCA output having daily output. Sub-daily projections created by statistical downscaling methods are very novel and none of the ESDMs listed here provide them as of yet. Though it is an area of active research, future releases of sub-daily products should be treated with caution until their reliability has been established. The datasets listed here are all gridded datasets, which to date is the only publically available form. Some ESDMs are able to produce output at the station-level, working with climate scientists on a particular project. In 2019 a station-downscaled (point-based) dataset is expected to be published, Seasonal Trends and Analysis of Residuals (STAR-ESDM), with CMIP5 GCMs (Hayhoe and Stoner, personal communication). Descriptions of each dataset as well as their spatial and temporal resolutions, number of GCMs and scenarios downscaled, and where to obtain the data, are listed in Appendix B.

BOTTOM LINE: ESDMs produce daily or monthly outputs at the spatial scale of the observations used to train the statistical model, which range from individual weather stations to regular grids. There is a broad range of datasets available; the most appropriate one(s) depends on the characteristics and the needs of the analysis.

4.2.10 Evaluating Climate Projections for Specific Applications

Practical and objective criteria should be used for evaluating the suitability of climate modeling outputs for engineering applications. In terms of practical criteria, does a given dataset provide the information needed at the spatial and temporal scale required? In terms of objective criteria,

does the data meet evaluation standards from both the climate science and engineering communities?

While GCM evaluation underlies the use and application of downscaled projections, as meaningful results can only be obtained from reliable inputs ("garbage in, garbage out"), downscaling methods themselves must be reliable as well. As discussed above, the characteristics of the analysis can and should be used to identify appropriate, or rule out inappropriate, methods. However, during design and development, all downscaling methods should undergo rigorous evaluation to demonstrate that they can produce reliable products, and the results of these tests should be provided in the journal article(s) introducing each downscaling method.

Typical criteria used to evaluate both RCM and ESDM approaches are listed in Table 4.7. The methods of evaluation listed are generally performed during the design and evaluation phase of creating downscaling techniques, but there are several independent reviews and comparisons of the ability of downscaling methods and products to reproduce certain aspects of climate variability available in the literature (e.g., Abatzoglou and Brown 2011, Benestad et al. 2007, Fowler et al. 2007, Gutmann et al. 2014, Yoon et al. 2012).

Table 4.7. Performance evaluation standards for downscaled global climate model output.

Performance Attribute	Description	Rationale
Climate Accuracy	Agreement with measurement distributions over a period of time.	Are RCMs and ESDMs able to recreate historical climate statistics?
Process Realism	Agreement with historical weather patterns and mechanisms for precipitation.	Do RCMs and ESDMs replicate weather processes?
Transferability	Agreement with measurement in regions separate from the model development region.	Do RCMs and ESDMs work well under climate conditions different from their development region? Are the models overfitting regional dynamics in their development region and performing poorly in other regions?
Within-sample versus out-of-sample accuracy	Agreement with measurement not used in model development.	Do RCMs and ESDMs perform poorly on historical data outside the period of model development? Are the models overfitting historical data and performing poorly on data outside the period of model development?
Sensitivity to nonstationarity	Agreement with future conditions substantially different than present.	Do ESDMs perform poorly when climate statistics have changed?

Some of these standards can be used to evaluate datasets through specific evaluation of bias, overfitting, and stationarity. First, ESDMs can be assessed for bias against data from the historical training period. The statistical properties of ESDM output should be virtually identical to that of the observations in the historical period, over climatological time scales of at least 20 to 30 years.

Second, ESDMs can be tested for overfitting by evaluating the bias for an independent evaluation period, i.e. a period of time that was not included to train the model. If a regression model uses too many parameters in creating a proper fit during the training period, it could be fitting the model to the noise or random variability rather than finding the underlying relationship between the observations and GCM output. If, for example, a historical period of 1950-2015 is used when building a statistical downscaling model, it can be divided into a period of years used to train the model and another used for evaluation (e.g., 1950-1995 for training and 1996-2005 for evaluation, or even years for training and odd years for evaluation, or more complex methods such as *k*-fold cross-validation).

Finally, an ESDM can be tested for stability, i.e. that the relationship between observations and historical simulations is stationary or valid in the future. This can be accomplished using the Perfect Model approach, where output from a higher-resolution GCM, RCM, or ESDM, for which future projections are available, takes the place of observations (e.g.,Vrac et al. 2007). Using the historical simulation from the model instead of observations to train the ESDM, downscaled future projections can be evaluated against future projections from the higher resolution model, not used in the process of training the ESDM or simulating future projections. Table 4.8 indicates whether the downscaled datasets have undergone and/or passed these three evaluation steps, as documented in peer-reviewed literature.

Table 4.8. Evaluation tool for US climate projection dataset suitability.

Dataset	Satisfactory Bias Evaluation	Overfitting Evaluation	Stationarity Evaluation
ARRM stations	Yes	Yes	Yes
ARRM gridded	Yes	Yes	Yes
BCCA gridded	Yes	No	No
BCSD gridded	Yes	No[2]	No[2]
LOCA gridded	Yes	Yes	Yes
MACAv2-METDATA gridded	Yes	No	No
MACAv2-Livneh gridded	Yes	No	No
NEX-DCP30 gridded	Yes	No	No
NEX-GDDP gridded	Yes	No	No
NARCCAP gridded	Yes[1]	N/A[3]	No
NA-CORDEX	Yes	N/A[3]	No

[1]RCMs participating in the NARCCAP program have individual evaluation schemes.
[2]Overfitting and stationarity evaluation documentation are not available in the public domain.
[3]Overfitting is not applicable to RCMs because they do not fit a statistical model to the data.

4.3. Guidance for Selecting Climate Modeling Outputs

The objective of this section is to provide guidance for selecting GCMs and scenarios appropriate for a given hydrologic design task (considering the appropriate level of analysis), and interpreting the resulting information in light of the uncertainty inherent in future projections. If

there were no logistical constraints on analyses, the first part of this guidance could be accomplished in one sentence: for analyses requiring quantitative inputs, consider all models that have appropriate outputs available, and—for analyses with time horizons longer than 30 years—a broad range of scenarios. The second aspect of this guidance is more challenging, but can be facilitated through awareness of the various sources of uncertainty in future projections and guidance regarding best practices on how to account for them in hydrologic analyses.

Although the default approach is recommended wherever possible, it is important to recognize that such an expansive approach is not feasible for most analyses, given real-world limits to budget and schedule. When logistical constraints demand a smaller range of future projections, this chapter also provides guidance regarding factors to consider depending on the level of analysis when narrowing the selection of climate inputs, from the criticality of the hydraulic structure to the range of uncertainty encompassed by climate projections based on a subset of available models and/or scenarios.

4.3.1 Selection of Climate Inputs by Level of Analysis

When it comes to selecting appropriate climate inputs for a given analysis, there is no one-size-fits-all selection for all applications. The scope of the hydrologic assessment defines what the most appropriate information may look like. Projects that require a qualitative assessment of change in design storms need guidance on whether or not there is an upward trend in the design storm, providing an indication of whether the project scope should be expanded. Projects that require site-specific quantitative assessment need guidance on climate outputs that can be manipulated and integrated into quantitative methods. Not all existing datasets of climate projections may be adequate for the wide range of temporal and spatial scales of engineering analysis and different levels of granularity in engineering assessments (e.g., Level 1 through Level 4 discussed in Chapter 3) – and for some applications, an appropriate dataset might not even exist yet.

For the hydrologic design of bridges with very large watersheds, daily, spatially-averaged precipitation from climate projections may be directly applicable; stormwater management and drainage design in smaller watersheds may require sub-daily information that is not typically available from climate projections. Similarly, coarse-scale climate projections may be sufficient to assess the direction of precipitation change; multi-decadal time series of downscaled precipitation may be needed to simulate stream flow.

Figure 4.11 outlines a conceptual decision tree that can be used as a tool to aid in the selection of appropriate climate inputs for levels of analysis 1 to 4. At all analysis levels, the design team should conduct an initial analysis using National Climate Assessment or other regional assessments described in Section 4.2.5 to qualitatively identify potential trends. Level 2 analyses should use these same assessments to determine a range of outcomes. Level 3 and 4 projects should use high-resolution climate datasets based on project scale and required precipitation duration. The input varies from the use of maps that show change in extreme precipitation, to downscaled climate projections. For the most comprehensive analysis (Level 4), engineers should consult with a climate scientist with relevant expertise at the beginning of the study to obtain expert guidance on the data source and methods used to generate metrics specifically for that study. The climate scientist should be experienced in development and/or application of climate projections at the regional to local scale.

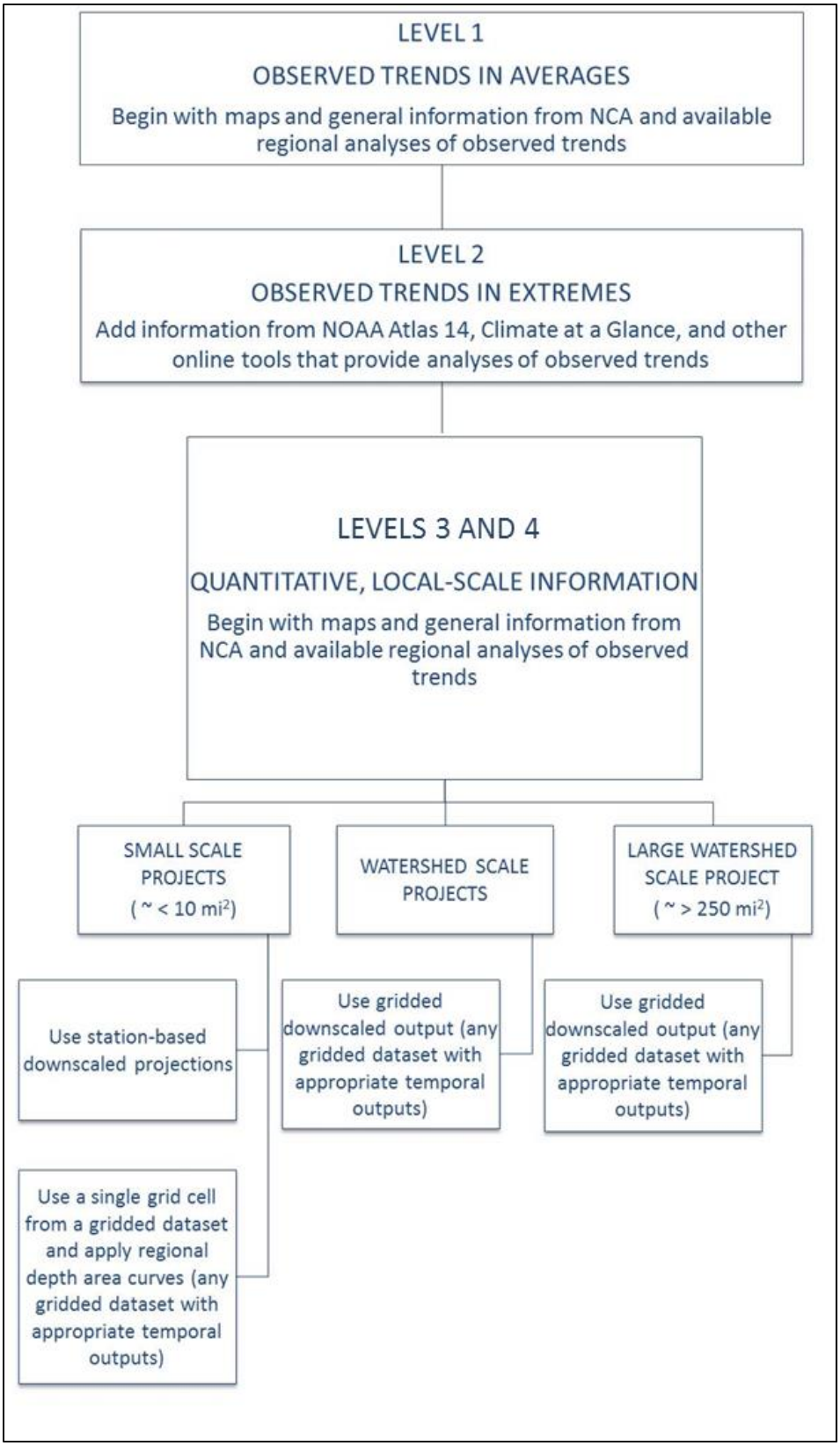

Figure 4.11. Decision tree for identifying appropriate climate projection information by level of analysis.

Table 4.9 lists recommended types of climate data along with examples of sources for the different levels of analysis for hydrologic design. For Level 1 and Level 2, climate information is required that enables *assessment of directionality* of change in precipitation extremes that influence the design storm. The relevant weather extreme may differ by basin size, characteristic hydrology, and the type of structure. For instance, design storms for small watersheds may have a direct correspondence with daily rainfall; whereas for large watersheds, design storms may be sensitive to a longer accumulation period such as weekly or monthly rainfall. It is critical that the engineering team has background knowledge of the relevant weather extremes.

Table 4.9. Potential climate resources for a range of levels of analysis.

Level of Analysis	Type of Climate Data	Examples of Climate Data Sources
Level 1: Historical Discharges	Maps showing observed regional change in mean or extreme rainfall.	Maps published in NCA and/or IPCC
Level 2: Historical discharges/confidence limits	Maps showing observed regional change in mean or extreme rainfall. Uncertainties associated with different return periods as mapped in NOAA Atlas 14.	Maps published in NCA and/or IPCC NOAA Atlas 14 maps.
Level 3: Projected discharges/confidence limits	Historical and projected daily or monthly future precipitation.	Daily or monthly future projections, more complex ESDMs or RCM output are necessary.
Level 4: Projected discharges/confidence limits with expanded evaluation	Historical projected daily future precipitation, custom derived metrics for that specific study.	Daily future projections, more complex ESDMs or RCM output are necessary.

Directionality should be determined from change in mean value of the relevant weather extreme. The change in weather extreme should be evaluated over a region rather than at specific locations. The need for a regional evaluation arises from the inherent isolated nature of extreme rainfall. This means the extreme rainfall is unlikely to occur at all locations within the dataset, even though the conditions that make it possible have changed. Maps, such as the ones shown in 4.2.5, showing the change in historically observed precipitation and the projected change in future precipitation for a number of extreme metrics, will most likely suffice for Levels 1 and 2.

For Level 3 and 4 analyses, ideal climate projections enable *assessment of site-specific quantitative design metrics*. This is relevant for infrastructure system assessments that intend to delve further into the direct vulnerabilities to find robust adaptation solutions, including assessments of systems that involve larger watersheds. Station level precipitation at daily or sub-daily temporal resolution is needed to resolve localized events, and a more complex statistical downscaling method is recommended in order to resolve rainfall events at the tails of the distribution. The climate projections will most often be used as input to hydrologic models.

A Level 3 analysis will require the use of high-resolution climate projections. For a small watershed, point-based station, downscaled projections for individual weather station(s) can provide an accurate estimate of future changes in extreme precipitation. An alternative is to use a minimum of three grid cells from a gridded dataset and apply areal reduction factors (ARFs) (see Section 5.3) to adjust the gridded information for differences in spatial scale between the grid

size and the project scale. For analysis of medium and larger watersheds, a larger collection of point-based downscaled projections or gridded downscaled projections can be used as input into hydrological models to determine design requirements.

For a study where an in-depth and customized Level 4 analysis is necessary, practitioners should consult with a climate scientist familiar with generating and applying high-resolution projections to impact analyses at the beginning of the analysis to determine which metrics can be calculated that will show the effect of climate change on vulnerabilities specific to the asset being studied. Such metrics could include, for example, the change in certain thresholds or return periods of precipitation events at certain periods into the future, or hybrid indices that combine different climatic variables such as amount of snowfall or heat index values.

BOTTOM LINE: Depending on the level of analysis of a hydrologic system or asset, different climate sources will be useful. For a small or relatively simple analysis where the direction of change is sufficient to determine vulnerabilities, maps showing the observed change in precipitation events will suffice, however, where a more in-depth analysis is needed, future climate projections or a custom climate assessment is necessary.

4.3.2 Model Selection

The default for any analysis with sufficient resources is to consider all models with appropriate outputs. Studies have shown that the multi-model mean is typically closer to reality than any individual model, regardless of the type of evaluations that have been conducted. In reality, however, practical considerations may limit the number of GCMs that can be used. Though computational resources have significantly increased over time, many impact assessments and engineering studies lack the resources or the decision-making framework to evaluate outputs from dozens of global climate models for multiple future scenarios and time periods, emphasizing the importance of understanding how to effectively and acceptably reduce the dimensionality of a multi-model ensemble.

One way is to reduce the dimensionality of the input by selecting a sparser matrix of input data that is still representative of the range of uncertainty in both model and scenario uncertainty. Often, the first instinct is to evaluate available models to select a "best" or a pool of "best" models. As discussed previously, however, it is not a simple matter of determining which model has the lowest bias for the region and variable in question, or which model reproduces a certain extreme event observed in the historical record. It is true that some GCMs are better than others at reproducing important large-scale features of certain regions. But sometimes it is not even possible to answer this question, as the ability to simulate one aspect of regional climate can be offset by its inability to reproduce another, both of which affect the variable in question.

Even if such evaluation were technically possible, it would need to be balanced against the body of literature that has found that model ability to simulate historical climate averages is not necessarily correlated with model ability to simulate observed and projected change (e.g., Ryu and Hayhoe 2017). In general, limitations are expected in any GCM, primarily because of a lack of spatial resolution rather than any inherent shortcoming in the physics of the model. However, it is reasonable to remove a model from consideration if extremely poor model performance indicates that the model cannot be trusted (Mendlik and Gobiet 2016). Depending on the region

and the variable, there may be detailed studies in the literature that demonstrate, for example, that specific GCMs are unable to reproduce a specific feature of regional climate that is essential to precipitation over that region, such as the North American monsoon. However, while it is possible in some cases to eliminate poorly performing models, it is not possible to select a set of "best" models. In fact, it is difficult, if not impossible, to identify a sub-set of generically "better" GCMs for the continental United States.

For analyses that cannot incorporate simulations from all available GCMs, then, how should they reduce the pool? In answering this question, it is important to note that many high-resolution datasets include only a limited number of GCMs, typically closer to 20. The goal is to use a collection of models and scenarios that capture both the spread of the model output (scientific or model uncertainty) as well as the possible range of future change (human or scenario uncertainty). Scientific consensus dictates that impact assessments should include a range of climate models and a range of future scenarios (Kotamarthi et al. 2016). Hosseinzadehtalaei et al. (2017) compare projections of extreme precipitation from 15 different GCMs and find that the choice of GCM accounts for up to 65 percent of the uncertainty in projected extreme precipitation for return periods ranging from 1 to 10 years.

In general, the scientific consensus tends to be that using more models is better than fewer; models should cover the range of accepted climate sensitivity, which ranges from 2 to 4.5^{o}C for a doubling of carbon dioxide in the atmosphere. It is generally preferable to prioritize models with a long and well-documented history of development and evaluation in the peer-reviewed scientific literature. While there is no standard for GCM selection, real-world examples of selection criteria are provided by FHWA pilot projects in New Jersey, Wisconsin, Iowa, and the Gulf Coast, all of which used a range of GCMs and scenarios to develop climate projections over a series of future time periods.

In New Jersey, GCMs were selected based on their ability to reproduce observed precipitation for the state. As described in detail above, this approach runs the risk of assessing models based on a factor that may be poorly correlated with their ability to simulate future change, and may not result in the intended subset of genuinely "best" models. In the Iowa pilot, the full set of nineteen CMIP3 GCMs was used, but GCMs were eliminated simply if they did not have a continuous daily time series for the study period (1960 to 2100), the model was new (one case), or if the scientific literature concluded the global climate simulation was unrealistic. For the Gulf Coast analysis, GCMs were eliminated if they did not have daily outputs and were not at least second generation, with each generation documented in the scientific literature (i.e. they were not the first version of the model to be published, but rather had a long history of development and evaluation stretching back years and even, in some cases, decades).

The Infrastructure and Climate Network (ICNet) provides an intercomparison tool prepared by Stoner and Hayhoe that includes a list of all CMIP3 and CMIP5 global climate models, as well as summary information about the individual models. It describes the 25 modeling centers or groups that participated in the CMIP5 effort and submitted model output that is available for applications (http://cmip-pcmdi.llnl.gov/cmip5/docs/CMIP5_modeling_groups.pdf). Each group ran at least one model and numerous groups ran more than one model or model version. Notably, the NOAA Geophysical Fluid Dynamics Laboratory submitted results from six different models. In total, there are 58 possible climate models that may potentially be used for climate studies. However, 12 of those models do not have output for any of the future scenarios. Of the remaining 46 models, 21 have output for all four scenarios, 8 are missing RCP6.0, 10 have only

RCP4.5 and RCP8.5, five have only RCP4.5, and two have only RCP8.5. These numbers are reduced further when daily output is required.

This analysis provides a consistent method for selecting GCMs, based on expert assessment of reliable GCMs and their estimated climate sensitivity (Table 9.5 in Flato et al. 2013). The ICNet has identified three groups of models:

- Group 1 Most Reliable: Models in this group represent the most recent versions of reliable, very well-documented, long-established global climate models from modeling groups that have been working in this area for decades.
- Group 2 New: The latest work in climate modeling circles is the development of "Earth System Models" that combine the traditional components of a global climate model (e.g., atmosphere, ocean, and biosphere) with other models (e.g., vegetation, hydrology). Adding brand-new components doesn't necessarily improve model performance and in many cases it actually degrades it - so these models can definitely be used for interest but should have a "caution" label attached as they are still very much in development.
- Group 3 Experimental: Models in this group represent brand-new global climate models, some from new modeling groups who are relatively inexperienced in the field or for versions of global models that have not submitted simulations to the CMIP archives. These models have not been extensively published and, with a few exceptions, are not based on previous versions. Again, they should be used with a "caution" label attached.

Group 1 models (15 CMIP3 and 21 CMIP5 GCMs) are listed in Table 4.10. Group 2 models and Group 3 models should be used with caution because they are either in development, are entirely new, or originate from modeling groups with less experience.

The recommended procedure is to prioritize Group 1 GCMs, and use as many GCMs as possible. To sample the climate sensitivity, the Group 1 GCMs have been ranked from lowest to highest climate sensitivity (a measure of the response of the climate system to increasing levels of carbon dioxide in the atmosphere), then divided into three tiers – high, medium, and low climate sensitivity. The Group 1 GCM tiers are provided in Table 4.10. GCM selection should include at least one GCM from each tier because this ensures the selected GCMs cover the range of likely values of climate sensitivity. When grouping GCMs by scenario, GCMs from CMIP3 and CMIP5 should not be mixed.

In general, a given project should use as many GCMs as logistics permits. However, the minimum number of GCMs depends on the analysis objectives. For a simple screening analysis, at least three Group 1 GCMs should be selected, one from each category of climate sensitivity (high, medium, and low). For example, in Table 4.10, three CMIP5 Group 1 models that encompass the range of climate sensitivity are MRI-CGCM3, CCSM4, and GFDL-CM3. For a Level 3 or 4 analysis requiring a mean value, confidence limits, or other statistics on the estimates of design precipitation values, enough GCMs should be selected to establish a plausible range of projections. If possible, all Group 1 GCMs should be used.

Table 4.10. Group 1 GCMs from the ICNet analysis and corresponding climate sensitivity (Randall et al. 2007; Flato et al. 2013).

CMIP	Low		Medium		High	
CMIP3 (15)	CCSM3	2.7°C	CGCM3.1 (T47)	3.4°C	IPSL-CM4	4.4°C
	GISS-EH	2.7°C	CGCM3.1 (T63)	3.4°C	MIROC3.2(hires)	4.3°C
	GISS-ER	2.7°C	CSIRO-Mk3.0	3.1°C	MIROC3.2(medres)	4.0°C
	INM-CM3.0	2.1°C	ECHAM5-MPI-OM	3.4°C	UKMO-HadGEM1	4.4°C
			GFDL-CM2.1	3.4°C		
			MRI-CGCM2.3.2	3.2°C		
			UKMO-HadCM3	3.3°C		
CMIP5 (21)	GISS-E2-H	2.3°C	BCC-CSM1.1	2.8°C	CSIRO-Mk3.6.0	4.1°C
	GISS-E2-H-CC	2.3°C	BCC-CSM1.1-m	2.9°C	GFDL-CM3	4.0°C
	GISS-E2-R	2.1°C	CCSM4	2.9°C	HadGEM2-A	4.6°C
	GISS-E2-R-CC	2.1°C	CNRM-CM5	3.3°C	HadGEM2-CC	4.6°C
	INM-CM4	2.1°C	CNRM-CM5-2	3.3°C	HadGEM2-AO	4.6°C
	IPSL-CM5B-LR	2.6°C	GFDL-CM2.1	3.4°C	IPSL-CM5A-LR	4.1°C
	MRI-CGCM3	2.6°C	HadCM3	3.3°C		
			MIROC5	2.7°C		

The second essential way to reduce the dimensionality of the future projections is to appropriately characterize the resulting envelope of model-based uncertainty using summary statistics such as means, standard deviations, and minimum and maximum values. When using multiple climate model simulations for an analysis, it is essential to derive these statistics across climate models as the very last step in the analysis; premature averaging will artificially dampen the variability and hence the extremes. In other words, each individual climate model simulation should be used as input to the analysis individually. Only after the metrics and impacts have been calculated should statistics be derived to characterize the envelope. These statistics could include the highest and lowest simulation, the standard deviation of the multi-model ensemble, or the multi-model ensemble average.

When calculating statistics such as the standard deviation or the mean, each model in a multi-model ensemble is often assumed to be independent, so when averaging the models, each is given a weighting factor of one. In the past, GCMs have sometimes been selected or weighted based on their historical performance relative to observed temperature and precipitation, but this practice has been largely discontinued in the climate science community. Though studies have shown that such selection and/or weighting may increase the risk of underestimating the range of uncertainty encompassed by the ensemble (USGCRP 2017), weighting is still relevant in that it can address the assumption that the models are independent. The reality, of course, is that GCMs build on previous generations and previous models, and are not independent from each other. As described by Knutti et al. (2013) and Sanderson et al. (2015), many share both ideas and model components or code. For this reason, for the first time, the upcoming Fourth U.S. National Climate Assessment uses an approach to jointly weight both performance and independence attributes by the Euclidian distance between the GCM output and observations (Hayhoe et al.

2017). These weighting scores are available for use in weighting multi-model ensembles for any analysis.

> *BOTTOM LINE: There is no perfect model; always use a selection of different GCMs, prioritizing Group 1 models. Typically, the more GCMs included, the better. Unless a full dynamical analysis of the processes and large-scale circulation patterns that drive precipitation over that region has been or can be conducted, do not attempt to select a "best" model or models for the region of interest. This is more likely to bias the sample than provide a reasonable estimate of the distribution of possible conditions. Unless there is substantial evidence in the climate science literature to justify such selection, using a large multi-model ensemble of climate models is nearly always better than attempting to select a smaller number of "better" models.*

4.3.3 Future Scenarios – Description and Guidance

Climate projections are typically presented for a range of plausible pathways, scenarios, or targets that capture the relationship between human choices, emissions, concentrations, and temperature change. Some scenarios are consistent with continued dependence on fossil fuels, while others can only be achieved by deliberate actions to reduce emissions. The resulting range reflects the uncertainty inherent in quantifying human influence on climate.

Most scenarios are time-dependent or transient scenarios that track how population, energy sources, technology, emissions, atmospheric concentrations, radiative forcing, and/or global temperature change over time. Other scenarios are simply expressed in terms of an end-goal or target, such as capping cumulative carbon emissions at a specific level, or stabilizing global temperature at or below a certain threshold. This section describes the different types of scenarios used today, and their relevance to assessing impacts and guiding future planning.

4.3.3.1 SRES and RCP Scenarios

The standard sets of time-dependent scenarios used by the climate modeling community as input to global climate model simulations provide the basis for the majority of the future projections available for use in hydrological modeling. The Special Report on Emission Scenarios (SRES) were developed in 2000 (Nakicenovic et al. 2000). SRES scenarios are used as input to CMIP3 simulations. SRES begin with a set of four socioeconomic storylines that inform Integrated Assessment Model (IAM) simulations that calculate emissions consistent with the four storylines: higher A1fi (fossil-intensive), mid-high A2, mid-low B2 and lower B1. Projections based on SRES scenarios were used in the second and third National Climate Assessments (Karl et al. 2009, Melillo et al. 2014) as well as the IPCC Third and Fourth Assessment Reports (Cubasch et al. 2000, Meehl et al. 2007).

The latest version of scenarios, called Representative Concentration Pathways (RCPs), were developed in 2010 (Moss et al. 2010). RCPs are not based on socioeconomic pathways; rather, each scenario is named after the change in radiative forcing at the tropopause by 2100 relative to preindustrial levels: +2.6, +4.5, +6.0 and +8.5 watts per square meter (W/m^2) (van Vuuren et al. 2011, Thomson et al. 2011, Masui et al. 2011, Riahi et al. 2011). Although multiple emissions pathways would lead to the same radiative forcing level in 2100, consistent pathways of carbon

dioxide and other anthropogenic emissions of greenhouse gases, aerosols, air pollutants, and those of short-lived species, have been identified for each RCP to use as input to future climate model simulations (e.g., Meinshausen et al. 2011, Cubasch et al. 2013). While RCP8.5 reflects the upper range of the open literature on emissions, it is not intended to serve as an upper limit, nor as a "business as usual" scenario for the other three scenarios. RCP-based projections are used in the third (Melillo et al. 2014) and upcoming fourth NCAs (USGCRP 2017) as well as the most recent IPCC Fifth Assessment Report (Collins et al. 2013).

Within the SRES and RCP families, individual scenarios have not been assigned a formal likelihood. Higher-numbered scenarios correspond to higher emissions and a larger and more rapid global temperature change as shown in Figure 4.12; the range of values covered by the scenarios was chosen to reflect the then-current range in the open literature. Since the choice of scenario constrains the magnitudes of future changes, most analyses quantify future change and corresponding impacts under a range of future scenarios – at minimum, one higher and one lower – that reflect the uncertainty in the consequences of human choices over the coming century. For example, the FHWA Gulf Coast assessment used the lower RCP4.5 and higher RCP8.5 scenarios to bound the range of plausible change.

BOTTOM LINE: SRES and RCP scenarios are transient pathways that quantify plausible changes in population, technology, energy use, and other aspects of human society consistent with a range of future emissions resulting from human choices, from low to high.

4.3.3.2 Global Mean Temperature Scenarios

The primary symptom of global change is the increase in global temperature that results from accumulation of carbon dioxide and other heat-trapping gases in the atmosphere. For this reason, many secondary physical changes and impacts scale with global mean surface temperature (GMT), including shifts in average precipitation, extreme heat, runoff, drought risk, wildfire, temperature-related crop yield changes, and more. GMT scenarios offer an alternative approach to quantifying the projected impacts that could occur under a given amount of warming, regardless of when that may occur.

An alternative to selecting individual transient scenarios is to use a global average temperature threshold. This approach allows the user to calculate projected impacts that would occur under a given global target such as the 2°C target in the Paris Agreement. Decades-long future simulations can be transformed into GMT scenarios by calculating the projected changes and resulting impacts that would occur under a transient warming of 1.5°, 2°, or 3°C or more. The 20 to 30 year period in each individual model simulation that corresponds to a given increase in global mean temperature can be identified, extracted, then averaged with the periods extracted from other simulations to generate an ensemble of climate model simulations corresponding to a world that has warmed by a given amount relative to any desired baseline, from preindustrial to a more recent time period such as 1976–2005.

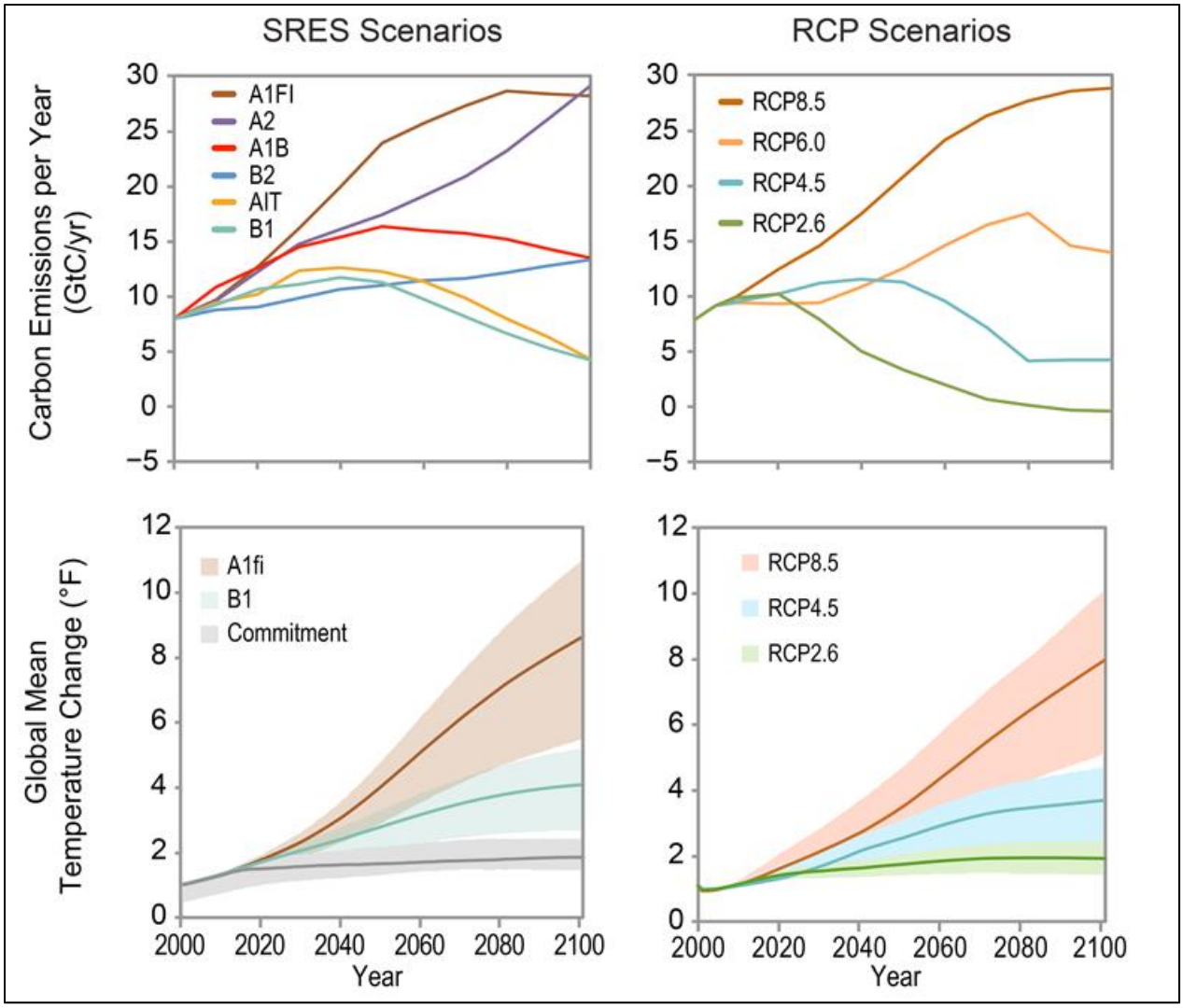

Figure 4.12. Comparison of projected carbon emissions (top) and resulting global mean temperature change that would result from the central estimate (lines) and the likely range (shaded areas) of climate sensitivity (bottom) for the 2000 SRES (left) with the 2010 RCPs (right). (Source: Hayhoe et al. 2017).

A National Research Council report (NRC 2011) states the primary justification for this approach is that "scientific research suggests that many key impacts can be quantified for given temperature increases." It finds the change per degree C of global warming is expected to have the following hydrological effects in the United States (NRC 2011, Swain and Hayhoe 2015):

- 3- to 10-percent increase rainfall from the heaviest 15 percent of daily rainfall.
- 5- to 10-percent change in streamflow in many river basins worldwide.
- Increasingly widespread spring dryness in the western United States and spring wetness in the northwest and central United States and Atlantic Coast.
- Increasingly widespread summer drought across the northern and southwestern United States and summer wetness along the West Coast.

There are multiple advantages of considering this approach for scenarios to inform future engineering design. For example, it enables the cost of adaptation to be compared to the cost of greenhouse gas reduction. Though engineering design cost-benefit analysis may not consider the cost of greenhouse gas reduction, the relative public investment in adaptation and reduction is important to public financing. In addition, adaptation and resilience planning can then be based on a future global temperature scenario that is consistent with global policy targets and for which the likelihood of reaching the temperature threshold can be determined. And finally, both SRES and RCP scenarios can be converted to global temperature scenarios, allowing analyses based on CMIP3 and CMIP5 models, and SRES and RCP scenarios, to be harmonized.

BOTTOM LINE: Global mean temperature thresholds offer a way to increase the sample size of future projections for estimating extremes while providing information at the local to regional scale that is consistent with global policy targets such as the Paris Agreement.

4.3.3.3 Guidance on Scenario Selection

For analyses with time horizons approximately 30 years or less, scenario selection is not critical. Because of the inertia of the climate system in responding to human emissions, as well as the inertia in socioeconomic systems in altering their emissions, there is no statistically significant difference between the climate changes that result from a higher versus a lower scenario over shorter time horizons. The dominant uncertainty for the near-term time scale is natural variability, compounded by scientific uncertainty. For such analyses, any or all available scenarios can be used as desired, with a focus on obtaining as many individual simulations as possible to capture the range of natural variability. Even historical climate information from recent decades can be used, if observed trends are accounted for (Meyer et al. 2014), because uncertainty in hydrological model parameters and flood frequency estimates, for example, is even larger than uncertainty in climate model output (Kjeldsen et al. 2013). Such analysis could relate to evaluating infrastructure repair or management plans, for example, that relate solely to performance within a horizon of 30 years or less.

For Level 1 and Level 2 analyses, scenarios are an important consideration, though not a choice, in interpreting the results of the pre-existing climate information (such as the precipitation maps shown in Section 4.2.5). The majority of assessments, including NCA and IPCC, provide projections for a higher and a lower scenario; some even show projections per degree of global temperature change, enabling the user to extrapolate to any given global temperature scenario. These resources enable users to quantify the uncertainty due to human choices, identifying the amount of change that is likely to occur even if emissions are significantly reduced, and the amount of change that may be avoided by following a lower as compared to a higher future scenario.

For Level 3 and Level 4 analyses of infrastructure with a 30 year or more service life, a lower and higher scenario, at a minimum, should be used because uncertainty in flood frequency estimates and the hydrological model parameters used becomes less significant compared to uncertainty in future scenarios (Kjeldsen et al. 2013). Multiple scenarios allows capture of a reasonable range of uncertainty in human choice and behavior (IPCC 2000, Meyer et al. 2014) – at minimum, a higher scenario (e.g., SRES A1fi or A2 for CMIP3 simulations and RCP8.5 for CMIP5 simulations) and a lower scenario (e.g., SRES B1 for CMIP3 simulations and RCP4.5 or

2.6 for CMIP5 simulations). If resources and budget are available, mid-range scenarios (SRES B1, A1T or RCP6.0) can also be included.

The IPCC states, "There is no single most likely, "central", or "best-guess" scenario, either with respect to SRES scenarios or to the underlying scenario literature. Probabilities or likelihood are not assigned to individual SRES scenarios." Although the SRES scenarios have been replaced with the RCP scenarios, the same statement applies equally to them. For average annual and seasonal precipitation, some research suggests that variability across models is more important than that from scenarios until mid-century, and this persists in all but the northern regions in the United States until 2100 (Northrop and Chandler 2014, Mora et al. 2013).

If an asset is a critical part of the infrastructure system and its loss would cause severe disruption or danger, a higher scenario should be used to ensure the design can withstand the impacts associated with the more extreme conditions expected under a higher scenario. If an asset is of lesser criticality and the difference in cost between designing for a lower or higher scenario is significant, in some cases it may suffice to design for a lower scenario. However, unless there is a specific reason not to consider one end of the scenario range or the other, at minimum one higher and one lower scenario should be considered in the design and resulting decision-making process.

Finally, when using multiple scenarios more than 30 years into the future, **never** average across the scenarios unless the analysis is being conducted on Global Mean Temperature thresholds as described in Section 4.3.3.2 and Hayhoe et al. (2017). Averaging will **NOT** improve the quality of the output because scenarios are entirely different possibilities of future development.

BOTTOM LINE: For applications with service lifetimes longer than 30 years in the future, it is important to use projections based on a range of future scenarios. For applications focusing on the next 30 years or less, there is no significant difference among scenarios and in some cases (depending on other associated uncertainties), even historical data can be used.

4.4. Incorporating New High-Resolution Climate Projections into Guidance

In the future, there will be new datasets of high-resolution climate projections with more refined temporal and spatial scales that may use existing or new downscaling methods. New GCMs and new model simulations will also become available after 2020, when the CMIP6 archive is completed. Subsequent CMIPs are likely to contain more new models, simulations, and ultimately even new scenarios. This section discusses how to incorporate new climate products that may become available within the next 20 years into the guidance described in this document. The goal is to develop guidance that is sufficiently robust that it can be adapted to new products rather than quickly becoming obsolete.

The climate science community continues to evolve in how it evaluates and presents its findings. For example, the World Meteorological Organization has adopted two tiers for climate norms for defining historical and future periods: 1) the standard sliding period, and 2) a fixed mid-20th century period. This section includes a discussion of the relevance of the definition of the historical baseline to transportation structures.

4.4.1 Future Advances in Climate Modeling

Experimental GCMs are being run at 25 km resolution at the global scale, providing output at a spatial scale previously only available from limited-area RCMs. Within the next decade, high-resolution GCM simulations at what used to be considered RCM scales are likely to become routine. Over the next two decades, as computing power evolves, both the spatial scale and the time step at which standard CMIP GCM simulations are conducted are expected to become much finer, matching the resolution of current experimental GCM and RCM simulations currently running at spatial resolutions of 5 to 25 km and temporal resolutions of minutes to hours.

CMIP6 simulations are currently underway, and the archive is scheduled for release in 2020 (Eyring et al. 2016a). Future CMIP phases are anticipated over the longer term. Like CMIP3 and CMIP5, CMIP6 will include historical and future simulations under a range of scenarios and a set of common experiments. The future simulations will use a new suite of scenarios that include the same range as the RCPs, but with updated datasets of current forcings. The number of GCM simulations is anticipated to exceed 70 and will include a dozen new modeling groups. CMIP6 evaluation and benchmark activities will use a series of tools such as the community-developed Earth System Model Evaluation Tool (ESMValTool) (Eyring et al. 2016b) that includes other software packages such as the National Center for Atmospheric Research (NCAR) Climate Variability Diagnostics Package (CVDP) (Phillips et al. 2014), and the Program for Climate Model Diagnostics and Intercomparison (PCMDI) Metrics Package (PMP) (Gleckler et al. 2015, 2016)) to produce well-established analyses as soon as CMIP model output is submitted (https://www.wcrp-climate.org/images/modelling/WGCM/CMIP/CMIP6FinalDesign_GMD_170726.pdf). Additional details are available in Eyring et al. (2016) or on the CMIP Phase 6 website (https://www.wcrp-climate.org/wgcm-cmip/wgcm-cmip6).

As the raw output from GCMs becomes higher-resolution, so too will downscaling efforts evolve. Even finer-resolution models will still require bias correction using ESDMs, but the need for regional climate models at the scales they are currently being run at will be obviated. Instead, regional models that are currently only run for urban areas at spatial scales of meters rather than kilometers may become viable over larger areas. As observations from both ground and satellite instruments increase in temporal and spatial resolution, so too will the resolution and geographic coverage of ESDM projections.

In addition to substantial increases in the spatial and temporal scales of climate model output, climate science will likely advance in other areas that are relevant to the end user community. Such advances are likely to include understanding the physical processes that affect climate at the regional to local scale, the appropriate use of model output, and measures of uncertainty, particularly those related to natural variability. For example, impacts analysis based on the global average temperature scenarios discussed in Section 4.3.3 rather than emission or radiative forcing scenarios, that more directly connect future planning to global policy targets, may become more commonplace as the IPCC is currently working on a new report to quantify impacts under a 1.5^{o}C warming. The emergence of higher performance computing, new modeling technology, observational datasets, and advanced approaches for analyzing data including data mining and machine learning, emphasize the importance of ensuring the guidance developed in this project will not become obsolete in the near future.

Over the next few years, other efforts underway tend to fall into four main categories: advances in climate information, observations, global models, and downscaling. GCM output used in engineering design will require update as simulations from CMIP6 and subsequent CMIP phases with enhanced resolution and updated future emissions scenarios become available and are downscaled and/or bias-corrected to relevant scales. For most future projections, the framework established in Section 4.3 can be used to determine which scenario(s), GCMs, and downscaling approaches to use, that is, consider as many models as possible, a range of representative scenarios, and an appropriate downscaling method. Below, known efforts are summarized and specific recommendations made for remaining up to date in each category.

First, in terms of the climate information required as input to Level 1 and 2 analyses, the latest U.S. National Climate Assessments will provide updated information on observed and projected trends and impacts for regions and sectors across the United States. NCA4 Vol. 1 was released in November 2017, and Vol. 2 is scheduled for release in December 2018. The IPCC Sixth Assessment Report is due to be released in 2022 and will contain further updates on observed and projected change at the global to regional scale. In addition, a special IPCC report is underway to quantify the impacts of a 1.5^{o}C warming consistent with the lower target of the Paris Agreement. And finally, new studies are being published in the peer-reviewed literature every day, many of which will contain relevant information on observed historical trends and future projections for specific variables and/or regions relevant to future analyses. While conducting a running and continuous evaluation of the peer reviewed literature is beyond the reasonable capacity of any program, there is value in maintaining a list of the latest and most up-to-date assessment and synthesis products available for the United States and for specific regions and states within the United States. Currently, a product compendium is not produced at a national level; **we recommend that both the engineering and climate science community consider strategies for creating and maintaining such a resource to support future updates to guidance on climate adaptation for transportation projects as well as other sectors**.

Second, in terms of the historical observations required as input to Level 2 through 4 analyses, these are increasing in extent as well as resolution and spatial coverage with each new satellite instrument or observing system, as well as with ongoing analyses and synthesis of existing observations. Lists of available datasets are typically maintained by NOAA. For example, a new observational precipitation dataset of 15-minute, 1-km areal average precipitation values derived from radar data from 1998 to present will be made available by NOAA through its NOAA Big Data Project (https://www.ncdc.noaa.gov/data-access/radar-data/noaa-big-data-project). This dataset will be useful for evaluation of the NA-CORDEX hourly precipitation data, as well as to provide input to a new generation of statistical downscaling methods and sub-daily projections. **We recommend maintaining a list of the latest and most up to date station and gridded observational products available for the United States.**

Third, in terms of the global climate model simulations that serve as the basis for climate projections, experimental simulations are constantly being conducted by various modeling groups but the simulations used for impact analyses should be obtained from the CMIP archives, as these provide the standard set of model output for use in engineering design. If possible, all GCMs should be still considered. When necessary to reduce the dimensionality of the input, a range of GCMs should still be used. Selection of the "best" models is to be avoided. The three GCM classifications described in Section 4.3.2 are recommended for upcoming CMIP phases. If available, climate experts can classify new GCMs and reclassify GCMs used in previous CMIP

phases. In the absence of expert guidance, GCMs that were previously identified as Group 1 models should remain in Group 1. New models should be categorized as Group 3. GCMs included in future CMIP phases that were previously categorized as Group 2 and Group 3 for CMIP5 may remain in the same category or become a Group 1 model if new peer-reviewed literature is able to show robust evaluations of the models. **We recommend prioritizing GCM simulations from Group 1-Type models for analyses where capacity is limited. If capacity is available, simulations from Group 2-Type models can be added.**

Although CMIP5 is the most recent archive, some of the recommended downscaled products were developed from CMIP3 simulations, and many pre-existing analyses also use CMIP3. Because there are minimal differences in CMIP3 and CMIP5 extreme precipitation across the United States, products generated from either or both archives can be used, particularly where resources are available to draw from a large ensemble that covers a broad range of variability. **We recommend using GCM simulations from the CMIP3 archive and onwards. While simulations from the most recent CMIP archive should be prioritized, CMIP3 simulations can be used if appropriate resources (including downscaled datasets and/or previously published analyses) are not available for more recent CMIPs and/or if the analysis is able to incorporate simulations from all available GCMs.**

Fourth, in terms of the scenarios used to drive global model simulations, it is unlikely that probabilities will be assigned to future scenarios. However, observed changes since the development of the RCPs used in CMIP5 may make some of those possible futures more or less likely, and inform the selection of scenarios from CMIP5 – just as changes since the SRES scenarios were developed informed the RCP scenarios. FHWA recommends use of a middle to above-middle scenario from the latest set of scenarios for design and a range of scenarios if the project justifies it (Kilgore et al. 2016). Using the nomenclature of the most current set of RCP pathways, RCP6.0 represents the middle to above-middle scenario. However, when a dataset does not include RCP6.0 output or equivalent, bracketing scenarios should be considered (i.e., RCP4.5 and RCP8.5). Traditionally, design guidance reflects the infrastructure criticality and informs whether the most pessimistic scenario or the most optimistic scenario is more appropriate than a mid-range scenario. **We recommend that users continue to consider at least two scenarios that cover a range from lower to higher, with appropriate emphasis on the greater risks of over- versus under-preparation for the given analysis.**

And lastly, regional climate models and empirical-statistical downscaling methods used to generate higher-resolution climate projections from global model output are advancing. For example, a dataset of gridded hourly precipitation projections at 0.44°, 0.22°, and 0.11° resolution generated by RCMs for the North American Coordinated Regional Climate Downscaling Experiment (NA-CORDEX) project is expected to be released in the next few years. Similarly, a dataset of more than 10,000 stations as well as gridded projections at 1/16th degree resolution covering North America using the new nonparametric STAR-ESDM (Stoner and Hayhoe, personal communication) is expected in 2019. Additional efforts similar to the NASA-NEX dataset, in which satellite data was downscaled using an ESDM, are also likely. **As described in Section 4.2.9, we recommend using high-resolution climate projections that are appropriate for the characteristics of the analyses. We also recommend updating Table** 4.4**, Table 4.6, and Table 4.8, which provide a complete list of available high-resolution datasets for the United States, at least every 5 years.** Currently, a product compendium equivalent to these tables is not produced at a national level; we recommend that an equivalent

resource be produced and maintained by the climate science community or NOAA to support climate adaptation for transportation projects as well as other sectors.

4.4.2 WMO Climatological Standard Normal Updates and Guidance

Summary statistics of both historical and future climate variables can be used to characterize climate over climatological time scales of 20 to 30 years. The World Meteorological Organization (WMO) provides an example of standards for climatological periods that may be applied or modified for application to engineering design. Historical climate normals have traditionally been summary statistics generated using 30-year periods that are updated every 10 years with the last year of the period ending with 0, such as January 1, 1971 to December 31, 2000. These *normals* provide a benchmark for comparison of recent observations, and are widely used as a predictive indicator of future conditions.

The WMO updated their definition of the standard climate normal: "The Climatological Standard Normal be calculated every 10 years at the start of every new decade having year digit 1; to serve as the updated official Climatological Standard Normal; that it applies to the most recent 30-year period, with 1981–2010 being the new current standard; and that for specific purpose of long-term climate change monitoring, the period 1961–1990 be retained as a reference period in perpetuity or until such time as a compelling scientific case to change it arises" (WMO 2018). This effectively established two types of climatalogical normals: the standard sliding period, and a fixed mid-20th century period (1961–1990). The WMO recommends that this fixed reference period should serve as reference period for analyzing climate change.

Future period(s) of interest can be identified in a similar manner, and statistics for these periods compared to baseline historical conditions. Future period(s) should include years at the end of the design lifetime, using a climatological period of 20 to 30 years that brackets that design lifetime. HEC-17 recommends baseline periods of at least 30 and preferably 50 years. HEC-17 additionally notes that, “there is also a risk that the sub-periods will be sufficiently short that they merely capture natural wet and dry periods that have been observed in the historic record rather than long-term nonstationary behavior. Further investigation of the validity of considering sub-periods for design purposes is a recommended future research effort.”

When using future projections, however, there are two reasons why this recommendation is overly narrow. First, for regions and variables with rapid trends, a 50-year and even potentially a 30-year period, compared to 20 years, may underestimate the rate of change. And second, as discussed in detail above, using multiple GCM simulations, particularly large ensembles for a given scenario, can significantly increase the sample variability available for the 20 to 30-year period – compare, for example, use of a single simulation (365 days times 20 years = 7,300 data points) with using 50 simulations (365,000 data points).

The use of climatological periods does address the uncertainty in future projections due to natural variability and climate projections, particularly if combined with large ensembles. Projected precipitation from the climatological period may be compared to a historical climatological period in order to determine whether the engineering design is likely to be significantly or notably altered under future climate conditions compared to historical data. Thus, a consistent definition of the historical period should be developed. The WMO reference period provides a reasonable period to use when transportation engineering does not have an existing standard for the analysis period. For example, the standard practice for Bulletin 17C and NOAA

Atlas 14 is to use all available historical data to estimate streamflow and precipitation extremes, respectively, and this document does not recommend changing that standard. However, the WMO reference period may be reasonable for hydrologic modeling studies or water quality analyses that do not have a specific standard. In addition, if analyses are conducted that compare observations or modeled data to a reference period, then the 1961–1990 WMO reference period is recommended as the default standard. While this period is intended to be a fixed period, the WMO may change it in the future. Thus, the current reference period should be confirmed prior to application by checking for updates to the WMO Guide to Climatological Practices at the WMO website:

http://www.wmo.int/pages/prog/wcp/ccl/guide/guide_climat_practices.php#updates

or by registering to receive update notices at:

http://www.wmo.int/pages/prog/wcp/ccl/guide/guide_climat_practices-registration.php

Chapter 5. Temporal and Spatial Adaptation of Projected Precipitation for Rainfall/Runoff Modeling

Increasingly, engineers, hydrologists, and other users of hydrologic technology must estimate discharge associated with a particular risk (or set of risks) to design a hydraulic structure or stormwater management facility. The desired value is often a peak discharge of runoff from a watershed with a particular annual exceedance probability (AEP). The AEP is the probability that the particular event of interest (peak discharge) will be equaled or exceeded each year.

This chapter discusses the precipitation inputs required for the use of hydrologic rainfall/runoff models. In some cases, an engineer requires these inputs on a daily time step, and in other situations, the engineer requires the data at a more temporally disaggregated sub-daily level of detail. Historical daily precipitation data are widely available, and historical sub-daily precipitation data are commonly available in the form of Intensity-Duration-Frequency (IDF) curves.

The development of IDF curves requires estimating the AEP of precipitation depths for durations ranging from 5 minutes to 24 hours using a variety of frequency distributions (e.g., Gumbel, Generalized Extreme Value, and log-Pearson Type III) and fitting methods (method of moments, maximum likelihood method, and L-Moments). The many IDF curves currently available for hydrologic design reflect this work based on historical conditions.

In addition, engineers have relied on the assumption of stationarity to apply historical information to future periods during which the transportation infrastructure will serve its intended purpose. However, with projections of a changing climate, engineers may need to consider the future without relying on stationarity. To accomplish this, engineers using rainfall/runoff models need estimates of daily and sub-daily precipitation as inputs at watershed-level spatial scales. As discussed in Chapter 4, suitable downscaled output from Global Climate Models (GCMs) is limited at a daily time-scale and is even more limited at a sub-daily time scale. Downscaled GCM output is also generally available on a spatial scale greater than required to model smaller watersheds.

If an engineer uses a hydrologic methodology that requires a 24-hour storm event (such as some of the Natural Resources Conservation Service [NRCS] distributions) or if the watershed is sufficiently large so that a 24-hour time step is appropriate, then the lack of projected sub-daily precipitation data is not problematic. However, for event-based or design storm modeling of small watersheds, estimates of projected sub-daily precipitation are necessary for hydrologic design of hydraulic structures, stormwater management facilities, and water quality analyses.

All of the rainfall/runoff modeling tools available to the practicing engineer for the design of highway drainage structures are based on the use of widely available historical precipitation data. To use these tools for evaluating potential future climate scenarios, it is necessary to identify common or overlapping domains in time and space between historical observations and GCM output and then find methods to adapt future climate data into the time and space resolution needed for the use of existing tools.

This chapter addresses techniques for estimating future sub-daily and daily precipitation data and offers recommendations for actionable guidance in these areas. Section 5.1 addresses a method

for estimating projected 24-hour duration precipitation. Section 5.2 addresses the identification, development, and application of sub-daily precipitation estimates. Finally, Section 5.3 describes methods for adapting the spatial scales of downscaled GCM output to watershed scales that engineers require.

A common theme of the recommendations in this chapter is the continued reliance on existing (stationary) engineering tools for rainfall/runoff modeling to adapt downscaled GCM output to temporal and spatial scales required for modeling of small watersheds. While these approaches rely on stationarity to varying degrees, they are actionable strategies for estimating the effects of future conditions on hydrologic designs until such time as nonstationary engineering design approaches are developed and accepted.

5.1. Projected 24-Hour Precipitation

This section describes a method for estimating a projected 24-hour precipitation design quantiles including, but not limited to, the 0.5, 0.1, 0.04, and 0.01 AEP. This method is appropriate for projects requiring a Level 3 analysis and some Level 4 analyses (see Chapter 3) to estimate a 24-hour duration precipitation as an input to rainfall/runoff modeling and other applications. The procedure also results in projected 24-hour precipitation confidence limits for each future scenario evaluated by the design team. As recommended in Chapter 4, the design team should evaluate multiple future climate scenarios, when feasible, to provide a more comprehensive understanding of possible future precipitation estimates.

5.1.1. Method

The recommended method is useful for estimating a future 24-hour duration rainfall frequency curve (RFC) with a range of AEP quantiles or for estimating a single future AEP quantile for one or more future scenarios. The method adjusts the historical observed AEP quantiles taken from established sources of historical precipitation data to future conditions based on information from high-resolution climate modeling datasets. Scenarios are used as input to GCMs, and GCM outputs are downscaled to create high-resolution climate modeling datasets also referred to as downscaled GCM output as described in Chapter 4.

Figure 5.1 summarizes the ten-step procedure. The procedure includes two loops repeated at the discretion of the design team based on the number of future scenarios and high-resolution climate modeling datasets (GCMs) determined to be appropriate for the project. As shown in Figure 5.1, Steps 5 through 9 are repeated for each future scenario considered, and Steps 5 and 6 are repeated for each GCM evaluated within a scenario. The following list summarizes each step, with more detail for each step provided after the summary:

1. Determine the historical observed 24-hour precipitation RFC (or single AEP quantile if only one is required) for the site.
2. Select baseline and future periods for analysis appropriate for the plan or project.
3. Identify the future scenarios and downscaled GCM outputs of interest from the most appropriate database of high-resolution climate projections using the recommendations in Chapter 4.

4. Determine the number of grid cells required to cover adequately the watershed of interest.
5. Acquire the daily precipitation values and extract an annual maximum series (AMS) for each grid cell for the selected future scenario and downscaled GCM output dataset. Adjust the AMS to unconstrained point values with an areal reduction factor and an unconstrained 24-hour correction factor appropriate for the location.
6. Compute the 24-hour precipitation RFC (or single AEP quantile) for the baseline period and for the future period from the AMS from Step 5 for each grid cell using an appropriate statistical distribution.
7. Repeat Steps 5 and 6 for each individual GCM simulation identified in Step 3. The result of this step is a set of estimates for a 24-hour RFC (or single AEP quantile) for each grid cell and each downscaled GCM output for both the baseline and future periods for the selected scenario.
8. Compute the ratios of the modeled (GCM based) future 24-hour precipitation RFC (or single AEP quantile) to the modeled baseline 24-hour precipitation RFC (or single AEP quantile) for all grid cells and simulations.
9. Estimate the projected 24-hour precipitation RFC (or single AEP quantile) from the historical observed 24-hour precipitation RFC (or single AEP quantile) from Step 1 and the ratio(s) from Step 8.
10. Repeat Steps 5 through 9 for each future scenario identified in Step 3.

In ***Step 1***, the engineer determines the appropriate source for the historical observed quantile estimates based on established guidance and datasets. Examples of such datasets include the National Oceanic and Atmospheric Administration (NOAA) Atlas 14 or a precipitation gauge at the site with a long record. Based on the appropriate source, the engineer estimates the 24-hour quantiles (the RFC) or a single AEP quantile based in the historical record in the same manner this task is accomplished without consideration of climate change. The engineer should also note the period of record for the source data for use in Step 2. As with most historical precipitation data sources, the historical record is based on gauging records of different lengths.

For large watersheds, the engineer may choose to estimate projected precipitation quantiles for multiple locations in the watershed. The engineer should base this decision on the level of disaggregation appropriate for the watershed when performing a hydrologic analysis without consideration of climate change. That is, the level of disaggregation required for an appropriate hydrologic analysis is generally not affected by potential changes in precipitation resulting from climate change.

In ***Step 2***, the engineer selects appropriate baseline and future periods for analysis. The baseline period should overlap as closely as possible the period of record used to develop the historical dataset selected in Step 1. For example, if the observed data from Step 1 covered a period from 1965 through 2010, the appropriate baseline period should be that entire period or a subset, but not less than 30 years. (Most volumes of NOAA Atlas 14 include data from 1948 to about 2005.)

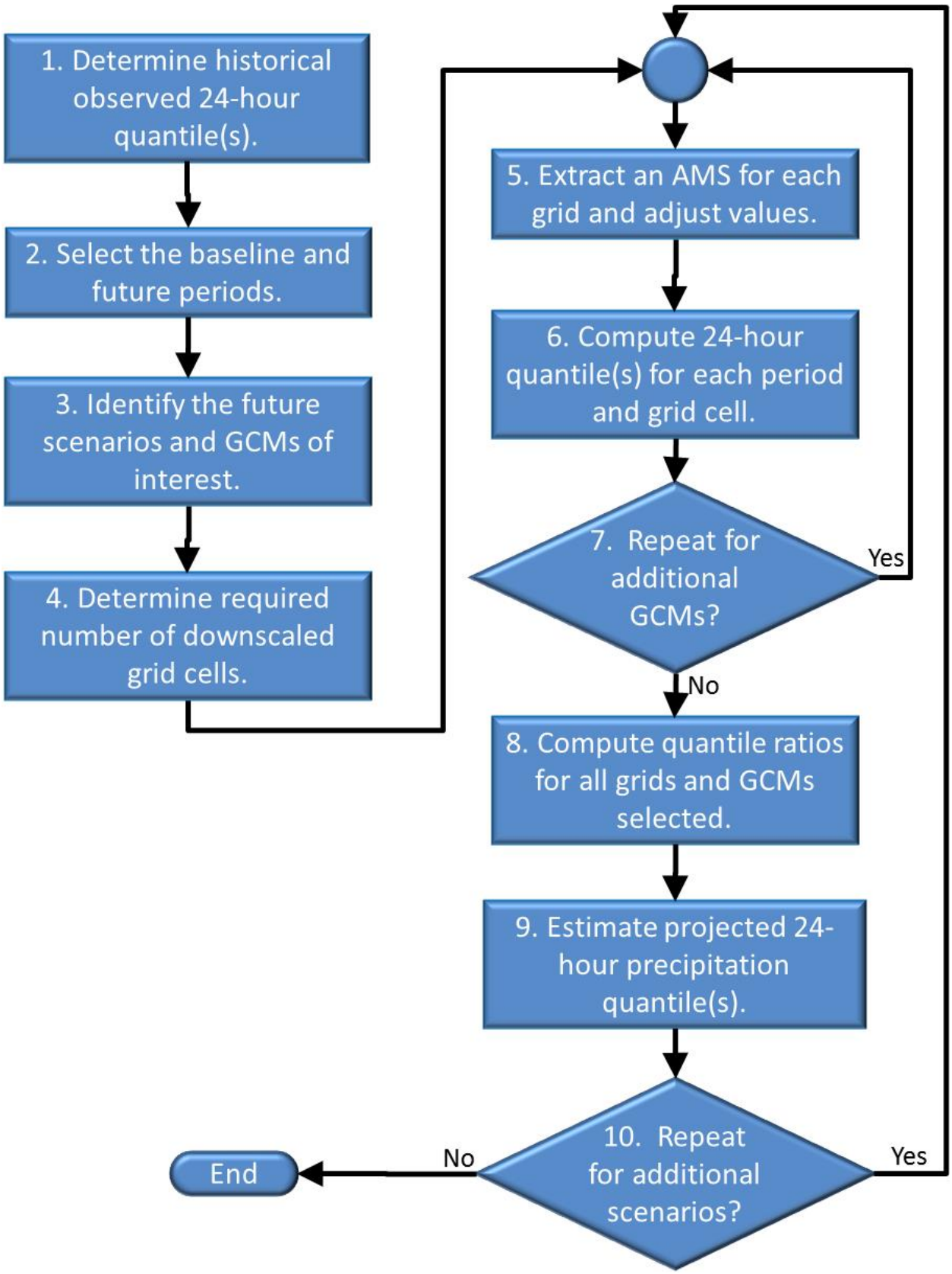

Figure 5.1. Recommended procedure for projecting 24-hour precipitation quantiles.

The engineer defines the future period considering the expected service life of the project. For example, the future period might begin as early as the end of the baseline period and extend through 2100. The entire projected record could be defined as the future period or a subset, but not be less than 30 years. A minimum of 30 years is recommended for both the baseline and future periods because the climate science community generally uses 30 years for defining a climatological period. (A climatological period is a length of time within which the statistical characteristics of a given climate are considered representative for that period.)

When selecting a future period, the engineer should consider the possibility that later periods may not always result in more extreme annual peak precipitation estimates than earlier periods. Therefore, it is recommended that the engineer inspect the behavior of the AMS developed in Step 5 before finalizing the selection of the future period. A visual inspection of a graphical representation of the AMS versus time is appropriate for this purpose.

In ***Step 3,*** the engineer or design team selects the future scenarios and GCMs to support the analysis. The use of multiple GCMs for each scenario allows analysis of scientific uncertainty as expressed by the variability of estimates among GCMs. Evaluation of multiple future scenarios permits assessment of the effects of alternative futures on the plan or design. Chapter 4 provides guidance for selecting appropriate high-resolution climate datasets as well as future scenarios and GCMs.

In ***Step 4,*** the engineer determines the high-resolution climate dataset grid cells required to cover the watershed of interest. (The high-resolution climate datasets recommended for this procedure are organized in a grid format with each grid defined by fractions of degrees latitude and longitude.) The engineer identifies the required grid cells by overlaying the climate projection grid on the watershed. For smaller watersheds, a single grid cell may be larger than the watershed and fully cover it. For larger watersheds, multiple grid cells may be required to cover the watershed. If the number of grid cells required to cover the watershed is less than three, it is recommended that three grid cells covering or adjacent to the watershed be identified. This minimum is recommended so that if there are anomalies in the data associated with a single grid cell, the engineer is more likely to identify the anomalies.

In ***Step 5***, the engineer acquires the daily precipitation values from one of the selected high-resolution climate projection datasets for the first of the selected scenarios and the first of the selected GCMs for each grid cell. For example, data from the Localized Constructed Analogs (LOCA) dataset recommended in Chapter 4 may be downloaded from the Downscaled CMIP3 and CMIP5 Climate and Hydrology Projections (DCHP) website (https://gdo-dcp.ucllnl.org/downscaled_cmip_projections/dcpInterface.html#Welcome). The LOCA dataset includes daily precipitation values from 1950 through 2100.

From the downloaded daily outputs, the engineer creates the ***unadjusted*** AMS for each grid cell for the entire downloaded period (historical and future) by taking the largest daily value from each year and discarding the other daily values. The engineer creates the ***adjusted*** AMS series by making two corrections to each value in the unadjusted AMS: 1) conversion from constrained daily values to unconstrained 24-hour values and 2) conversion from spatially averaged values to point values. HEC-17 describes both adjustments (Kilgore et al. 2016).

In ***Step 6***, the engineer separately estimates the 24-hour precipitation RFC (or single AEP quantile) from the AMS for the baseline and future periods for each grid cell. Estimating the 24-

hour quantile(s) requires the use of an appropriate statistical distribution. HEC-17 provides guidance for selecting an appropriate distribution (Kilgore et al. 2016).

In ***Step 7***, the engineer repeats Steps 5 and 6 for each simulation (GCM/scenario combination). In general, including a larger ensemble of GCMs provides a greater opportunity to capture variability in the projections and generate more representative confidence limits for the estimates for the chosen future scenario. (See Chapter 4 for more information about GCM ensembles.)

In ***Step 8***, the engineer computes the ratio of the future and baseline modeled 24-hour quantiles for each grid cell and each simulation as described in Equation 5.1.

$$RFB_{q,n,m} = \frac{PF_{q,n,m}}{PB_{q,n,m}} \tag{5.1}$$

where:

$RFB_{q,n,m}$ = *Ratio of the future to baseline 24-h precipitation quantile for grid (n), model (m).*

$PF_{q,n,m}$ = *Future 24-h precipitation quantile for grid (n), model (m).*

$PB_{q,n,m}$ = *Baseline 24-h precipitation quantile for grid (n), model (m).*

The subscripts in the equation indicate the following:

- The subscript (*n*) indicates the grid cell and ranges from 1 to the number of grid cells (N).
- The subscript (*m*) indicates the GCM from which the estimate is derived and ranges from 1 to the number of models (M).
- The subscript (*q*) indicates the quantile, e.g., 0.5, 0.1, 0.04, and 0.01 AEP.

The computations for Step 8 generate a total of N x M ratios for a single AEP as illustrated in Table 5.1. These ratios represent estimates of the change in the future 24-hour precipitation quantile compared with the baseline 24-hour precipitation quantile for each grid cell based on each GCM. As shown in Table 5.1, the information for each grid cell should be analyzed to estimate useful statistics such as the mean ratio (assuming that each model output is equally likely) and upper and lower confidence limits of the ratios (assuming a normal distribution) for a given grid cell.

Table 5.1. Example matrix of future/baseline ratios by grid cell and model for a future scenario.

	Model (m = 1, 2,…, M)						
Grid Cell (n = 1, 2,…, N)	**1**	**2**	**…**	**M**	**Mean**	**Lower Confidence Limit (LCL)**	**Upper Confidence Limit (UCL)**
1	$RFB_{q,1,1}$	$RFB_{q,1,2}$	…	$RFB_{q,1,M}$	$\overline{RFB}_{q,1}$	$RFB_{q,1}^{LCL}$	$RFB_{q,1}^{UCL}$
2	$RFB_{q,2,1}$	$RFB_{q,2,2}$	…	$RFB_{q,2,M}$	$\overline{RFB}_{q,2}$	$RFB_{q,2}^{LCL}$	$RFB_{q,2}^{UCL}$
…	…	…	…	…	…	…	…
N	$RFB_{q,N,1}$	$RFB_{q,N,2}$	…	$RFB_{q,N,M}$	$\overline{RFB}_{q,N}$	$RFB_{q,N}^{LCL}$	$RFB_{q,N}^{UCL}$

The engineer evaluates the information in the table to confirm consistency among the means, lower confidence limits, and upper confidence limits between the grid cells. For example, if all of the grid cell mean ratios typically range from 1.2 to 1.5 except for a single grid cell that has a significantly different ratio of 2.5, then the engineer should examine the outlier grid cell to assess whether there is a reasonable explanation for the departure from the other grid cells.

If a single estimate of precipitation was considered appropriate to represent the watershed in Step 1, then a single estimate of the mean ratio from Table 5.1 is usually sufficient for assessing potential effects of climate change. However, the level of spatial disaggregation of precipitation determined in Step 1 may be modified if large variations in the ratios are observed as a function of location in the watershed. Depending on this evaluation, the selected *RFB* value for each quantile may represent a watershed average of the ratios or may spatially vary.

In most cases, the engineer will select the mean estimate of the ratio for each quantile for use in Step 9. The engineer should also use the ratios from the lower and upper confidence limits to consider design sensitivity to the variation in downscaled GCM outputs for that future scenario.

In ***Step 9***, the engineer estimates the projected 24-hour precipitation quantile(s) by multiplying the historical precipitation quantile from Step 1 by the ratio of future to baseline model estimates from Step 8 as shown here:

$$P_{q,p} = P_{q,h}\left(RPB_q\right) \tag{5.2}$$

where:

$P_{q,p}$ = *Projected 24-hour precipitation quantile.*

$P_{q,h}$ = *Historical 24-hour precipitation quantile.*

RFB_q = *Ratio of the model future to model baseline 24-hour precipitation quantile.*

Equation 5.2 is not recommended for quantiles more extreme than the 0.1 AEP quantile because the current ability of high-resolution climate datasets to represent precipitation extremes (in the engineering hydrology sense) is limited. Therefore, Equation 5.3 is recommended for more extreme quantiles, including the 0.04 and 0.01 AEP quantiles. In this equation, the ratio associated with 0.1 AEP quantile is substituted for the ratios estimated for the more extreme quantiles:

$$P_{q,p} = P_{q,h}(RPB_{0.1}) \tag{5.3}$$

where:

$RFB_{0.1}$ = *Ratio of the model future to model baseline for the 24-hour precipitation 0.1 AEP quantile.*

The engineer should also consider the uncertainty in the estimate(s) of the projected 24-hour precipitation quantile(s) by using the upper and lower confidence limits of the ratios. This will provide insight into the potential variation in these estimates resulting from scientific uncertainty based on the ensemble of GCMs.

In ***Step 10***, the engineer repeats Steps 5 through 9 for each additional future scenario selected in Step 3. Analysis of multiple scenarios provides further insight into potential future precipitation and the resultant vulnerabilities of infrastructure. In general, the longer the relevant service life,

the more important it is to consider multiple scenarios, as differences between scenarios become most apparent after mid-century.

5.1.2. Example

This example illustrates application of the ten-step procedure for estimating future 24-hour duration precipitation quantiles. The site is a small watershed in the Denver, Colorado, region (latitude = 39.6875 degrees, longitude = -104.8125 degrees).

Step 1. Determine the historical observed 24-hour precipitation RFC (or single AEP quantile if only one is required) for the site.

NOAA Atlas 14 is used to determine the historical 24-hour precipitation quantiles for the site. Table 5.2 summarizes the results for four AEPs from the existing RFC. The table also shows the corresponding lower (5 percent) and upper (95 percent) confidence limits from NOAA Atlas 14 for each quantile.

Table 5.2. NOAA Atlas 14 24-hour precipitation quantiles for Denver, Colorado, example.

AEP	P (in)	5% Confidence Limit (in)	95% Confidence Limit (in)
0.5	1.84	1.52	2.22
0.1	3.00	2.56	3.65
0.04	3.72	2.96	4.69
0.01	4.89	3.67	6.37

Step 2. Select baseline and future periods for analysis appropriate for the plan or project.

The engineer selects a baseline period of 1950 through 1999, which roughly corresponds to the period of record for NOAA Atlas 14. The engineer also selects two future periods to compare potential variation introduced by future period selection: 1) the first half of the 21st century (2000 through 2049) and 2) the second half of the 21st century (2050 through 2099). As described in the description of the method, baseline and future periods should be at least 30 years.

Step 3. Identify the future scenarios and downscaled GCM outputs of interest from the most appropriate database of high-resolution climate projections using the recommendations in Chapter 4.

The RCP6.0 scenario is selected for illustrating the method. The engineer should also consider a second scenario to evaluate sensitivity of results between scenarios. For the RCP6.0 scenario, an ensemble of 12 GCMs from the CMIP5 archive will be used. The downscaled Bias-Correction Constructed Analogues (BCCA) information was used for this analysis. Results from LOCA or other downscaled datasets will differ, but the methodology is the same.

Step 4. Determine the number of grid cells required to adequately cover the watershed of interest.

Since the watershed is small, one grid cell is sufficient to cover the watershed. Two additional cells should also be analyzed per the recommendations to ensure that the analyzed cell is not an outlier; however, only the computations for the single cell will be illustrated in this example.

Step 5. Acquire the daily precipitation values and extract an annual maximum series (AMS) for each grid cell for the selected future scenario and downscaled GCM output dataset. Adjust the AMS to unconstrained point values with an areal reduction factor and an unconstrained 24-hour correction factor appropriate for the location.

The engineer downloads the data from the DCHP website described earlier and extracts the AMS for each GCM. The engineer adjusts the AMS values to unconstrained point values by multiplying the unadjusted values by an areal reduction factor (1.04) and an unconstrained 24-hour correction factor (1.13). See Section 5.3.3 for the areal reduction factor and Kilgore et al. (2016) for information on the unconstrained 24-hour correction factor.

Step 6. Compute the 24-hour precipitation RFC (or single AEP quantile) for the baseline period and for the future period from the AMS from Step 5 for each grid cell using an appropriate statistical distribution.

The engineer estimates the RFC, represented by the 0.5, 0.1, 0.04, and 0.01 AEP quantiles, from the AMS from each high-resolution dataset (model) and summarizes the results in Table 5.3, Table 5.4, and Table 5.5 for the baseline period, the first future period, and the second future period, respectively. These tables also summarize the mean, standard deviation, and skew estimated for each model and period.

Because of the variation in moments across models, most notably the skew, the estimated quantiles also vary across models. However, all models underestimate the quantiles for the baseline period (Table 5.3) compared with the NOAA Atlas 14 values (Table 5.2). This is one reason that high-resolution climate datasets are never used directly, but always as differences or ratios between future and baseline periods. This methodology uses ratios.

Step 7. Repeat Steps 5 and 6 for each individual GCM simulation identified in Step 3. The result of this step is a set of estimates for a 24-hour RFC (or single AEP quantile) for each grid cell and each downscaled GCM output for both the baseline and future periods for the selected scenario.

The tables referenced in Step 6 show the results for each of the models (high-resolution datasets). Only one cell is used for this example, but a minimum of three is recommended in the procedure.

Step 8. Compute the ratios of the modeled (GCM based) future 24-hour precipitation RFC (or single AEP quantile) to the modeled baseline 24-hour precipitation RFC (or single AEP quantile) for all grid cells and simulations.

Table 5.6 and Table 5.7 summarize the computed ratios for the 2000-2049 and 2050-2099 periods, respectively. By considering an ensemble of GCMs, the engineer can evaluate the varied outcomes from different models. Referencing the ratios from the first future period to the baseline period (Table 5.6) the following outcomes are notable in this example from Denver:

- The Model 1 ratios show a ***decline*** in the ratios from 1.21 for the 0.5 AEP to 1.07 for the 0.01 AEP. This result suggests that the RFC will ***flatten*** in the future compared with the historical RFC.

Table 5.3. Estimated moments and quantiles for the baseline period (1950-1999).

Quantity	Model 1	Model 2	Model 3	Model 4	Model 5	Model 6	Model 7	Model 8	Model 9	Model 10	Model 11	Model 12
Mean	0.0291	-0.0051	0.0077	0.0160	-0.0286	0.0034	0.0013	0.0001	-0.0089	0.0044	-0.0001	0.0442
Standard Deviation	0.1381	0.1504	0.1437	0.1606	0.1387	0.1497	0.1501	0.1507	0.1404	0.1500	0.1517	0.1586
Skew	0.6	0.4	-0.1	0.3	-0.7	-0.1	0.2	0.6	0.6	0.1	0.7	-0.4
AEP=0.5 Precip. (in)	1.04	0.97	1.02	1.02	0.97	1.01	0.99	0.97	0.95	1.00	0.96	1.13
AEP=0.1 Precip. (in)	1.63	1.56	1.55	1.68	1.37	1.56	1.57	1.59	1.51	1.58	1.59	1.74
AEP=0.04 Precip. (in)	1.98	1.90	1.80	2.06	1.51	1.82	1.88	1.96	1.83	1.87	1.99	1.99
AEP=0.01 Precip. (in)	2.57	2.44	2.15	2.66	1.67	2.19	2.36	2.60	2.39	2.31	2.68	2.32

Table 5.4. Estimated moments and quantiles for the future period (2000-2049).

Quantity	Model 1	Model 2	Model 3	Model 4	Model 5	Model 6	Model 7	Model 8	Model 9	Model 10	Model 11	Model 12
Mean	0.0995	-0.0152	0.0102	0.0121	0.0245	0.0063	0.0432	0.0301	0.0177	0.0196	-0.0094	0.0281
Standard Deviation	0.1412	0.1330	0.1332	0.1650	0.1594	0.1502	0.1375	0.1393	0.1425	0.1406	0.1171	0.1766
Skew	0.1	-0.1	0.2	0.4	-0.2	0.5	0.2	0.1	-0.1	0.1	-0.1	0.6
AEP=0.5 Precip. (in)	1.25	0.97	1.01	1.00	1.07	0.99	1.09	1.07	1.05	1.04	0.98	1.02
AEP=0.1 Precip. (in)	1.91	1.42	1.53	1.70	1.68	1.60	1.67	1.62	1.58	1.59	1.38	1.83
AEP=0.04 Precip. (in)	2.25	1.63	1.79	2.10	1.96	1.96	1.96	1.90	1.83	1.86	1.55	2.35
AEP=0.01 Precip. (in)	2.74	1.92	2.19	2.78	2.35	2.57	2.42	2.31	2.18	2.27	1.80	3.27

Table 5.5. Estimated moments and quantiles for the future period (2050-2099).

Quantity	Model 1	Model 2	Model 3	Model 4	Model 5	Model 6	Model 7	Model 8	Model 9	Model 10	Model 11	Model 12
Mean	0.0604	-0.0059	0.0327	0.0264	0.0624	-0.0045	0.0019	0.0780	0.0612	-0.0251	0.0334	0.0425
Standard Deviation	0.1662	0.1490	0.1418	0.1390	0.1377	0.1547	0.1566	0.1440	0.1356	0.1646	0.1147	0.1728
Skew	0.0	-0.4	0.3	0.2	-0.1	0.0	0.8	0.0	0.3	-0.4	0.1	0.0
AEP=0.5 Precip. (in)	1.15	1.01	1.06	1.05	1.16	0.99	0.96	1.20	1.13	0.97	1.08	1.10
AEP=0.1 Precip. (in)	1.88	1.50	1.65	1.61	1.73	1.56	1.63	1.83	1.73	1.51	1.52	1.84
AEP=0.04 Precip. (in)	2.25	1.71	1.97	1.90	1.99	1.85	2.06	2.14	2.05	1.73	1.73	2.21
AEP=0.01 Precip. (in)	2.57	2.44	2.15	2.66	1.67	2.19	2.36	2.60	2.39	2.31	2.68	2.32

Table 5.6. Estimated quantile ratios future period (2000-2049) to baseline.

Quantity	Model 1	Model 2	Model 3	Model 4	Model 5	Model 6	Model 7	Model 8	Model 9	Model 10	Model 11	Model 12
AEP=0.5 Ratio	1.21	1.00	0.99	0.98	1.10	0.97	1.10	1.10	1.10	1.04	1.02	0.90
AEP=0.1 Ratio	1.17	0.91	0.98	1.01	1.23	1.03	1.06	1.02	1.05	1.01	0.87	1.05
AEP=0.04 Ratio	1.13	0.86	1.00	1.02	1.30	1.08	1.04	0.97	1.00	1.00	0.78	1.18
AEP=0.01 Ratio	1.07	0.79	1.02	1.04	1.41	1.17	1.03	0.89	0.91	0.98	0.67	1.41

Table 5.7. Estimated quantile ratios future period (2050-2099) to baseline.

Quantity	Model 1	Model 2	Model 3	Model 4	Model 5	Model 6	Model 7	Model 8	Model 9	Model 10	Model 11	Model 12
AEP=0.5 Ratio	1.11	1.04	1.04	1.03	1.19	0.98	0.97	1.24	1.19	0.96	1.12	0.97
AEP=0.1 Ratio	1.15	0.97	1.07	0.96	1.26	1.00	1.03	1.15	1.15	0.95	0.95	1.06
AEP=0.04 Ratio	1.13	0.90	1.10	0.92	1.32	1.01	1.10	1.09	1.12	0.93	0.87	1.11
AEP=0.01 Ratio	1.09	0.81	1.15	0.88	1.41	1.03	1.21	0.99	1.07	0.88	0.76	1.20

- The Model 5 ratios show an ***increase*** in the ratios from 1.10 for the 0.5 AEP to 1.41 for the 0.01 AEP. This downscaled GCM output projects that the RFC will become ***steeper*** compared with the historical RFC.
- Models 3 and 4 show ***relatively constant*** ratios across the range of AEPs. These ratios are also close to unity, suggesting that the future RFC will be ***nearly the same*** as the historical RFC.
- Model 2 provides an example of ***declining*** ratios as was noted for Model 1, but also exhibits ratios that are ***less than one***. Model 2 projects that the more extreme precipitation events, e.g., AEP = 0.01, will be less than the historical precipitation amount for that AEP.

Comparing the ratios for the later future period (Table 5.7) with those for the earlier future period (Table 5.6), one would expect to see higher ratios for the later period as global mean temperatures are projected to increase under the RCP6.0 scenario. In most cases, the ratios support this hypothesis. However, in a few cases such as for Model 4 and Model 6, the opposite is estimated.

An important part of Step 8 is to assess these ratios for patterns and anomalies. Table 5.8 and Table 5.9 summarize mean, standard deviation, and confidence limits (CLs) for the ensemble of ratios for 2000-2049 and 2050-2099, respectively. In both tables, the mean values of the ratios are roughly constant across the AEPs, ranging from 1.03 to 1.04 for the early future period and from 1.04 to 1.07 for the later future period. In this example, the models with higher and lower ratios offset each other, though this may not occur at all locations and for all model ensembles.

Examination of the 90 percent confidence interval – bounded by the 5 percent and 95 percent confidence limits – shows that in both tables, the confidence interval widens as the AEP becomes more extreme. That is, the confidence interval is much wider for the 0.01 AEP compared with the 0.5 AEP. Not surprisingly, this suggests greater uncertainty in the estimates of more extreme AEPs.

Based on an assessment of the ratios, the engineer may discard models or grid cells that exhibit anomalous behavior. This assessment requires engineering judgement and the engineer should document the rationale for any discarded models or grids. For this example, none of the models are discarded.

Step 9. Estimate the projected 24-hour precipitation RFC (or single AEP quantile) from the historical observed 24-hour precipitation RFC (or single AEP quantile) from Step 1 and the ratio(s) from Step 8.

The engineer obtains the projected 24-hour precipitation quantiles from the mean values or confidence limit values of the ratios multiplied by the estimate of the existing quantiles. In this example, the existing quantiles were taken from NOAA Atlas 14 in Step 1 and are reproduced in Table 5.8 and Table 5.9. These tables also summarize estimates of the projected future quantiles using Equation 5.2 for the 0.5 and 0.1 AEP quantiles and Equation 5.3 for the 0.04 and 0.01 AEP quantiles. To illustrate a computation, the projected 0.01 AEP precipitation estimate in Table 5.9 is 1.06 x 4.89 inches = 5.18 inches.

Table 5.8. Ensemble summary of ratios and projections for 2000-2049.

AEP	Number of Models	Mean of Ratios	Std Dev. of Ratios	5% CL of Ratios	95% CL of Ratios	NOAA 14 Precip. (in)	Projected Precip. (In)
0.5	12	1.04	0.082	1.01	1.08	1.84	1.92
0.1	12	1.03	0.098	0.99	1.08	3.00	3.10
0.04	12	1.03*	0.137	0.97	1.10	3.72	3.84
0.01	12	1.03*	0.220	0.93	1.14	4.89	5.05

*Ratio of 1.03 for the 0.1 AEP should be used for the more extreme AEPs. In this case, this represents no change to the estimated ratios for these AEPs.

Table 5.9. Ensemble summary of ratios and projections for 2050-2099.

AEP	Number of Models	Mean of Ratios	Std Dev. of Ratios	5% CL of Ratios	95% CL of Ratios	NOAA 14 Precip. (in)	Projected Precip. (In)
0.5	12	1.07	0.099	1.02	1.12	1.84	1.97
0.1	12	1.06	0.101	1.01	1.11	3.00	3.18
0.04	12	1.05*	0.128	0.99	1.11	3.72	3.94
0.01	12	1.04*	0.189	0.95	1.13	4.89	5.18

*Ratio of 1.06 for the 0.1 AEP should be used for the more extreme AEPs. In this case, 1.06 is greater than the estimated ratios for these AEPs.

Figure 5.2 displays the projected precipitation quantiles along with the NOAA Atlas 14 historical AEP precipitation estimates. For this example, the projected change in 24-hour precipitation using the RCP6.0 scenario is not significant. In the context of the confidence limits for the NOAA Atlas 14 estimates in Table 5.2, the projected change in the 0.01 AEP precipitation is well within the 90 percent confidence interval based on the historical record (3.67 to 6.37 inches). Therefore, it may be advisable for the engineer in this example to evaluate project sensitivity to the variability in the historical record using the NOAA Atlas 14 confidence limits rather than focusing on the projections of future precipitation under climate change scenarios. Alternatively, further analysis in this example of this future scenario could be conducted using the 95 percent confidence limit ratios to estimate alternative projected estimates.

Step 10. Repeat Steps 5 through 9 for each future scenario identified in Step 3.

In this Denver example, the initial analysis was conducted using RCP6.0. It is recommended that more than one scenario be evaluated when the project and resources justify further analysis. In this case, the first scenario did not result in significant changes in the estimates of the 24-hour precipitation quantiles.

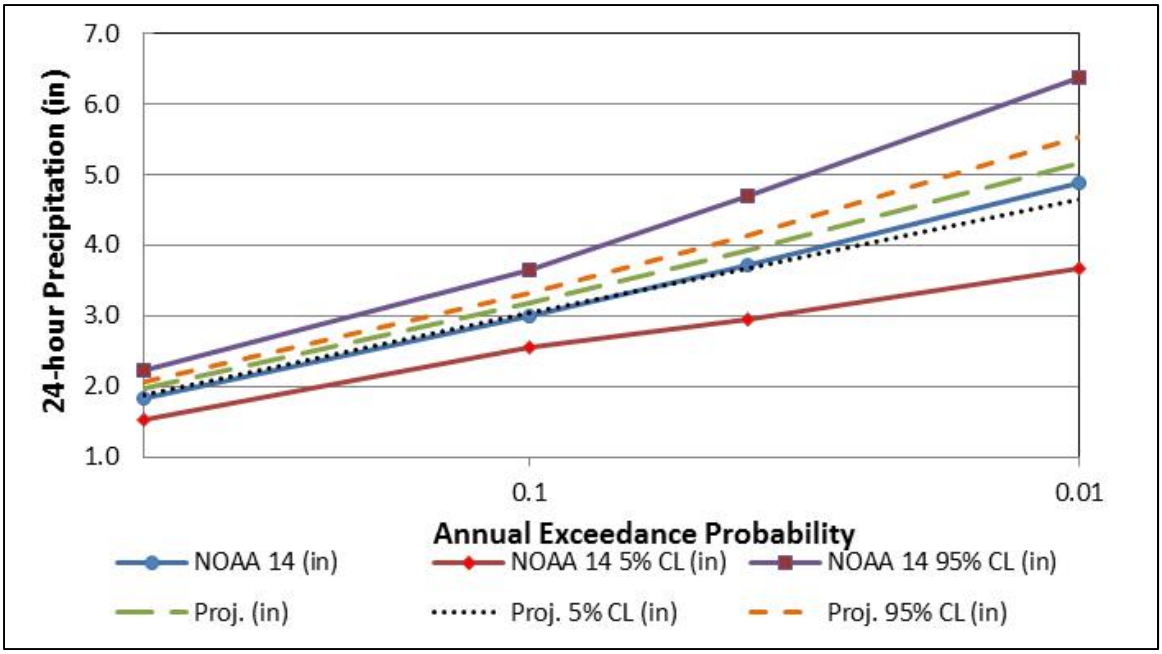

Figure 5.2. Projected (2050-2099) estimates of the 24-hour precipitation for Denver, Colorado.

5.1.3. Applicability and Limitations

The ten-step method for estimating projected 24-hour precipitation, including, but not limited to, the 0.5, 0.1, 0.04, and 0.01 AEP quantiles, is applicable to projects requiring a Level 3 analysis and some Level 4 analyses requiring a 24-hour duration precipitation depth as an input to rainfall/runoff modeling. The rainfall/runoff modeling tools in which the projected 24-hour duration precipitation estimates can be applied include the SCS graphical peak discharge method, many unit hydrograph procedures, and others.

As recommended in Chapter 4, the design team should evaluate multiple future climate scenarios, when feasible, to provide a more comprehensive understanding of possible future precipitation estimates. Results will be more informative when a larger ensemble of GCMs are considered, giving a larger potential range of outcomes.

This procedure is limited by the ability of high-resolution climate datasets to represent historical and future extreme precipitation, particularly those extremes greater than the 0.1 AEP quantiles. As described in the introduction of the method and as illustrated in the example application, the high-resolution climate datasets tend to underestimate extremes. The procedure mitigates this limitation by using the 0.1 AEP ratio for estimating projected precipitation values for the more extreme quantiles, including the 0.04 and 0.01 AEPs.

The projected changes in precipitation illustrated in this example as shown in Figure 5.2 are not notable. However, application of this methodology using different scenarios, GCMs, and future periods might result in larger changes. In addition application of the methodology in other parts of the country could exhibit different results.

The example demonstrates that engineers should consider confidence limits based on the historical data in the design process more often than is typical today. Recall that the confidence limits, such as those shown in Figure 5.2, are derived from historical data. The range represented

in the confidence limits tells engineers that precipitation estimates are far from certain and should be considered in designing some projects even without considering a changing climate.

The ten-step procedure is intended to be used by hydrologic engineers without special training in climate change modeling or technology. The procedure uses existing hydrologic analysis tools and assumes that some relationships in the observed record will remain constant even though projected estimates will increase (or decrease) relative to historical estimates.

Finally, the ten-step procedure relies on the use of gridded datasets of projected precipitation. Station-based alternatives may eventually be available for purposes of estimating projected precipitation values.

5.1.4. Discussion and Other Resources

More complex approaches are available and are described in Kilgore et al. (2019). However, these require specialized skills and resources to implement. In some cases, regional or state organizations may collaborate to develop tools such as a NOAA Atlas 14 type resource for projected conditions so that design engineers could use such a tool in the same way they do for existing conditions.

The ten-step procedure introduces innovations for estimating projected 24-hour precipitation quantiles. Components of this procedure where further research might improve the methodology include answering the following questions:

- How sensitive are projected precipitation quantiles to the selection of the baseline and future periods?
- Is the analysis of a minimum of three grid cells for small watersheds necessary?
- What difference does the use of a ratio rather than a difference (delta) make in the estimate of the projected 24-hour precipitation quantiles?
- Does projecting the more extreme AEP quantiles, e.g., the 0.04 and 0.01 AEP, using the model ratio for the 0.1 AEP quantile provide a more accurate projection of the extreme AEP quantiles?

A challenge for further research is that because what may happen in the future is being considered, there is no objective reference with which to compare. However, through application of these procedures to examples, one can compare the results from the recommended procedure and other approaches to assess whether there are major differences and, if so, which appears to provide more reasonable results.

The following sections summarize additional evaluation of the issues for capturing extreme precipitation quantiles from existing high-resolution climate datasets related to the fourth bullet above. First, a discussion of the general issue of the potential underestimation of precipitation quantiles is presented. Then, an evaluation of using the 0.1 AEP quantile ratio for more extreme quantiles is provided.

5.1.4.1. Underestimation of Precipitation Quantiles

Although high-resolution climate datasets continue to improve, they exhibit limitations as evidenced by the example in Section 5.1.2. First, the high-resolution climate datasets for the

historical period underestimate the observed estimates even adjusted to unconstrained point values. This is clearly evident when comparing the observed NOAA Atlas 14 quantiles (Table 5.2) with the baseline period downscaled GCM quantiles (Table 5.3).

As shown in Table 5.3, none of the 12 high-resolution datasets produced quantile estimates higher than those from NOAA Atlas 14 for the Denver location. In fact, most were notably lower. This outcome was also observed in analyses in the Eastern United States with BCCA downscaled data including Baltimore, Maryland; Philadelphia, Pennsylvania; and Pittsburgh, Pennsylvania. (As described in Chapter 4, the LOCA climate dataset is considered to be an improvement over the BCCA dataset for this application.)

Figure 5.3 displays the precipitation quantiles estimated from the downscaled CSIRO GCM dataset for a location in Baltimore, Maryland, compared with the NOAA Atlas 14 quantiles. The baseline period (1950-1999) model estimates are well below the NOAA Atlas 14 estimates, although the two curves show a similar shape. The figure also shows the projected model estimates for the two future periods.

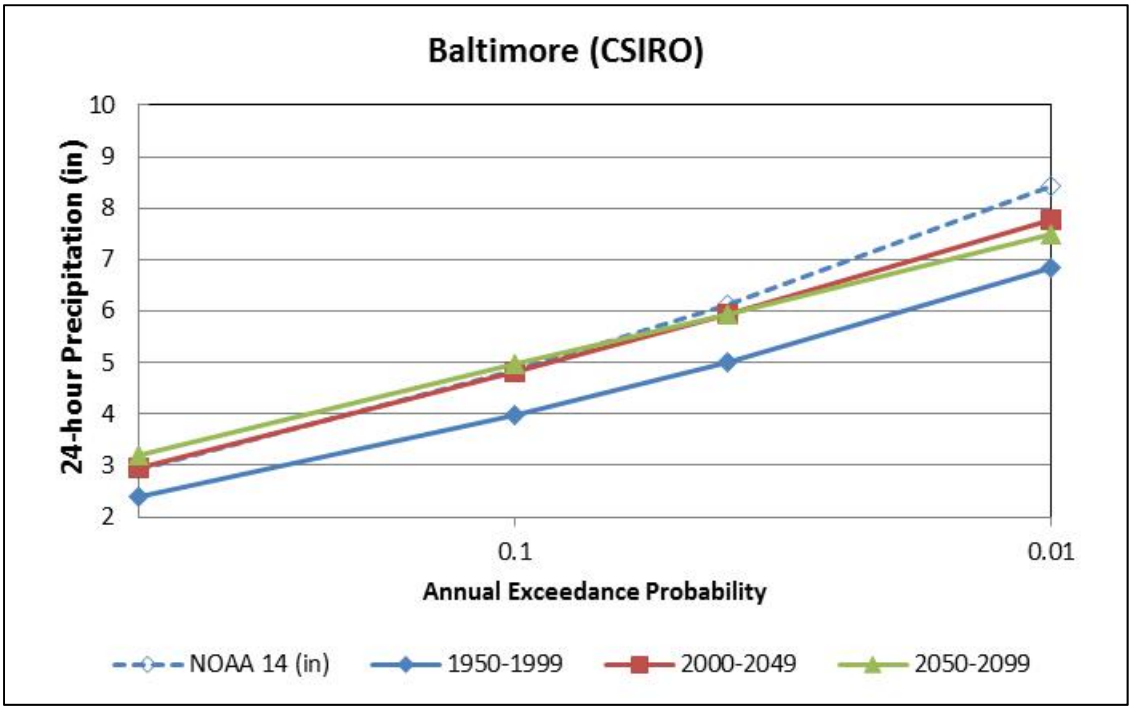

Figure 5.3. Baseline and future (RCP8.5) model estimates for 24-hour precipitation for Baltimore from the CSIRO GCM.

Figure 5.4 displays the same type of information from the downscaled MIROC5 GCM dataset for a location in Philadelphia, Pennsylvania. Again, the baseline model estimates are well below the NOAA Atlas 14 estimates (and the future periods are relatively unchanged from the baseline). In this case, the GCM RFC is flatter than historical NOAA Atlas 14 estimates. Similarly, Figure 5.5 shows the findings for the downscaled CCSM GCM dataset for a location in Pittsburgh, Pennsylvania.

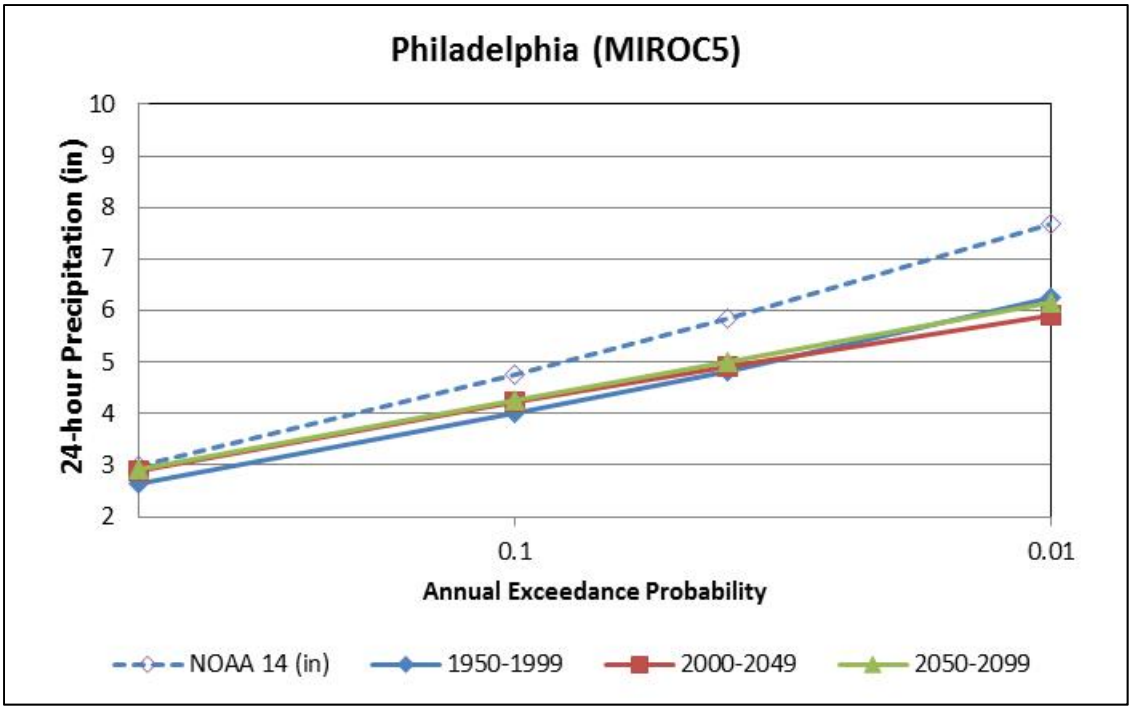

Figure 5.4. Baseline and future (RCP8.5) model estimates for 24-hour precipitation for Philadelphia from the MIROC5 GCM.

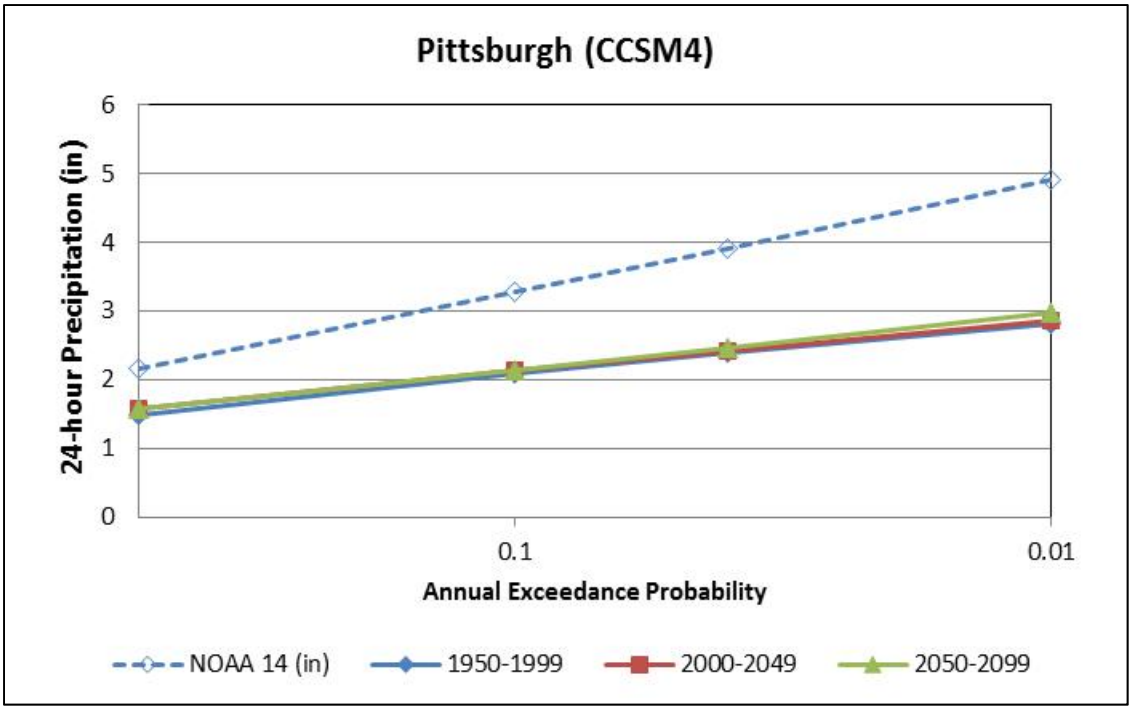

Figure 5.5. Baseline and future (RCP8.5) model estimates for 24-hour precipitation for Pittsburgh from the CCSM4 GCM.

Overall, the high-resolution datasets from the three GCMs (CSIRO, CCSM4, and MIROC5) at all three locations produced baseline quantiles significantly lower than the NOAA Atlas 14 estimates as was observed for the 12 downscaled GCM output datasets in the Denver example. The procedure addresses this limitation in the downscaled GCM output datasets by using NOAA Atlas 14 estimates as the starting point for estimates of projections with the ratio of the modeled future to modeled baseline as the basis for future estimates.

5.1.4.2. Calculating More Extreme Quantiles with the 0.1 AEP Ratio

It is unclear whether the changes in ratios observed between future and baseline periods with AEP from the example as summarized in Table 5.6 and Table 5.7 are artifacts of the high-resolution climate datasets or are true representations of change in the shape of the RFC according to the GCM and downscaling. As previously noted, some downscaled GCM outputs show increases in the ratios with more extreme AEP and others show decreases.

As discussed in Chapter 4, current high-resolution climate datasets are limited in their ability to capture precipitation extremes. Therefore, the ten-step procedure assumes that the most extreme quantiles are mathematical artifacts. As artifacts, the computed moments (especially standard deviation and skew) are not likely to be truly as variable as they seem to be within different periods for a given GCM. Therefore, the ten-step procedure uses the 0.1 AEP ratio as an "***index***" for the more extreme AEPs as illustrated in the example in Table 5.8 and Table 5.9. That is, Equation 5.2 is used for AEPs of 0.1 and less extreme while Equation 5.3 is used for AEPs more extreme than the 0.1 AEP.

An alternative approach is to assume that the results for the extreme AEPs are true representations of the future RFC as projected by each downscaled GCM output. That is, the results from each GCM showing decreases and for others showing increases represent physics-driven changes in the RFC. If this is true, then a "***direct***" application of the computed ratio for the extreme AEPs (e.g., 0.04 and 0.01) is appropriate and Equation 5.3 is used for all AEPs.

For the Denver example in Section 5.1.2, the choice between the "direct" method and the "index" method was inconsequential as the more extreme AEP ratios were not significantly different from the 0.1 AEP ratios in the aggregate. Using three downscaled GCM outputs (CSIRO, CCSM4, and MIROC5) for the RCP8.5 scenario from the BCCA data archive, the two methods were further compared in three additional locations: Baltimore, Philadelphia, and Pittsburgh.

Figure 5.6 summarizes the projected estimates using the mean ratios from the ensemble of three GCMs for Baltimore. For the 0.5 and 0.1 AEP, the estimates from the Index and Direct methods are identical by definition. In this case, the Index method results in a higher estimate of the projected 0.01 AEP precipitation driven largely because one of the downscaled GCM output datasets (MIROC5) results in low ratios (less than one) for the more extreme AEPs. A larger ensemble might moderate this result.

Similarly, Figure 5.7 displays the quantiles for Philadelphia where the Index method results in a higher estimate for the 0.01 AEP precipitation than the Direct method. In both this case and the Baltimore case, the Direct method produces a "future" estimate that is roughly the same as the baseline estimate represented by NOAA Atlas 14. (Under no circumstance would using a projected precipitation value less than the historical precipitation value be recommended because the built infrastructure would need to meet requirements today and in the future.)

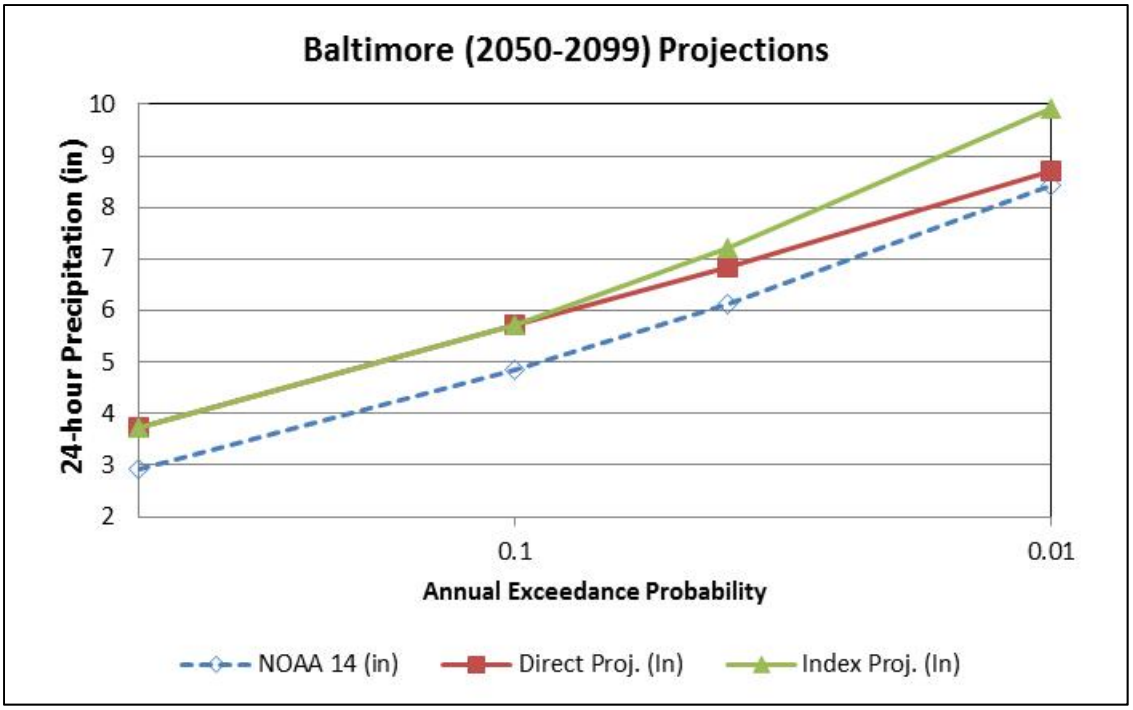

Figure 5.6. Future (RCP8.5) model estimates for 24-hour precipitation for Baltimore (2050-2099) from an ensemble of the three CCMs.

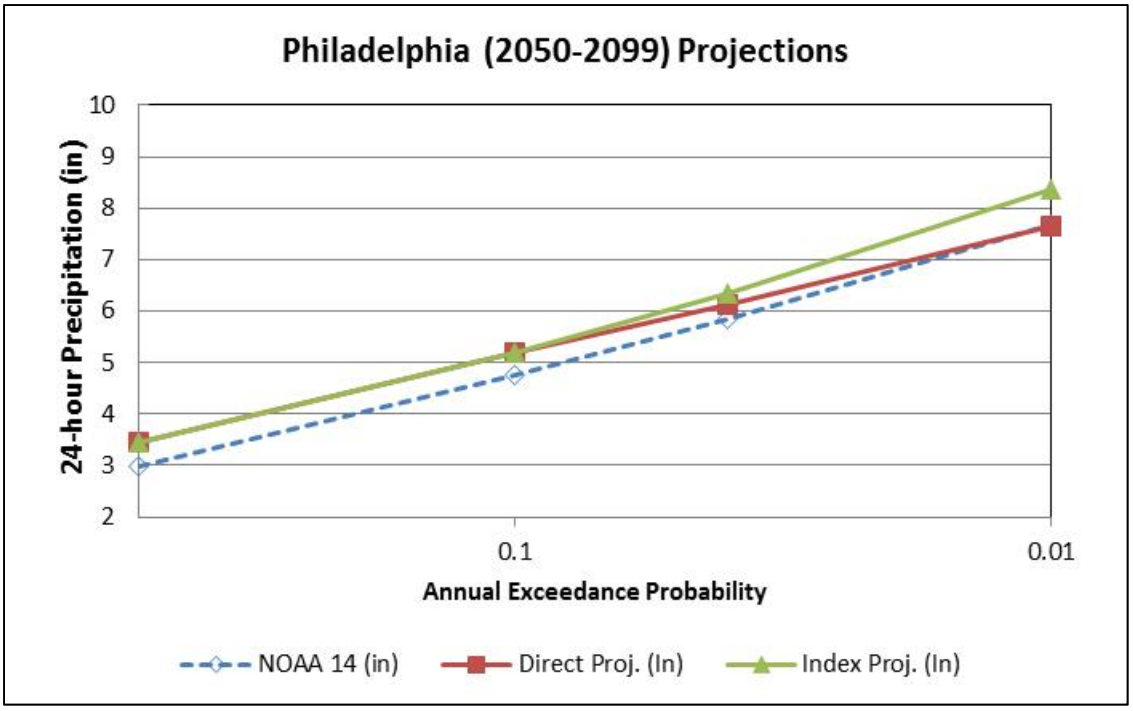

Figure 5.7. Future (RCP8.5) model estimates for 24-hour precipitation for Philadelphia (2050-2099) from an ensemble of the three CCMs.

A different result is observed for Pittsburgh for the earlier future as shown in Figure 5.8. In this case, the Direct method results in a higher estimate of the 0.01 AEP precipitation. In all three locations, the differences between methods might be moderated by larger ensembles as was observed in the Denver example.

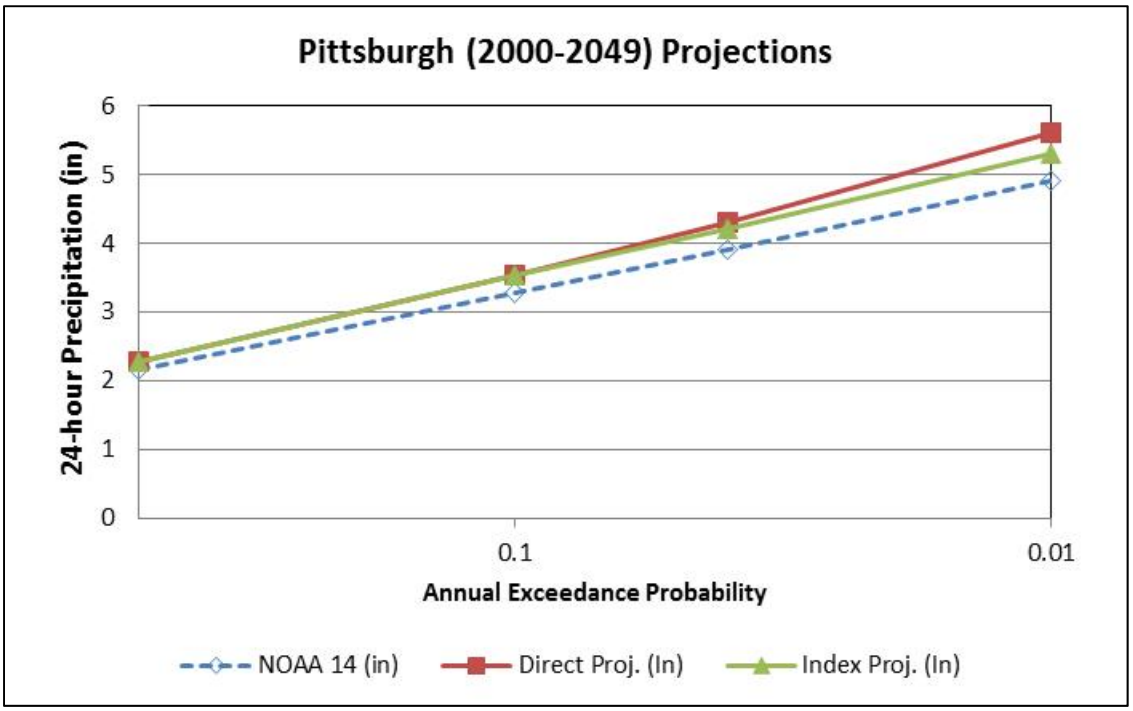

Figure 5.8. Future (RCP8.5) model estimates for 24-hour precipitation for Pittsburgh (2000-2049) from an ensemble of the three CCMs.

As described previously, the Direct method implicitly places a higher level of confidence on the high-resolution climate datasets for estimating extreme events such as the 0.01 AEP than does the Index method. For example, the Direct method assumes that the variations in the statistical moments (particularly the standard deviation and skew) from the annual maximum series of precipitation represent meaningful physics-based responses from the GCMs. In the Denver example, the variations in the moments can be seen in Table 5.3, Table 5.4, and Table 5.5. By contrast, the Index method relies on the downscaled GCM output datasets for quantiles less than or equal to 0.1 AEP but uses the 0.1 AEP ratio for more extreme AEPs. This essentially assumes that the shape of the future RFC for more extreme AEPs than the 0.1 AEP is the same as the historical RFC.

One strategy for further evaluation could be to apply both methods and use the larger of the two to be conservative. Another strategy would be to use larger ensembles than three GCMs as recommended in Chapter 4 to reduce the sensitivity of the result to a single downscaled GCM output dataset. As applied in the Denver example, the use of the Index approach with a larger ensemble is recommended. However, the engineer may choose to use the Direct method if it appears justified in a particular situation.

In all cases, the engineer should compare future estimates of the T-year 24-hour precipitation with the confidence limits of the historical estimates (e.g., NOAA Atlas 14) to assess whether

projected changes in precipitation are significant within the context of historical variability. The Climate Change Indicator (CCI) is one tool for assessing whether projected precipitation changes are significant (Kilgore et al. 2016). If projected precipitation is not significantly different than historical precipitation, it is recommended that the engineer consider the historical precipitation estimates, including the appropriate confidence limits, in designing resilient infrastructure. Estimates for projected precipitation should be documented and placed within the historical context.

5.2. Sub-Daily Precipitation/IDF Curves

Several engineering methods for estimating discharge use design rainfall quantiles as input, including the Rational Method, the NRCS graphical peak discharge method, and unit hydrographs (Kilgore et al. 2016). That input may be in the form of rainfall depth for a specific duration of rainfall or rainfall intensity (rainfall depth divided by the specific duration) and is often required at sub-daily durations.

Reliable projections of sub-daily precipitation values from high-resolution climate datasets are generally not available from broadly accessible databases such as the following:

- The Downscaled CMIP3 and CMIP5 Climate and Hydrology Projections (DCHP).
- The USGS GeoData Portal (http://cida.usgs.gov/gdp/).

These databases include historical and projected future daily precipitation data from several GCMs for several future scenarios. The historical data generally cover the period from 1950 to 1999, and future estimates generally span the period from 2000 to 2100. However, these databases do not include projections of sub-daily precipitation data commonly required by engineers for hydrologic analysis. (See Chapter 4 for more information on these and other high-resolution climate datasets.)

Temporal adaptation of downscaled GCM output for hydrologic design generally involves adjusting 24-hour projection results to sub-daily time scales needed for rainfall/runoff modeling. Estimating 24-hour duration precipitation quantiles was discussed in Section 5.1. This section describes the general characteristics of IDFs and several approaches identified in the literature for estimating these for future conditions. This discussion is followed by recommendations for appropriate approaches to use for hydrologic design.

5.2.1. General Description of IDF Relations

Total precipitation depth occurring in a storm increases with duration of the storm as well as with the severity of the storm. Historical depth-duration (DD) relations express the accumulation of depth of rainfall with time for a given AEP based on the analysis of observed storms over the period of record. Because it is an accumulation, curves representing DD relations are monotonically increasing. The rate of accumulation of rainfall (intensity) always diminishes with increasing duration; DD curves increase rapidly at short durations and continue increasing, but at a diminishing rate. For example, the accumulation of rainfall between time equal 0 and time equal 1 hour is greater than the accumulation between time equal 1 hour and time equal 2 hours. Thus, DD curves are monotonically increasing, with “downward” concavity; the rate of change of depth diminishes with time, as illustrated in Figure 4.1.

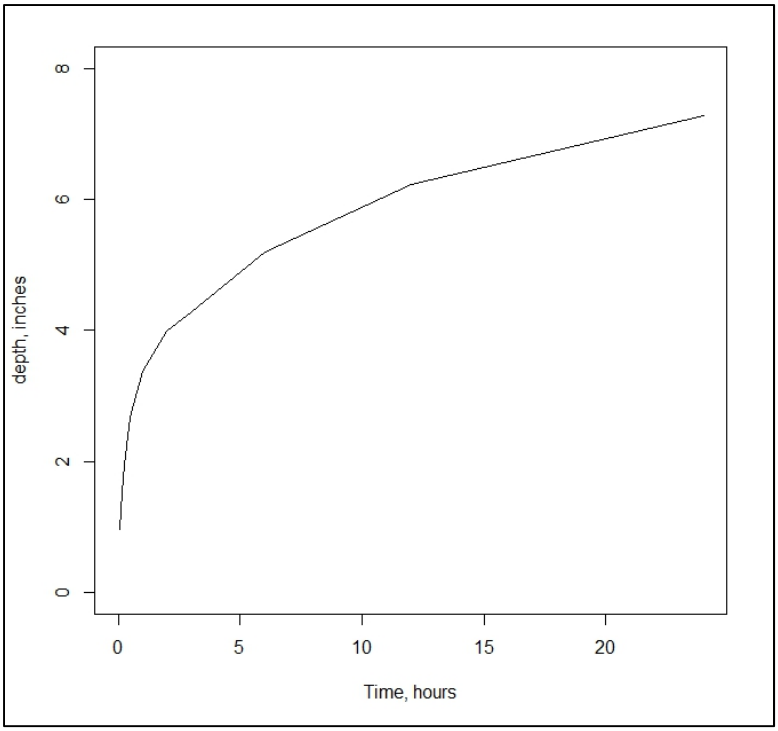

Figure 5.9. Depth-duration curve for an AEP of 0.01 for Roxboro, NC (data from NOAA Atlas 14).

Intensity, as used in the context of rainfall, denotes the time-averaged rate of rainfall accumulation for a given duration. Engineers calculate intensity by dividing the accumulated depth at any time, by the time of accumulation. Units are length per unit time, usually inches per hour (or millimeters per hour). Intensity is invariably high for short durations, diminishing with time. Intensity-duration (ID) curves, therefore, are monotonically decreasing curves, and always exhibit "upward" concavity; the rate of change of intensity diminishes with time, as illustrated in Figure 5.10.

Values of depth-duration and intensity-duration are linked to their respective probabilities of exceedance (expressed as "frequency"). Depth-duration-frequency (DDF) relations have been developed from historical point precipitation measurements or from generalized publications such as National Weather Service Technical Paper 40 (TP-40) (U.S. Department of Commerce 1961), which was developed with data from many stations. Currently, NOAA is developing Atlas 14 to serve as a nationwide source of DDF information. Regardless of the source, the DDF relations are developed based on assumptions of stationarity over the period of record.

DDF curves are developed by statistical processes that yield an expected (most likely) value and a range of values called confidence limits that describe the variability in the estimates. Table 4.1 summarizes the DDF values for precipitation for the Roxboro, North Carolina, station, taken from NOAA Atlas 14. The table shows expected depth values for selected durations from 5 minutes to 24 hours and AEPs of 0.5 to 0.01. Alongside the expected value in each cell are the lower and upper 90 percent confidence limit depths in parentheses.

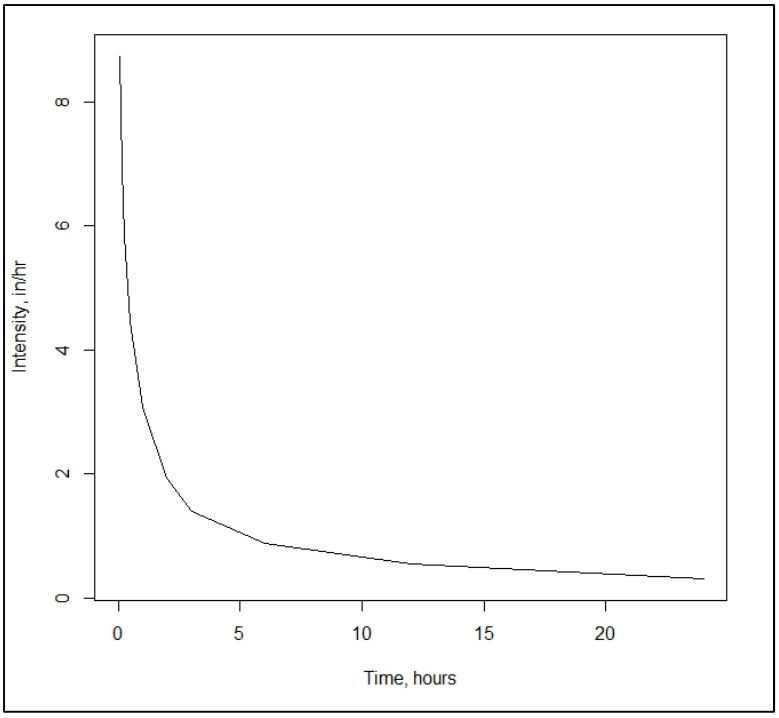

Figure 5.10- Intensity-duration curve for an AEP of 0.01 for Roxboro, NC (NOAA Atlas 14).

While the set of DDF curves for each station or point may be unique, the basic shape at each station is necessarily reasonably consistent across magnitude (associated with AEP). Were this not true, DDF curves for a given station may cross one another, which is a logical inconsistency. The basic shape of a DDF curve may be represented as non-dimensional depth ratios by dividing all depths by the largest depth, which is associated with the longest duration in the curve. Figure 5.11 shows non-dimensional DDF curve shapes for AEP values of 0.5 and 0.01 for five randomly selected US stations: Roxboro, North Carolina; Venus, Florida; Milford, Kansas; Moreno Valley, California; and Mountain City, Nevada. For each station, the non-dimensional curves exhibit some separation. However, the separation among curves for each station is smaller by comparison than the separation among curves for different stations. Therefore, the figure demonstrates that while DDF curves exhibit variation with location, variation with magnitude of rainfall represented by various AEP values at any given location exhibit inconsequential variation.

The separation among curves for a particular station is also generally small compared to the width of the confidence limits for each curve. Figure 5.12 shows the non-dimensional DDF curve shapes for the 0.5, 0.04, and 0.01 AEP values for Roxboro, North Carolina, plotted along with the non-dimensional upper- and lower-90-percent confidence limits for the 0.04 AEP relation. All three of the AEP curves fall within the 90-percent confidence limits, indicating relative indifference of shape of the DDF curves with AEP for a given location. From a practical standpoint, considering the size of the interval represented by the confidence limits, Figure 5.12 supports the observation that the basic shape of DDF curves in a given location is sufficiently invariant to allow the acceptance of the assumption of stationarity of shape, until future data confirms or contradicts that assumption.

Table 5.10. Precipitation depth (inches) from NOAA Atlas 14 for AEP 0.5 to 0.01 and durations from 5 min. to 24 h for Roxboro, NC.

Duration	Annual Exceedance Probability					
	0.5	0.2	0.1	0.04	0.02	0.01
5-min	0.452 (0.413-0.494)	0.524 (0.478-0.572)	0.582 (0.531-0.635)	0.644 (0.585-0.701)	0.688 (0.622-0.749)	0.728 (0.655-0.793)
10-min	0.722 (0.660-0.789)	0.838 (0.765-0.915)	0.931 (0.848-1.01)	1.03 (0.932-1.12)	1.10 (0.990-1.19)	1.16 (1.04-1.26)
15-min	0.908 (0.830-0.992)	1.06 (0.968-1.16)	1.18 (1.07-1.28)	1.30 (1.18-1.42)	1.39 (1.25-1.51)	1.46 (1.32-1.59)
30-min	1.25 (1.15-1.37)	1.51 (1.38-1.65)	1.71 (1.56-1.86)	1.93 (1.75-2.10)	2.09 (1.89-2.28)	2.24 (2.02-2.44)
60-min	1.57 (1.44-1.72)	1.93 (1.76-2.11)	2.22 (2.03-2.42)	2.57 (2.33-2.79)	2.83 (2.56-3.08)	3.09 (2.78-3.36)
2-hr	1.87 (1.70-2.04)	2.31 (2.10-2.52)	2.68 (2.43-2.92)	3.13 (2.83-3.42)	3.51 (3.15-3.82)	3.87 (3.45-4.21)
3-hr	2.00 (1.83-2.19)	2.47 (2.25-2.71)	2.88 (2.62-3.15)	3.38 (3.05-3.69)	3.79 (3.41-4.13)	4.20 (3.75-4.57)
6-hr	2.42 (2.22-2.66)	2.99 (2.73-3.29)	3.50 (3.18-3.84)	4.15 (3.74-4.54)	4.70 (4.21-5.13)	5.25 (4.67-5.73)
12-hr	2.89 (2.66-3.18)	3.60 (3.29-3.94)	4.23 (3.85-4.63)	5.07 (4.59-5.53)	5.80 (5.20-6.30)	6.55 (5.81-7.10)
24-hr	3.39 (3.17-3.66)	4.24 (3.95-4.56)	4.90 (4.56-5.27)	5.82 (5.38-6.25)	6.54 (6.03-7.04)	7.29 (6.70-7.86)

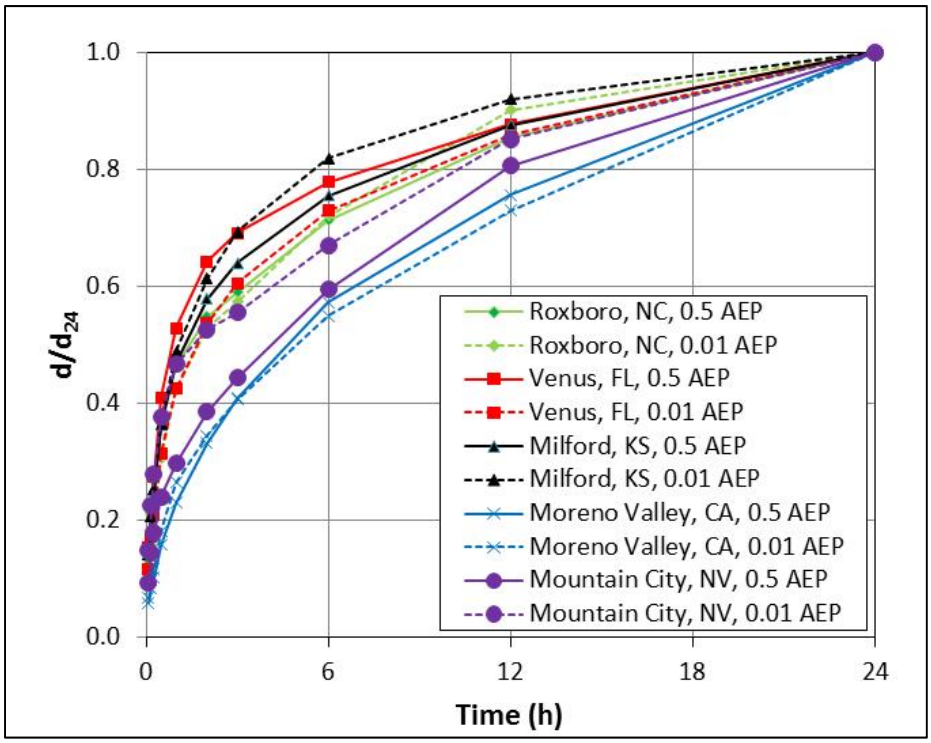

Figure 5.11. 24-h depth-duration-frequency curves for AEP values of 0.5 and 0.01 for five randomly selected stations reduced to non-dimensional shapes by normalizing on the largest value (d_{24}).

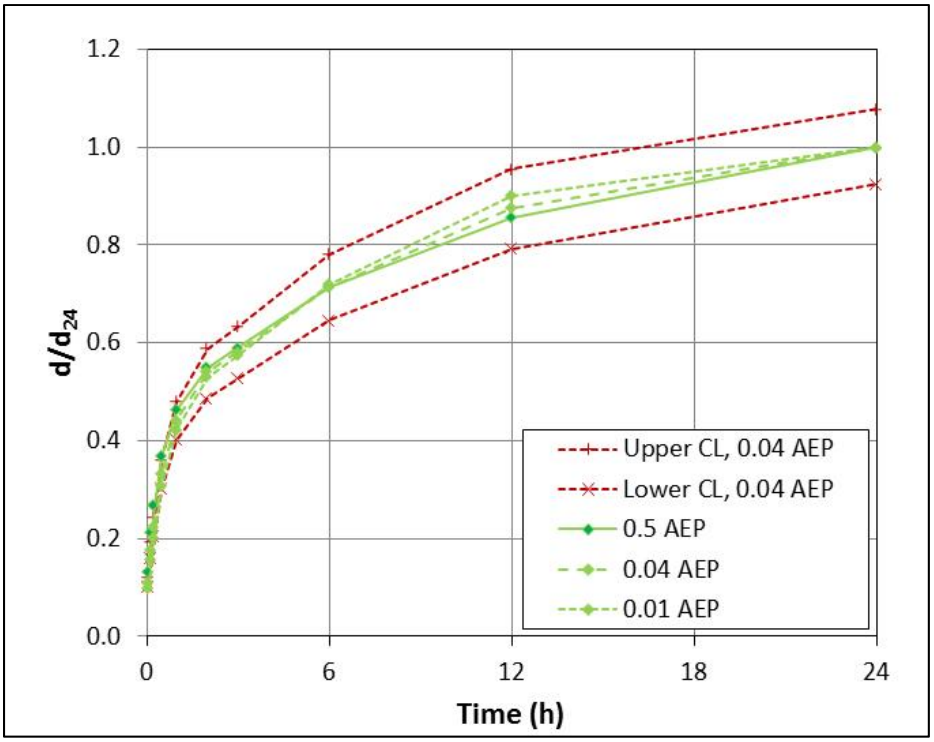

Figure 5.12. DDF curves (0.5, 0.04, and 0.01 AEP) for Roxboro, NC, normalized to the largest value (d_{24}) augmented by the 90th percentile curves for the 25-year curve, also normalized by dividing all values by the 25-year 24-h depth.

5.2.2. Sub-Daily Precipitation from the Climate Science Community

As described in Chapter 4, actionable sub-daily precipitation information is generally not available from current high-resolution climate datasets prepared by the climate science community. In part, this is because historical trends and future changes in sub-daily precipitation and their relationship to climate change are not as well understood because historical observations of sub-daily precipitation in the United States are more limited than daily data and there is additional uncertainty regarding the estimates of sub-daily precipitation. For most applications in the climate science community, historical sources of sub-daily data are limited to the 114 stations in the U.S. Climate Reference Network (USCRN). With fewer observations, it is more difficult to identify trends and to understand the physical mechanisms that cause short duration, intense precipitation.

While climate models often use computational time steps less than 24 hours, this sub-daily information is often not saved. Furthermore, the sub-daily precipitation may not be appropriate for engineering purposes where extreme (0.1 to 0.01 AEP) values are required because of the spatial incongruity between the large model grid size and, in some cases, smaller watershed sizes.

In this section, two potential tools for estimating sub-daily precipitation for engineering applications from climate community products are described: 1) sub-daily estimates based on changes in air temperature and 2) higher resolution modeling. Advances in either of these

emerging areas have the potential to improve climate model sub-daily output beyond the approaches that are currently available.

5.2.2.1. Precipitation Extremes Related to Air Temperature

Climate scientists primarily attribute increases in some measures of extreme precipitation in historical observations and GCM simulations to a warming atmosphere that is able to hold more moisture that contributes to approximately a 7 percent per °C rate for daily precipitation extremes (the upper 75th, 90th, 99th, and 99.9th percentiles of daily values) (Westra et al. 2014). There is some observational evidence that increases to sub-daily precipitation extremes are greater than the 7 percent per °C rate for daily precipitation extremes (Westra et al. 2013). One possible outcome from research in this area is a set of relations linking increases in sub-daily precipitation quantiles to increases in average air temperatures.

This research recognizes that thermodynamic processes controlled by the availability of moisture in the atmosphere primarily drive precipitation extremes. The Clausius–Clapeyron (CC) equation states that as the air temperature increases, the atmospheric water holding capacity exponentially increases by approximately 7 percent per degree of surface air temperature warming at 0°C and approximately 6 percent per degree at 24°C (Westra et al. 2014). Precipitation intensity is a function of the water in the atmosphere and, in many regions, precipitation extremes occur when the atmosphere profile is nearly saturated. GCM simulations on average show an increase in the 0.05 AEP daily precipitation quantile by about 6 percent per ^{o}C globally, similar to the CC rate, although rates differ among GCMs and by location (Kharin et al. 2007, Kharin et al. 2013).

The top left panel of Figure 5.13 shows relative changes in globally averaged 0.05 AEP (20-year return period) of daily precipitation extremes (ΔP_{20}) plotted on a log scale as a function of globally averaged changes in annual mean near surface temperature simulated by the CMIP5 models in the RCP2.6, RCP4.5, and RCP8.5 experiments in 2046-2065 and 2081-2100. The dashed line indicates the linear regression fit. In the top right panel of the figure, a histogram of extreme precipitation sensitivities simulated by the CMIP5 models in the three scenarios for the two time periods is shown. The median value and the inter-quartile range are indicated by the vertical dashed and dotted lines, respectively. The two bottom panels in the figure show the same information as the top panels, but for changes in global annual mean precipitation instead of ΔP_{20}. (Kharin et al. 2013). The sensitivity of the 0.05 AEP precipitation to changes in global temperature is much higher than the sensitivity annual mean precipitation to the same changes in global temperatures. Currently, these results represent global averages, and additional research is needed to understand how these results may be applied to specific sites and the application to AEP value other than the 0.05 AEP.

The use of the CC approach for estimating sub-daily precipitation is appealing because it removes many of the spatial and temporal resolution issues associated with using downscaled precipitation model output. Increases in historical AEP design values could be based on anticipated increases in global mean surface air temperature as opposed to local values and would not require sub-daily temperatures. Thus, estimates of changes in AEP precipitation would only require the global average temperature change. As reviewed by Westra et al. (2014), numerous studies using observational datasets have concluded that sub-daily (hourly and less) extreme rainfall is intensifying more rapidly than rainfall measured at daily time scales. This "super CC rate" results in approximately a doubling of increases in hourly rainfall extremes as compared to daily extremes. This is largely a result of increases in convective rainfall. However,

as temperatures increase still further, a decrease in extremes is evident, which may result from limits on moisture availability at high temperatures.

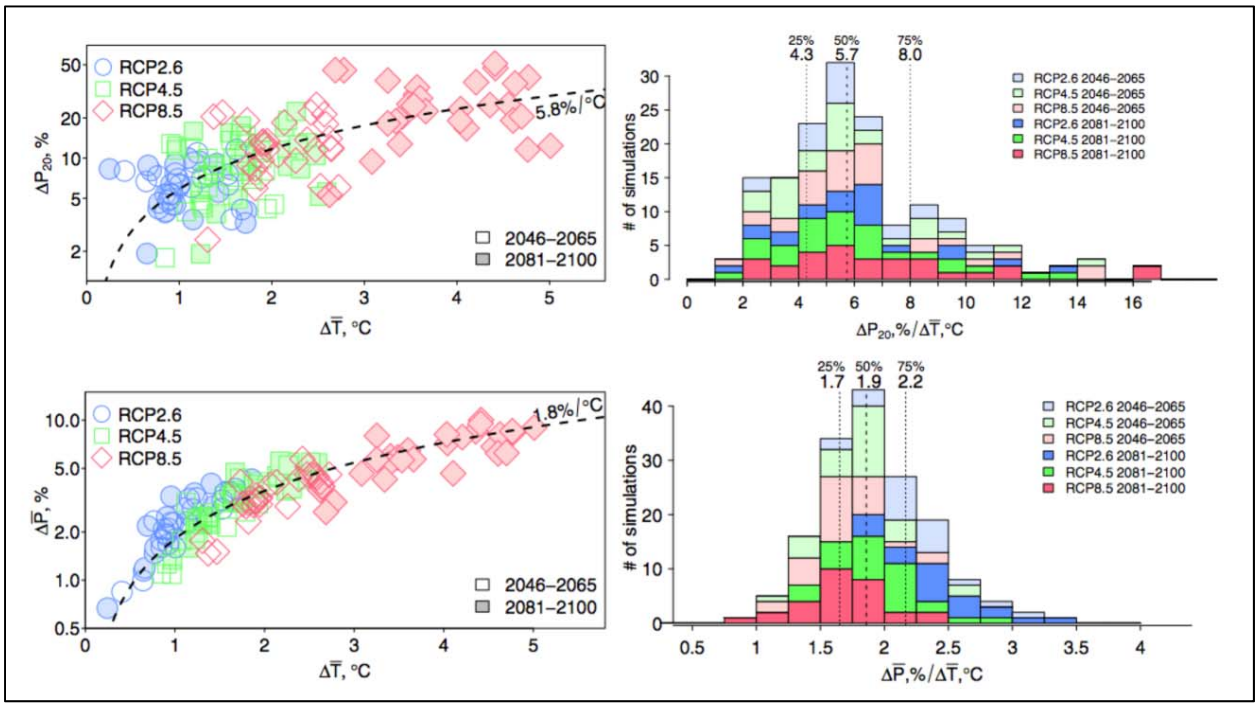

Figure 5.13. Projected increases in precipitation measures with changes in temperature [Kharin et al. 2013] Top left: Relative changes (%) in globally averaged 20-year return values of annual daily precipitation extremes versus globally averaged changes in annual mean near surface temperature simulated by the CMIP5 models for the RCP2.6, RCP4.5 and RCP8.5 in 2046–2065 and 2081–2100. Top right: Histograms of the ratio of globally averaged 20-year return values of annual daily precipitation extremes to the globally averaged changes in annual mean near surface temperature. Bottom figures same as top except for mean annual precipitation.

While these results have been found throughout the globe, the generalization of the method is not yet recommended for several reasons: 1) there is limited availability of high quality sub-daily precipitation observations, 2) there are differences among the methods used to establish the precipitation intensity rate increases using the CC increases for daily versus sub-daily precipitation data, and 3) a better understanding of the physical mechanisms governing site-specific atmospheric water content is needed (Prein et al. 2017, Wang et al. 2017). Consensus by the research community regarding these issues is needed prior to applying the super CC rate approach to design practice. As summarized by (Zhang et al. 2017), "In the interim, it would be prudent for those undertaking adaptation planning and requiring engineering design values for long-lived infrastructure to be guided by the CC relationship in most mid-latitude locations, consistent with results for extreme daily precipitation from observations and models, bearing in mind that the levels of uncertainty in future projection is high and may remain so for some time."

5.2.2.2. Higher Resolution Modeling

Another approach to improving sub-daily estimates of extreme precipitation from the climate science community is to leverage future advances in higher resolution models that offer the potential to capture small-scale storm dynamics. While thermodynamics and the water holding capacity of the atmosphere are important considerations for precipitation extremes, local conditions such as those found in subtropical regions or local features such as mountains and water availability status (e.g., deserts, large water bodies) can play a significant role at site and watershed scales. For example, the 2013 Boulder, Colorado, flood resulted from both dynamic and thermodynamic processes and caused by rainfall where the source water was from hundreds of miles away (Eden et al. 2016).

A subclass of regional climate modeling, convection-permitting models (CPMs) have emerged as a promising approach to capture small-scale storm dynamics and, therefore, better represent extreme precipitation at spatial and temporal scales more appropriate for engineering design. CPMs typically have a spatial resolution of less than 4 km. At that spatial scale, CPMs may represent larger convective storms in a more realistic manner. Prein et al. (2015) concluded that CPMs should be able to capture the diurnal cycle of precipitation. This ability can add value in regions where precipitation results from deep convective processes or where precipitation is highly spatially variable (e.g., mountains and urban areas). When sub-daily precipitation extremes occur in the summer, CPMs may be able to eliminate biases that result in lower precipitation intensities and longer duration storms in most Regional Climate Models (RCMs) (Kendon et al. 2014).

Current limitations of CPMs include high computational costs, a limited number of independently developed models, and a limited range of future periods. The upcoming CMIP6 GCMs will not include CPMs. Other coordinated RCM downscaling efforts that generate multi-model ensembles (e.g., NARCCAP and CORDEX) do not use CPMs but have developed a roadmap for coordinated, focused experiments. Kendon et al. (2017) call for a similar coordinated multi-model experiments over common domains using CPMs.

If such an experiment occurs in the future and meets the criteria for downscaling established in Chapter 4, it might provide the basis to improve estimates of future sub-daily extreme precipitation for engineering practice. In addition, future model results should be reviewed to determine if they look realistic with regard to extreme precipitation events of interest and if the results make physical sense on the broader scale for the system of interest. If the results do not make physical sense, there may be a deeper underlying problem with the simulation that could affect the overall credibility of the findings (personal communication, S. McGinnis, NCAR). For example, in some regions, convective events typically occur within a specific time window in the afternoon. If the timing of events does not match historical observations then the results "might not make sense." In other cases, local convective storms "pop up" in clusters with some areas being hot spots for events resulting from uplift from terrain or local warm temperature anomalies. If the location or clustering of events does not match baseline positions, then the results "might not make sense."

More generally, even if a model provides sub-daily precipitation values, the model's ability to capture the diurnal cycle of precipitation must be verified. Evaluation metrics for the diurnal cycle could include: 1) total precipitation, 2) frequency of precipitation occurrence, 3) local time of peak intensity, and 4) intensity of precipitation per occurrence on an hourly basis averaged

over the baseline 20- to 30-year period (Mooney et al. 2017). Model results should be compared to local or regional observations and examined for biases such as overestimation of occurrences and underestimation of intensities. Ideally, a national comparison would be conducted in a consistent manner that provides results at a range of scales.

An additional evaluation metric is the joint probability distribution function between duration and peak intensity of precipitation events (Kendon et al. 2014; Lee et al. 2017). For example, in regions where convection is important (Southwestern and Southeastern United States in the summer) or where precipitation has an intense diurnal cycle (night-time precipitation in the central United States associated with the Great Plains Low Level Jet), a model should be able to adequately represent this cycle (personal communication, F. Dominguez, University of Illinois).

BOTTOM LINE: Projected sub-daily precipitation estimates from climate modeling are not currently available for hydrologic modeling inputs. However, advances are being made that may provide such estimates directly in the future.

5.2.3. Sub-Daily Precipitation and Development of IDF Curves

As described in the previous section, actionable estimates of future sub-daily precipitation from the climate science community are not yet available. This section describes several engineering approaches for filling this need. This section also proposes criteria for evaluating the suitability of these methods for engineering design and provides recommendations for those methods that are most appropriate.

The literature documents several approaches for estimating future sub-daily precipitation values, including development of IDF curves. Table 5.11 lists several efforts that may be categorized in four groups based on the primary strategy used for disaggregation: 1) quantile to quantile mapping, 2) curve fitting, 3) linear scaling, and 4) stochastic sampling. Each is described in the following sections.

Table 5.11. Methods and examples of sub-daily disaggregation.

Application	Method	Source
City of Saskatoon (Canada)	Quantile to quantile mapping	Hassanzadeh et al. 2014
New York State	Quantile to quantile mapping	Castellano and DeGaetano 2015
Canada	Quantile to quantile mapping	Simonovic et al. 2016
Mid-Atlantic region	Curve fitting	Moglen and Vidal 2014
Texas	Stochastic sampling	Socolofsky et al. 2011, Choi et al. 2008
Nationwide	Linear scaling	Kilgore et al. 2016
Nationwide	Linear scaling	NRCS 2015

5.2.3.1. Quantile to Quantile Mapping

Quantile to quantile mapping seeks to develop relationships between GCM daily data and sub-daily and daily historical data through techniques such as regression and genetic programming. These relations are then used to disaggregate projected daily climate model outputs. Three example variations on this approach are described in the following sections.

5.2.3.1.1. Genetic Programming for the City of Saskatoon

Hassanzadeh et al. (2014) describe an approach for developing IDF curves that accounts for future climate change and demonstrates the approach for an application to the City of Saskatoon, Saskatchewan, Canada. The approach uses Genetic Programming to establish a relation between daily annual maximum precipitation (AMP) as estimated by the Canadian global climate model CGCM3 for the period 1961 to 1990 and the corresponding daily and sub-daily estimates as observed in the City of Saskatoon. Genetic Programming uses artificial intelligence and tree structures to develop the needed relations. The authors use a special form of Genetic Programming, genetic symbolic regression (GSR), to seek optimum equations that relate the predictor (daily AMP quantiles at the GCM scale) to the dependent variables (daily and sub-daily locally observed estimates) through an adaptive random search. One of the advantages of GSR over other regression techniques is its ability to provide insight into the functional (structural) form of the relation between inputs and outputs.

The GSR approach used in this study is an example of statistical downscaling whereby a relation is developed between large-scale GCM outputs and point-scale precipitation observations. Assuming the mapping between climate variables at the large scale (GCM scale) and point scale (local observations) is stationary in time, projected local climate variables can be estimated using future projections of GCMs and the mapping relations. Hassanzadeh et al. (2014) note this approach can be applied for either continuous or frequency-based precipitation records:

- For ***continuous records,*** the mapping relations (equations) are determined using the continuous daily precipitation from the GCM and the continuous daily or sub-daily data observed locally. This approach is appropriate for developing projected precipitation for continuous simulation modeling.
- For ***frequency-based records,*** the mapping relations (equations) are determined using the daily AMP quantiles from the GCM and quantiles of the annual maximum daily or sub-daily data observed locally. This approach is appropriate for developing quantiles for event or design-storm modeling.

Hassanzadeh et al. (2014) used the frequency-based approach for the City of Saskatoon study because their objective was to construct IDF curves for future conditions under climate change. The training period for the GSR relations was the period 1961 to 1990 and used the daily AMP quantiles from the GCM as the predictor variables and the quantiles for the annual maximum 1-hour to 24-hour durations (24 relations) based on local observed data. The GCM data were based on CGCM3.1 predictions for the A1B, A2, and B1 scenarios. The general steps for developing the mapping relations are as follows:

1. Fit the Generalized Extreme Value (GEV) frequency distribution assuming a stationary time series using the maximum likelihood method to estimate the quantiles for the GCM and locally observed data.
2. Analyze hindcasted data for the A1B, A2, and B1 scenarios from the CGCM3.1 model. (For the training period 1961 to 1990, the outputs were similar across all scenarios so one set of daily AMP quantiles were used for the GCM data.)
3. Apply the GSR routines to develop relations for each of the 24 durations between the GCM and local data based on a multi-criteria goodness-of-fit measure that included the root

mean-square error, correlation coefficient, mean absolute relative error, and mean bias. These relations are applicable for the three scenarios.

The authors used the projected daily precipitation values from the three scenarios for the ninety-year period 2010 to 2100 and the 24 mapping relations to estimate projected 1-hour to 24-hour precipitation values and new IDF curves. (While a ninety-year projected period was used in the study for comparison with the baseline conditions, other projected periods, e.g., the 30-year period from 2070 to 2100, could have been used.)

For this study, projected IDF values increased across all scenarios for AEPs of 0.1 and greater and durations up to 6 hours. For the 0.04 AEP and durations higher than 2 hours, the future IDF values declined in the B1 scenario and increased in the A1B and A2 scenarios. For the 0.01 AEP, the projected IDF values increased in the A2 scenario and decreased in both the B1 and A1B scenarios. The increases and decreases in projected IDF curves were illustrated in figures, but the actual percentage changes were not reported.

5.2.3.1.2. Empirical Relations Applied to New York State

The Northeast Regional Climate Center at Cornell University in Ithaca, New York, estimated IDF curves for both historical and future periods (Castellano and DeGaetano 2015). Castellano and DeGaetano performed frequency analyses at 157 weather stations in New York and portions of adjacent states and Canada using daily precipitation (based on a partial duration series) for the period 1970-1999. They used L-moments to fit the Generalized Extreme Value (GEV) distribution to the daily data, assuming a stationary time series.

For estimated future conditions, the authors obtained 49 projections of daily data from three downscaling techniques, two scenarios (the lower RCP4.5 and the higher RCP8.5), and three future periods (2010-2039, 2040-2069, and 2070-2099). The three downscaling methods are as follows:

- Quantile to quantile mapping to bias correct daily precipitation extremes dynamically downscaled from regional climate models run at 50-km resolution and driven by CMIP5 global models from CORDEX. This method provided four model projections for each scenario and future period.
- A variation of the delta method to compute differences in simulated precipitation extremes between CMIP5 projected estimates and the historical period (1970-1999) and apply these differences to the observed precipitation extremes. This method provided 25 CMIP5 model projections for each scenario and future period.
- A combination of quantile to quantile mapping with a unique approach for downscaling daily precipitation extremes from historical analogs. The analog approach involves a multi-step procedure in which the occurrence of extreme precipitation on a given CMIP5 model day is first predicted based on the observed probability of extreme precipitation on that day's closest historical analog day(s). Then, if extreme precipitation occurred on the selected analog day(s), the precipitation observations associated with the historical analog day(s) are used to ascribe the precipitation amounts on the corresponding model day. This method provided 20 CMIP5 model projections for each scenario and future period.

The n-hour (sub-daily) values for the downscaled data were obtained by adjusting the daily data based on the factors from Table 5.12 developed by McKay and Wilks (1995). These factors are

based on daily data at 256 stations in the northeastern United States with at least 30 years of record. Partial duration series data were developed with the sample size equal to the number of years of record. The partial duration series data were ranked, divided by the daily amount, and averaged for each station and then averaged across all 256 stations in the study.

The L-moment frequency method was applied to the downscaled projected daily precipitation estimates for the three periods to estimate quantiles. Frequency analyses were also performed for the 1-, 2-, 3-, 6-, 12-, 18- and 24-hour durations, to develop IDF curves based on the ratios in Table 5.12 applied to the daily AEP frequency curves. The assumption is that these ratios will not change with increasing temperatures. The daily data used in the McKay and Wilks (1995) study were based on recording times of approximately 8 a.m. each day. Therefore, it is possible to have a larger precipitation total in 24 consecutive hours than in a set 24-hour period from 8 a.m. to 8 a.m.; hence the ratio of 1.13 for the 24-hour duration. The analyses by McKay and Wilks (1995) also indicated a ratio greater than 1.0 for the 18-hour duration data.

Table 5.12. Factors for adjusting daily values.

Duration	Northeast Average
1-hour	0.43
2-hour	0.54
3-hour	0.62
6-hour	0.79
12-hour	0.97
18-hour	1.07
24-hour	1.13

Based on the ensemble mean of the 49 individual projections, IDF curves for 157 locations in New York and the surrounding area are provided online at http://ny-idf-projections.nrcc.cornell.edu/. IDF curves are available for the 0.5, 0.2, 0.1, 0.04, 0.02, and 0.01 AEP rainfall depths from the greater RCP8.5 scenario and the lesser RCP4.5 scenario for a historical period (defined by NOAA Atlas 14) and three future periods (2010-2039, 2040-2069, and 2070-2099). The online resource also provides graphical comparisons between the historical IDF curves and those for future time periods and scenarios.

New York City (2017) has developed guidelines based on the work at the Northeast Regional Climate Center. This kind of tool provides a consistent resource for engineers to design facilities that are resilient to changing climate conditions. Included in these guidelines are baseline and projected design storm events for the 1- and 24-hour duration precipitation for the 0.2, 0.02, and 0.01 AEP design storms for the baseline and future periods described previously.

To develop the tool, New York City made policy decisions regarding the levels of risk and conservativism. These decisions resulted in basing the projected precipitation values on the 90th percentile of the higher RCP8.5 scenario. With this selection, the 0.01 AEP 24-hour precipitation depth increased by 20 percent for the period 2010-2039, 40 percent for the period 2040-2069, and 52 percent for the period 2070-2099 compared with the baseline.

5.2.3.1.3. Quantile Regression Analyses Applied in Canada

Simonovic et al. (2016) developed a web-based tool (IDF_CC) for use by water professionals in Canada to estimate IDF curves incorporating climate change for approximately 700 weather stations in the Environment Canada database. The IDF_CC tool provides estimates of future IDF curves from 22 CMIP5 GCMs (ensemble option) or the user can choose an individual GCM. The ensemble option represents the median of all models.

The tool allows the user to select a 20-year period for any time between 2006 and 2100 for three future scenarios: RCP2.6, RCP4.5, and RCP8.5. It uses the Gumbel distribution and the method of moments for estimating the AMP. Precipitation estimates are provided for AEPs of 0.50, 0.20, 0.10, 0.02, and 0.01 and durations of 5, 10, 15 and 30 minutes and 1, 2, 6, 12, and 24 hours.

The major steps in the development of the IDF curves in this study are as follows:

1. Extract sub-daily annual maximums from the observed data at a given location (5, 10, 15, and 30 minutes and 1, 2, 6, 12, and 24-hour durations) from the historical baseline period. Fit the annual maximum series (AMS) for each duration to a Gumbel distribution, assuming a stationary time series to determine the quantiles.
2. Extract daily annual maximums for the historical baseline period from the selected GCM. Fit the AMS to a Gumbel distribution, assuming a stationary time series to determine the quantiles.
3. Extract daily annual maximums from the projected RCP scenarios (RCP2.6, RCP4.5, and RCP8.5) for the selected GCM output. Fit the annual maximum series to a Gumbel distribution to determine the quantiles.
4. Establish a statistical relation between the GCM baseline daily quantiles and the sub-daily baseline observed quantiles.
5. Establish a quantile-based statistical relation between the projected GCM simulations of daily maximums to the baseline historical GCM daily maximums.
6. Use the statistical (regression) relations in Steps 4 and 5 and the projected GCM daily quantiles to generate projected sub-daily data to develop IDF curves for a given scenario and future period.

5.2.3.2. Curve Fitting - Mathematical Relations for the Mid-Atlantic Region

Curve fitting assumes IDF curve shapes derived from historical data and applies these shapes to extend projected GCM output to finer temporal disaggregation. One example of this approach is described here.

Moglen and Vidal (2014) describe an approach for developing IDF curves for future conditions that incorporates climate change for the Mid-Atlantic region of the United States. They obtained downscaled climate model precipitation output for four GCM/regional model pairs from the NARCCAP (Mearns et al. 2009) at a 3-hour resolution for a future (2041-2070) scenario based on the A2 scenario and a historical (1971-2000) period.

The historical and future model outputs were aggregated into 3-, 6-, 12-, 24- and 48-h durations on an annual basis and a frequency analysis was performed on the annual maximums for each duration and time period by fitting a log-Pearson Type III distribution to the data. Because the

historical and future periods were 30 years, the authors chose to analyze only the 0.5 and 0.10 AEP rainfall depths.

The authors based their methodology on the observation that IDF curves for durations less than one hour follow an inverse relation between intensity and duration and for durations greater than one hour follow a power law relation (McCuen 2005). The methodology is summarized in the following steps:

1. For each AEP and time period (historical and future), fit the modeled estimates for the five durations (3-, 6-, 12-, 24-, and 48-h) to a power law relation of intensity as a function of duration.
2. Using the fitted relations, compute the ratio of future to historical precipitation for each duration and AEP.
3. Adjust the observed NOAA Atlas 14 rainfall intensities by the ratios computed in Step 2 to estimate future rainfall intensities for each duration and AEP.
4. Fit the adjusted future intensities from Step 3 to the power law relation to obtain revised IDF curves. These curves represent the future IDF relations for durations greater than 1 hour.
5. Determine the equation for durations less than one hour by assuming that at the 1-hour duration, both the IDF equation for less than one hour and for more than one hour: 1) produce the same intensity value and 2) exhibit the same curve slope.

The results of this process are two equations describing the IDF for each AEP for a given GCM/regional model pair. These steps are repeated for each of the GCM/regional model pair of interest.

Cook et al. (2017) also analyzed the 3-hour data from NARRCAP for a single grid cell in Pittsburgh. For the historical (1971-2000) and future (2041-2070) periods, precipitation depths were estimated for the 3-, 6-, 12-, 24-, 48- and 72-hour durations and for the 0.50, 0.20, 0.10, 0.04, 0.02, and 0.01 AEPs. Based on five different RCM-GCM simulations, change factors representing the ratio of future precipitation depths to historical depths for each duration and AEP were estimated. The median change factors for each RCM-GCM combination were greater than 1.0, indicating DDF precipitation values will likely increase in the future. There was no consistent pattern in the increase in DDF values across durations or AEPs. As noted above, the results are only applicable to the A2 scenario.

5.2.3.3. Stochastic Sampling - Application of Historical Storm Patterns in Texas

Stochastic sampling establishes precipitation depth cumulative distribution functions from observed historical data and uses these data to randomly sample from the historical database to generate storms from daily data. One example of this approach is described here.

Socolofsky et al. (2001) developed a stochastic approach for disaggregating daily precipitation data using hourly data from other gauges. In this method, the hourly precipitation data are grouped into individual storm events where an event is defined as a continuous sequence of uninterrupted hourly rainfall. All storm events are grouped by month where each group contains multiple years of data. Each monthly dataset of storm event depths is sorted in ascending order based on their total accumulated rainfall depth, resulting in a cumulative distribution function

(CDF) for storm depth for each month for each station. Each entry in the CDF corresponds to a measured storm event in the hourly precipitation database. (Because the daily precipitation data will be disaggregated one day at a time, simulated storm events compiled from the hourly data are not allowed to extend beyond midnight.)

The daily rainfall depth in the daily database is defined as D_T. Storms from the CDFs are randomly selected to disaggregate each daily rainfall depth. To constrain the search for a randomly selected event, the index "*a*" is found in the CDF such that the corresponding event depth is equal to the depth D_T. All events with indices less than "*a*" then have a total event depth less than or equal to D_T. A storm event is selected by generating a uniformly distributed random number between zero and "*a*" and selecting the corresponding event from the CDF. The selected storm event depth is then subtracted from the initial value of D_T to obtain an updated value of D_T. The algorithm continues until D_T is zero. Once completed for all daily values, a new CDF of the selected events is created for each month. One constraint on this method is separates storms in the daily data that span midnight into two separate storms – one before midnight and one after.

Choi et al. (2008) applied this approach using hourly data at 532 precipitation stations in Texas. Although their primary purpose was to generate hourly precipitation time series for calibration and verification of continuous simulation models, a time series of hourly data could also be used to generate an IDF curve with a lower limit on the duration of one-hour.

The result of the work of Choi et al. was development of an intensity versus AEP curve for a typical station in central Texas. Their overall evaluation of the stochastic storm simulation method was that the intensity-exceedance curves matched the majority of the moderate rainfall events very closely. However, the curves both over- and under-predicted the extreme events with systematic under-prediction for events above 75 mm/h. They also observed that the simulated data overestimated the maximum intensity by up to 17 percent.

The application of Choi et al. did not include evaluation of this method for projected daily precipitation data derived from GCM output. However, the method does represent a potential strategy for disaggregating daily data to sub-daily values regardless of whether the daily data are historical or projected from GCMs.

5.2.3.4. Linear Scaling

Linear scaling uses observed historical ratios between daily and sub-daily quantiles and applies them to projected daily precipitation values to estimate the sub-daily quantiles. Two examples of this approach are described here.

5.2.3.4.1. Adjustment of Historical Data from NOAA Atlas 14

Kilgore et al. (2016) recommended an approach for estimating the projected change in the 24-hour precipitation for selected AEPs. The downscaled daily precipitation data are first downloaded from the DCHP website or equivalent database (such as the Localized Constructed Analogs [LOCA]) for the baseline period and projected period. The authors recommend using an ensemble of climate model outputs for multiple scenarios that includes the RCP6.0 scenario. The approach uses quantile ratios in NOAA Atlas 14 to produce sub-daily estimates of future precipitation. The steps in the process are summarized as follows:

1. Determine the historical 24-hour and sub-daily precipitation estimates for a selected AEP from an accepted source and calculate the ratio of each sub-daily value to the 24-hour value.
2. Estimate the future 24-hour precipitation depth for the selected AEP using the ten-step procedure in Section 5.1 or other suitable approach.
3. Apply the sub-daily ratios computed in Step 1 to the future 24-hour precipitation estimated in Step 2 to compute the future sub-daily values for the selected AEP.
4. Repeat Steps 1 through 3 for each AEP of interest.

This approach assumes that historical ratios calculated in Step 1 are indicative of ratios that could be expected in the future. Such a stationarity assumption is required in this method and other statistically based approaches.

5.2.3.4.2. Natural Resources Conservation Service Temporal Distributions

The Natural Resources Conservation Service (NRCS) developed an approach for linking daily rainfall to shorter duration events. The NRCS used data from TP-40 (1961) and Hydro-35 (U.S. Department of Commerce 1977) to develop the Type I, Type IA, Type II, and Type III temporal distributions. The temporal distributions are the ratios of 5-minute/24-hour precipitation values up to the 12-hour/24-hour precipitation values. NRCS developed each temporal distribution using the frequency data in the above-mentioned reports. These distributions varied across AEP values, but NRCS averaged them so that one shape represented all AEPs to simplify the application process for engineers. Engineers use these NRCS temporal distributions in event-based hydrologic models such as WinTR-20 and HEC-HMS.

The National Weather Service of NOAA is updating TP-40 (1961) and Hydro-35 (1977) as part of its development of NOAA Atlas 14. Based on these new data, NRCS developed new regional temporal distributions using the ratios of 5-minute/24-hour precipitation through the 12-hour/24-hour precipitation values from NOAA Atlas 14. An example of regional NOAA Atlas 14 temporal distributions is given in Figure 5.14 for Volume 2 of NOAA Atlas 14 (Ohio Valley and neighboring states) (Merkel et al. 2015). The differences in the four temporal distributions for the Ohio Valley and neighboring states are relatively small. The NRCS temporal distributions essentially disaggregate the 24-hour data into sub-daily values for modeling small watersheds.

Figure 5.15 shows the states in the continental United States for which NOAA Atlas 14 temporal distributions are available as of January 2016 (NRCS 2015). In September 2018, the National Weather Service released Volume 11 of NOAA Atlas 14 for Texas, and NRCS is developing new temporal distributions for Texas. Temporal distributions based on NOAA Atlas 14 are also available for Hawaii, Alaska, Puerto Rico, the U.S. Virgin Islands, and selected Pacific Islands. For states where NOAA Atlas 14 has not been updated, NRCS recommends the use of the Type 1, Type 1A, Type II, or Type III temporal distributions for the appropriate location as shown in Figure 5.15 (NRCS 2015).

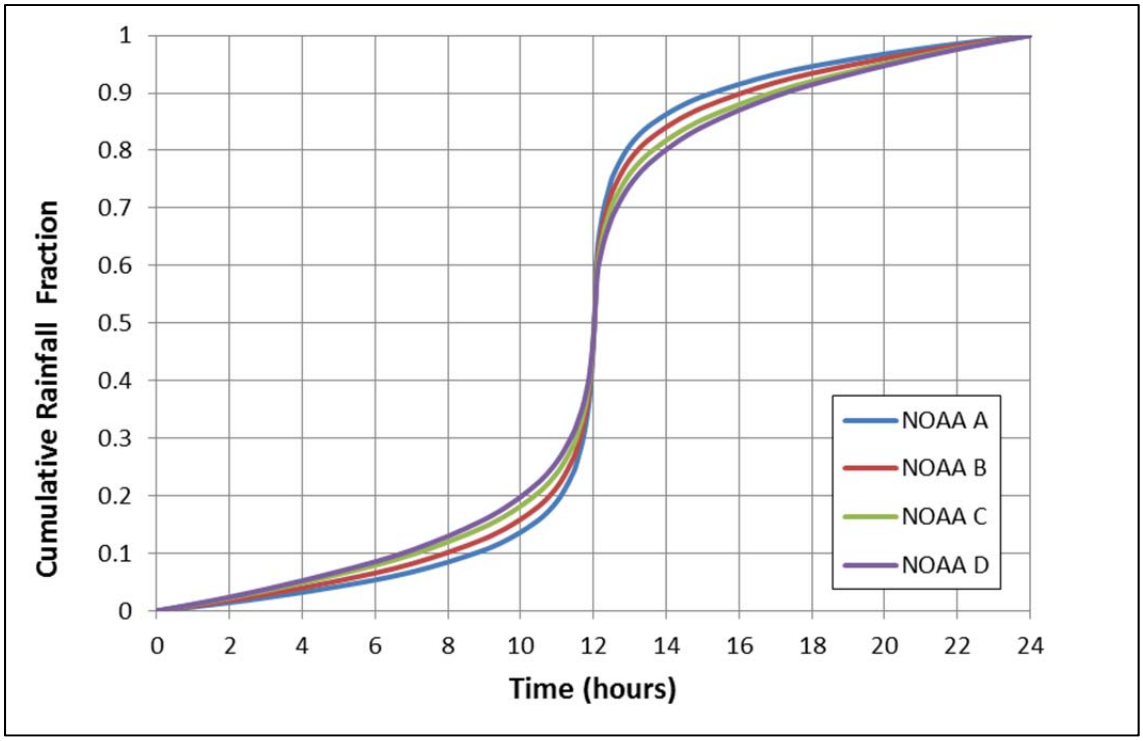

Figure 5.14. Four regional 24-hour rainfall distributions from Volume 2 of NOAA Atlas 14 (Ohio Valley and neighboring states).

The use of the NRCS synthetic temporal distributions only requires the 24-hour precipitation for selected annual exceedance probabilities for use in event based hydrologic models. Temporal distributions such as those shown in Figure 5.14 define the relation between the shorter durations (sub-daily) and the 24-hour precipitation. Therefore, the NRCS temporal distributions can effectively utilize the projected daily precipitation data available from selected GCM output databases to estimate sub-daily quantiles. The approach assumes that the temporal distributions based on NOAA Atlas 14 are stationary.

An example application of the NRCS synthetic temporal distributions to estimate precipitation depth for various AEPs for future climate change is described by the Minnesota Department of Transportation (MnDOT 2014). MnDOT evaluated the potential effects of climate change on two small (less than 20 square miles) watersheds using the NRCS temporal distributions and WinTR-20. They developed precipitation AEPs using daily (24-hour) data from the DCHP website for baseline and three future periods based on the output from 22 GCMs. The median percentage change for the 24-hour precipitation was calculated and applied to the NOAA Atlas 14 data for current conditions to obtain future precipitation for selected AEPs. The inherent assumption in this approach is that sub-daily values estimated from the temporal distributions increased by the same percentage as the 24-hour values. The increased precipitation values were input in the WinTR-20 model to estimate increases in the AEP discharges resulting from climate change. Across the three scenarios for one culvert site, a 3.8 to 32.4 percent increase in the 0.01 AEP 24-hour precipitation resulted in a 16 to 60 percent increase in the 0.01 AEP discharges. For the other culvert site, a 3.2 to 27.1 increase in the 0.01 AEP precipitation resulted in a 5 to 36 percent increase in the 0.01 AEP discharges.

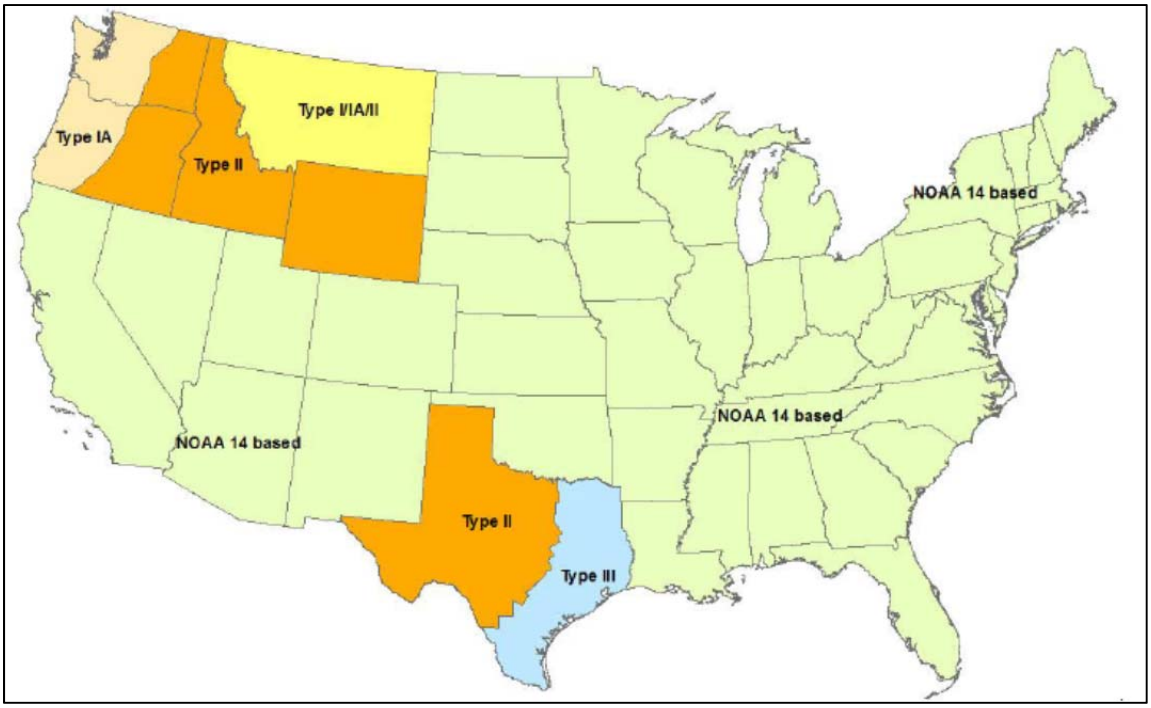

Figure 5.15. Map of the synthetic rainfall distributions used by NRCS as of January 2016 (NRCS 2015).

5.2.3.5. Recommendations for Development of IDF Curves

As described in the previous section, several approaches to estimating future sub-daily quantiles and IDF curves have been tested and applied. However, such tools do not currently exist in most places. Some exceptions have been mentioned including New York City (New York City 2017), Canada (Simonovic et al. 2016), and the Netherlands (Fortuin 2017).

The Netherlands Ministry of Infrastructure and Environment developed DDF curves for 5- to 120-minute durations for the 0.1, 0.02, and 0.004 AEP events for 2030, 2050, and 2085 for designing roads, bridges, and tunnels in the Netherlands (Fortuin 2017). The set of recommended IDF curves for projected conditions were based on an analysis of a nationwide network of precipitation gauges and internally derived future scenarios.

Each of these approaches assumes that the relation between sub-daily and daily data will remain stationary for the future to some degree. The differences between the methods are in defining where those relationships are fixed and the degrees of freedom in developing the resulting relationships between daily and sub-daily data.

Important differences between the approaches are the selections of the GCMs, downscaling, and scenarios used. As described in Chapter 4, a range of projected outputs should be considered, but in many of the described approaches, resource constraints limited the research and demonstration efforts to smaller subsets of outputs. Other differences include choices of analytical techniques and future period horizon. In some cases, a responsible government entity makes a policy decision about one or more of these choices based on their degree of conservatism. These choices vary from place to place and affect the estimates of change between historical and projected conditions.

Regardless of these differences, in those areas with official sub-daily data or IDF curves for future conditions, engineers will directly use those tools in the same way they use historical sub-daily and IDF tools. Developing and publishing IDF or DDF information for a community or region provides consistent guidelines for designing facilities and reduces the need to conduct site-specific studies.

For those areas where no such tool or resource providing estimates of future sub-daily information exists, recommended strategies are needed. The strategies must employ accessible data, incorporate reasonable assumptions, and reflect reproducible outcomes.

Engineers face resource constraints in project budgets. Except for infrequent projects involving large capital expenditures and critical risks, the engineer will require straightforward methods for estimating future sub-daily data. For these situations, the recommended approaches are the two linear scaling methods described in the previous section:

- Adjustment of historical data based on at-site data in NOAA Atlas 14.
- Use of regional temporal distributions developed by the NRCS (NRCS 2015).

The linear scaling methods are based on widely available tools and data and represent a straightforward approach that is readily incorporated into the design process. As recommended in Chapter 4, these approaches should be implemented using multiple downscaled GCM outputs and scenarios. The mean curve for each given scenario should be selected for design of the project, but other scenarios should also be evaluated to determine how the proposed design could vary.

Confidence limits are recommended to define the higher and lower curves rather than taking the highest and lowest curves generated. Simply using the highest and lowest curves does not provide insight into the potential variability of the IDF estimates and the range of data that is appropriate to use for design. Table 5.13 provides guidance on the confidence limits appropriate for the hydrologic service life of the project (Kilgore et al. 2016). The procedure for estimating confidence limits for multiple GCMs is described in Kilgore et al. (2016) and Anderson et al. (2015).

Table 5.13. Confidence intervals based on hydrologic service life.

Hydrologic Service Life (years)	Confidence Interval
Less than 30	38%
Between 30 and 75	68%
Greater than 75	90%

For Level 4 projects (and potentially selected Level 3 projects) with high project costs and risks, linear scaling approaches may not be sufficient to support design decision-making. In such cases, the more rigorous quantile mapping approach is recommended, specifically, the "Simonovic approach" (Simonovic et al. 2016). It employs relatively straight-forward concepts that can be applied to multiple gauges for a project-specific study or to a larger area to develop regional or national tools. Further recommendations for adapting this approach to the United States, along with an example application to a single gauge are described in Section 5.2.4.

BOTTOM LINE: Linear scaling is a reasonable approach for estimating sub-daily precipitation quantities for most projects. Development of state or region-wide sub-daily databases for projected precipitation based on the Simonovic approach is recommended as a cost-effective strategy to support a broader range of projects with more sophisticated estimates.

5.2.4. Adaptation of the Simonovic Approach to the United States

The approach of Simonovic et al. (2016) summarized in Section 5.2.3.1.3 is recommended for some Level 4 analyses and for the development of regional tools for generating future sub-daily precipitation estimates. The assumption in the Simonovic approach is that accurate sub-daily precipitation estimates are not available from RCMs for a wide range of models and scenarios. Therefore, sub-daily precipitation for future time periods are estimated from future daily precipitation data. The following sections describe modifications of the approach for the United States and provide an example application.

5.2.4.1. Modification of the Approach

In the Simonovic approach (Steps 1 and 4), the procedure includes developing frequency curves and estimating quantiles for observed sub-daily precipitation for selected durations ranging from 5 minutes to 24 hours. For application to Canada, the required data were obtained from a nationwide network of precipitation gauges. Therefore, to adapt the method to a site-specific location in the United States, NOAA Atlas 14 could be used for estimating quantiles of sub-daily precipitation for the states covered by NOAA Atlas 14, as well as Puerto Rico, the U.S. Virgin Islands, and selected Pacific Islands. Other precipitation atlases and reports are available for the states where NOAA Atlas 14 is not available. Therefore, the quantiles for the sub-daily precipitation can be obtained from existing atlases and reports that will enable the application of the Simonovic approach in the U.S.

In the method, a relation is developed between the observed sub-daily quantiles from NOAA Atlas 14 and the GCM daily quantiles for the historical period. For the sub-daily data archived at the National Data Climatic Center (NCDC) and used in the development of Atlas 14, the period of record begins about 1948. Volumes 1 and 2 of Atlas 14 used data through 2000 with the more recent volumes having a few additional years of record. The NCDC data are the majority of the hourly and 15-minute data used in NOAA Atlas 14. Therefore, the period of record for much of sub-daily precipitation data in NOAA Atlas 14 is from 1948 to the early 2000s. This period of record is reasonably consistent with the base period of observed data (1950-99) that is available in the commonly used databases with projected climate data.

The steps in the application of the Simonovic approach adapted to the United States include the following:

1. Obtain the sub-daily observed (historical) quantiles from NOAA Atlas 14 for several sub-daily durations such as 5-, 10-, 15-, 30- and 60-minutes and 2-, 3-, 6-, 12- and 24-hours.
2. Extract the daily annual maximums for each downscaled GCM output for the baseline (historical) period for each grid cell, convert the gridded daily data to 24-hour point

data, and estimate the quantiles using an appropriate three-parameter frequency distribution assuming a stationary time series.

3. Extract the daily annual maximums for each downscaled GCM output and scenario for each future period, convert the gridded daily data to 24-hour point data, and estimate the quantiles as described in Step 2.
4. Establish statistical relations between the downscaled GCM output historical 24-hour quantiles (Step 2) and the sub-daily observed (historical) quantiles obtained from NOAA Atlas 14 (Step 1). Need sufficient durations to represent adequately the IDF curves.
5. Establish a statistical relation between the downscaled GCM output 24-hour quantiles for the baseline period (Step 2) and projected GCM simulations for the future periods (Step 3) (One relation for each future period, GCM, and scenario).
6. Use the two statistical relations in Steps 4 and 5 and future downscaled GCM output 24-hour quantiles to estimate future sub-daily precipitation quantiles for development of IDF curves for a given future time period and scenario.

Many three-parameter frequency distributions may be used, such as the Generalized Extreme Value (GEV), Pearson Type III, and log-Normal distributions. In producing Atlas 14, NOAA analyzed the historical data to evaluate the most appropriate data fit. In most regions, NOAA determined that the GEV distribution using L-moments to compute the parameters was the most appropriate. Although it is unknown whether the frequency distributions will shift with future climate conditions, Kilgore et al. (2016) recommends using the distributions chosen in the development of NOAA Atlas 14 for a given location. However, the project design team should always choose the distribution determined to be appropriate based on project-specific conditions.

5.2.4.2. Site-Specific Example Application

The Simonovic approach is illustrated using information derived from a Pennsylvania Department of Transportation study (PennDOT 2017). In that study, the CSIRO-Mk3.6.0 (CSIRO) GCM was one of three GCMs used with the RCP8.5 scenario. Typically, the engineer should use multiple GCMs and scenarios as described by Simonovic et al. (2016), but focusing on a single model/scenario will allow demonstration of the method.

The downscaled GCM output for one grid in the Philadelphia, Pennsylvania, area was obtained from the DCHP website where each grid cell is approximately 12 km by 12 km or 56 square miles. The gridded daily data were converted to point data by multiplying by 1.04 (TP-40 1961) (see Section 5.3 for a discussion of this conversion) and converted to 24-hour data using the conversion factor 1.13 (see NOAA Atlas 14, Volume 2). The conversion to point data was needed for consistency because the observed (historical) sub-daily data estimated from NOAA Atlas 14, Volume 2 are point data.

For Step 1, the observed sub-daily AEP quantiles for five selected durations are extracted from NOAA Atlas 14 (Volume 2) and summarized in Table 5.14 to illustrate the technique. Additional quantiles could be added.

Table 5.14. Summary of observed sub-daily AEPs for selected durations from NOAA Atlas 14 for Philadelphia, PA.

Duration	AEP (0.50) (inches)	AEP (0.10) (inches)	AEP (0.04) (inches)	AEP (0.01) (inches)	AEP (0.002) (inches)
5-minute	0.38	0.53	0.60	0.68	0.76
15-minute	0.77	1.08	1.21	1.37	1.52
60-minute	1.33	2.03	2.38	2.89	3.47
6-hour	2.16	3.37	4.05	5.15	6.58
24-hour	2.99	4.76	5.83	7.67	10.20

To estimate the quantiles for Steps 2 and 3 of the procedure, the AMS of daily downscaled GCM output were fit to the Pearson Type III distribution assuming a stationary time series to determine the daily quantiles for the baseline period (1950-1999) and the future period (2000-2049, RCP8.5). Other three-parameter distributions could be used and the appropriate one selected based on site-specific considerations. Other time period windows could also be chosen for the analysis and should consider the hydrologic service life of the project. A shorter future time horizon, but not less than 30 years, may provide additional insight into the direction of climate change as opposed to longer time periods that may obscure changes estimated in the future.

The precipitation depths for selected AEPs for the two periods are given in Table 5.15. The future daily quantiles range from 12 to 15 percent higher than estimated during the baseline period. The mean, standard deviation and skew are also provided for the two periods to illustrate the increase in future precipitation is primarily related to the increase in the mean.

Table 5.15. Summary of model-based (GCM) 24-hour quantiles for the example.

AEP	Baseline Period (1950-1999) Precipitation Depth (inches)	Future Period (2000-2049) Precipitation Depth (inches)	Ratio of Future to Historical
0.50	2.737	3.079	1.125
0.10	4.217	4.788	1.135
0.04	5.011	5.709	1.139
0.01	6.259	7.159	1.144
0.002	7.835	8.994	1.148
mean	0.444541 log units	0.495706 log units	---
std deviation	0.137665 log units	0.140828 log units	---
skew	0.31763	0.30834	---

In Step 4, a series (one for each duration) of statistical relations between the observed (historical) sub-daily quantiles and the GCM daily quantiles estimated for the 1950-99 baseline period is developed. Each row in Table 5.14 (representing a duration) is regressed against the baseline GCM daily quantiles in Table 5.15, pairing the data by AEP. For example, the data and resulting relation for the 60-minute duration are plotted in Figure 5.16. With linear regression of the logarithms, the relation in the figure is as follows:

$$P_{1,\mathrm{h}} = 0.5375\left(P_{24,b,m}\right)^{0.9144} \quad (5.4)$$

where:

$P_{1,h}$ = *Historical precipitation for a 1-hour duration.*

$P_{24,b,m}$ = *Baseline period 24-hour precipitation from the GCM.*

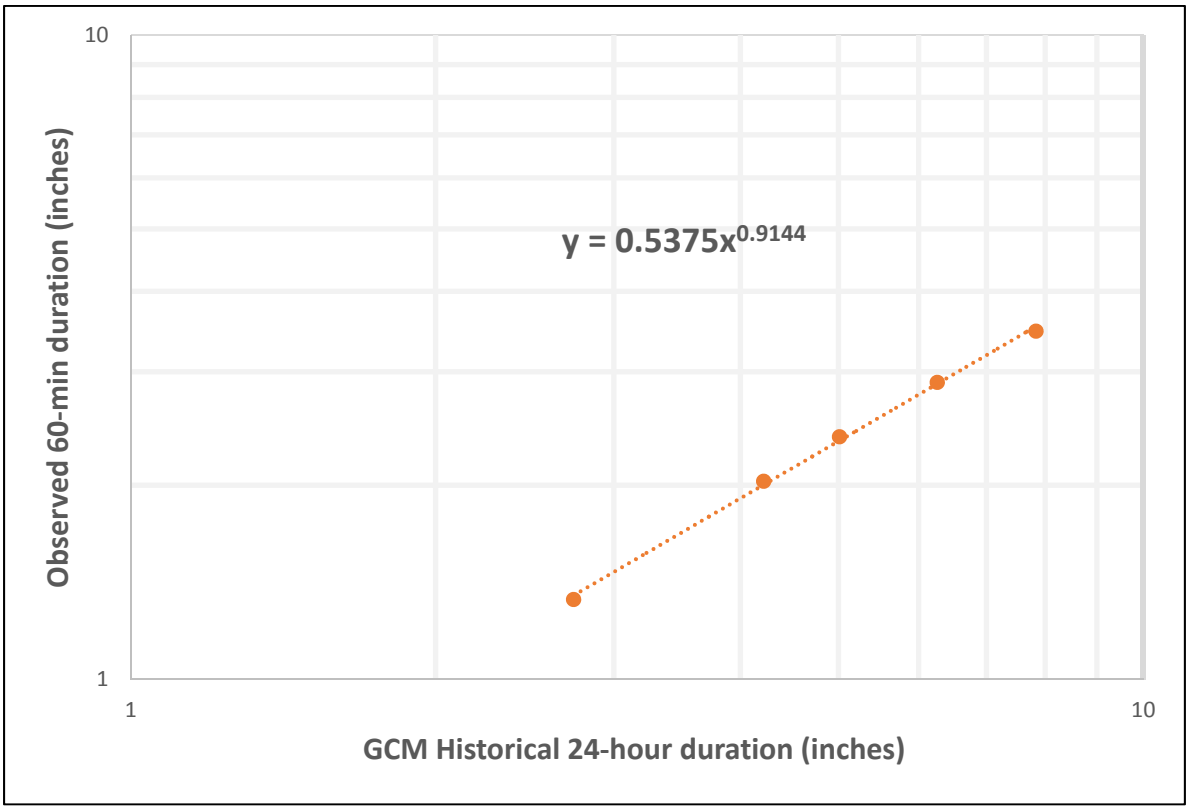

Figure 5.16. Relation between observed 60-minute duration quantiles and baseline GCM 24-hour quantiles for the example application to Philadelphia, PA.

In Step 5, a single statistical relation between future GCM quantiles and the baseline GCM quantiles is developed for each GCM, scenario, and future time period. For this example, both sets of quantiles are shown in Table 5.15 and are plotted in Figure 5.17. With linear regression of the logarithms, the relation shown in the figure is defined as follows:

$$P_{24,\mathrm{f,m}} = 1.1038\left(P_{24,\mathrm{b,m}}\right)^{1.0193} \quad (5.5)$$

where:

$P_{24,f,m}$ = *Future period 24-hour precipitation from the GCM.*

$P_{24,b,m}$ = *Baseline period 24-hour precipitation from the GCM.*

For Step 6, the previous two equations are transformed to generate projected sub-daily quantiles. First, Equation 5.4 is redefined for the future rather than baseline period by assuming the future 60-minute quantiles and the future daily quantiles will have the same relation as in Equation 5.4. Then, Equation 5.5 is substituted into Equation 5.4 to yield:

$$P_{1,\mathrm{f}} = 0.588\left(P_{24,b,m}\right)^{0.932} \tag{5.6}$$

where:

$P_{1,f}$ = *Future precipitation for a 1-hour duration.*

While it appears from Equation 5.6 that the projected 24-hour precipitation information is no longer needed to compute the future sub-daily information, it is actually incorporated (in a smoothed form) through Equation 5.6. Also, in Equation 5.6, the AEP for the future 60-minute quantile is the same as the AEP for the 24-hour historical GCM daily quantile.

The historical and future quantiles for the 60-minute duration are given in Table 5.16. The increase in the 60-minute quantile from historical to future for the given GCM and scenario conditions ranges from 11 to 13 percent. That is consistent with the 12- to 15-percent increase in the 24-hour quantiles in Table 5.15 because the observed 60-minute values are being scaled by the increase (or decrease) in the historical 24-hour quantiles.

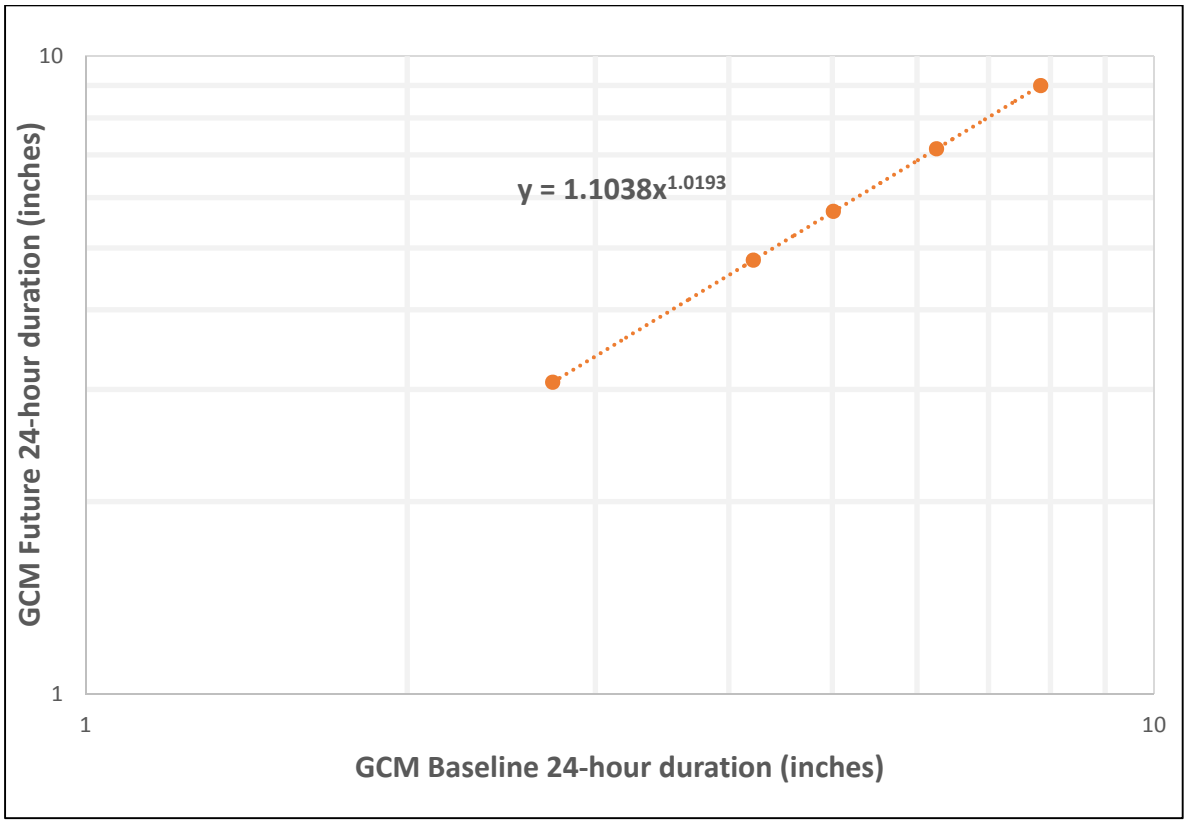

Figure 5.17. Relation between the GCM future and baseline 24-hour quantiles for the example application to Philadelphia, PA.

Following the same procedure, future quantiles for the 5- and 15-minute durations, and the 6- and 24-hour durations are computed and summarized in Table 5.17. The quantiles for the 5- and 15-minute durations increased 6 to 13 percent from historical to future conditions while the quantiles for the 6- and 24-hour durations increased 12 to 18 percent.

Table 5.16. Summary of historical and future 60-minute quantiles for Philadelphia, PA.

Exceedance Probability	Historical 60-minute precipitation depth (inches)	Future (2000-2049) 60-minute precipitation depth (inches)	Ratio of Future to Historical
0.50	1.33	1.50	1.13
0.10	2.03	2.25	1.11
0.04	2.38	2.64	1.11
0.01	2.89	3.25	1.12
0.002	3.47	4.00	1.13

Table 5.17. Summary of historical and future (2000-2049, RCP8.5) quantiles for the 5- and 15-minute and 6- and 24-hour durations for Philadelphia, PA.

AEP	5-min historical (inches)	5-min future (inches)	15-min historical (inches)	15-min future (inches)	6-hour historical (inches	6-hour future (inches)	24-hour historical (inches)	24-hour future (inches)
0.50	0.381	0.422	0.766	0.854	2.16	2.43	2.99	3.36
0.10	0.532	0.566	1.06	1.14	3.37	3.88	4.76	5.62
0.04	0.598	0.636	1.21	1.28	4.05	4.67	5.83	6.90
0.01	0.682	0.739	1.37	1.48	5.15	5.94	7.67	9.00
0.002	0.762	0.860	1.52	1.72	6.58	7.57	10.2	11.75

IDF curves for existing conditions can now be constructed from data in Table 5.14, while IDF curves for future conditions can be constructed from Table 5.16 and Table 5.17. For example, the historical and future IDF curves for the 0.01 AEP are summarized in Table 5.18. As shown in Table 5.18, the increases for the 0.01 AEP precipitation vary from 8 percent for the 5-minute duration to 17 percent for the 24-hour duration. This example illustrates that the shorter duration events do not necessarily change in the same proportion as the 24-hour events. In addition, the future IDF curve would vary with model and scenario.

Table 5.18. Summary of historical and future (2000-2049) precipitation depths for the 0.01 AEP for Philadelphia, PA for the CSIRO model and the RCP8.5 scenario.

Duration (hours)	Historical precipitation depth (inches)	Future (2000-2049) precipitation depth (inches)	Ratio of Future to Historical
0.083	0.682	0.739	1.08
0.25	1.37	1.48	1.08
1	2.89	3.25	1.12
6	5.15	5.94	1.15
24	7.67	9.00	1.17

The 0.01 AEP curves are shown in Figure 5.18 with the ordinate converted to intensity illustrating the increase in precipitation intensity for the 0.01 AEP event from historical to future (2000-2049) conditions for Philadelphia, Pennsylvania, using data for one GCM (CSIRO), one

scenario (RCP8.5), and one time period. Application of the method should use multiple GCMs and scenarios creating a series of IDF curves. The mean IDF curve with the associated confidence limits from all GCMs for a given scenario provides a design tool for estimating future sub-daily precipitation. Repeating the process for multiple scenarios allows consideration of a possibly broader range of future outcomes.

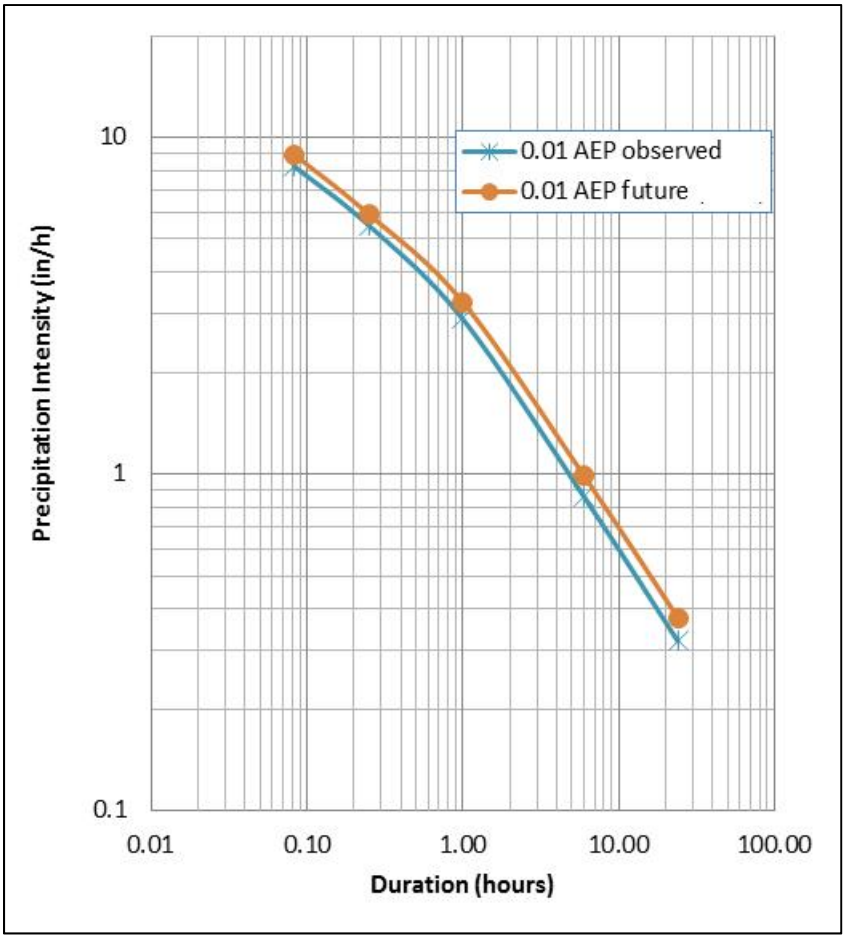

Figure 5.18. IDF curves for historical and future conditions for the 0.01 AEP for Philadelphia, PA.

5.2.4.3. Discussion of Application

The CSIRO model results for the 2000-2049 period (RCP8.5 scenario) were chosen for the example because this scenario exhibited an increase in the extreme AEP events such as the 0.01 AEP (100-year) event from the historical to future periods. However, there is significant variability in the projections.

Limited frequency analyses were also performed for locations in the Baltimore, MD and Pittsburgh, PA areas using projected data for three GCMs (CSIRO, CCSM4, and MIROC5). Estimates of the 0.01 AEP daily events both increased and decreased from historical to future periods. However, the mean of annual maximum daily precipitation values always increased with time suggesting that more frequent quantiles may consistently increase even though more extreme quantiles do not. As with any dataset, the absence or presence of extreme events will likely affect the computed standard deviation and skew more than the mean. This absence or

presence of extreme events from a particular downscaled GCM output dataset may be random or may reflect that some modeling approaches do not capture the extremes of the AEP distribution very well.

The Simonovic approach (Simonovic et al. 2016) is computationally intensive. To assist with these computations, Simonovic et al. created a web-based tool (IDF_CC) for Canada that includes downloading the required data from the appropriate climate websites. A similar computational package would be very beneficial for use in the United States.

Whether the complexity of the Simonovic approach is worthwhile for a single project depends on the project. One potentially important difference between the linear scaling methods and the quantile mapping approach of Simonovic et al. is that the former, assumes the same percentage change in the sub-daily quantiles as is estimated for the 24-hour quantile. As shown in Table 5.18, the Simonovic method may result in different percent changes for each duration.

5.3. Spatial Scale Compatibility

This section addresses the use of gridded downscaled GCM precipitation output in hydrologic analysis and design. Engineers recognize that real rainfall fields may vary widely in time and space. Typically, engineers use point estimates or spatially adjusted point estimates compatible with the scale of the watershed of interest whereas the gridded downscaled GCM precipitation is spatially-averaged over the grid area. For larger watersheds, engineers may use multiple point estimates to represent the precipitation in different parts of the watershed. Therefore, there is a need for a method to convert spatially-averaged grid precipitation estimates from downscaled GCM output to the appropriate watershed scale. As described in Chapter 4, some downscaled GCM outputs provide point estimates, but these are not broadly available; therefore, such datasets are not discussed in this section.

Downscaled GCM outputs are generally available as spatially-averaged precipitation on regular grids. For example, the DCHP 1/8th degree downscaled data is available on 1/8 degree by 1/8 degree grids, which is roughly equivalent to 7.5 mile by 7.5 mile (12 km by 12 km) rectangles at mid-latitudes (56 square miles). The LOCA dataset is available on with 1/16 degree by 1/16 degree grid cells (14 square miles) and one version of the MACA dataset is 1/24 degree by 1/24 degree grid cells (approximately 6 square miles). The smaller a watershed is relative to these grid sizes, the greater the gap between the available spatially-averaged precipitation from the gridded output and then required point precipitation estimate for hydrologic analysis.

The initial question is how to define a small watershed? The term “small watershed” is often not well defined and depends on the limits of the tools applied and the data required to develop the hydrologic estimates. NRCS personnel use a cutoff drainage area of 25 square miles to determine whether a watershed qualifies as “small” (WinTR-55 Workgroup 2009). Black (2005) states that a watershed is small if the drainage area is sufficiently small such that the rainfall fields that affect it can be treated as homogeneous. Such a definition would result in a watershed scale of a few square miles up to perhaps the suggestion of NRCS (25 square miles), depending on the geographic location of the watershed.

Similar to Black’s reasoning, an alternative approach is to consider the time response characteristic of the watershed. If the time response of the watershed is such that rainfall can be treated as homogenous in time and space, then the watershed can be defined as “small.”

However, watershed drainage area is only one component used for estimating the time response characteristic of a watershed. Others are roughness, shape, and slope.

For the purpose of this report, a "small watershed" is defined as one with a drainage area less than a downscaled data grid cell. While it is unlikely that a watershed with an area the size of a grid cell would overlay only that grid, this definition is intended to focus on rough scale. The use of other existing or future downscaled GCM output with differing grid cell sizes will require an adjustment of that numeric threshold.

Section 5.1.1 describes a procedure for estimating 24-hour precipitation quantiles from gridded downscaled precipitation projections and recommends that precipitation from at least three downscaled grid cells be downloaded and analyzed. The recommendation is intended to avoid using a single cell for small watersheds that may turn out to be an outlier for some reason. For large watersheds extending beyond the minimum recommended number of grid cells, the guidance recommends using all grid cells overlaying the watershed.

The following sections provide background information on the general engineering practice of adjusting point rainfall estimates for watersheds of varying sizes for use in rainfall/runoff modeling. Although most GCM output is available at spatially-averaged grids, a discussion of available point GCM output is included. Finally, recommended procedures for adapting downscaled GCM outputs to the appropriate watershed spatial scale are discussed.

5.3.1. Background and Development

Rainfall is highly variable in both space and time. A single point precipitation estimate may sufficiently represent local conditions for watersheds of very small contributing area for engineering estimation purposes. However, with increasing watershed contributing area, the likelihood that the statistically computed point estimate of rainfall depth or intensity (for a given AEP) would be observed over the entire watershed decreases. That is, average precipitation depth for a given AEP quantile and duration decreases with increasing area. Therefore, at some watershed area scale, it becomes prudent for the engineer to quantitatively discount, or reduce, the estimated rainfall depth developed from point rainfall statistics to account for the tendency of rainfall fields to decrease in average depth/intensity over increased area of the rainfall field (and watershed drainage area).

Recognition of the diminishing average precipitation depth with increase in watershed area led to the development of areal reduction factors (ARFs). Technical Paper 29 (TP 29) (U.S. Department of Commerce 1957) and Technical Report 24 (NWS-24) (U.S. Department of Commerce 1980) are commonly used sources for ARFs. Figure 5.19 displays an example ARF chart from NWS-24. ARFs are often obtained by reading monotonically decreasing graphs of a discount factor over the closed interval [0,1] on the ordinate versus contributing area on the abscissa.

Both rainfall depth/duration/frequency information and ARF information have historically assumed stationary processes. However, decades have passed since many of the national ARF curves were developed and whether changes have been detected the past 40 to 60 years represents a potential research opportunity.

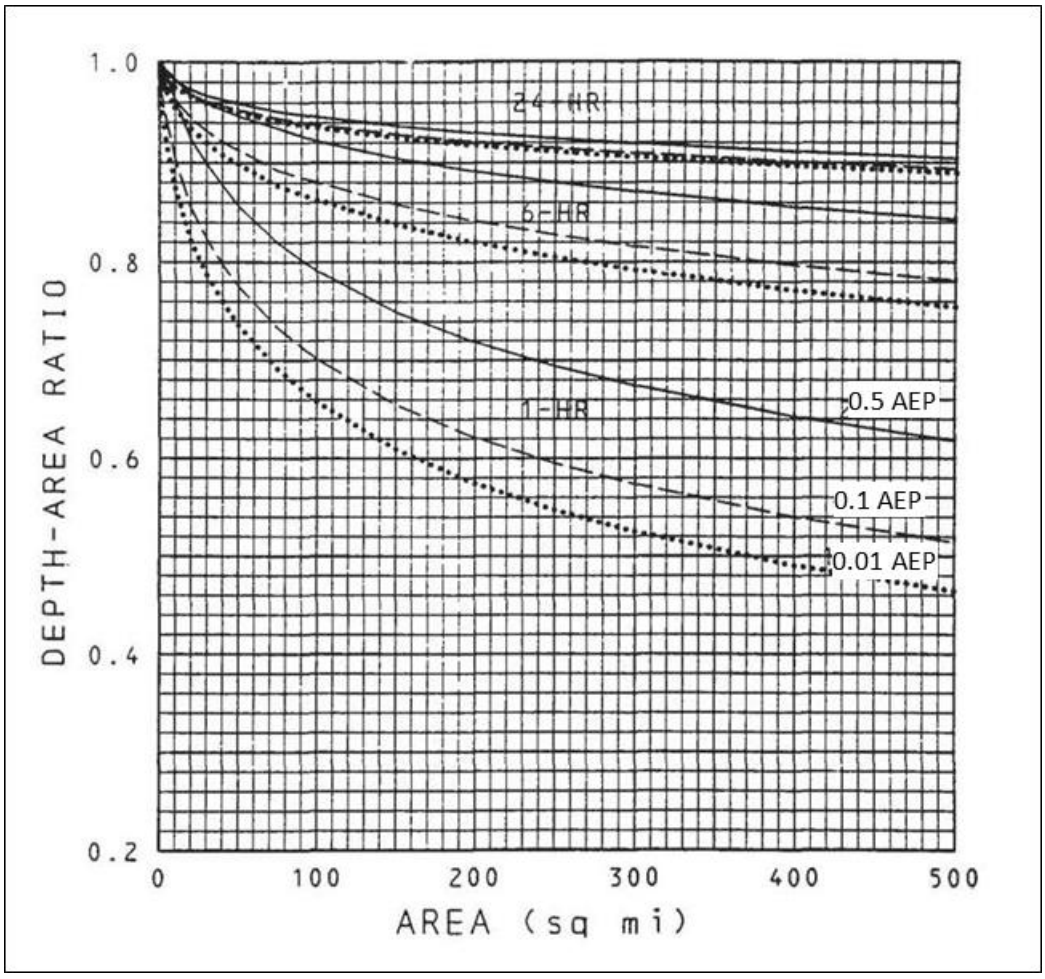

Figure 5.19. Areal reduction factor graph for 0.5, 0.1, and 0.01 AEP and 1-, 6-, and 24-hour durations (NWS-24).

Along with the methods for developing ARF curves that have been published in guidance documents by US Federal agencies (e.g., NWS-24 and TP-29), other, similar work is documented in the literature. Asquith and Famiglietti (1999) used a variation of these methods that specifically considers the distribution of concurrent precipitation surrounding annual precipitation maxima. The use of annual peak rainfall as a basis of analysis conceptually fits with the use of annual peak rainfall for the development of DDF relations.

Several regional and local studies on ARFs have been conducted (e.g., Allen and DeGaetano 2015, Asquith 1999, Svensson and Jones 2010, and Wright et al. 2014), but a broad development of updated ARFs for engineering design has not been completed. Radar information is also available for evaluating assumptions built into ARFs and this may be a research area that results in improvement in ARFs. However, generally applicable techniques for analyzing radar information have not been developed. Until more insight is developed from these various research efforts, the assumption that ARFs are stationary is necessary if engineers are to have useful tools for considering future conditions resulting from climate change.

Another limitation of ARFs is that the methods of analyzing for ARF values generally involve distances calculated from point to point of discrete stations without considering direction, implying that the distances are radial and that areal distribution is circular, and direction is irrelevant (the rainfall field is isotropic). This is also an approximation useful for engineering purposes.

With the assistance of an ARF graph, or a functional relationship for a particular region, a decreasing reduction or discount factor less than 1 is estimated as watershed area increases. That factor is then multiplied by the point design rainfall depth obtained for the appropriate duration and desired AEP from historical or projected information as shown in the following equation:

$$P_{\mathrm{A,W}} = \mathrm{ARF}_W \times P_{Point} \quad (5.7)$$

where:

$P_{A,W}$ = *Spatially-averaged precipitation for the watershed, inches.*

P_{Point} = *Point precipitation (from a rain gauge, NOAA Atlas 14, or equivalent), inches.*

ARF_W = *Areal reduction factor for the watershed, dimensionless.*

5.3.2. Identification of Projected Point Precipitation Data

GCMs and RCMs produce spatially-averaged precipitation data at a spatial resolution set by the model element size and, over time, these spatial resolutions have become finer. Statistically downscaled GCM output developed using precipitation (weather) gauges may include point (or station) projections of precipitation.

Downscaled GCM point data, such as that generated using the ARRM for the U. S. DOT Gulf Coast climate vulnerability transportation study, has been applied for engineering analysis (U.S. DOT 2014). However, at this time there are no broadly accessible regional or national databases containing projected point-based (station-based) precipitation data. Therefore, generation of point-based data is currently a project-specific decision and would likely only be justified for large-scale projects or efforts with a research and development component, that is, only for selected Level 4 projects.

This raises the question of whether engineering analyses would be better supported by an increase in the availability of point precipitation estimates from downscaled GCM outputs or better tools for adjusting spatially-averaged GCM output. The answer is likely that it depends on how each of the alternatives are pursued and what progress is achieved with each strategy. For now, engineers and hydrologists will continue to use spatially-averaged precipitation data for the vast majority of projects falling into levels 3 and 4.

5.3.3. Application of an Areal Reduction Factor

Spatially averaged downscaled GCM output is currently the predominant source of projected precipitation information. As described previously, if the watershed drainage area is less than the area of a downscaled grid cell, then the watershed is "small" relative to the downscaled data. Under this condition, an engineer could reasonably expect that the downscaled precipitation data represents less precipitation on the watershed than what might be expected for a particular exceedance probability because it is averaged over a larger area. Therefore, similar to the

problem associated with using point estimates of design precipitation on watersheds that are clearly not well represented by point estimates, design estimates of precipitation depth could be developed using an approach to "inflate" the spatially-based estimate (from the downscaled data). That approach is to use the ARF developed from historical data as an "inflator" for spatially-averaged precipitation.

Applying the ARF concept expressed in Equation 5.7 to gridded precipitation estimates from high-resolution climate datasets, the relation is rewritten to estimate a point precipitation from the spatially-averaged gridded value, $P_{A,G}$, as follows:

$$P_{\text{Point}} = P_{A,G}\ x\ \frac{1}{ARF_G} \tag{5.8}$$

where:

$P_{A,G}$ = *Spatially-averaged precipitation from the high-resolution climate dataset grid cell, inches.*

ARF_G = *Areal reduction factor for the high-resolution climate dataset grid cell, dimensionless.*

Taking the process one step further, conversion from a gridded precipitation from a high-resolution climate dataset to an appropriate areal average for the watershed of interest is accomplished by substituting Equation 5.8 into Equation 5.7, resulting in the following:

$$P_{\text{A,W}} = P_{A,G}\ x\ (ARF_W/ARF_G) \tag{5.9}$$

For application of Equation 5.9, the engineer should use the recommended ARF from the applicable jurisdiction or agency or developed from local/regional data. If locally applicable ARFs are not available, the designer should consult the applicable volume of NOAA Atlas 14 (e.g., Bonin et al. 2005, Perica et al. 2013). While NOAA Atlas 14 does not provide new ARFs, each provides references to appropriate documents containing ARFs for the location.

The general procedure for areal adjustment of gridded high-resolution climate dataset precipitation is summarized in the following steps for the required AEP and duration:

1. Determine the watershed size and the corresponding ARF for the watershed.
2. Determine the grid size and average precipitation for the grid along with the ARF for the gridded high-resolution climate dataset precipitation.
3. Calculate the adjustment using Equation 5.9.

Step 1 represents the standard adjustment that engineers make for converting point precipitation to an appropriate areas average for large watersheds. The watershed area is determined and the corresponding value of ARF_W is estimated from a tool such as shown in Figure 5.19. For many smaller watersheds, the value is 1 indicated no areal adjustment from point values is necessary.

For **Step 2**, the engineer determines the grid size and average precipitation for the grid. Based on the grid size, the engineer determines the ARF to adjust the gridded precipitation value to a point value. The value of ARF_G is estimated using the same tool used in Step 1.

Finally, in **Step 3**, the engineer uses Equation 5.9 to compute the adjusted precipitation value for the watershed given the information developed in Steps 1 and 2. If more than one AEP or duration is required, the steps are repeated with the new information.

BOTTOM LINE: Areal reduction factors, such as those used to reduce point estimates of precipitation depth from tools such as NOAA Atlas 14 to the watershed drainage area scale, can be used as a method for estimating a point precipitation from an spatially-averaged precipitation such as those generated by downscaling GCM estimates of precipitation until such time as climate model outputs are available at more detailed spatial resolutions, use of the ARF is an effective tool for adjusting precipitation estimates.

Chapter 6. Statistical and Index Methods for Projecting Discharges

This chapter addresses statistical and index methods for estimating future design discharges, including trend projections, regression analyses, and index flood methods. The following sections provide an introduction to these methods and, where applicable, describes efforts by others to apply these methods to future climate projections. Finally, recommendations of when and how each method might be applied to future conditions are described.

6.1. Trend Projection Based on Historical Discharges

In this section, tools for estimating projected design discharges based on the analysis of trends in historical discharges are explored, with recommendations of when these tools are applicable. In addition, possible pitfalls in the use of historical data exhibiting trends are described.

6.1.1. Trends and Nonstationarity in Historical Peak Discharges

The two major sources of trends and nonstationarity in annual flood peak discharges are land use changes and climate change. Land use change is often directly observable and its effects can be quantified using data such as housing density (Ries and Dillow 2006, Over et al. 2016), population density (Allen and Bejcek 1979, Moglen and Shivers 2006), impervious area (Moglen and Shivers 2006, Thomas and Moglen 2016), and runoff curve number (Hejazi and Markus 2009). The effects of climate change can be indirectly evaluated by analyzing trends in annual flood discharges using streamflow records for basins with no significant upstream regulation or changes in land use (urbanization). That is, trends that are observed in annual peak flows may be attributed to changes in climatic variables if other directly observable watershed explanations are eliminated or quantified.

Several nationwide studies, including those by Hirsch (2011), Lins and Cohn (2011), Petersen et al. (2013), and Archfield et al. (2016), evaluated trends in annual flood peak discharges using long-term streamflow records with no significant effects of regulation or urbanization. Villarini et al. (2011) analyzed annual flood peak discharges in the Midwestern United States using long-term streamflow records that included data influenced by regulation and urbanization. The objectives of these studies were to document the magnitude and extent of trends on a nationwide or regional basis. The results of these studies varied, but generally they indicated more streamflow records had no significant trend or more of a downward trend than an upward trend in annual flood peak discharges. These studies suggest there is considerable uncertainty over the effects of climate change on annual peak discharges in the historical record. Cohn and Lins (2005) concluded that long-term persistence of climatic systems, combined with the paucity of observational records and their natural variability, made it difficult to distinguish between stationary and nonstationary processes. Salas et al. (2018) observes that nonhomogeneity in a time series may result from stationary processes such as the low-frequency (cyclic) components of the atmospheric and oceanic system.

While there is no general agreement within the hydrologic community that annual flood peak discharges are uniformly increasing in the historic record as a result of climate change, there is a need to evaluate trends and nonstationarity in flood data prior to frequency analysis. Land use change, long-term persistence, and changing regional climate contribute to nonstationarity in

annual peak discharges. There are many statistical tests documented in the literature for evaluating nonstationarity of data. Kilgore et al. (2016) describe the Mann-Kendall test for detecting gradual trends and the Pettitt test for detecting abrupt changes in hydrologic data. The Mann-Kendall test is available in several statistical packages and is now available in the U.S. Geological Survey (USGS) PeakFQ flood frequency program (https://water.usgs.gov/software/PeakFQ/). England et al. (2018) describe several tests for detecting trends and shifts in annual flood peak discharges prior to frequency analysis. The U.S. Army Corps of Engineers (USACE) developed a Nonstationarity Detection Tool (Friedman et al. 2016) to detect nonstationarities in annual flood peak discharges that includes several statistical tests for detecting changes in the mean, variance/standard deviation, and underlying distribution of the data. This tool is intended for use as part of a climate hydrology assessment that is described in the USACE Engineering and Construction Bulletin (ECB) (USACE 2016).

When a significant trend exists, the engineer must consider what the trend implies for hydrologic design since stationarity cannot be assumed. USACE (2016) describes the climate hydrology assessment as having three major components:

- Detection: Determine if there are increases or decreases in the observed hydrologic record in magnitude or variability. As described above, there are many statistical tests for making this determination.
- Attribution: If a change is detected through statistical analysis, attribute the change to one or more causes.
- Projection: Use climatological, hydrological, or land use data to adjust the observed record to current conditions or project the trend into the future.

Several approaches are available for estimating design discharges (current and projected) when trends are suspected in the historical data:

- Development of time-varying statistical distribution parameters (Section 6.1.2).
- Adjustment of historical data to current conditions (Section 6.1.3).
- Analyzing recent sub-periods of the historical record (Section 6.1.4).

6.1.2. Time-Varying Statistical Distribution Parameters

Changing land use conditions and climate variability have prompted several researchers to propose and describe frequency analyses in which the parameters of a given frequency distribution vary with time. Salas and Obeysekera (2014) describe an approach using the GEV distribution where the mean and standard deviation vary with time. Obeysekera and Salas (2014) describe three approaches for defining confidence intervals if the distribution parameters are estimated with the method of maximum likelihood. Vogel et al. (2011) and Read and Vogel (2015) describe a nonstationary flood model using the 2-parameter lognormal distribution. Salas et al. (2018) provide a review of current techniques for nonstationary frequency analysis and point out some of the challenges ahead in future development and applications. Read and Vogel (2015) show that the coefficient of variation (standard deviation divided by the mean) is relatively constant for most real-space flood data (no transformation to logarithms) with significant trends. This implies the mean and standard deviation of the untransformed data are increasing together. However, for logarithmic transformed data, only the mean is increasing, so a

single nonstationary model for the logarithmic mean is sufficient for most applications. Recent research by Hecht and Vogel (personal communication) of a large national dataset of streamflow stations with 30 or more years of record indicated that about 90 percent of the stations with a statistically significant increase in the mean did not experience a concurrent significant change in the coefficient of variation. Serago and Vogel (2018) describe the advantages of varying the distribution parameters with a single parameter time (parsimonious model) versus the development of other more complicated models and propose a nonstationary model coupled with the Pearson Type III distribution in which the mean of the logarithms of the annual flood peak discharges is a linear function of time.

6.1.2.1. Application to the Northeast Branch of the Anacostia River

The Northeast Branch of the Anacostia River at Riverdale, Maryland is located in Prince George's County, just a few miles east of Washington, DC. The watershed draining to Riverdale Road (East Riverdale) (station 01649500) has a drainage area of 73.35 square miles and is shown in Figure 6.1. The upper part of the watershed is in the Piedmont Region (17 percent) and the lower part is in the Western Coastal Plain Region (83 percent) of Maryland.

Several major highway systems within the watershed are indicative of extensive development. The western and southern portion of the watershed is more heavily urbanized and includes the cities of Calverton, Beltsville, College Park (and the University of Maryland), Greenbelt, and East Riverdale. Major Federal installations within the watershed include the U.S Department of Agriculture Beltsville Agricultural Research Center (BARC) (approximately 6,500 acres) and the National Aeronautical and Space Administration (NASA) (approximately 300 acres). The steps and data used in this analysis include:

1. Determine if there is a statistically significant trend in the annual peak discharges.
2. Develop an equation that defines the trend in the annual peak discharges.
3. Use the time varying mean approach to estimate the design flood discharges for current conditions.
4. Determine the cause for the increasing trend in annual peak discharges.
5. Use local rainfall data to determine the potential historical impact of climate on annual peak discharges.
6. Determine if the causative factor for the trend can be extended into the future (determine impervious area for ultimate development conditions or projections for precipitation when applicable).

The annual maximum peak discharge record for the Northeast Branch Anacostia River at Riverdale, Maryland consists of a historical flood in 1933 and a systematic record from 1939 to 2016. The annual maximum peak discharges shown in Figure 6.2 are plotted versus time in years since 1933 and indicate an increasing trend with time. Lower annual peaks are evident in the 1950s, and higher annual peaks occurred in the 1970s. These variations from the trend line reflect the long-term persistence of wet and dry periods in climatic systems discussed by Cohn and Lins (2005) that can complicate the detection of a trend related to land use or climate change.

If these data were analyzed assuming stationarity (ignoring the trend), the engineer would fit the logarithms of the full annual maximum series using the Pearson Type III distribution based on Bulletin 17C guidelines (England et al. 2018). The resulting discharges for the 0.5, 0.10, and 0.01 Annual Exceedance Probabilities (AEPs) are summarized in the second column of Table 6.1. However, because the data clearly illustrate an upward trend in annual peak discharges, these estimates likely underestimate the design discharges. A gradual increase in annual peak flows like those exhibited in Figure 6.2 is commonly evaluated using the Mann-Kendall test (Helsel and Hirsch 1992, McCuen 2003) with a significance level of 5 percent (percent chance of rejecting no trend when there is a trend). The Mann-Kendall test is now included in the USGS PeakFQ program and is discussed in Appendix 4 of Bulletin 17C (England et al. 2018). The estimation of Kendall's tau for the Northeast Branch Anacostia River at East Riverdale is described by Kilgore et al. (2016).

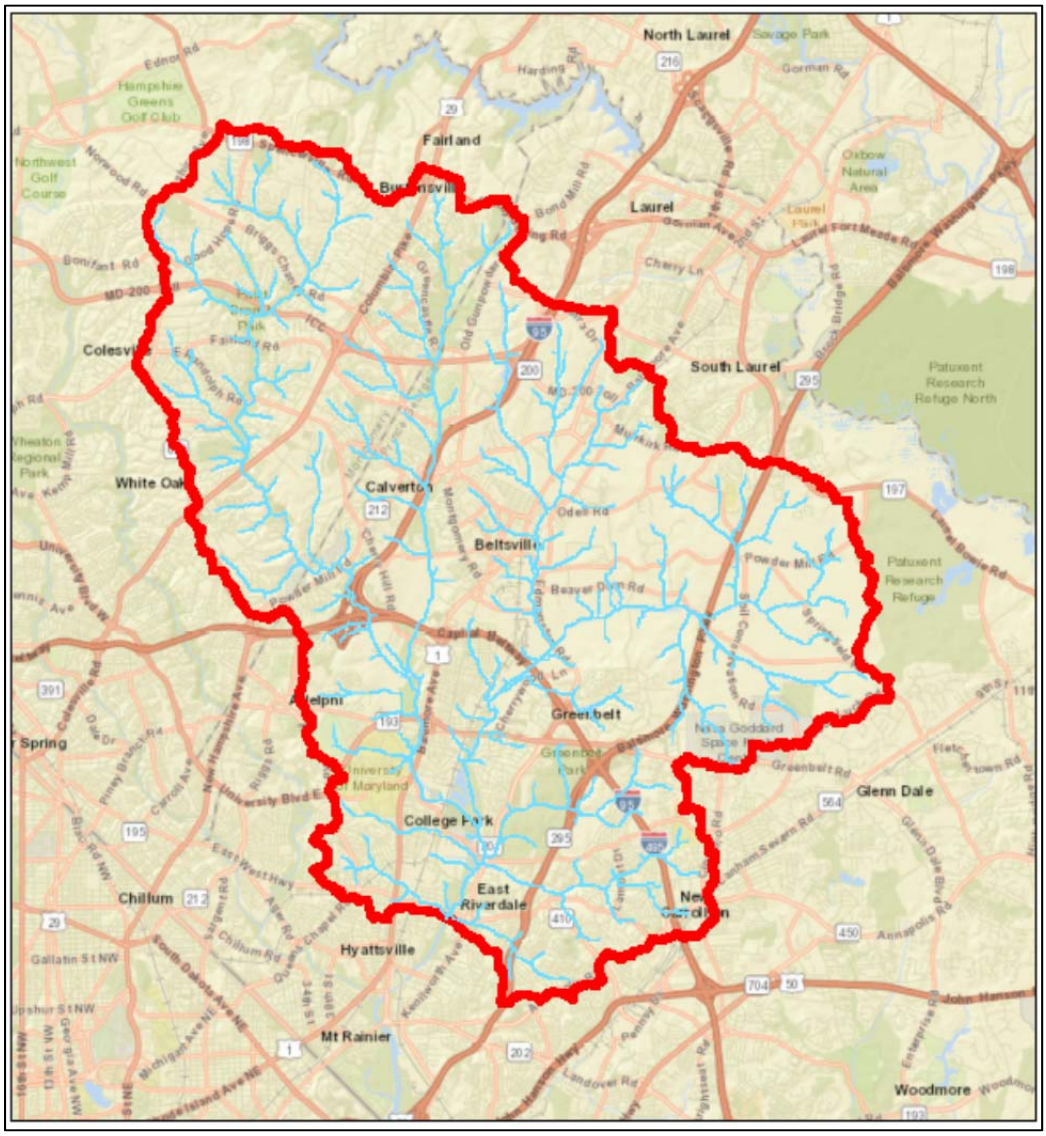

Figure 6.1. Watershed map for the Northeast Branch of the Anacostia River upstream of East Riverdale, Maryland.

As shown in Figure 6.2, the large historic flood in 1933 departs significantly from the trend line. The 1933 flood occurred when the watershed was essentially rural and does not provide meaningful information about the slope of the trend line when the watershed was undergoing urbanization. The residuals about the trend line should be distributed normally, but inclusion of the 1933 flood resulted in the residuals being highly skewed. Therefore, the historic flood was omitted from the trend analysis and the systematic data from 1939 to 2016, as shown in Figure 6.3, were used in the following time-varying mean analyses. The effect of omitting the 1933 historic flood is minimal because the slope of the trend line increases slightly, offsetting a slight decrease in skew of the logarithms of the annual peak discharges. However, the historic flood was deleted because data used to estimate a time-varying mean should be indicative of the trend in the annual data.

The identification of a trend does not tell the engineer whether the trend is the result of urbanization, climate, other factors, or a combination of several. However, it is known that the Northeast Branch of the Anacostia River at Riverdale, Maryland is a watershed where urbanization has increased significantly during the period of systematic record from 1939 to 2016.

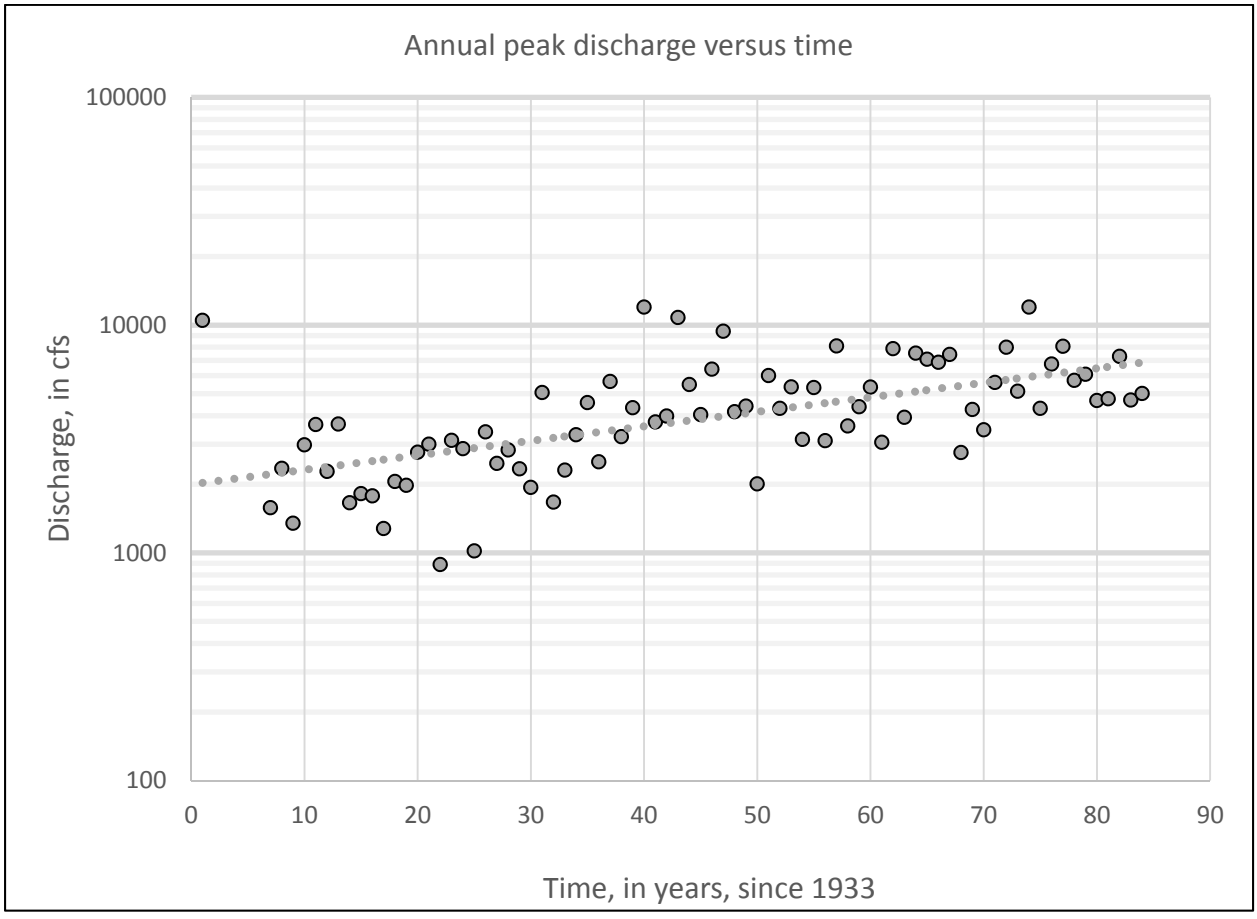

Figure 6.2. Time series of annual maximum peak discharges from 1933 to 2016 for the Northeast Branch of the Anacostia River at Riverdale, Maryland.

Table 6.1. Summary of AEP discharges using different periods of record and the time-varying mean approach for the Northeast Branch of the Anacostia River at Riverdale, Maryland.

AEP	Full period – 1933, 1939-2016 (cfs)	Period 1972 to 2016 (cfs)	Period 1985 to 2016 (cfs)	Time varying mean (cfs)
0.50	3,970	5,340	5,370	7,350
0.10	7,940	8,890	8,480	12,200
0.01	13,200	13,500	12,300	17,700

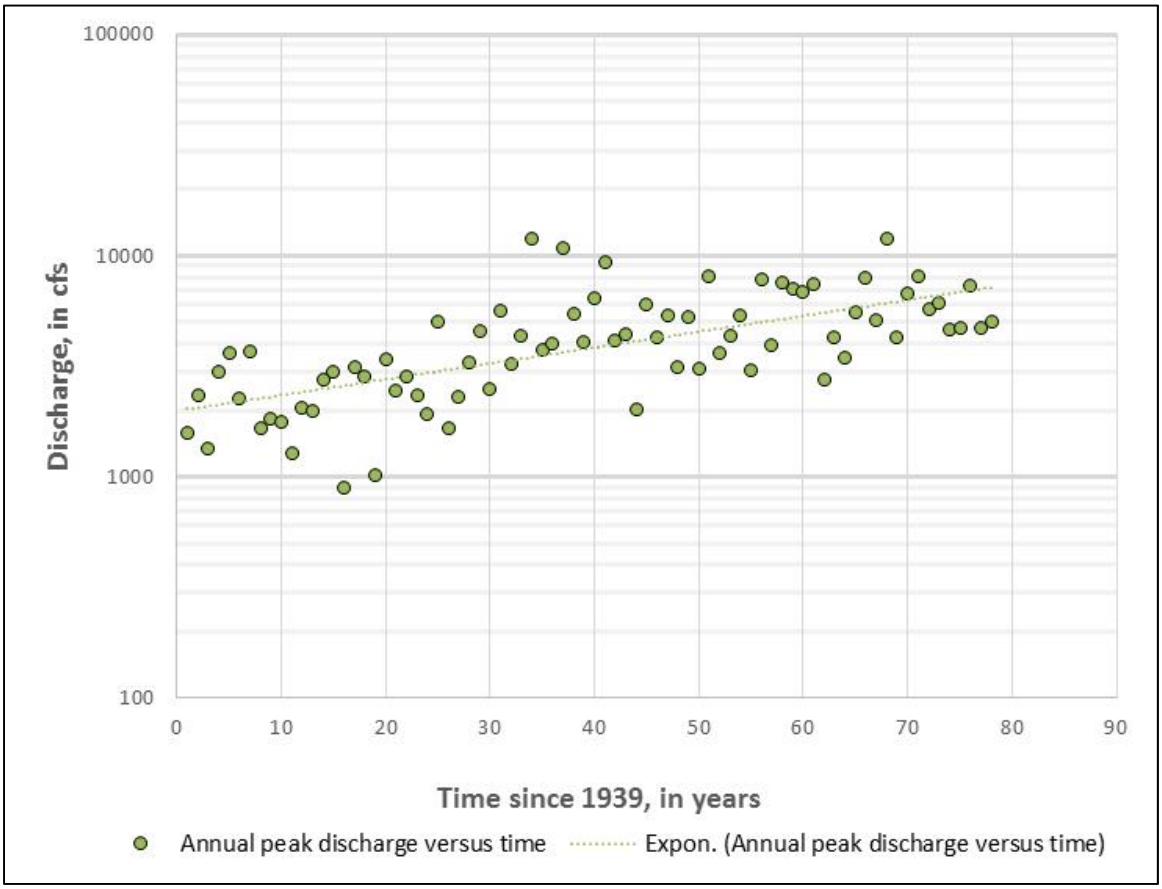

Figure 6.3. Time series of annual maximum peak discharges from 1939 to 2016 for the Northeast Branch of the Anacostia River at Riverdale, Maryland.

Regardless of the drivers for the trend, the annual peak discharges are clearly increasing with time so a frequency analysis with a time varying mean is performed following procedures described in Serago and Vogel (2018).

The linear trend line in Figure 6.3 illustrates that the logarithmic mean of the annual peak discharges is increasing with time and this relation is estimated as:

$$\log_{10}(Q) = 3.29852 + 0.00717\ t \tag{6.1}$$

where:

Q = *Annual peak flow, cfs.*

t = *Time since the beginning of the record (i.e., 1939 = 1 and 2016 = 78), years.*

The slope of the trend line (0.00717) is statistically significant and represents a 0.717-percent annual increase in logarithms of peak flows. (Kendall's τ is 0.483 and the p-value is less than 0.0001.) Equation 6.1 can be rewritten using the mean of $\log_{10}(Q)$ $(\overline{LQ})$ and the mean of t $(\bar{t})$ as follows:

$$\log_{10}(Q) = \overline{LQ} + 0.00717\ (t - \bar{t}) \tag{6.2}$$

In this equation, t ranges from 1 to 78 with $\bar{t} = \frac{(n+1)}{2}$ and n is the years of record. Equation 6.2 can be rewritten as:

$$\log_{10}(Q) = \overline{LQ} + 0.00717\ \left(t - \frac{(n+1)}{2}\right) \tag{6.3}$$

The equation for estimating the x AEP discharge $(\log_{10}(Q_x))$ assuming the logarithms are Pearson Type III distributed is:

$$\log_{10}(Q_x) = \overline{LQ} + B\ \left(t - \frac{(n+1)}{2}\right) + K_x(S_Y^2 - B^2 * S_t^2)^{0.5} \tag{6.4}$$

where:

$\overline{LQ}$ = *Mean of the logarithms of the historical AMS.*

Q_x = *Flow quantile associated with the x AEP.*

B = *Slope of the regression trend line.*

S_Y = *Standard deviation of the logarithms of the historical AMS.*

S_t = *Standard deviation of the time variable t.*

K_x = *Pearson Type III frequency factor that is a function of the x AEP and skew (G_Y) for the logarithms of the historical AMS.*

t = *Time since the beginning of the record, years.*

n = *Number of years in the record.*

The quantity $(S_Y^2 - B^2 * S_t^2)^{0.5}$ is the standard deviation of the logarithmic residuals about Equation 6.1.

Equation 6.4 indicates that the x AEP discharge $(\log_{10}(Q_x))$ varies with time (t). Solving Equation 6.4 for x = 0.50, 0.10, and 0.01 AEP floods and t = 78 (2016 conditions) results in the design discharges given in the last column of Table 6.1. These discharge estimates are

significantly larger than previously estimated when ignoring the trend and are more representative of 2016 land use conditions.

If the trend continues and the hydraulic structure has a long service life, the time-varying mean estimate of design flow might prove to be an underestimate. Conversely, projecting further into the future without knowledge that the underlying causes of the trend will continue could result in an overestimate of the design discharge. Therefore, it is critical to identify the underlying causes of a trend before projecting it into the future. For this case, the role of increases in urbanization and precipitation in the historical record was examined.

Estimates of impervious area in the Northeast Branch Anacostia River watershed are available for 1985, 1990, 1997, 2002, and 2010 and are plotted versus time since 1939 in Figure 6.4. The latest estimate of impervious area for the watershed is 28.4 percent, taken in 2010. It was assumed the watershed was essentially rural in 1939 (impervious area of 1 percent) and this assumption agrees well with the near linear trend in impervious area since 1985. The impervious areas for the years noted above were estimated based on the average percentage of each land use category that is covered with impervious area as found in land use data available from the Maryland Department of Planning (Moglen and Kim 2007). Clearly, a trend in increasing impervious area correlates with the increase in annual peak flows. (This approach for estimating impervious area is different than estimating the impervious area directly using spectral measurements from satellite data to define land cover (e.g., grass, forest, roads, and buildings). Moglen and Kim (2007) developed relationships between impervious area determined through land use versus land cover and showed that estimates using land use data are higher than those using land cover data.)

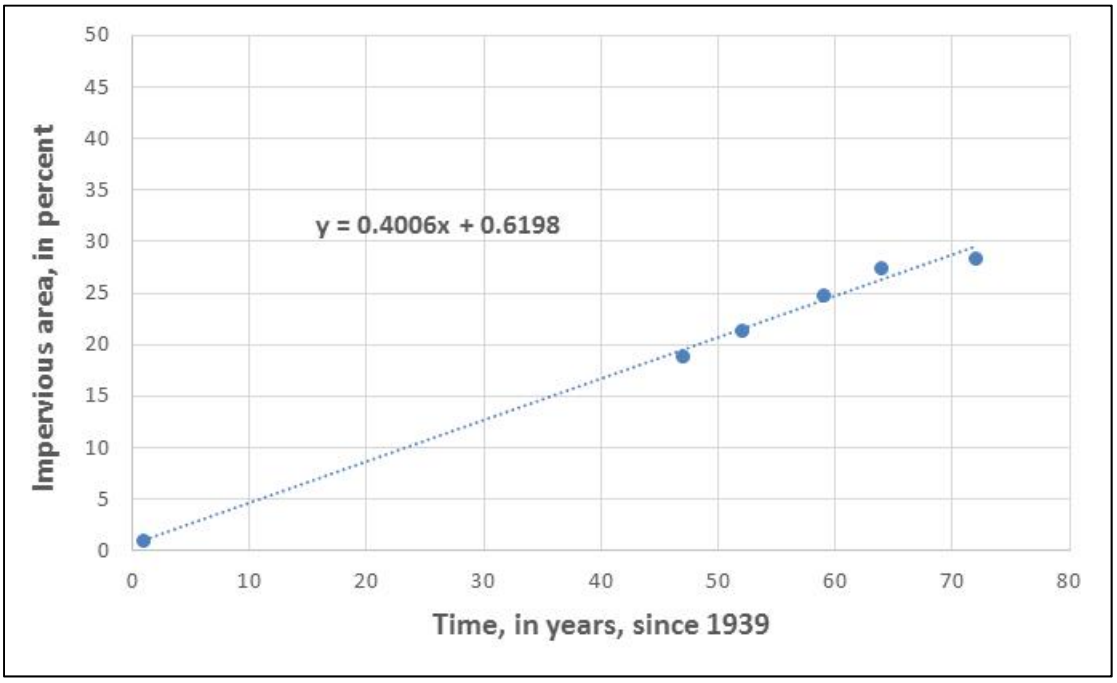

Figure 6.4. Impervious area since 1939 for the Northeast Branch of the Anacostia River at Riverdale, Maryland.

Identifying the potential contribution of climate variables such as precipitation to a trend in annual maximum flows is more challenging because there are many precipitation statistics available (e.g., mean annual precipitation and numerous AEP values for different durations). Other factors, such as antecedent moisture and precipitation intensity and duration, also influence the link between rainfall and runoff. With this caution, the 24-hour annual maximum precipitation is plotted in Figure 6.5 for a rainfall station within the watershed (Beltsville) for the period 1941 to 2016. The precipitation trend line is slightly downward and visual inspection clearly shows no increase in the 24-hour annual maximum precipitation with time.

Even though the rainfall station is located near the center of the watershed, the annual maximum precipitation did not always occur at the same time as the annual maximum peak discharge. An extreme example is the 9.43 inches of rainfall that occurred in August 1955 (Hurricane Connie), while the annual maximum peak discharge occurred in January 1955. While data for one rainfall station (point values) do not adequately reflect the basin-wide precipitation for a 73.35-square-mile watershed, the point precipitation data suggest that the increasing annual peak discharges are not related to increasing precipitation.

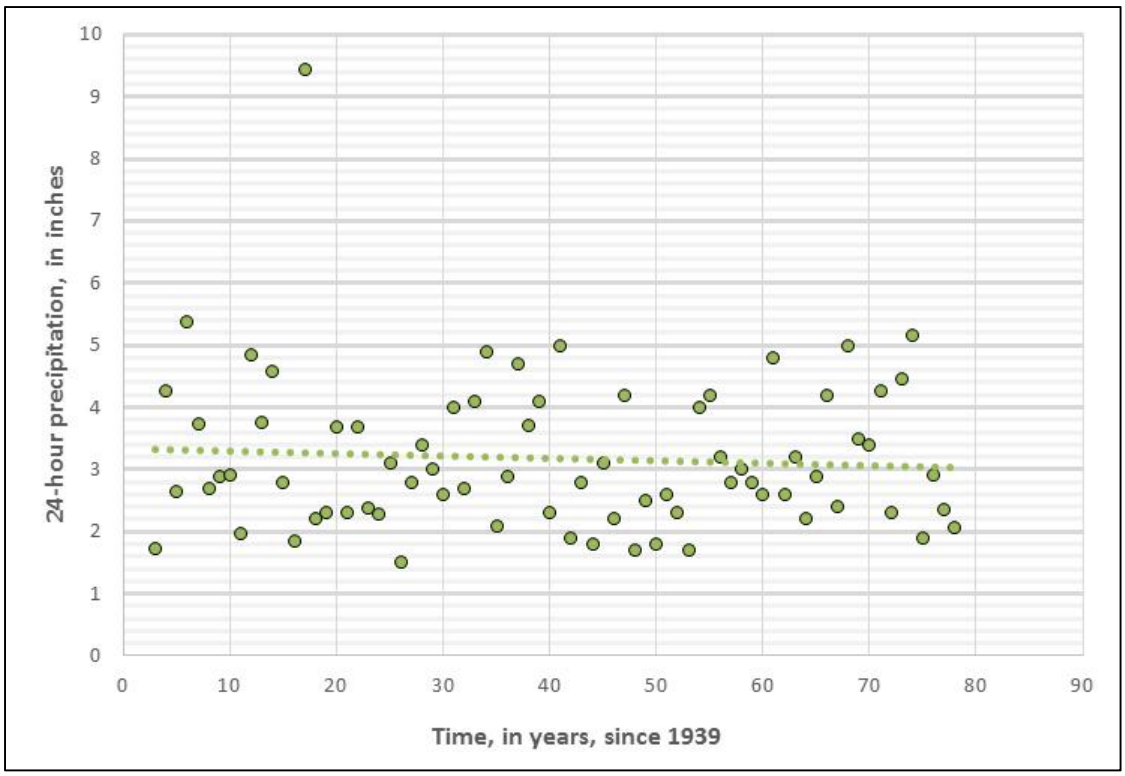

Figure 6.5. The 24-hour annual maximum precipitation at Beltsville, Maryland from 1941 to 2016.

Based on the historical land use and precipitation data, it appears that the trend in annual peak flow that has been quantified can be expected to continue if the driving cause continues. In this case, the driving cause is increasing urbanization, not precipitation changes. Read and Vogel (2015) and Salas et al. (2018) have stressed that the trend in the mean should only be extrapolated if there is some physically meaningful covariate (like land use change) that defines the trend into the future. However, there are no standardized protocols for drawing quantitative conclusions. Salas et al. (2018) note it may be reasonable to use the historical trends resulting

from urbanization to simply update a flood frequency analysis to reflect current urbanization conditions, which may remain roughly constant for the near term or for a short time into the foreseeable future.

It is likely that urbanization will continue to increase in the Northeast Branch of the Anacostia River and the Maryland State Highway Administration designs bridges based on ultimate development conditions in the watershed. An impervious area for ultimate development conditions was estimated to be 34.9 percent for the Northeast Branch Anacostia River at Riverdale, Maryland. If the trend line in Figure 6.4 is extended upward to 34.9 percent, this will occur in 2024 (or year 86), indicating the watershed is near its ultimate development conditions. This assumes the linear trend will continue for the next 8 years. As noted above, the BARC occupies about 6,500 acres of the watershed (approximately 14 percent of the watershed) and most of the research center is agriculture with no plans to develop. Therefore, reaching ultimate development conditions in the watershed by 2024 is a reasonable assumption.

Projection of historical discharges using a time-varying mean is applicable when:

- There is a statistically significant trend in the mean of the logarithms of the annual maximum discharges based on at least 30 years of record;
- The trend can be attributed to some hydrologically meaningful covariate like land use change that can be projected into the future; and
- The trend in the logarithms of the annual maximum discharges exceeds about +/-0.25 percent a year (Yu and Stedinger 2018).

Yu and Stedinger (2018) indicate that adjustment of the mean and variance is advantageous when the trend exceeds +/-1 percent a year. However, this is likely an extreme trend for flood data and the adjustment for the mean and standard deviation is more complicated than the example discussed in this section. Therefore, the recommendation is to apply the time-varying mean for trends greater than +/-0.25 percent per year assuming trends greater than +/-1 percent will be rare. For example, for the Northeast Branch Anacostia River Watershed, the annual peak discharges increased by 0.717 percent per year while the impervious area increased significantly, from about 1 percent to over 30 percent during the period of record. When procedures for adjusting the mean and standard deviation are adequately documented and tested, these procedures will become more operational.

6.1.2.2. Application to Stockley Branch

Another application of the time-varying mean approach is demonstrated for a rural watershed in southern Delaware, Stockley Branch at Stockley (station 01484500), taken from Kilgore et al. (2016). The AMS displayed in Figure 6.6 from Kilgore et al. (2016) exhibits an upward linear increase in annual peak discharges implying an increasing design discharge with time. No land use changes occurred in the watershed during the period of record. The upward trend in annual flood discharges is correlated to increased precipitation near the end of the record. (The gauging station was discontinued in 2004.) This increasing trend can likely be attributed to long-term persistence in the precipitation, but there is no assurance that the trend will continue into the

future. In this case, the trends should not be projected into the future, although incorporating the trend into the frequency analysis is valuable for estimating design flows for current conditions.

6.1.3. Adjusting Historical Discharge Records for Land Use or Climate Change

Several investigators have developed methods for adjusting annual peak discharges to current land use or climate conditions (McCuen 1989, Ries and Dillow 2006, Beighley and Moglen 2003, Over et al. 2016a and Over et al. 2016b) and performing frequency analysis on the homogeneous adjusted data. This approach is often referred to as an index adjustment method. Adjusting annual peak discharges to current land use or climate conditions is a reasonable approach, but often the adjustment results in a significant reduction in variance such that the adjusted discharges provide lower estimates of the extreme AEP discharges than using the unadjusted data.

Beighley and Moglen (2003) developed an approach for adjusting for the effects of land use change on flood discharges for eight watersheds in the Washington, DC to Baltimore, MD corridor. The adjustment procedure involved land use changes over time and used the HEC-HMS watershed model to determine the precipitation that caused the observed annual peak discharges. The inferred precipitation was then used with land use conditions for the year 2000 and the calibrated HEC-HMS model to estimate adjusted annual peak discharges for a constant land use condition for use in frequency analyses.

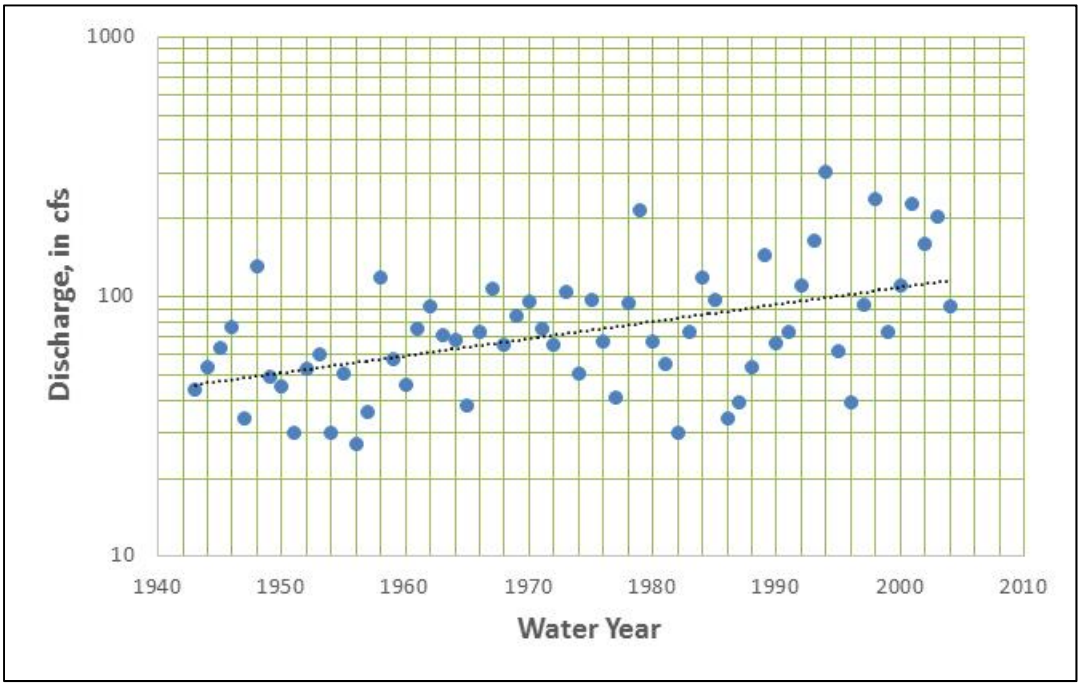

Figure 6.6. Annual peak discharges for Stockley Branch at Stockley, Delaware from 1943 to 2004.

Hejazi and Markus (2009) evaluated the impact of urbanization and climate variability on flood discharges for 12 small urbanizing watersheds in Northeastern Illinois. The HEC-HMS model was calibrated to major rainfall-runoff events in 1954 and 1996 using land use conditions at the time of the flood events. Isolated effects of urbanization and climate change were evaluated for

the 100-year flood by running various combinations of land use data (1954 and 1996-1999) and design precipitation (TP-40 (Hershfield 1961) and NOAA Atlas 14 (Bonnin et al. 2005)). TP-40 was based on precipitation data through 1958 and NOAA Atlas 14, Volume 2, was based on data through 2000, representing an additional 42 years of record. Increasing precipitation and urbanization were both contributors to increased flood peaks for the 12 small watersheds, but the average contribution of urbanization was 34 percent higher than the increase in precipitation.

Over et al. (2016a; 2016b) used a panel regression approach for adjusting annual peak discharges for several Northeastern Illinois gauging stations to 2010 land use conditions using a fraction of urban area in the watershed and daily precipitation. Housing density data were used to develop a complete time series of a fraction of urban area for each studied watershed. The analyses by Over et al. (2016a; 2016b) are described in more detail in Section 6.2.2.3.

6.1.4. Analyzing Recent Homogeneous Sub-Periods of Record

Kilgore et al. (2016) proposed using only the most recent, homogeneous portion of the record to address an AMS of discharge when a trend is known to exist. This simple strategy may be appropriate regardless of whether the trend is caused by urbanization or climate change. Challenges for this approach are both the necessity to use a shorter period of record than is available and the possibility that extreme flood data points may be excluded.

Returning to the Northeast Branch of the Anacostia River as an example, the period 1985 to 2016 (32 years) is reasonably homogeneous with respect to land use change, with impervious area increasing from 18.9 percent to about 31 percent in 2016 (Figure 6.4). However, choosing this period ignores four of the five largest floods of record as shown in Table 6.2. The floods occurring in 1979 or in prior years would have been much larger if they occurred in 2016 when the impervious area was 31 percent. The period 1972 to 2016 includes the three large floods in the 1970s, but the impervious area changes more significantly over the analysis period (15 to 31 percent). There is no statistically significant trend (at the 5-percent level of significance) in annual peak discharges for either the 1985 to 2016 or the 1972 to 2016 periods.

Table 6.2. Largest floods of record for the Northeast Branch of the Anacostia River at Riverdale, Maryland (station 01649500).

Year	Discharge (cfs)	Imperviousness (%)
1933	10,500	Rural
1972	12,000	15
1975	10,800	16
1979	9,410	18
2006	12,000	28

To evaluate the effect analyzing various sub-periods of the record might have on design discharges, flood frequency analyses were performed for the two more recent periods: 1) 1972 to 2016 and 2) 1985 to 2016. The results are summarized in Table 6.1 and indicate increases in the 0.5 and 0.1 AEP discharges compared to the full record. However, estimates of the 0.01 AEP flood are comparable to the results assuming stationarity and using the full record. All estimates,

regardless of AEP, are lower than those estimated using the time-varying mean. Based on engineering judgment, the estimates from the sub-periods are low given that four floods exceeded 10,000 cfs in 79 years. Choosing sub-periods of record sometimes underestimates the variability of the annual peak discharges and decreases estimates of extreme flood discharges.

6.1.5. Summary and Recommendations

Land use and climate change or climate variability can lead to trends and nonstationarity in the annual flood series that violate the assumption that the data are independent in time. Most research has concentrated on detecting trends in streamflow or adjusting annual flood peak discharges to current land use conditions with no intent of extending the trends into the future. Uncertainty in future climate change generally precludes extending historical discharge trends into the future based on climate. Read and Vogel (2015) and Salas et al. (2018) have stressed that the trend in historical data should only be extrapolated if there is some physically meaningful covariate (like land use change) that defines the trend into the future. Historical land use change is a single observable variable that can be projected into the future by estimating ultimate development as was illustrated by the Northeast Branch Anacostia River example discussed in Section 6.1.2.1.

The time-varying mean approach is applicable for projects where the design team is evaluating projected changes in climate or land use (Level 3 or Level 4 as defined in Chapter 3). Several researchers have described other approaches for varying the parameters of the frequency distribution with time to account for a nonstationary time series, but there have been limited applications in practice and more research is needed (Salas et al. 2018). Serago and Vogel (2017) point out that despite the tremendous increase in attention given to nonstationary flood frequency analysis, there is still no consensus on the methodology for performing the analysis or the need for nonstationary flood frequency analysis (Serinaldi and Kilsby 2015). Other than the methods described by Obeysekera and Salas (2014) requiring the use of the method of maximum likelihood, there are no well-defined approaches for estimating confidence of quantiles estimated from the time-varying mean approach. The results from the time-varying mean approach should be compared to results from other methods in making decisions about a given project design.

BOTTOM LINE: Where trends in annual maximum series discharge measurements can be identified in the historical record, these trends can be used to estimate changes in historical discharge estimates and in the near future. However, unless sound evidence can be provided that a trend will continue in the future, including the cause of the trend and how the trend will change in the future, trend extrapolation is not recommended.

6.2. Regression Approaches for Projecting Discharges

Another potential tool for projecting discharges to represent future conditions is regression. Multiple linear regression (MLR) equations are widely used by engineers for estimating design discharges based on historical data. In addition, new techniques such as panel regression are finding applications for hydrologic design. This section provides an overview of both regression approaches and discusses their potential for estimating future design discharges.

6.2.1. Traditional Multiple Linear Regression Hydrologic Equations

Many state DOTs use regression equations to estimate flood discharges for bridge and culvert design. Generally, the USGS develops these regression equations through cooperative projects with the state DOTs and equations are available for all 50 states and Puerto Rico. In some cases, state or local agencies or consultants also develop regression equations. The standard approach for developing these equations is MLR. The following sections provide a general overview of MLR techniques for hydrologic design and offer several examples of how these tools have and can be used to estimate future design flows.

6.2.1.1. Overview of Multiple Linear Regression

The MLR approach for estimating flood discharges is to relate a quantile discharge, such as the 0.01 AEP discharge, to watershed, climatic, and land use characteristics for many watersheds in a region over a period of time when the land use and climatic characteristics are considered relatively static. In this framework, each gauging station is considered one observation and equally weighted with all other gauging stations used in the analysis when using ordinary least square regression. If the period of record is the same for all gauging stations (one segment of time), which is generally not the case, Steinschneider et al. (2013) refers to this process as cross-sectional regression. MLR analysis utilizes a large number of watersheds with a wide variation in land use and climatic characteristics and different periods of flood records to evaluate the hydrologic response under different land cover and climatic regimes. The objective is to estimate a quantile such as the 0.01 AEP discharge for current drainage basin and climatic characteristics. The approach uses the concept that space (many stations with different periods of record) can be substituted for time but **the predictor variables do not vary with time.**

Current USGS regression equations for estimating flood discharges (and mean and low flows) are available through the USGS National Streamflow Statistics (NSS) web page (https://water.usgs.gov/osw/programs/nss/NSSpubs_Rural.html.). These regression equations are primarily applicable for rural watersheds, but regression equations for estimating flood discharges for urban watersheds are available for metropolitan areas in 18 states. In addition to the urban regression equations for statewide or metropolitan areas, nationwide urban regression equations are also available in Sauer et al. (1983). The flood discharge regression equations historically developed by USGS are MLR equations and have the following attributes:

- The dependent variable is a peak discharge value for a given AEP (such as the 0.01 AEP [100-year] discharge) estimated by applying the Pearson Type III frequency distribution to the logarithms of the annual peak discharges assuming a stationary time series (Interagency Advisory Committee on Water Data 1982, England et al. 2018).
- The AEP discharge is based on a homogeneous period of record available at the gauging station assuming no significant trends or land use change. Each gauging station has a different period of record as the objective is to use the longest period of homogeneous record at each gauging station.
- Watershed and climatic characteristics are determined using GIS data layers or topographic maps, precipitation atlases, and land use databases (Ries 2007). The

watershed and climatic characteristics are assumed to be stationary for the homogeneous period of record used in estimating the AEP discharges.

- The regression equations are developed using ordinary least squares regression or weighted/generalized least squares regression (Tasker and Stedinger 1989, Ries 2007, Eng et al. 2009). The weighted and generalized least squares regression techniques are applied to account for unequal record lengths at the gauging stations or unequal variances of the dependent variable and the cross correlation of the dependent variable across gauging stations.
- Typically, the regression equations are developed for homogeneous hydrologic regions where flood characteristics are similar. On average, there are four hydrologic regions in each state (Ries 2007). The use of homogeneous regions often limits the applicability of precipitation variables in the regression equations because of limited variability over the homogeneous hydrologic region. Therefore, many USGS regression equations do not include a climatic variable.

The NSS program facilitates application of the USGS regression equations, but the estimates of watershed and climatic characteristics must be input by the user. To provide for easier application of the regression equations, USGS developed the StreamStats Program, a web-based application that computes the required watershed and climatic characteristics using GIS data layers (Ries et al. 2008) (https://water.usgs.gov/osw/streamstats). As of 2017, the USGS StreamStats Program is fully functional in 36 states and under implementation in seven additional states.

In some areas, the USGS regression equations include a precipitation variable such as the mean annual precipitation or the 2-year 24-hour precipitation. At least half the states have at least one hydrologic region where a precipitation variable is statistically significant in the regression equation. For the urban equations, there are only two states (Ohio and Tennessee) where a precipitation variable and an urbanization variable are included in the equations. An example regression equation with a precipitation variable for estimating the 0.01 AEP ($Q_{0.01}$) is shown below (Lumia et al. 2006):

$$Q_{0.01} = 1.91A^{0.98}SL^{0.636}P^{0.590} \quad (6.5)$$

where:

A = *Drainage area, mi^2.*

SL = *Channel slope, ft/mi.*

P = *Mean annual precipitation, inches.*

In this equation, the mean annual precipitation is based on the historical period 1951-80. USGS regional regression equations are among the most commonly used and useful tools for estimating design discharges for transportation infrastructure. They are broadly applicable throughout the United States, as long as values of the independent variables are within the ranges of the data used when the USGS developed the equations.

Their primary limitations are that they rely on statistical correlation between computed discharge quantiles and the corresponding independent variables from gauged watersheds and that they are limited by the form of the equation chosen. These two factors combine such that the equations do

not fully explain variations in the discharge quantiles computed from gauged records. Therefore, uncertainty remains in the estimates for ungauged watersheds derived from these equations. Each USGS regional regression equation has a ***standard error of estimate*** that is a measure of the reliability of the equation. The larger the standard error of estimate, the less reliable the equation is for estimating the discharge. (See McCuen et al. (2002) for more information on the standard error of estimate.)

These limitations apply to all applications of USGS regression equations. When applying USGS regional regression equations for projected precipitation, as described in the previous sections of this chapter, additional caution is appropriate.

First, if the applicable equation(s) for the project location does not have an independent variable for precipitation, the equation is not equipped to estimate future conditions. As noted previously, many states and regions do not currently have equations with precipitation as an independent variable.

Second, as with traditional applications of USGS regression equations, the values of projected precipitation should remain within the range of the precipitation values used by USGS to generate the equation. Furthermore, this report recommends that projected precipitation values should be estimated by adjusting the historical values by multiplying them by the ratio of modeled (GCM) future and modeled (GCM) baseline conditions. This process was illustrated in the previous sections.

Third, because USGS develops these equations using information from the historical record, they implicitly assume that the relationships between the independent variables and discharge will remain the same, that is, the relationships are stationary. Because this procedure is accommodating a future precipitation that differs from the historical precipitation, this assumption is not strictly true. In the future, the relationship between the independent variables and discharge may change, new variables may become more important and enter the equation, and other variables in the current equation may become less important and drop out.

Recall that USGS regional regression equations do not fully explain variations in discharge even considering only historical information. This degree of reliability is measured by the standard error of estimate described previously. Use of future precipitation may reduce the reliability of the equation to an unknown degree because changes in precipitation may be accompanied by changes in related physical phenomena such as soil moisture, vegetation, evapotranspiration, etc. that are presumed to be encapsulated in the correlated behavior of the precipitation variable.

Urbanization may also alter the interrelationships within watersheds that contribute to discharges, but engineers frequently use regression equations with independent variables like impervious area to assess the effects of future urbanization on discharges. While the large-scale effects of climate change may alter watershed processes more fundamentally than urbanization, application of USGS regression equations for evaluating the effects of climate is a useful tool when used within prudent limits. For this report, “prudent limits” means that the values of projected precipitation must remain within the range of precipitation values used when developing the equation.

BOTTOM LINE: When USGS regional regression equations include a precipitation variable, they can be used for estimating the effects on design discharge as long as the value for the precipitation variable is within the range of values for that variable used in the development of the equation.

6.2.1.2. Hypothetical Example with USGS Regression Equation

Kilgore et al. (2016) provides an example application of an existing USGS equation for evaluating potential future conditions. In a hypothetical watershed for which climate projections suggest increasing precipitation, for an existing structure that was designed based on a 0.02 AEP (50-year) design event for an estimated 100-year service life, what is the change in the risk profile as a result of the changing conditions should they occur?

The applicable regression equations used for the original design are provided by the USGS and include the Mean Annual Precipitation (MAP) as one of the variables (Asquith and Roussel 2009). The watershed has a drainage area of 100 square miles and the MAP for the site is 26 inches. Future projections indicate that the median MAP value of an ensemble of projections for a particular scenario will increase to 32.5 inches over the structure service life, which is within the range of MAP used to develop the equation. Applying the regression equations for both the existing and future MAP results in the discharge estimates that are summarized in Table 6.3.

Table 6.3. MAP results for hypothetical example.

Annual Exceedance Probability	0.5	0.2	0.1	0.04	0.02	0.01
Flow with Current MAP (ft^3/s)	2,280	5,240	7,800	12,000	15,800	20,500
Flow with Future MAP (ft^3/s)	3,110	7,020	10,200	15,500	20,300	26,000

The original 50-year (AEP = 0.02) design flow was 15,800 ft^3/s and the structure was built for that flow. Under future conditions, one can observe that a flow of that magnitude is associated with a 25-year (AEP = 0.04) return period. The projection of climate change, therefore, suggests that a 15,800 ft^3/s (or 15,500 ft^3/s, which is essentially the same) event will be exceeded on average twice as frequently. Rather than the design value being experienced once every 50 years on average, it is now expected once every 25 years. The existing USGS regression equation is useful for revealing this potential shift in design discharge.

6.2.1.3. New York State Department of Transportation Example

In cooperation with the New York State Department of Transportation, the USGS developed a web-based tool based on the USGS StreamStats Program for estimating future flows under various climate change scenarios (Burns et al. 2015) (https://ny.water.usgs.gov/maps/floodfreq-climate/). The purposes of the tool are to provide estimates of peak flows in ungauged basins under current and future conditions for any stream in New York State (exclusive of Long Island) and the Lake Champlain Basin of Vermont.

For New York, the approach incorporates the previously developed regression equations by Lumia et al. (2006) that include one climate variable, either runoff or precipitation. Annual runoff is described as a climate variable here because it is computed as the difference between annual precipitation and annual evapotranspiration (ET). Infiltration is assumed to be a constant. Based on data for the period 1951 to 1980, Lumia et al. divided the state into six hydrologic regions with mean annual precipitation as the climatic variable in two regions and mean annual runoff as the climate variable in the other four regions.

For Vermont, the approach uses the previously developed regression equation by Olson (2014). In Vermont, there is only one set of regression equations and this set uses average annual precipitation as the climatic variable.

With these regression equations, the USGS based its tool on the following data and assumptions:

- Projections of future annual precipitation are derived from five CMIP5 GCMs using two future scenarios (lower RCP4.5 and higher RCP8.5) (The specific GCMs and downscaling technique are not noted in the documentation).
- The five climate models were selected based on discussions with climate scientists on those that best represent historic trends in precipitation in the Lake Champlain Basin (Guilbert *et al.* 2014).
- Projections were averaged over three future periods: 2025 to 2049, 2050 to 2074, and 2075 to 2099 using the National USGS Climate Change Viewer.
- The relation between annual precipitation or runoff and the peak flows is assumed to be the same in future as for the historical time periods from which the regression equations were developed.
- The ET to precipitation ratio was held constant and future changes in annual runoff are governed by changes in precipitation and the resulting changes in ET.

Burns et al. (2015) discuss several sources of uncertainty in this approach including the uncertainty in the peak flow estimates, inaccuracies in determining the prediction variables, uncertainty embedded in each climate model and scenario, uncertainty with respect to the future ET to precipitation ratio, and uncertainties in downscaling from the GCMs.

For the New York regression equations, mean annual runoff was the predictor variable for four of the six hydrologic regions, leading Burns et al. (2015) to use a water balance model and the assumption that the ET to precipitation ratio is constant for future conditions to convert to annual runoff. Future modeled precipitation values were compared to the historical precipitation and runoff used to develop the regression equations. Preliminary results indicate that larger increases in the 0.02 and 0.01 AEP discharges are projected for the near future period 2025-2049 for the lower scenario RCP4.5 than for the period 2050-2074 and the higher scenario RCP8.5. Possible reasons for results contrary to expectation include the following:

- The regression equations may be extrapolated too far beyond the precipitation data on which they are based.
- The projected precipitation may not be reasonable for the future period 2050-2074.

- Comparisons of regression estimates based on projected model precipitation to regression estimates based on historical precipitation and runoff for the period 1951-80 may be contributing to the irrational results.

The recommendation by Burns et al. (2015) is to use this tool in an exploratory manner and to consider the results along with other sources of information to decide how future climate change may affect peak flow magnitudes. There are several sources of uncertainty in the analysis as documented by Burns et al. (2015). However, the tool provides estimates of future discharges that may be useful for qualitative assessments.

6.2.1.4. Pennsylvania Department of Transportation Example

A regression equation was also used in a recent planning study by the Pennsylvania Department of Transportation (PennDOT) to estimate future 0.01 AEP discharges to evaluate the potential future flooding of roadways and bridges from climate or land use change (PennDOT 2017). Data for the 0.01 AEP discharges and watershed characteristics for gauging stations were obtained from USGS published reports and databases. These data were also used in a nationwide climate change study for FEMA (Kollat et al. 2012). The precipitation data were obtained from the DCHP website (http://gdo-dcp.uclinl.org/downscaled_cmip_projections). A regression equation for the 0.01 AEP discharge ($Q_{0.01}$) was developed using data for 230 gauging stations in and near Pennsylvania with the following form:

$$Q_{0.01} = aDA^{b1}SL^{b2}(ST+1)^{b3}(IA+1)^{b4}P^{b5} \quad (6.6)$$

where:

a = *Regression constant.*

b1 to b5 = *Regression exponents.*

DA = *Drainage area.*

SL = *Main channel slope.*

ST = *Percent of the watershed area covered by lakes and ponds.*

IA = *Percent of the watershed covered by impervious surfaces.*

P = *Mean of the annual maximum daily precipitation for the historic period 1950-99 from the DCHP website.*

The objective was to use the same precipitation variable in developing the regression equations for which projected values were available from the DCHP website. All of the independent variables in Equation 6.6 were statistically significant at the 5-percent level, with all coefficients positive except *ST*.

Data for gauging stations in New York, New Jersey, Delaware, and Maryland were used in the analysis to increase the variability in the time varying parameters *IA* and *P* that were projected into the future. There are a limited number of urban gauging stations (impervious area greater than 10 percent) in Pennsylvania with sufficient record for frequency analysis with the majority of the urban gauging stations in southeast Pennsylvania. Urban gauging stations from New Jersey, Maryland, and Delaware were used in the analysis to increase the variability in *IA*. The highest annual maximum precipitation in Pennsylvania is in the southeast corner of the state near

Philadelphia and the lowest annual maximum precipitation is in the southwest corner of the state near Pittsburgh. Precipitation decreases from east to west across the Commonwealth of Pennsylvania. Annual maximum precipitation is greater in New Jersey, Delaware, and Maryland so adding gauging stations from those states also increased the variability in the annual maximum precipitation.

The equation was used to estimate 0.01 AEP discharges for future time periods based on changing land use conditions and changes in the mean of the annual maximum precipitation. Future land use projections were obtained from the Integrated Climate and Land Use Scenarios (ICLUS) database developed by the U.S. Environmental Protection Agency (U.S. EPA 2009). Projected precipitation was obtained from the DCHP website. The study parameters were:

- Future estimates of the mean of the annual maximum precipitation for three GCMs obtained from the DCHP website. Three GCMs were chosen that were reasonably independent using criteria on the ICNet website (http://theicnet.org/?page_id=50).
- Future periods were 2000-2049 and 2050-2099.
- Because the objective was to perform a conservative assessment of potential future impacts on PennDOT infrastructure, the higher RCP8.5 scenario was used.
- Increases in future precipitation were estimated by comparing downscaled GCM precipitation for future time periods to downscaled GCM precipitation for the baseline period 1950-99.
- A ratio of future and existing conditions gives the increase in the 0.01 AEP for a given future period and a given GCM. The ratios were averaged for the three GCMs for each period and the average ratio was applied to the observed estimate of the 0.01 AEP discharge to obtain estimates for future periods.

The increases in the 0.01 AEP discharges were used to estimate increases in flood depths, which were applied to depth grids for the effective Flood Insurance Rate Maps (FIRMs) for three pilot counties to produce new floodplain boundary maps. These new maps were used to determine the increase in flooding at bridges and roadways in the PennDOT transportation network.

As previously discussed, one of the concerns in using regional regression equations for projecting flood discharges is applying the regression equations outside the range of data used to develop the equations. For the PennDOT study, data were used from surrounding states to increase the variability in the land use and climate data variables. For the pilot county in the southeast corner of the state, the regression equations were occasionally extrapolated beyond the precipitation data used to develop them, but the potential effects on the study were not evaluated. For the county in the southwest corner of the state where precipitation is lower, the regression equations were not extrapolated beyond the range of precipitation used to develop them. With respect to land use change, extrapolation was not an issue because highly urbanized watersheds were used in developing the regression equations. The approach used for the PennDOT (2017) study provides estimates of future discharges that may be useful for a Level 3-type analysis.

BOTTOM LINE: Traditional multiple linear regression tools including existing USGS regional equations with one or more climate variables or new equations developed explicitly for evaluating climate change (such as the PennDOT example) can be useful for evaluating changes in discharge when used within the bounds of the data used to develop the tools.

6.2.2. Panel Regression Techniques for Projecting Flood Discharges

As defined by Steinschneider et al. (2013), panel regression is a statistical technique that pools multidimensional data recorded across several watersheds and through time (panel data) to identify response characteristics unique to each watershed and those common across watersheds. The panel regression procedure essentially combines the strengths of MLR and time series analysis into a single statistical framework.

The time series approach employs analyses on individual watersheds that are known to have undergone some level of land use change over the analysis period. The analyst determines whether land use change trends in the watershed can be used to explain any trends in flow statistics for that watershed. However, climatic variability can mask the detection of any relation between land use and streamflow. By examining only one watershed at a time, it is difficult to separate the effects of trending climate and land use variables on streamflow. This is the classic multicollinearity problem where trending climate and land use characteristics could be highly correlated.

The dependent variable in a panel regression is a single flow variable, such as the annual maximum peak discharge or the annual runoff, and there is an observation for each year of record for each gauging station in the panel regression analysis. In addition, the **predictor variables can vary in time,** which is a key difference from MLR analysis. Steinschneider et al. (2013) identify three primary benefits of panel regression:

- Annual data across all watersheds through time are used simultaneously in the analysis to increase the sample size and improve the efficiency of parameter estimation.
- A means for handling unobservable heterogeneity between watersheds is available.
- The ability to examine time series trends across several watersheds simultaneously helps distinguish between land use and climate variability signals.

6.2.2.1. Panel Regression Overview

The use of panel regression in hydrologic analyses is relatively new concept discussed and illustrated by Steinschneider et al. (2013). The limited published examples have used mean annual flow data as the dependent variable. If all sites in the panel regression have equal record lengths, the panels are considered balanced; if the sites have unequal record lengths, the panels are considered unbalanced. The panel regression equation has the following form:

$$Q_{i,t} = B_o + \mu_i + \sum\left(B_k * x_{i,t}^k\right) + \epsilon_{i,t} \quad (6.7)$$

where:

$Q_{i,t}$ = *Flow or the logarithm of flow for watershed i at time t.*

B_o = *Mean intercept that applies to all watersheds.*

B_k = *Regression coefficients describing the influence of the* k^{th} *predictor.*

$x^k_{i,t}$ = k^{th} *predictor (or its logarithm) for watershed i and time t (could be a climatic or a land use variable).*

μ_i = *Watershed-specific term describing the time-averaged differences in flow between watersheds.*

$\varepsilon_{i,t}$ = *Residual error term for watershed i and time t with an expected value of zero and constant variance.*

The B_k and $x^k_{i,t}$ account for variability in the streamflow response within each watershed across time, referred to as the "within" variability, while the term μ_i accounts for the variability across watersheds, referred to as the "between" variability. In a panel regression, the "between" variability may not be well described by available predictor variables because certain time-invariant characteristics of each watershed may be difficult to quantify. In this situation, the parameter estimates of the model can become biased.

In a panel regression, the watershed-specific term μ_i can be used to account for differences in the time-averaged streamflow responses across watersheds not accounted for by the available predictors, thus removing parameter estimation bias. This property is potentially very powerful if variables not included in the model have significant effects on streamflow and lead to unobservable heterogeneity between individual watersheds, a common situation in the traditional regression analysis. One key assumption implicit in the panel regression model formulation is that the structural heterogeneity between watersheds (e.g., time-invariant characteristics), as quantified by μ_i, does not change over time. Furthermore, it is assumed that each of the *k* predictors has the same effect on the streamflow response across all watersheds (Steinschneider et al. 2013).

Bassiouni et al. (2016) indicate that multicollinearity (correlation between predictor variables) and omitted-variable bias are major limitations to developing MLR models to estimate streamflow characteristics for ungauged areas for varying precipitation conditions. Estimated coefficients of the MLR offer important information about the elasticity of streamflow characteristics to the predictor variables and therefore it is important to obtain robust estimates of the regression coefficients. Elasticity provides a measure of the sensitivity of streamflow to changes in the predictor variables. For example, Sankarasubramanian and Vogel (2001) discussed the sensitivity of streamflow to changes in precipitation, described several models for estimating the precipitation elasticity of streamflow, and developed a nationwide map of precipitation elasticity of streamflow.

Panel regression has the potential to overcome both the statistical challenges of multicollinearity and omitted-variable bias in MLR and to give more robust estimates of the elasticity of streamflow to predictor variables such as precipitation (Bassiouni et al. 2016). Panel regression structure can be varied depending on the characteristics of the heterogeneity in the streamflow response and the assumptions on model residuals. Briefly, the alternative approaches are:

- Pooled panel regression. The watershed-specific term μ_i is set to zero with no heterogeneity allowed between watersheds. This approach is often used for comparison purposes with other approaches.
- Fixed-effects panel regression. The watershed-specific term μ_i is treated as a dummy or binary variable (0,1) that assumes omitted factors controlling the behavior of streamflow are correlated with other predictor variables in the model and the individual watershed effects are not random variables.
- Random-effects panel regression. The watershed-specific term μ_i is treated as a random variable and constant in time for each watershed *i*. The assumption is that there are omitted predictor variables that are not correlated with other predictor variables and can be incorporated in the model through the stochastic component of the response variable.

A pooled panel regression can be expressed in the vector form $\mathbf{Q} = \mathbf{XB} + \boldsymbol{\varepsilon}$ with predictors stacked in the design matrix **X** across watersheds for a balanced panel model as follows (Steinschneider et al. 2013):

$$\mathbf{X} = \begin{bmatrix} x^1_{1,1} & \cdots & x^K_{1,1} \\ \vdots & \cdots & \vdots \\ x^1_{1,T} & \cdots & x^K_{1,T} \\ \vdots & \cdots & \vdots \\ x^1_{N,1} & \cdots & x^K_{N,1} \\ \vdots & \cdots & \vdots \\ x^1_{N,T} & \cdots & x^K_{N,T} \end{bmatrix}$$

Here **X** is a matrix of dimension NT x K where N is number of watersheds, K is the number of predictor variables and T is the length of record at each gauging station. In addition, **B** is a column vector of length K and **Q** and **ε** are column vectors of length NT. The design matrix includes a column of ones to account for the intercept term B_o. The matrix formulation is shown to illustrate that each row in **X** is a different year of record for watershed i for the period of record T. Each year of record is used in the regression analysis in contrast to traditional regression analysis that uses a quantile statistic for the period of record. Ordinary least squares regression is used to compute the model.

For the fixed-effects panel regression (balanced panels), the **X** matrix is augmented to include the watershed-specific intercept terms (μ_i) as follows (Steinschneider et al. 2013):

$$\mathbf{X}_{\mathrm{FE}} = \begin{bmatrix} x^1_{1,1} & \cdots & x^K_{1,1} & 1 & \cdots & 0 \\ \vdots & \cdots & \vdots & \vdots & \cdots & \vdots \\ x^1_{1,T} & \cdots & x^K_{1,T} & 1 & \cdots & 0 \\ \vdots & \cdots & \vdots & \vdots & \cdots & \vdots \\ x^1_{N,1} & \cdots & x^K_{N,1} & 0 & \cdots & 1 \\ \vdots & \cdots & \vdots & \vdots & \cdots & \vdots \\ x^1_{N,T} & \cdots & x^K_{N,T} & 0 & \cdots & 1 \end{bmatrix}$$

Here the $\mathbf{X_{FE}}$ matrix has the original predictors ($x^k_{i,t}$) in the first K columns followed by N columns of zeros and ones that specify a specific intercept for each watershed. These are the dummy or binary variables (0,1) that are used to describe a watershed-specific response across the watersheds. Each station has a 1 and N-1 zeroes for the watershed-specific effect. Ordinary least squares regression is used to compute the model.

For the random-effects panel regression, the terms μ_i are considered normally distributed random variables that are eventually manifested in the covariance matrix of the error term and are by assumption not correlated with the predictor variables $x^k_{i,t}$ or the residuals $\varepsilon_{i,t}$. The dependent variables are also correlated in this approach so generalized least squares regression is used to compute the model. Because the variance of the dependent variable is used in the analysis, the **X** matrix is more complicated than in the fixed-effects panel regression and Steinschneider et al. (2013) provide the details.

6.2.2.2. Example Panel Regression Analyses by Steinschneider et al.

Steinschneider et al. (2013) illustrate panel regression approaches by examining the influence of urbanization on the annual runoff coefficient for 19 gauging stations in New England for the period 1977-2007 (equal record lengths at all stations). The period of record was limited to 1977-2007 because measures of urbanization could be estimated for that period. The annual runoff coefficient was defined as the ratio of cumulative streamflow to cumulative precipitation.

The hypothesis was that increased urbanization will increase the runoff volumes from individual storms and increase the annual runoff coefficient. The annual runoff coefficient was related to three predictor variables that varied with time: the cumulative annual precipitation, the cumulative annual potential evapotranspiration (ET), and a measure of urban land cover. Using data for the 19 watersheds for 31 years of record, Steinschneider et al. (2013) performed five different modeling experiments:

- **Cross-sectional regression** analysis for the year 2007 for the 19 gauging stations (space-only model): The analysis indicated a statistically significant relation between the annual runoff coefficient and urbanization, but not with precipitation or potential ET. This result is likely because the variability in urbanization across watersheds was greater than the variation in precipitation and potential ET for a given year.
- **Time-series regression** for one station chosen at random for all 31 years of record (time-only model): The analysis for a single station indicated no statistically significant relation between annual runoff coefficient and urbanization and

precipitation was the only significant variable. This result is likely because the variation in precipitation over the period of record was greater than the variation in urbanization for this single watershed.

- **Pooled regression** analysis assuming no variation across watersheds: The analysis that included data for all 19 stations for the 31 years of record indicated all three predictor variables – precipitation, potential ET, and urbanization – were statistically significant. However, there was significant variation in residuals across the 19 watersheds leading to the conclusion that a pooled regression model was not valid.
- **Fixed-effects** regression assuming a qualitative (binary) variable for variation across watersheds.
- **Random-effects** regression assuming the variation across watersheds is a random variable.

The fixed- and random-effects regression analyses indicated no significant relation between the annual runoff coefficient and urbanization, but it did result in statistically significant relations with precipitation and potential ET. The results from the fixed- and random-effects model were considered the most reasonable because the standard errors were lower and both spatially and temporally varied data were used for all gauging stations for the period of record. In general, the urbanization changes were not large over the 31-year period 1977-2007 with 10 of the 19 watersheds having less than a 10-percent change in urbanization. Therefore, the hypothesis that urbanization increases the annual runoff coefficient was rejected for the given dataset.

The objective of Steinschneider et al. (2013) was to determine if the annual runoff coefficient increased with increasing urbanization based on data for the 19 gauging stations. The objective was not to project the climatic data and land use conditions into the future although the panel regression approach could be used for this purpose.

6.2.2.3. Example Panel Regression Analyses by Over et al.

An example is provided of adjusting annual peak discharges for land use change for 183 gauging stations in the Chicago, Illinois metropolitan area. Over et al. *(*2016a) describes the methodology and Over et al. (2016b) describes application of the methodology. Over et al. used a two-step regression procedure, longitudinal and quantile regression, to adjust annual peak discharges where the longitudinal regression used by Over et al. was consistent with the panel regression described earlier. The end product of the Over et al. study was conventional regression equations for estimating the x-percent chance flood discharges based on watershed characteristics (drainage area, urbanization measure, basin soil wetness measure, and basin slope measure).

Most gauged watersheds in the Chicago metropolitan area have experienced urbanization over the period 1940 to 2010. Over et al. chose to use this 70-year period because decadal housing density data (1940, 1950, 1960, etc.) are available from Theobald (2005) for this period. Theobald (2005) defined 11 categories of housing density, and Over et al. used four of them to estimate the fraction of developed land. The four categories are:

- Category 7 – 1.7 to 10 acres per housing unit;
- Category 8 – 0.6 to 1.7 acres per housing unit;

- Category 9 – Less than 0.6 acres per housing unit; and
- Category 10 – Commercial/industrial/transportation.

Based on these four land use categories, the fraction of developed land (U) was estimated for each gauged watershed for each year of record between 1940 and 2010. The annual data were obtained by linear interpolation between the decadal points. Panel and quantile regression were used to adjust the annual peak discharges to 2010 land use conditions to achieve a homogeneous sample of data for flood frequency analysis. Initially there were 181 gauging stations in the study area but many of the stations had redundant data (watersheds nested within other watersheds) so Over et al. reduced the number of gauging stations to 117.

The first step was to perform a panel regression whereby each annual peak discharge for each watershed was related to daily precipitation (P) and fraction of urban land (U) as defined above. Daily precipitation was used for each annual flood because there are many more daily precipitation stations than hourly stations in the study area, and high quality NEXRAD data were not available before the mid-1990s. The panel regression equation has the following form:

$$y_i(t) = a_i + b_1 P_i(t) + b_2 U_i(t) + e_i(t) \quad (6.8)$$

where:

$y_i(t)$ = *Base-10 logarithm of the annual maximum peak discharge (log_{10} $Q_i(t)$)at the ith segment during year t.*

a_i = *Intercept of the ith segment where N is the number of segments (usually one segment per gauging station.,*

$P_i(t)$ = *Precipitation for the ith segment during year t.*

$U_i(t)$ = *Urban fraction for the ith segment during year t.*

b_1, b_2 = *Regression coefficients for precipitation and urban fraction, respectively.*

$e_i(t)$ = *Regression error for the ith segment during year t.*

i = *segment, i = 1,2, … N.*

The intercept a_i is unique to each segment. It represents the difference in flood response between watershed and accounts for watershed characteristics not used in the analysis. Over et al. indicate that a_i is related closely to the drainage area. The segment generally refers to a gauging station, but 18 of the 117 stations had more than one segment due to some change in the watershed during the period of record.

For panel regression, each observation in the analysis represents a given year for a gauging station and all gauging stations are included in the same analysis (117 stations for this analysis). Not all gauging stations have record for the full period 1940 to 2010. Equation 6.8 could be used for adjusting for the effect of future precipitation, but projections of future precipitation are very uncertain. For this study, the annual peak discharges are only adjusted for the effect of land use change or urbanization.

Based on the analysis for 117 gauging stations, the coefficient for precipitation (b_1) was 0.110 and the coefficient for urban fraction (b_2) was 0.508. Both coefficients were large with respect to

their standard errors implying the coefficients are highly significant. Equation 6.8 without the error term can be expressed as:

$$y_i(t) = a_i + 0.110\ P_i(t) + 0.508\ U_i(t) \quad (6.9)$$

where a_i is unique to a given watershed and accounts for watershed characteristics not in the model, like drainage area. Over et al. obtained a segment-independent dataset of $y_i(t)$ by adding a weighted mean of the segment intercepts and subtracting each specific segment intercept. The resultant annual peak discharges ($y_i(t)$) vary according to the impact of precipitation and urban fraction and not watershed characteristics.

Quantile regression is used in the second step because it provides an estimate of the coefficients of the regression model for different quantiles (annual exceedance probabilities). A regression model of the same form as Equation 6.8 was assumed except the dependent variable was a quantile—a discharge for a given annual exceedance probability. The regression analysis was performed on quantiles because it is well known that urbanization has more impact on the frequent floods than on the more extreme floods. The quantile regression analysis can account for this disparate effect.

The output from the quantile regression analysis was the determination of quantile regression coefficients of the urban fraction (U) for selected annual exceedance probabilities. Figure 6.7 summarizes the coefficients for urban fraction as a function of annual exceedance probability (Over et al. 2016b). A boot strap resampling approach was applied to obtain unbiased mean coefficient values and their standard errors. A seventh-order polynomial fit to the mean quantile regression coefficients provides a continuous relation between the urban fraction coefficient and exceedance probability.

As shown in Figure 6.7, the urban fraction coefficient for the 0.01 exceedance probability flood is 0.312 while the coefficient for the 0.99 exceedance probability is 0.929, illustrating that urbanization has a much larger impact on the more frequent floods. The urban fraction coefficients illustrated in Figure 6.7 were then used to adjust the annual peak discharges for each gauging station for the period of record.

The third step in the analysis was to assign each peak discharge an exceedance probability by a procedure described in Over et al. (2016a). Using the exceedance probability (p) assigned to each peak discharge observation and the continuous fraction coefficient function ($b_2^*(p)$ from Figure 6.6, the annual maximum peak discharges were adjusted to 2010 land use conditions using the following equation:

$$y_i^*(t) = a_i^* - a_i + y_i(t) + b_2^*(p)[U_i(t^*) - U_i(t)] \quad (6.10)$$

where:

$y_i^*(t)$ *and* $y_i(t)$ = *Base-10 logarithms of the adjusted and unadjusted, respectively peak discharge value for year t and segment i.*

a_i^* *and* a_i = *Segment intercept values for the most recent and current segments, respectively, of the stream gauge record containing segment i.*

$b_2^*(p)$ = *Urban fraction coefficient value corresponding to the exceedance probability (p) assigned to the peak discharge value* $y_i(t)$.

$U_i(t^*)$ and $U_i(t)$ = *Urban fraction values for the basin corresponding to segment i during the year t* to which peak discharges are being adjusted (2010) and the year t of the observation of the peak discharge $y_i(t)$, respectively.*

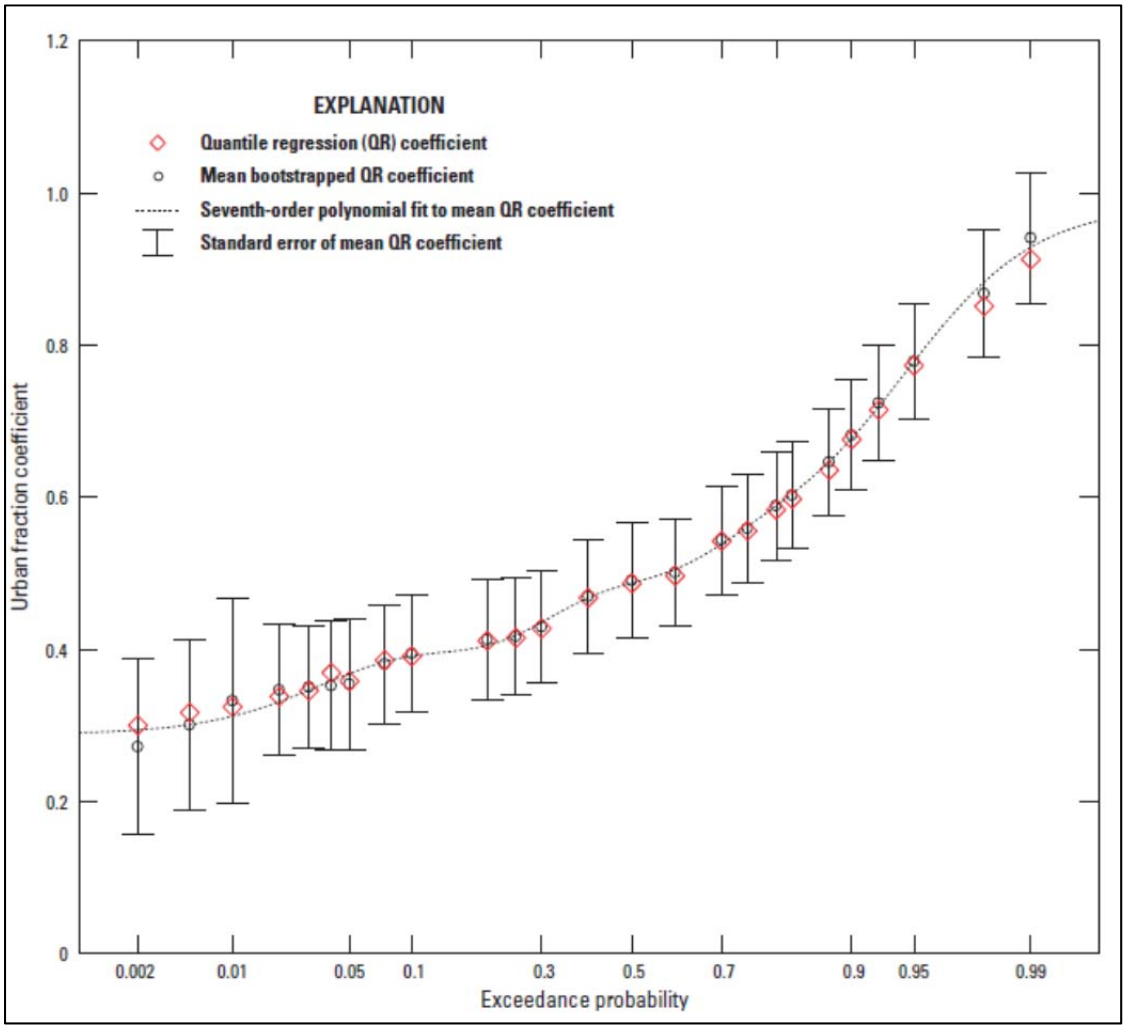

Figure 6.7. Urban fraction coefficients from temporal regression analysis of 117 stream gauges in northeastern Illinois and adjacent states as a function of exceedance probability (Over et al., 2016b).

Notice that if a stream gauge record has only one segment, then $a_i^* = a_i$ and the quantity $a_i^* - a_i$ drops out of Equation 6.10. Only 18 of the 117 stream gauges in this study had more than one segment. For those watersheds, hydrologic conditions changed over the period of record (detention storage, channelization, etc.) and separate analyses were conducted for each segment of record.

Annual peak discharges adjusted to 2010 land use conditions were estimated for all 117 stream gauging stations. An example of the observed and adjusted annual peak discharges for the Skokie River at Lake Forest, Illinois (05535000) are given in Figure 6.8.

The dotted line in Figure 6.8 is the change in the urban fraction over time from 0.211 in 1952 to 0.850 in 2009. As shown in Figure 6.8, the peak discharges in the early part of the record when

the watershed was more rural are adjusted upward more than in the latter part of the record when the watershed was more urbanized. There is an upward trend in the observed peak discharges but the adjusted peak discharges do not exhibit an upward trend.

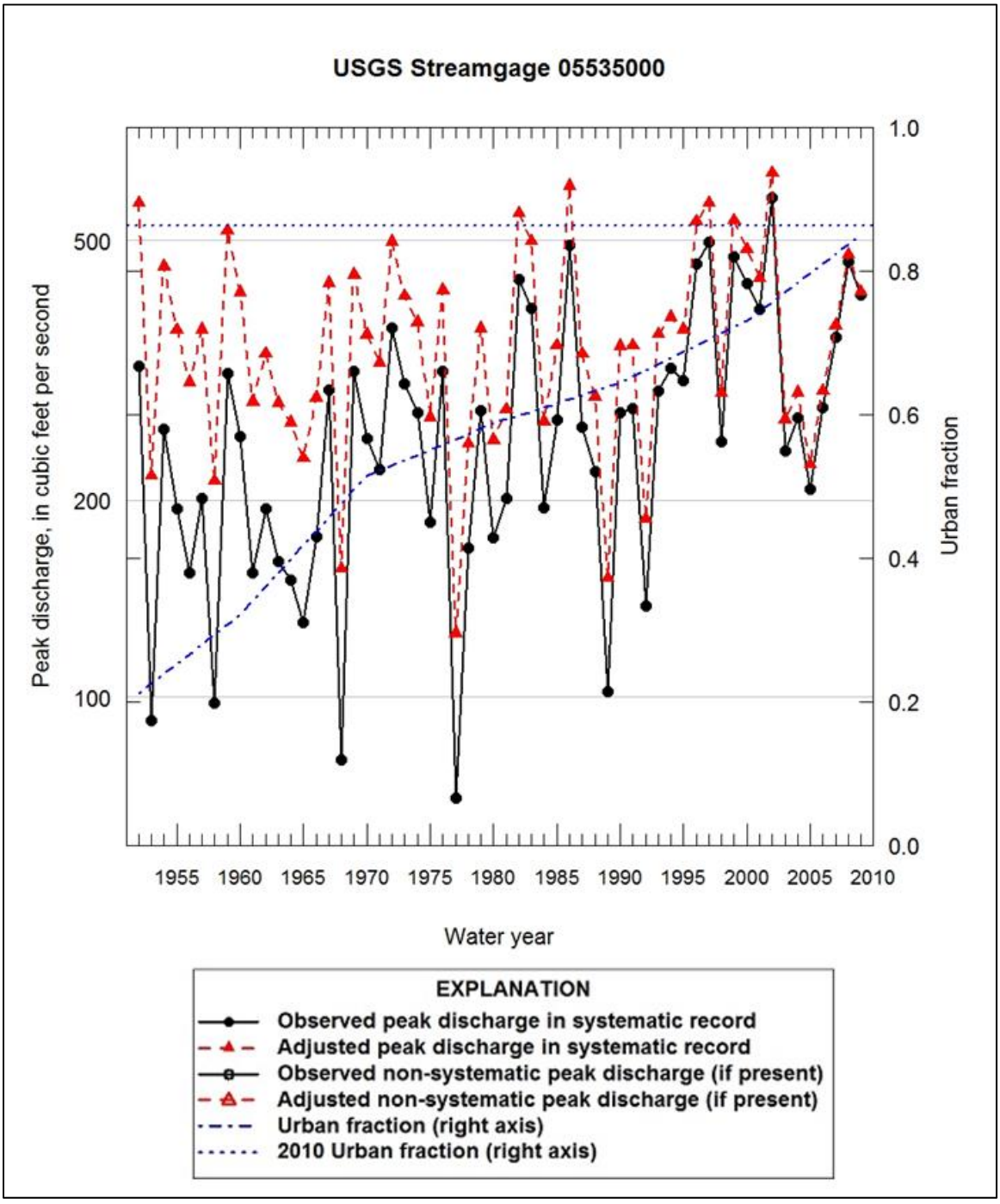

Figure 6.8. Observed and adjusted annual peak discharges for the Skokie River at Lake Forest, IL (05535000).

The fourth step in the process was to perform flood frequency analyses at the 117 gauging stations using the adjusted annual peak discharges based on 2010 land use conditions. Over et al. (2016b) used the USGS PeakFQ Version 7.1 program to perform the frequency analyses using Bulletin 17C procedures. A Bayesian Generalized Least Squares (GLS) analysis was employed to derive an equation for estimating regional skew as a function of the level of urbanization.

The final step in the analysis was to perform a spatial GLS regression analysis to develop equations for estimating x-percent chance floods at ungauged locations. The final regression equations are documented in Over et al. (2016b) and are based on the drainage area (A) in square miles, an urbanization measure (U) as a decimal fraction, basin soil wetness measure (W) as a decimal fraction, and a basin slope measure (S) in feet per mile.

This study represents an example of how panel regression can be used to adjust annual peak discharges for urbanization to achieve homogeneous flood records for frequency analysis. The homogeneous flood records, representing 2010 land use conditions, were used to define spatial or conventional regression equations for estimating flood discharges for ungauged watersheds. The same approach could be used for adjusting for the effects of climate change if reliable estimates of future precipitation were available for the Chicago, Illinois metropolitan area.

The study was completed by the USGS in cooperation with the USACE−Chicago District, the Illinois Center for Transportation, the Illinois Department of Transportation, and the Federal Highway Administration. Considerable resources were expended for this study and state-of-the-art statistical procedures were employed (panel or longitudinal regression, quantile regression, boot strap resampling, and regional skew analysis using Bayesian GLS analysis). This level of effort is appropriate for a regional-scale study where the results can be applied at many locations.

BOTTOM LINE: Panel regression techniques implemented by Over et al. (2016b) for evaluating the effects of land use change could also be used for estimating the potential changes in flood flow resulting from climate change.

6.2.3. Summary and Recommendations

MLR analysis techniques are frequently used to estimate a quantile such as the 0.01 AEP discharge for an ungauged watershed. The annual peak discharges and land use conditions are assumed stationary in time. Each watershed in the MLR analysis is one observation in the regression analysis. MLR equations such as those developed by USGS are typically used by state DOTs for estimating design flood discharges for ungauged watersheds. USGS regression equations are published and readily available for all 50 states and Puerto Rico. Two published reports by state DOTs were used to illustrate examples of projecting discharges using MLR equations. The pertinent points and recommendations relative to using MLR equations to project flood discharges are:

- A major concern with using regression equations to project flood discharges is their potential extrapolation beyond the data used to develop them that may lead to irrational results.
- Use of MLR equations, when they include the appropriate independent variables, should not be ruled out as long as the values are not extrapolated beyond their limits of applicability.

- Projected discharges from MLR equations should be used in an exploratory manner with other sources of information to estimate how future climate change may affect flood discharges.
- An alternative approach to using existing equations may be to develop new regression equations using data beyond the limit of study area to increase the variability in the time varying parameters such as precipitation and land use conditions (one example is the PennDOT [2017] study).
- In developing new regression equations, climatic and land use characteristics for which there are projected values from readily available sources should be used.

Panel regression analysis differs from MLR analysis because it pools multidimensional data across several watersheds and through time (panel data) to identify response characteristics unique to each watershed and those common across watersheds. In panel regression analysis, the dependent variable is an annual flow value like the annual runoff coefficient. The predictor variables like precipitation or land use conditions are also annual values that vary with time. Panel regression analysis combines spatial data and temporal data into a single analysis and provides a comprehensive approach for simultaneously evaluating time series trends across several watersheds and distinguishing between land use and climate variability signals. Panel regression provides more robust regression coefficients for evaluating the sensitivity (elasticity) of streamflow to climate and land use variables. In addition, panel regression can be used with projected annual climate and land use data to estimate future annual values of streamflow. Frequency analyses can then be performed on the future annual flows to estimate the needed design flows.

Panel regression analysis has only recently been applied to hydrologic data and there are two useful approaches. The fixed-effects panel regression analysis treats the impact of time invariant watershed characteristics as dummy or binary variables (0,1) and is appropriate for evaluating the effects of climatic and land use change on streamflow response at gauging stations. The random-effects panel regression treats the impact of time invariant watershed characteristics as random variables and can also be used for evaluating changes for ungauged watersheds.

The two examples of panel regression described in this section analyzed the impact of land use change on annual runoff and annual peak discharges. Annual and daily precipitation were used as explanatory variables in the panel regression analysis so the impact of precipitation on annual runoff and annual peak flows could have been analyzed. Panel regression offers promise for:

- Determining the simultaneous effect of climate and land use at gauging stations.
- Analyzing the effects of projected climate and land use on streamflow data for ungauged watersheds.

The use of panel regression is new in hydrologic analyses and limited examples of using this technique were found in the literature. The study by Over et al. was a good example of using panel regression to adjust annual peak flow data to current land use conditions. Considerable resources and expertise are needed to conduct a similar study. This level of effort is appropriate for a regional-scale study where the results can be applied across many projects.

6.3. Index Flood Methods for Accommodating Climate Change

The Index Flood Method is a method for estimating design discharges at ungauged sites based on flood frequency analysis of historical data at gauged sites. Since the advent of USGS Regional Regression Equations, it has seen little use in the United States, but it is still popular in many other areas of the world. Despite having fallen into disuse in this country, the concept on which the method is based offers a means for using the technique to incorporate climate change into projected design flow estimates. Flood frequency curves (FFCs) are the foundation on which the Index Flood Method is based. This section describes the Index Flood Method and how it can be applied in the context of climate change. Background information is provided in Appendix D.

6.3.1. The Index Flood Method

The FFC for each watershed is unique. To compare shapes of FFCs between watersheds, or to adapt an FFC from one watershed to another, requires a common coordinate system. A convenient approach is to normalize the quantile values for each curve about a selected quantile – the index flood – by dividing each quantile magnitude by the magnitude of the index flood. The transformed value of the selected quantile becomes unity. Flood values smaller in magnitude (higher AEP) are transformed to fall between 0 and 1 and flood values larger in magnitude (lower AEP) are transformed to take on values greater than 1. The transformed values are "flood ratios" for their respective quantiles. The flood ratios represent multipliers on the index flood, and thus a growth rate or slope of the curve (Dalrymple 1960). The USGS departed from using the Index Flood Method in the early 1970s because the slope of the regional frequency curve was a constant (based on the growth factors). Based on studies by Manual Benson, regression on quantiles was adopted because the slope of the frequency curve varied as a function of watershed characteristics (e.g., steeper slopes for smaller watersheds than for larger watersheds).

The Index Flood Method was developed to estimate flood frequency curves on ungauged sites by aggregating information on the slopes of the curves obtained from stream gauge data. Dalrymple (1960) presented the "mean annual flood" as the index flood. It was defined as the arithmetic average of flood discharges and was assigned the return period of 2.33 years (AEP=0.43) based on the Gumbel distribution. The Gumbel distribution was the distribution of choice for the USGS at that time.

The median of the flood ratios for each quantile value was considered characteristic and representative over a region for that quantile. To apply the Index Flood Method, the index (mean annual) flood was estimated from watershed characteristics and then multiplied by the representative ratios to obtain flood frequency values for each quantile. The Index Flood Method was, in effect, a predecessor to regression equations as a flood estimation technique in the era before computers were available for general use.

The selection of the mean annual flood as the index flood was made for convenience; the arithmetic mean was easy to calculate, even with only pencil and paper. The assignment of the mean annual flood to a return period of 2.33 years is attributable to the institutional selection of the Gumbel distribution as the distribution of choice for flood frequency. The association of mean annual and the 2.33-year return period has persisted in the hydrologic community, even though the mean annual flood does not have the same AEP for all statistical distributions

If an FFC can be developed, any convenient quantile value, or one that shows particular advantages, can be selected as the index flood. The index flood serves as an "anchor point" for

FFCs generalized by this method. The use of the mean annual flood as the index flood places the anchor point at or near one end (the frequent end) of the curve. In the manner of a lever, uncertainty and error grow in proportion to distance. To minimize such leverage, an index flood located somewhere in the middle portion of the part of the FFC of principal interest (0.5, 0.2, 0.1, 0.04, 0.02, and 0.01 AEP quantiles) would exhibit less sensitivity to error than the mean annual flood. Errors in either the estimation of the index flood or the flood ratios would be subject to less inflation by leverage.

Reviewing the information available on annual peak series gauge analysis for regression equations, confidence limits and standard errors of estimate often minimize in the neighborhood of the 0.1 AEP estimate. There appears to be some loss of resolution at frequent AEP values for annual peak series that increases uncertainty for those values, while data series are seldom long enough to provide good resolution for infrequent values. Use of the 0.1 AEP (10-year return period) flood estimate as an index flood provides balance between the extremes. The 10-year flood discharge can be thought of as sufficiently rare to avoid the loss of information resolution apparent in frequent flood values obtained using annual peak series, yet sufficiently frequent as to fall well within the data range of many gauge data series. The result is thus a balancing of competing deficiencies in information.

The idea underlying the Index Flood Method is that the flood ratios encapsulate the shape and slope of FFCs in a dimensionless form. Preserving the shape in this way facilitates the adaptation of an entire FFC for changing conditions by the estimation of change in only one value—the index flood. In this case, the Index Flood Method is a method of translating the properties of FFCs from one set of conditions to another; some initial estimates of the index flood magnitude and flood ratios are needed in order to apply it.

In the absence of a stream gauge and existing FFC at a site of interest, flood ratios may be computed for nearby gauges with similar characteristics. Documentation of past analyses, such as USGS Regional Regression Equation publications, can be exploited as source material for flood ratios. Flood ratios may be compared among any number of appropriate gauges and appropriate values selected or calculated. Flood ratios may be transposed from one or more gauged to an ungauged watershed in a manner similar to the transposition of gauge analysis, if a suitable estimate and scaling of the index flood is available.

FFCs are continuous, connected entities in magnitude and probability, rather than being discreet, disjoint values associated with particular probabilities as would be derived from regression equations. Among the advantages of FFCs are proportionate responses to changes in conditions, sharing of information from one location to another, and understanding behavior.

6.3.1.1. A Broad Look at Flood Ratios

Over time, the Index Flood Method of Dalrymple (1960) fell into disuse in the United States, because other methods, many requiring more intensive computing, replaced it. It is still used in other places, and research on the estimation of the mean annual flood still finds publication. Flood ratios and index floods are of interest in this study because flood ratios capture the slope and shape of flood frequency curves and relate them to a single quantity: the index flood magnitude. Renewed interest in flood ratios has occurred, in part, because some common methods of estimating FFCs tend to distort the shape of individual FFCs.

To illustrate the variety of FFC shapes, flood ratios for FFCs for 637 gauged watersheds in and around Texas were calculated, indexed about the 10-year discharge for each watershed, and plotted in Figure 6.9. (Data are from the USGS website pertaining to Asquith and Roussel [2009]). The flood ratios for the 100-year return period (0.01 AEP) magnitude range from 1.039 (Q_{100} is only 3.9 percent greater than Q_{10}) to 27.5 (Q_{100} is 27.5 times Q_{10}). A range in magnitude of flood ratios as great as this (over 700 times) indicates that the preservation of shape may be an important topic in estimating FFCs on ungauged watersheds, as well as estimating the change in FFCs under changing precipitation conditions. The figure also displays the median, 25th, and 75th percentile curves showing the general distribution of the watershed FFCs.

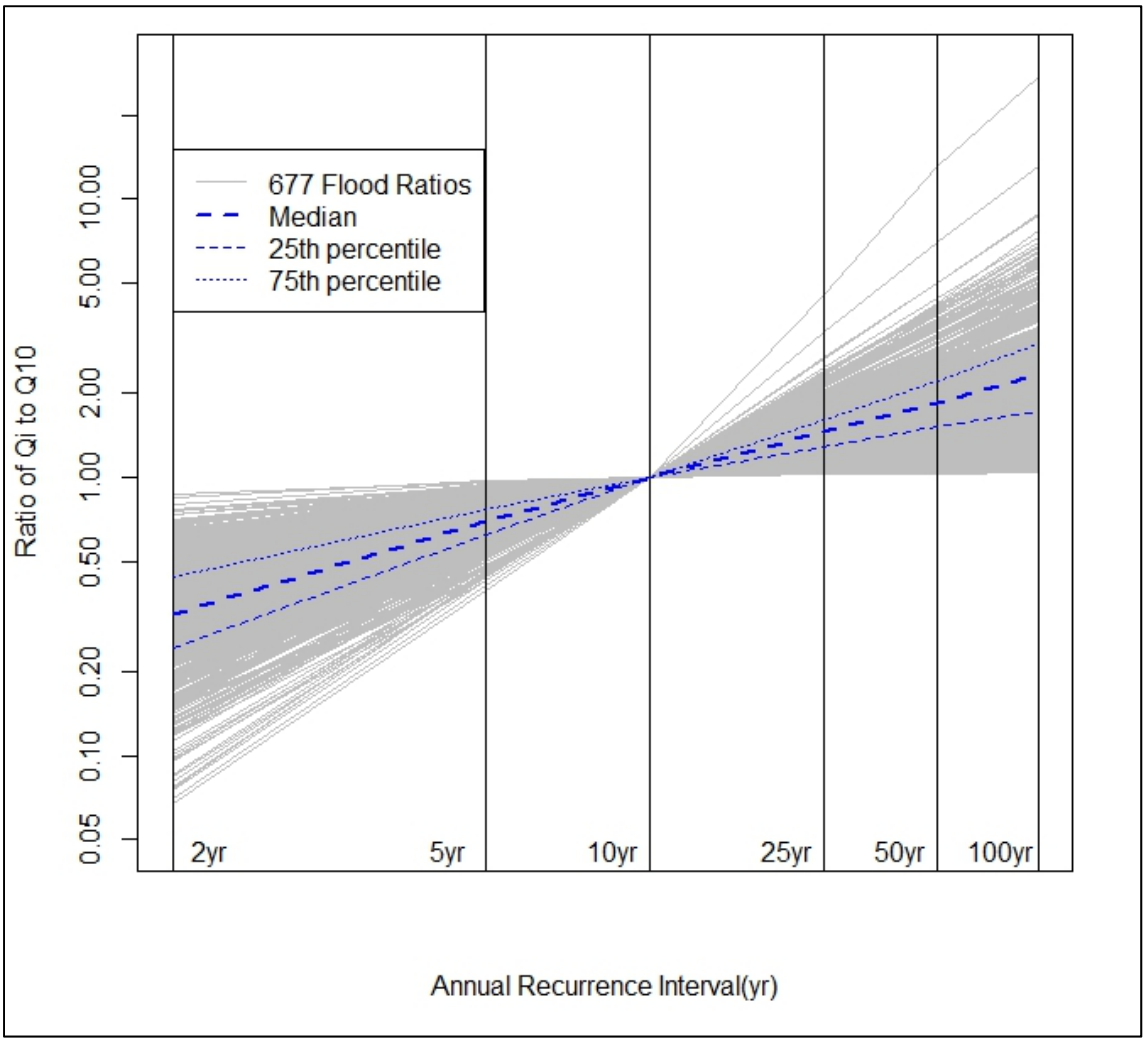

Figure 6.9. Flood ratios for 677 Texas watersheds using the 0.1 AEP (10-year) flood discharge as the index flood. Ratios are plotted with the median, 25th, and 75th percentile values.

The choice of the 10-year return period flood as the index flood stems from discussions in Asquith and Roussel (2009) showing that statistics representing uncertainty in the prediction of regression equations (in this case the PRESS and AIC statistics) minimize at the 10-year prediction. This minimization is consistent with observations of confidence limits computed for gauge data, which often minimize in "width" at the 10-year level. Overall, both formal analysis

and experience indicate that the ability to estimate the discharge/probability relationship optimizes at or near the AEP of 0.1, likely because of information balance as discussed previously. The use of flood ratios preserves the continuity of individual flood frequency curves in the form of shape. This allows a comparison of shape among curves of different magnitudes and from different watersheds.

6.3.1.2. Comparison of Flood Ratios and Rainfall Ratios

Rainfall ratios may also be computed to compare shapes of rainfall frequency curves and to demonstrate that rainfall frequency curves have different shapes than FFCs and cannot be used to estimate FFCs directly. To illustrate this, depth-duration-frequency values for five counties in Texas were obtained and tabulated for AEP values of 0.5, 0.2, 0.1, 0.04, 0.02, and 0.01, and for durations of 0.25, 0.5, 1, 2, 3, 6, 12, and 24 hours. The five counties (McCulloch, El Paso, Jasper, Hidalgo, and Lipscomb) are located at the center and the extremities of the state as shown in Figure 6.10. Five counties at the extremes and the center of the state were selected for comparison of rainfall ratios with flood ratios to provide geographical and climatic variation in rainfall that is comparable to the variation in flood ratios shown in Figure 6.9. Precipitation metrics generally decrease from east-southeast to west-northwest, with some topographical influence from sharp elevation changes (the Balcones Escarpment.)

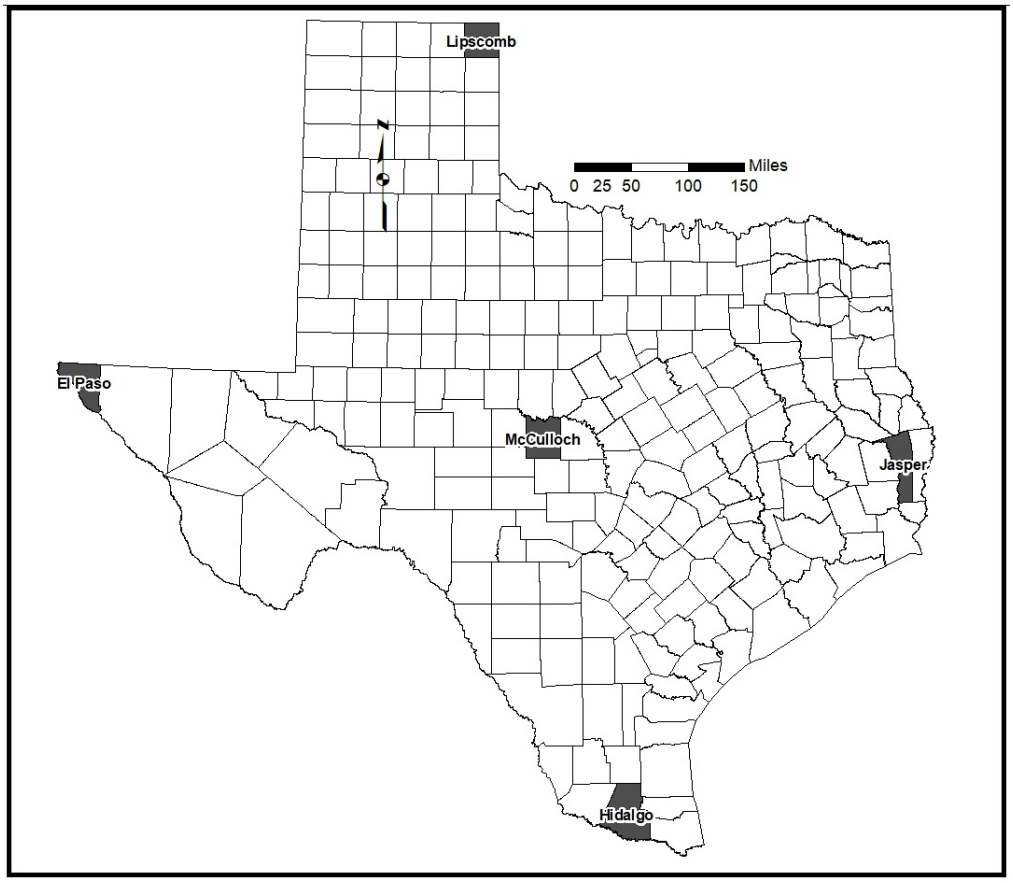

Figure 6.10. Five counties in Texas selected for DDF analyses.

Depth, duration, and frequency values of rainfall for these five counties are tabulated in Table 6.4. Dividing by the 10-year return period depth results in rainfall ratios for each curve, mimicking the derivation of flood ratios. The ratios of each depth value to the value for the 10-year return period (AEP=0.1) are shown in Table 6.5. Computation of these ratios allows direct comparison of rainfall frequency curves at all five locations for the eight durations. The minimum rainfall ratio for the 100-year return period is 1.38 in Hidalgo County for the 0.25-hour duration, while the maximum is 1.85 in Lipscomb County for the same 0.25-hour duration.

To visually compare these representative rainfall ratios with the FFCs, the rainfall ratios are plotted in Figure 6.11 with the median, 25-percent, and 75-percent values of flood ratios. The largest rainfall ratios are very near the 25-percent flood ratio line. The influence on runoff rate exerted by watershed processes converting rainfall into runoff is not proportional to rainfall.

An example is the influence of the "initial abstraction," a quantity of rainfall that is presumed to fall on the watershed that wets exposed surfaces, satisfies initially high soil uptake rates, and fills small depressions in the landscape before runoff can begin. If a rainfall event does not exceed the initial abstraction, no runoff occurs at all. However, if rainfall drastically exceeds the initial abstraction depth, the effect of the initial abstraction may be small. Particularly in arid areas where initial abstractions are large and typical rainfall event depths are small, the initial abstraction alone can result in a substantial alteration of flood ratios as compared to rainfall ratios (Herrmann and Cleveland 2009).

Thus, while rainfall ratios are derived from statistical analysis of the entire population of recorded rainfall events, flood ratios (in the simplest view) are derived from analysis of a subset of rainfall events that are censored by watershed processes involved in converting rainfall into runoff (loss processes.)

The fundamental assumptions underlying the use of an index flood and flood ratios are that the basic shape of FFCs is encapsulated in the flood ratios and factors that affect the magnitude of the index flood exhibit a proportional effect across the entire curve without significant alteration of shape. The same ideas are implicit in all methods of hydrologic flood frequency estimation, whether it is gauge analysis, regression equations, or watershed modeling. Discharge is expected to monotonically increase with diminishing probability of exceedance in a smooth and continuous manner. Flood ratios provide a way to compare *relative* growth of discharge with return period among curves.

The fundamental attractiveness of the use of an index flood and flood ratios evaluation of the effects of climate change on design flood estimates is that deriving an estimated FFC for changing conditions is reduced to estimating changes only to the index flood, relying on the flood ratios to expand the estimate across the entire curve, assuming those ratios are stationary over time.

Table 6.4. Depths of rainfall for various durations and return periods for five Texas counties.

County	Duration (hr)	Depth (in)					
		AEP=0.5	AEP=0.2	AEP=0.1	AEP=0.04	AEP=0.02	AEP=0.01
McCulloch	0.25	0.85	1.1	1.3	1.5	1.7	1.85
	0.5	1.15	1.5	1.75	2.05	2.3	2.6
	1	1.4	1.9	2.3	2.65	3.1	3.4
	2	1.7	2.3	2.8	3.5	4.1	4.8
	3	1.8	2.5	3.1	3.8	4.4	5.25
	6	2	2.8	3.5	4.5	5.35	6.1
	12	2.3	3.25	4.15	5.5	6.25	7.1
	24	2.6	3.75	4.7	6.25	7.2	7.9
Jasper	0.25	1.05	1.35	1.5	1.8	1.95	2.2
	0.5	1.5	1.9	2.1	2.5	2.8	3.1
	1	1.9	2.5	2.8	3.3	3.8	4.2
	2	2.5	3.4	3.8	4.7	5.5	6.3
	3	2.8	3.6	4.3	5.3	6	7.2
	6	3.2	4.3	5	6	7.2	8.5
	12	3.8	5.15	6.2	7.3	8.5	10.2
	24	4.2	6	7.5	9	10.5	12.5
El Paso	0.25	0.65	0.9	1.1	1.25	1.4	1.6
	0.5	0.8	1.1	1.3	1.5	1.7	1.95
	1	0.85	1.2	1.6	2	2.2	2.5
	2	0.92	1.25	1.75	2.15	2.4	2.75
	3	1	1.3	1.8	2.25	2.5	2.9
	6	1.1	1.4	1.95	2.4	2.7	3.2
	12	1.2	1.6	2.15	2.6	3	3.5
	24	1.4	2	2.5	3	3.5	4
Hidalgo	0.25	1.05	1.35	1.6	1.8	2.1	2.2
	0.5	1.5	1.9	2.2	2.6	2.9	3.2
	1	1.9	2.5	2.9	3.5	4	4.6
	2	2.4	3.2	3.6	4.4	5.2	5.8
	3	2.8	3.45	4	4.8	5.8	6.4
	6	3	4	4.8	6	7	8
	12	3.2	4.4	5.5	7	8.2	9
	24	3.8	5	6.5	8	9	10
Lipscomb	0.25	0.8	1.1	1.3	1.7	2	2.4
	0.5	1.05	1.4	1.6	2	2.4	2.8
	1	1.25	1.8	2.2	2.7	3.2	3.8
	2	1.45	2	2.5	3.2	3.8	4.4
	3	1.6	2.2	2.7	3.4	4	4.75
	6	1.8	2.6	3.2	3.8	4.5	5.5
	12	2.1	2.9	3.6	4.35	5	6
	24	2.4	3.25	4.2	5	5.6	6.5

Table 6.5. Depth Ratios to 10-year for various durations and return periods for Texas.

County	Duration (hr)	Depth (in)					
		AEP=0.5	AEP=0.2	AEP=0.1	AEP=0.04	AEP=0.02	AEP=0.01
McCulloch	0.25	0.65	0.85	1.00	1.15	1.31	1.42
	0.5	0.66	0.86	1.00	1.17	1.31	1.49
	1	0.61	0.83	1.00	1.15	1.35	1.48
	2	0.61	0.82	1.00	1.25	1.46	1.71
	3	0.58	0.81	1.00	1.23	1.42	1.69
	6	0.57	0.80	1.00	1.29	1.53	1.74
	12	0.55	0.78	1.00	1.33	1.51	1.71
	24	0.55	0.80	1.00	1.33	1.53	1.68
Jasper	0.25	0.70	0.90	1.00	1.20	1.30	1.47
	0.5	0.71	0.90	1.00	1.19	1.33	1.48
	1	0.68	0.89	1.00	1.18	1.36	1.50
	2	0.66	0.89	1.00	1.24	1.45	1.66
	3	0.65	0.84	1.00	1.23	1.40	1.67
	6	0.64	0.86	1.00	1.20	1.44	1.70
	12	0.61	0.83	1.00	1.18	1.37	1.65
	24	0.56	0.80	1.00	1.20	1.40	1.67
El Paso	0.25	0.59	0.82	1.00	1.14	1.27	1.45
	0.5	0.62	0.85	1.00	1.15	1.31	1.50
	1	0.53	0.75	1.00	1.25	1.38	1.56
	2	0.53	0.71	1.00	1.23	1.37	1.57
	3	0.56	0.72	1.00	1.25	1.39	1.61
	6	0.56	0.72	1.00	1.23	1.38	1.64
	12	0.56	0.74	1.00	1.21	1.40	1.63
	24	0.56	0.80	1.00	1.20	1.40	1.60
Hidalgo	0.25	0.66	0.84	1.00	1.13	1.31	1.38
	0.5	0.68	0.86	1.00	1.18	1.32	1.45
	1	0.66	0.86	1.00	1.21	1.38	1.59
	2	0.67	0.89	1.00	1.22	1.44	1.61
	3	0.70	0.86	1.00	1.20	1.45	1.60
	6	0.63	0.83	1.00	1.25	1.46	1.67
	12	0.58	0.80	1.00	1.27	1.49	1.64
	24	0.58	0.77	1.00	1.23	1.38	1.54
Lipscomb	0.25	0.62	0.85	1.00	1.31	1.54	1.85
	0.5	0.66	0.88	1.00	1.25	1.50	1.75
	1	0.57	0.82	1.00	1.23	1.45	1.73
	2	0.58	0.80	1.00	1.28	1.52	1.76
	3	0.59	0.81	1.00	1.26	1.48	1.76
	6	0.56	0.81	1.00	1.19	1.41	1.72
	12	0.58	0.81	1.00	1.21	1.39	1.67
	24	0.57	0.77	1.00	1.19	1.33	1.55

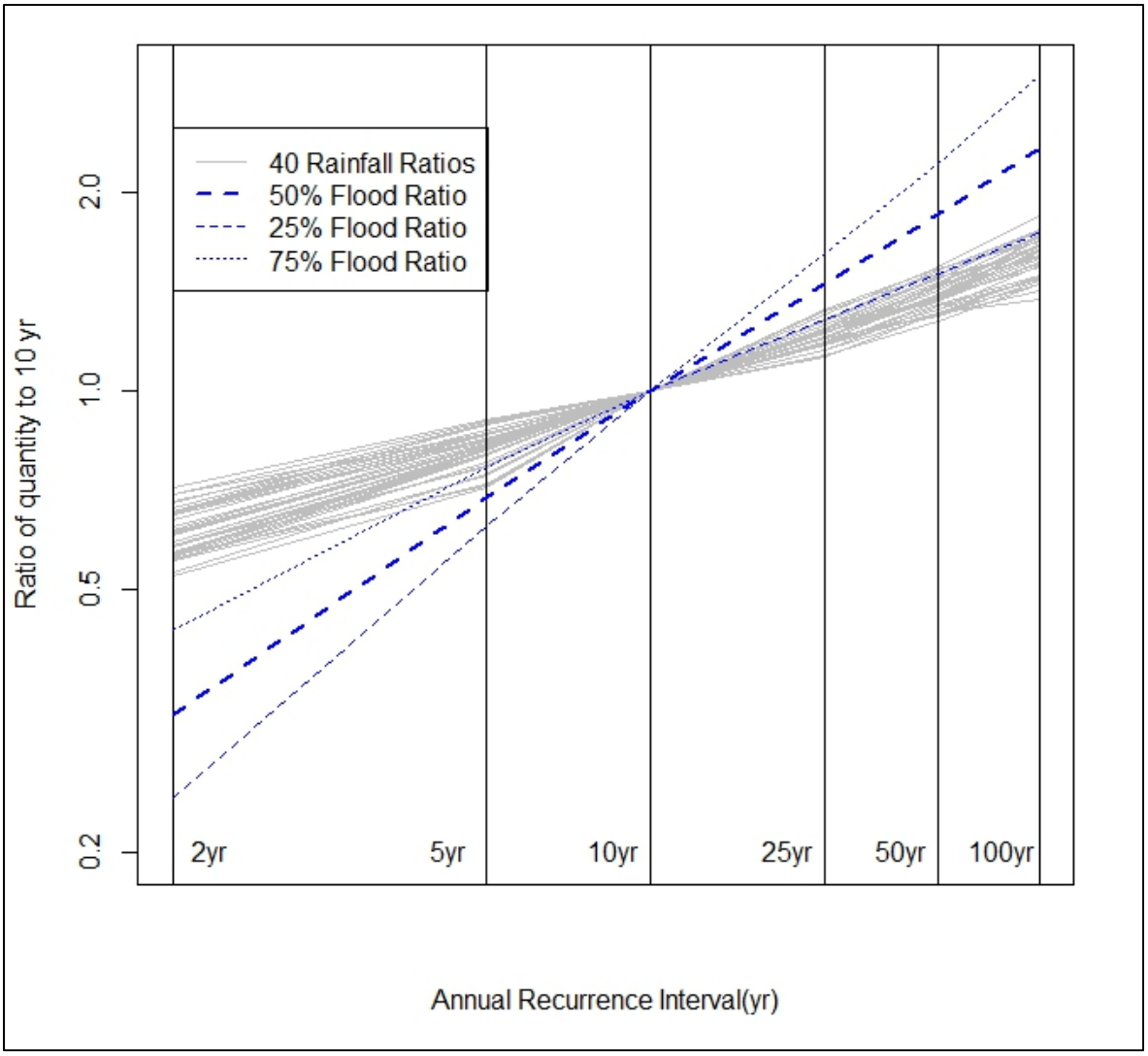

Figure 6.11. Comparison of the middle 50 percent of flood ratios to rainfall ratios for 40 rainfall ratio curves for Texas.

6.3.2. Application of the Index Flood Method for Climate Change

The Index Flood Method offers an analytical framework to estimate design discharges for projected climate change using a variety of tools within that framework. The appropriate tools will depend on the characteristics of the watershed, available data, and the judgment of the design team. The overall framework is described in the following three steps:

1. Compute historical quantiles and flood ratios based on the 10-year index flood using either:
    a. An appropriate gauge record.
    b. Applicable regression equations.
    c. Flood ratios transposed from one or more nearby, similar watersheds.

2. Estimate the baseline and future conditions 10-year flood for the watershed of interest using either:
    a. A rainfall/runoff model.
    b. Regression equations (if they consider climatic variables).
    c. Identifiable trends in FFCs.
3. Estimate the required design quantiles from the future conditions 10-year flood and the flood ratios.

6.3.2.1. Computing Flood Ratios Based on the 10-year Index Flood

The selection of the 10-year flood as the index flood in Step 1 is based on statistical evidence that the prediction error in the 10-year return period discharge is minimized. Using the concept of the 10-year index flood and flood ratios to capture and preserve the shape of the FFC, adjusting an FFC for changing rainfall expectation (or any other phenomenon expected to alter the curve) simplifies to adjusting only the 10-year value, then applying the flood ratios. However, it is critical to define criteria for which index flood and ratios can appropriately be applied to any given ungauged watershed of interest.

In addition, as has been discussed in Chapter 4, the ability of downscaled GCM outputs to generate extreme statistics (e.g., AEPs of 0.04, 0.02, and 0.01) for existing or projected conditions is limited. Focusing on a less extreme index such as the 0.1 AEP event is more likely to yield representative results. The flood ratios, rather than the downscaled GCM outputs are used to compute more extreme floods.

Flood ratios are computed for existing conditions. The preferred approach is to establish the flood ratios based on an appropriate stream gauge record that is representative of the watershed of interest for design, although any method of developing an FFC that has traditionally been deemed satisfactory for design discharge estimation can be used. The considerations for selecting such a stream gauge were previously discussed. Several stream gauges may be evaluated and compared. Judgment about weighted averaging or selection of a single curve should be exercised to preserve important aspects of the shape.

If data from an appropriate stream gauge (or stream gauges) are not available, then the applicable regression equations for the area may be used to establish the flood ratios based on existing conditions. Since this step applies to existing conditions, the applicable regression equations do not need to include climatic parameters among the predictor variables. As described previously, regression equations do not necessarily preserve the FFC shape, which is why this option is recommended only if appropriate gauges are not available.

Flood ratios computed from stream gauges on nearby, similar watersheds may be evaluated for use as an alternative to those developed from regression equations. Comparison among regression equation results and ratios from several appropriate gauge analyses may yield insight into local or regional tendencies in the shape of FFCs for similar watersheds. The result might be the selection of a surrogate FFC to provide ratios, or an average among a number of FFCs might be considered representative. Flood ratios from regression equation-derived discharges tend to be similar to a regional average value; comparison of them to average flood ratios from several

nearby, similar watersheds should provide information on the influence of various characteristics on the shape of the FFC.

6.3.2.2. Baseline and Future Conditions for the Index (10-year) Flood

For Step 2 of the basic procedure, a baseline and future conditions Index Flood is calculated using the same methodology and a ratio of future to baseline conditions is estimated. The design team should evaluate and select the most appropriate method, regardless of the AEP required. If the method used to develop the historical FFC in Step 1 is adaptable to future conditions, that method may also be used in this step. Chapter 5 and earlier sections in this chapter discuss options for estimating design discharges under future conditions.

A common approach is likely to be a calibrated rainfall/runoff model. The engineer first calibrates the rainfall/runoff model to baseline (historical) conditions and estimates a 10-year design flow based on those conditions. Then, using the guidance in Chapter 5, the engineer determines the appropriate precipitation inputs to the rainfall/runoff model for estimating a 10-year design flow for future conditions. An ensemble of projected precipitation values should be used to provide greater insight into the uncertainty regarding the 10-year flood estimate (e.g., Anderson *et al.* 2015).

In some cases, regional regression equations may be available that include precipitation, or another climatic parameter, as a predictor variable. If available, these equations may provide a method for estimating a future 10-year flood discharge as described in Section 6.2.1. The 10-year flood for existing conditions would also be calculated using the applicable regression equation.

6.3.2.3. Future Conditions AEP Design Discharge

With the flood ratios and historical 0.1 AEP discharge from Step 1 and the ratio of projected (future) conditions to baseline conditions from Step 2, any single design quantile or the complete FFC curve may be estimated by the following equation:

$$Q_{q,p} = Q_{0.1,h}(R_q)(RPB_{0.1}) \tag{6.11}$$

where:

$Q_{q,p}$ = *Projected discharge for quantile, q.*

$Q_{0.1,h}$ = *Historical discharge for the 0.1 AEP quantile (from Step 1).*

R_q = *Flood ratio for the AEP quantile q (from Step 1).*

$RFB_{0.1}$ = *Ratio of the future to baseline 0.1 AEP discharge (from Step 2).*

For example, if a 0.01 AEP design discharge is desired, q is set to 0.01. The primary advantage of using the flood index framework for estimating design discharges is that it does not rely on the ability of a downscaled GCM output to reasonably produce extreme projected climate variables while preserving the historical relationship of the FFC at a site. The disadvantage is that the method assumes that climate change does not alter the historic shape of the FFC. Use of the 10-year event as the index flood mitigates this concern by using a relatively extreme event as the basis for the computed flood ratios.

BOTTOM LINE: Estimating extreme discharge quantiles such as the 100-year flood flow under conditions where climate may be changing is limited because climate modeling temporal and spatial scales, while improving, result in averaging that can reduce extremes. Therefore, estimating a less extreme discharge quantile such as the 10-year flood flow and scaling that up has the potential for providing a better estimate for design.

6.3.3. Estimation of Uncertainty

The use of both gauge analysis and regression equations imply a degree of uncertainty in estimates. Transposing analyses from one watershed to another can only be expected to increase the degree of uncertainty to an unknown degree, a subject for future research.

Adjustment of the magnitude of the index flood for anticipated future conditions can also be expected to increase the level of uncertainty of the resulting curve as some combination of the uncertainty of the original curve and the uncertainty involved in the prediction of future conditions; however, that same increase can be implied for any method used to adjust to accommodate predicted conditions. Total uncertainty in projections of the future is a function of the uncertainty in historical analysis and uncertainty of the projected change.

The principle of parsimony implies that minimizing the number of calculations that directly involve prediction of future conditions should minimize the growth of uncertainty attributable to the prediction process. Within the index flood method framework, direct adjustment of discharge values is only performed on the index flood; discharges at the other quantile values are calculated from flood ratios and preserve the historically derived shape of the FFC.

Chapter 7. Adaptation of Projected Precipitation Time Series for Continuous Simulation

This chapter addresses how to develop time series data for future scenarios that can be used for continuous simulation modeling to support stormwater management and water quality infrastructure. Though stormwater management and water quality facilities are frequently designed based on design storms, stormwater management and water quality analyses sometimes require a continuous simulation model. Depending on applicable design standards and/or requirements, hydrologic design applications may also require low-flow statistics, flood-volume statistics, or flow-duration curves. All of these applications require daily time series data.

Low-flow statistics, such as the 7Q10 (a 7-day average low flow with a 0.10 annual non-exceedance probability), are generated based on an analysis of daily streamflow. Likewise, flood-volume statistics, such as the 30-day average flood flow with a 0.01 annual exceedance probability, are generated based on an analysis of daily streamflow. In some areas of the country, the USGS and others have developed regression equations to estimate these statistics for ungauged watersheds. Future low-flow and flood-volume statistics can also be estimated by inputting climate projections into continuous simulation hydrologic models.

Flow-duration or precipitation-duration curves are developed based on daily streamflow or precipitation data, respectively. Engineers use these curves when design criteria require water quality treatment for a particular percentile rainfall, for example. Flow duration curves can be developed using continuous simulation hydrologic models driven with future climate projections.

Many researchers have assessed the hydrological consequences of climate change using a variety of continuous simulation models (Kour et al. 2016). These include studies by Xu et al. (2014), Masood et al. (2014), Piniewski et al. (2013), Maurer et al. (2009), and Shrestha (2014).

For continuous simulation modeling, a continuous series of precipitation, and often temperature, at hourly or daily durations is a required input. This chapter provides an overview of, and guidance for, using continuous simulation for assessing the effects of climate change on stormwater management and water quality analyses.

7.1. Modeling Framework

Application of continuous simulation modeling for assessing the effects of climate change requires the appropriate tools, selection of the appropriate level of analysis, and a structured modeling approach. The following sections discuss each of these.

7.1.1. Available Modeling Tools

The potential effects of climate change on hydrology and water quality can be evaluated using any hydrologic or water quality modeling tool, such as Hydrological Simulation Program–FORTRAN (HSPF), Soil Water and Analysis Tools (SWAT), or the Storm Water Management Model (SWMM). Future conditions representing precipitation, temperature, wind speed, etc. are derived from a downscaled GCM output (using a range of scenarios and models as described in Chapter 4). The resulting scenarios are then provided as inputs to the appropriate modeling tool.

In some cases, the hydrologic and water quality modeling tools provide pre-processors that support development of future scenarios, such as the BASINS Climate Assessment Tool (CAT) or SWMM-CAT. As an example, BASINS CAT provides the capability to incorporate potential climatic data input changes into different watershed models in BASINS (HSPF, SWAT, and SWMM are currently available) through adjustments to historical datasets.

While there are many similarities, the climatic input requirements for continuous simulation models differ among models. For example, HSPF requires hourly precipitation and temperature, while SWAT requires only daily precipitation and minimum/maximum air temperatures. Therefore, one of the primary differences for using these models for future climate studies is obtaining future climatic variables at the appropriate spatial and temporal scales.

Of the continuous simulation models, state Departments of Transportation most frequently use SWMM; therefore, this discussion focuses on the SWMM model. However, much of the guidance and discussion is also relevant to similar models, such as HSPF and SWAT, which are described in Appendix C. The appendix provides a discussion of the application of HSPF and SWAT for future climate studies, as well as descriptions of the BASINS CAT and EPA's National Stormwater Calculator Tool.

Engineers can apply the SWMM model to a range of watershed sizes to support hydraulic structure and water quality design. Other modeling tools have been developed for nationwide assessments of the effects of climate change on water resources. Though the time and spatial scales of these tools are not generally appropriate for design, a description of one such model, the Variable Infiltration Capacity (VIC) model, is provided in Section 7.5.2.

7.1.1.1. SWMM and SWMM-CAT

SWMM simulates the water quality and quantity of urban stormwater runoff and combined sewer overflows (Rossman 2016). It is used to analyze single events or for a long-term (continuous) simulation of runoff quantity and quality from primarily urban areas. SWMM is used throughout the world for planning, analysis, and design related to stormwater runoff, combined and sanitary sewer analysis, and other drainage systems in urban areas. There are also many applications for drainage systems in non-urban areas.

Engineers can evaluate climate scenarios by generating a time series of climate inputs that represent a range of possible futures and comparing the results with existing conditions. The future time series for each scenario can be custom developed or adjusted from existing conditions using the SWMM-CAT pre-processor that the EPA developed in 2014.

SWMM-CAT provides a set of location-specific adjustments to historical precipitation and temperature data that can be used to represent future scenarios. These adjustments are derived from CMIP3 global climate model simulations (see Chapter 4) and are stored in EPA's Climate Resilience Evaluation and Analysis Tool (CREAT) database (see Section 7.5.2). CREAT (version 3) includes projections from CMIP5. EPA might update SWMM-CAT to use CREAT 3.0. Also, the EPA recently updated SWMM to accept user-supplied monthly adjustment factors for time series that could be used to represent future climate scenarios. The adjustment factors modify input time series corresponding to precipitation, evaporation, and air temperature.

The adjustments, referred to as ***change factors***, are retrieved from the CREAT database corresponding to the station closest to the study area. Adjustments are made to temperature and

evaporation on a monthly basis as additive (delta) changes, while rainfall values are adjusted using a multiplier. (The climate science community applies the word "delta" for both additive and multiplicative change factors (CFs). Here, "delta" applies to additive changes only.) The engineer chooses the adjustments from any of the three CREAT scenarios (Hot/Dry, Median, and Warm/Wet) for the near term (2035) or the far term (2060) (see Section 7.5.2). SWMM-CAT also provides an option to adjust the 24-hour design storms for any scenario/time period (near/far term) combination when SWMM is used for design storm analyses.

7.1.1.2. Variable Infiltration Capacity Model

The VIC model is a large (macro-) scale, semi-distributed hydrologic model that solves full water and energy balance equations (Liang et al. 1994). VIC represents the land surface as a uniform grid with a user-defined cell size. The cell sizes are typically set within the range of 1/16th to 1/4th degree for large-scale studies. Land cover and elevation within individual cells can be proportioned within different land cover and elevation bands (e.g., 60 percent agricultural land, 40 percent forest). Each grid cell can have a lake/wetland system contained within one of its land cover tiles. The lake/wetland model (Bowling and Lettenmaier 2010) handles the impoundment of surface water within a grid cell. Gao et al. (2010) provides an example application of the lake model.

The model uses daily or sub-daily time series of meteorological data including precipitation, air temperature, and wind speed as input to simulate a full set of hydrological variables for each grid cell. Hydrologic variables for each grid cell are simulated first and any fluxes between grid cells are calculated before moving on to the next time step. VIC routes streamflow using a routing model developed by Lohmann et al. (1996 and 1998). Each grid cell is represented as a node in the channel network. The flow from each grid cell enters the channel network and is routed through it using the linearized St. Venant equations. Figure 7.1 shows a schematic representation of land surfaces and functionality within the VIC model. VIC can represent multiple soil layers, but three layers are typically used as depicted in the figure.

One of the uses for VIC has been to evaluate the effects of climate change on regional hydrology over areas typically covering multiple 8-digit HUCs. For example, Hayhoe et al. (2007) used VIC to estimate past and future changes in hydrologic indicators, including the timing of spring peak discharge and the 7-day low flow values in the Northeast United States. Yan et al. (2015) applied the VIC model to assess the effects of climate change on seasonal discharge and extreme flows within the Pearl River Basins in China using a range of future climate scenarios. Oubeidillah et al. (2014) used the VIC model to study the effects of climate change hydrology for the conterminous United States.

Because VIC is generally applied on a large geographic scale and at relatively coarse resolutions, VIC has not been used for the hydrologic design of transportation assets. For these reasons, it is unlikely that hydrologic design engineers will begin to use VIC for specific project needs in the near term, though this may change as the resolutions improve and the VIC model becomes more broadly accessible. However, existing datasets of projected flows generated by VIC in a watershed of interest may provide insight into possible future changes in discharges affecting a specific project.

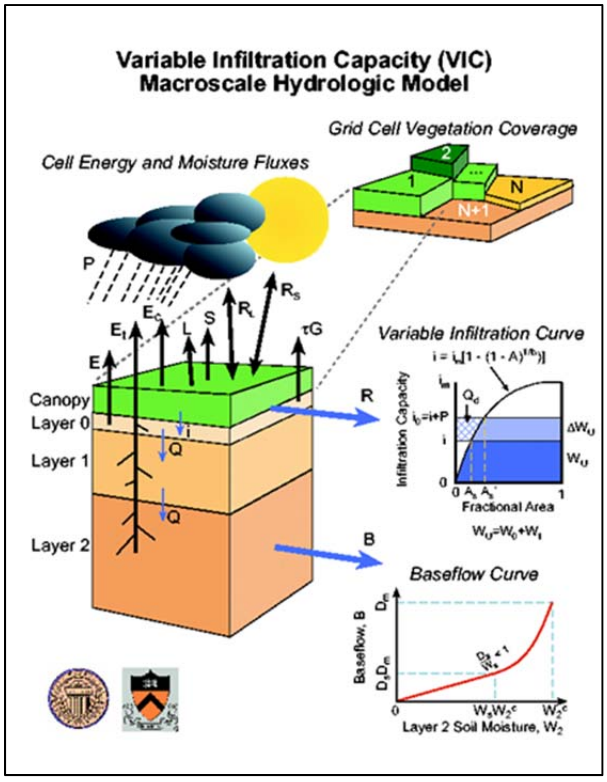

Figure 7.1. Schematic representation of VIC model components (University of Washington 2017).

7.1.2. Levels of Analysis

As summarized in Chapter 3, a Level 1 analysis represents the application of standard hydrologic design techniques for estimating a design discharge based on historical climate and watershed data. It includes a qualitative assessment of future conditions and a determination of the significance of those conditions for the plan or project. Hence, a Level 1 analysis using a continuous model will use historical climate data only.

For a Level 2 analysis, the design team explicitly identifies an appropriate range of historical conditions. The continuous simulation of a hydrologic/water quality model uses historical data that ranges over various flow regimes and considers various climatic conditions (both wet and dry). The output from such a model run can be used to obtain the required confidence limits. The design team will need to consider the uncertainty in model input parameters. For example, SWMM model input parameters such as sub-basin width, connected impervious percentage, impervious depression storage coefficient, watershed slope, groundwater flow coefficient, initial upper zone moisture, and Manning's roughness coefficient are considered during a hydrology calibration. When performing a Level 2 analysis, a probability distribution can be selected for these parameters.

If the design team determines that Level 3 or 4 analyses are needed, then the continuous simulation model runs need to incorporate quantitative future climate projections, particularly precipitation. A generalized modeling framework is discussed in the following section.

7.1.3. Generalized Modeling Approach for Climate Change

The general approach for incorporating downscaled GCM precipitation outputs into watershed models is depicted in Figure 7.2 using SWMM as an illustration. The basic steps for deriving and using CFs in SWMM are as follows (using precipitation as an example):

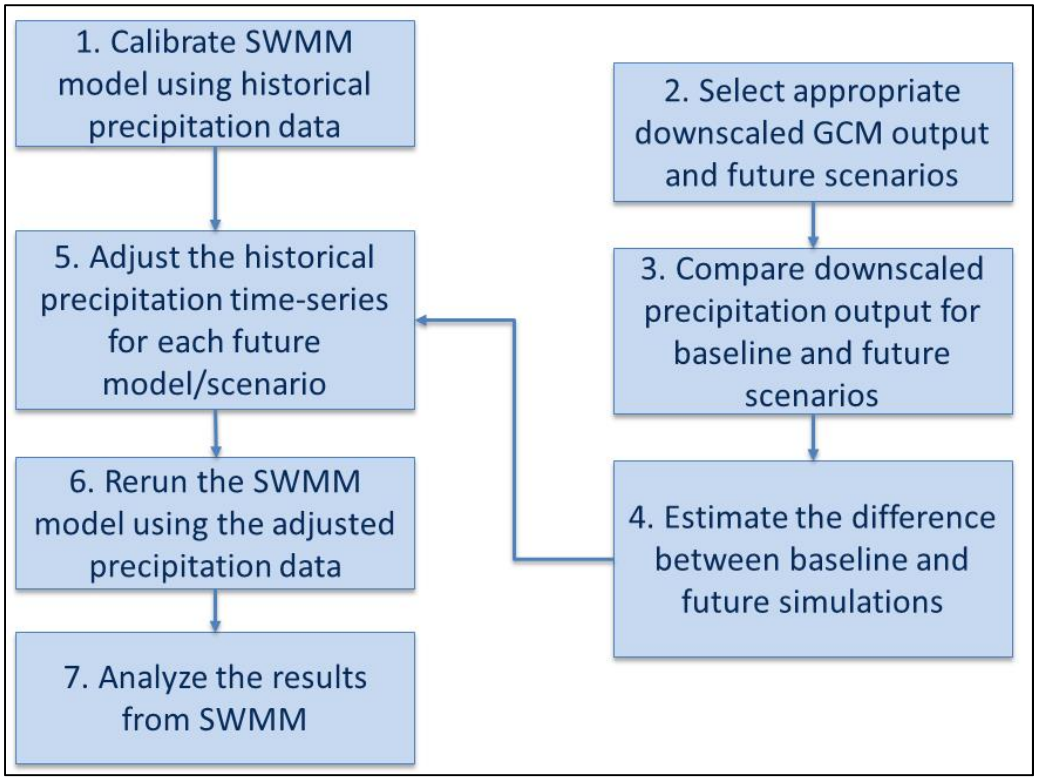

Figure 7.2. Flow chart showing the general approach for incorporating Downscaled GCM precipitation data into continuous simulation.

1. Calibrate and run the SWMM model using historical precipitation data.
2. Obtain downscaled GCM outputs for both baseline (historical) conditions and future scenarios. (Chapter 4 describes appropriate data sources.)
3. Calculate the appropriate precipitation depth statistics for both the baseline conditions and future scenarios for the type of CFs that are desired. The temporal domain for both baseline and future periods should be no less than 30 years.
4. Compute the multiplicative change factor based on the downscaled GCM future precipitation compared to the baseline scenario:

$$CF_{mul} = \left(\frac{\bar{P}_{GCM,future}}{\bar{P}_{GCM,\text{baseline}}} \right)$$

5. Adjust the historical observed precipitation time series used in the SWMM model to evaluate existing conditions with the multiplicative CF:

$$P_{i,future} = P_{i,observed} \times CF_{mul}$$

6. Rerun the SWMM model using the adjusted precipitation data.
7. Evaluate the differences between historical and projected SWMM results to develop a robust stormwater management/water quality design.

With respect to Step 1, it is important to evaluate sensitivity to temporal aggregation. For example, if SWMM is calibrated with sub-hourly data, aggregate the data to hourly then daily to determine any simulation error that could result from limitations imposed by climate projection data that lacks sub-daily data.

7.2. Change Factor Methodology

The change factor methodology (CFM) is one approach for incorporating projected future climate conditions into continuous simulation models. The CFM (available in SWMM-CAT) involves adjusting an observed climate data time series by adding a difference (additive) or by multiplying by a factor (multiplicative) based on future projections. Change factor approaches have been widely applied in climate impact studies, typically using changes to monthly mean or seasonal precipitation totals to develop change scenarios (Anandhi et al. 2011, Prudhomme et al. 2010, Kay and Jones 2012). Recent experimentation has included sub-daily change factors in SWMM (Cook et al. 2017).

Change factors (CFs) may be categorized by how they address temporal scale and domain, their mathematical formulation, or the number of change factors (Anandhi et al. 2011). Temporal scale refers to the disaggregation of time (e.g., daily, monthly, seasonal, and annual) used to compute CFs. Temporal domain refers to both the time of year (e.g., monthly, seasonal, or annual) and the beginning and ending dates of the historical observed, historical modeled, and future modeled values to be included in the analysis (e.g., 1981–2000 compared to 2046–2065). CFs may also be categorized by their mathematical formulation, that is, whether the CF is added to or multiplied by the base information. Finally, CFs are categorized based on the number of CFs used in an analysis. For example, a single CF for precipitation could be used or multiple CFs representing different months could be applied.

7.2.1. Additive and Multiplicative Change Factors.

Additive and multiplicative CFs are conceptually straight-forward and are based on comparing projected and historical downscaled GCM output and applying the computed CF to historical data to estimate projected future conditions. An additive CF for a given temporal scale and domain at a given location is computed as follows:

$$CF_{add} = (\overline{CV}_{GCM,f} - \overline{CV}_{GCM,h}) \quad (7.1)$$

where:

CF_{add} = *Additive change factor for climate variable CV.*

$\overline{CV}_{GCM,h}$ = *Average of the downscaled GCM climate variables over the historical time domain.*

$\overline{CV}_{GCM,f}$ = *Average of the downscaled GCM climate variables over the future time domain.*

The CF is added to each observed data value over the historical time domain to obtain a time series of estimated future values for that climate variable as follows:

$$CV_{i,future} = CV_{i,observed} + CF_{add} \quad (7.2)$$

where:

$CV_{i,observed}$ = *The i^{th} value of the observed climate variable time series.*

$CV_{i,future}$ = *The i^{th} value of the future climate variable time series.*

Multiplicative CFs are analogous to additive CFs except that the ratio, rather than arithmetic difference, is required and computed as follows:

$$CF_{mul} = \left(\frac{\overline{CV}_{GCM,future}}{\overline{CV}_{GCM,historical}}\right) \quad (7.3)$$

where:

CF_{mul} = *Multiplicative change factor for climate variable CV.*

To compute the future time series, the observed values are multiplied by the CF as follows:

$$CV_{i,future} = CV_{i,observed} \times CF_{mul} \quad (7.4)$$

Typically, an additive CF is used for temperature and a multiplicative CF is used for precipitation. The additive CF assumes that, regardless of limitations in the future climate projections, the differences between the future and historical information are reasonable estimates of change. Similarly, the multiplicative CF assumes that the percentage change is reasonable.

7.2.2. Single and Multiple Change Factors

In many situations, when not only the mean, but also the shape of the distribution of daily or hourly precipitation is altered by a changing climate, a single CF will not adequately represent the change over the full range of values. For example, a multiplicative CF between may decrease with increasing precipitation magnitude. In such cases, multiple or continuous change factors should be considered. Multiple CFs are calculated separately for different magnitudes of a variable of interest. For example, one can empirically calculate separate CFs for different percentile ranges such as 0–10, 10–20, and so on, for any given meteorological parameter.

The first step to calculate multiple CFs is to estimate the empirical cumulative distribution function for the historical and future time series. Second, percentile values are selected and the CF for each percentile range is calculated. When applying CFs to the historical observed data, the same percentiles are used to group the observed data so that the appropriate CF is applied.

It is also possible to calculate continuous parametric CFs. Here, the first step is to fit a continuous function (using linear regression, piece-wise linear regression, or a polynomial fit) to the quantile-quantile plot of the observed versus modeled variable. Second, the CF for any given quantile or percentile can then be derived from the resulting function. In this way, no grouping is needed and "jumps" in CFs between quantile groups are avoided.

Finally, if there is a specific threshold of interest, multiple CFs can be applied using any threshold of percentiles appropriate for a given project. For example, calculating a CF above the 70th percentile, another CF for values below the 30th percentile, and a third CF for values between the 30th and 70th percentiles may be an appropriate strategy.

BOTTOM LINE: Change factors provide a simple way to adjust historical continuous simulation precipitation and temperature times series (at a variety of temporal resolutions) to assess the effects of future climate scenarios.

7.2.3. Customized Change Factors

CFs can be customized on a seasonal, monthly, weekly, or daily basis by developing specific time-based, threshold-based, and/or quantile-based analyses. The goal is to identify and resolve the data in a way that is most relevant to the analysis or that resolves changes across the distribution, by quantile (Cook et al. 2017). Individual or customized CFs can then be applied based on both months and threshold values in the data.

While customized, quantile-specific CFs can be developed using annual data; a monthly or seasonal approach is recommended because of physical differences in the weather patterns that bring precipitation in different seasons (e.g., large-scale winter low pressure systems versus convective precipitation from summer thunderstorms). GCMs differ in their ability to simulate those patterns, and the effect of climate change on those systems differs as well. Both of these factors imply that CFs for the identical threshold may differ substantially from one season to the next.

Customized CFs can be developed in one of three ways. The first is discrete empirical quantile mapping where, for example, all the rainfall events greater than or equal to a specific threshold, such as the 80th percentile value, are adjusted by a different (possibly higher) CF than the events less than the 80th percentile. The selection of the threshold is based on predefined criteria or site-specific evaluation. This method is discrete because it is derived for one or more specific thresholds and empirical because it calculates the change factor directly from the model output.

The second is continuous empirical quantile mapping, where a CF is calculated for each quantile or for a range of quantiles from zero to 100. This method is continuous because it derives a CF for each quantile or range of quantiles and is empirical because the CF is calculated directly from model output.

The third approach is parametric empirical quantile mapping. This method is continuous but differs because it uses a function to fit the quantile-quantile plot. This creates a map informed collectively by a range of quantiles (i.e., that fit a line) rather than CFs defined for each quantile independently. It also allows a CF to be derived for any desired quantile.

The first approach is demonstrated by the precipitation data and projections in Table 7.1 for the Philadelphia, Pennsylvania site discussed previously. However,10 percentile intervals of the Downscaled GCM output for the baseline period are used to identify potential thresholds. CFs are computed for the cumulative rainfall amounts above the threshold. (This table uses annual values for illustrative purposes. As noted above, in practice it is recommended that quantile-based CFs be calculated from monthly or seasonal downscaled GCM outputs.)

In this example, a breakpoint appears where the CF transitions from 1.09 to a higher value. Breakpoints can be seen even more clearly when daily modeled versus observed precipitation is plotted in a quantile-quantile plot. Depending on its relevance to the analysis, the engineer could select the 70th, 80th, or 90th percentile value as the appropriate threshold.

Table 7.1. Percentile thresholds of baseline precipitation and total precipitation above the threshold calculated based on observed period (1950-1999) and future period (2000-2049) for the CCSM4 model for RCP8.5 in Philadelphia, PA.

Percentile	Baseline Threshold (mm)	Total precipitation above threshold		CF
		Baseline (mm)	Future (mm)	
10	0.00	54,102	58,916	1.09
20	0.00	54,102	58,916	1.09
30	0.01	54,100	58,914	1.09
40	0.06	54,052	58,868	1.09
50	0.22	53,816	58,636	1.09
60	0.63	53,089	57,891	1.09
70	1.57	51,204	55,998	1.09
80	3.69	46,678	51,370	1.10
90	9.11	35,843	40,463	1.13

To compute the CF for the precipitation values less than the chosen threshold, the data must be formatted as shown in Table 7.2. Because the chosen threshold was the 80th percentile, the CF for precipitation less than the threshold value can be taken from the table as 1.017. Therefore, the CFs for above and below the chosen (80th percentile) precipitation value are 1.10 and 1.017, respectively.

To apply these CFs, the engineer calculates the 80th percentile value for the observed time series dataset and applies the appropriate CF for each value in the observed time series to compute the future time series.

For the second approach, this method would be expanded to calculate appropriate values for each quantile or quantile range. Taking this method to its extreme, as used in the empirical quantile mapping approach that generates climate inputs for the VIC model described above, a CF is calculated for each point in the distribution.

For the third approach, a parametric function such as a linear regression, a piecewise linear regression, a polynomial, or other type of numerical function is fit to the quantile-quantile plot and the resulting function is used to derive a CF for any desired quantile. This last parametric approach has the benefit of avoiding potential noise and discontinuities, focusing instead on the larger relationship between modeled and observed precipitation and how it changes over the distribution.

Table 7.2. Percentile values of baseline precipitation and the total precipitations below the percentile calculated based on observed period 1950-1999 and future period 2000-2049 for the CCSM4 model for RCP8.5 in the Philadelphia, PA area.

Percentile	Baseline Threshold (mm)	Total precipitation below the thresholds		CF
		Baseline (mm)	Future (mm)	
10	0.00	0	0	
20	0.00	0	0	
30	0.01	2	2	0.934
40	0.06	50	48	0.958
50	0.22	285	279	0.978
60	0.63	1,013	1,025	1.012
70	1.57	2,898	2,918	1.007
80	3.69	7,423	7,546	1.017
90	9.11	18,258	18,452	1.011

7.3. Projected Time Series

Projected time series of precipitation and temperature are often required for continuous simulation. In some cases, other climatic variables are also needed.

7.3.1. Precipitation Time Series

The basic steps for generating time series of projections for precipitation as input to SWMM, using the framework described in Figure 7.2, can follow two alternative paths: 1) derivation and use of CFs and 2) customized high-resolution projections of precipitation time series. Following discussion of these two options, sub-daily precipitation data are discussed and then recommendations for precipitation time series data are provided.

7.3.1.1. Derivation and Use of Change Factors

Several approaches to deriving CFs are available and consideration of their limitations is critical to avoid misleading projections. (Some approaches can be facilitated by tools such as SWMM-CAT.) Many of the limitations have been evaluated with monthly to annual data. However, the CF methods affect characteristics of distributions differently regardless of whether the distributions are composed of annual, monthly, or daily data. Thus, lessons learned in applying CF to annual and monthly data are valid for daily data.

Use of a single multiplicative CF is the simplest approach but will not be adequate to represent projected changes in precipitation time series if changes in sub-annual precipitation are a concern. In other words, this approach will accurately reflect projected changes in annual averages but cannot resolve how changes in annual mean values are distributed across the calendar year. Future projections clearly indicate that changes in mean precipitation are likely to vary significantly from one season to the next, with overall wetter conditions in the northern

United States in winter and spring, and drier conditions in summer in the south and western United States (see Chapter 4). To address this issue, it is common to either obtain and apply high-resolution or station-level downscaled projections directly or estimate and apply a multiplicative CF for each season or month.

As an example, compare annual with monthly CFs for Philadelphia using precipitation data derived from the CCSM4 model and the higher RCP8.5 scenario, as summarized in Table 7.3 and Figure 7.3. The CF shown in the table is the ratio of the future to the baseline precipitation values. Monthly CFs range from a low of 0.96 in May (indicating a decrease of 4 percent in monthly precipitation) to a high of 1.23 in August (indicating an increase of 23 percent), but the annual mean CF is 1.09. If only one CF was used, an increase of 9 percent would be uniformly applied to all months, obscuring the fact that the largest cumulative increases are projected for the warm season, specifically July through September. With the monthly CFs, all the precipitation data in the SWMM model within January are adjusted using the January CF of 1.08, while all February data are adjusted using a CF of 1.16, and so on.

Table 7.3. Downscaled GCM monthly average values based on a baseline period 1950-1999 and a future period 2000-2049.

Month	Baseline Average Monthly Precipitation (mm)	Future Average Monthly Precipitation (mm)	CF
Jan	78.8	84.8	1.08
Feb	77.3	89.6	1.16
Mar	100.3	104.7	1.04
Apr	87.5	95.5	1.09
May	95.5	91.6	0.96
Jun	88.4	93.1	1.05
Jul	104.0	120.2	1.16
Aug	104.9	129.0	1.23
Sep	83.4	100.5	1.21
Oct	84.7	86.8	1.02
Nov	87.7	93.2	1.06
Dec	89.7	89.4	1.00
Annual	1082.2	1178.4	1.09

Use of monthly or seasonal CFs meets the need of assessments concerned with sub-annual precipitation. Precipitation is typically projected to differ from one season to the next (Melillo et al. 2014); thus, seasonal or monthly CFs provide a more useful representation of possible future conditions compared with a single CF which would only be representative of changes in annual mean values.

But what about assessments concerned with projected changes in sub-monthly precipitation, that is, shifts in the amount and frequency of precipitation on an hourly, daily, or weekly time scale? As discussed in Chapter 4, increases in the frequency and intensity of precipitation above the daily 99th historical percentile have been observed across the entire United States. In most

regions, these indicators are projected to continue to increase. If these changes are relevant for the assessment, a monthly CF approach will still be inadequate.

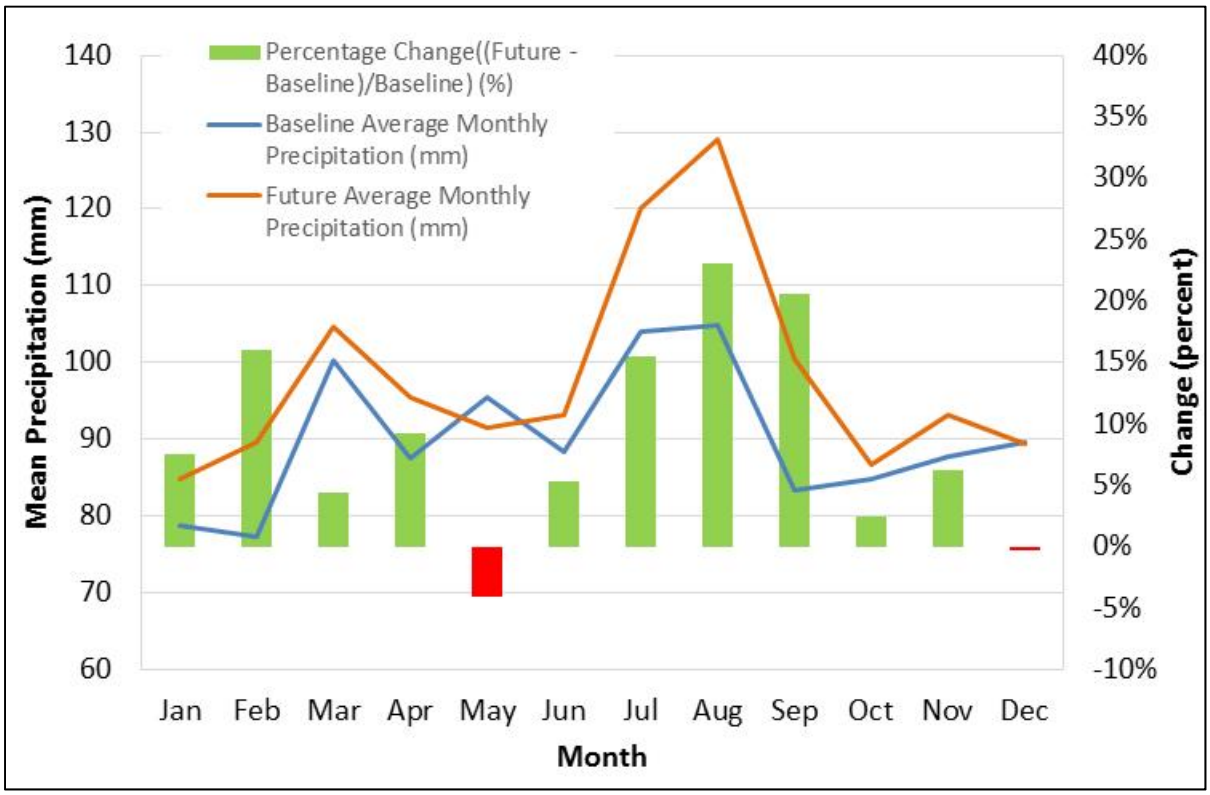

Figure 7.3. Comparison of average monthly future (2000-2049) and baseline (1950-1999) precipitation for the CCSM4 model and the RCP8.5 scenario in Philadelphia, PA.

7.3.1.2. Use of Customized High-Resolution Projections

The second path is to use customized high-resolution precipitation time series projections. This customization might be appropriate for a Level 4 analysis and would replace Steps 2 through 5 of the general procedure. Customization would start with a qualified climate expert obtaining high-resolution daily precipitation projections which would be more appropriate for the project goals, including being able to better resolve the distribution of change in daily and monthly values beyond a simple annual or monthly CF approach.

7.3.1.3. Sub-Daily Precipitation

When sub-daily (e.g., hourly) precipitation data are used as input for SWMM, the use of either CFs or customized projections can be more challenging because hourly (or other sub-daily) output from climate projections is highly experimental and not widely tested. If the CF approach is desired, then several options may be considered:

- Option 1 is to aggregate historical precipitation data to the precipitation time increment available in climate projection data (e.g., aggregate hourly to daily), calculate CF for the aggregate data, and run SWMM with the aggregate data. This approach requires a companion evaluation to determine whether error from using

aggregate data is larger than the magnitude of the climate change impact (Anderson et al. 2015, Cook et al. 2017).

- Option 2 is to include a temporal disaggregation method. As in Option 1, the historical data are first aggregated to the time increment of the climate projection data, and CF is calculated for the aggregate data. After applying the CF to the aggregate data, the disaggregation method is applied to return to the original time increment of the historical data.
- Option 3 is to use CFs computed based on daily data and apply them to sub-daily data.

7.3.1.4. Recommendations for Precipitation

Three general CF approaches for precipitation have been described in Section 7.2: 1) single CF, 2) seasonal/monthly CFs, and 3) CFs for individual thresholds or quantiles. The latter can be calculated for individual thresholds for a continuous range of quantiles or as a parametric equation providing a customized CF for any quantile.

In developing climate inputs for SWMM or other uses, engineers are encouraged to consider the following points carefully:

1. Whether to calculate CFs themselves or obtain high-resolution climate projections directly.
2. If calculating CFs, whether to derive them on an annual, seasonal, or monthly basis.
3. Whether to focus on CFs that resolve changes in the mean or CFs that represent changes in specific thresholds, quantiles, or percentages.
4. Selecting an appropriate range of GCMs and scenarios on which to base the CFs, as described in detail in Chapter 4.

For a given future climate scenario, CFs for an ensemble of GCMs can be computed. The mean value of these CFs can be computed along with the appropriate confidence limits (e.g., 90 percent). The observed precipitation time series can then be adjusted by the mean and upper and lower confidence level CFs to generate three SWMM output files representing potential future conditions under that scenario. The process of generating mean values and confidence limits may be repeated for other future scenarios and the implications of the series of SWMM outputs for developing a resilient stormwater management/water quality design evaluated.

7.3.2. Time Series for Other Climate Variables

The approach to incorporating the projected air temperature, solar radiation, relative humidity, evaporation, and wind speed from Downscaled GCM datasets into watershed models such as SWMM is similar to that described for precipitation. One difference is that SWMM, and other continuous simulation models, generally requires less detailed temporal resolution of these other climatic parameters. While continuous simulation models generally use sub-daily precipitation data, they use daily or monthly values of temperature and other parameters. (SWMM does not use solar radiation or relative humidity, but other models do.)

The climate variables required by the hydrologic continuous simulation model may restrict the potential sources of Downscaled GCM data if those variables are not available within the dataset. Surface air temperature can be obtained from most common datasets. However, humidity, wind speed, and solar radiation are available only for a subset of these datasets. See Appendix 4A for a listing of datasets and available data.

7.3.2.1. Temperature

If the design team determines that a Level 3 analysis is needed, then the continuous model simulations should incorporate projections for other climatic variables, including temperature. The incorporation of future temperature scenarios can be achieved by the same approaches described above: obtaining high-resolution climate projections directly or calculating and applying an appropriate CF using an additive rather than multiplicative approach.

The time series input for temperature data used in SWMM can be in hourly or daily time steps. The basic steps for generating a projected temperature time series for SWMM is also based on the framework described in Figure 7.2 and can follow either of two alternative paths: 1) derivation and use of CFs or 2) customized high-resolution projections of temperature time series. The basic steps for deriving and using CFs in SWMM are as follows:

1. Calibrate and run the SWMM model using historical temperature data.
2. Obtain downscaled GCM data for both baseline (historical) conditions and future scenarios. (Chapter 4 describes appropriate data sources.)
3. Calculate the appropriate temperature statistics for both the baseline conditions and future scenarios for the desired CF approach. The temporal domain for both the baseline and future should be the same domain that was applied for the precipitation analyses.
4. Compute the additive CF based on downscaled GCM output for the future temperature compared to the baseline scenario for each month:

$$CF_{j,add} = (\bar{T}_{j,GCM,future} - T_{j,GCM,historical})$$

5. Adjust the historical observed temperature time series used in the SWMM model to evaluate existing conditions using the monthly CFs:

$$T_{i,j,future} = T_{i,j,observed} + CF_{j,add}$$

6. Rerun the SWMM model using the adjusted temperature data.
7. Evaluate the differences between historical and projected SWMM results to develop a robust stormwater management/water quality design.

Similar to the example for precipitation above, the process of estimating temperature change factors is illustrated with downscaled output from the CCSM4 model and the higher RCP8.5 scenario in Fairfax, Virginia. Table 7.4 summarizes mean monthly temperatures for a baseline period (1950-1999) and a future period (2000-2049) for the given model, scenario, and location. The resulting additive CF is also shown in the table. Figure 7.4 presents the same information graphically.

Table 7.4. Monthly average temperatures based on baseline period 1950-1999 and future period 2000-2049 for the CCSM4 model for RCP8.5 scenario in Fairfax, VA.

Month	Baseline Average Monthly Temperature (^{0}F)	Future Average Monthly Temperature (^{0}F)	Additive CF (^{0}F)
Jan	33.4	35.7	2.3
Feb	36.0	39.4	3.4
Mar	44.1	47.1	3.0
Apr	54.7	56.5	1.8
May	63.9	67.0	3.2
Jun	72.0	75.0	2.9
Jul	76.6	80.1	3.6
Aug	75.0	78.4	3.4
Sep	68.0	71.5	3.4
Oct	56.4	59.8	3.4
Nov	46.0	48.6	2.5
Dec	36.6	41.7	5.1
Annual	55.2	58.4	3.2

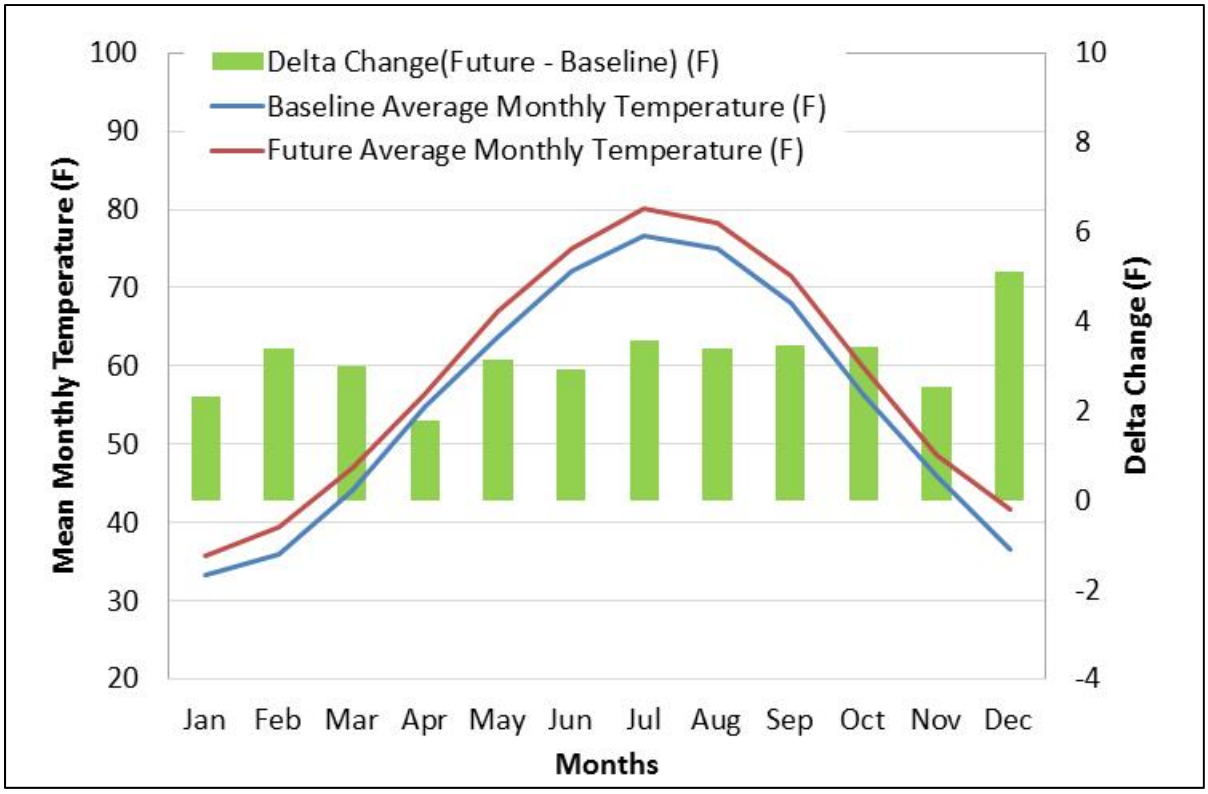

Figure 7.4. Monthly average temperature for future (2000-2049) and baseline (1950-1999) periods and the corresponding monthly change factor for a location in Fairfax, VA (CCSM4 model and RCP8.5).

The annual average CF shows an increase of +3.2°F. If used annually, this CF would be applied equally to every day in the year. As Table 7.4 and Figure 7.4 illustrate, however, more warming is projected for certain months as compared to others. Application of an annual CF would under-estimate projected change for July through October, while over-estimating it in April through June. This again emphasizes the need for monthly or at least seasonal CFs if sub-annual conditions are at all relevant to the analysis.

This CF is applied on a monthly basis to the historical temperature time series as part of Step 5. For example, the temperature data in SWMM within January will be adjusted using the CF calculated for January. (SWMM includes a monthly adjustment option.) Once the adjustments are completed, the engineer continues with Steps 6 and 7 of the process.

7.3.2.2. Other Climatic Variables

The approach for incorporating other climatic variables, such as solar radiation, relative humidity, evaporation, and wind speed, is analogous to that provided for temperature. Generally, either high-resolution projections are obtained directly from a regional climate model (see Chapter 4), or an additive CF is estimated on a monthly basis for these variables. Some empirical-statistical downscaling models can downscale solar radiation, relative humidity, and evaporation, and combined with climatological observed wind speed (because projected changes in wind speed in the future are highly uncertain), these can also be used.

For the SWMM model specifically, evaporation data can be adjusted to represent future conditions using monthly adjustment factors (+/- in/day or mm/day) through the SWMM Climatology Editor. If an external climate file with evaporation and wind speed is used with SWMM, this file can be manually modified to incorporate the future scenario. Daily evaporation rates and wind speeds are adjusted using monthly CFs.

BOTTOM LINE: The range of complexity and detail offered by change factors for precipitation and other parameters allows the engineer to pick a strategy that is compatible with project objectives and budget.

7.4. Autocorrelation Structure of Climatic Time Series Data

Temperature data, and to a lesser extent precipitation data, tend to be autocorrelated (serially correlated) in time to a certain degree, meaning that the values at a given time step are dependent on the values at previous time steps. Autocorrelation is the strength of the linear relationship between observations in a given time series as a function of the time lag between them. Temperature data have diurnal and seasonal variations that contribute to the serial correlation. Precipitation data are intermittent time series that include intervals with zero precipitation. Therefore, there is less autocorrelation in precipitation data than temperature data. As the time step increases (e.g., hourly to daily to monthly), the autocorrelation increases.

In time series analysis, an autocorrelation function (ACF) describes the extent of autocorrelation of the current value with previous values. The partial autocorrelation function (PACF) gives the partial correlation of a time series with its own lagged values, controlling for the values of the time series at all shorter lags than the defined limit. For example, the partial autocorrelation at lag k is the correlation that results after removing the effect of any correlations resulting from terms at shorter lags. The PACF and ACF at lag 1 are the same.

As described earlier, differences (multiplicative or additive) between future and baseline downscaled GCM outputs are typically used to scale or modify observed historical data to create future time series data. Single multiplicative or additive CFs do not alter the autocorrelation structure in the observed time series. However, scaling monthly data by different amounts or adjusting data only above a given percentile may affect the autocorrelation. For these adjustments, the autocorrelation of the projected time series should be compared to the baseline time series data. Much of the concern about autocorrelation structure in projected time series may be avoided if the projected time series are obtained from downscaled projections directly or using a continuous quantile mapping approach rather than CFs.

Figure 7.5 shows an example of a PACF against the lag for a sample dataset using the three multiplicative CF options: 1) single (option 1), 2) seasonal/monthly (option 2), and 3) threshold (option 3). This chart shows that the PACF values corresponding to the historical data and the future projections produce similar values, confirming that the autocorrelation structure was maintained in these cases. This example confirms that the single CF (option 1) does not change the autocorrelation structure.

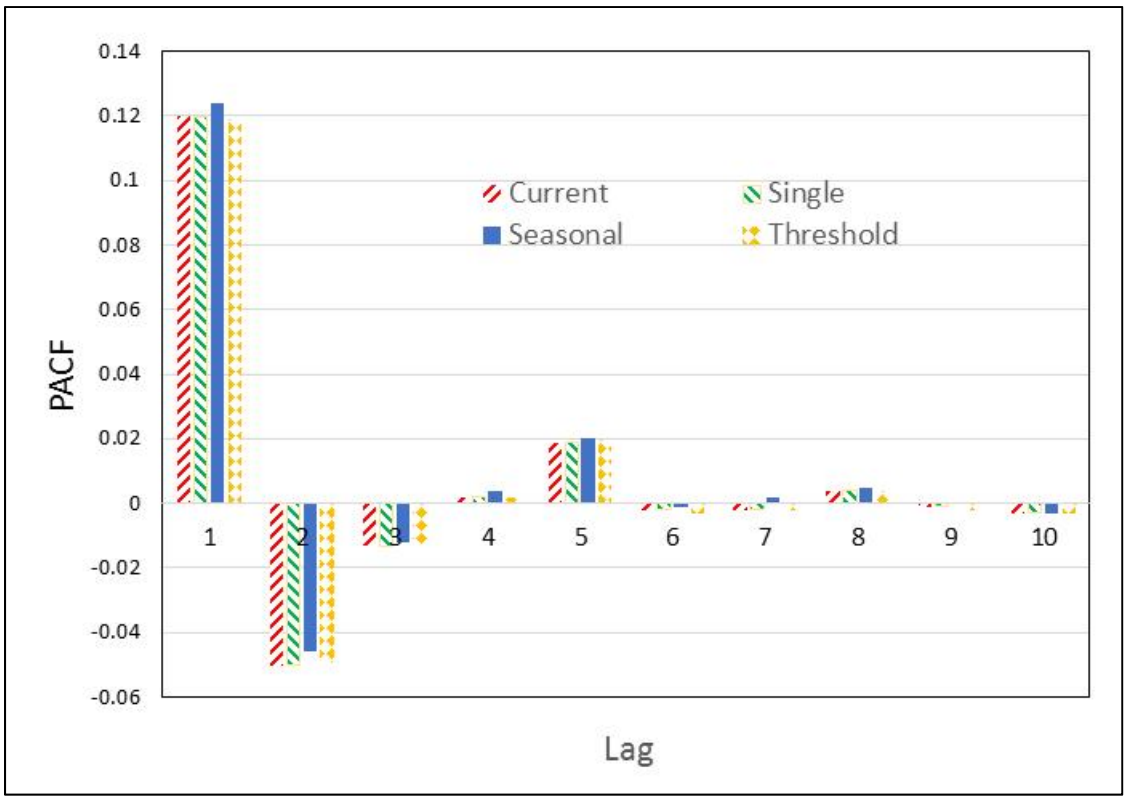

Figure 7.5. Example partial autocorrelation function values for a baseline precipitation time series and three future precipitation series using single, seasonal, and threshold CFs.

Figure 7.6 shows an alternative example of PACF values against the lag for a case where hypothetical projected precipitation values show a different behavior than the historical data. The historical precipitation shows a comparatively higher PACF for a lag of 1 compared to the projected precipitation PACF value. Lags other than one did not display reasonable correlation at all. If the autocorrelation structure of the projected precipitation data differs from the historical

data, the project team needs to decide whether it is reasonable to use the projected data in the analysis.

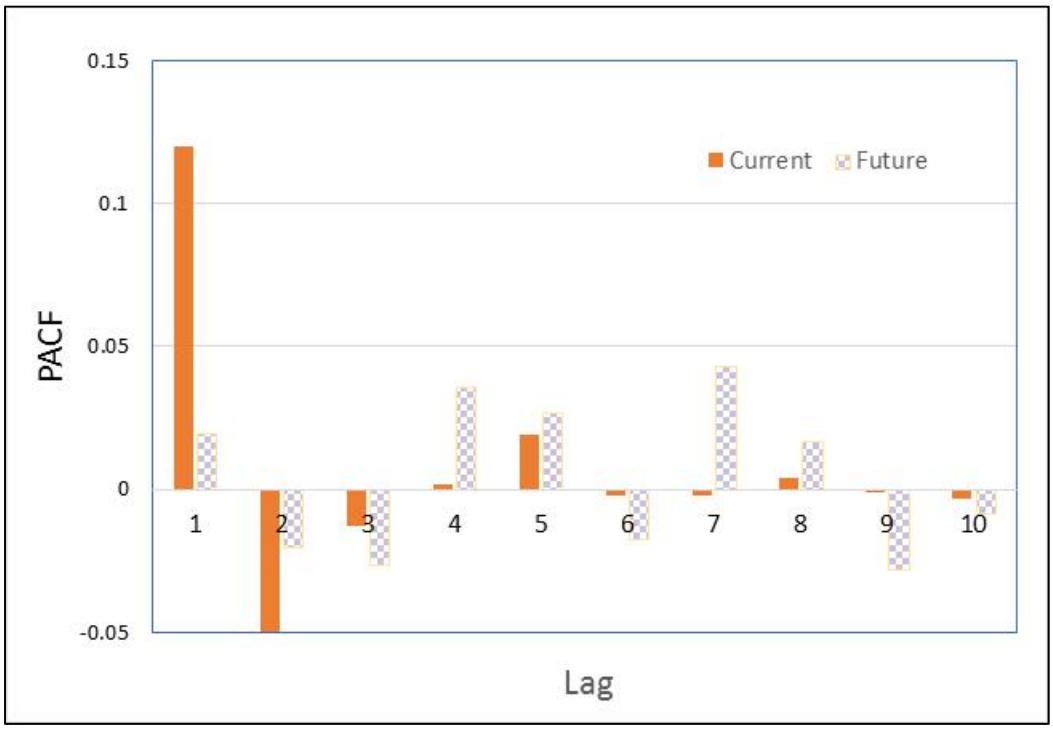

Figure 7.6. Example partial autocorrelation function values for baseline and projected future precipitation time series.

7.5. Obtaining Projected Data for Continuous Simulation

The preceding sections assume that data derived from GCMs for baseline and future conditions, including that from existing high-resolution climate datasets, are available at an appropriate spatial and temporal scale. Chapter 4 describes these databases, including the climate variables available and their temporal and spatial scales. The following sections provide guidance related to the acquisition and use of these data for continuous simulation modeling.

7.5.1. Mapping Climate Stations to Downscaled GCM Grid Data for Change Factors

Future climate projections are generally available at three different types of spatial resolutions. The first is gridded GCM output, which typically ranges from one to three degrees per side. The second is high-resolution gridded downscaled output, which for regional climate model output typically ranges from 10 to 25 km per side, and for an empirical statistical downscaling model typically matches the spatial resolution of the observations used to train the model, usually 1/16th or 1/8th degrees. Finally, high-resolution climate projections that have been downscaled to an individual weather station using an empirical-statistical downscaling model are available for individual point sources corresponding to the long-term weather station or gauge used to train the model. When CFs are being used, although derived from GCM output, they are applied to observations at their native spatial scale. So depending on whether the observations are gridded or station-based, they would fall under either the second or third category.

For watershed analysis, the engineer needs a minimum of one time series for each climate variable at or near the watershed of interest to provide a basis for generating projected future time series for that variable. Depending on the size of the watershed, either a continuous grid or an individual point may be used. The larger the watershed, the more likely there are spatial variations in temperature, precipitation, and other aspects of climate across the region, and the more important it becomes to use high-resolution gridded data (the second category above) rather than a single point source (the third category above). For gridded data, the relationship between the watershed drainage area and the grid size will vary from cases where the watershed (or the drainage area for the hydraulic structure) is covered by only a few high-resolution grids (e.g., a few grid cells up to about a 5x5 or 6x6 area), to where the watershed encompasses a substantial number of grids (e.g., possibly 10x15 or larger). In the former case, a single point source may be adequate whereas in the latter case a continuous grid covering the region should be used. (Section 5.3 discusses matching watershed and GCM data grid size.)

If an individual point is deemed adequate for the analysis, this information can be obtained in one of three ways. First, if high-resolution gridded projections have been obtained directly, the small number of grids overlapping the watershed drainage area can be averaged to obtain a single time series for the area. Second, if high-resolution projections for a single representative weather station have been obtained directly, they can be used directly. Third, if a CF is being derived from GCM output and used to modify a single weather station time series or a gridded average, then those observed station data or observed areal average data can be selected to be representative of the drainage area. In this last case, if more than one GCM data grid overlies the drainage area, multiple GCM grid cells should be area-weighted to produce a single time series, and the CF calculated from that area-weighted time series.

If multiple climate stations are used to obtain the historical climate data and to calibrate the continuous simulation model, then mean change in precipitation should be calculated for each historical climate data station. The area of influence for each historical climate data station is estimated using a strategy such as Thiessen polygons. Then each climate station is mapped to the GCM gridded data as described above. If a Thiessen polygon comprises many GCM data grids and the grids are completely within the polygon, then a mean of the statistics corresponding to each grid can be used in the analysis. If a Thiessen polygon comprises only portions of some or all GCM grids, then an area-weighted approach should be used to calculate the change in input precipitation values.

7.5.2. The Climate Resilience Evaluation and Analysis Tool Database

The Climate Resilience Evaluation and Analysis Tool (CREAT) is a decision support tool developed primarily to assist drinking water, wastewater, and stormwater utility owners in understanding, evaluating, and addressing climate change risks. It contains a database of climate projections across the United States, downscaled using a CF approach to a grid of 1/2 degree in latitude and longitude (about 48 km square) that may also be used for environmental analyses relevant for state DOTs. The database includes historical climate information as well as changes in monthly average precipitation, monthly average temperature, and 24-hour rainfall amounts for return periods of 5, 10, 15, 30, 50, and 100 years. A part of the database is available from the CREAT Climate Scenarios Project Map with a limited dataset showing changes in average annual temperature, average annual precipitation, and 100-year storm intensity

(https://epa.maps.arcgis.com/apps/MapSeries/index.html?appid=3805293158d54846a29f750d63c6890e).

Historical annual and monthly climate data in CREAT are from the (Parameter-elevation Regressions on Independent Slopes Model) PRISM dataset from 1981 to 2010. As previously noted, changes in the tails of the distribution may not scale with changes in the mean, so methods that use mean rather than quantile-based CFs may not be reliable for extreme precipitation. For this reason, historic precipitation extremes were developed using NOAA station data to develop series of annual maxima daily precipitation that are fit to a Generalized Extreme Value (GEV) distribution to estimate AEP quantiles.

Projected information in CREAT is based on 38 CMIP5 GCMs for the higher RCP8.5 scenario. The projections cover two 20-year time domains: 2025 to 2045 and 2050-2070. (Note that this is 10 years shorter than the WMO climate normal definition of 30 years.) By only including the higher RCP8.5 scenario and limited time domains, the CREAT database may be inappropriate for some applications. CREAT developers are currently considering adding the Localized Constructed Analogs (LOCA) statistically downscaled climate projections for North America to CREAT (Fries 2017).

The ensemble of projections was consolidated in CREAT to three groups: Hot/Dry, Central, and Warm/Wet. The Warm/Wet group includes the average of the five models that were nearest to the 5th percentile of annual temperature change and the 95th percentile of annual rainfall change. The Central group includes the average of the five models nearest to the median temperature and rainfall changes. The Hot/Dry group includes the average of the five models that were closest to the 95th percentile temperature change and 5th percentile rainfall change.

The ensemble averages for each group of the annual and monthly changes for temperature and precipitation were calculated. CREAT includes a database of percent changes in monthly average precipitation and absolute changes in monthly average temperature for each group and each of the projected time domains at each grid cell across the United States.

The CREAT database also includes information on the projected changes to the magnitude and frequency of precipitation extreme events. The historical GEV curve for the 5-, 10-, 15-, 30-, 50-, and 100-year return intervals were developed for precipitation stations that have data from 1981 through 2010, using the annual maxima time series for 24-hour precipitation. The changes in precipitation per degree of warming (global), scalars, for the different storm events were determined for each GCM mode from a subset (22 out of 38) of GCMs. This set of spatially distributed scalars was collected in cooperation with ClimSystems (http://www.climsystems.com). The models were ranked based on the scalars for the storm events with a 5-year return interval. The five models having the highest scalars were averaged to describe a “Stormy Future,” while the five models with the lowest scalars were averaged to describe a “Not as Stormy Future.” The historical GEVs were then adjusted using the ensemble averaged scalars and the change in global mean temperature from the same model, thus creating a new GEV curve for each of the future time periods.

The intent of calculating the scalar and the modified GEV is that future design rainfall values (5-year, 10-year, 15-year, 30-year, 50-year, and 100-year) may be determined by multiplying the historical design rainfall by the averaged scalars and the change in global temperature. However, because the methodology for developing the scalars is undocumented, this approach is not recommended for design.

BOTTOM LINE: The CREAT tool embeds a series of assumptions about GCMs and scenarios. The user should be familiar with these assumptions to ensure that they are compatible with the project objectives before using the tool.

Chapter 8. Evaluation of Climate Outputs and Design for Coastal Transportation Assets

Transportation infrastructure along the coast is being exposed to several impacts from a changing climate, including rising sea levels, higher storm surges, changing freshwater inputs, increased risk of heavy precipitation, and the potential for stronger storms. The design environment consists of water levels, currents, waves and sediment transport. Design decisions within this coastal environment are influenced by the ecosystems and habitats (e.g., beaches, dunes, estuaries, and reefs) that exist along the coast and are highly valuable to society. Coastal engineering is influenced by a broad spectrum of coastal marine sciences (e.g., oceanography, geology, ecology). The scientific advances occurring in these coastal marine sciences, such as improved numerical modeling of coastal processes, are altering the coastal engineering design environment.

Uniformly, all future projections of global sea levels show that they will continue to increase with time. That sea level rise will progressively make coastal infrastructure more vulnerable and less functional has been recognized for years. This is true for coastal infrastructure in general (NRC 1987, IPCC 1990) and transportation infrastructure specifically (Titus 2002, Hyman et al. 2008, Kafalenos and Leonard 2008). As the 2017 Fourth National Climate Assessment (NCA4) states (Sweet et al. 2017b):

> *"… it is virtually certain that sea level rise this century and beyond will pose a growing challenge to coastal communities, infrastructure, and ecosystems from increased (permanent) inundation, more frequent and extreme coastal flooding, erosion of coastal landforms, and saltwater intrusion within coastal rivers and aquifers."*

This chapter evaluates climate outputs with a focus on those most critical in the design of coastal transportation assets. The primary goals are providing guidance on selecting sea level rise scenarios for design and on the use of storm surge/wave hazard information with sea level rise scenarios for design. The level of damage caused by coastal storms in the past two decades makes it clear that some of our coastal transportation infrastructure is already highly vulnerable to extreme events, and climate change will increase this vulnerability incrementally and progressively through sea level rise. Information on the effects of climate change on other related coastal issues, including watershed contributions to water levels at the coast and coastal geomorphology, are discussed, but actionable design guidance in these areas is not presented.

8.1. Selecting Sea Level Rise for Design

As the planet warms, one of the more predictable outcomes of this warming has been, and will continue to be, increasing sea levels. An estimated 93 percent of the additional heat trapped inside the earth's climate system by emissions is going into the ocean (Jewett and Romanou 2017), resulting in thermal expansion of ocean water and subsequent global mean sea level rise (GMSLR). Sea level is also rising as land-based ice sheets and glaciers melt; this is the primary cause of the observed acceleration in the rate of GMSLR over the past 30 years (Sweet et al. 2017b). Although global sea level has been gradually increasing for thousands of years, and the overall location and geological character of our coastal shorelines reflect that sea level history, GMSLR rates have more than doubled over the last 25 years compared to the past century, and

they are projected to increase substantially over the remainder of this century (Sweet et al. 2017b). The latest conclusions from the Climate Science Special Report, Volume 1 of the Fourth National Climate Assessment (NCA4), find that:

"Global mean sea level (GMSL) is very likely to rise by 0.3–0.6 feet by 2030, 0.5–1.2 feet by 2050, and 1.0–4.3 feet by 2100. Future pathways have little effect on projected GMSL rise in the first half of the century, but significantly affect projections for the second half of the century. Emerging science regarding Antarctic ice sheet stability suggests that, for high emission scenarios, a GMSL rise exceeding 8 feet by 2100 is physically possible, although the probability of such an extreme outcome cannot currently be assessed." (Sweet et al. 2017b)

This increase is of concern because of the potential for extensive effects on the coastal environment and population including effects on transportation infrastructure, such as more frequent and more severe flooding of low-lying assets, and increased exposure to waves during extreme events.

Much of the literature stresses the significant levels of uncertainty related to the selection of any specific value as an estimate of a future sea level for design, as well as the critical upper bounds of sea level rise projections. However, water resources engineers often address significant uncertainty in other areas of design analysis (e.g., Manning's coefficient, rainfall-runoff models, risk-based design). They accomplish this by understanding the causes of, and ranges of, the uncertainty involved in the important physical processes and analyses, and then use judgment in design including appropriate factors of safety. **There is no need to wait for any future reduction in uncertainty in our projections of future sea level rise**. **The tools are available for its regular inclusion in the design of coastal transportation assets today**.

Below is a detailed summary of some of the physical processes and uncertainties inherent in the use of sea level rise projections for design. The purpose is to inform the design engineer about these physical processes and their uncertainties with the understanding that proper use in design will remain in the realm of project specific engineering judgment. This section provides an overview of the current understanding regarding sea level rise, available sea level rise projections, issues surrounding the selection of sea level rise scenarios for design, and recommendations for selection of sea level rise values for planning and design.

8.1.1. Current Understanding of Sea Level Rise and Variations

Methods to measure and estimate past sea levels include paleoclimate data such as sediments that document the geologic record for past millennia, tide gauge records for the past century and a half, and satellites for the past several decades. All these data indicate global sea levels are rising. Between the last glacial maximum and peak temperature during the Holocene, they rose an estimated 100 meters (m) over the course of 10,000 years. Since then, they continued to rise at a much slower rate, but a rate that has significantly accelerated in the past few decades (see Church et al. 2013).

Relative sea level (RSL) is the difference between sea surface and land surface elevations at a specific place. Changes in RSL over time, relative sea level rise (RSLR), vary by location. They depend on global mean sea level, on ocean circulation that can affect the relative height of sea level compared to the global average, and on subsidence or uplift of local land masses that result from both natural and human causes. RSLR is the primary concern for coastal engineering, since each design is site-specific.

RSL changes are measured by **tide gauges**. A wealth of data and analysis on tide gauge records is available online at the National Oceanic and Atmospheric Administration (NOAA) Tides and Currents website (U.S. Department of Commerce 2017). Monthly average sea levels measured by the tide gauge for New York City are shown in Figure 8.1, with the seasonal trend removed, as an example. The gauge record extends back to the 1850's (with a gap in the data in the 1870-1890's). At this location, the average annual rate of rise is 2.84 millimeters (mm)/year, which is equivalent to 0.93 feet per century. However, there are significant fluctuations in average sea level month to month which appear as the "spikiness" of the data plot, as well as yearly and multi-year time periods that have different trends. Similar tide gauge records can be obtained at the same website for many other locations around the United States. **Design engineers should obtain the plot and analysis from the tide gauges nearest to their project site to begin to understand the historical RSLR and vertical land movement (VLM) rates, and how they vary from the global average**.

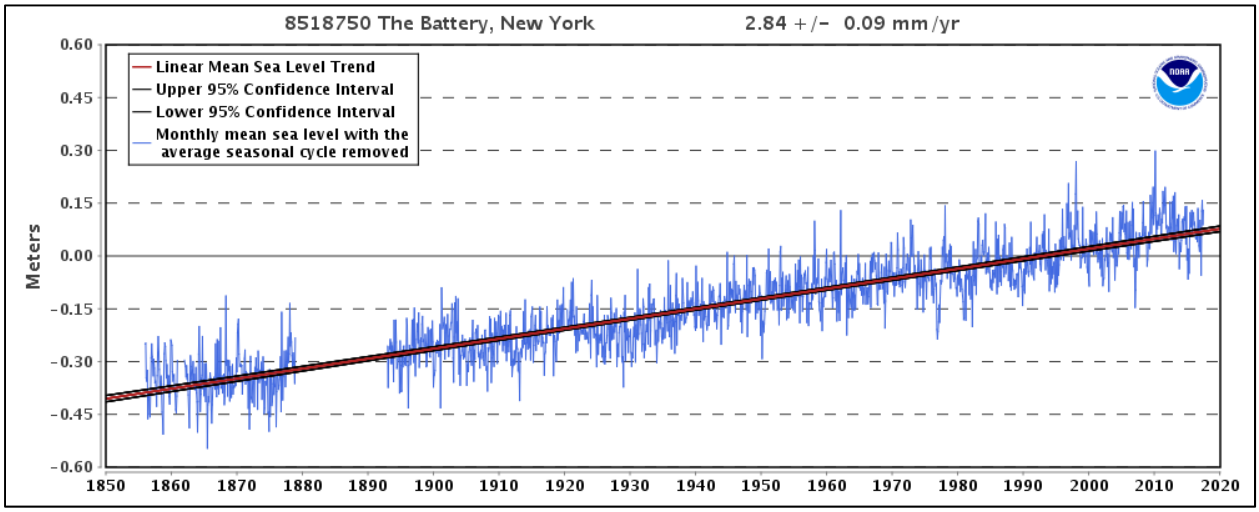

Figure 8.1. Relative sea level rise trend for New York City based on tide gauge data (downloaded from www.tidesandcurrents.noaa.gov/sltrends Sept. 30, 2017).

Figure 8.2 summarizes the long-term RSL trends as measured by tide gauges around the United States. The small arrows represent the direction and magnitude of the linear RSL trend (upward-pointing arrows indicate RSL rise, and downward-pointing arrows represent RSL fall; the length and the color of the arrows represent the magnitude of the trend). Again, **sea level is rising along most of the coast.** The rates of rise vary by location due to local and regional mechanisms, including VLM and ocean dynamics, discussed below. Most of the US gauge locations have rates of rise less than 6 mm/year (the yellow and green upward arrows on Figure 8.2). This rate corresponds to less than 2 feet per century. In a few locations, particularly Alaska and some Pacific Northwest areas, the RSL tendency is negative; in other words, RSL is falling. This happens when the rate at which land is rising exceeds the rate at which the sea level is rising at a specific location. Zervas (2009) presents a detailed analysis of the sea level changes at all the US tide gauges, similar to those on the NOAA Tides and Currents website.

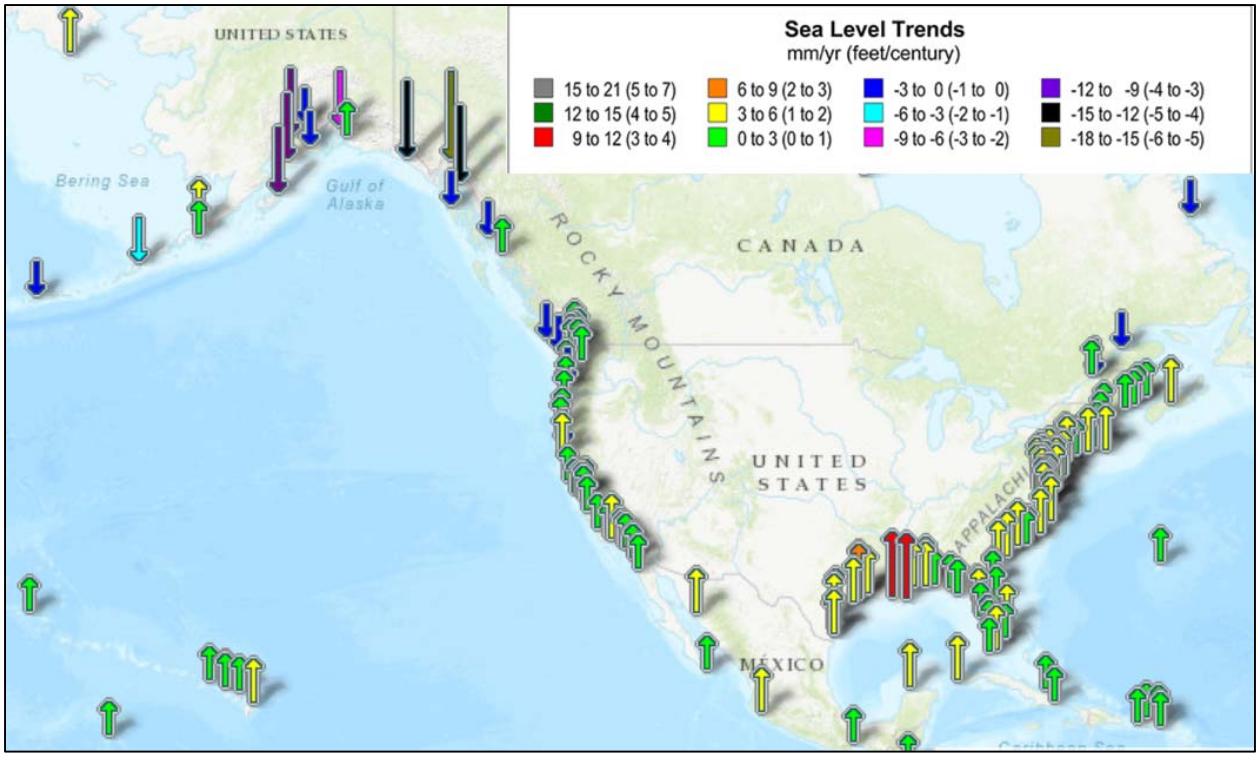

Figure 8.2. RSL trends based on tide gauges around the US (Adapted from www.tidesandcurrents.noaa.gov/sltrends, downloaded September 30, 2017)

The information derived from tide gauge RSLR records can be improved through smoothing and the application of different averaging periods. For example, annual rather than monthly average sea levels for Dauphin Island, Alabama are shown in Figure 8.3. That tide gauge has only been operational since 1967 and years with significant data gaps are not shown. By smoothing the data, one concludes that:

- The average sea level along the Alabama coast in 2016 was the highest ever on record at almost 7 inches higher than the average in the 1980s and 1990s.
- The 2016 record was 2.5 inches higher than the previous record high year.
- Six of the highest years in history for average sea level along the Alabama coast have occurred in the last 8 years.

While the data did not change with the averaging period, these characterizations of the dataset are not as obvious with NOAA's monthly average plot. The relatively high sea level shown for Alabama in 2016 is generally consistent with other gauges along this portion of the northern Gulf of Mexico coast. It also likely reflects the inter-annual variability due to regional weather patterns that year, superimposed on the longer-term trends in land subsidence and GMSLR observed along the US coastline and throughout the Gulf of Mexico.

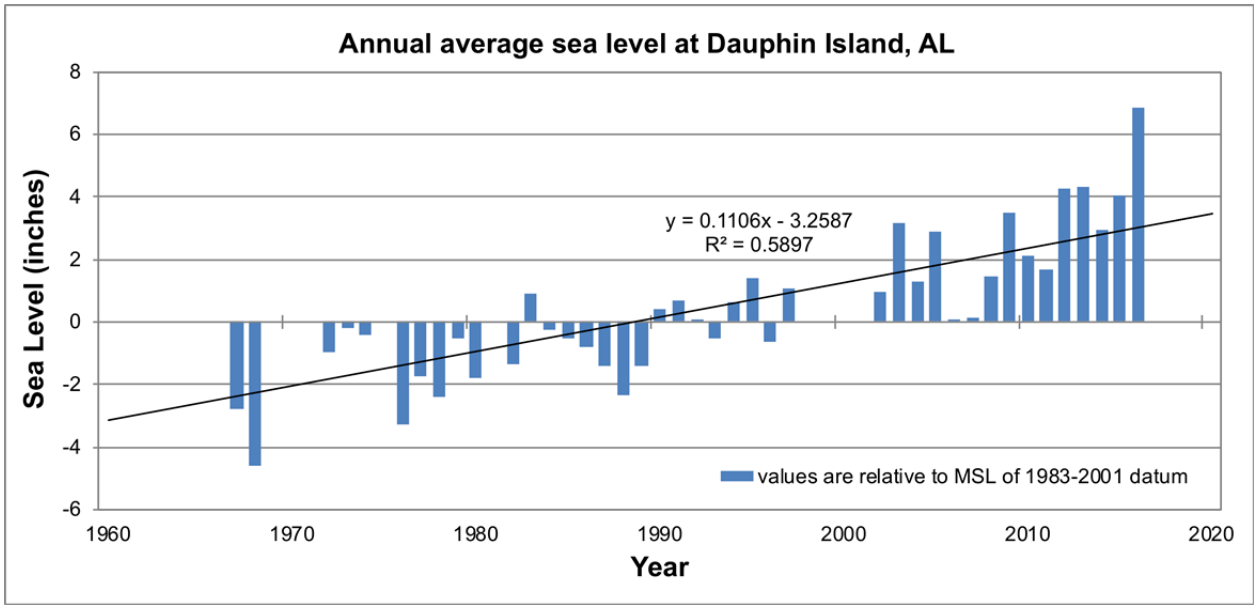

Figure 8.3. Annual average RSL at Dauphin Island, Alabama.

Sea levels can also be measured by **satellite altimetry**. The sea surface has been mapped by satellites several times per month since 1992. Sea level is measured across large portions of the earth's oceans and measurements are not geographically limited, in contrast to the locations of the long-term tide gauges that are all on the coast and mostly in the northern hemisphere. The global average rate of GMSLR measured by satellites has been 3.4 mm/year (0.13 inch/year) since 1992 (JPL 2017). This rate corresponds to about 1.1 foot/century. The satellite results are a direct estimate of the GMSLR.

Changes in RSL depend on the simultaneous interaction of the following general types of physical mechanisms:

1. Global mean sea level rise (GMSLR).
2. Vertical land movement (VLM).
3. Other regional variations in RSL (e.g., oceanic currents and land ice melt signatures).

Each of these, and the complexities of the physical processes involved, is briefly introduced below as scientific background related to sea level rise projections and their uncertainty.

8.1.1.1. Global Mean Sea Level Rise

Global mean sea level rise (GMSLR) results from eustatic change, meaning a change in the global volume of water in the oceans. Over the 20th and early 21st century, the two primary contributors to GMSLR have been thermal expansion of seawater and melting of land ice (glaciers and ice sheets located on land masses such as Greenland and Antarctica) in response to warming temperatures. The long-term potential contribution of globally distributed glaciers to GMSLR is small when compared to the potential contribution of continental-scale ice sheets on Greenland and Antarctica. There are several other contributors to the global volume of water in the ocean which have smaller effects on GMSLR. Dams impound water and slightly reduce the

volume of water in the oceans. Groundwater extraction adds to the overall surface water budget including the ocean volume. Both of those contributions are smaller in magnitude than the thermal expansion of seawater and the melting of land ice. Thermal expansion, melting glaciers, and terrestrial water storage explains approximately 65 percent of the observed GMSLR for 1901-1990 and 90 percent for 1971-2010 and 1993-2010 (Church et al. 2013). Later in the 21st century, ice melt from Greenland and Antarctica is expected to play an increasingly important, and likely a dominant, role in GMSLR (Rignot et al. 2011).

8.1.1.2. Vertical Land Movement

Vertical land movement (VLM) includes changes in the land surface elevation at a location (either uplift or subsidence) that affect the relative sea level. These changes can be naturally caused by factors such as glacio-isostatic adjustment (GIA), tectonics, and natural sediment compaction. These changes may also be human-induced, including subsidence due to groundwater and hydrocarbon extraction. GIA includes the vertical rebound of the Earth's surface occurring in response to unloading following the retreat of glaciers. Tectonic uplift dominates RSLR at specific locations such as the northern California Coast south of Cape Mendocino where the Earth's surface is rising at rates up to 3 mm/year because of building strains along the Cascadia Subduction Zone (NRC 2012). Sediment compaction, either natural or human-induced, is often referred to as subsidence.

VLM is responsible for significant variations in RSLR rates around the US, as measured by tide gauges in the last century (e.g., see Figure 8.2). For example, the extremely high rates of RSLR experienced in coastal Louisiana result from natural compaction of ancient Mississippi River sediment deposits, which can be the dominant VLM mechanism in some locations. In contrast, the very high rates of RSLR in the Galveston, Texas area are primarily caused by subsidence related to both groundwater and hydrocarbon extraction. Finally, the negative values of RSLR (i.e., relative sea level is falling) experienced in Alaska are due to GIA. The magnitude of both natural and human-induced local variations can exceed the magnitude of regional and global sea level change in some locations (Nicholls et al. 2014).

8.1.1.3. Other Regional Variations in Relative Sea Level

In addition to variations caused by VLM, sea level rise is not evenly distributed across the oceans because of other regional variations in some of the controlling physical processes. Regional variations in relative sea level result from differences in thermal expansion, long term fluctuations in meteorological conditions (wind and atmospheric pressure patterns due to decadal-scale phenomena), changes in ocean circulation, and changes in the regional gravity field caused by the redistribution of ice melting from continental-scale ice sheets that exert a gravitational pull on the ocean water. Changes in the location and strength of ocean currents and/or prevailing winds, as well as in the distribution of heat and salt in the ocean, can induce "dynamic" sea level changes. One type of dynamic change that would affect the US Atlantic coast would be a change in the amount of heat being transported poleward by the Gulf Stream (Kopp 2013, Sallenger et al. 2012). Another dynamic change would result from Antarctic melt: as very large ice sheets melt, their gravitational pull is reduced, causing migration of water away from the ice sheet. Near the ice sheet, sea levels fall despite the addition of melt water and beyond that distance, ocean levels increase at a rate greater than GMSLR (Mitrovica et al. 2011). The effect of melting Antarctic ice sheets will be significantly increased RSLR in the Boston

area and other northern latitudes as discussed in the next section (Douglas et al. 2016a). This effect is sometimes referred to in the literature as ice sheet fingerprinting.

Coastal engineering practice has traditionally considered GMSLR and VLM when evaluating RSLR at specific locations for design, but not these other regional phenomena affecting RSLR. That is likely changing now, as new tools like Sweet et al. (2017a) become available (see Section 8.1.3).

BOTTOM LINE: GMSLR is occurring and coastal transportation projects will be exposed to the effects of RSLR, which varies from the GMSLR (higher at many locations) because of VLM and other regional variations in oceanography and meteorology, each providing their own unique contributions.

8.1.2. Sea Level Rise Projections

Future sea levels are a key issue for design of coastal infrastructure. The rate of GMSLR has already doubled since 1993 compared to the rise observed since 1900 (Sweet et al. 2017b) and future predictions using empirical and theoretical models of ice sheet processes, global sea level, and global climate all confirm that continued warming will contribute to melting of land-based ice in glaciers and ice sheets, as well as continued thermal expansion of the ocean (NRC 2012, Church et al. 2013). This section outlines current projections of future sea levels, discusses the science underlying those projections, and presents the ranges of uncertainties in those projections.

An example of a scientific projection of future GMSLR is shown in Figure 8.4. This projection is for GMSLR of 83 centimeters (cm) by the year 2100. The low and high range of estimates are shown to account for the uncertainties in the best-available science. The range is from 50 to 140 cm by 2100. The detailed explanation of the projection and its range can be found in NRC (2012). Figure 8.4 illustrates several characteristics typical of GMSLR projections. **First, all the projections are for increasing sea levels and almost all of them are for increasing rates of sea level rise (i.e., positive curvature). Second, all investigators are aware of and stress the uncertainty in the projected values.** This includes model uncertainties inherent in simplified models of the physical processes and data uncertainties attributed to natural variability in the oceans and atmosphere as well as those related to social behavior leading to alternative scenarios for future emissions of greenhouse gases.

The range of probabilistic uncertainty for sea level rise projections is represented schematically in Figure 8.5. Any projection will have a distribution of possible results (black lines) around a central estimate (red line) as shown for Representative Concentration Pathway (RCP) 2.6. Within that range will be a probabilistic distribution of values also shown schematically and labelled "Conditional Probabilities." As can be seen in the figure, the three conditional RCP distributions overlap though their central estimates remain unique.

Another example of scientific projections of future GMSLR is shown in Figure 8.6 (Kopp et al. 2014). These projections correspond to three RCPs and include the median values of GMSLR from 2000 as well as estimates of the probability distribution about those median values. **The median value by 2100 for RCP4.5/6.0 is 0.59 m of rise,** with a 90-percent confidence the value

will be between 0.36 m and 0.93 m. The RCP8.5 projections are higher (median of 0.79 m), and the RCP2.6 projections are lower (median of 0.50 m).

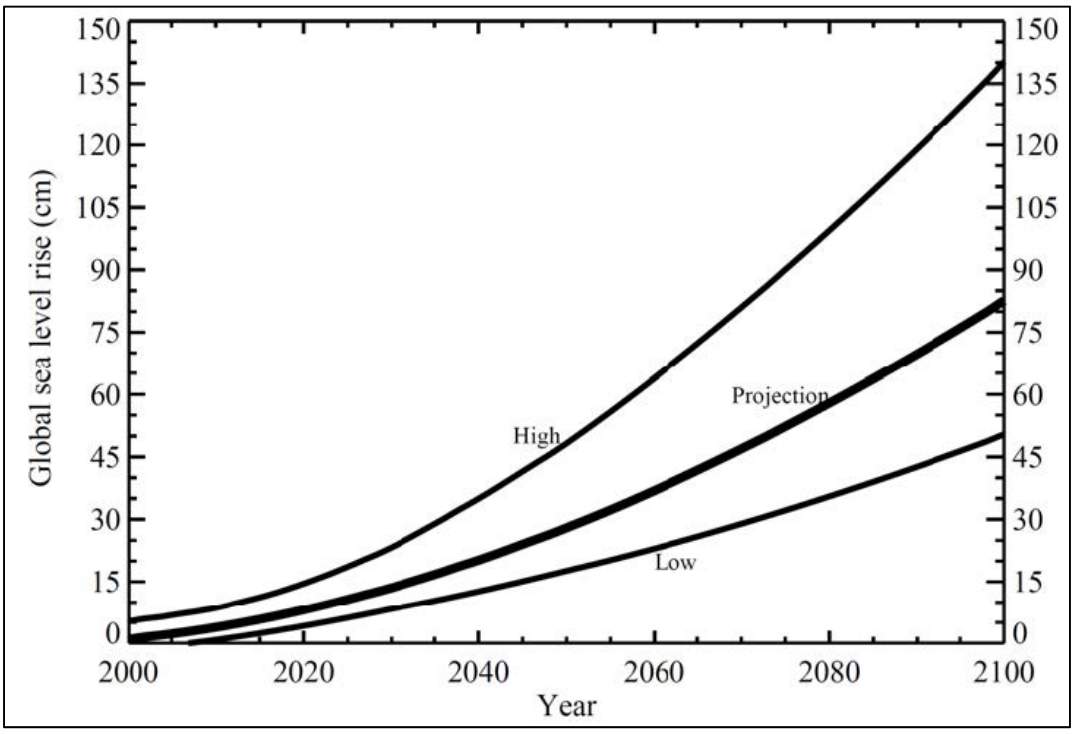

Figure 8.4. Global mean sea level rise projection (from NRC 2012).

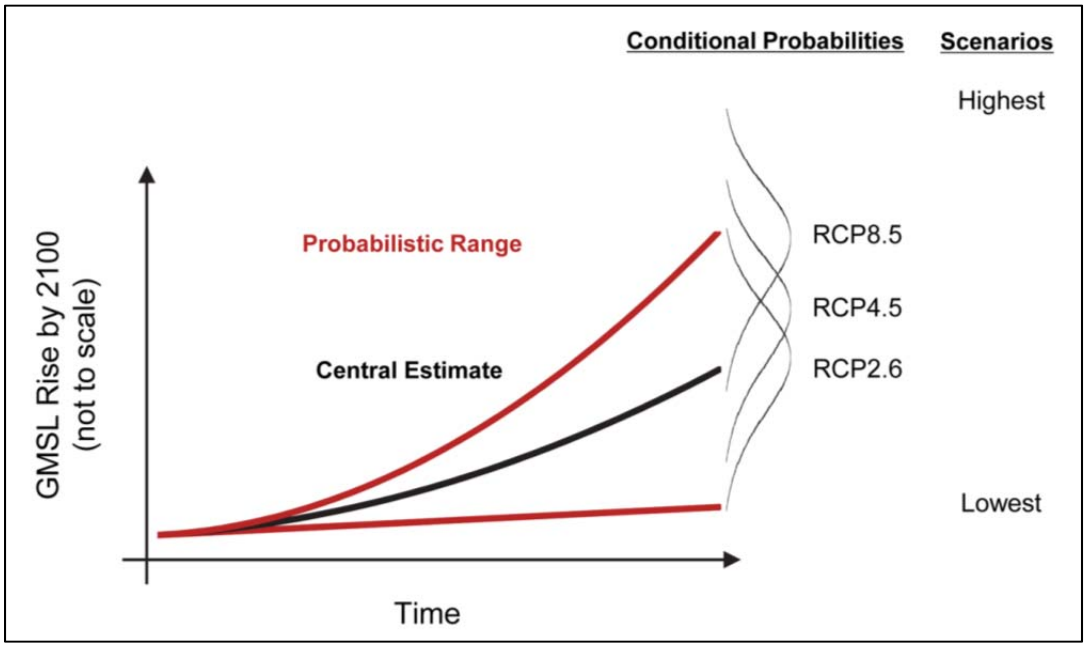

Figure 8.5. General relationship between the central estimate and probabilistic range of sea level rise and the relationship between RCP-based scenarios (from Sweet et al. 2017a).

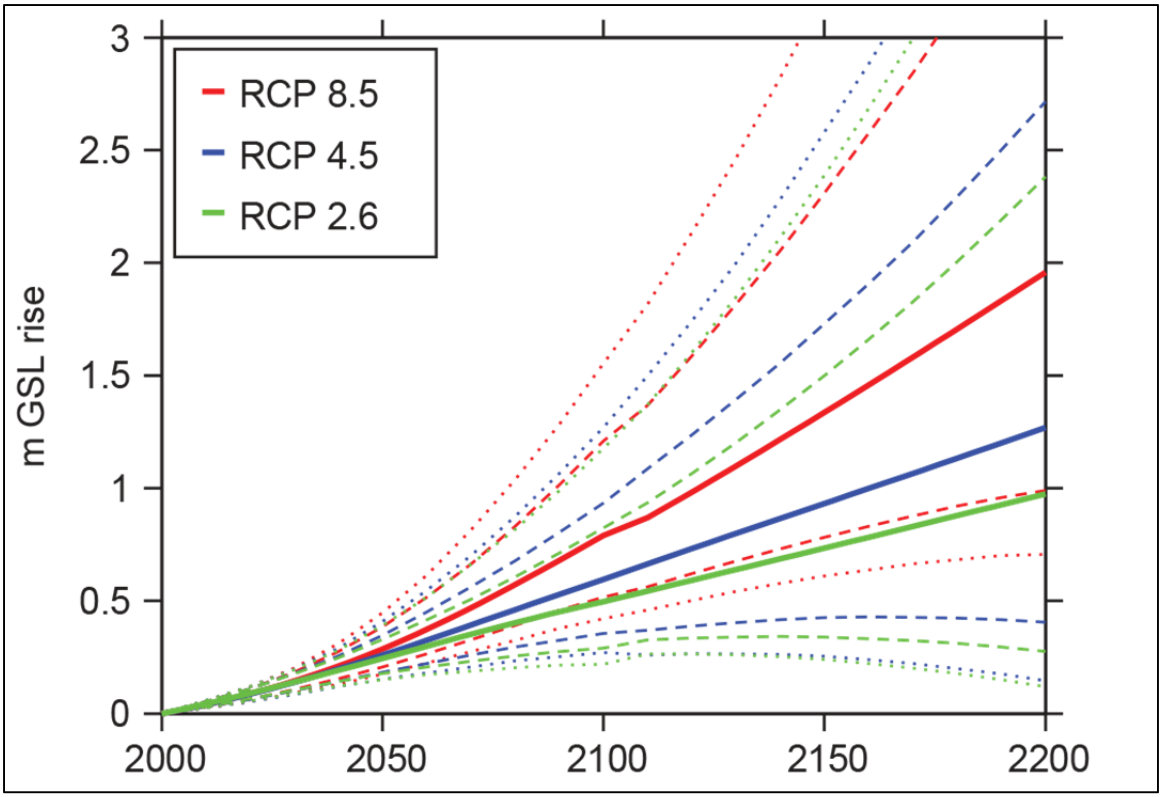

Figure 8.6. Global mean sea level rise (GMSLR) projections with probabilities (from Kopp et al. 2014; solid lines = median, dashed = 5th-95th percentile, dotted = 0.5th-99.5th percentile).

Scientific estimates of projected sea levels can be developed using several methods:

1. Extrapolating historical trends.
2. Using process-based physical models that simulate the effects of future warming.
3. Using semi-empirical models that employ a hybrid process-empirical model.

Extrapolating historical trends ideally requires at least 50 years of record and can be useful for projecting RSLR but does not account for anticipated sea level rise acceleration. Because of this, extrapolation is generally only adequate for near-term projections (Nicholls et al. 2014). Such near-term (i.e., a few years) projections are impractical for engineering design that requires longer project lifespans. Process-based models, such as GCMs, simulate the physics of thermal expansion and ocean dynamics, but require projected changes resulting from land-based ice simulated by ice sheet dynamic model output to be added. Semi-empirical models link global temperatures and sea level and assume historical relationships between GMSLR rise and global temperatures will persist. Interpolation of the historical trend and semi-empirical models are much less computationally intensive than process-based models but can suffer from oversimplification.

Figure 8.7 compares future GMSLR projections (from a baseline year of 2005) for a site in New England, using all three projection methods. Linear extrapolation (represented by the green line) yields the lowest value and is likely to underestimate future sea level rise because it only represents the mechanisms that dominated in the past and assumes that the rate of change

remains constant into the future. Thermal expansion, melting glaciers, and terrestrial water storage explains approximately 65 percent of the observed GMSLR for 1901–1990 and 90 percent for 1971–2010 and 1993–2010 (Church et al. 2013). Later in the 21st century, ice melt from Greenland and the Antarctic are expected to play an increasingly important, and likely dominant, role in GMSLR (Rignot et al. 2011). Hence, projections from linear extrapolation will increasingly underestimate GMSLR beyond the current timeframe.

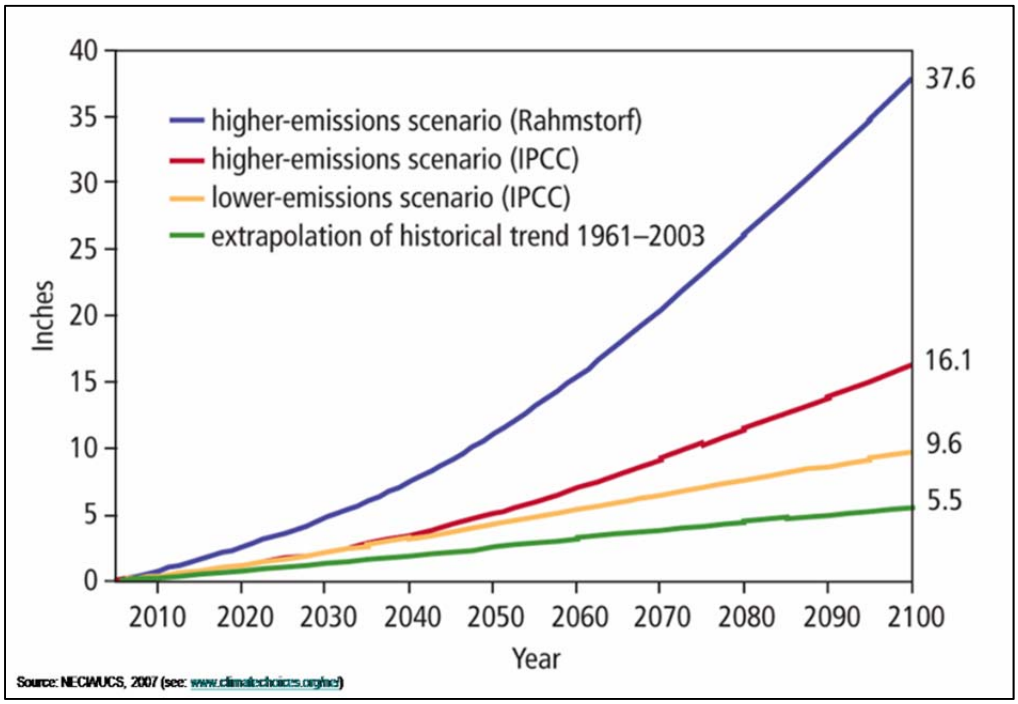

Figure 8.7. Example of sea level rise projections (baseline 2005) using linear extrapolation of historical sea level trend (green), lower and higher emissions estimates from process-based models (yellow and red; from IPCC 2007) and higher emissions estimates a semi-empirical model (blue; from Vermeer and Rahmstorf 2009). Source: unpublished figure from Frumhoff et al. 2007.

The yellow and red lines in Figure 8.7 represent GMSLR projections resulting from thermal expansion alone from process-based models, under emission scenarios predating the RCP scenarios, from IPCC (2007). These methods yield estimates of GMSLR by 2100 that are nearly double and triple, respectively, the linear interpolation method even though they are only based on thermal expansion and ignore land-based ice melt. Finally, the purple line shows GMSLR estimates from a semi-empirical modeling approach (Vermeer and Rahmstorf 2009) that includes both thermal expansion and land-based ice melt, emphasizing the importance of understanding the method, and its limitations, used in estimating future GMSLR projections.

Ranges of available projections of GMSLR vary significantly, as shown in Figure 8.8. The overall spread of these projections should provide the design engineer with an appreciation of the level of uncertainty involved in future sea level rise estimation. Table 8.1 lists the upper and lower bounds of GMSLR projections shown in Figure 8.8 and their sources. All of these projections were published since the IPCC fourth assessment report (AR4) was released in 2007. However, these do not include the most recent estimates of Sweet et al. (2017a, 2017b) that include revisions to the upper bound based on emerging research on ice sheet stability.

The IPCC (2013) offered "likely" ranges for GMSLR, but did not offer "very likely" ranges because of the limitations of process-based models, especially with respect to ice sheet dynamics. As with the IPCC (2007) estimates, the range of projected GMSLR reported by the IPCC (2013) is generally thought to be an underestimate. In general, GMSLR projections made since 2007 are constrained between 0.2 and 2 m, although there are some exceptions. The median, 25th, and 75th percentiles of the upper and lower bounds of these projections are also presented in Table 8.1. The median lower bound GMSLR projection is 0.5 m (with 0.2 and 0.7 m as 25th and 75th percentiles, respectively). The median upper bound GMSLR projection is 1.4 m (with 0.9 and 2.0 m as 25th and 75th percentiles, respectively). The range of GMSLR projections by semi-empirical models tends to be higher than those reported by the IPCC. For instance, none of the IPCC "likely" range projections (source numbers 1, 2, 16, 17) exceeds 1 m by 2100, while the projections based on semi-quantitative models (source numbers 3 through 8) exceed 1 m in five out of six cases.

According to Nicholls et al. (2014), 21st century GMSLR less than 1 m is still considered more likely. In fact, **an elicitation of expert opinion by Horton et al. (2014) reports a median likely range of 0.4 to 0.6 m by 2100**, which offers hope that limiting GMSLR to less than 1 m is still possible with climate mitigation initiatives. However, under the higher warming scenarios the median likely range of expert elicitation was 0.7 to 1.2 m of GMSLR by 2100. Bamber and Aspinall (2013) elicited expert opinion focused on ice sheet dynamics and reported a range of 0.33 to 1.32 m by 2100 under the RCP4.5 emissions scenario. However, there is still considerable scientific support for GMSLR up to and even exceeding 2 m by 2100; thirteen out of the 90 experts surveyed by Horton et al. (2014) estimated a 17-percent probability of exceeding 2 m by 2100. Sweet et al. (2017b) concludes that "emerging science regarding Antarctic ice sheet stability suggests that, for high emissions scenarios, a GMSLR rise exceeding 8 feet (2.4 m) by 2100 is physically possible." **Hence, selecting mid-range estimates for adaptation strategies related to GMSLR may not offer the protectiveness that engineering typically requires**.

It is common practice for planning purposes to develop a range of scenarios of future sea levels that are consistent with these scientific estimates, but not specifically based on any one of them. *Scenarios* are defined typically by the increase in GMSLR by the year 2100 in equal increments (NRC 1987, Parris et al. 2012, Melillo et al. 2014, USACE 2014, Sweet et al. 2017a).

Historical sea level rise data and future sea level rise projections as scenarios from the third National Climate Assessment (NCA3, Melillo et al. 2014) are shown in Figure 8.9. For the fourth National Climate Assessment (NCA4, Sweet et al. 2017b), these have been updated to use the Interagency sea level rise scenarios from Sweet et al. (2017a), which are presented in the subsequent text. However, this figure still illustrates two important aspects of sea level rise projections: first, a lower limit projection of 0.66 feet (0.2 m) considers only the existing background rate; and second, the upper limit may be significantly higher than 4 feet (and in fact NCA4 uses an upper bound of 8 feet; Sweet et al. 2017b) because of inherent uncertainties primarily related to ice sheet dynamics.

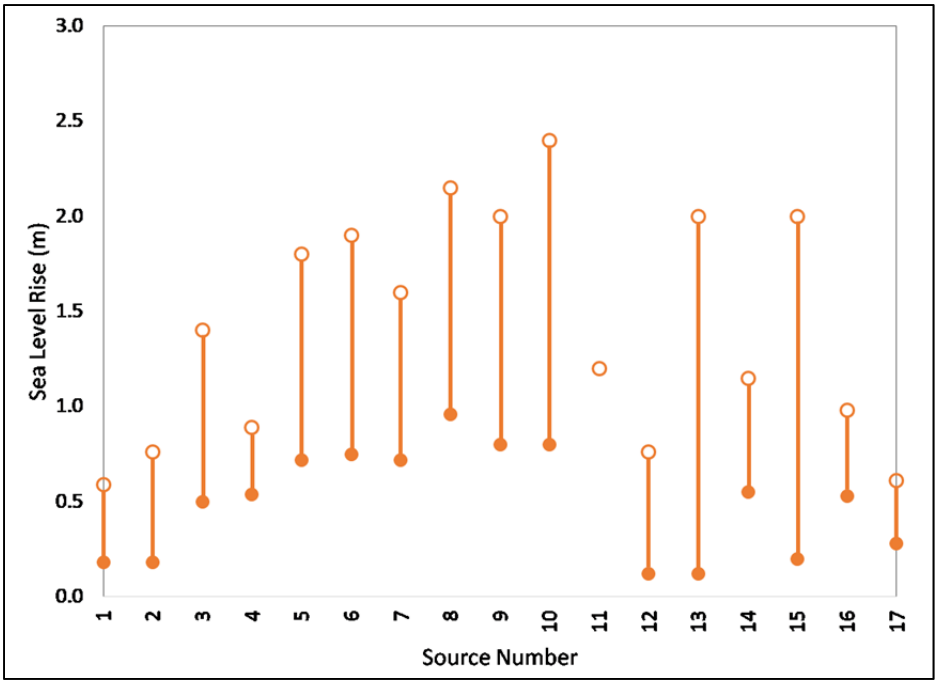

Figure 8.8. Range of global mean sea level rise (GMSLR) projections for the 21st century (adapted from Nicholls et al. 2014; used with permission). Sources listed in Table 8.1.

Table 8.1. Comparison of global mean sea level rise (GMSLR) projections for the 21st century. (Source: modified from Table 3 in Nicholls et al. 2014; used with permission).

Number	Source[A, B]	Type[A]	Lower (m)	Upper (m)	Comments[A]
1	IPCC AR4 (2007)	Physical model	0.18	0.59	without future ice sheet melt acceleration
2	IPCC AR4 (2007)	Physical model	0.18	0.76	with future ice sheet melt acceleration
3	Rahmstorf (2007)	Semi-empirical	0.5	1.4	
4	Horton (2008)	Semi-empirical	0.54	0.89	
5	Vermeer & Rahmstorf (2009)	Semi-empirical	0.72	1.8	includes upper & lower uncertainty bounds
6	Jevrejeva (2010)	Semi-empirical	0.75	1.9	
7	Grinsted (2010)	Semi-empirical	0.72	1.6	based on Moberg temperatures
8	Grinsted (2010)	Semi-empirical	0.96	2.15	based on Jones and Mann temperature
9	Pfeffer (2008)	Evidence based	0.8	2	based on physical constraints
10	Rohling (2008)	Evidence based	0.8	2.4	based on surrogate data
11	Grant (2012)	Evidence based		1.2	only upper limit given
12	UKCP09 (2009)	Expert reasoning	0.12	0.76	from IPCC range
13	UKCP09 (2009)	Expert reasoning	0.12	2	from H++ range
14	Katsman (2011)	Expert reasoning	0.55	1.15	
15	Parris et al (2012)	Combination	0.2	2.0	lower bound from linear interpolation
16	IPCC AR5 (2013)	Physical model	0.53	0.98	medium confidence likely range for RCP 8.5
17	IPCC AR5 (2013)	Physical model	0.28	0.61	medium confidence likely range for RCP 2.6
Note: [A]see Nicholls et al., 2014 for details.					
[B]Vermeer & Rahmstorf (2009), Parris et al. (2012) and IPCC (2013) results added to projections in Table 3 of Nicholls et al., 2014.					
		Summary statistics			
		N	16	17	
		Upper quartile	0.7	2.0	
		Medan	0.5	1.4	
		Lower quartile	0.2	0.9	

HEC-25 Volume 2 recommends the use of the NCA3 values in Figure 8.9 or the NRC (2012) values in Figure 8.4 in coastal vulnerability assessments when VLM is accounted for to develop an estimate of future RSLR (Douglass et al. 2014). The procedure outlined in HEC-25 Volume 2 does not account for the other regional processes that can affect RSLR including changes in ocean currents and land ice melt effects (see Section 8.1.1.3). Furthermore, future VLM rates are assumed to remain unchanged.

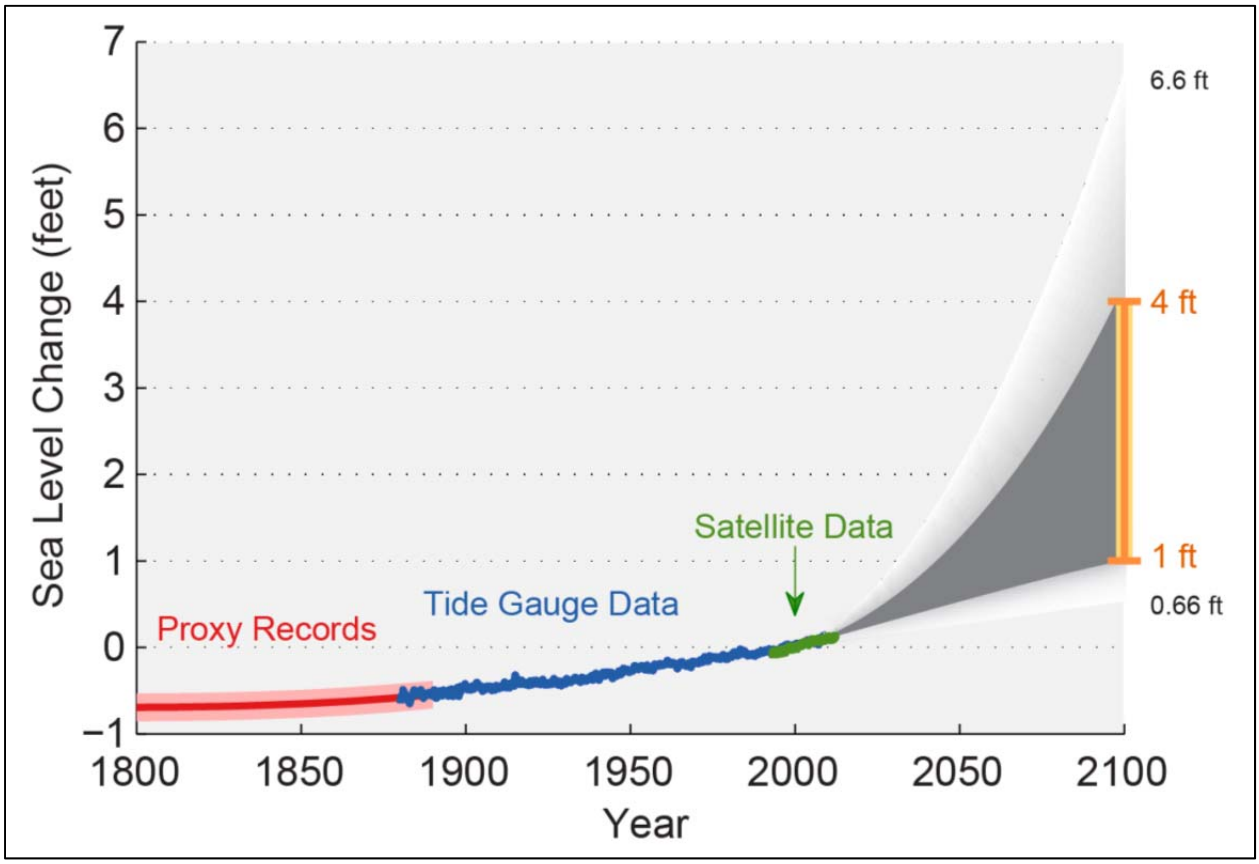

Figure 8.9. GMSLR data and projections from NCA3 (Melillo et al. 2014).

Hall et al. (2016) developed detailed scenarios of RSLR at Department of Defense facility locations based on five GMSLR scenarios. The RSLR scenarios included all the physical process components of sea level discussed above: GMSLR, VLM, and other processes including regional differences in thermal expansion and meteorology, changes in ocean circulation, and land ice melt effects.

The most recently published set of GMSLR and RSLR scenarios for the US coast are those of Sweet et al. (2017a); these are also used in NCA4 (Sweet et al. 2017b). Sweet et al. (2017a) is a NOAA Technical Report from the Sea Level Rise and Coastal Flood Hazard Scenarios and Tools Interagency Task Force jointly convened by the U.S. Global Change Research Program (USGCRP) and the National Ocean Council. The task force charge was to develop and disseminate, through interagency coordination and collaboration, future RSLR and associated coastal flood hazard scenarios and tools for the entire United States. The report provides detailed estimates of projected RSLR at thousands of locations, including at all the tide gauges around the

US coast for each decade in the 21st century, plus several other times extending to the year 2200. A table with detailed projections can be downloaded from the NOAA website. The RSLR projections include both the GMSLR and the regional differences including all the other physical process components of sea level rise as in Hall et al. (2016). The RSLR projections were developed for six GMSLR scenarios of 0.3, 0.5, 1.0, 1.5, 2.0, and 2.5 m of GMSLR between 2000 and 2100. These GMSLR scenarios are shown in Figure 8.10 with historical sea level rise data. Sweet et al. (2017a) increases the lower bound suggested by Parris et al. (2012) and used in the NCA3 by 0.1 m to 0.3 m and increases the upper bound by 0.5 m to 2.5 m. The reader is alerted to the fact that GMSLR increments may also vary across studies due to the initial year to which they are referenced. For example, the values provided in NCA3 are referenced to the midpoint of the 1983-2001 National Tidal Datum epoch, whereas newer values provided in NCA4, and some other recent studies, use the year 2000.

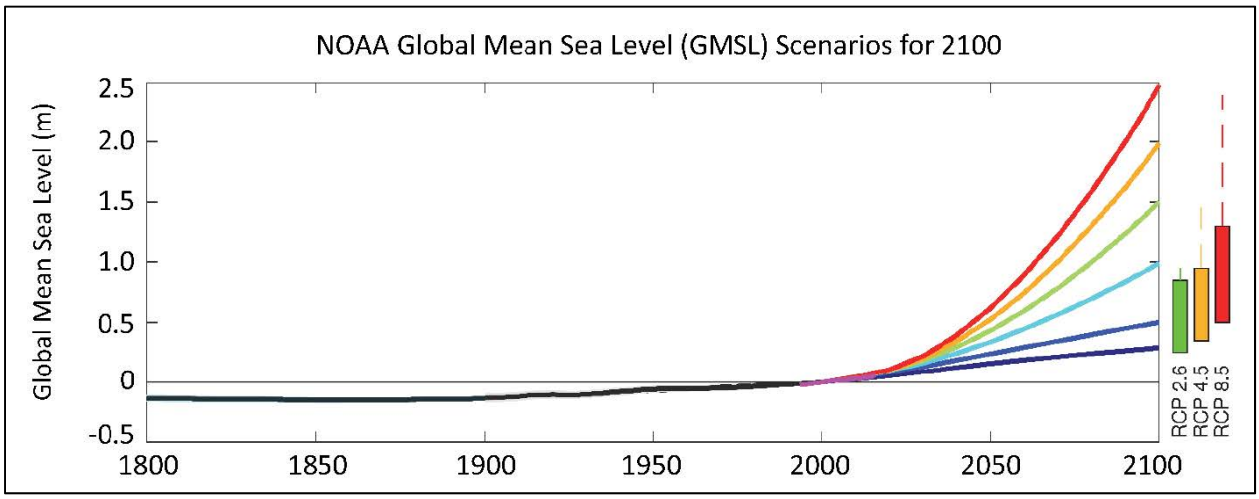

Figure 8.10. GMSLR data and projections from Sweet et al. (2017a) with central probability ranges and extremes of RCP-based projections, as used in NCA4 (Sweet et al. 2017b).

Figure 8.10 displays the 90-percent probability range of RCP-based GMSLR projections. The dashed lines above the boxes indicate the magnitude of higher estimates resulting from ice sheet processes (see Sweet et al. 2017a). These RCP-based projections are not those from IPCC (Church et al. 2013) but are from more recent, similar analyses by Kopp et al. (2014). These RCP-based projections have slightly increased values and broader ranges than those from the IPCC. It should be noted that the probabilities, or likelihoods, of these GMSLR projections, as well as their uncertainties, are tempered by the epistemic uncertainty associated with the RCP assumptions regarding human intervention in future emissions.

Figure 8.11 shows RSLR scenario projections from Sweet et al. (2017a) at four locations on the US coast. The scenario names are defined as the following quantities of GMSLR in the 21st century: Low = 0.3 m, Intermediate-Low = 0.5 m, Intermediate = 1.0 m, Intermediate-High = 1.5 m, High = 2.0 m, and Extreme = 2.5 m. The Low and Extreme scenarios represent the scientifically plausible lower and upper limit to GMSLR, and the other four scenarios are set at 0.5 m intervals within those limits.

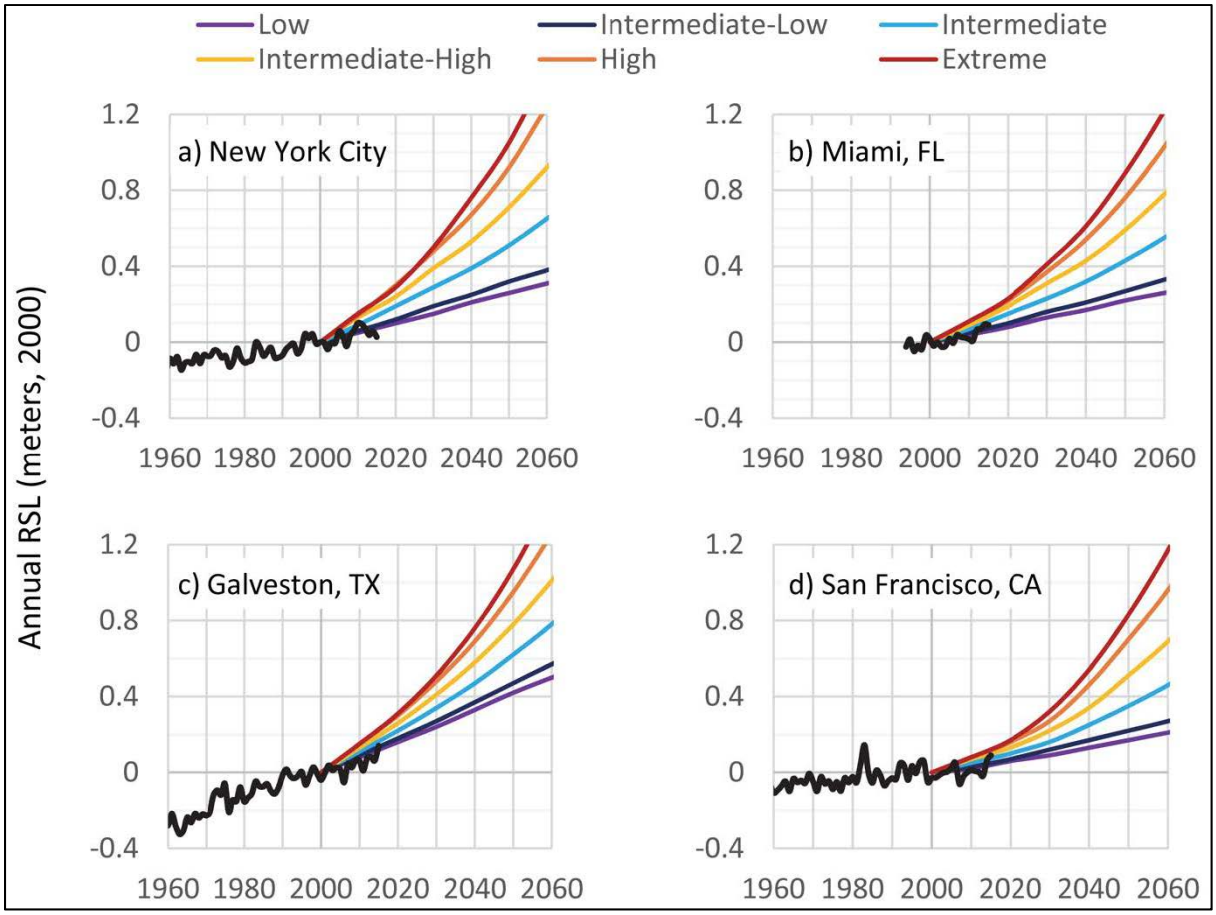

Figure 8.11. RSLR, scenario projections at four US locations (from Sweet et al. 2017a).

The RSLR rates in Figure 8.11 vary with location for the same GMSLR because of VLM and the other processes influencing RSLR. Also shown in the plots are the actual measured RSL values from those tide gauges (annual averages) from 1960 to 2015. Plotted this way, the gauge data show the annual variability of RSL including a 15-year period of overlap with the projections. In general, visual inspection of Figure 8.11 indicates that the range of the annual variability is bounded by the Intermediate-High (1.5 m) scenario and the trend is very roughly similar to the Intermediate-Low (0.5 m) scenario.

Figure 8.11 shows the median value of the RSLR projections for each scenario. An estimate of the range about that median, suitable for probabilistic analysis, is also provided in the data output tables of Sweet et al. (2017a). For each of the six GMSL scenarios, at each location, there is a low, medium and high sub-scenario, corresponding to the 17th, 50th, and 83rd percentile of the climate-related sea level projections consistent with the seven GMSLR scenarios. The Sweet et al. (2017a) scenarios, including median and probability distributions, are included in a recent version of the USACE Sea Level Change Curve Calculator (USACE 2017a).

BOTTOM LINE: The rate of GMSLR is projected to increase significantly throughout this century (and the next). The median projections for GMSLR this century range from about 0.5 m to 0.8 m depending on RCP. The uncertainty in those values is significant with a scientifically plausible upper bound of 2.5 m.

8.1.3. Selecting Sea Level Rise Scenarios for Design

Coastal engineering practice has evolved over the past several decades toward including sea level rise in design and planning as the long-term effects of the process have become more obvious. Prior to this period, there was a realization of the role of sea level rise in the geomorphological shaping of the coast, but its importance in establishing design water levels was largely minimized by assuming a rate of 1 to 2 mm/year for consideration in the design of projects with 50-year life spans (USACE 1984). Previously, the order of magnitude of sea level rise was dwarfed by the other factors involved in design water level decisions including tides and storm surge elevations (and the uncertainties in estimating those values).

NRC (1987) began to change the perception of the importance of sea level rise within the coastal engineering practice community. USACE guidance evolved to discussions of sea level rise and provided limited recommendations to use RSLR based on projections of the historical linear rate (USACE 2006). Considerations of sea level rise projections are now frequently included in planning and design, both in government and private practice. This is true for both the design of traditional infrastructure (seawalls, jetties, etc.) as well as the nature-based solutions (e.g., beach nourishment and living shorelines). The USACE now has explicit guidance on the inclusion of sea level rise for planning and design which is evolving to continue to reflect the best available science (e.g., USACE 2014, Hall et al. 2016, USACE 2017a). The USACE guidance includes tools for assessing local relative sea level change, as well as the uncertainty in that assessment, and it explains the assumptions for non-linear additions to direct extrapolation from gauge records.

Within FHWA guidance, the consideration of sea level rise has similarly evolved. HEC-25 (second edition) discussed sea level rise along with tides and storm surge, but did not provide specific guidance (Douglass and Krolak 2008). It was recognized that historical sea level rise has been indirectly accounted for in design of coastal transportation infrastructure because of its effect on epoch-based tidal datums and its fundamental controlling influence on other coastal processes. In HEC-25 Volume 2, sea level rise was given emphasis because of its critical role and recommendations were provided on how to incorporate sea level rise in vulnerability assessments of coastal transportation infrastructure to extreme events and climate change (Douglass et al. 2014). The approach recommended in that document was to incorporate GMSLR projections from either the NCA3 (Melillo et al. 2014) or NRC (2012) with local estimates of VLM derived from the NOAA tide gauges. The simple, second-order polynomial model (NRC 1987, USACE 2014) was recommended for developing the timing of the curves up to a designer-selected magnitude of sea level rise at the year 2100. No specific recommendation for appropriate 2100 values was provided for either planning or design because of the uncertainties in the science and the need to allow the engineer/decision maker flexibility in determining the appropriate level of risk tolerance for any specific project. As expected, newer GMSLR guidance in the forms of NCA4 (Sweet et al. 2017b), and many of the documents cited previously, has been developed in the intervening period. It is expected that the FHWA guidance in HEC-25 will be similarly updated in an upcoming third edition.

8.1.3.1. Factors of Safety and Conservatism

Most of the recent literature focuses on the critical upper bounds of sea level rise to be "conservative," i.e., higher than the median, for planning and engineering purposes. The median values of the sea level rise projections are not as frequently discussed in the literature, yet there are design situations where their use would be valuable. Coastal engineering has a tradition of application of analysis tools and inputs which are not "conservative" by themselves. It is incumbent on the engineer to address the appropriate factor of safety at some point in the design process. This is largely the result of the implicit uncertainties associated with describing the magnitudes of the coastal hazards themselves.

For example, Hudson's Equation, the most commonly used method for selecting the weight of armor stones in a revetment or seawall exposed to waves, has no inherent factor of safety. For a given weight, 5 percent of the stones will experience movement for those wave conditions according to the original laboratory tests by Hudson. Thus, designers often increase the median weight of the stones estimated from the equation, or alternatively, use a "conservatively" high estimate of design wave height in the equation. This type of approach is commonplace in coastal engineering design.

Formal design codes have not been developed for many coastal engineering situations, so engineering judgment is commonly used in such design decisions. There are a few exceptions where formal guidance has been developed, such as wave-induced loads on coastal highway bridge piles. In those areas the "factor of safety" is addressed through load factors that have been developed (as high as 1.75) to account for the uncertainties in the underlying analysis approach.

With respect to the effect of sea level rise on design water levels, the engineer will almost certainly choose to use a more conservative value, say the 95th percentile value of the projections, for design of components and projects that are extremely sensitive to sea level (e.g., the low-chord elevation of new bridges over coastal waters exposed to hurricane waves). However, there are situations where an estimate of the median (50th percentile) value of the sea level rise projection will be valuable for planning and design. Many design decisions present trade-offs, and **there is a need for guidance on the median sea level rise projections for coastal engineering design** with the expectation that conservative engineering decisions will account for: the aleatory uncertainty related to the hazard; the epistemic uncertainty associated with the selection of a scenario; and the importance, or criticality, of the infrastructure.

8.1.3.2. Selection Criteria

Given the historical practices in coastal engineering design and the use of safety factors, selecting appropriate sea level rise projections for engineering assessment and design requires consideration of the following decision criteria:

- Risk tolerance, system sensitivity and redundancy (if little redundancy or high system sensitivity, then low risk tolerance and higher projection needed for design).
- Policy choices, e.g., protection or retreat.
- Timeframe, e.g., short term preparation versus long term planning.

To date, engineering and planning studies have generally selected a range of low and high estimates to test the robustness of assessments and design parameters within this range.

Sensitivity analysis using extreme (upper bound) estimates are also recommended to highlight the limitation of current policies or thresholds for new actions, for example, when to consider switching from protection strategies to accommodation or retreat strategies (Nicholls et al. 2014). Selecting projections that represent multiple time frames can also elucidate when policy or design changes should be considered.

For example, the vulnerability assessment of the Central Artery/Tunnel system in Boston, Massachusetts (Bosma et al. 2015, Douglas et al. 2016a) selected several points along the highest GMSLR curve presented by Parris et al. (2012), which also coincided with later times along a lower curve. For example, point 2 in Figure 8.12 represents GMSLR by 2030 under the highest emissions scenario, and the same elevation at point 2a represents GMSLR by 2070 under the intermediate low emissions scenario (based on Parris et al. 2012). This is a particularly important point for design engineering decisions for projects that will have very long lives: future sea levels will most likely not be going down or leveling off; they are only going up for the foreseeable future. **Moreover, multiple pathways, or emission scenarios, may be followed to reach the same future global sea level; the only difference between them is the time required to reach that level**. Using this strategic selection of GMSLR estimates, three values were used to simulate six scenarios, offering a sensitivity analysis of both risk and timeframe.

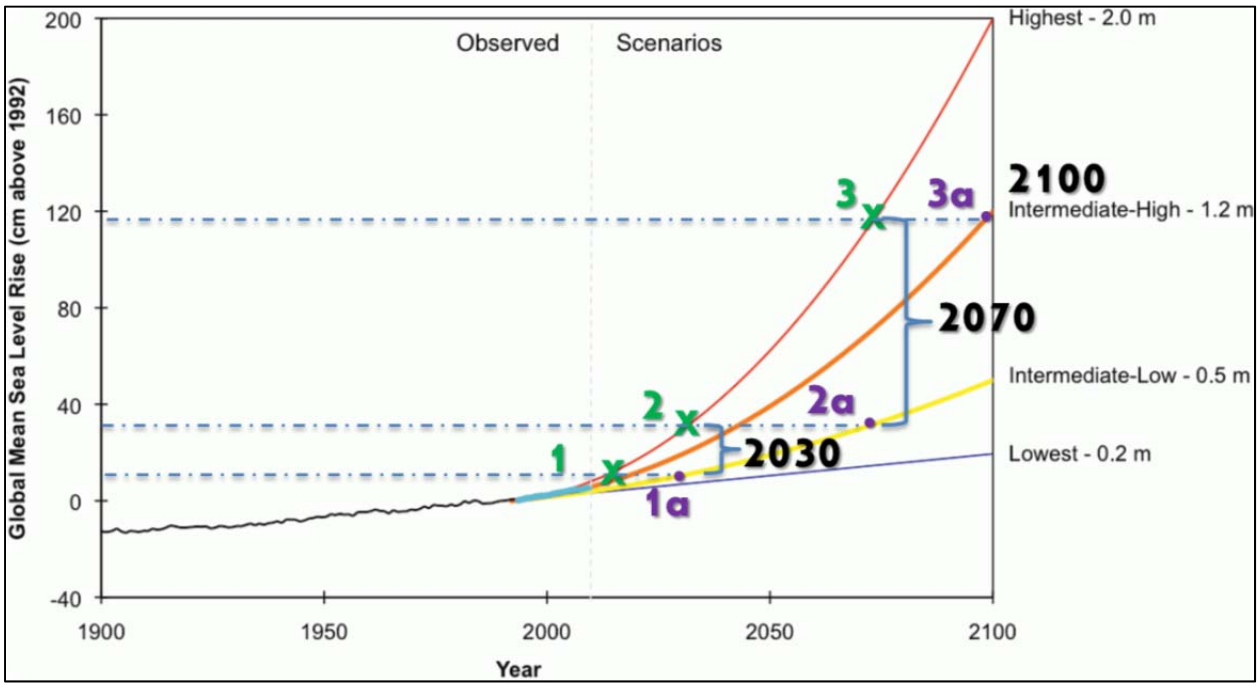

Figure 8.12. Selection of GMSLR projections for vulnerability assessment and adaptation strategies for the Central Artery/Tunnel system in Boston, MA Source; Bosma et al. (2015), Douglas et al. (2016a). Used with permission.

The RSLR projections presented in Douglas et al. (2016b) are an example of a probabilistic approach that accounts for the physical processes of importance (described in Section 8.1.1). The methodology produced a continuum of location-specific probability distributions (in this case, based on the tide gauge at Boston Harbor), informed by state-of-the-art process modeling, expert assessment, and expert elicitation. The RSLR projections shown in Table 8.2 aggregate the

components of sea level rise, including thermal expansion, regional ocean dynamics, changes in alpine glacier and ice sheet mass, land-water storage, and land subsidence, following the method outlined in Kopp et al. (2014). The script for this method is published with the supplemental materials and allows the user to apply this method to other locations with available tide gauge observations. The exceedance probabilities of future RSLR (converted from the cumulative probabilities output by the method) can be linked to the analysis of specific threats such as storm surge and the time-evolving flood protection appropriate for specific assets.

Table 8.2. RSLR projections (in feet above year 2000 sea level) by exceedance probability and representative concentration pathway (RCP) for Boston Harbor, following Kopp et al. (2014). (Modified from Table 1-1 in Douglas et al. 2016b).

			Likely range					Maximum
	0.99	0.95	0.833	0.5	0.167	0.05	0.01	0.001
RCP8.5								
2030	-0.1	0.1	0.3	0.5	0.7	0.9	1.0	1.2
2050	0.1	0.4	0.7	1.1	1.5	1.8	2.1	2.4
2070	0.6	1.0	1.5	2.2	3.1	3.7	4.3	4.8
2100	1.6	2.4	3.2	4.9	7.4	8.6	9.5	10.5
2200	18.9	19.9	21.4	26.1	32.8	34.1	35.3	36.9
RCP4.5								
2030	-0.1	0.1	0.3	0.5	0.7	0.9	1.0	1.2
2050	0.1	0.4	0.7	1.0	1.4	1.7	2.0	2.3
2070	0.4	0.9	1.3	1.9	2.6	3.1	3.6	4.1
2100	0.9	1.7	2.4	3.6	5.1	6.1	7.0	8.0
2200	5.5	6.2	7.2	10.9	16.5	18.0	19.3	20.9
RCP2.6								
2030	-0.1	0.1	0.3	0.5	0.7	0.9	1.0	1.2
2050	0.1	0.4	0.6	1.0	1.4	1.7	2.0	2.3
2070	0.3	0.7	1.1	1.7	2.3	2.7	3.1	3.6
2100	0.4	1.2	1.8	2.8	3.8	4.6	5.3	6.2
2200	3.6	4.4	5.2	6.4	7.7	8.8	9.9	11.8

While sea level rise is being considered increasingly often in planning and design of transportation assets, its consideration is not universal, and there is confusion about the complexities of the science and the multiple scenarios. There is a need for sea level rise projection tools for engineering design which:

- Are simple to apply as a first approximation of the likely value of RSLR.
- Are scientifically complete and correct including uncertainties.

- Allow for quantitative risk-based sea level rise decisions.

The need for projection guidance that is simple to apply stems from the realization that sea level rise is an active area of highly technical scientific research. Highway engineers may not be able to follow the extensive scientific literature related to sea level rise projections, but need basic guidance. The focus of many of the sea level rise projections on the critical upper bounds of uncertainty may be obscuring the median value projections. **The need for scientifically complete/correct projections is met by much of the literature summarized above and the need for quantitative risk-based estimates, i.e., probabilities, is met by the most recent literature.**

While there is significant uncertainty related to the selection of any specific value as an estimate of a future sea level for design, hydraulic engineers often address significant uncertainty in other areas of design analysis through an understanding of the ranges and causes of the uncertainty in future sea level rise estimates.

BOTTOM LINE: Selecting appropriate sea level rise projections for engineering assessment and design requires consideration of risk tolerance, system sensitivity, and redundancy. To date, engineering and planning studies have generally selected a range of low and high estimates in order to test the robustness of assessments and design parameters within this range.

8.1.4. Recommendations

This section outlines recommendations concerning sea level rise for engineers tasked with design of coastal transportation infrastructure. There are three primary recommendations:

1. Future sea level rise should be included in coastal asset planning and design.
2. A specific set of values for projections of sea level throughout the remainder of this century are suggested for situations where an estimate of the median RSLR is appropriate.
3. Use more conservative estimates of future sea level rise when overall project performance is very sensitive to design sea levels, and/or when designing critical transportation infrastructure.

8.1.4.1. Include Sea Level Rise Projections in Design

Sea level rise should be considered in the design of transportation assets near the coast. Sea level rise is a well understood physical process that is a component of the coastal design environment (along with tide range, storm surge, waves, winds, soils, etc.) which is specific to every site. **Rising mean sea level can have significant effects on the long-term functionality and vulnerability of built transportation infrastructure near the coast and estimates of future RSLR projections should be used in planning and design**.

Many governmental organizations (including federal agencies, state governments and state DOTs, and local governments) have implemented guidance regarding appropriate sea level rise assumptions for planning and design. FHWA, through HEC-25 Volume 2, provides guidance using the GMSLR projections from either the NRC (2012) or the NCA3 (Melillo et al. 2014) for coastal vulnerability assessments. FHWA outlines a procedure similar to guidance developed by

the USACE (2014). Both recommend estimating future RSLR as the sum of GMSLR and "local" VLM. First, GMSLR is selected based on a year 2100 value (e.g., 4.0 feet by 2100 from one projection in Melillo et al. [2014]). Second, VLM is estimated based on the historical NOAA tide gauge linear rise rate minus the generally accepted value of the GMSLR for the past century (1.7 mm/year). The ***time rate*** of RSLR is estimated using the second-order polynomial equation from NRC (1987) with the linear coefficient set to 1.7 mm/year and the non-linear coefficient set to reach the 2100 value previously selected.

The guidance in this document recognizes that many choices are possible. Therefore, nothing in this guidance should be interpreted as countervailing to existing guidance.

8.1.4.2. Recommended Sea Level Rise Estimates

This section provides a simple set of recommendations for a range of very likely GMSLR outcomes by the year 2100. The range is bound by a specific recommendation for a minimum GMSLR of 0.59 m (1.94 feet) by the end of this century and an alternative scenario that yields a GMSLR of 1.21 m (3.96 feet) over that same time period. These recommendations are consistent with the latest guidance provided in USGCRP (2017), which describes the range of very likely GMSLR as 0.5 to 1.3 m (1.6 to 4.3 feet) by 2100 under RCP8.5. The next section provides a separate set of recommendations for estimating risk-based sea level rise for conservatism in planning and/or the design of critical infrastructure.

Planning and design should consider a range of sea level rise scenarios to properly account for uncertainties and risk, hence the minimum and alternative GMSLR scenarios described here. There are often trade-offs in design decisions and some engineering projects near the coast will not be particularly sensitive to the specific assumed design value of sea level rise. The recommended minimum GMSLR scenario is likely an appropriate design value under those circumstances. For infrastructure that is more sensitive to sea level rise, or a project with a longer service life, a practitioner may also want to consider the impacts of the alternative GMSLR scenario on project performance.

Developing an estimate of the recommended minimum value of RSLR for the planning or design horizon is the first step and considerations of uncertainty in that estimate for design can then be evaluated as needed by the design engineer. For these situations, the following simple procedure is recommended for developing an estimate of the median value of RSLR:

1. Develop an estimate of the existing, historical RSLR using the available nearby NOAA tide station analyses.
2. Adjust that value to develop an estimate of the VLM and other local effects/components by subtracting the longer term historical GMSLR rate (1.7 mm/year) from the historical RSLR rate, and convert the result to an elevation change by end of the desired time period (e.g., middle or end of the planning horizon).
3. Develop an estimate of the total GMSLR with any of the available projections discussed above (except the linear background rate) or the values shown in Table 8.3.
4. Combine the two elevation components, Step 2 and Step 3, to estimate the total RSLR for the planning horizon.
5. If needed for design, adjust that RSLR value to the NAVD88 datum.

Table 8.3. Recommended minimum GMSLR estimates for use in planning and design.

	Unit	2020	2030	2040	2050	2060	2070	2080	2090	2100
GMSLR (relative to MSL of 2000: mid-point of 1991-2009)	m	0.08	0.12	0.18	0.23	0.29	0.36	0.43	0.51	0.59
	ft	0.26	0.41	0.58	0.76	0.96	1.18	1.42	1.67	1.94

Table 8.3 provides estimates of GMSLR by decade for the remainder of this century. These are estimates for the 19-year averages centered on the decade relative to that of 2000. They must be adjusted with VLM and other local effects to obtain an estimate of RSLR at a specific location. The values shown in Table 8.3 were developed by using a second order polynomial equation (following NRC 1987 and USACE 2014) to model the GMSLR rate throughout the century to reach the target GMSLR by 2100 using the following equation:

$$GMSLR(\mathrm{t}) = \mathrm{a}(\mathrm{t} - 2000) + \mathrm{b}(\mathrm{t} - 2000)^2 \quad (8.1)$$

where:

a = 0.0034 m/yr or 0.011155 ft/yr.

b = 0.000025 m/yr^2 or 0.000082 ft/yr^2.

t = Time in years (≥ 2000).

A GMSLR of 0.59 m (1.94 feet) is the median (50th percentile exceedance probability estimate) for RCP4.5/6.0 from Kopp et al. (2014). This value is slightly higher than the IPCC mid-range projection for RCP4.5 of 0.52 m (Church et al. 2013), and it is lower than the mid-range projections for RCP8.5 (0.79 m).

The initial linear rate of rise in the equation is set to 3.4 mm/year. This initial rate corresponds to an estimate of the rate of GMSLR for the past two decades. Therefore, it is the most reasonable way to represent GMSLR from approximately the year 2000 to present. The values in Table 8.3 are within 0.02 m of the median projections of Kopp et al. (2014) for RCP4.5 throughout the century (and exactly equal in 2100).

This equation and the values in Table 8.3 are proposed here as a simple, reasonable estimate of the minimum projection of GMSLR for the design of transportation in the coastal environment. It is not a "conservative" projection as it is the median (50th percentile) value of the RCP4.5/6.0 scenario and it does not explicitly include any consideration of upper bound possibilities. It is essentially one reasonable answer to the question "What is likely to occur?" As a 50th-percentile estimate, there is a 50-percent probability that the actual value will be greater than this and a 50-percent probability that the actual value will be less than this (for that RCP4.5/6.0, based on Kopp et al. 2014).

The values in Table 8.3 are shown with the NOAA GMSLR projection scenarios from Sweet et al. (2017a) in Figure 8.13. The values of this recommendation are close to the NOAA Intermediate-Low scenario (0.5 m of GMSLR between 2000 and 2100). Recall (see Figure 8.10) that this Intermediate-Low scenario is relatively close to the middle of all three of the RCP-based projections from Kopp et al. (2014).

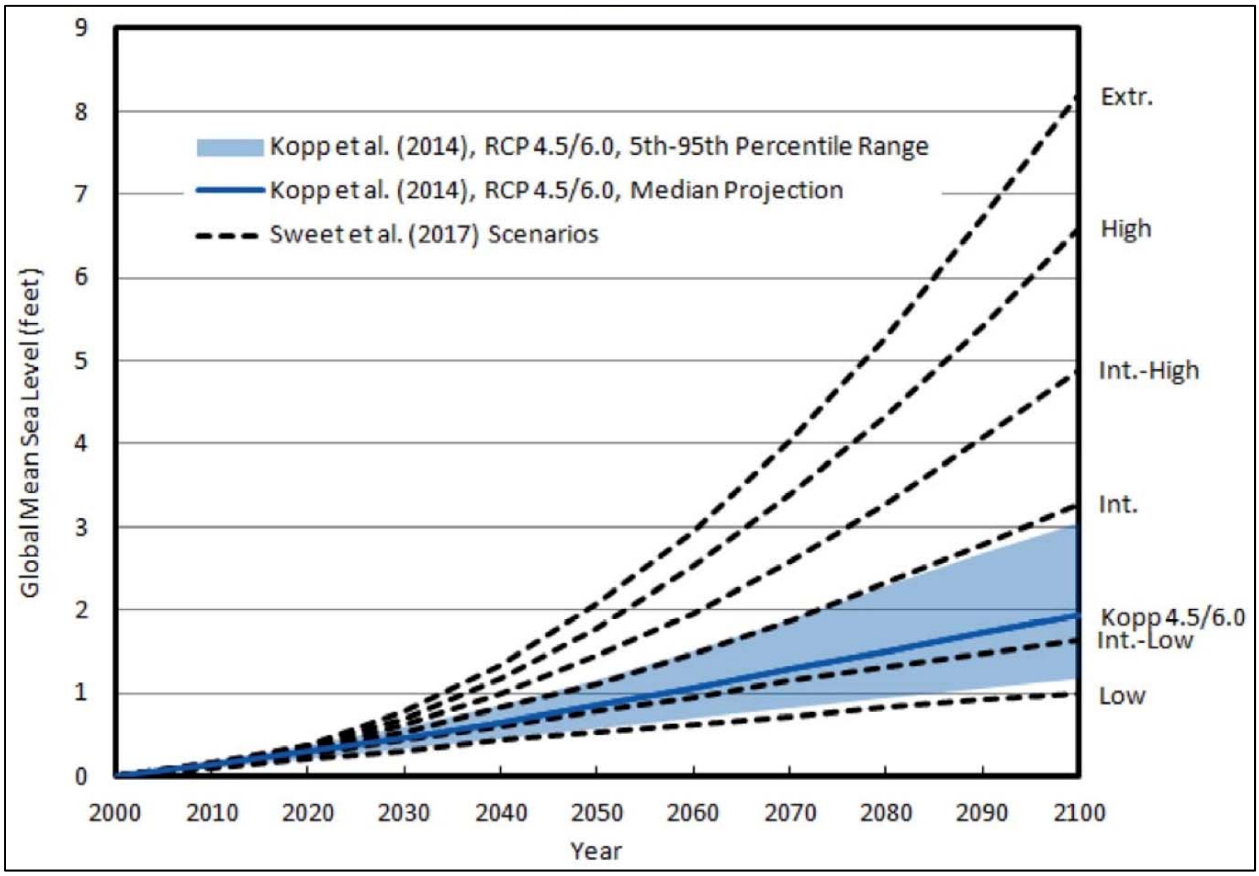

Figure 8.13. Recommended minimum (solid blue line) projection of GMSLR with the NOAA scenarios (dashed lines) from Sweet et al. (2017a).

For transportation projects that are more sensitive to sea level rise, or for projects expected to function well beyond 2100, consideration of a higher GMSLR outcome is appropriate as part of the engineering design process. The alternative GMSLR scenario recommended here, 1.21 m (3.96 feet), is the 95th percentile value for RCP8.5, as defined by Kopp et al. (2014). This GMSLR scenario is shown relative to the scenarios from Sweet et al. (2017a) in Figure 8.14. The 95th percentile scenario in that figure is represented by the upper edge of the blue shaded region. This alternative GMSLR outcome of 1.21 m (3.96 feet) lies between the Intermediate and Intermediate-High scenarios of Sweet et al. (2017a). When taken together with the recommended minimum GMSLR value of 0.59 m (1.94 feet), this alternative recommendation defines a reasonable range for the design of coastal transportation infrastructure.

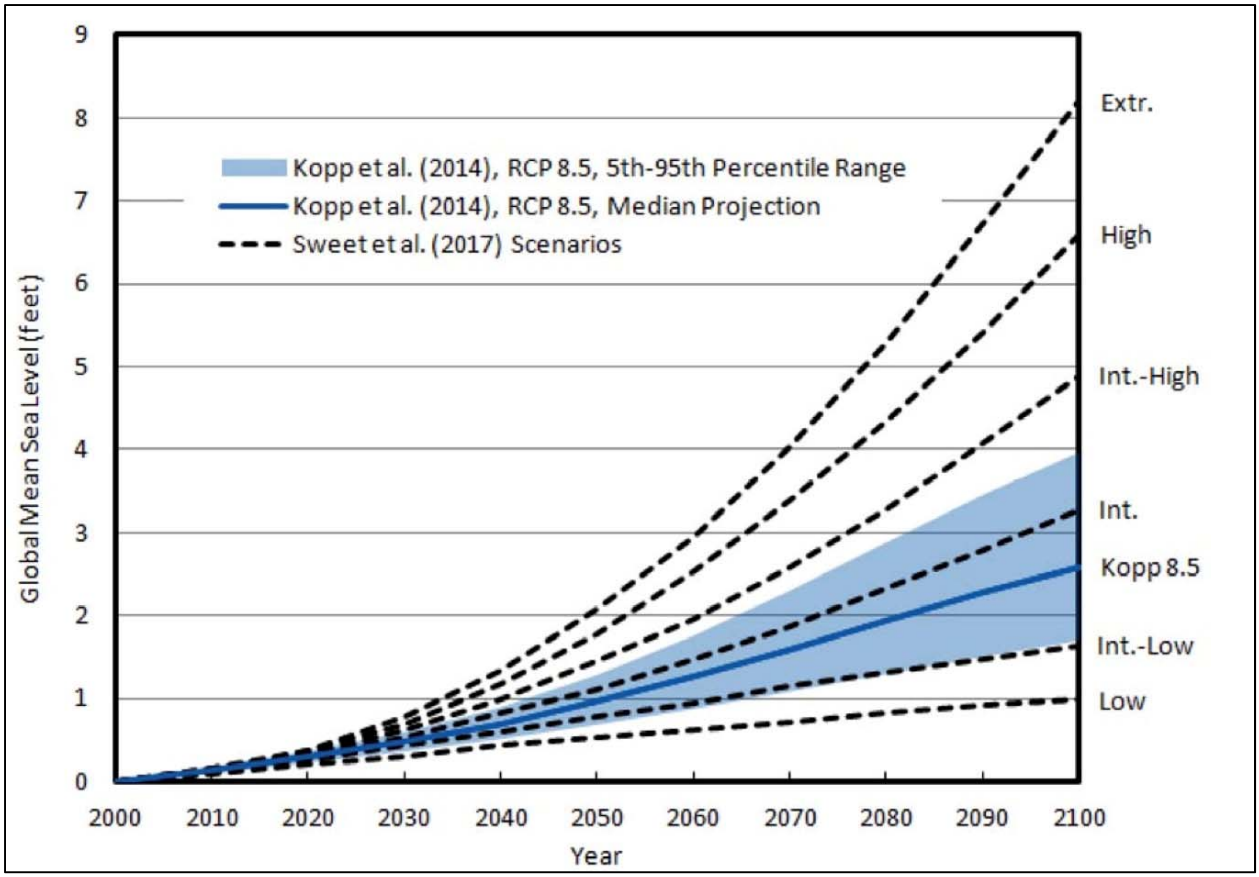

Figure 8.14. Recommended alternative RCP8.5 (solid blue line) projection of GMSLR with the NOAA scenarios (dashed lines) from Sweet et al. (2017a).

Following the simple procedures outlined above neglects some of the future changes in the regional/local non-GMSLR rate components of RSLR including regional differences in thermal expansion, long term changes in meteorological conditions (wind and atmospheric pressure), changes in ocean circulation, and changes in the regional gravity field caused by the redistribution of ice melting from continental-scale ice sheets. It only accounts for the existing VLM and/or local effects as measured at the tide gauges. It has been shown that these other processes will have a significant effect on RSL at the northern latitudes and along the north Atlantic, particularly later in the century, as discussed above. Thus, this simple approach of Table 8.3 is recommended only as an approximation that can be improved with the use of the methodology of Kopp et al. (2014) and/or the tables in Sweet et al. (2017a).

Since the NOAA tide gauge data are presented in terms of the 1983-2001 datum, the values in Table 8.3 can be adjusted to the NAVD88 by adjusting to the 1983-2001 MSL datum and then adjusting to NAVD88 using data available online for each NOAA tide station. The first adjustment can be done by obtaining the monthly average data from the NOAA website and calculating the average of the 1991-2009 MSL data. Then combine that value (typically a small (~0.01m), positive value due to sea level rise in "half" of an epoch) with the adjustment between MSL (of 1983-2001) and the NAVD88 for that gauge. Note that the USACE Sea Level Change Curve Calculator performs these calculations for the user.

The values presented in Figure 8.3 do not include any range of uncertainty. In addition to the uncertainty associated with natural variability, there is scientific (model) uncertainty, and there is scenario (human) uncertainty. The general magnitudes of uncertainties for sea level rise can be mostly understood by consideration of the range of projections discussed in Section 8.1.2. These uncertainties may be compounded by the epistemic uncertainty inherent in the selection of a sea level rise scenario.

A specific idea of the model uncertainty can be obtained by considering that the 50th percentile value of 0.59 m is bracketed at the 17th to 83rd percentile range of 0.45 to 0.77 m, and at the 5th to 95th percentile range of 0.36 to 0.93 m (e.g., see Figure 8.6 above; Kopp et al. 2014). In other words, there is a 90-percent chance that the GMSLR will be between 0.36 m and 0.93 m (roughly 1 foot and 3 feet) this century under that RCP4.5/6.0 scenario. There is a 95-percent probability that the GMSLR will be below 0.93 m (3 feet) at the end of this century under that RCP.

An example of the recommended procedure with Table 8.3 in **a site-specific case study** follows. The design of a reconstruction of an existing roadway near the coast is to be informed with an estimate of the recommended minimum projection for sea level rise since the road is occasionally flooded in extreme events today. The planning horizon is 50 years, so it is assumed for this analysis that performance period ends in 2070. The nearest NOAA tide gauge to the site is the Pensacola, Florida gauge. The long-term average RSLR rate from the NOAA Tides and Currents website for that gauge is 2.31 mm/year. Adjusted for the assumed GMSLR rate of 1.7 mm/year, the remaining 0.61 mm/year, which is 0.04 m of rise (70 years from 2000 to 2070), is attributed to VLM and the other regional effects. The GMSLR component from Table 8.3 is 0.36 m for the epoch centered on 2070. Therefore, the RSLR is 0.40 m (1.3 feet). This is a recommended minimum projection of RSLR at this location (from 2000 to 2070).

If a conversion of the MSL values to NAVD88 is required for design, the NAVD88 at the Pensacola gauge is 0.091 m (0.30 feet) below the MSL of 1983-2001 (from the "Datums" NOAA website for that gauge) and the MSL of 1991-2009 was 0.02 m higher than the MSL of the 1983-2001 epoch (computed from the monthly means available online) and so the projected value of MSL of 2070 will be +0.51 m NAVD88 (+1.6 feet NAVD88). These calculations can be performed, or checked for accuracy, using the USACE Sea Level Change Curve Calculator if desired.

It is noted that this projected value of RSLR for this case study is 0.40 m (1.3 feet) higher than would be considered if sea level rise were ignored in the design analysis and more than double the historical trend.

BOTTOM LINE: If a design is sensitive to future sea level, and the range defined by the recommended minimum and alternative is not appropriate for engineering design, then one of the methods outlined in the next section can be used at any risk tolerance level.

8.1.4.3. Recommended Sea Level Rise in Design – All Situations

Any of the primary sea level rise projections discussed above can be used in the planning and design of coastal transportation assets (except for linear extrapolation of historical rates).

Preference may be given to the most recent scientific information as it typically accounts for improved understanding of the physical processes and dynamic results. Specifically, these are:

- The procedure outlined by Kopp et al. (2014).
- The 4th National Climate Assessment (Sweet et al. 2017b).
- The tabular values of RSLR from Sweet et al. (2017a).
- The results of Hall et al. (2016).
- The Climate Science Special Report (USGCRP 2017).
- The regional and GMSLR projections of NRC (2012).
- The procedure outlined in HEC-25 Volume 2 (Douglass et al. 2014).
- The procedures and equations in USACE (2014) and in the USACE Sea Level Change Calculator (USACE 2017a).
- The GMSLR projection estimates of IPCC (Church et al. 2013).
- The GMSLR projection scenarios of Parris et al. (2012).
- The 3rd National Climate Assessment (Melillo et al. 2014).

The first four bullets are similar, closely related approaches and may be the most comprehensive to date, particularly since they include estimates of likelihood (e.g., Sweet et al. 2017a, 2017b has the high and low values tabulated with the mid-range values that are estimates of the 17th and 83rd percentile for a full range of GMSLR scenarios). They also address other regional processes affecting RLSR beyond VLM, which are expected to become more significant later in this century.

The USACE (2014) and Douglass et al. (2014) are similar approaches that consider VLM and can be applied to any range of GMSLR scenarios including those of Parris et al. (2012), the NCA3 (Melillo et al. 2014), or the projections of NRC (2012). The GMSLR projections of the IPCC (Church et al. 2013) are included above primarily because they represent the most recent internationally accepted values (and it is noted that the mid-range values are not much different than those of the RCP-based scenarios of Kopp et al. 2014). **The GMSLR scenario values should be adjusted for at least the VLM (and other local effects) for use as RSLR values for design**.

The USACE Sea Level Change Calculator is recommended for design estimates of RSLR since most of the recent approaches listed above are explicitly included in the most recent version (USACE 2017a). This web-based calculator also provides the added benefits of performing epoch and/or datum adjustments. It also contains the Sweet et al. (2017a) data at 1-degree intervals along the coastline, which may provide useful information between tide gauge locations.

Selection of a design still water level is a part of many coastal engineering analyses and sea level rise should be included in that analysis. **For major projects and projects that have long planning horizons, particularly those with severe consequences of exceedance, a broad range of potential RSLR projections should be evaluated**. For those types of projects, an important question beyond "what is likely to occur?" is "how bad can things get?" Examples of

coastal transportation assets which may be extremely sensitive to design elevation decisions are a major bridge over water or the entrance to a major tunnel. In those situations, increased design elevation decisions can provide for both future sea levels and a lower risk of damage during extreme events.

Design decisions should be made with a probabilistic justification and the specifics of the decision will include conservative engineering judgment and existing policy guidance. The methods outlined above that address the risk-based probabilities (within a future scenario) are the first four bullets. For example, as outlined above for the Pensacola case study, there is a 95-percent probability that the GMSLR will be below 0.93 m (3 feet) at the end of this century under that RCP. This sort of value can be used for design decisions for coastal projects that are sensitive to design water levels.

BOTTOM LINE: It is recommended that future sea level rise estimates be incorporated in the planning and design of coastal transportation infrastructure. A minimum sea level rise projection (based on RCP4.5/6.0) is presented for situations where an asset is not considered critical or when it is not sensitive to sea level rise. Any of the sea level rise projections and scenarios discussed above (except linear extrapolation of the historical rate) are recommended for use in design. The selection of a sea level rise value for use in establishing future design water levels should include application of engineering judgment considering the uncertainties in the science.

8.2. Combining Coastal Hazard and Climate Change Information

This section provides guidance on combining various existing sources of coastal hazard and climate change information for the purpose of design. Methods for incorporating pertinent climate change information into hydrodynamic modeling are also described. The specific climate change addressed in this section is sea level rise. Higher future sea levels are expected to increase the vulnerability of coastal structures to wave attack; low-lying coastal roads to flooding and embankment damage attributable to overtopping; and foundations to changes in local pier and abutment scour. It is unclear whether potential changes in hydraulic conditions will substantially impair the function or safety of transportation infrastructure over the anticipated service life. For example, could wave-induced loads exceed the AASHTO recommended load factor of 1.75 because of sea level rise during the service life of the structure and, if so, what is the associated probability?

The following information addresses three major topics followed by two relevant case studies. First, relevant sources of coastal hazard data are identified and their practical uses for transportation design in the coastal environment are described in Section 8.2.1. Methods for combining existing coastal hazard data and sea level rise projections are presented in Section 8.2.2. The coastal hazards addressed in this section include storm water levels, wave characteristics, and water velocity. The methods presented can be used without the need for any hydrodynamic modeling, but only in cases where existing hazard data are available and appropriate for use. Where coastal hazard data are absent or insufficient, or for major infrastructure projects, original hydrodynamic modeling is identified as the preferred alternative. Methods for incorporating climate change impacts in hydrodynamic modeling are presented in Section 8.2.3.

This section concludes with two case studies that demonstrate practical applications of the tools and methods described. First, existing sources of coastal hazard data are combined with sea level projections to demonstrate the vulnerability of a coastal highway to flooding and wave attack over time. Second, original hydrodynamic modeling is used to describe how sea level rise has already increased the vulnerability of an interstate bridge to wave damage since the time it was designed. In addition to the increases in storm surge and wave heights that have resulted from sea level change, its effects on local pier scour and abutment scour are also briefly addressed.

8.2.1. Sources of Coastal Hazard Data

Obtaining data for the purpose of engineering design in coastal regions has long been a challenge. Sources of measured and analyzed data tend to be distant from where they are needed for transportation design. Some form of modeling, ranging from simple to complex, is typically needed in order to overcome the geographic gap between where data exist and where they are needed. In recent years the availability of coastal hazard data, particularly storm water levels and wave characteristics, has improved greatly including resources available from federal agencies, state agencies, universities, and private consultants. Only a limited subset of potential data sources is described here.

As a component of the North Atlantic Coast Comprehensive Study (NACCS), **the US Army Corps of Engineers initiated development of the Coastal Hazards System, which contains high resolution hazard data** in coastal regions including the Northeast Atlantic Coast, the Gulf of Mexico, and the Great Lakes (USACE 2017c). This system contains densely spaced points of hydrodynamic data along the coast in open water and on the coastal floodplain. These data were generated by performing extensive hydrodynamic modeling, but the effects of future sea level rise were not included. The density, location, and data available at each point make this dataset very useful for some coastal transportation projects. Most data points provide water level, depth averaged water velocity, wave height, wave period, wave direction, wind velocity, and atmospheric pressure time-series and/or representative statistics for each of the synthetic storms (hundreds or thousands) simulated with storm surge and wave models. Each point will also provide annual exceedance probabilities (AEPs) for water levels, wave height, and wave period ranging from 0.1 percent to 10 percent (10-, 20-, 50-, 100-, 200-, 500-, and 1000-year return periods). In addition to the median value AEP for each parameter, the 68-percent, 85-percent, 95-percent, and 98-percent confidence limits are also given.

An example of these data from the Texas coast is provided in Figure 8.15. That figure shows the median AEP and associated 98-percent confidence interval for water level, significant wave height, and peak wave period for a point near the CR257 bridge that crosses San Luis Pass in between Galveston Island and Follets Island. Again, these model data do not currently account for the effects of future sea level rise. There are plans to perform such modeling in the future.

The US Army Corps of Engineers maintains a database of hindcast offshore wave characteristics at thousands of locations in the Atlantic, Gulf of Mexico, Pacific, Alaskan waters, and Great Lakes. These data are collectively named the Wave Information Studies (WIS) (USACE 2017b). The data locations are unique geographic points, typically found in deeper water (> 20 m), where 20- to 30-year records (or longer) of winds have been used to hindcast wave conditions using wind-wave generation models. Those hindcast data are available in raw or processed forms and show trends in wave direction, height, period, and frequency. The wave

height data are analyzed using rank order statistics and those results are presented in the form of return period values at each station.

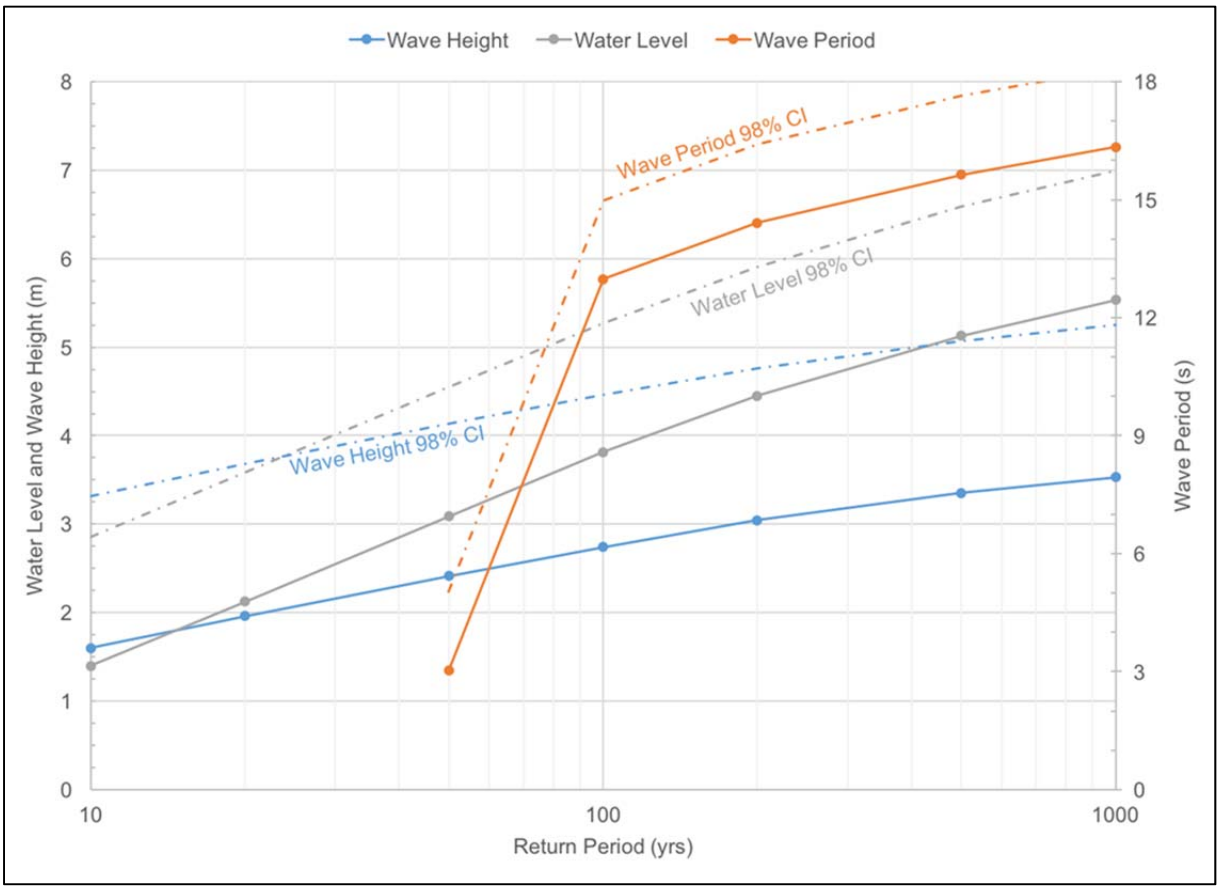

Figure 8.15. Water level, wave height, and wave period AEP values near San Luis Pass, Texas.

An example from a water depth of 19 m offshore of Hatteras Island, NC is shown in Figure 8.16. The estimated 100-year return period (0.01 AEP) wave height is just over 8 m. The extreme value analysis is performed only for wave height and not for wave period and/or direction. As a result, the information given below the extreme value plot must be used, in addition to judgment and site-specific considerations, to assign an appropriate wave period and direction. Like the NOAA tide gauge data, these return period wave height values are often located a considerable distance from any potential transportation project. As a result, these two sources of data would likely be used to describe the forcing for a hydrodynamic model simulation.

Coastal and Great Lakes water levels are measured by NOAA at hundreds of continuously operating tide gauges around the United States (U.S. Department of Commerce 2017). These stations provide 1-, 6-, and/or 60-minute water level measurements referenced to tidal or survey (i.e., map) datums. Many stations also provide other summarized data, such as daily or monthly high and low water elevations, relative sea level trends, and extreme water level data. Stations containing extreme water level data represent a potentially useful source of information, with some notable limitations. First, monthly exceedance probabilities and AEPs are only available at a subset of NOAA tide gauges, and only at those containing at least 30 years of data. Second, tide gauges containing the exceedance probability data are likely quite distant from a

transportation project. Third, the exceedance probabilities do not directly correlate with Base Flood Elevations shown on FEMA flood maps because the tide gauges do not measure wave runup. These gauges are, however, measuring all other potential contributions to the total water level including the astronomical tide, barometric tide, wind stress tide, and wave setup effects. Because of these substantial limitations, the NOAA extreme water level data do not typically reflect the flood hazard well at any location other than that of the tide gauge.

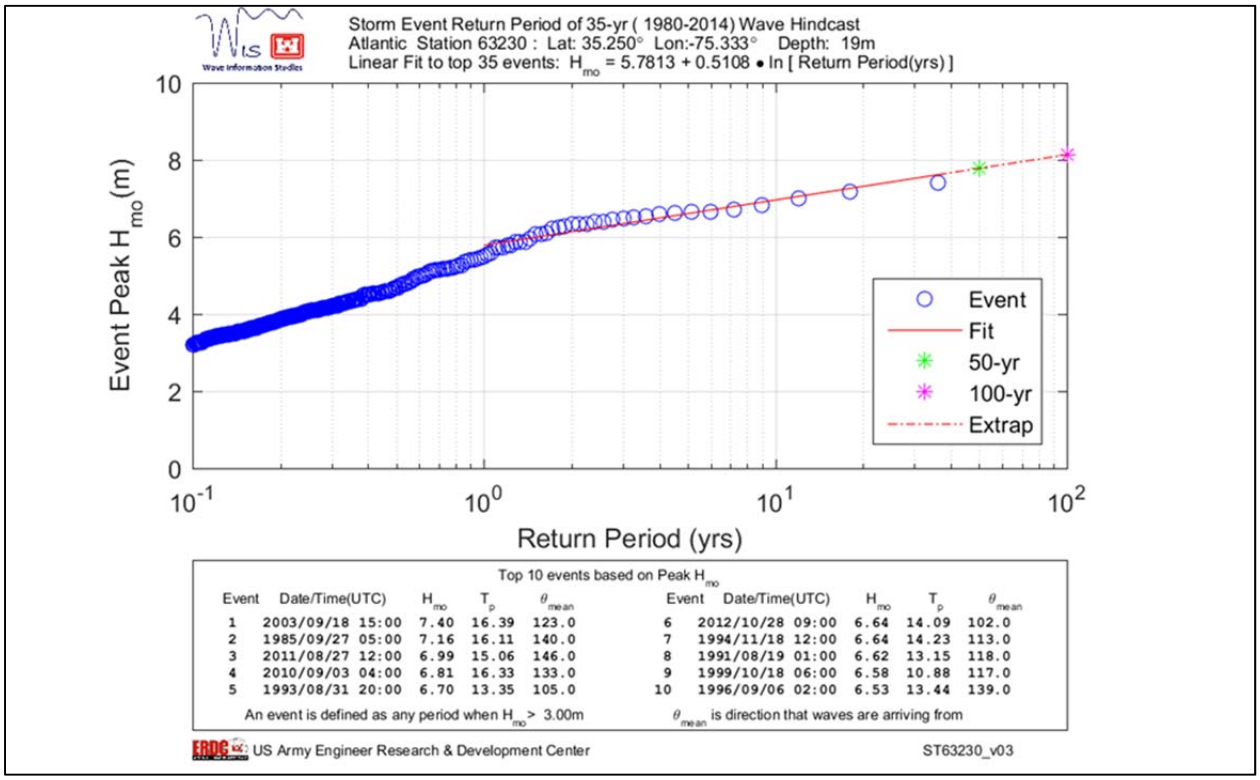

Figure 8.16. Return period (spectrally) significant wave heights in 19 m depth offshore of Hatteras Island, NC.

An example of water level exceedance probabilities, relative to the Mean Higher High Water (MHHW) tidal datum for the Sandy Hook, NJ tide gauge is shown in Figure 8.17. The trend and confidence intervals shown are determined by fitting three parameters of the Generalized Extreme Value (GEV) probability distribution function to annual maximum water levels using an iterative maximum likelihood estimation technique. As shown in the figure, the 1-percent-annual-chance still water flood elevation at this gauge is estimated at 2.06 m (6.76 feet) above MHHW. Also shown are the 10-, 50-, and 99-percent AEPs.

As previously mentioned, the usefulness of a dataset will ultimately be determined by the data it provides and its location relative to a project or site of interest. Some form of simple or comprehensive modeling may be needed when data either do not exist or are too distant from where they are needed. In such cases, the data resources described above are useful for developing the required model forcing in a way that allows the results to be described relative to the event exceedance probability of interest. Note that this does not necessarily require or involve the hindcast simulation of a specific storm of interest. However, the characteristics of

past storms that have contributed to peak water levels or maximum wave heights of interest provide useful context when developing required model input.

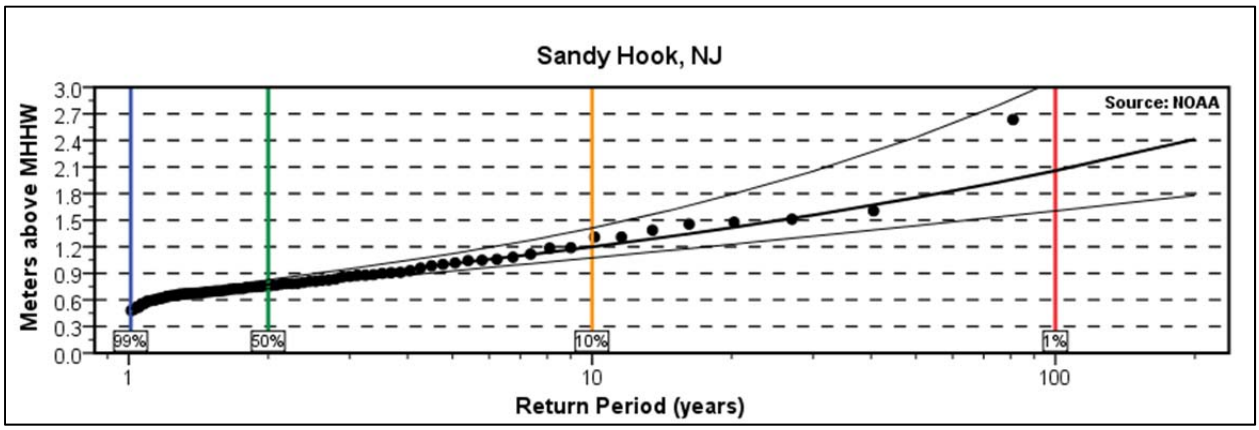

Figure 8.17. Water level exceedance probabilities for Sandy Hook, NJ above the MHHW tidal datum. The thick black line is the GEV fit and the thin black lines above and below are the 95-percent confidence intervals.

BOTTOM LINE: There are useful sets of coastal hazard data available for the purpose of engineering planning and design. The USACE ERDC Coastal Hazards System will contain the most comprehensive inventory of coastal hazard information with associated exceedance probabilities.

8.2.2. Modifying Coastal Hazards to Account for Sea Level Rise

As discussed in the previous section most existing coastal hazard datasets provide parameter values that have been developed through hindcasting or analysis of past storm events, or by using a statistically determined set of synthetic storm events, but do not account for the potential effects of sea level rise. In this section simple methodologies for adjusting water level and storm surge, wave height and period, and velocity data for sea level rise are presented. This is still an emerging area of research and there are no widely accepted or established methods for performing these adjustments. The methodologies presented are verified against a limited set of hydrodynamic modeling data for a specific location and storm event, but caution should be exercised in generalizing these results. However, the relationships given below each have strong physical justification and can be easily modified to account for site-specific concerns.

The methods presented below were developed using hydrodynamic simulations of a specific storm event for two different mean sea level positions. The dynamically coupled versions of the Advanced Circulation model (ADCIRC) (Luettich et al. 1992, Westerink et al. 1994), and Simulating Waves Nearshore model (SWAN) (Booij et al. 1999) were used to simulate Hurricane Ivan, a major hurricane of record in the Gulf of Mexico that made landfall near the Alabama-Florida border. The models were simulated on a medium-resolution mesh containing over 0.5 million nodes, including points on dry land up to the 60-foot elevation contour in parts of Northwest Florida and the two coastal counties of Alabama. One simulation was a true model hindcast of the conditions and mean sea level position of Ivan when it made landfall in 2004. Those results were validated using available tide gauge data and surveyed high water marks.

Good agreement was found between model results and measured data. That storm was then simulated again but with a mean sea level position in the model that was 10 cm lower than the true storm hindcast to reflect a condition in the year 1970. This was done to evaluate the degree to which sea level change affected coastal hazards over a 30-plus year period at that location. Methods for incorporating climate change data in hydrodynamic modeling are provided in Section 8.2.3, and specific details about the storm event and sea level rise scenario used are presented in Section 8.2.5.

8.2.2.1. Water Levels and Storm Surge

The most common approach to combining sea level rise and extreme water levels, in lieu of hydrodynamic modeling, is to simply add them together. In other words, an existing flood elevation and a RSLR of interest would be added together through linear superposition to describe how that flood hazard potentially changes in the future:

$$\eta_2 = \eta_1 + SLR \tag{8.2}$$

where:

η_2 = *Flood elevation of interest in the future.*

η_1 = *Flood elevation of interest today.*

SLR = *Relative sea level rise increment for a given scenario.*

This methodology could also work for relative sea level decrease if the sea level rise increment were negative. When evaluated against the results of the hydrodynamic model simulations, this simple combination of storm surge and sea level rise yields a root mean square error (RMSE) of 1.8 cm, or approximately 18 percent of the sea level rise increment used between the simulations. This was determined by comparing the hydrodynamic model simulation results for maximum still water level in 2004 to those predicted using Equation 8.2, where η_1 was a maximum still water level from the 1970 simulation. The results of that direct comparison are shown graphically in Figure 8.18, which shows the agreement between the predicted and simulated maximum still water levels for all points that were "wet" in the model simulations (N=278255).

This is a straightforward procedure that ignores the potential for non-linear behavior when flood elevations and sea level changes are combined. Such non-linear effects have been noted in the published literature (Smith et al. 2010, Bilskie et al. 2014) and tend to exhibit the most variability in what is normally very shallow water and/or on the coastal floodplain. The degree of non-linearity may also be a function of the size of the sea level change increment to the total depth (i.e., normal depth plus storm tide) of the water body. However, there is currently no empirical method for estimating the magnitude of the non-linearity that leads to amplification or attenuation of the surge and sea level rise combination.

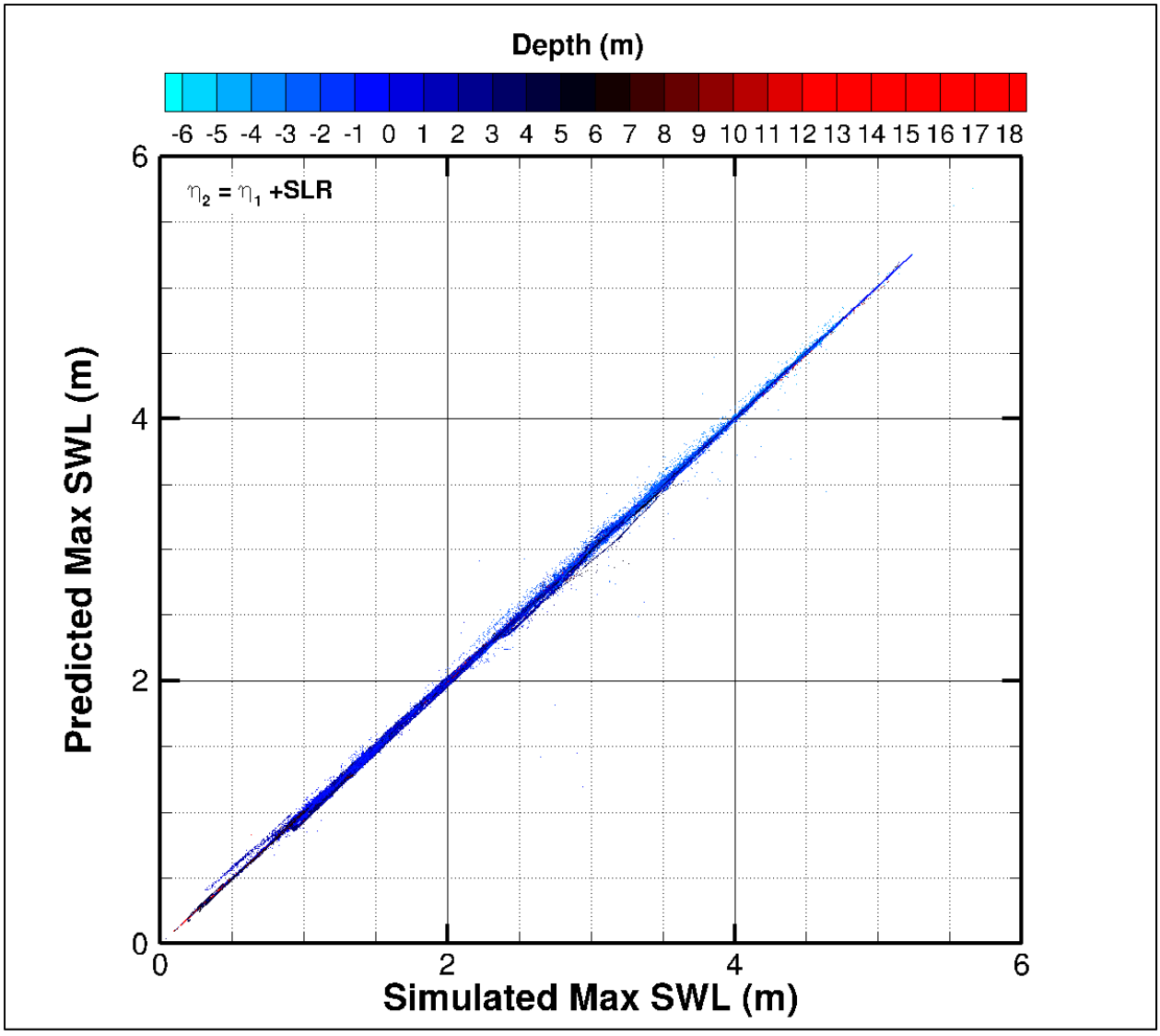

Figure 8.18. Comparison of simulated (hydrodynamic models) maximum still water level (SWL) and predicted (Equation 8.2) maximum still water level. The color of each point (N=278255) represents the depth, relative to mean sea level, at that location under non-storm conditions.

The non-linear coupling between sea level rise and storm surge is further evaluated as a potential source of error. As demonstrated in the subsequent sections, the ability to predict future values of wave height, wave period, or water velocity are dependent upon an accurate estimation of the future flood elevation at a specific location. Therefore, error in the estimation of a future flood will propagate to the other predicted values. Here, an amplification ratio is defined as the difference between maximum still water elevations divided by the sea level rise increment used between the two modeled scenarios:

$$AR = \frac{\hat{\eta}_2 - \hat{\eta}_1}{SLR} \tag{8.3}$$

where:

AR = *Amplification ratio.*

$\hat{\eta}_2$ = *Future flood elevation modeled with the sea level rise increment of interest.*

$\hat{\eta}_1$ = *Modeled (or a known) flood elevation under present sea levels.*

When Equation 8.3 yields a value of one, the effects of sea level rise on storm surge are linear. However, when values of *AR* are greater (less) than one, the sea level rise increment results in a non-linear amplification (attenuation) in maximum still water levels.

The 1970 and 2004 hydrodynamic model simulation results are used to characterize the non-linear coupling between surge and sea level rise to better understand its significance. The dependence of the amplification ratio on depth is shown graphically in Figure 8.19. All of the computed *AR* values are shown in the top two panels with respect to depth and are colored by their corresponding maximum still water level from the 1970 simulation. The mean and standard deviation of all *AR* values in the model domain is 1.028 ± 0.178. The average value is likely closer to 1.0 because all model mesh nodes were used in the computation. Note that some values of *AR* are large (e.g., -6 to 18), but those specific points tend to fall in locations just above or below mean sea level for either scenario. In other words, if a point had no flooding in the 1970 simulation but did flood during the 2004 simulation, the *AR* value will obviously be much larger. However, this isn't a non-linear effect.

The statistical analysis of *AR* values as a function of depth (Figure 8.19) reveals two important results. First, assuming a linear superposition of sea level rise and storm surge (*AR* = 1.0) in open water conditions is a reasonable approximation. For depths greater than 5 m the mean *AR* value is approximately equal to 1.0 with a small standard deviation. There is a notable increase in the mean *AR* value in water depths ranging from 0 to 5 m, along with a corresponding increase in standard deviation. The mean *AR* value over the coastal floodplain is very close to 1.0, but with the largest standard deviation. Second, the variability (standard deviation) in *AR* values increases, almost monotonically, from open water to the coastal floodplain.

Consider the potential impacts of non-linearity where different types of transportation projects are found. The mean and standard deviation of *AR* on the coastal floodplain is 1.0091 ± 0.279. If a designer is concerned about potential future flood elevations for a coastal roadway or bridge approach on land, an assumed linear superposition of sea level rise and surge may be appropriate. While the associated uncertainty is larger on the floodplain than it is elsewhere, it can be argued that there is considerably more uncertainty in the magnitudes of future sea level rise.

On the other hand, if a designer is concerned about the non-linear effects in open water where you might be evaluating a bridge design, the mean and standard deviation of AR there are 1.032 ± 0.152. So while there is more of a tendency for the non-linear effect to influence water levels, and subsequently other hazard values as will be shown, the variability around that mean value is almost 50 percent less than it is on land. In other words, assuming some modest non-linear effect (especially in cases where water depths are 0 to 5 m) may be justified, but the potential exceedance of that value is rather small.

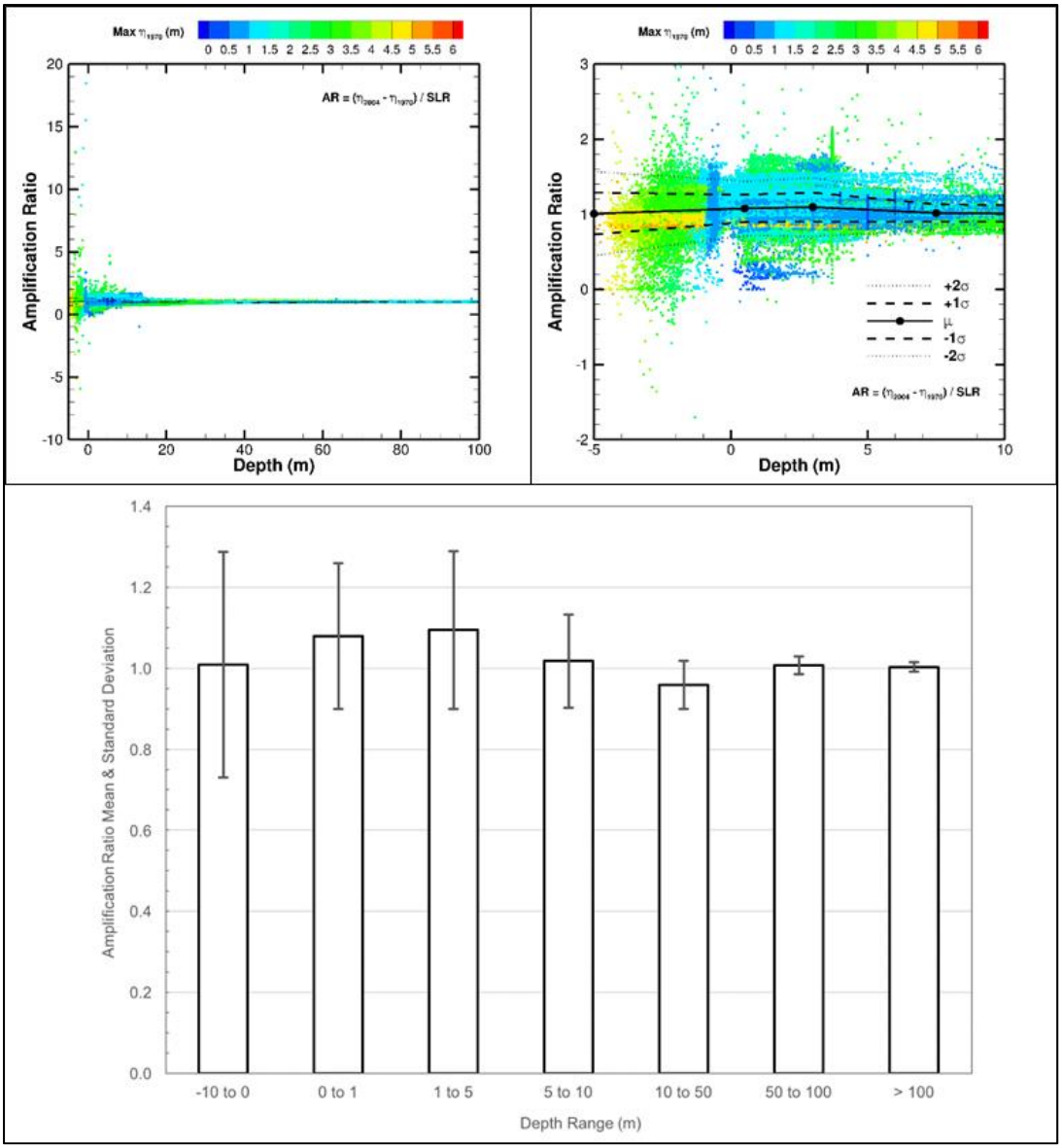

Figure 8.19. The variation of amplification ratio with depth for each model node colored by its maximum SWL in 1970 (top two panels) along with the means and standard deviations by depth range (lower panel).

If one were to account for the potential non-linear effects for the purpose of planning or design, it is easily incorporated into Equation 8.2 as follows:

$$\eta_2 = \eta_1 + (AR)(SLR) \tag{8.4}$$

All terminology is as previously defined, and the sea level rise increment of interest is simply multiplied by a reasonable *AR* value. Without performing site-specific hydrodynamic modeling, selecting a reasonable *AR* value may be difficult. The variation of *AR* values about the mean is not exactly described by a normal probability distribution, but the fit is robust. Almost 99 percent of all *AR* values determined from these specific model simulations fall in the range of 0.6 to 1.6.

A normal distribution fit to the data show a slightly smaller range, with 99 percent of all values falling between 0.7 and 1.5.

The actual distributions and assumed (normal) distributions of *AR* values are shown in Figure 8.20. In that figure, the Relative Frequency and Cumulative Frequency curves show the actual data while the Normal CDF and Normal PMF curves show the cumulative normal distribution and normal probability mass functions, respectively, fit to the mean and standard deviation of the *AR* values. Since 68 percent of all potential values fall within one standard deviation of the mean value in a normal distributed process, the variability or uncertainty in the assumed *AR* value can be assessed in design.

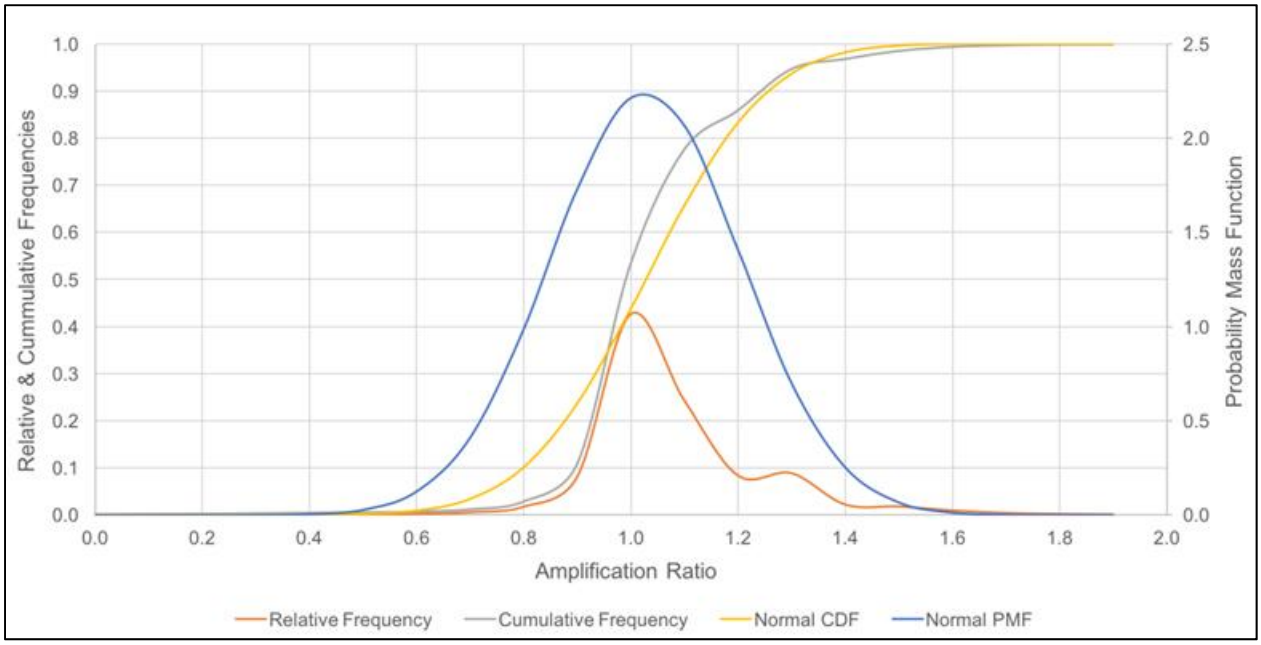

Figure 8.20. Comparison of actual *AR* value statistics (relative and cumulative frequency) to those fit by a normal probability distribution (normal CDF, normal PMF).

8.2.2.2. Wave Heights and Periods

Future sea level change, particularly sea level rise, will lead to changes in wave characteristics mainly through changes in water depth. The relationship between water depth and wave height is important in two ways: through depth-limited wave breaking and through wind-wave generation. As depths on the coastal floodplain change with future sea levels, their corresponding depth-limited wave heights will change proportionally. Changes in depth also affect wind-wave growth where depth and wave height are directly proportional to each other. As a result, a sea level rise increment could potentially lead to larger wave heights in the future through either of those mechanisms.

Using the hydrodynamic model data from the 1970 and 2004 simulations, **a simple predictive relationship can be developed to estimate changes in wave height resulting from sea level rise**. It is assumed that a wave height statistic, like the zero-moment wave height (H_{mo}), will grow proportionally to the increase in total water depth over time. If relative sea level were

decreasing, the wave height would decrease by a similar proportion. The suggested equation for estimating wave heights under sea level rise scenarios is:

$$H_2 = H_1 \left(\frac{d+\eta_2}{d+\eta_1}\right) \tag{8.5}$$

where:

H_2 = *Future zero moment wave height.*

H_1 = *Present zero moment wave height.*

d = *Present water depth.*

Note that Equation 8.4 can be substituted into Equation 8.5 such that:

$$H_2 = H_1 \left(\frac{d+\eta_1+(AR)(SLR)}{d+\eta_1}\right) \tag{8.6}$$

In this equation, the *AR* value may be set to 1.0 when ignoring potential non-linear effects. In this way, potential sources of error associated with assumed values of *AR* = 1.0 propagate to the estimation of wave heights.

As with still water levels, the relationship presented in Equation 8.6 is tested against the hydrodynamic model results from the 1970 and 2004 simulations. Figure 8.21 shows the comparison of the predicted maximum zero moment wave heights (Equation 8.6) to their simulated (modeled) counterparts yields an RMSE of 1.4 cm, or 14 percent of the sea level increment used between the scenarios.

In addition to wave height, a representative statistic of the wave period distribution is often needed in coastal engineering design. Wind-wave generation equations also suggest that wave periods will grow with respect to water depth, though in a somewhat non-linear fashion. Also, there are existing relationships between wave height and wave period in the SPM (1984), USACE (2006), and Goda (2003). Here, we present a modification of Goda's (2003) relationships for estimating peak wave period using the zero-moment wave height. The suggested equation for predicting peak wave period is simply:

$$T_2 = T_1\sqrt{\frac{H_2}{H_1}} \tag{8.7}$$

where:

T_2 = *Future peak wave period.*

T_1 = *Present peak wave period.*

Substituting Equation 8.4 and Equation 8.6 into Equation 8.7 yields an alternative form that is a function only of depth, the sea level increment, and amplification ratio:

$$T_2 = T_1\sqrt{\frac{d+\eta_1+(AR)(SLR)}{d+\eta_1}} \tag{8.8}$$

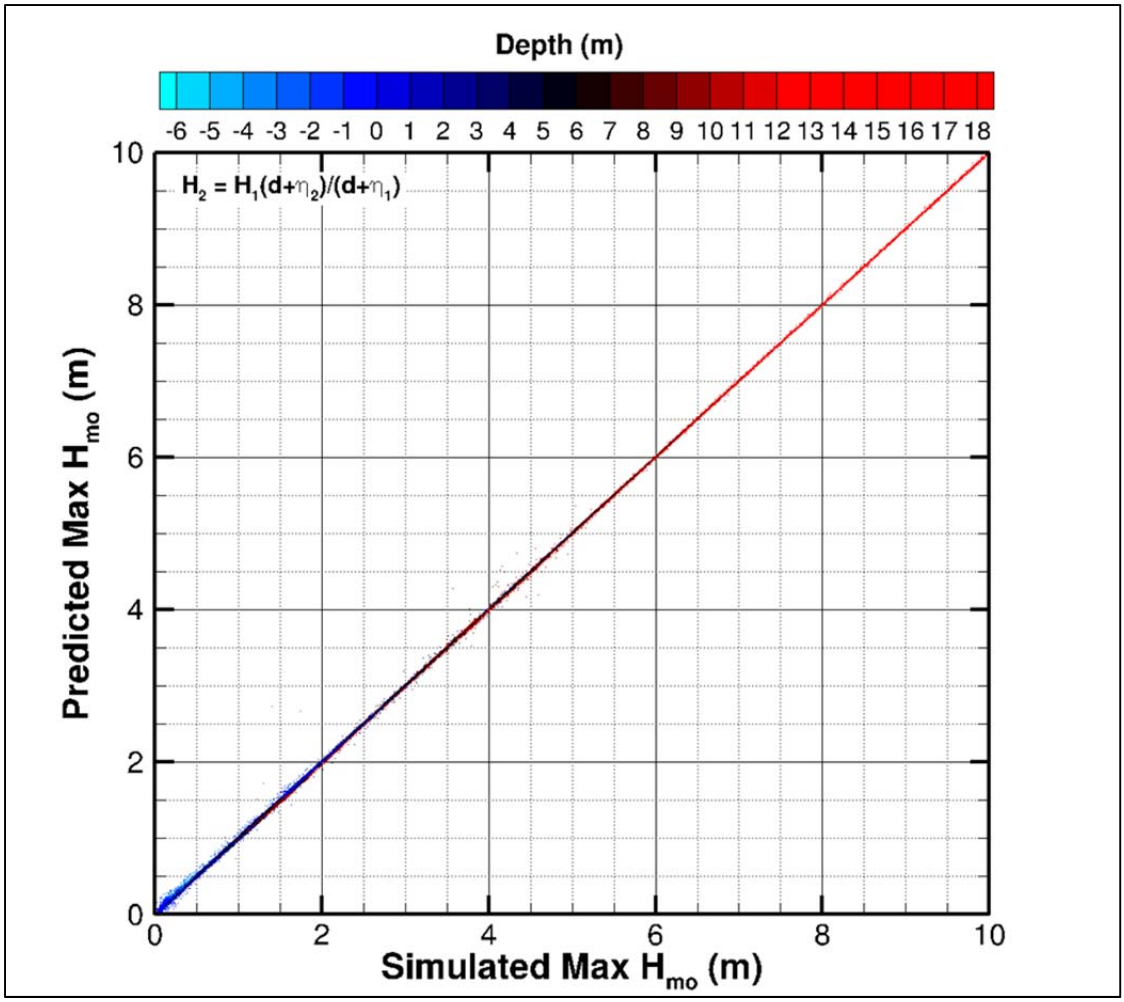

Figure 8.21. Comparison of simulated (modeled) and predicted maximum zero moment wave height. Each point (*N*=278255) is colored by its depth relative to the given scale.

The potential for error in estimating peak wave periods in the absence of guidance for selecting appropriate values of *AR* is evident. Even without considering the non-linear effects, the simple relationship proposed in Equation 8.7 or Equation 8.8 is in very good agreement with the hydrodynamic model results. The RMSE for the predicted peak wave period is only 0.64 s when applied in cases where the present wave height is nonzero (i.e., $H_1 > 0$). The RMSE for peak wave period in open water conditions only ($d > 0$) is reduced to 0.42 s. A graphical comparison of simulated (modeled) and predicted (Equation 8.8) peak wave periods is provided in Figure 8.22. Unlike the previous comparisons shown in Figure 8.18 and Figure 8.21, the simple predictive equation for peak wave period yields more scatter about the expected value. The variability in peak wave period values tends to be more pronounced for values less than 5 s and greater than 15 s. However, even the larger RMSE of 0.64 s is still less than 13 percent of a 5-s peak wave period.

8.2.2.1. Velocity Changes

In addition to changing flood elevations and wave characteristics, sea level rise will also impact water velocity magnitude (i.e., current speed). Understanding changes in coastal water velocities is important for characterizing potential changes in local pier scour at bridge foundations under future sea levels. The previous methods for estimating flood elevation, wave height, and wave period all demonstrate that higher future sea levels will lead to larger values of each parameter. Coastal water velocities, however, behave differently.

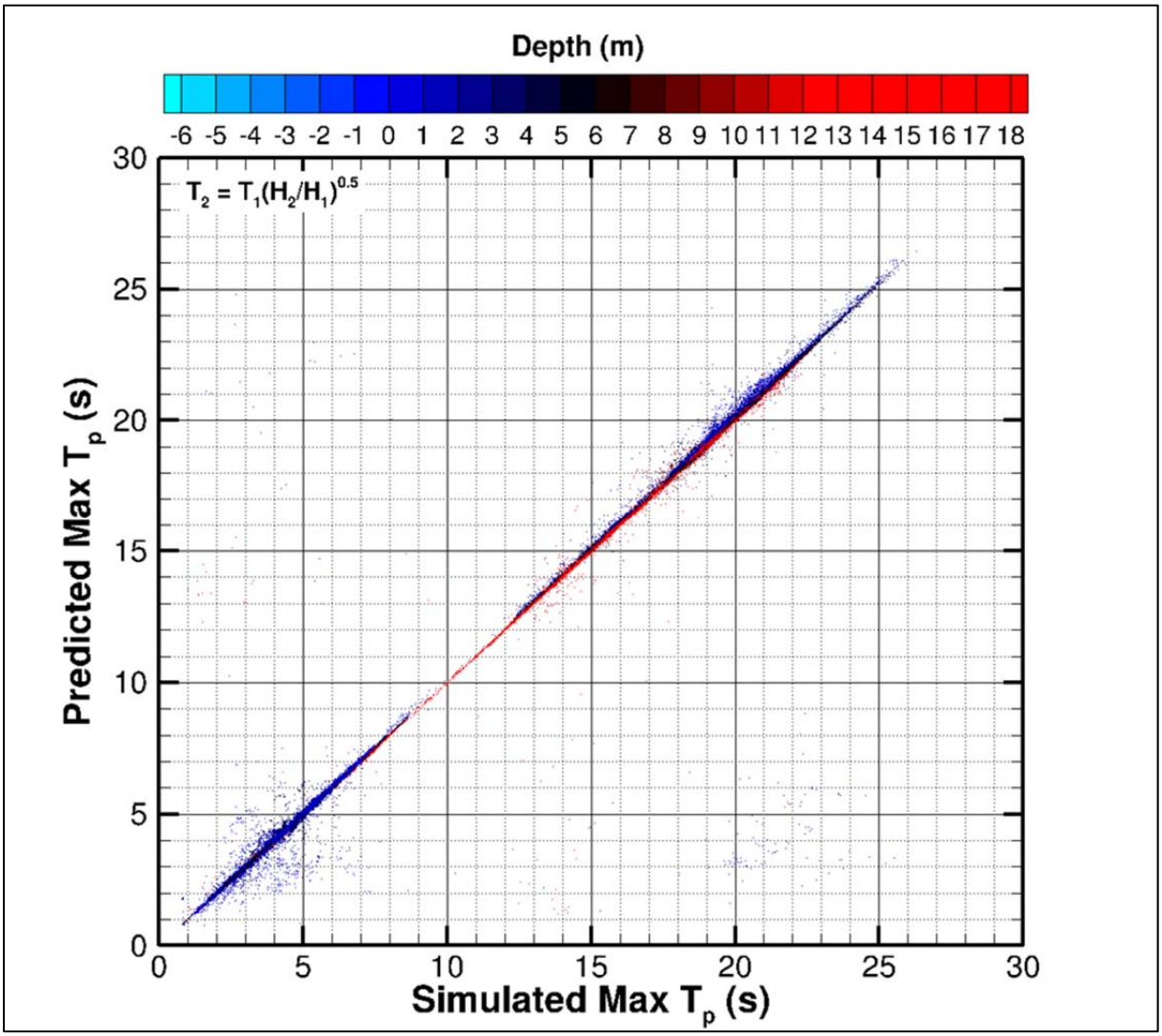

Figure 8.22. Direct comparison of simulated (modeled) and predicted peak wave periods. Each point (N=278255) is colored by its depth relative to the given scale.

The modification of water velocity is assumed to be constrained by the continuity equation, in terms of flow per unit width. Higher future sea levels will lead to an expansion of the water column. This expansion results in a decrease in coastal water velocities. An example would be a storm surge hydrograph that shifts vertically with sea level rise, but without modifying the time base, in a manner that preserves the total volumetric discharge over the duration of the event.

Note that the velocity magnitude is the only coastal hazard mentioned in this section that has an indirect, or inverse, relationship to sea level change. The resulting approximation is written as:

$$V_2 = V_1 \left(\frac{d+\eta_1}{d+\eta_2}\right) \tag{8.9}$$

where:

V_2 = *Water velocity magnitude under future sea levels.*

V_1 = *Water velocity magnitude under present sea levels.*

By substitution of Equation 8.4 the relation becomes:

$$V_2 = V_1 \left[\frac{d+\eta_1}{d+\eta_1+(AR)(SLR)}\right] \tag{8.10}$$

This simple approximation ignores the lateral expansion of the floodplain that occurs during overland coastal flooding. It also ignores changes in velocity direction, where increasing sea levels may result in additional net landward flow both during storm and non-storm conditions. The approximation given above is also limited to describing changes in velocity magnitude associated with coastal hydrodynamics. This does not address potential changes in fluvial contributions as a result of a persistently high tailwater condition. These limitations are best overcome by performing a hydrodynamic model simulation that includes the effects of sea level rise and potential fluvial inputs.

Although the conservation argument above does have some limitations, the predictive results of Equation 8.10 are strong. A direct comparison of predicted (Equation 8.10) and simulated velocity magnitude yields an RMSE of 4.5 cm/s for all points in the simulations, even those with zero velocity (N=446459). For non-zero velocities, the RMSE is 5.06 cm/s (N=278079). The direct comparison of all non-zero velocity values is shown graphically in Figure 8.23. There is considerably more scatter about the trend in Equation 8.10 as compared to the relationships shown in prior figures. However, the RMSE magnitude and relative percentage, by velocity range, as shown in Table 8.4 are not considerably larger than those described previously.

Table 8.4. Analysis of velocity magnitude error associated with Equation 8.10.

Velocity Range (m/s)	Number of Points	RMSE (m/s)	Error Relative to Mid-Range Velocity
$0 < V < 1$	184009	0.0510	10.2%
$1 \le V < 2$	93855	0.0583	3.9%
$2 \le V < 3$	2663	0.151	6.0%
$3 \le V < 4$	307	0.258	7.4%
All $V > 0$	278079	0.0506	n/a

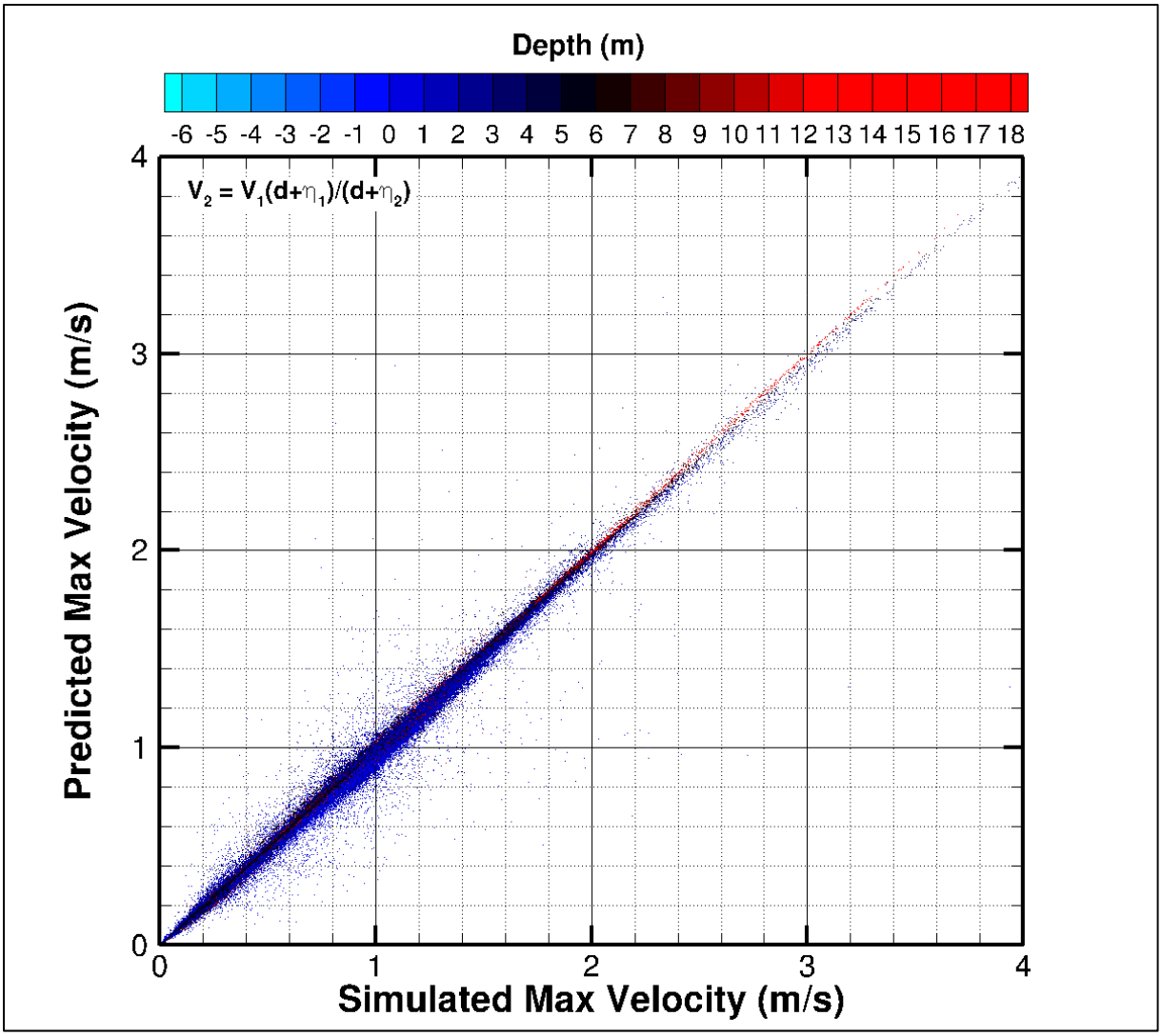

Figure 8.23. Comparison of simulated (model) and predicted maximum water velocity magnitude for all non-zero velocity values in the model simulation (*N*=278079).

8.2.2.2. Example of Combining Coastal Hazards and Sea Level Rise

This section provides a site-specific example of how existing coastal hazard data can be combined with a relative sea level rise scenario of interest using the methods described above. This example uses the coastal hazard data presented in Figure 8.15, which were taken from the USACE ERDC Coastal Hazards System near San Luis Pass between Galveston and Follets Islands, Texas (Save Point 2322). As shown previously, these data provide AEPs for water levels, wave heights, and wave periods.

For this example, the 0.01 AEP values are used in the calculations. A graphical representation of these calculations will be given later showing how both the 0.01 AEP (100-year) and 0.02 AEP (50-year) values change over time under different relative sea level rise scenarios. Also, since the Coastal Hazards System does not provide AEPs for depth-averaged velocities, a representative value is used instead. The representative value was determined by sampling storm scenarios from

the database that yielded a maximum still water level close to that of the given 0.01 AEP value. The corresponding depth-averaged velocity from that scenario is used in the calculation below, and a similar procedure was followed for finding the 0.02 AEP value shown graphically after the calculations.

The USACE (2017a) Sea Level Change Calculator is used, along with the Sweet et al. (2017a) GMSLR projections, for the NOAA tide gauge at Freeport, TX. This tide gauge is less than 15 miles from the example location and is the closest tide gauge. Two other tide gauges are within 20 miles of this location. The VLM rate at the Freeport gauge is -0.00587 m/year. For this example, we assume that the given 0.01 AEP values are appropriate at the year 2000 and we will calculate their values in 2100 under the Intermediate-High GMSLR scenario (+1.5 m) described in Sweet et al. (2017a).

The USACE Sea Level Change Calculator returns a local MSL of +2.38 m in 2100 at the Freeport, TX tide gauge. Note that the value of MSL in the year 2000 at this location is +0.03 m, giving an RSLR increment of +2.5 m over the time period 2000 to 2100. Accounting for the +1.5 m increase in GMSLR, and another 0.617 m in VLM, leaves a balance of 0.233 m in RSLR not accounted for by VLM at this location. This balance represents the other regional impacts on RSLR (e.g., ice sheet gravitational affects).

With the RSLR increment now determined (+2.35 m), the calculations for maximum water level, significant wave period, peak wave period, and velocity can be determined. The estimated 0.01 AEP maximum still water level is (using Equation 8.4):

$$\eta_{2100} = 3.8\ m + (1.0)(2.35\ m) = \ 6.15\ m$$

In this example, the amplification ratio value *AR* is assumed to be 1.0 (no non-linear effects), the current 0.01 AEP maximum water level is 3.8 m above MSL, and η_{2100} is the estimated 0.01 AEP maximum still water level in the year 2100 relative to MSL of the year 2000. Now using the results from above with Equation 8.6, the estimated maximum significant wave height is:

$$H_{2100} = 2.7\ m\left(\frac{7\ m+3.8\ m+(1.0)(2.35\ m)}{7\ m+3.8\ m}\right) = 3.29\ m$$

In this example, a depth of 7 m was used to represent the depth at the location from which the coastal hazards data were obtained at San Luis Pass, TX, the 0.01 AEP value of the maximum significant wave height is 2.7 m, and H_{2100} represents the estimated maximum significant wave height (H_{mo}) resulting from RSLR. The ratio of the two wave heights can now be used to estimate the future peak wave period using Equation 8.7, or as below in Equation 8.8:

$$T_{2100} = 13\ \text{s}\sqrt{\frac{7\ m+3.8\ m+(1.0)(2.35\ m)}{7\ m+\ 3.8\ m}} = 14.3\ s$$

The current 1-percent AEP for peak wave period is 13 s, and T_{2100} is the estimated peak period value in the year 2100 under the Intermediate-High RSLR scenario. Finally, using the modified continuity equation described in Equation 8.10, the change in velocity due to RSLR can be estimated as:

$$V_{2100} = 2.3\ m/s\left[\frac{7\ m+3.8\ m}{7\ m+3.8\ m+(1.0)(2.35\ m)}\right] = 1.9\ m/s$$

The value of 2.3 m/s is used as a proxy for the 0.01 AEP velocity under present sea levels, and V_{2100} is the estimated velocity in the year 2100 based on the other assumed and/or calculated values. Again, note that the tendency is for velocity to decrease with increasing sea levels.

The 0.01 AEP (100-year) and 0.02 AEP (50-year) values for maximum water level, significant wave height, and velocity (wave period is excluded here for brevity) are modified to account for the effects of relative sea level rise. Three sea level rise scenarios from Sweet et al. (2017) are used to demonstrate how the existing AEP values change with time: Intermediate-Low, Intermediate-High, and Extreme. The plots for maximum water levels, wave heights, and velocities are shown in Figure 8.24, Figure 8.25, and Figure 8.26, respectively. The MSL trends for each relative sea level rise scenario are also shown in Figure 8.24 for comparison.

Without accounting for non-linear effects of sea level rise on water levels, the tendency for maximum still water level is to simply follow the RSLR trend offset by the amount of today's 0.01 or 0.02 AEP water level. Some notable changes in the AEP trends do occur over time across different sea level rise scenarios. For example, today's 0.01 AEP water level at this location becomes a 0.02 AEP by approximately 2065, 2045, and 2035 under the Intermediate-Low, Intermediate-High, and Extreme RSLR scenarios, respectively. **So as sea levels rise, the frequency at which today's event thresholds are exceeded will increase**.

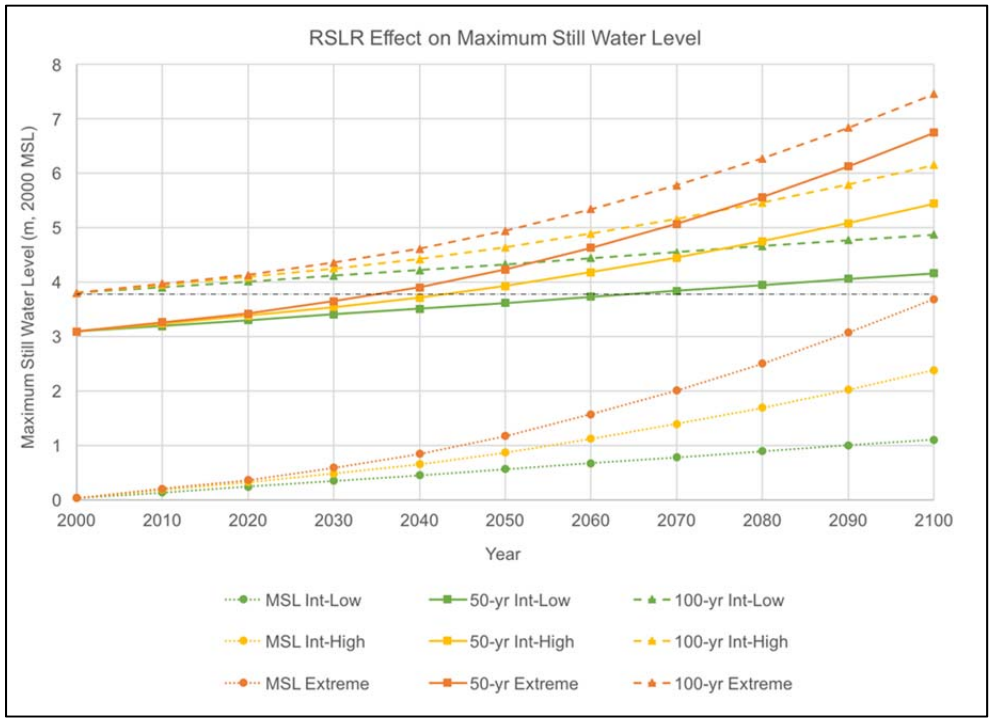

Figure 8.24. Estimated 100-year and 50-year maximum still water level at San Luis Pass, TX for three sea level rise scenarios adjusted for regional effects. The black dashed line shows the baseline 100-year still water level.

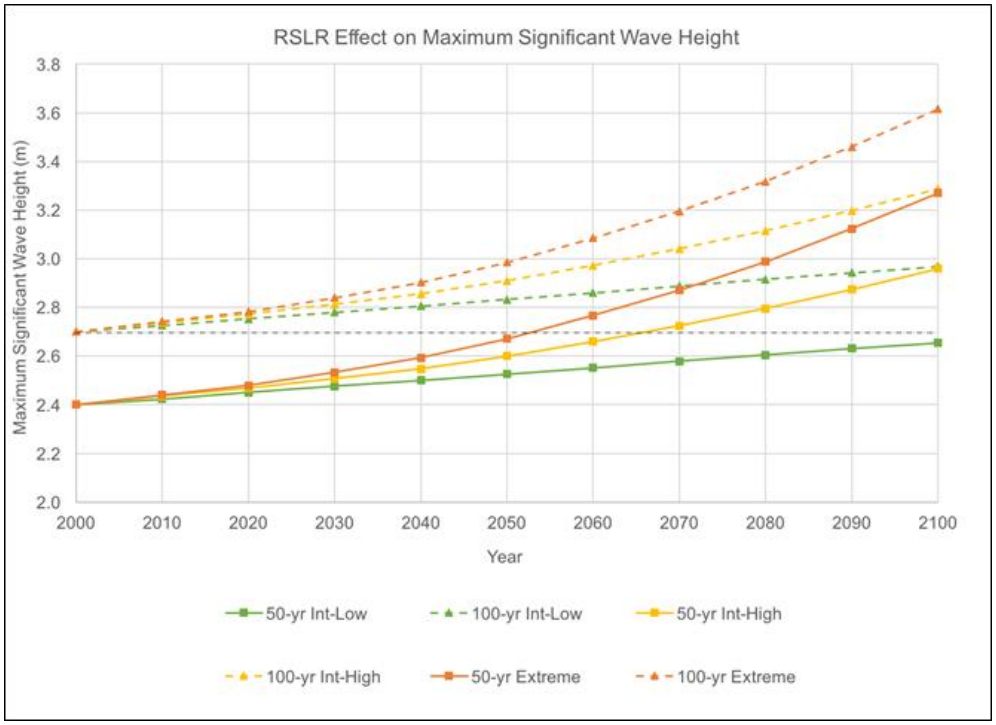

Figure 8.25. Estimated 100-year and 50-year maximum significant wave height (Hmo) at San Luis Pass, TX for three sea level rise scenarios adjusted for regional effects. The black dashed line shows the baseline 100-year wave height.

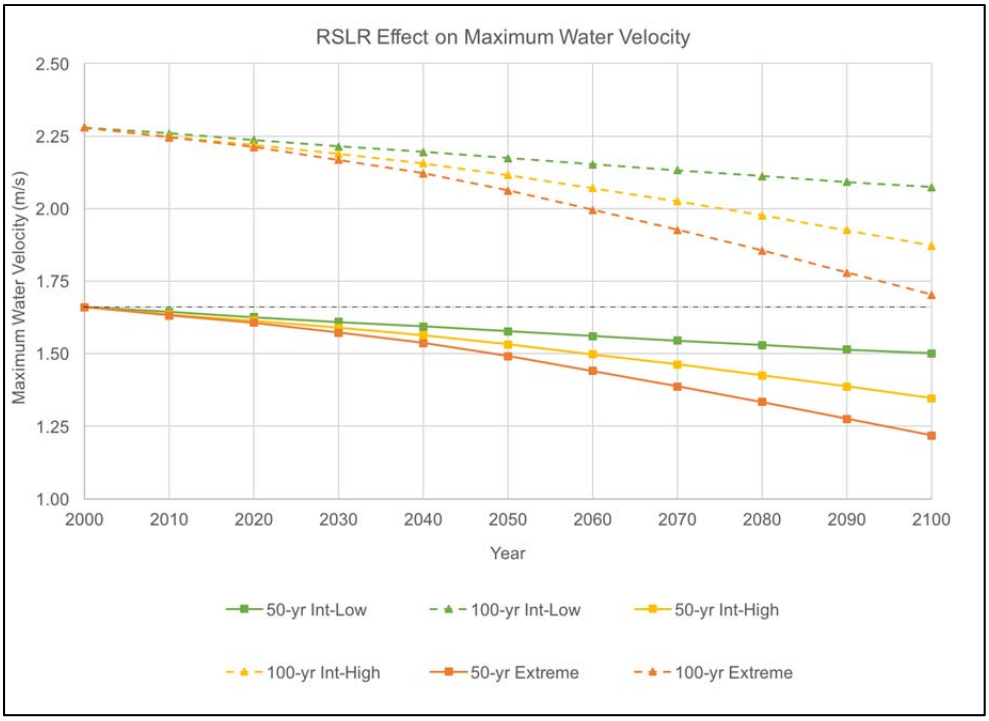

Figure 8.26. Estimated 100-year and 50-year maximum water velocity at San Luis Pass, TX for three sea level rise scenarios adjusted for regional effects. The black dashed line shows the baseline 50-year velocity.

A similar case can be made for the trend in significant wave heights in Figure 8.25, though with slightly less overlap between the various scenario results. For example, today's 0.01 AEP for significant wave height changes to a 0.02 AEP by 2055 under the Extreme scenario, and by 2070 under the Intermediate-High scenario. The value of today's 0.02 AEP wave height does not reach the 0.01 AEP value by 2100 under the Intermediate-Low scenario.

As described earlier, the anticipated effect of sea level rise on velocity is for present values to decrease over time due to an expansion of the water column and increase in overall flow area. Again, this finding is predicated on the assumption of a storm of similar magnitude with the only difference being a higher future sea level. As with changes in water levels and wave heights, the anticipated changes in water velocity are not trivial. Figure 8.26 shows the reduction in assumed 0.01 and 0.02 AEP maximum velocities with times for the three sea level rise scenarios chosen for this location. Unlike in the previous examples, however, the velocity values do not overlap between return period or sea level rise scenarios.

BOTTOM LINE: Simple methods can be used to combine existing coastal hazard data, with or without probabilities, with appropriate sea level rise projections to estimate their future values for the purpose of planning or the design of minor, non-critical infrastructure. Original hydrodynamic modeling of the potential non-linear coupling between sea level rise and coastal hazards is recommended for major projects, or those where failure leads to severe consequences.

8.2.3. Incorporating Climate Change Information into Hydrodynamic Modeling

The most appropriate way to simulate the potential effects of climate change on relevant coastal hazards is by incorporating them into hydrodynamic simulation models. For most major transportation planning or design projects, original hydrodynamic modeling is justifiable, and it would be highly preferable to the simple methods outlined above. Any potential non-linear effects that arise from climate change impacts are better captured by the hydrodynamic model, which would provide the type of site-specific information needed for the engineering design of a highway, bridge, or tunnel. This section briefly describes some common ways in which climate change data can be incorporated into hydrodynamic model simulations.

Most hydrodynamic models can be easily adapted to simulate the effects of a relative sea level change. A relative sea level rise is incorporated into a hydrodynamic model by raising the water surface, or lowering the land elevations, with an increment equal to the relative sea level rise of interest. A relative sea level decrease is incorporated by lowering the water surface, or increasing the land elevations, with an increment equal to the relative sea level decrease of interest. There are some limitations to these methods. When incrementally adjusting the water surface up or down relative to land, it must be done uniformly across the entire model domain. If the modeling domain covers a broad geographic region with significant variability in regional sea level change, this method may not capture all the potential effects of future sea level change on a process of interest. While the regional variability can be incorporated by accounting for it in terms of land elevation changes in the model grid, doing so would be quite tedious. The potential benefits of using such a method may only be realized if the hydrodynamic model is being used to develop regional information (i.e., across multiple states).

The change in bottom friction should be addressed when incorporating a relative sea level change into a hydrodynamic model. Many models that simulate coastal flooding do so through a Manning's-type formulation of frictional resistance. The frictional resistance of the coastal floodplain today is potentially much higher than it will be under a future sea level rise scenario, as macro roughness features on the upland terrain are eliminated or changed through conversion of the upland to open water. Conversely, as relative sea level falls in some places (e.g., Alaska and the Great Lakes), the present frictional resistance of the shallow water environment is lower than it may be under a future scenario of lower sea level. Future changes in land use and land cover will also drive frictional changes that could potentially be captured in the hydrodynamic modeling. These changes in frictional resistance can be incorporated into hydrodynamic model simulations by appropriately adjusting the friction coefficients, like Manning's *n* values, wherever necessary. The degree to which modifying the frictional resistance affects simulation results is not presently known, but there are published studies that account for the effect in sea level rise simulations (Smith et al. 2010, Bilskie et al. 2014, Bosma et al. 2015).

Some potential climate change impacts can also be incorporated into hydrodynamic models as boundary conditions. For study regions that reside in a coastal setting where water levels and circulation are overwhelmed by inputs from the coastal watershed, specifying inflow boundary conditions may be necessary (Webb and Marr 2016). This is typically achieved by specifying a time-series of stage and/or discharge values on an open boundary of a model that is coincident with a stream or river cross-section. If the potential effects of a climate change scenario on streamflows or watershed inputs can be described, then these changes too can be incorporated into the hydrodynamic model boundary conditions. The results of hydrodynamic simulations may also be used as downstream boundary conditions for hydraulic or hydrologic models applied within the coastal watersheds. Some information about the potential importance of watershed contributions to coastal areas is provided in Section 8.3.1.

If they can be properly described, the future effects of climate change on storm characteristics (e.g., wind speed, pressure, track, forward speed, etc.) can also be incorporated into hydrodynamic model simulations. This was done in a limited fashion in the Gulf Coast 2 Study. The anticipated changes to hurricane wind speed and central pressure for the year 2100, as described by Knutson and Tuleya (2004), were incorporated into the characteristic storm parameters used to define the meteorological forcing in a hydrodynamic simulation of storm surge and waves on a projected 2100 sea level.

Expected changes in future morphologic conditions have not typically been accounted for *a priori* in hydrodynamic simulations of future scenarios. Where known, local rates of shoreline retreat can be incorporated into a future sea level rise scenario by accounting for the horizontal change in shoreline position, and lateral translation of the resulting shoreline profile, that would occur over the period in question. Modifying other large-scale morphologic features, like ebb or flood tidal shoals, would require site specific knowledge about the potential effects of sea level rise on those features, but could similarly be accounted for in the bathymetry of the hydrodynamic models. Additional comments on sea level rise impacts on geomorphology are provided in Section 8.3.2

BOTTOM LINE: Many climate impacts can be easily incorporated into hydrodynamic modeling, including sea level rise, changes in watershed inputs to the coast, and tropical cyclone characteristics.

8.2.4. Case Study: Climate Change Impacts on a Coastal Roadway – Brookhaven, NY

This case study demonstrates how existing coastal hazard data can be combined with sea level rise projections to illustrate the vulnerability of a coastal roadway to storm surge and wave action over time. The "bottom-up" approach is used to identify future dates by which some form of action may be needed considering alternative future climate scenarios.

The road considered for this case study parallels Mt. Sinai Harbor in the Town of Brookhaven located on the north shore of Long Island, New York as shown in Figure 8.27. The coastal roadway is a low-volume, two-lane, flexible asphalt pavement road. Mt. Sinai Harbor is a small coastal bay with a substantial tide range of more than 2 m adjacent to Long Island Sound. Erosion of the roadway embankment has been a problem for many years, and some sections of the road flood during extremely high tides. The edge of pavement has an elevation of approximately +1.8 m MSL, which is less than 0.7 m above the elevation of the Mean Higher High Water (MHHW) tidal datum.

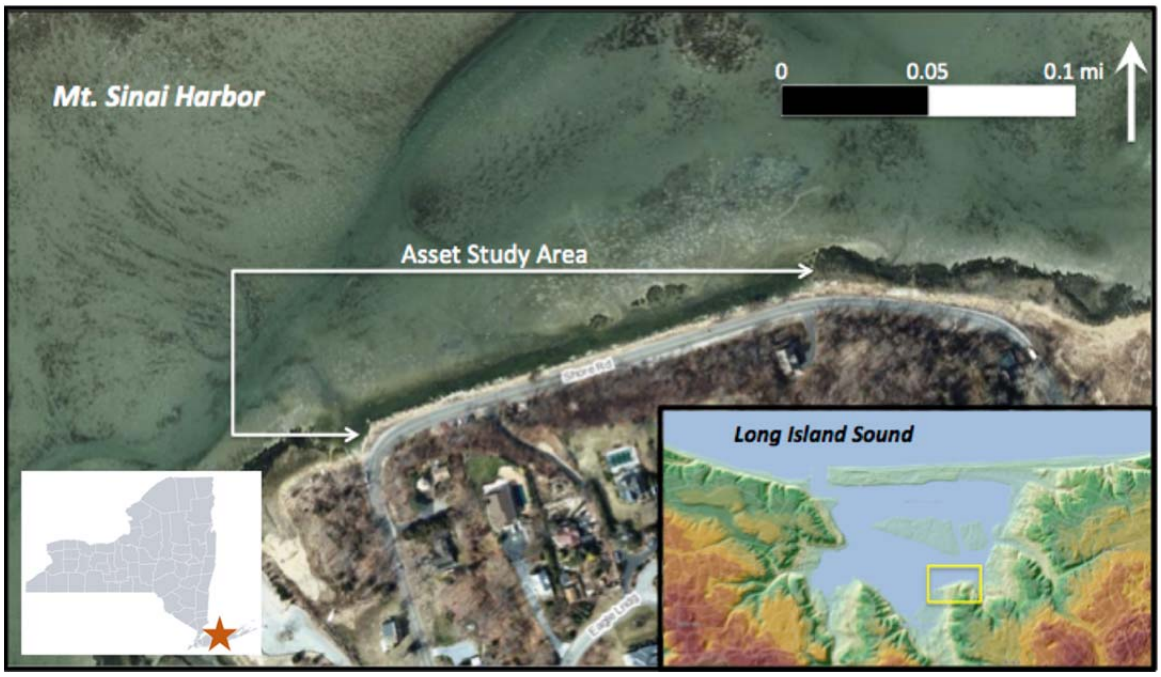

Figure 8.27. Case study: Shore Road, Brookhaven, NY location overview map.

This roadway is believed to have been in use in some form since the late 17th century when the town was established. Based on an extrapolation of the historical rate of 2.44 mm/year measured at the Port Jefferson tide gauge (1957-1992), the road has already experienced nearly 0.5 m of relative sea level rise. The road is also subject to flooding and erosion during storms including hurricanes and more frequently occurring nor'easters. Susceptibility of the road to nuisance and storm-induced flooding, as well as wave overtopping, for alternative future sea level rise scenarios is evaluated using the "bottom-up" approach.

The following analysis uses sea level rise projections from Sweet et al. (2017a), return period coastal hazard data from the USACE ERDC Coastal Hazards System (USACE 2017c), and tidal datums from the Port Jefferson NOAA tide gauge (U.S. Department of Commerce 2017). The

methods of Section 8.2.2 are used to demonstrate how tidal datums, storm water levels, and the potential for wave overtopping change under alternative future climate scenarios.

Three RSLR projections (Intermediate-Low, Intermediate-High, and Extreme), based on Sweet et al. (2017a), were obtained from the USACE (2017a) Sea Level Change Calculator and are summarized in Table 8.5. Storm water levels and significant wave heights at a location near Shore Road were obtained from the USACE ERDC Coastal Hazards System and are summarized in Table 8.6. For the 5-year event and greater, estimated storm water levels exceed the roadway elevation today and are therefore excluded from this analysis.

Table 8.5. Relative sea level by year for three scenarios from Sweet et al. (2017a). Values are relative to the MSL tidal datum of 1983-2001 for Port Jefferson, NY.

Year	Intermediate-Low (m, MSL)	Intermediate-High (m, MSL)	Extreme (m, MSL)
2000	0.03	0.03	0.03
2010	0.09	0.16	0.17
2020	0.16	0.28	0.32
2030	0.22	0.43	0.53
2040	0.28	0.58	0.81
2050	0.35	0.75	1.10
2060	0.42	0.95	1.49
2070	0.48	1.18	1.89
2080	0.53	1.43	2.34
2090	0.59	1.72	2.92
2100	0.64	2.00	3.46

Table 8.6. Return period storm water levels and significant wave heights at a location near Shore Road obtained from the USACE ERDC Coastal Hazards System.

Return Period (yrs)	Still Water Level (m, MSL)	Wave Height (m)
1	0.95	0.98
2	1.36	1.30
5	1.81	1.62
10	2.10	1.85

The resulting combinations of the relative sea level projections, tidal datums, storm water levels, and wave effects are summarized shown in Figure 8.28, Figure 8.29, and Figure 8.30 for the intermediate-low, intermediate-high, and extreme scenarios, respectively. In these examples, the tidal datums of Mean Lower Low Water (MLLW) and MHHW are combined linearly using Equation 8.4, similar to how storm water levels are adjusted to account for future sea level rise.

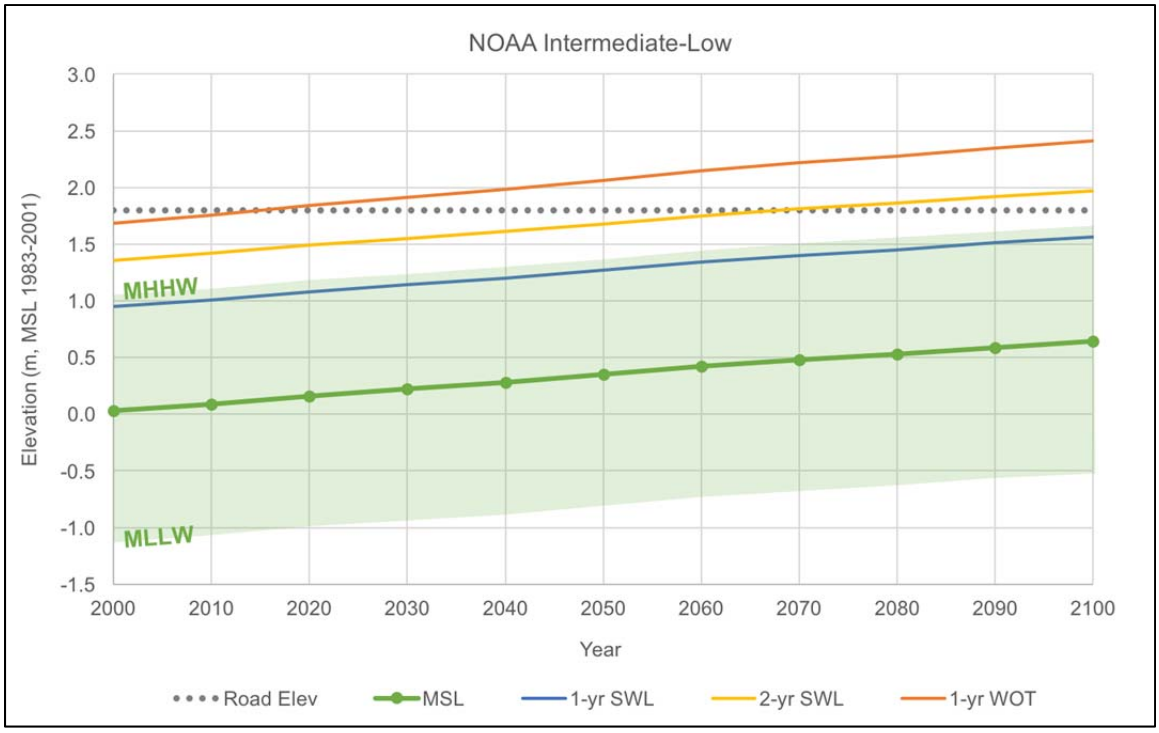

Figure 8.28. Projections of mean sea level, tidal datums (MLLW, MHHW), storm water levels, and wave overtopping elevations (WOT) for the intermediate-low scenario at Shore Road, NY.

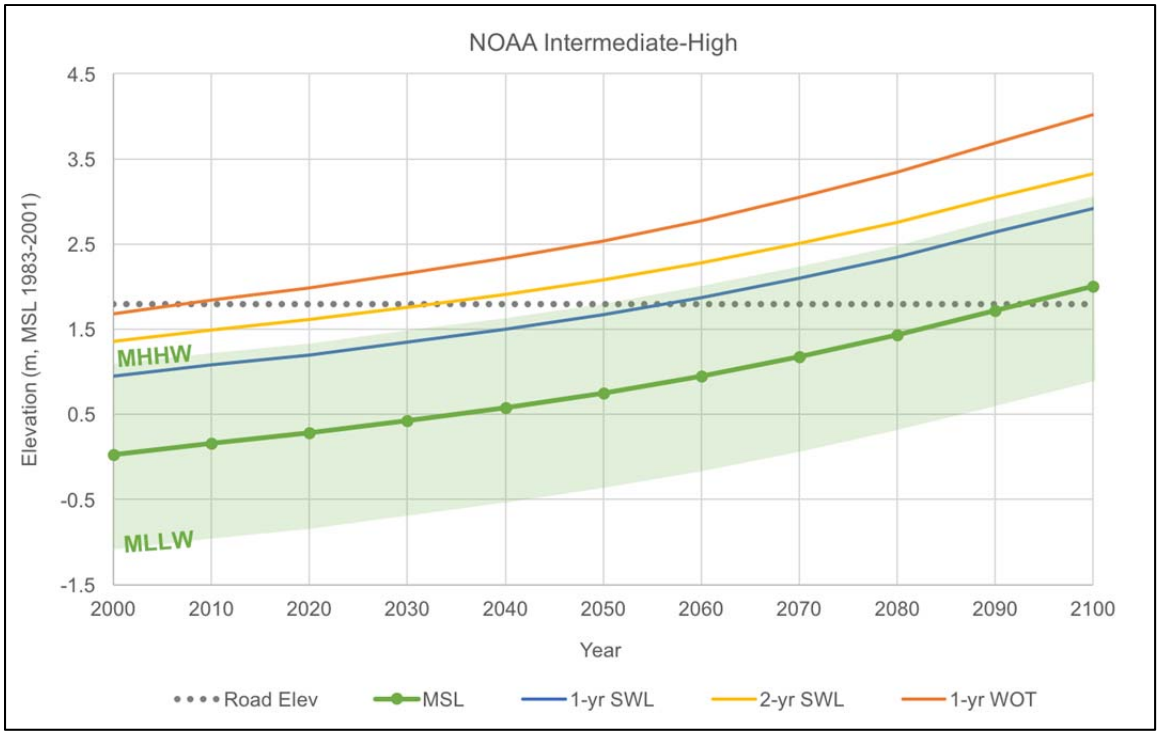

Figure 8.29. Projections of mean sea level, tidal datums (MLLW, MHHW), storm water levels, and wave overtopping (WOT) elevations for the intermediate-high scenario at Shore Road, NY.

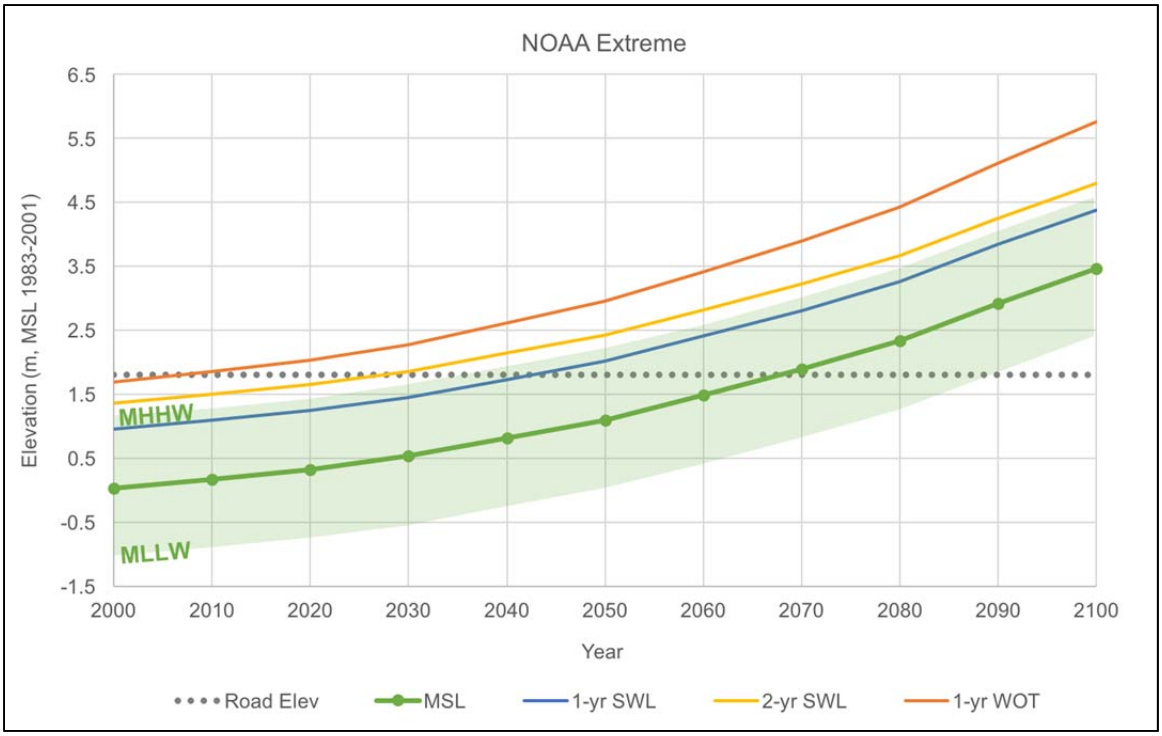

Figure 8.30. Projections of mean sea level, tidal datums (MLLW, MHHW), storm water levels, and wave overtopping (WOT) elevations for the extreme scenario at Shore Road, NY.

The tidal range in each figure is shaded green. Because of the large tide range at this site, the MHHW elevation is greater than the still water elevation produced by the annual (1-year) storm. The series labeled "1-yr WOT" represents the crest elevation of the significant wave height, which is estimated as the still water level added to 75 percent of the corresponding significant wave height. This method is used as a proxy for wave overtopping vulnerability since the existing revetment protecting the roadway is essentially a vertical wall. If the roadway were protected by a sloping revetment, wave overtopping would be more appropriately estimated by calculating the wave runup above the storm water level. Therefore, in this approach the "1-yr WOT" represents the elevation at which waves substantially contribute to flooding of the roadway.

Threshold (bottom-up) design is a process where the vulnerabilities of existing infrastructure or preliminary designs of new infrastructure are identified so that potential conditions that expose the infrastructure to these vulnerabilities can be quantified. The threshold at which the infrastructure becomes vulnerable is called the "threshold." In threshold design the goal is to assess vulnerabilities and seek robust solutions. The "bottom-up" approach to vulnerability analysis does not require the selection of any one specific sea level rise scenario or projection. Instead, the times at which a future hazard intercepts a known, critical elevations are identified for one or more future scenarios. In this case, the critical elevation is that of the roadway (+1.8 m MSL) since the focus is on roadway flooding. Therefore, any scenario that results in a tidal datum, storm water level, or wave overtopping that exceeds the roadway elevation of +1.8 m MSL is identified and the time at which it occurs is noted. By doing so, a range of potential decision or management timeframes is established.

The results of the bottom-up approach under the Intermediate-Low RLSR scenario, shown in Figure 8.28, show that the roadway is currently vulnerable to frequent wave overtopping. The 1-year storm water levels with wave effects are already affecting the roadway. Excluding wave effects, the roadway may be subject to flooding during the 2-year return period (50 percent AEP) storm as early as 2070. Neither the 1-year storm water level nor the MHHW tidal datum exceeds the roadway elevation before the year 2100. Note that both elevations are very similar to one another, further demonstrating the substantial tide range at this location.

When considering a potentially higher rate of RSLR, the Intermediate-High projection essentially slides the vulnerability forward in time (earlier). It also suggests that the roadway may be vulnerable to more frequent flooding well before 2100. Figure 8.29 shows that the roadway elevation is exceeded by the 2-year return period water level by 2040, or about 30 years sooner than in the Intermediate-Low scenario. It also shows that the roadway will likely experience more frequent nuisance flooding as both the 1-year storm water level and MHHW tidal datum elevations exceed that of the roadway by the year 2060. However, under this scenario the elevation of MSL exceeds that of the roadway before 2100, suggesting that the roadway would be completely under water for a substantial period every day. As before, the roadway is clearly already vulnerable to flooding due to wave action combined with the annual storm event (and MHHW tidal datum for that matter).

Under the Extreme RSLR scenario, flooding from tides, water levels, and wave action occurs even sooner. In Figure 8.30, the 2-year return period storm event may flood the roadway as early as 2030 even in the absence of wave action. The possibility for frequent nuisance flooding may occur sometime between 2040 and 2050. The consequence of this much higher rate of sea level rise is that MSL exceeds the roadway elevation by the year 2070, and that the MLLW tidal datum captures the roadway by 2090. If this projection occurs, the road would be completely flooded all of the time by or shortly after the year 2090.

BOTTOM LINE: Existing coastal hazard data, when combined with plausible future sea level rise scenarios, can be used in a bottom-up approach to identify times at which transportation infrastructure will become vulnerable to frequent flooding and/or wave action.

8.2.5. Case Study: Climate Change Effects on an Interstate Bridge –Pensacola, FL

This case study demonstrates how sea level rise information can be integrated into original hydrodynamic modeling to describe the vulnerability of a major interstate bridge to coastal hazards. The focus of this case study is to describe how sea level rise contributed to the failure of the Interstate 10 twin span bridge over Escambia Bay near Pensacola, FL during Hurricane Ivan in 2004. The major results of the hydrodynamic modeling—storm surge and wave characteristics—are highlighted in this case study for their role in the displacement of bridge decks during the storm event. However, additional descriptions of potential changes in scour are also provided because of the impact of sea level rise on waves and water velocity.

Interstate 10 (I-10) crosses Escambia Bay just east of Pensacola, FL on elevated twin span bridges (Figure 8.31). Like many other bridges, the decks are simply supported atop bent beams with minimal structural connections between the deck girders and bent beams. Hurricane Ivan made landfall near the Alabama-Florida border in 2004, causing substantial damage throughout

the adjacent coastal counties including the displacement of multiple spans of the I-10 bridge (*Damage W* and *Damage E* in Figure 8.31). The bridge decks were displaced by waves riding on top of the elevated storm water levels. This bridge was replaced with higher elevation twin spans following Hurricane Ivan.

Figure 8.31. Location map and damage overview for the I-10 Escambia Bay Bridge in Florida.

Two hydrodynamic model simulations were developed using ADCIRC and SWAN. The simulations were performed to compare the magnitude of wave loads in 2004 when the bridge was damaged with conditions of mean sea level 34 years prior when the bridge was designed. The mean sea level trend at the Pensacola, FL NOAA tide gauge (2.31 mm/year) was used to estimate the MSL position for the year 1970. The linear trend and data are shown in Figure 8.32. After accounting for seasonal variations in the MSL trend at this location, a MSL difference of 10 cm was determined between the two scenarios (1970 and 2004). After performing the 2004 hindcast of Hurricane Ivan and making the necessary adjustments for the MSL value of that time, a second simulation was performed using a water surface that was offset 10 cm lower in the models (1970 condition). **The models capture all the potential non-linear hydrodynamic effects that lead to changes in storm water levels, waves, and velocities between the two different time periods.**

The HEC-25 method (Douglas and Krolak 2008) is used to estimate the maximum vertical wave loads for the 1970 and 2004 condition simulations. The only variable in the HEC-25 method that changes between the two simulations is the elevation of the maximum wave crest. That value increased from +7.42 m MSL in 1970 to +7.56 m MSL in 2004 at location Damage W, and from +7.65 m MSL in 1970 to +7.79 m MSL in 2004 at location Damage E. A representative

comparison of the time-series from the 1970 and 2004 simulations is shown in Figure 8.33 and for a shorter time period to enhance the contrast between the values in Figure 8.34. The time-series results from other locations along the bridge behave in a similar fashion, though the values are lower relative to the low chord elevation of the bridge in sections of the bridge that survived.

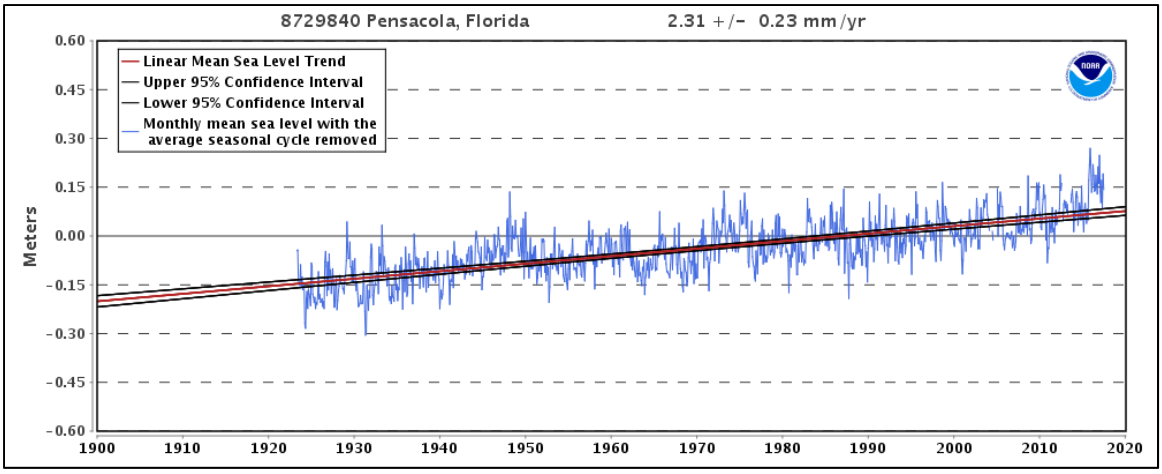

Figure 8.32. Mean sea level data, trend, and confidence intervals for Pensacola, FL.

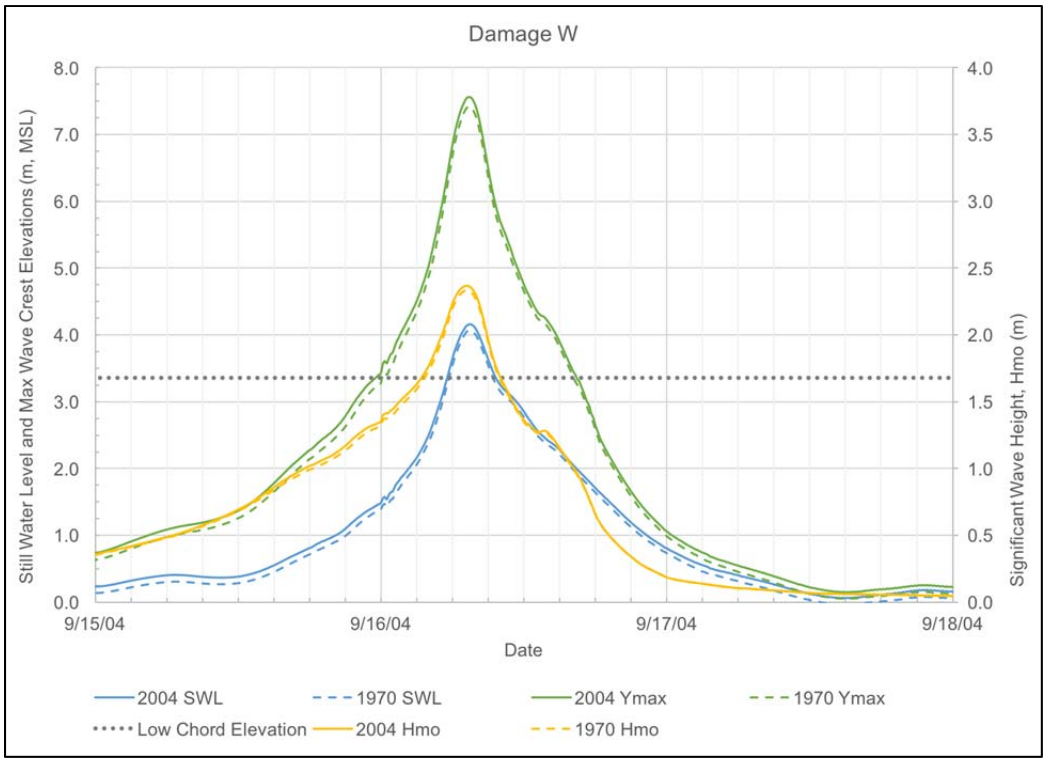

Figure 8.33. Time-series results from the 1970 and 2004 hydrodynamic model simulations of Hurricane Ivan at location Damage W.

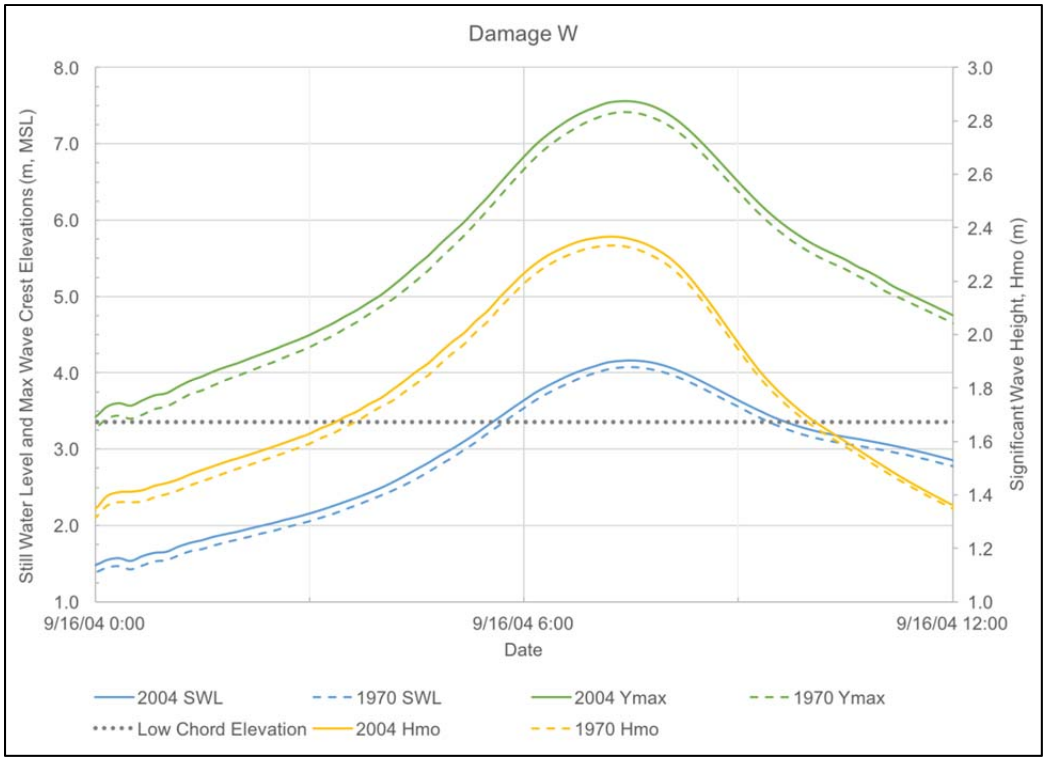

Figure 8.34. Time-series results from the 1970 and 2004 hydrodynamic model simulations of Hurricane Ivan at location Damage W, shown for a shorter time period during the storm event.

After accounting for the increase in maximum wave crest elevation between the two scenarios, the resultant wave loads would have potentially increased by 315 kN (~70 kips) due to RSLR alone. This is within the range of the resistance that the minimal connections between the deck girders and bent beams would have provided in the storm event. These results demonstrate the sensitivity of wave loads to changes in MSL and the storm surge elevation over time due to sea level rise. Also, the higher elevation MSL and maximum wave crest elevations lead to a prolonged duration of wave attack during the storm event. The increased time during which the bridge may have been exposed to very large waves in the storm would have been almost 2 hours. Using the peak wave period values extracted from the model simulations at the bridge (~6 s), that extended 2-hour duration would have been equivalent to the bridge being hit by an additional 1200 waves. **In summary, this bridge may not have been damaged, or would not have experienced as much damage, if MSL had not risen in between the time of construction and the landfall of Hurricane Ivan.**

The 34 years of increasing MSL also contributed to changes in local pier scour, wave scour, and abutment scour, though in different ways. As demonstrated earlier, the relationship between MSL and water velocity is an inverse proportionality. Therefore, as sea level increased from 1970 to 2004, the maximum water velocity experienced during Ivan would have decreased. The decreases in velocities at selected locations along the bridge alignment, however, were small and ranged from 1 to 3 cm/s. Since local pier scour (Florida DOT 2011, Arneson et al. 2012) is directly proportional to flow velocity, reductions in flow velocity would yield decreases in local pier scour. On the other hand, wave scour (Webb and Matthews 2014) and abutment scour (USACE 2006) are directly proportional to wave height. With wave height increases from the

1970 to 2004 scenarios, the corresponding scour would have similarly increased. While pier scour and scour in general were not the cause of damage to this bridge, this case study is used as an example of how changes to wave heights and flow velocities, as a result of sea level rise, may lead to changes in scour potential.

BOTTOM LINE: Sea level rise scenarios can be incorporated into hydrodynamic modeling in order to determine its effects on storm water levels, wave characteristics, and flow velocity for the purpose of coastal highway planning and design. Sea level rise has already significantly contributed to damage of one major US bridge during a hurricane.

8.3. Selected Coastal Issues

Several other considerations in the coastal environment will continue to be affected by climate change and sea level rise. Issues surrounding watershed contributions to coastal water levels and potential impacts to coastal geomorphological features are summarized in this section. Areas of potential future study are highlighted, but this section does not provide any specific design guidance.

8.3.1. Watershed Contributions to the Coast

The combination of coastal storm surge and heavy upland rainfall can cause an increased potential for flooding, which poses a threat to coastal transportation infrastructure. This effect will be exacerbated by several climate change effects, including rising sea levels.

The combined streamflow and storm surge hydrograph related to a coastal storm can show greatly increased flow volume and magnitude. Combined hydraulic and hydrodynamic simulations of flow and water levels reveal that rainfall-runoff can significantly affect coastal water levels and that the presence of storm surge generally results in higher flood levels upstream. Important to these results are locale: the topography of the watershed and an associated time lag between the rainfall event and the storm surge require careful consideration (Blumberg et al. 2015, Klerk et al. 2015, McGuigan et al. 2015, Torres et al. 2015).

When considered individually or as components, the peak flow resulting from storm surge tends be much higher than that from rainfall-runoff, owing to the intense flood and ebb of storm surge during a short duration storm event. However, **the total flood volume draining toward the coast tends to be dominated by rainfall-runoff** (Torres et al. 2015).

Hydraulic design associated with peak flow (e.g., bridge foundation, culvert, drain, etc.) would likely be sensitive to the increased flows associated with the rushing flood or ebb of storm surge. Design that is most concerned with flow volumes (e.g., detention basins, routing reservoirs, stormwater wetlands, etc.) would be more sensitive to long-lasting or delayed drainage due to combined rainfall-runoff and storm surge.

Because this compound flooding is so dependent on location-specific characteristics, the joint probability of rainfall-runoff and storm surge requires consideration. This effect is more likely on the Atlantic and Gulf coasts than on the Pacific Coast, for instance. The frequency of such events has increased in the last century. Sea level rise is one major cause of increased coastal flooding,

but climate change effects will likely increase the probability of compound events (surge and heavy precipitation), augmenting flooding potential in some areas (Wahl et al. 2015).

8.3.2. Evaluating the Effects of Sea level Rise on Coastal Geomorphology

Sea level is a critical component of coastal geology, and rising sea levels will impact bluff erosion, intertidal marsh location, barrier island behavior, and shoreline positions. As sea levels rise, waves will impact shorelines at higher elevations, causing increased erosion and retreat of bluffs, with the side effect of adding sediment to coastal systems. Some intertidal marshes will be able to keep pace with local sea level rise, increasing in elevation or migrating. Unprotected wetlands with sediment shortages can become inundated and transition to shallow-water habitat, as in coastal Louisiana.

Most barrier islands will likely be able to adjust to rising sea levels through storm-induced overwash processes causing increases in island elevations. The US barrier islands have existed, but moved and changed shape, throughout the past 6,000 years in response to sea level fluctuations, wave-driven longshore sand transport, cross-shore sand transport including storm tide overwash, inlet formation and closure, and winds blowing sand into dunes. The barrier overwash or rollover process is a typical response of all barrier islands as they migrate toward the mainland across the shallow continental shelf. These barrier island migration processes will be affected by accelerated sea level rise rates (Fitzgerald et al. 2008).

Shorelines will respond in different ways to sea level rise, though in general they are anticipated to be recessional. Local considerations such as weather impacts and anthropogenic activities can affect this response. The most common method to describe changes to beaches and barrier island positions has been the Bruun rule, which states that the wave climate under a higher water level adjusts the beach profile by shifting subaerial material offshore, thereby causing the shoreline to recede (Bruun 1988). However, the Bruun rule can be considered overly simplistic, limited, and inaccurate in many cases (Cooper and Pilkey 2004). Beach nourishment as an adaptation strategy may be able to offset the recessional effects of sea level rise for most sea level rise projections this century (Houston 2017).

A number of coastal geomorphology models have been developed to address changes in response to sea level rise. The Probabilistic Coastline Recession (PCR) model provides probabilistic estimates of shoreline recession induced by sea level rise (Ranasinghe et al. 2012). The model is relatively simple to develop, easy to apply, and appropriate for use with any coastline. Use of the model entails the implementation of a storm time-series with long-term measurements of tides and waves. Such measurements are available along the US coastline from NOAA and other agencies. The Coastal Storm Modeling System (CoSMoS) has been developed by the USGS (2017) to predict coastal flooding from both future sea level rise and storms integrated with long-term coastal evolution (e.g., beach changes and cliff/bluff retreat). Lentz et al. (2015) developed a coastal geomorphology model which predicts landform change with sea level rise with particular emphasis on inundation. Nearly 70 percent of the coastal landscape has some capacity to respond dynamically to sea level rise and inundation models overpredict land likely to submerge (Lentz et al. 2016).

Climate change may also impact coastal morphology through fluvial processes. Precipitation and runoff are the main drivers of the movement of sediment to the coast, and augmentations to the sediment supply can have a pronounced effect on shoreline positions (Blum and Törnqvist 2000).

The degree to which these processes change and what effects those changes have may be an area of study in the future.

BOTTOM LINE: Potential effects of climate outputs on watershed contributions to coastal water levels and on coastal geomorphological features are both important research areas.

References

Abatzoglou, J.T. and T.J. Brown. 2011. "A Comparison of Statistical Downscaling Methods Suited for Wildfire Applications." *Intl. J. Climatology*, Vol. 32, pp. 772–780.

Adler, R.F., G.J. Huffman, A. Chang, R. Ferraro, P. Xie, J. Janowiak, B. Rudolf, U. Schneider, S. Curtis, D. Bolvin, A. Gruber, J. Susskind, and P. Arkin. 2003. "The Version 2 Global Precipitation Climatology Project (GPCP) Monthly Precipitation Analysis (1979–Present)." *J. Hydrometeorology*, Vol. 4, pp. 1147–1167.

Allen, H.E., and R.M. Bejcek. 1979. *Effects of Urbanization on the Magnitude and Frequency of Floods in Northeastern Illinois*, U.S. Geological Survey Water Resources Investigations, 79-36, 48 pp.

Allen, R.J. and A.T. DeGaetano. 2015. "Areal Reduction Factors for Two Eastern United States Regions with High Rain-Gauge Density." *Journal of Hydrologic Engineering*, Vol. 10, No. 4 (July) ASCE.

Alley, R.B.,J. Marotzke, W.D. Nordhaus, J.D. Overpeck, D.M. Peteet, R.A. Pielke, R.T. Pierrehumbert, P.B. Rhines, T.F. Stocker, L.D. Talley, and J.M. Wallace. 2003. "Abrupt Climate Change." *Science*, Vol. 299, No. 5615, pp. 2005–2010.

American Association of State Highway and Transportation Officials (AASHTO). 2007. "Highway Drainage Guidelines." Washington, D.C.

Anandhi, A., A. Frei, D.C. Pierson, E.M. Schneiderman, M.S. Zion, D. Lounsbury, and A.H. Matonse. 2011. "Examination of Change Factor Methodologies for Climate Change Impact Assessment." *Water Resources Research*, Vol. 47, W03501, doi: 10.1029/2010WR009104.

Anarde, K.A., S. Kameshwar, J.N. Irza, J.A. Nittrouer, J. Lorenzo-Trueba, J.E. Padgett, A. Sebastian, and P.B. Bedient. 2017. "Impacts of Hurricane Storm Surge on Infrastructure Vulnerability for an Evolving Coastal Landscape." *Natural Hazards Review,* Vol. 19, No. 1, 14 pp.

Anderson, C., R. Arritt, Z. Pan, E. Takle, W. Gutowski, F. Otieno, R. da Silva, D. Caya, J. Christensen, D. Lüthi, M. Gaertner, C. Gallardo, F. Giorgi, R. Laprise, S. Hong, C. Jones, H. Juang, J. Katzfey, J. McGregor, W. Lapenta, J. Larson, J. Taylor, G. Liston, R. Pielke, and J. Roads. 2003. "Hydrological Processes in Regional Climate Model Simulations of the Central United States Flood of June–July 1993." *Journal of Hydrometeorology*, Vol. 4, No. 3, pp. 584–598.

Anderson, C., D. Claman, and R. Mantilla. 2015. *Iowa's Bridge and Highway Climate Change and Extreme Weather Vulnerability Assessment Pilot*. Final Report HEPN-707, Institute for Transportation, Iowa State University, Ames, IA.

Arneson, L.A., L.W. Zevenbergen, P.F. Lagasse, and P.E. Clopper. 2012. *Evaluating Scour at Bridges.* Hydraulic Engineering Circular No. 18, Fifth Ed., FHWA-HIF-12-003.

Asadieh, B. and N.Y. Krakauer. 2015. "Global Trends in Extreme Precipitation: Climate Models Versus Observations." *Hydrology and Earth System Sciences*, Vol 19, No. 2, pp.877–891.

Asquith, W. H. 1999. *Areal-Reduction Factors for the Precipitation of the 1-day Design Storm in Texas*. U.S. Geological Survey, Water-Resources Investigations Report 99-4267, Austin, TX.

Asquith, W.H. and R.W. Slade. 1996. *Regional Equations for Estimation of Peak-Streamflow Frequency for Natural Basins in Texas*. U. S. Geological Survey Water-Resources Investigations Report 96-4307, U.S. Geological Survey, Reston, VA.

Asquith, W.H. and J.S. Famiglietti. 1999. "Precipitation Areal-Reduction Factor Estimation Using an Annual-Maxima Centered Approach." *Journal of Hydrology*, Vol. 230, pp. 55–69.

Asquith, W.H. and D.B. Thompson. 2008. *Alternative Regression Equations for Estimation of Annual Peak-Streamflow Frequency for Undeveloped Basins in Texas Using PRESS-Minimization*. U.S. Geological Survey Scientific Investigations Report 2008-5084, U.S. Geological Survey, Reston, VA.

Asquith, W. H. and M.C. Roussel. 2009. *Regression Equations for Estimation of Annual Peak-Streamflow Frequency for Undeveloped Basins in Texas Using an L-Moment-Based, PRESS-Minimized, Residual-Adjusted Approach*, U.S. Geological Survey Scientific Investigations Report 2009-5087, U.S. Geological Survey, Reston, VA.

Archfield, S.A., R.M. Hirsch, A. Viglione, and G. Bloschi. 2016. "Fragmented Patterns of Flood Change Across the United States." *Geophysical Research Letters*, Vol. 43, 8 pp.

Bamber, J.L. and W.P. Aspinall. 2013. "An expert judgment assessment of the future sea level rise from the ice sheets." *Nature Climate Change*, Vol. 3, pp. 424–427.

Bassiouni, M., R.M. Vogel, and S.A. Archfield. 2016. "Panel Regression to Estimate Low-flow Response to Rainfall Variability in Ungaged Basins." *Water Resources Research*, Vol. 52, pp. 1–25.

Beighley, R.E. and G.E. Moglen. 2003. "Adjusting Measured Peak Discharge from an Urbanizing Watershed to Reflect a Stationary Land Use Signal." *Water Resources Research*, Vol. 39, No. 4, p. 1093.

Benestad, R.E., I. Hanssen-Bauer, and E.J. Førland. 2007. "An Evaluation of Statistical Models for Downscaling Precipitation and their Ability to Capture Long-Term Trends." *International Journal of Climatology*, Vol 27, pp. 649–665.

Bicknell, B.R., J.C. Imhoff, J.L. Kittle, Jr., A.S. Donigian, Jr., and R.C. Johanson. 1997. "Hydrological Simulation Program—Fortran, User's Manual for Version 11." U.S. Environmental Protection Agency, National Exposure Research Laboratory, Athens, GA, EPA/600/R-97/080, 755 pp.

Bilskie, M.V., S.C. Hagen, S.C. Medeiros, and D.L. Passeri. 2014. "Dynamics of Sea Level Rise and Coastal Flooding on a Changing Landscape." *Geophysical Research Letters*., Vol. 41, doi: 10.1002/2013GL058759.

Black, P.E. 2005. *Watershed Hydrology*. Wiley Online Library.

Blum, M.D., and T.E. Törnqvist. 2000. "Fluvial Responses to Climate and Sea-level Change: A Review and Look Forward." *Sedimentology*, Vol. 47, No. s1, pp. 2–48.

Blumberg, A.F., N. Georgas, L. Yin, T.O. Herrington, and P.M. Orton. 2015. "Street-Scale Modeling of Storm Surge Inundation along the New Jersey Hudson River Waterfront." *Journal of Atmospheric and Oceanic Technology*, Vol. 32, No. 8), pp. 1486–1497.

Bonnin, G.M., D. Martin, B. Lin, T. Parzybok, M. Yekta, and D. Riley. 2005. "Precipitation-Frequency Atlas of the United States." *NOAA Atlas 14*, Vol. 2, Version 3.0: Ohio River Basin and Surrounding States, National Weather Service, Silver Spring, MD.

Booij, N., R.C. Ris, L.H. Holthuijsen. 1999. "A Third-Generation Wave Model for Coastal Regions. 1. Model Description and Validation." *Journal of Geophysical Research,* Vol. 104, No. C4, pp. 7649–7666.

Bosma, K., E. Douglas, P. Kirshen, S. Miller, K. McArthur, and C. Watson. 2015. MassDOT-FHWA Pilot Project Report: Climate Change and Extreme Weather Vulnerability and Adaptation Options for the Central Artery/Tunnel System in Boston, MA.

Bowling, L.C., and D.P. Lettenmaier. 2010. "Modeling the Effects of Lakes and Wetlands on the Water Balance of Arctic Environments." *Journal of Hydrometeorology*, Vol. 11, pp. 276–295, doi:10.1175/2009JHM1084.1.

Brohan, P., J.J. Kennedy, I. Harris, S.F. Tett, and P.D. Jones. 2006. "Uncertainty Estimates in Regional and Global Observed Temperature Changes: A New Data Set from 1850." *Journal of Geophysical Research: Atmospheres*, Vol. 111, No. D12.

Bruun, P. 1988. "The Bruun Rule of Erosion by Sea Level Rise: A Discussion on Large-scale Two- and Three-dimensional Usages." *Journal of Coastal Research*, Vol. 4, pp. 627–648.

Burns, D.A., M.J. Smith, and D.A. Freehafer. 2015. "Development of Flood Regressions and Climate Change Scenarios to Explore Estimates of Future Peak Flows." U.S. Geological Survey Open-File Report 2015-1235, 11 pp.

Castellano, C. M. and A.T. DeGaetano. 2015. "Downscaled Projections of Extreme Rainfall in New York State." Technical Document of the Northeast Regional Climate Center, Cornell University, Ithaca, New York.

CCSP. 2008. *Abrupt Climate Change. A Report by the U.S. Climate Change Science Program and the Subcommittee on Global Change Research* [Clark, P.U., A.J. Weaver (coordinating lead authors), E. Brook, E.R. Cook, T.L. Delworth, and K. Steffen (chapter lead authors)]. U.S. Geological Survey, Reston, VA, 459 pp.

Choate, A., W. Jaglom, R. Miller, B. Rodehorst, P. Schultz, P. and C. Snow. 2012. "Impacts of Climate Change and Variability on Transportation Systems and Infrastructure: The Gulf Coast Study, Phase 2: Climate Variability and Change in Mobile, Alabama: Final Report, Task 2." FHWA-HEP-12-053, 228pp.

Choi, J., S.A. Socolofsky, and F. Oliver. 2008. "Hourly Disaggregation of Daily Rainfall in Texas Using Measured Hourly Precipitation at Other Locations." *Journal of Hydrologic Engineering*, ASCE, Vol. 13, No. 6, pp. 476–487.

Chow, V.T., D.R. Maidment, and L.W. Mays. 1988. *Applied Hydrology*, McGraw-Hill, New York, NY.

Church, J.A., P.U. Clark, A. Cazenave, J.M. Gregory, S. Jevrejeva, A. Levermann, M.A. Merrifield, G.A. Milne, R.S. Nerem, P.D. Nunn, A.J. Payne, W.T. Pfeffer, D. Stammer, and A.S. Unnikrishnan. 2013. "Sea Level Change." In *Climate Change 2013: The Physical Science Basis*. Contribution of Working Group I to the Fifth Assessment Report of the Intergovernmental Panel on Climate Change [Stocker, T.F., D. Qin, G.-K. Plattner, M. Tignor, S.K. Allen, J. Boschung, A. Nauels, Y. Xia, V. Bex and P.M. Midgley (Eds.)]. Cambridge University Press, Cambridge, United Kingdom and New York, NY, USA.

Cohn, T.A. and H.F. Lins. 2005. "Nature's Style: Naturally Trendy." *Geophysical Research Letters*, Vol. 32, L23402, doi: 10.1029/2005GL024476.

Collins, M., R. Knutti, J. Arblaster, J.-L. Dufresne, T. Fichefet, P. Friedlingstein, X. Gao, W.J. Gutowski, T. Johns, G. Krinner, M. Shongwe, C. Tebaldi, A.J. Weaver, and M. Wehner. 2013. "Long-term Climate Change: Projections, Commitments and Irreversibility." In *Climate Change 2013: The Physical Science Basis. Contribution of Working Group I to the Fifth Assessment Report of the Intergovernmental Panel on Climate Change* [Stocker, T.F., D. Qin, G.-K. Plattner, M. Tignor, S.K. Allen, J. Boschung, A. Nauels, Y. Xia, V. Bex and P.M. Midgley (Eds.)], Cambridge University Press, Cambridge, United Kingdom and New York, NY, USA.

Connecticut Department of Transportation. 2014. "Climate Change and Extreme Weather Vulnerability Pilot Project." Final Report, December.

Cook, L.M., C.J. Anderson, and C. Samaras. 2017. "Framework for Incorporating Downscaled Climate Output into Existing Engineering Methods: Application to Precipitation Frequency Curves." *Journal of Infrastructure Systems*, ASCE, Vol. 23, No. 4, pp. 1–15.

Cooper, J.A.G., and O.H. Pilkey. 2004. "Sea-level Rise and Shoreline Retreat: Time to Abandon the Bruun Rule." *Global and Planetary Change*, Vol. 43, No. 3-4, pp. 157–171.

Croissant, Y. and G. Milo. 2008. "Panel Data Econometrics in R: The plm Package." *Journal of Statistical Software*, Vol. 27, No. 2, 51 pp.

Cubasch, U., G. Meehl, G. Boer, R. Stouffer, M. Dix, A. Noda, C. Senior, S. Raper, and K. Yap. 2001. "Projections of Future Climate Change." *Climate Change 2001: The Scientific Basis. Contribution of Working Group I to the Third Assessment Report of the Intergovernmental Panel on Climate Change.*

Cubasch, U., D. Wuebbles, D. Chen, M.C. Facchini, D. Frame, N. Mahowald, and J.-G. Winther. 2013. "Introduction. Climate Change 2013: The Physical Science Basis." Contribution of Working Group I to the Fifth Assessment Report of the Intergovernmental Panel on Climate Change. Stocker, T.F., D. Qin, G.-K. Plattner, M. Tignor, S.K. Allen, J. Boschung, A. Nauels, Y. Xia, V. Bex, and P.M. Midgley, Eds. Cambridge University Press, Cambridge, United Kingdom and New York, NY, USA, pp. 119–158.

Cunnane, C. 1978. "Unbiased Plotting Positions—A Review," *Journal of Hydrology*, Vol. 37, pp. 205–222.

Dalrymple, T. 1960. "Flood-Frequency Analyses." *Manual of Hydrology: Part 3. Flood-Flow Techniques*, Geological Survey Water-Supply Paper 1543-A, U.S. Geological Survey, Reston, VA.

Dawdy, D.R., V.W. Griffis, and V.K. Gupta. 2012. "Regional Flood Frequency Analysis: How We Got Here, and Where We Are Going." *Journal of Hydrological Engineering,* 10.1064(ASCE) HE, 1943-5584.0000584, pp. 953–959.

Deltacommissie 2008. "Working Together with Water: A Living Land Builds for Its Future." The Hague: Delta Committee.

Dixon, K.W., J.R. Lanzante, M.J. Nath, K. Hayhoe, A. Stoner, A. Radhakrishnan, V. Balaji, and C. Gaitán. 2016. "Evaluating the Stationarity Assumption in Statistically Downscaled Climate Projections: Is Past Performance an Indicator of Future Results?" *Climatic Change*, Vol. 135, pp. 395–408.

Dompe, P.E., J.M. McBee, and H. Demir. 2015. "Storm Surge and Wave Vulnerability Assessment of Coastal Bridges." *Proceedings of the World Environmental and Water Resources Congress: Floods, Droughts, and Ecosystems*. ASCE, Reston, VA: pp. 1256–1263.

Douglas, E.M., P. Kirshen, K. Bosma, C. Watson, S. Miller, and K. McArthur. 2016a. "Simulating the Impacts and Assessing the Vulnerability of Boston's Central Artery/Tunnel System to Sea Level Rise and Increased Coastal Flooding." *Journal of Extreme Events*, Vol 3, No. 4, 1650013, https://doi.org/10.1142/S2345737616500135.

Douglas, E., P. Kirshen, R. Hannigan, R. Herst, and A. Palardy. 2016b. *Climate Change and Sea Level Rise Projections for Boston*. Boston Research Advisory Group for Climate Ready Boston.

Douglass, S. L., and J. Krolak 2008. *Highways in the Coastal Environment*. Hydraulic Engineering Circular No. 25, Vol. 1, FHWA-NHI-07-096.

Douglass, S.L., B.M. Webb, and R. Kilgore 2014. *Highways in the Coastal Environment: Assessing Extreme Events.* Hydraulic Engineering Circular No. 25 (Vol. 2), Federal Highway Administration, FHWA-NHI-14-006.

Easterling, D. R., K.E. Kunkel, J.R. Arnold, T. Knutson, A.N. LeGrande, L.R. Leung, R.S . Vose, D.E. Waliser, and M.F. Wehner. 2017. "Precipitation Change in the United States." In *Climate Science Special Report: Fourth National Climate Assessment*, Vol. I [Wuebbles, D.J., D.W. Fahey, K.A. Hibbard, D.J. Dokken, B.C. Stewart, and T.K. Maycock (Eds.)]. U.S. Global Change Research Program, Washington, DC, pp. 207–230, doi: 10.7930/J0H993CC.

Eden, J.M., K. Wolter, F.E.L. Otto, and G.J. van Oldenborgh. 2016. "Multi-method Attribution Analysis of Extreme Precipitation in Boulder, Colorado." *Environmental Research Letters*, Vol. 11.

Eng, K., Y. Chen, and J.E. Kiang. 2009. "User's Guide to the Weighted-Multiple-Linear Regression Program (WREG version 1.0)." U.S. Geological Survey Technique and Methods 4-A8, 21 pp.

England, J.F., Jr., T.A. Cohn, B.A. Faber, J.R. Stedinger, W.O. Thomas, Jr., A.G. Veilleux, J.E. Kiang, and R.R. Mason 2018. "*Guidelines for Determining Flood Flow Frequency – Bulletin 17C*." U.S. Geological Survey Techniques and Methods 4-B5, Reston, VA, 164 pp.

Environment Agency. 2009. "Thames Estuary 2100: Managing Flood Risk through London and the Thames Estuary." Environment Agency, London, United Kingdom, 28 pp.

Eyring, V., S. Bony, G.A. Meehl, C.A. Senior, B. Stevens, R.J. Stouffer, and K.E. Taylor. 2016a. "Overview of the Coupled Model Intercomparison Project Phase 6 (CMIP6) Experimental Design and Organization." *Geoscientific Model Development*, Vol 9, pp. 1937–1958, doi: 10.5194/gmd-9-1937-2016.

Eyring, V., M. Righi, A. Lauer, M. Evaldsson, S. Wenzel, C. Jones, A. Anav, O. Andrews, I. Cionni, E.L. Davin, C. Deser, C. Ehbrecht, P. Friedlingstein, P. Gleckler, K. D. Gottschaldt, S. Hagemann, M. Juckes, S. Kindermann, J. Krasting, D. Kunert, R. Levine, A. Loew, J. Mäkelä, G. Martin, E. Mason, A.S. Phillips, S. Read, C. Rio, R. Roehrig, D. Senftleben, A. Sterl, L.H. van Ulft, J. Walton, S. Wang, and K.D. Williams. 2016b. "ESMValTool (v1. 0)–a Community Diagnostic and Performance Metrics Tool for Routine Evaluation of Earth System Models in CMIP." *Geoscientific Model Development*, Vol. 9, pp. 1747–1802, doi: 10.5194. gmd-9-1747-2016.

Fitzgerald, D.M., M.S. Fenster, B.A. Argow, and I.V. Buynevich. 2008. "Coastal Impacts due to Sea Level Rise." *Annual Review of Earth and Planetary Sciences*, Vol. 36, pp. 601–647.

Flato, G., J. Marotzke, B. Abiodun, P. Braconnot, S.C. Chou, W. Collins, P. Cox, F. Driouech, S. Emori, V. Eyring, C. Forest, P. Gleckler, E. Guilyardi, C. Jakob, V. Kattsov, C. Reason, and M. Rummukainen. 2013. "Evaluation of Climate Models." In *Climate Change 2013: The Physical Science Basis*. Contribution of Working Group I to the Fifth Assessment Report of the Intergovernmental Panel on Climate Change [Stocker, T.F., D. Qin, G. K. Plattner, M. Tignor, S.K. Allen, J. Boschung, A. Nauels, Y. Xia, V. Bex and P.M. Midgley (Eds.)]. Cambridge University Press, Cambridge, United Kingdom and New York, NY, USA.

Florida DOT. 2011. *Bridge Scour Manual*. Tallahassee, FL.

Fortuin, P. 2017. "Severe Rain Showers, Implications for Design of Roads, Bridges and Tunnels." Rijkswaterstaat, Netherlands Ministry of Infrastructure and Environment, presentation in April 2017.

Fowler, H.J., S. Blenkinsop, and C. Tebaldi. 2007. "Review: Linking Climate Change Modeling to Impacts Studies: Recent Advances in Downscaling Techniques for Hydrological Modeling," *International Journal of Climatology*, Vol. 27, pp. 147–178.

Friedman, D.J., J. Schecter, B. Baker, C. Mueller, G. Villarini, and K. White. 2016. *U.S. Army Corps of Engineers Nonstationarity Detection Tool User Guide*. User Guide Version 1.1, January 2016, U.S. Army Corps of Engineers, Climate Preparedness and Resilience Community of Practice, Washington, DC.

Fries, S. 2017. *Personal Communication*. August 16, 2017, U.S. EPA.

Frumhoff, P.C., J.J. McCarthy, J.M. Melillo, S.C. Moser, and D.J. Wuebbles. 2007. *Confronting Climate Change in the U.S. Northeast: Science, Impacts, and Solutions.* Synthesis Report of the Northeast Climate Impacts Assessment (NECIA). Cambridge, MA: Union of Concerned Scientists (UCS).

Gao, H., Q. Tang, X. Shi, C. Zhu, T.J. Bohn, F. Su, J. Sheffield, M. Pan, D.P. Lettenmaier, and E.F. Wood. 2010. "Water Budget Record from Variable Infiltration Capacity (VIC) Model." In *Algorithm Theoretical Basis Document for Terrestrial Water Cycle Data Records* (in review).

Giambelluca, T.W., Q. Chen, A.G. Frazier, J.P. Price, Y.L. Chen, P.S. Chu, J.K. Eischeid, and D.M. Departe. 2013. "Online Rainfall Atlas of Hawaii." *Bulletin American Meteorological Society*, Vol. 94, No. 3, pp. 313–316.

Gleckler, P. 2015. "Community-Based Benchmarking of the CMIP DECK Experiments." AGU Fall Meeting Abstracts.

Gleckler, P. 2016. "Making Objective Summaries of Climate Model Behavior More Accessible." AGU Fall Meeting Abstracts.

Goda, Y. 2003. "Revisiting Wilson's Formulas for Simplified Wind-Wave Prediction." *Journal of Waterway, Port, Coastal, and Ocean Engineering,* Vol. 129, No. 2, pp. 93–95.

Guilbert, J., B. Beckage, J.M. Winter, R.M. Horton, T. Perkins, and A. Bomblies. 2014. "Impacts of Projected Climate Change over the Lake Champlain Basin in Vermont." *Journal of Applied Meteorology and Climatology*, Vol. 53, pp. 1861–1875.

Gutmann, E., T. Pruitt, M.P. Clark, L. Brekke, J.R. Arnold, D.A. Raff, and R.M. Rasmussen. 2014. "An Intercomparison of Statistical Downscaling Methods Used for Water Resource Assessments in the United States." *Water Resources Research*, Vol. 50, pp. 7167–7186.

Hall, J.A., S. Gill, J. Obeysekera, W. Sweet, K. Knuuti, and J. Marburger. 2016. *Regional Sea Level Scenarios for Coastal Risk Management: Managing the Uncertainty of Future Sea Level Change and Extreme Water Levels for Department of Defense Coastal Sites Worldwide.* U.S. Department of Defense, Strategic Environmental Research and Development Program. 224 pp.

Hassanzadeh, E., A. Nazemi, and A. Elshorbagy. 2014. "Quantile-Based Downscaling of Precipitation Using Genetic Programming: Application to IDF Curves in Saskatoon." *Journal of Hydrologic Engineering*, Vol. 19, No. 5, pp. 943–955.

Hawkins, E., and R. Sutton. 2009. "The Potential to Narrow Uncertainty in Regional Climate Predictions." *Bulletin of the American Meteorological Society*, Vol. 90, pp. 1095–1107. doi: 10.1175/2009BAMS2607.1.

Hawkins, E., and R. Sutton. 2011. "The Potential to Narrow Uncertainty in Regional Precipitation Change." *Climate Dynamics*, Vol. 37, pp. 407–418. doi: 10.1007/s00382-010-0810-6.

Hay L.E, R.L. Wilby, and G.H. Leavesley. 2000. "A Comparison of Delta Change and Downscaled GCM Scenarios for Three Mountainous Basins in the United States." *Journal of the American Water Resources Association*, Vol. 36, pp. 387–397. doi: 10.1111/j.1752-1688.2000.tb04276.x.

Hayhoe, K., J. Edmonds, R.E. Kopp, A.N. LeGrande, B.M. Sanderson, M.F. Wehner, and D.J. Wuebbles. 2017. "Climate Models, Scenarios, and Projections." In *Climate Science Special Report: Fourth National Climate Assessment, Volume I* [Wuebbles, D.J., D.W. Fahey, K.A. Hibbard, D.J. Dokken, B.C. Stewart, and T.K. Maycock (Eds.)]. U.S. Global Change Research Program, Washington, DC, USA, pp. 133–160, doi: 10.7930/J0WH2N54.

Hayhoe, K., C.P. Wake, T.G. Huntington, L. Lou, M.D. Schwartz, J. Sheffield, E. Wood, B. Anderson, J. Bradbury, A. DeGaetano, T.J. Troy, and D. Wolfe. 2007. "Past and Future Changes in Climate and Hydrological Indicators in the U.S. Northeast." *Climate Dynamics*, Vol. 28, pp. 381–407.

Hecht and R.M. Vogel (in review). *Updating Design Flood Estimates Using Regression*.

Hejazi, M.I. and M. Markus 2009. "Impacts of Urbanization and Climate Variability on Floods in Northeastern Illinois." *Journal of Hydrologic Engineering*, Vol. 14, No. 6, pp. 606–616.

Helsel, D.R. and R.M. Hirsch. 1992. "Statistical Methods in Water Resources." Elsevier, New York, 55 pp.

Herrmann, G.R. and T.G. Cleveland. 2009. "Consideration of Fundamental Loss Components, Rational Coefficients, and Arid Climate." In Proceedings, *AIH/AHS HydroSymposium*, American Institute of Hydrology, Arizona Hydrological Society, American Institute of Hydrology.

Hershfield, D.M. 1961. *Rainfall Frequency Atlas of the United States for Durations of 30 Minutes to 24 Hours and Return Periods from 1 to 100 Years*, Technical Paper 40, U.S. Department of Commerce, Weather Bureau, Washington, D.C.

Hidalgo, H.G., M.D. Dettinger, and D.R. Cayan. 2008. *Downscaling with Constructed Analogues: Daily Precipitation and Temperature Fields over the United States*. PIER Energy-Related Environmental Research, California Energy Commission, Sacramento, CA.

Hirsch, R.M. 2011. "A Perspective on Nonstationarity and Water Management." *Journal of the American Water Resources Association*, Vol. 47, No. 3, pp. 436–446. doi: 10.1111/j.1752-1688.2011.00539.

Horton, B.P., S. Rahmstorf, S.E. Engelhart, and A.C. Kemp. 2014. Expert Assessment of Sea-level Rise by AD 2100 and AD 2300, *Quaternary Science Reviews*, Vol. 84, No. 15, 1–6.

Hosseinzadehtalaei, P., H. Tabari and P. Willems. 2017. "Uncertainty Assessment for Climate Change Impact on Intense Precipitation: How Many Model Runs Do We Need?" *International Journal of Climatology*, Vol. 37, pp. 1105–1117, doi: 10.1002/joc.5069.

Houston, J. 2017. "Shoreline Change in Response to Sea-Level Rise on Florida's West Coast." *Journal of Coastal Research*, http://www.jcronline.org/doi/abs/10.2112/JCOASTRES-D-17-00024.1.

Hyman, R.C., J.R. Potter, M.J. Savonis, V.R. Burkett, and J.E. Tump. 2008. "Chapter 1: Why Study Climate Change Impacts on Transportation?" *Impacts of Climate Change and Variability on Transportation Systems and Infrastructure*: Gulf Coast Study, Phase I U.S. Climate Change Science Program Synthesis and Assessment Product 4.7.

IPCC. 1990. *First Assessment Report*. Working Group II: Impacts Assessment of Climate Change.

IPCC. 2007. *Climate Change 2007: The Physical Science Basis*. Contribution of Working Group I to the Fourth Assessment Report of the Intergovernmental Panel on Climate Change, Solomon, S., D. Qin, M. Manning, Z. Chen, M. Marquis, K.B. Averyt, M. Tignor and H.L. Miller (Eds.), Cambridge University Press, Cambridge, United Kingdom and New York, NY, USA

IPCC. 2012a. "Glossary of Terms." In *Managing the Risks of Extreme Events and Disasters to Advance Climate Change Adaptation* [Field, C.B., V. Barros, T.F. Stocker, D. Qin, D.J. Dokken, K.L. Ebi, M.D. Mastrandrea, K.J. Mach, G.-K. Plattner, S.K. Allen, M. Tignor, and P.M. Midgley (Eds.)]. A Special Report of Working Groups I and II of the Intergovernmental Panel on Climate Change (IPCC). Cambridge University Press, Cambridge, United Kingdom, and New York, NY, USA, pp. 555—564.

IPCC. 2012b. *Managing the Risks of Extreme Events and Disasters to Advance Climate Change Adaptation.* A Special Report of Working Groups I and II of the Intergovernmental Panel on Climate Change [Field, C.B., V. Barros, T.F. Stocker, D. Qin, D.J. Dokken, K.L. Ebi, M.D. Mastrandrea, K.J. Mach, G.-K. Plattner, S.K. Allen, M. Tignor, and P.M. Midgley (Eds.)], Cambridge University Press, Cambridge, United Kingdom, and New York, NY, USA, 582 pp.

IPCC. 2013. *Climate Change 2013: The Physical Science Basis*. Contribution of Working Group I to the Fifth Assessment Report of the Intergovernmental Panel on Climate Change [Stocker, T.F., D. Qin, G.-K. Plattner, M. Tignor, S.K. Allen, J. Boschung, A. Nauels, Y. Xia, V. Bex and P.M. Midgley (Eds.)]. Cambridge University Press, Cambridge, United Kingdom and New York, NY, USA, 1535 pp.

Interagency Advisory Committee on Water Data. 1982. "Guidelines for Determining Flood Flow Frequency." Bulletin 17B of the Hydrology Subcommittee, U.S. Geological Survey, Office of Water Data Coordination, Reston, VA.

Jacob, D., J. Peterson, B. Eggert, and 36 coauthors. 2014. "EURO-CORDEX: New High-Resolution Climate Change Projections for European Impact Research." *Regional Environmental Change*, Vol. 14, pp. 563–578, doi: 10.1007/s10113-013-0499-2.

Jewett, L. and A. Romanou. 2017. Ocean Acidification and Other Ocean Changes. In *Climate Science Special Report: Fourth National Climate Assessment, Volume I* [Wuebbles, D.J., D.W. Fahey, K.A. Hibbard, D.J. Dokken, B.C. Stewart, and T.K. Maycock (Eds.)]. U.S. Global Change Research Program, Washington, DC, USA, pp. 364–392, doi: 10.7930/J0QV3JQB.

Johnson, T.E. and C.P. Weaver. 2009. "A Framework for Assessing Climate Change Impacts on Water and Watershed Systems." *Environmental Management*, Vol. 43, pp. 118–134.

JPL. 2017. Jet Propulsion Laboratory website on Ocean Surface Topography from Space, accessed October 4, 2017. (see http://sealevel.jpl.nasa.gov/)

Kafalenos, R.H. and K.J. Leonard. 2008. "What are the Implications of Climate Change and Variability for Gulf Coast Transportation?" Chapter 4, *Impacts of Climate Change and Variability on Transportation Systems and Infrastructure: Gulf Coast Study*, Phase I U.S. Climate Change Science Program Synthesis and Assessment Product 4.7.

Karl, T.R., J.T. Melillo, and T.C. Peterson (Eds.). 2009. *Global Climate Change Impacts in the United States*, Cambridge University Press, 189 pp. [http://downloads.globalchange.gov/usimpacts/pdfs/climate-impacts-report.pdf]

Kates, R.W., W.R. Travis, and T.J. Wilbanks 2012. "Transformational Adaptation when Incremental Adaptations to Climate Change are Insufficient." Proceedings of the National Academy of Sciences, Vol. 109, pp. 7156–7161.

Kay, A.L. and R.G. Jones. 2012. "Comparison of the Use of Alternative UKCP09 Products for Modelling the Impacts of Climate Change on Flood Frequency." *Climatic Change*, Vol. 114, No. 2, pp. 211–230.

Kendon, E.J., N.M. Roberts, H.J. Fowler, M.J. Roberts, S.C. Chan, and C.A. Senior. 2014. "Heavier Summer Downpours with Climate Change Revealed by Weather Forecast Resolution Model." *Nature Climate Change*. Vol. 4, pp. 570–576.

Kendon, E.J., N. Ban, N.M. Roberts, H.J. Fowler, M.J. Roberts, S.C. Chan, J.P. Evans, G. Fosser, and J.M. Wilkinson. 2017. "Do Convection-Permitting Regional Climate Models Improve Projections of Future Precipitation Change?" *Bulletin of the American Meteorological Society* Vol. 98, pp. 79-+.

Kharin, V.V., F.W. Zwiers, and X. Zhang. 2005. "Intercomparison of Near Surface Temperature and Precipitation Extremes in AMIP-2 Simulations, Reanalyses and Observations." *Journal of Climate*, Vol. 18, pp. 5201–5223.

Kharin, V.V., F.W. Zwiers, X. Zhang, and G.C. Hegerl. 2007. "Changes in Temperature and Precipitation Extremes in the IPCC Ensemble Global Coupled Model Simulations." *Journal of Climate*, Vol 20, pp. 1419–1444.

Kharin, V., F. Zwiers, X. Zhang, and M. Wehner. 2013. "Change in Temperature and Precipitation Extremes in the CMIP5 Ensemble." *Climatic Change*, Vol. 119, No. 2, 345–357.

Kilgore, R., G.R. Herrmann, W.O. Thomas, Jr., and D.B. Thompson. 2016. *Highways in the River Environment – Floodplains, Extreme Events, Risk, and Resilience*. Hydraulic Engineering Circular No. 17 (HEC-17), Federal Highway Administration, FHWA-HIF-16-018.

Kilgore, R.C. Anderson, J.M. Jacobs, K. Hayhoe, G.R. Herrmann, A.Stoner, W.O. Thomas, Jr., and D.B. Thompson. 2019. *Applying Climate Change Information to Hydrologic and Hydraulic Design of Transportation Infrastructure*. Project NCHRP 15-61 Final Report, Transportation Research Board, NAS-NRC.

Kinnison, H.B. and B.R. Colby. 1945. "Flood Formulas Based on Drainage-Basin Characteristics." ASCE Trans. 100, pp. 849–904.

Kjeldsen, T.R., J.D. Miller, and J.C. Packman. 2013. "Modelling Design Flood Hydrographs in Catchments with Mixed Urban and Rural Land Cover." *Hydrology Research*, Vol. 44, No. 6, pp. 1040–1057.

Klerk, W.J., H.C. Winsemius, W.J. van Verseveld, A.M.R. Bakker, and F.L.M. Diermanse. 2015. "The Co-incidence of Storm Surges and Extreme Discharges within the Rhine–Meuse Delta." *Environmental Research Letters*, Vol. 10, No. 3, 035005.

Knutti, R., D. Masson, and A. Gettelman. 2013. "Climate Model Genealogy: Generation CMIP5 and How We Got There." *Geophysical Research Letters,* Vol. 40, pp. 1194–1199. http://dx.doi.org/10.1002/grl.50256.

Knutti, R., and J. Sedláček. 2013. "Robustness and Uncertainties in the New CMIP5 Climate Model Projections." *Nature Climate Change*, Vol. 3, pp. 369–373, doi: 10.1038/nclimate1716.

Knutson, T.R. and R.E. Tuleya. 2004. "Impact of CO2-induced Warming on Simulated Hurricane Intensity and Precipitation: Sensitivity to the Choice of Climate Model and Convective Parameterization." *Journal of Climate,* Vol. 17, No. 18, p. 3477.

Kollat, J.B., J.R. Kasprzky, W.O. Thomas, Jr., A.C. Miller, and D. Divoky. 2012. "Estimating the Impacts of Climate Change and Population Growth on Flood Discharges in the United States." *Journal of Water Resources Planning and Management*, Vol. 138, No. 5, pp. 442–452.

Kopp, R.E. 2013. "Does the Mid-Atlantic United States Sea Level Acceleration Hot Spot Reflect Ocean Dynamic Variability?" *Geophysical Research Letters,* Vol. 40, pp. 3981–3985. doi: 10.1002/grl.50781

Kopp, R.E., R.M. Horton, C.M. Little, J.X. Mitrovica, M. Oppenheimer, D. Rasmussen, and C. Tebaldi. 2014. Probabilistic 21st and 22nd Century Sea-level Projections at a Global Network of Tide-Gauge Sites. *Earth's Future*, Vol. 2 No. 8, pp. 383–406.

Kopp, R.E., A.C. Kemp, K. Bittermann, B.P. Horton, J.P. Donnelly, W.R. Gehrels, C.C. Hay, J.X. Mitrovica, E.D. Morrow, and S. Rahmstorf. 2016. "Temperature-driven Global Sea-level Variability in the Common Era." *Proceedings of the National Academy of Sciences*, Vol. 113, pp. E1434–E1441, http://dx.doi.org/10.1073/pnas.1517056113.

Kopp, R.E., K. Hayhoe, D.R. Easterling, T. Hall, R. Horton, K.E. Kunkel, and A.N. LeGrande. 2017a. "Potential Surprises – Compound Extremes and Tipping Elements. In *Climate Science Special Report: Fourth National Climate Assessment, Volume I* [Wuebbles, D.J., D.W. Fahey, K.A. Hibbard, D.J. Dokken, B.C. Stewart, and T.K. Maycock (Eds.)]. U.S. Global Change Research Program, Washington, DC, USA, pp. 411–429, doi: 10.7930/J0GB227J

Kopp, R.E., R.M. DeConto, D.A. Bader, C.C. Hay, R.M. Horton, S. Kulp, M. Oppenheimer, D. Pollard, and B.H. Strauss. 2017b. "Evolving Understanding of Antarctic Ice-sheet Physics and Ambiguity in Probabilistic Sea-level Projections. *Earth's Future*, Vol. 5, No. 12, pp. 1217–1233, doi:10.1002/2017EF000663.

Kotamarthi, R., C. Castro, K. Hayhoe, L. Mearns, and D. Wuebbles. 2016. *Use of Climate Information for Decision-Making and Impacts Research: State of our Understanding*, U.S. Department of Defense Strategic Environmental Research and Development Program.

Kour, R., N. Patel, and A.P. Krishna. 2016. "Climate and Hydrological Models to Assess the Impact of Climate Change on Hydrological Regime: a Review." *Arabian Journal of Geosciences,* Volume 9, No. 9.

Koutroulis, A.G., M.G. Grillakis, I.K. Tsanis, and L. Papadimitriou. 2016. "Evaluation of Precipitation and Temperature Simulation Performance of the CMIP3 and CMIP5 Historical Experiments." *Climate Dynamics*, Vol. 47, No. 5-6, pp. 1881–1898.

Krajewski, W.F. and R. Mantilla. 2008. "Why Were the 2008 Floods so Large," *A Watershed Year: Anatomy of the Iowa Floods of 2008*, pp. 19–30.

Krakauer, N.Y. and B.M. Fekete. 2014. "Are Climate Model Simulations Useful for Forecasting Precipitation Trends? Hindcast and Synthetic-Data Experiments." *Environmental Research Letters*, Vol. 9, No. 2, p. 024009.

Kumar, D., E. Kodra, and A.R. Ganguly. 2014. "Regional and Seasonal Intercomparison of CMIP3 and CMIP5 Climate Model Ensembles for Temperature and Precipitation." *Climate Dynamics*, Vol. 43, 2491–2518, doi: 10.1007/s00382-014-2070-3.

Lee, H., D.E, Waliser, R. Ferraro, T. Iguchi, C.D. Peters-Lidard, B. Tian, P.C. Loikith, and D.B. Wright. 2017. "Evaluating Hourly Rainfall Characteristics over the U.S. Great Plains in Dynamically Downscaled Climate Model Simulations Using NASA-Unified WRF." *Journal of Geophysical Research: Atmospheres*, Vol. 122, No. 14, pp.7371–7384.

Lentz, E.E., Stippa, S.R., Thieler, E.R., Plant, N.G., Gesch, D.B., and Horton, R.M. 2015. Evaluating Coastal Landscape Response to Sea-level Rise in the Northeastern United States—Approach and Methods (ver. 2.0, December 2015): U.S. Geological Survey Open-File Report 2014–1252, 27 pp., http://dx.doi.org/10.3133/ofr20141252

Lentz, E.E., E.R. Thieler, N.G. Plant, S.R. Stippa, R.M. Horton, and D. B. Gesch. 2016. "Evaluation of Dynamic Coastal Response to Sea-level Rise Modifies Inundation Likelihood." *Nature Climate Change*, Vol. 6, pp. 696–700, doi:10.1038/nclimate2957.

Liang, X., D.P. Lettenmaier, E.F. Wood, and S.J. Burges. 1994. "A Simple Hydrologically Based Model of Land Surface Water and Energy Fluxes for GSMs," *Journal of Geophysical. Research*, Vol. 99, No. D7, pp. 14,415–14,428.

Lindquist, E. 2011. *Transportation Planning, Policy and Climate Change: Making the Long-Term Connection.* College Station, TX: Texas Transportation Institute.

Lins, H.F. and T.A. Cohn. 2011. "Stationarity: Wanted Dead or Alive?" *Journal of the American Water Resources Association* (JAWRA) Vol. 47, No. 3, pp. 475–480. doi: 10.111/j.1752-1688.2011.00542.

Liu, C., K. Ikeda, R. Rasmussen, M. Barlage, A.J. Newman, A.F. Prein, F. Chen, L. Chen, M. Clark, A. Dai, and J. Dudhia. 2016. "Continental-Scale Convection-Permitting Modeling of the Current and Future Climate of North America." *Climate Dynamics*, pp.1–25.

Livneh, B., E.A. Rosenberg, C.Y. Lin, B. Nijssen, V. Mishra, K.M. Andreadis, E.P. Maurer, and D.P. Lettenmaier. 2013. "A Long-Term Hydrologically Based Dataset of Land Surface Fluxes and States for the Conterminous United States: Update and Extensions," *Journal of Climate*, Vol. 26, No. 23, pp. 9384–9392. (available at https://www.esrl.noaa.gov/psd/data/gridded/data.livneh.html)

Lohmann, D., E. Raschke, B. Nijssen, and D.P. Lettenmaier. 1998. "Regional Scale Hydrology: I. Formulation of the VIC-2L Model Coupled to a Routing Model," *Hydrological Science Journal*, Vol. 43, No. 1, pp. 131–141.

Lohmann, D., R. Nolte-Holube, and E. Raschke. 1996. "A Large-Scale Horizontal Routing Model to be Coupled to Land Surface Parametrization Schemes." *Tellus*, 48(A), pp. 708–721.

Luettich, R.A., J.J. Westerink, and N.W. Scherffner. 1992. *An Advanced Three-Dimensional Circulation Model for Shelves, Coasts, and Estuaries. Theory and Methodology of ADCIRC-2DDI and ADCIRC-3DL. Report 1 (No. Technical Report DRP-92-6)*. U.S. Army Corps of Engineers, Washington, D.C.

Lumia, R., D.A. Freehafer, and M.J. Smith. 2006. "Magnitude and Frequency of Floods in New York." *U.S. Geological Survey Scientific Investigations Report 2006-5112*, 153 pp.

Maidment, D.R. (Ed.). 1993. *Handbook of Hydrology*. McGraw-Hill, New York, NY.

Mantilla, R. and V.K. Gupta. 2005. "A GIS Numerical Framework to Study the Process Basis of Scaling Statistics in River Networks." *IEEE Geoscience and Remote Sensing Letters*, Vol. 2, No. 4, pp. 404–408.

Maryland Hydrology Panel. 2016. *Application of Hydrologic Methods in Maryland*. Fourth Edition, July, http://www.gishydro.eng.umd.edu/panel.htm.

Masood M., P.J.F. Yeh, N. Hanasaki, and K. Takeuchi. 2014. "Model Study of the Impacts of Future Climate Change on the Hydrology of Ganges-Brahmaputra-Meghna (GBM) Basin." *Hydrology and Earth System Sciences*, Vol. 11, pp. 5747–5791.

Masui, T., K. Matsumoto, Y. Hijioka, T. Kinoshita, T. Nozawa, S. Ishiwatari, E. Kato, P.R. Shukla, Y. Yamagata, and M. Kainuma. 2011. "An Emission Pathway for Stabilization at 6 W/m^2 Radiative Forcing." *Climatic Change,* Vol. 109, No. 59. http://dx.doi.org/10.1007/s10584-011- 0150-5.

Mauran, D. 2013. "Bias Correction, Quantile Mapping, and Downscaling: Revisiting the Inflation Issue." *Journal of Climate*, Vol 26, No. 6, pp. 2137–2143.

Maurer, E.P., L. Brekke, T. Pruitt, and P.B. Duffy. 2007. "Fine-Resolution Climate Projections Enhance Regional Climate Change Impact Studies." *Eos Transactions of the American Geophysical Union,* Vol. 88, No. 47, p. 504.

Maurer E.P., J.C. Adam, and A.W. Wood. 2009. "Climate Model Based Consensus on the Hydrologic Impacts of Climate Change to the Rio Lempa Basin of Central America." *Hydrology and Earth System Sciences*, Vol. 13, pp. 183–194.

McCuen, R. H. and B. S. Levy. 2001. "Evaluation of Peak Discharge Transposition." *Journal of Hydrologic Engineering*, Vol. 5, No. 3, American Society of Civil Engineers.

McCuen, R.H., P.A. Johnson, and R.M. Ragan. 2002. *Highway Hydrology*. Hydraulic Design Series 2 (HDS 2), Second Edition, FHWA-NHI-02-001.

McCuen, R.H. 2003. "Modeling Hydrologic Change – Statistical Methods." Lewis Publishers, A CRC Press Company, 433 pp.

McCuen, R.H. 2005. *Hydrologic Analysis and Design*. Third Edition, Pearson Prentice Hall, Englewood Cliffs, NJ.

McGinnis S.,D. Nychka, and L.O. Mearns. 2015. "A New Distribution Mapping Technique for Climate Model Bias Correction." In Lakshmanan V., Gilleland, E., McGovern A., Tingley M. (Eds.) *Machine Learning and Data Mining Approaches to Climate Science*, Springer.

McGuigan, K.,T. Webster, and K. Collins. 2015. "A Flood Risk Assessment of the LaHave River Watershed, Canada Using GIS Techniques and an Unstructured Grid Combined River-Coastal Hydrodynamic Model." *Journal of Marine Science and Engineering*, Vol. 3, No. 3), pp. 1093–1116.

McKay, M. and D.S. Wilks. 1995. *Atlas of Short Duration Precipitation Extremes for the Northeastern United States and Southeastern Canada*. Northeast Regional Climate Center Publication No. RR 95-1, March.

Mearns, L.O., W.J. Gutowski, R. Jones, L.Y. Leung, S. McGinnis, A.M.B. Nunes, and Y. Qian. 2009. "A Regional Climate Assessment Program for North America." *EOS*, Vol. 90, No. 36, pp. 311–312.

Mearns, L. O. 2009. "The North American Regional Climate Change Assessment Program (NARCCAP): Overview of Phase II Results." *Earth and Environmental Science Transactions,* Vol. 6,p. 022007.

Mearns, L.O., S. Sain, L.R. Leung, M.S. Bukowsky, S. McGinnis, S. Biner, D. Cava, R.W. Arritt, W. Gutowsky, E. Takle, M. Snyder, R.G. Jones, A.M.B. Nunes, S. Tucker, D. Herzmann, L. McDaniel, and L. Sloan. 2013. "Climate Change Projections of the North American Regional Climate Change Assessment Program (NARCCAP)." *Climatic Change*, doi: 10.1007/s10584-013-0831-3.

Meehl, G.A., C. Covey, T. Delworth, M. Latif, B. McAvaney, J.F.B. Mitchell, R.J. Stouffer, and K.E. Taylor. 2007. "The WCRP CMIP3 Multi-Model Dataset: A New Era in Climate Change Research." *Bulletin of the American Meteorological Society*, Vol. 88, pp. 1383–1394.

Mehran, A., A. AghaKouchak, and T.J. Phillips. 2014. "Evaluation of CMIP5 Continental Precipitation Simulations Relative to Satellite-Based Gauge-Adjusted Observations." *Journal of Geophysical Research – Atmospheres*, Vol. 119, No. 4, pp. 1695–1707.

Meinshausen, M.,S.J. Smith, K. Calvin, J.S. Daniel, M.L.T. Kainuma, J.-F. Lamarque, K. Matsumoto, S.A. Montzka, S.C.B. Raper, K. Riahi, A. Thomson, G.J.M. Velders, and D.P.P. van Vuuren. 2011. "The RCP Greenhouse Gas Concentrations and Their Extensions from 1765 to 2300." *Climatic Change,* Vol. 109, pp. 213–241, http://dx.doi.org/10.1007/s10584-011-0156-z.

Melillo, J. M., T. C. Richmond, and G. W. Yohe (Eds.). 2014. *Climate Change Impacts in the United States: The Third National Climate Assessment*. U.S. Global Change Research Program, 841 pp. doi:10.7930/J0Z31WJ2.

Mendlik, T., and A. Gobiet. 2016. "Selecting Climate Simulations for Impact Studies Based on Multivariate Patterns of Climate Change." *Climatic Change*, Vol. 135, No. 3-4, pp. 381–393.

Mengel, M., A. Levermann, K. Frieler, A. Robinson, B. Marzeion, and R. Winkelmann. 2016. "Future Sea Level Rise Constrained by Observations and Long-term Commitment." *Proceedings of the National Academy of Sciences*, Vol. 113, pp. 2597–2602. http://dx.doi.org/10.1073/pnas.1500515113.

Menne, M.J., I. Durre, R.S. Vose, B.E. Gleason, and T.G. Houston. 2012. "An overview of the Global Historical Climatology Network-Daily Database." *Journal of Atmospheric and Oceanic Technology*. Vol 29, pp. 897–910, doi.10.1175/JTECH-D-11-00103.1

Merkel, W.H., H.F. Moody, and Q.D. Quan. 2015. *Design Rainfall Distributions Based on NOAA Atlas 14 Rainfall Depths and Durations*. Proceedings of the 2015 Federal Interagency Hydrologic Modeling Conference in Reno, NV, April 19–23, 2015.

Meyer, M., M. Flood, J. Keller, J. Lennon, G. McVoy, C. Dorney, K. Leonard, R. Hyman, and J. Smith. 2014. "Volume 2: Climate Change, Extreme Weather Events, and the Highway System: Practitioner's Guide and Research Report." NCHRP Report 750.

Minnesota DOT. 2014. *MnDOT Flash Flood Vulnerability and Adaptation Assessment Pilot Project*. Final Report, November 5, 2014.

Mitrovica, J. X., N. Gomez, E. Morrow, C. Hay, K. Latychev and M. E. Tamisiea. 2011. "On the Robustness of Predictions of Sea Level Fingerprints." *Geophysical Journal International,* 2011 Vol. 187, pp. 729–742.

Moglen, G.E. and D.E. Shivers 2006. "Methods for Adjusting USGS Rural Peak Discharges in an Urban Setting." *U.S. Geological Survey Scientific Investigations Report*, 2006-5270, 65 pp.

Moglen, G.E. and S.Kim. 2007. "Limiting Imperviousness." *Journal of the American Planning Association*, Vol. 73, No. 2, pp. 161–171.

Moglen, G.E. and G.E. R. Vidal. 2014. "Climate Change and Storm Water Infrastructure in the Mid-Atlantic Region: Design Mismatch Coming?" *Journal of Hydrologic Engineering*, ASCE.

Mooney, P.A., C. Broderick, C.L. Bruyere, F.J. Mulligan, and A.F. Prein. 2017. "Clustering of Observed Diurnal Cycles of Precipitation over the United States for Evaluation of a WRF Multi-Physics Regional Climate Ensemble." *Journal of Climate*, American Meteorology Society.

Mora, C., A. Frazier, R. Longman, R. Dacks, M. Walton, E. Tong, J. Sanchez, L. Kaiser, Y. Stender, J. Anderson, C. Ambrosino, I. Fernandez-Silva, L. Guiseffi, and T. Giambelluca 2013. "The Projected Timing of Climate Departure from Recent Variability." *Nature*, Vol. 502, pp. 183–188.

Moss, R.H., J.A. Edmonds, K.A. Hibbard, M.R. Manning, S.K. Rose, D.P. van Vuuren, T.R. Carter, S. Emori, M. Kainuma, T. Kram, G.A. Meehl, J.F.B. Mitchell, N. Nakicenovic, K. Riahi, S.J. Smith, R.J. Stouffer, A.M. Thomson, J.P. Weyant, and T.J. Wilbanks. 2010. "The Next Generation of Scenarios for Climate Change Research and Assessment." *Nature,* Vol. 463**,** pp. 747–756, http://dx.doi.org/10.1038/nature08823.

Nakicenovic, N., J. Alcamo, G. Davis, B. de Vries, J. Fenhann, S. Gaffin, K. Gregory, A. Grübler, T.Y. Jung, T. Kram, E. Lebre La Rovere, L. Michaelis, S. Mori, T. Morita, W. Pepper, H. Pitcher, L. Price, K. Riahi, A. Roehrl, H.-H. Rogner, A. Sankovski, M. Schlesinger, P. Shukla, S. Smith, R. Swart, S. van Rooijen, N. Victor, and Z. Dadi. 2000. *Special Report on Emissions Scenarios (SRES)*, IPCC, Cambridge University Press, Cambridge, United Kingdom.

Natural Resources Conservation Service. 2015. "Chapter 4: Storm Rainfall Depth and Duration," Part 630 Hydrology, *National Engineering Handbook*, 69 pp.

Neitsch, S., J.G. Arbold, J.R. Kinry, and J.R. Williams, Jr. 2011. "Soil and Water Assessment Tool Theoretical Documentation."

New York City. 2017. "Preliminary Climate Resiliency Design Guidelines." NYC Mayor's Office of Recovery and Resiliency, April 21, 2017, Version 1.0.

Nicholls, R.J., S.E. Hanson, J.A. Lowe, R.A. Warrick, X. Lu and A.J. Long. 2014. "Sea-level Scenarios for Evaluating Coastal Impacts." *WIREs Climate Change*, Vol. 5, pp. 129–150, doi:10.1002/wcc.253.

Northrop, P.J. and R.E. Chandler. 2014. "Quantifying Sources of Uncertainty in Projections of Future Climate." *Journal of Climate*, Vol 27, pp. 8793–8808.

NRC. 1987. *Responding to Changes in Sea Level: Engineering Implications*. National Research Council, The National Academies Press, Washington, DC, 160 pp. (http://www.nap.edu/catalog/1006.html).

NRC. 2011. *Climate Stabilization Targets: Emissions, Concentrations, and Impacts over Decades to Millennia.* Washington, DC: The National Academies Press, https://doi.org/10.17226/12877.

NRC. 2012. *Sea-Level Rise for the Coasts of California, Oregon, and Washington: Past, Present, and Future*. National Research Council, National Academy Press, Washington D.C. 201 pp.

Obeysekera, J. and J.D. Salas. 2014. "Quantifying the Uncertainty of Design Floods under Nonstationary Conditions." *Journal of Hydrologic Engineering*, Vol. 19, No. 7, pp. 1438–1446.

Olson, S.A. 2014. "Estimation of Flood Discharges at Selected Annual Exceedance Probabilities for Unregulated, Rural Streams in Vermont," with a section on "Vermont Regional Skew Regression" by Veilleux, A.G., *U.S. Geological Survey Scientific Investigations Report 2014-5078*, 27 p.

Oubeidillah, A.A., S.C. Kao, M. Ashfaq, B.S. Naz, and G. Tootle. 2014. "A Large-Scale, High-Resolution Hydrological Model Parameter Data Set for Climate Change Impact Assessment for the Conterminous US." *Hydrology and Earth System Sciences*, Vol. 18, No. 1, pp. 67–84, doi:10.5194/hess-18-67-201.

Over, T.M., R.J. Saito, and D.T. Soong. 2016a. "Adjusting Annual Maximum Peak Discharges at Selected Stations in Northeastern Illinois for Changes in Land-Use Conditions." *U.S. Geological Survey Scientific Investigations Report 2016-5049*, 33 pp.

Over, T.M, R.J. Saito, A.G. Veilleux, J. Sharpe, D.T. Song, and A. Ishii. 2016b. "Estimation of Peak Discharge Quantiles for Selected Annual Exceedance Probabilities in Northeastern Illinois." *U.S. Geological Survey Scientific Investigations Report 2016-5050*, 50 pp.

Parris, A., P. Bromirski, V. Burkett, D. Cayan, M. Culver, J. Hall, R. Horton, K. Knuuti, R. Moss, J. Obeysekera, A. Sallenger, and J. Weiss. 2012. "Global Sea Level Rise Scenarios for the US National Climate Assessment." NOAA Tech Memo OAR CPO-1, 37 pp.

Pennsylvania DOT (PennDOT). 2017. *PennDOT Extreme Weather Vulnerability Study, Phase I,* Appendix D Methodology for Forecasting Flooding Vulnerabilities, April.

Perica, S., D. Martin, S. Pavlovic, I. Roy, M. St. Laurent, C. Trypaluk, D. Unruh, M. Yekta, and G. Bonnin. 2013. "Precipitation-Frequency Atlas of the United States." *NOAA Atlas 14*, Volume 8 Version 2.0: Midwestern States, National Weather Service, Silver Spring, MD.

Peterson, T.C., R.R. Heim, Jr., R. Hirsch, D.P. Kaiser, H. Brooks, N.S. Diffenbaugh, R.M. Dole, J.P. Giovannettone, K. Guirguis, T.R. Karl, R.W. Katz, K. Kunkel, D. Lettenmaier, G.J. McCabe, C.J. Paciorek, K.R. Ryberg, S. Schubert, V.B.S. Silva, B.C. Stewart, A.V. Vecchia, G. Villarini, R.S. Vose, J. Walsh, M. Wehner, D. Wolock, K. Wolter, C.A. Woodhouse, and D. Wuebbles. 2013. "Monitoring and Understanding Changes in Heat Waves, Cold Waves, Floods, and Droughts in the United States." American Meteorological Society, pp. 821–834, June.

Phillips, A.S., C. Deser, and J. Fasullo. 2014. "Evaluating Modes of Variability in Climate Models." *Eos Transactions of the American Geophysical Union,* Vol. 95, pp. 453–455.

Piniewski M., F. Voss, I. Barlund, T. Okruszko, and Z.W. Kundzewicz. 2013. "Effect of Modelling Scale on the Assessment of Climate Change Impact on River Runoff." *Hydrological Sciences Journal,* Vol. 58, pp. 737–754.

Pierce, D.W., D.R. Cayan, and B.L. Thrasher. 2014. "Statistical Downscaling Using Localized Constructed Analogs (LOCA)." *Journal of Hydrometeorology*, Vol. 15, pp. 2558–2585.

Prein, A.F., W. Langhans, G. Fosser, A. Ferrone, N. Ban, K. Goergen, M. Keller, M. Tölle, O. Gutjahr, F. Feser. 2015. "A Review on Regional Convection-Permitting Climate Modeling: Demonstrations, Prospects, and Challenges." *Reviews of Geophysics*, Vol. 53, pp. 323–361.

Prein, A.F., R.M. Rasmussen, K. Ikeda, C.H. Liu, M.P. Clark, and G.J. Holland. 2017. "The Future Intensification of Hourly Precipitation Extremes." *Nature Climate Change*, Vol. 7, pp. 48-+.

Prudhomme, C., R.L. Wilby, S. Crooks, A.L. Kay, and N.S. Reynard. 2010. "Scenario-Neutral Approach to Climate Change Impact Studies: Application to Flood Risk," *Journal of Hydrology*, Vol. 390, No. 3–4, pp. 198–209.

Ranasinghe, R., D. Callaghan, and M.J.F. Stive. 2012. "Estimating Coastal Recession due to Sea Level Rise: Beyond the Bruun Rule." *Climatic Change*, Vol. 110, No. 3-4, pp. 561–574.

Read, L.K. and R.M. Vogel. 2015. "Reliability, Return Periods, and Risk under Uncertainty." *Water Resources Research*, Vol. 51. doi: 10.1002/2015WR017089.

Regan, R.S., S.L. Markstrom, L.E. Hay, R.J. Viger, P.A. Norton, J.M. Driscoll, and J.H. LaFontaine. 2018. Description of the National Hydrologic Model for use with the Precipitation-Runoff Modeling System (PRMS): U.S. Geological Survey Techniques and Methods, Book 6, Chapter B9, 38 pp., https://doi.org/10.3133/tm6B9.

Riahi, K., S. Rao, V. Krey, C. Cho, V. Chirkov, G. Fischer, G. Kindermann, N. Nakicenovic, and P. Rafaj. 2011. "RCP 8.5—A Scenario of Comparatively High Greenhouse Gas Emissions." *Climatic Change,* Vol. 109, pp. 33–57. http://dx.doi.org/10.1007/s10584-011-0149-y.

Ries, K.G. and J.A. Dillow. 2006. "Magnitude and Frequency of Floods on Nontidal Streams in Delaware." *U.S. Geological Survey Scientific Investigations Report 2006-5146*, 38 pp.

Ries, K.G. 2007. "The National Streamflow Statistics Program: A Computer Program for Estimating Streamflow Statistics for Ungaged Sites." U.S. Geological Survey Techniques and Methods 4-A6, 37 pp.

Ries, K.G., P.A. Steeves, J.D. Coles, A.H. Rea, and D.W. Stewart. 2008. "StreamStats: A Water Resources Web Application." U.S. Geological Survey Fact Sheet 2008-3067, 4 pp.

Rignot, E., I. Velicogna, M. van den Broeke, A. Monaghan, and J. Lenaerts. 2011. "Acceleration of the Contribution of the Greenland and Antarctic Ice Sheets to Sea Level Rise." *Geophysical Research Letters.* doi:10.1029/2011GL046583.

Rosner, A., R.M. Vogel, and P.H. Kirshen. 2014. "A Risk-Based Approach to Flood Management Decisions in a Nonstationary World." *Water Resources Research*.

Rossman, L. 2016. *Storm Water Management Model User's Manual Version 5.1*, EPA/600/R-14/413b. U.S. Environmental Protection Agency, National Risk Management Research Laboratory, Cincinnati, OH.

Ryu, J.-H. and K. Hayhoe. 2015. "Regional and Large-Scale Influences on Seasonal to Interdecadal Variability in Caribbean Surface Air Temperature in CMIP5 Simulations." *Climate Dynamics*, Vol. 45, No. 1-2, pp. 455–475.

Ryu, J.-H. and K. Hayhoe. 2017. "Observed and CMIP5 Modeled Influence of Large-Scale Circulation on Summer Precipitation and Drought in the South-Central United States," *Climate Dynamics*, https://doi.org/10.1007/s00382-017-3534-z.

Salas, J.D. and J.Obeysekera. 2014. "Revisiting the Concepts of Return Period and Risk for Nonstationary Hydrologic Extreme Events." *Journal of Hydrologic Engineering*, Vol. 19, No. 3, pp. 554–568.

Salas, J.D., J. Obeysekera, and R.M. Vogel. 2018. "Techniques for Assessing Water Infrastructure for Nonstationary Extreme Events." *Hydrological Sciences Journal*, International Association of Hydrological Sciences, pp. 1–28.

Sallenger, A.H., K.S. Doran, and P.A Howd. 2012. "Hotspot of Accelerated Sea-level Rise on the Atlantic Coast of North America." *Nature Climate Change*, Vol. 2, pp. 884–888. doi:10.1038/nclimate1597.

Sanderson, B.M., R. Knutti, and P. Caldwell. 2015. "A Representative Democracy to Reduce Interdependency in a Multimodel Ensemble." *Journal of Climate,* 28, pp. 5171–5194. http://dx.doi.org/10.1175/JCLI-D-14-00362.1.

Sanderson, B.M., M. Wehner, and R. Knutti. 2017. "Skill and Independence Weighting for Multi-Model Assessments." *Geoscientific Model Development*, Vol. 10, pp. 2379–2395.

Sankarasubramanian, A. and R.M. Vogel. 2001. "Climate Elasticity of Streamflow in the United States." *Water Resources Research*, Vol. 37, No. 6, pp. 1771–1781.

Sauer, V.B. 1973. ''Flood Characteristics of Oklahoma Streams.'' *Water Resources Investigations Report*. 73-52, U.S. Geological Survey, Oklahoma City, OK.

Sauer, V.B., W.O. Thomas, Jr., V.A. Stricker, and K.V. Wilson. 1983. "Flood Characteristics of Urban Watersheds in the United States." U.S. Geological Survey Water-Supply Paper 2207, 63 pp.

Seneviratne, S.I., N. Nicholls, D. Easterling, C.M. Goodess, S. Kanae, J. Kossin, Y. Luo, J. Marengo, K. McInnes, M. Rahimi, M. Reichstein, A. Sorteberg, C. Vera, and X. Zhang. 2012. "Changes in Climate Extremes and Their Impacts on the Natural Physical Environment." In *Managing the Risks of Extreme Events and Disasters to Advance Climate Change Adaptation* [Field, C.B., V. Barros, T.F. Stocker, D. Qin, D.J. Dokken, K.L. Ebi, M.D. Mastrandrea, K.J. Mach, G.-K. Plattner, S.K. Allen, M. Tignor, and P.M. Midgley (Eds.)]. *A Special Report of Working Groups I and II of the Intergovernmental Panel on Climate Change (IPCC)*, Cambridge University Press, Cambridge, United Kingdom, and New York, NY, USA, pp. 109–230.

Serago, J.M. and R.M. Vogel. 2018. "Parsimonious Nonstationary Flood Frequency Analysis." *Advances in Water Resources,* Vol. 112, Elsevier, pp. 1–16.

Serinaldi F. and C.G. Kilsby. 2015. "Stationarity is Undead: Uncertainty Dominates the Distribution." *Advances in Water Resources*, Vol. 77, Elsevier, pp. 17–36.

Sheffield, J., A.P. Barrett, B. Colle, D.N. Fernando, R. Fu, K. L. Geil, Q. Hu, J. Kinter, S. Kumar, B. Langenbrunner, K. Lombardo, L.N. Long, E. Maloney, A. Mariotti, J.E. Meyerson, K.C. Mo, J.D. Neelin, S. Nigam, Z. Pan, T. Ren, A. Ruiz-Barradas, Y.L. Serra, A. Seth, J.M. Thibeault, J.C. Stroeve, Z. Yang, and L. Yin. 2013. "North American Climate in CMIP5 Experiments. Part I: Evaluation of Historical Simulations of Continental and Regional Climatology." *Journal of Climate,* Vol. 26, pp. 9209–9245. http://dx.doi.org/10.1175/jcli-d-12-00592.1.

Sheffield, J., *et al*. 2014. *Regional Climate Processes and Projections for North America: CMIP3/CMIP5 Differences, Attribution and Outstanding Issues*. NOAA Climate Program Office, 47pp.

Shrestha, S. 2014. "Assessment of Water Availability under Climate Change Scenarios in Thailand," *Journal of Earth Science and Climatic Change,* Vol. 5, pp. 1–7.

Simonovic, S., A. Schardong, D. Sandink, and R. Srivastav. 2016. "A Web-Based Tool for the Development of Intensity Duration Frequency Curves under Climate Change." *Environmental Modelling & Software,* Vol. 81, pp. 136–153.

Smith, J.M., M.A. Cialone, T.V. Wamsley, and T.O. McAlpin. 2010. "Potential Impact of Sea Level Rise on Coastal Surges in Southeast Louisiana. *Ocean Engineering*, Vol. 37, pp. 37–47.

Socolofsky, S., E.E. Adams, and D. Entekhabi. 2001. "Disaggregation of Daily Rainfall for Continuous Watershed Modeling." *Journal of Hydrologic Engineering*, Vol. 6, No. 4, pp. 300–309.

Steinschneider, S., Y.E. Yang, and C. Brown. 2013. "Panel Regression Techniques for Identifying Impacts of Anthropogenic Landscape Change on Hydrologic Response." *Water Resources Research*, Vol. 49, pp. 7874–7886.

Stoner, A., K. Hayhoe, X. Yang, and D. Wuebbles. 2012. "An Asynchronous Regional Regression Model for Statistical Downscaling of Daily Climate Variables." *International Journal of Climatology*, doi: 10.1002/joc.3603.

Stoner, A., K. Hayhoe, X. Yang, and D.J. Wuebbles 2013. "An Asynchronous Regional Regression Model for Statistical Downscaling of Daily Climate Variables." *International Journal of Climatology,* Vol. 33, No. 11, pp. 2473–2494.

Stoner, A., K. Hayhoe, K. Dixon, J. Lanzante, and I. Scott-Fleming. 2017. "Comparing the Performance of Multiple Statistical Downscaling Approaches Using a Perfect Model Framework." Annual Meeting of the American Meteorological Society, Seattle, WA.

Svensson, C. and D.A. Jones. 2010. "Review of Methods for Deriving Areal Reduction Factors." *Journal of Flood Risk Management*.

Swain, S. and K. Hayhoe. 2015. "CMIP5 Projected Changes in Spring and Summer Drought and Wet Conditions over North America." *Climate Dynamics,* Vol. 44, pp. 2737–2750, http://dx.doi.org/10.1007/s00382-014-2255-9.

Sweet, W., R. Kopp, C. Weaver, J. Obeysekera, R. Horton, R. Thieler, and C. Zervas. 2017a. "Global and Regional Sea Level Rise Scenarios for the United States." *NOAA Technical Report NOS CO-OPS 083*.

Sweet, W., R. Horton, R.E. Kopp, A.N. LeGrande, and A. Romanou. 2017b. "Sea Level Rise." In *Climate Science Special Report: Fourth National Climate Assessment, Volume I* [Wuebbles, D.J., D.W. Fahey, K.A. Hibbard, D.J. Dokken, B.C. Stewart, and T.K. Maycock (Eds.)]. U.S. Global Change Research Program, Washington, DC, USA, pp. 333–363, doi: 10.7930/J0VM49F2.

Tasker, G.D. and J.R. Stedinger. 1989. "An Operational GLS Model for Hydrologic Regression." *Journal of Hydrology*, Vol. 3, pp. 361–375.

Tebaldi, C. and R. Knutti. 2007. "The Use of the Multi-Model Ensemble in Probabilistic Climate Projections." *Philosophical Transactions of the Royal Society A,* Vol. 365, pp. 2053–2075, doi: 10.1098/rsta.2007.2076.

Theobald, D. 2005. "Landscape Pattern of Exurban Growth in the USA from 1980 to 2020." *Ecology and Society*, Vol. 10, No. 1, Article 32, 29 pp.

Themeßl, M. J., A. Gobiet, and G. Heinrich. 2011. "Empirical-Statistical Downscaling and Error Correction of Regional Climate Models and Its Impact on the Climate Change Signal." *Climatic Change*, doi: 10.1007/s10584-011-0224-4.

Thomas, W.O., Jr. and G.E. Moglen. 2016. *Regression Equations for Estimating Flood Discharges for the Piedmont, Blue Ridge and Appalachian Plateau Regions in Western Maryland*, Maryland State Highway Administration Research Report MD-15-SP309B4D, March, 35 pp.

Thomson, A.M., K.V. Calvin, S.J. Smith, G.P. Kyle, A. Volke, P. Patel, S. Delgado-Arias, B. Bond-Lamberty, M.A. Wise, and L.E. Clarke. 2011. "RCP4.5: A Pathway for Stabilization of Radiative Forcing by 2100." *Climatic Change,* Vol 109, pp. 77–94. http://dx.doi.org/10.1007/s10584- 011-0151-4.

Titus, J. 2002. *Does Sea Level Rise Matter to Transportation Along the Atlantic Coast? The Potential Impacts of Climate Change on Transportation.* U.S. DOT Workshop 1002. Web, accessed March 9, 2017, https://climate.dot.gov/documents/workshop1002/titus.pdf.

Torres, J.M., B. Bass, N. Irza, Z. Fang, J. Proft, C. Dawson, M. Kiani, and P. Bedient. 2015. "Characterizing the Hydraulic Interactions of Hurricane Storm Surge and Rainfall–Runoff for the Houston–Galveston Region." *Coastal Engineering*, Vol. 106, pp. 7–19.

University of Washington. 2017. "Variable Infiltration Capacity (VIC) Macroscale Hydrologic Model - How to Run VIC," available online at http://www.hydro.washington.edu/Lettenmaier/Models/VIC/Documentation/HowtorunVIC.shtml, accessed August 2017.

USACE. 1984. *Shore Protection Manual*.

USACE. 2006. *Coastal Engineering Manual, EM 1110-2-1100*.

USACE. 2014. *Procedures to Evaluate Sea Level Change: Impacts, Responses, and Adaptation*. U.S. Army Corps of Engineers, ETL 1100-2-1, June 30, 2014, 254 pp.

USACE. 2016. "Guidance for Incorporating Climate Change Impacts to Inland Hydrology in Civil Works Studies, Designs and Projects." Engineering and Construction Bulletin No. 2016-25, September 16, 2016, U.S. Army Corps of Engineers.

USACE. 2017a. Sea Level Change Curve Calculator, version 2017.55, (see http://corpsclimate.us/ccaceslcurves.cfm)

USACE. 2017b. Wave Information Studies website (see http://wis.usace.army.mil/)

USACE. 2017c. Coastal Hazards System website (see https://chs.erdc.dren.mil)

USBR. 2013. *Downscaled CMIP3 and CMIP5 Climate Projections: Release of Downscaled CMIP5 Climate Projections, Comparison with Preceding Information, and Summary of User Needs,* U.S. Department of the Interior, Bureau of Reclamation, Technical Service Center, Denver, CO, 116 pp.

USGCRP. 2017. *Climate Science Special Report: Fourth National Climate Assessment, Volume I* [Wuebbles, D.J., D.W. Fahey, K.A. Hibbard, D.J. Dokken, B.C. Stewart, and T.K. Maycock (Eds.)]. U.S. Global Change Research Program, Washington, DC, USA, 470 pp, doi: 10.7930/J0J964J6.

USGCRP. 2018. *Impacts, Risks, and Adaptation in the United States: Fourth National Climate Assessment, Volume II* [Reidmiller, D.R., C.W. Avery, D.R. Easterling, K.E. Kunkel, K.L.M. Lewis, T.K. Maycock, and B.C. Stewart (Eds.)]. U.S. Global Change Research Program, Washington, DC, USA, 1515 pp. doi: 10.7930/NCA4.2018.

USGS. 2017. Coastal Storm Modeling System: CoSMoS, (see https://walrus.wr.usgs.gov/coastal_processes/cosmos/)

U.S. Department of Commerce. 1957. "Rainfall Intensity-Frequency Regime," Technical Paper No. 29, Weather Bureau, Washington, D.C.

U.S. Department of Commerce. 1961. "Rainfall Frequency Atlas of the United States for Durations from 30 Minutes to 24 Hours and Return Periods from 1 to 100 Years," Technical Paper No. 40 (TP-40), Weather Bureau, Washington, DC.

U.S. Department of Commerce. 1977. "Five- to 60-Minute Precipitation Frequency for the Eastern and Central United States," NOAA Technical Memorandum NWS HYDRO-35, National Weather Service, Silver Spring, MD.

U.S. Department of Commerce. 1980. "A Methodology for Point-to-Area Rainfall Frequency Ratios," NOAA Technical Report NWS 24, Washington, D.C.

U.S. Department of Commerce. 2017. Tides and Currents website, National Oceanic and Atmospheric Administration, https://tidesandcurrents.noaa.gov/ visited Oct 2017.

U.S. DOT. 2014. "Engineering Assessments of Climate Change Impacts and Adaptation Measures (Task 3.2)" Impacts of Climate Change and Variability on Transportation Systems and Infrastructure – The Gulf Coast Study, Phase 2, FHWA-HEP-15-004, August.

U.S. EPA. 2009. "Land-Use Scenarios: National-Scale Housing-Density Scenarios Consistent with Climate Change Storylines," Global Change Research Program, National Center for Environmental Assessment, EPA/600/R-80/076F, Washington, DC.

U.S. EPA. 2010. *Climate Change Vulnerability Assessments: A Review of Water Utility Practices,* EPA 800-R-10-0001, Office of Water.

U.S. EPA. 2013. *Watershed Modeling to Assess the Sensitivity of Streamflow, Nutrient and Sediment Loads to Potential Climate Change and Urban Development in 20 U.S. Watersheds*, National Center for Environmental Assessment, Washington, DC, EPA/600/R-12/058F.

U.S. EPA. 2014a. National Stormwater Calculator. Cincinnati OH: National Risk Management Research Laboratory. Available at http://www2.epa.gov/water-research/national-stormwater-calculator.

U.S. EPA. 2014b. *National Stormwater Calculator User's Guide*. (EPA/600/R-13/085c) Revised September 2014. Cincinnati, OH: National Risk Management Research Laboratory, 75pp. Available at http://nepis.epa.gov/Adobe/PDF/P100LOB2.pdf.

U.S. EPA. 2014c. SWMM-CAT User's Guide. (EPA/600/R¬14/428). Cincinnati, OH: National Risk Management Research Laboratory. 16pp. Available at

http://nepis.epa.gov/Exe/ZyPDF.cgi/P100KY8L.PDF?Dockey=P100KY8L.PDF.

U.S. EPA. 2015. *BASINS 4.1 (Better Assessment Science Integrating Point and Non-point Sources) Modeling Framework,* National Exposure Research Laboratory, Research Triangle Park, North Carolina.

U.S. EPA. 2016. Climate Resilience Evaluation and Awareness Tool, Version 3.0 Methodology Guide. https://www.epa.gov/sites/production/files/2016-05/documents/creat_3_0_methodology_guide_may_2016.pdf

U.S. EPA. 2017. *Updates to the Demographic and Spatial Allocation Models to Produce Integrated Climate and Land Use Scenarios (ICLUS)* (Final Report, Version 2), Washington, DC, EPA/600/R-16/366F, (https://cfpub.epa.gov/ncea/iclus/recordisplay.cfm?deid=322479)

van Vuuren, D.P., J. Edmonds, M. Kainuma, K. Riahi, A. Thomson, K. Hibbard, G.C. Hurtt, T. Kram, V. Krey, J.-F. Lamarque, T. Masui, M. Meinshausen, N. Nakicenovic, S.J. Smith, and S.K. Rose. 2011. "The Representative Concentration Pathways: An Overview." *Climatic Change*, Vol. 109, pp. 5–31.

Vermeer, M. and S. Rahmstorf. 2009. "Global Sea Level Linked to Global Temperature," *Proceedings of the National Academy of Sciences*, Vol. 106, No. 51, pp. 21527–21532, doi: 1073/pnas.0907765106.

Villarini, G., J.A. Smith, M.L. Baeck, and W.F. Krajewski. 2011. "Examining Flood Frequency Distributions in the Midwest US." *Journal of the American Water Resources Association* (JAWRA), Vol. 47, No. 3, pp. 447–463. doi: 10.111/j.1752-1688.2011.00540.

Vogel, R.M., C. Yaindl, and M. Walter. 2011. "Nonstationarity: Flood Magnification and Recurrence Reduction Factors in the United States." *Journal of the Water Resources Association* (JAWRA), Vol. 47, No. 3, pp. 464–474. doi: 10.1111/j.1752-1688.2011.00541.

Vrac, M., M.L. Stein, K. Hayhoe, and X.-Z. Liang. 2007. "A General Method for Validating Statistical Downscaling Methods under Future Climate Change." *Geophysical Research Letters*, Vol. 34, L18701, doi:10.1029/2007GL030295.

Wahl, T., S. Jain, J. Bender, S.D. Meyers, and M.E. Luther. 2015. "Increasing Risk of Compound Flooding from Storm Surge and Rainfall for Major U.S. Cities." *Nature Climate Change*, Vol. 5, No. 12, pp. 1093–1097.

Walsh, J., D. Wuebbles, K. Hayhoe, J. Kossin, K. Kunkel, G. Stephens, P. Thorne, R. Vose, M. Wehner, J. Willis, D. Anderson, S. Doney, R. Feely, P. Hennon, V. Kharin, T. Knutson, F. Landerer, T. Lenton, J. Kennedy, and R. Somerville. 2014. "Chapter 2: Our Changing Climate. Climate Change Impacts in the United States." *The Third National Climate Assessment*, J.M. Melillo, T.C. Richmond, and G. W. Yohe, Eds., U.S. Global Change Research Program, 19-67. doi:10.7930/J0KW5CXT.

Wang, G.L., D.G. Wang, K.E. Trenberth, A. Erfanian, M. Yu, M.G. Bosilovich, and D.T. Parr. 2017. "The Peak Structure and Future Changes of the Relationships Between Extreme Precipitation and Temperature." *Nature Climate Change*, Vol. 7, pp. 268-+.

Webb, B.M. and C.D. Marr. 2016. "Spatial Variability of Hydrodynamic Timescales in a Broad and Shallow Estuary: Mobile Bay, Alabama." *Journal of Coastal Research*, Vol. 32, pp. 1374–1388.

Webb, B.M., and M.T. Matthews. 2014. Wave-induced Scour at Cylindrical Piles. *Transportation Research Record: Journal of the Transportation Research Board*, Vol. 2436, pp. 148–155.

Wehner, M. 2013. "Very Extreme Seasonal Precipitation in the NARCCAP Ensemble: Model Performance and Projections." *Climate Dynamics*, Vol. 40, No 1, pp. 59–80.

Wehner, M.F., J.R. Arnold, T. Knutson, K.E. Kunkel, and A.N. LeGrande. 2017. "Droughts, Floods, and Wildfires." In *Climate Science Special Report: Fourth National Climate Assessment, Volume I* [Wuebbles, D.J., D.W. Fahey, K.A. Hibbard, D.J. Dokken, B.C. Stewart, and T.K. Maycock (Eds.)]. U.S. Global Change Research Program, Washington, DC, USA, pp. 231–256, doi: 10.7930/J0CJ8BNN.

Westra, S.,L.V. Alexander, and F.W. Zwiers. 2013. "Global Increasing Trends in Annual Maximum Daily Precipitation." *Journal of Climate*, Vol. 26, pp. 3904–3918.

Westra, S., H.J. Fowler, J.P. Evans, L.V. Alexander, P. Berg, F. Johnson, E.J. Kendon, G. Lenderink, and N.M. Roberts. 2014. "Future Changes to the Intensity and Frequency of Short-Duration Extreme Rainfall." *Reviews of Geophysics*, Vol. 52, pp. 522–555.

WinTR-55 Workgroup. 2009. *WinTR-55 User's Guide, Technical Report*. Natural Resources Conservation Service.

Wood, A.W., L.R. Leung, V. Sridhar, and D.P. Lettenmaier. 2004. "Hydrologic Implications of Dynamical and Statistical Approaches to Downscaling Climate Model Outputs." *Climatic Change*, Vol. 15, pp. 189–216.

World Meteorological Organization (WMO). 2018. *Guide to Climatological Practices.* WMO-No. 100. Secretariat of the World Meteorological Organization. ISBN 978-92-63-10100-6.

Wright, D.B., J.A. Smith, and M.L. Baeck. 2014. "Critical Examination of Area Reduction Factors." *Journal of Hydrologic Engineering*. Volume 19, No. 4 (April), ASCE.

Wuebbles, D., G. Meehl, K. Hayhoe, T.R. Karl, K. Kunkel, B. Santer, M. Wehner, B. Colle, E.M. Fischer, R. Fu, and A. Goodman. 2014. "CMIP5 Climate Model Analyses: Climate Extremes in the United States." *Bulletin of the American Meteorological Society*, Vol. 95, No. 4, pp.571–583.

Xu Y., X. Gao, Q. Zhu, Y. Zhang, and L. Kan. 2014. "Coupling a Regional Climate Model and a Distributed Hydrological Model to Assess Future Water Resources in Jinhua River Basin, East China." *Journal of Hydrologic Engineering*, Vol. 20, No. 04014054.

Yan, D., S.E. Werners, F. Ludwig, and H.Q. Huang. 2015. "Hydrological Response to Climate Change: The Pearl River, China under Different RCP Scenarios." *Journal of Hydrology: Regional Studies*, Vol. 4, pp. 228–245.

Yoon, J.-H., L.R. Leung, and J. Correia, Jr. 2012. "Comparison of Dynamically and Statistically Downscaled Seasonal Climate Forecasts for the Cold Season over the United States." *Journal of Geophysical Research*, Vol. 117, No. D21109, doi: 10.1029/2012JD017650.

Yu, X., and J.R. Stedinger. 2018. "LP3 Flood Frequency Analysis Including Climate Change." Proceedings of the World Environmental and Water Resources Congress, ASCE, pp. 459–467.

Zervas, C. 2009. "Sea Level Variations of the United States 1854-2006." *Technical Report NOS CO-OPS 053*. 194 pp. (http://www.coops.nos.noaa.gov/publications/Tech_rpt_53.pdf)

Zhang, X., F. Zwiers, G. Hegerl, F.H. Lambert, N. Gillett, S. Solomon, P. Stott, and T. Nozawa. 2007. "Detection of Human Influence on Twentieth-Century Precipitation Trends." *Nature*, Vol. 448, pp. 461–465.

Zhang, X., H. Wan, F. Zwiers, G. Hegerl, and S. Min. 2013. "Attributing Intensification of Precipitation Extremes to Human Influence." *Geophysical Research Letters*, Vol. 40, No. 19, pp. 5252–5257.

Zhang, X.B., F.W. Zwiers, G.L. Li, H. Wan, and A.J. Cannon. 2017. "Complexity in Estimating Past and Future Extreme Short-Duration Rainfall." *Nature Geoscience.*, Vol. 10, pp. 255-+.

Abbreviations

AASHTO	American Association of State Highway and Transportation Officials
AEP	Annual Exceedance Probability
AMS	Annual Maximum Series
AR4	Fourth Assessment Report (IPCC)
AR5	Fifth Assessment Report (IPCC)
ARF	Areal Reduction Factor
ARRM	Asynchronous Regional Regression Model
ASCE	American Society of Civil Engineers
BCCA	Bias-Correction Constructed Analogues
BCSD	Bias-Correction Spatial Disaggregation
CCI	Climate Change Indicator
CF	Change Factor
CMIP	Coupled Model Intercomparison Project
CO_2	Carbon Dioxide
CREAT	Climate Resilience Evaluation and Analysis Tool
DCHP	Downscaled Climate and Hydrology Projections
ENSO	El Niño Southern Oscillation
ESDM	Empirical-Statistical Downscaling Model
FEMA	Federal Emergency Management Agency
FFC	Flood Frequency Curve
FHWA	Federal Highway Administration
FIRM	Flood Insurance Rate Map
GC2	Gulf Coast Study, Phase 2
GEV	Generalized Extreme Value
GIS	Geographic Information System
GCM	Global Climate Model (or General Circulation Model)
GHG	Greenhouse Gases
GMSLR	Global Mean Sea Level Rise
GrIS	Greenland Ice Sheet
H&H	Hydrologic and Hydraulic
HCDN	Hydro-Climatic Data Network

HDG	Highway Drainage Guidelines
HDS	Hydraulic Design Series
HEC	Hydraulic Engineering Circular
HEC-HMS	Hydrologic Engineering Center – Hydrologic Modeling System
HWM	High Water Mark
ICLUS	Integrated Climate and Land Use Scenarios
ICNet	Infrastructure and Climate Network
IDF	Intensity-Duration-Frequency
IPCC	Intergovernmental Panel on Climate Change
LOCA	Localized Constructed Analogs
LULC	Land Use/Land Cover
MACA	Multivariate Adaptive Constructed Analogs
MHHW	Mean Higher High Water
MHW	Mean High Water
MSL	Mean Sea Level
NA-CORDEX	North American Coordinated Regional Downscaling Experiment
NARCCAP	North American Regional Climate Change Assessment Program
NAVD	North American Vertical Datum
NCA	National Climate Assessment
NCHRP	National Cooperative Highway Research Program
NEX-DCP30	NASA Earth Exchange Downscaled Climate Projections (30 arcsec resolution)
NEX-GDDP	NASA Earth Exchange Global Daily Downscaled Projections
NFIP	National Flood Insurance Program
NHC	National Hurricane Center
NOAA	National Oceanic and Atmospheric Administration
NOS	National Ocean Service
NRC	National Research Council
NRCS	Natural Resources Conservation Service
NWS	National Weather Service
PDO	Pacific Decadal Oscillation
RCM	Regional Climate Model
RCP	Representative Concentration Pathway
RFC	Rainfall Frequency Curve

RSL	Relative Sea Level
RSLR	Relative Sea Level Rise
SCS	Soil Conservation Service (now the NRCS)
SERDP	Strategic Environmental Research and Development Program
SLR	Sea Level Rise
SRES	Special Report on Emission Scenarios
SWL	Still Water Level
SWMM	Stormwater Management Model
USACE	U.S. Army Corps of Engineers
USGCRP	U.S. Global Change Research Program
USGS	United States Geological Survey
VLM	Vertical Land Movement
WAIS	Western Antarctic Ice Sheet

Glossary

Abrupt or rapid climate change. The non-linearity of the climate system may lead to rapid climate change, sometimes called abrupt events or even surprises. These are defined as large-scale changes in the climate system that take place over a few decades or less, persist for at least a few decades, and cause substantial disruptions in human and natural systems (IPCC 2013). Some abrupt future events may be imaginable, such as a dramatic reorganization of the thermohaline circulation, rapid deglaciation, or massive melting of permafrost leading to fast changes in the carbon cycle. Others may be truly unexpected, a consequence of a strong, rapidly changing, forcing of a non-linear system.

Accuracy. How close measurements are to the actual or true value. Climate model accuracy can be evaluated for weather aggregated over time periods (climate accuracy) and decadal forecasts for near-term climate (forecast accuracy). In the context of climate model projections, accuracy refers to model ability to reproduce the aggregate statistical properties of real-world weather and climate patterns, not specific historical events. Most model simulations develop their own pattern of internal natural variability, making them accurate at climatological time scales of 20 to 30 years, but not at weather-relevant time scales of days to years.

Adaptation. Preparing for the effects of extreme events and climate change on transportation infrastructure and systems. Adaptation refers to the planning, designing, constructing, operating, or maintaining transportation infrastructure while incorporating consideration of extreme events and climate change.

Adaptive capacity. The degree to which the system containing the asset (road, bridge, etc.) can adjust or mitigate the potential for damage or service interruption resulting from climatic hazards.

Annual exceedance probability. The probability that the magnitude of the random variable (for example annual maximum flood peak) will be equaled or exceeded in a single year.

Bankfull. Water level in a stream corresponding to where water is flowing within the banks just before it spills out into the floodplain.

Beach. The zone of unconsolidated material, typically sand, that extends landward from closure depths, where sand is moved by waves, to the place where there is marked change in material or physiographic form, or to the line of permanent vegetation (usually the effective limit of storm waves).

Boundary conditions. Environmental conditions, e.g., water levels, waves, currents, drifts, etc. used as input for numerical models.

Bottom-up analysis. A process where the vulnerabilities of existing infrastructure or draft designs of new infrastructure are identified so that potential conditions that expose the infrastructure to these vulnerabilities can be quantified.

Climate. The characteristic weather of a region, particularly temperature and precipitation, averaged over some significant interval of time (20 to 30 years or longer). A specific event is weather; the risk of such a weather event occurring during a significant time interval is climate.

Climate change. 1) A significant and lasting shift in the statistical distribution of weather patterns around the average conditions (e.g., more or fewer extreme weather events) over periods

ranging from decades to millions of years. 2) Any significant shift in the measures of climate lasting for an extended period of time, including major alterations in temperature, precipitation, coastal storms, or wind patterns, among others, that occur over several decades or longer. 3) A non-random shift in climate that is measured over several decades or longer. The change may result from natural or human causes.

Climate change detection and attribution. Detection builds the statistical evidence for a change in climate without providing a reason for that change. Attribution establishes the most likely causes for the detected change and assigns a level of confidence or certainty to those causes.

Climate projections. Output from global climate model simulations that attempts to estimate the future evolution of the climate system, given a specific set of plausible external forcings that can include both natural (e.g., changes in solar energy, volcanic eruptions) and human (greenhouse gas emissions, soot and dust) factors. Simulations from multiple models are typically combined into a probabilistic multi-model ensemble of future projections.

Climate sensitivity. The change in global mean temperature from a doubling of atmospheric carbon dioxide levels relative to a pre-industrial base. The current estimate of this value is 3^{o}C, with a range from 2.0 to 4.5^{o}C.

Climatological standard normal. A climatological standard normal is a consecutive 30-year period of observations.

Coastal engineering. The planning, design, construction, and operation of infrastructure in the wave, tide, and sand environment that is unique to the coast. A well-established specialty area of civil engineering that focuses on the coastal zone and coastal processes.

Coastal environment. The sum of all external conditions (e.g., tides, waves, sediments) affecting built infrastructure near the coast.

Coastal processes. Collective term covering the action of natural forces on the shoreline and nearshore seabed.

Confidence interval. An interval estimated from data that has a stated probability of including the true value of a statistic. The limits of the interval are called **confidence limits**.

Confidence limits. Limits that define an interval in which the true value of a statistic is expected to lie with the stated probability.

Conservative estimate. To a climate scientist, this refers to a "best-case scenario," which in the context of climate projections would be the lowest estimate of future emissions or climate change. To an engineer, this refers to a "worst case scenario," which in the context of climate projections would be a higher estimate of future emissions or change.

Datum. Any permanent line, plane, or surface used as a reference point for elevations.

Design flood. The peak discharge, volume (if appropriate), stage, or wave crest elevation of the flood associated with the annual exceedance probability (AEP) selected for the design of a transportation asset.

Design storm (coastal). Hypothetical extreme storm that coastal protection structures may be designed to withstand. The severity of the storm (i.e. return period) is chosen given an acceptable level of risk of damage or failure. A design storm consists of a design wave condition, design

water level, and duration. In coastal flood analysis, the design storm frequently refers to water level elevation.

Deterministic. A prediction or projection where each state develops in a predictable manner from the previous state, according to known principles or processes. For example, climate models are based on physical equations that produce one and only one output sequence for a given set of input and boundary conditions.

Discharge. Volume of water passing a given point per unit time. Also known as flow.

Downscaling. A procedure to develop higher-resolution information from lower-resolution information.

El Niño. Phenomenon characterized by a large-scale weakening of the trade winds and warming of the surface layers in the eastern and central equatorial Pacific Ocean. El Niño events occur irregularly at intervals of 2 to 7 years, although the average is about once every 3 to 4 years. They typically last 12 to 18 months and are accompanied by swings in the Southern Oscillation, an interannual see-saw in tropical sea level pressure between the eastern and western hemispheres. During El Niño, unusually high atmospheric sea level pressures develop in the western tropical Pacific and Indian Ocean regions, and unusually low sea level pressures develop in the southeastern tropical Pacific. Southern Oscillation tendencies for unusually low pressures west of the date line and high pressures east of the date line have also been linked to periods of anomalously cold equatorial Pacific sea surface temperatures, sometimes referred to as La Niña.

El Niño Southern Oscillation (ENSO). The atmospheric component of El Niño.

Epoch. 1) Tidal epoch is a time related to astronomical cycles of the earth-moon-sun system lasting about 19 years. 2) Geological epoch is a subdivision of the geologic timescale that is longer than an age and shorter than an era.

Eustatic sea level change. Change in sea level resulting from change in the volume of the world's ocean basins and the total amount of ocean water. Vertical land movement is not included. See Global Sea Level Rise.

Exposure. The frequency, nature, and degree to which a transportation asset (road, bridge, etc.) will experience a climatic hazard.

Extratropical. A term used in advisories and tropical summaries to indicate that a cyclone has lost its "tropical" characteristics. The term implies both poleward displacement of the cyclone and the conversion of the cyclone's primary energy source from the release of latent heat of condensation to baroclinic (the temperature contrast between warm and cold air masses) processes. Cyclones can become extratropical and still retain winds of hurricane or tropical storm force.

Extreme event. Severe and rare natural occurrence that may pose significant risks of damage, destruction, or loss of life.

Extreme flood event. Specific type of extreme weather event that is manifested as flooding.

Extreme weather event. Significant anomalies in temperature, precipitation, and winds that may manifest as heavy precipitation and flooding, heatwaves, drought, wildfires, or windstorms (including tornados and tropical storms). They are rare, weather-induced events that usually cause damage, destruction, or severe economic loss.

Flood. A general and temporary condition of partial or complete inundation of normally dry land areas resulting from the overflow of inland or tidal waters.

Flood frequency curve. A curve relating a range of flood flows to their respective annual exceedance probabilities (frequencies).

Floodplain. The land area susceptible to being inundated by flood waters.

Flow. Volume of water passing a given point per unit time. Also known as discharge.

Forcing. Factors that affect the Earth's climate. For example, natural factors such as volcanoes and human factors such as the emission of heat-trapping gases and particles through fossil fuel combustion.

Freeboard. Vertical distance above a design water-surface elevation that provides a safety factor for waves, surges, drift, uncertainty in hydrologic estimates, and other contingencies.

Geomorphology. 1) The branch of physical geography that deals with the form of the Earth, the general configuration of its surface, the distribution of the land, water, etc. 2) The investigation of the history of geologic changes through the interpretation of topographic forms.

Global sea level rise. The sea level rise averaged across the world's oceans. This is the average change in sea level resulting from a change in the volume of the world's ocean basins and the total amount of ocean water. Vertical land movement is not included. See Eustatic Sea Level Change.

Hazard. Something that is potentially dangerous or harmful, often the root cause of an unwanted outcome.

High-resolution. Climate information on a spatial and/or temporal scale that is finer than standard GCM output. At present, spatial grids at or less than 25 km and daily time increments or less are considered high resolution.

Hindcasting. Application of a numerical model to simulate a past event. Often used in model validation to see how well the output matches known events or historical statistics.

Hurricane. An intense tropical cyclone in which winds tend to spiral inward toward a core of low pressure, with maximum sustained (1-minute average) surface wind velocities that equal or exceed 75 mph or 65 knots (120 km/h). Term is used in the Atlantic, Gulf of Mexico, and eastern Pacific.

Hydrodynamic. Having to do with the science of moving water.

Hydrograph. 1) Time series of flow (discharge) or stage at a particular location in a watershed. 2) The graph of the variation of still water level with time (coastal).

Hyetograph. Time series of rainfall, which can be expressed as intensity (rate), depth per incremental time unit, or total (accumulated) rainfall from the beginning of the storm (mass hyetograph).

Hydrology. The earth science that considers the occurrence, distribution, and movement of water in the atmosphere, between the atmosphere and the Earth's surface, and on the Earth.

Hydraulics. The applied science and engineering of the mechanical properties of water.

Likelihood. A probabilistic estimate of the occurrence of a single event or of an outcome - for example, a climate parameter, observed trend, or projected change - lying within a given range. Likelihood may be based on statistical or modeling analyses, elicitation of expert views, or other quantitative analyses. The engineer will tend to use the term "likelihood" to refer to general, or non-numeric, matters and use the term probability to refer to computed, or numerical, values. The climate scientist may rely more on the statistical definitions of likelihood and probability, where the terms may be used interchangeably.

Mean sea level. The average height of the surface of the sea for all stages of the tide over a 19-year period, usually determined from hourly height readings. Not necessarily equal to mean tide level.

Monte Carlo. A class of computational algorithms that use repeated random sampling to obtain risk estimates.

Morphology. The form and structure, and the changes of form and structure, of the Earth's surface.

Nonstationarity. A characteristic of time series data where statistical parameters of the series, such as trend, variability, or temporal dependence change over time. Such changes over time complicate the use of historical data for estimating future conditions.

Nor'easter. Common storm type in the North Atlantic Ocean that produces northeast winds along the U.S. Atlantic seaboard.

Pacific Decadal Oscillation. A long-lived El Niño-like pattern of Pacific climate variability.

Perfect model approach. A method for evaluating the stationarity of downscaling approaches against future projections from a high-resolution global climate model. This approach assumes the high-resolution projections from the global model represent "truth," relative to which projections that have been downscaled from a coarser global climate model grid can be compared and their biases quantified.

Precipitation. Water in the form of rain, hail, sleet, or snow that forms in the atmosphere and falls to the Earth's surface.

Projection. A potential future evolution of a quantity or set of quantities, often computed with the aid of a model. Unlike predictions, projections are conditional on assumptions concerning, for example, future socio-economic and technological developments that may or may not be realized.

Quantile. Value in a distribution of a random variable representing a certain probability threshold. For example, the 0.1 AEP discharge quantile is the discharge that is equaled or exceeded in a given year with a probability of 0.1.

Relative sea level change. Sea level change at a coastal location relative to the land. This includes both the eustatic sea level rise component and local components such as the vertical land movement. This is the sea level change measured by long-term tide gauges.

Resilience. The ability to anticipate, prepare for, and adapt to changing conditions and withstand, respond to, and recover rapidly from disruptions.

Resilient. Capable of maintaining or rapidly recovering functionality in response to changing conditions or disruptions.

Return period. The average length of time, *T,* between occurrences in which the value of a random variable (e.g., flood magnitude) is equaled or exceeded. Actual times between occurrences may be longer or shorter, but the return period represents the average interval. The return period is the inverse of the AEP. For example, if the AEP equals 0.01 (or 1 percent), the return period, *T*, is 100 years.

Risk. The consequences associated with hazards (including climatic) considering the probabilities of those hazards. More specifically for this document, risks are the consequences associated with the probability of flooding attributable to an encroachment. It shall include the potential for property loss and hazard to life during the service life of the highway (23 CFR 650 A).

Runoff. The portion of a rainfall event discharged from a watershed into the stream network during and immediately following the rainfall.

Runup. The upper level reached by a wave on a beach or coastal structure relative to the still water level.

Scenarios. Sets of assumptions used to help understand potential future conditions such as population growth, land use, and sea level rise. Scenarios are neither predictions nor forecasts. Scenarios are commonly used for planning purposes.

Sea level rise. A rising long-term trend in mean sea level.

Sensitivity. The degree to which an asset is damaged or service is interrupted by a climatic hazard.

Shoreline. The intersection of a specified plane of water with the shore or beach (e.g., the high-water shoreline would be the intersection of the plane of mean high water with the shore or beach). The line delineating the shoreline on National Ocean Service nautical charts and surveys approximates the mean high-water line.

Standard error. A measure of the sampling variation of a statistic.

Stationarity. A characteristic of time series data where the statistical properties of the series do not change over time. There are no trends or other changes that would prevent historical data from being used to estimate future conditions.

Still water level. The elevation of the water surface if all wave and wind action were to cease.

Stochastic. A climate process or its functional representation that contains unpredictable components. In climate projections, weather sequences are considered stochastic; climate statistics are a combination of stochastic and deterministic processes. In hydrology, a stochastic process is a phenomenon (e.g., rainfall, streamflow) whose variation in time or space includes a random component.

Storm surge. A rise in average (typically over several minutes) water level above the normal astronomical tide level caused by the action of a storm. Storm surge results from wind stress, atmospheric pressure differences, and wave setup.

Storm surge hydrograph. Graph of the variation in the rise and fall of the still water level with time during a storm.

Submarine. The surface of the Earth under the ocean.

Tidal epoch. A 19-year cycle in the astronomical (sun and moon) producing tide forces that are averaged to obtain a tidal datum.

Tide. The periodic rising and falling of water that results from the gravitational attraction of the moon, sun, and other astronomical bodies acting upon the rotating Earth. Although the accompanying horizontal movement of the water resulting from the same cause is also sometimes called the tide, it is preferable to designate the latter as “tidal current,” reserving the name “tide” for the vertical movement.

Top-down analysis. A process where a defined set of information, design procedures, and design criteria is applied to a project to determine the resulting solution or to evaluate an existing solution.

Tropical storm. A tropical cyclone with maximum winds less than 75 mph (119 km/h) and greater than 39 mph (63 km/h). Tropical storms are characterized by less strength than hurricanes or typhoons.

Tsunami. A long-period wave caused by an underwater disturbance such as a volcanic eruption or earthquake. Commonly (non-technical usage) called "tidal wave."

Uncertainty. A state of incomplete knowledge that can result from a lack of information or from disagreement about what is known or even knowable. It may have many types of sources, such as imprecision in the data, ambiguously defined concepts or terminology, or uncertain projections of human behavior (IPCC 2013). Uncertainty can be represented by quantitative measures, such as a probability-density function, or by qualitative statements.

Validation. The process of determining the degree to which a model is an accurate representation of the real world from the perspective of the intended uses of the model.

Verification. A term used in reference to the accuracy of forecast values.

Vulnerability. The extent to which a transportation asset is susceptible to sustaining damage from hazards (including climatic). Vulnerability is a function of exposure, sensitivity, and adaptive capacity.

Water year. The 12-month period from October 1 for any given year through September 30 of the following year, according to the USGS. The water year is designated by the calendar year in which it ends and which includes 9 of the 12 months.

Weather. Meteorological conditions (including, but not limited to, temperature, moisture, precipitation, and wind) and the resulting events at a particular place over a short period of time.

Appendix A. Literature Review

This literature review was completed in fulfillment of Task 1 for NCHRP project 15-61 "Applying Climate Change Information to Hydrologic and Hydraulic Design of Transportation Infrastructure." It is divided into four major sections. The primary purpose of this project is to "**develop a design guide of national scope to provide hydraulic engineers with the tools needed to amend practice to account for climate change**."

Because design is essentially a decision-making process, the first section describes literature on decision-making frameworks.

Next, the literature review discusses high-resolution climate projections, including global climate model simulations, future scenarios, downscaling models, and their application to quantify future trends and distributions.

The third major section reviews the literature applicable to integrating climate inputs into hydrologic design for inland applications. Topics include nonstationarity, climate inputs for hydrologic design, sub-daily rainfall, and confidence limits.

The final major section reviews the literature related to the effects on coastal processes of climate change, with an emphasis on those topics with potential for immediate integration into coastal design applications. Topics include sea level rise, increasing ground water levels, changes in tropical and extratropical cyclones, watershed contributions to total water level at the coast, storm surges and wave hazards, and changes to coastal morphology.

Table of Contents

Appendix A. Literature Review A-1

Table of Contents A-2

List of Figures A-3

List of Tables A-4

Chapter 1. Decision-Making Frameworks A-5

Chapter 2. Hydrologic Outputs from Climate Modeling and Downscaling A-8
2.1. Reliability of Global Climate Model Simulations A-8
2.2. CMIP5 Simulations and Precipitation A-10
2.3. Translating Global Model Output into Higher-Resolution, Localized Information A-12
2.4. Selecting Global Climate Models A-16
2.5. Scenario Selection A-19
2.6. Abrupt Climate Change and Surprises A-20

Chapter 3. Nonstationarity, Uncertainty, and Climate Inputs for Inland Hydrology Applications A-22
3.1. Nonstationarity and Hydrologic Frequency Analysis A-22
3.2. Incorporating Climate Change into Hydrologic Analysis A-23
3.2.1. Event-Based Versus Continuous Simulation Hydrologic Modeling A-23
3.2.2. Hydrologic Design of Small Watersheds A-24
3.2.3. Stormwater Management and Water Quality Analysis and Design A-26
3.3. Sub-Daily Precipitation A-26
3.3.1. Historical Data A-27
3.3.2. Projected Data A-28
3.4. Confidence Limits and Uncertainty Bounds A-29

Chapter 4. Climate Changes to Coastal Processes Affecting Coastal Design Applications A-32
4.1. Global Sea-Level Rise A-32
4.1.1. Factors Contributing to Global Mean Sea Level Rise A-33
4.1.2. Local Factors in Sea Level Rise A-34
4.1.3. Global Sea-Level Rise and Projected Probabilities A-35
4.1.4. Sea-level Rise Scenario Selection A-37
4.2. Increasing Coastal Groundwater Levels A-39
4.3. Changes in Tropical and Extratropical Cyclones A-40
4.4. Watershed Contributions to Total Water Level at the Coast A-43
4.5. Climate Change and Historical Storm Surge and Wave Hazard Information A-44
4.6. Climate Induced Changes to Coastal Morphology Including Erosion and Deposition A-46

References A-49

Annex A1: Collaborative Research Opportunity: Global Climate Model Datasets A-64

Annex A2: Summary of Evaluations of Downscaled Daily and Sub-Daily Precipitation. A-65

List of Figures

Figure 2.1. Percent increases in the amount of precipitation falling in very heavy events (defined as the heaviest 1% of all daily events) from 1958 to 2012 for each region of the continental United States. These trends are larger than natural variations for the Northeast, Midwest, Puerto Rico, Southeast, Great Plains, and Alaska. The trends are not larger than natural variations for the Southwest, Hawai'i, and the Northwest.(Source: Walsh *et al.* 2014) A-11

Figure 2.2. Proportion of the total uncertainty in future annual mean precipitation projections corresponding to the internal natural variability of the climate system (orange), scientific or model uncertainty (blue) and human or scenario uncertainty (green). Source: Hawkins and Sutton 2011..... A-17

Figure 3.1. Frequency curves for the Cedar River and Skunk River in Iowa. A-31

Figure 4.1. Projected changes in global mean sea level and their associated averages and uncertainties for the period 2081-2100 (vertical bars). A-36

Figure 4.2. An ensemble of many combined cumulative probability distributions showing the effect of sea-level rise on the Gulf of Finland. A-37

Figure 4.3. Screening analysis flowchart for consideration of sea-level rise. A-38

Figure 4.4. Schematic of marine and groundwater inundation due to sea-level rise in the southern Oahu aquifer. A-40

Figure 4.5. Time-series of discharge for hindcast simulations of Hurricane Ike accounting for rainfall-runoff, storm surge, and combinations thereof. A-44

Figure 4.6. Non-linearity of storm surge due to a 15.2-cm sea-level rise for Hurricane Katrina in the northcentral Gulf coast. Values > (<) 0 show amplification (attenuation). A-46

List of Tables

Table 2.1. Valid performance evaluation standards for global climate model output..... A-9
Table 2.2. Standard 'extreme' precipitation indices used by the international climate science community. A-12
Table 2.3. Valid performance evaluation standards for downscaled global climate model output. A-14
Table 4.1. Global climate model collaborative research opportunities..... A-64
Table 4.2. Validity of available high-resolution climate projections..... A-65

Chapter 1. Decision-Making Frameworks

Because of the numerous sources of uncertainty involved with climate modeling and hydrologic analysis alternative decision-making frameworks are being developed or introduced to these areas. These **bottom-up** frameworks are alternatives to the **top-down** decision-making dominate in engineering analyses. With the top-down approach, scenarios of future climate applied to hydrologic models provide a range of hydrologic outcomes that are applied to various planning and design strategies; conversely, with the bottom-up approach, the vulnerabilities or tipping points of a location or system are assessed and the possibilities of those conditions occurring are evaluated (U.S. EPA 2010).

Weaver *et al.* (2013) describes this dichotomy as a contrast between two paradigms: 1) Predict then act, and 2) Seek Robust solutions. For the more traditional engineering approach of predict-then-act, one tries to assess the most likely future outcomes and then designs the best policy or design for that future. The relevant question is what is most likely to happen and the goal is to maximize expected utility. For the paradigm of seek robust solutions, one tries to identify the greatest vulnerabilities across a range of futures and identifies a range of policies or designs that perform reasonably well across the range of futures. The relevant question under this paradigm is how does my system work and under what circumstances might it fail. The goal is to minimize regret.

Another common way of characterizing top-down versus bottom-up decision approaches is c**ontext-first versus science-first** as described in Weaver *et al.* (2013) and Reeder and Ranger (2011). The predominant approach to adaptation planning has been a science-first approach where the process is: 1) generate/interpret climate projections, 2) analyze their impacts, and 3) design adaptation options to mitigate those impacts. An alternative approach, context-first, encourages beginning at the level of the adaptation problem first, then specifying objectives and constraints, and finally identifying appropriate adaptation strategies and (if necessary) appraising their desirability against a set of projections (Reeder and Ranger 2011).

There are many examples where future scenarios are chosen and then impacts are assessed (see for example USDOT 2014, Anderson *et al.* 2015, Mishra and Herath 2014, LaFontaine *et al.* 2015, Selvanathan *et al.* 2016, Moglen and Vidal 2014). However, the tools used in the analyses do not define which paradigm is applied, but rather it is the approach that reveals the paradigm. For example, the Federal Highway Administration (FHWA) completed a new guidance document "Highways in the River Environment- Floodplains, Extreme Events, Risk, and Resilience" (known as HEC-17) that provides recommendations on the selection of climate scenarios to generate precipitation information to feed into hydrologic models for design, analysis, and planning (Kilgore *et al.* 2016). The recommended framework in HEC-17 attempts to use confidence limits, where uncertainty can be quantified, to generate the most likely discharge appropriate for design along with a range of discharges that can be used to assess design performance. While designing only for the most likely discharge is representative of top-down evaluation, considering effects of a possible range of discharges, and making design adjustments to avoid unacceptable outcomes, moves to more of a bottom-up decision process.

The **design storm** concept is another example of a top-down decision process typical in hydrologic modeling. The design storm is the precipitation that corresponds to a predetermined level of risk (usually expressed as a probability of exceedance). The hydraulic facility, e.g. a culvert or storm drain system, is then configured to pass the design storm while satisfying one or

more design criteria. The effects of storms larger or smaller on system performance are generally not considered.

Traditional **risk analysis** and **benefit cost analysis** also tend to be top-down in the sense that uncertainty is quantified**.** Risk analysis incorporates probabilities of damages and provides some measure of the costs and consequences (monetary and other) associated with damages and performance interruptions to facilitate the comparison of alternatives (Kilgore *et al.* 2016). From this information, benefit cost ratios or net benefits can be calculated and the alternatives with the most desirable metrics are selected. Because these approaches, as well as the design storm approach rely on historical probabilities, they do not readily inform decision-making with uncertain futures.

To respond to this limitation, a growing suite of bottom-up decision-making tools are being applied to quantify vulnerability and resilience in a changing climate. One of these tools is the concept of **regret**. Regret is the difference between the benefits associated with a particular option and the benefits associated with the best option available if one had perfect foresight (Rosner *et al.* 2014). The concept of regret is two-sided because it considers the costs of underpreparing and overpreparing for climate change. Regret-based methods include, for example, **regret minimization** and **minimax regret** (Garcia *et al.* 2014, Kirshen *et al.* 2014, van der Pol *et al.* 2016, Rosner *et al.* 2014). Within this context, some decisions or adaptions can be considered **low (no) regrets** if they perform well under most or all future scenarios (Kirshen *et al.* 2014). Regret minimization and minimax regret (minimize the maximum regret) both require scenarios from which to estimate regret, but minimax regret does not require probabilities associated with the scenarios (van der Pol *et al.* 2016).

The decision-making literature is replete with a variety of other bottom-up decision frameworks that facilitate decisions with uncertainty. These include:

- **Robust Decision Making (RDM)** (Weaver *et al.* 2013, Garcia *et al.* 2014, Fischbach *et al.* 2015, Clark *et al.* 2016). RDM uses an iterative decision framework to identify strategies that perform reasonably well over a wide range of plausible future scenarios (Garcia *et al.* 2014)
- **Information Gap** (Weaver *et al.* 2013, Clark *et al.* 2016). RDM and info-gap emphasize the evaluation of the performance of different options within the context of declared uncertainties and the minimization of potential regrets (Clark *et al.* 2016).
- **Decision Scaling** (Weaver *et al.* 2013). Decision scaling is a process incorporating both stakeholder involvement and data analysis to distinguish between important uncertainties that can be informed by further analysis versus those uncertainties that are not critical for the policy or decision being evaluated.
- **Real Options** (Garcia *et al.* 2014, Kirshen *et al.* 2014). Real options is a probabilistic decision process by which adaptability can be explicitly incorporated into project designs in an effort to avoid potential regrets associated with either over-investment or under-investment. It encourages staged decision-making where more expensive and highly-irreversible decisions are reserved until more information is available on which to make those decisions (Garcia *et al.* 2014)
- **Route-Map Approach** (also known as decision pathways) (Reeder and Ranger 2011). The route-map approach encourages postulation of "what if" outcomes and seeks flexible approaches where decisions are made over time allowing continuous adaptation. It emphasizes

the creation of sets of measures that can be implemented over time rather than more irreversible major strategies (Reeder and Ranger 2011)

These bottom-up approaches have reinforced decision-making more suited to the uncertainties of climate change than were needed under assumptions of nonstationarity. The inability to assign probabilities to future projections of climate is related to the **deep uncertainty** associated with the projections. Walker *et al.* (2003) defines five levels of uncertainty between certainty and total ignorance. Level 5 uncertainty means that we only know that we do not know, that is, we recognize our ignorance. This is referred to as deep uncertainty. Example discussions of deep uncertainty are found in Weaver *et al.* (2013), Haasnoot *et al.* (2012), Reeder and Ranger (2011) and Walker *et al.* (2003).

The bottom-up approach is applicable in cases where **tipping points** may be experienced (Haasnoot *et al.* 2012). A tipping point is where the magnitude of change due to climate change or sea level rise is such that the current management strategy will no longer be able to meet the objectives. Bottom-up approaches also generally encourage or facilitate **adaptive management.** Adaptive management promotes flexible decision making that can be adjusted in the face of uncertainties as outcomes from management actions and other events become better understood (NRC 2004).

Most examples of bottom-up decision making in the literature apply this approach to larger systems with complex physical and operational characteristics. Overall, our transportation systems exhibit these same kinds of complexities. This study, however, is focused on tools for designing specific elements of the transportation system such as bridges, culverts, and stormwater management facilities. These are usually designed and built at a fixed scale intended to serve its function for a certain design life. While such infrastructure may have adaptable features, such as additional bridge width to add lanes later, the design choices are largely binary. Still, the bottom-up approach for considering climate projection and hydrologic modeling uncertainty has potential for informing infrastructure design.

Chapter 2. Hydrologic Outputs from Climate Modeling and Downscaling

Global climate modeling and associated downscaling models produce projections of future precipitation and temperatures that are used as inputs for hydrologic models. In this section of the literature review, hydrologic outputs of climate models are considered.

2.1. Reliability of Global Climate Model Simulations

Climate model projections play a growing role in informing policy decisions at every level, from the individual city to international negotiations. Global climate models (GCMs) are subjected to vast, comprehensive, and continuous scrutiny and testing. Determining the accuracy and reliability of climate model projections is a unique challenge, however, as climate change models produce projections, not predictions or forecasts. Climate scientists use the term **prediction** in reference to the evolution of specific weather events and **forecast** for future weather events under known forcing factors. **Projection** is used for aggregate weather under plausible future forcing factors. Climate model projections cannot be used as a long-term weather forecast model, to predict the chances of rain on July 18, 2064, or by how much the average temperature in January 2032 will exceed the long-term average. Rather, they are intended to accurately project the behavior of the climate system averaged over climate timescales of twenty to thirty years, and the most likely response of the climate system to the specific emissions trajectory -- of heat-trapping greenhouse gases and other radiatively-active species -- used as input to that specific climate model simulation. The response to future greenhouse gases is evaluated with projections rather than predictions because the uncertainty in the amount of future greenhouse gas emissions and resulting climate change is human, rather than physical, in origin.

Model reliability cannot be demonstrated by validation of future projections. To use future projections for validation purposes, it would be necessary to: (a) have the entire world adopt a specific emissions trajectory exactly as forecast, including associated changes in population, demographics, technological development, and energy use, such as one of the Representative Concentration Pathways and its associated Shared Socioeconomic Pathway (Moss *et al.* 2010); (b) follow this pathway precisely for multiple decades, to mid-century or beyond; then (c) look backwards to assess the accuracy of projections made today. This process is clearly impossible from a logistical perspective, as it would require an unprecedented level of international and national coordination. It is also futile from a utilitarian perspective, as it precludes the primary use of climate models today, which is to quantify the impacts of a range of future scenarios on human society and infrastructure in order to select the most viable pathway forward that minimizes the costs of both adaptation and mitigation. By the time the projection was validated, that amount of climate change would be inevitable due to the emissions that had occurred while the pathway was being followed.

Model reliability cannot be demonstrated by assessing whether the model reproduces a specific historical event in the year in which it occurred, such as the 1995 Chicago heat wave, or the 2011 drought. Climate model projections are initialized with conditions from the 1800s and then allowed to generate their own chaotic patterns of internal natural variability that evolve over time into a different temporal sequence than experienced in the real world. This means that, while climate models are generally able to simulate a heatwave of the magnitude and geographic location observed in 1995 sometime in the 30-year climatological period surrounding 1995, there is no reason *per se* to expect that event to occur in 1995.

In addition, model reliability cannot be demonstrated by calculating model bias: comparing, for example, the absolute value of seasonal or annual mean precipitation for a given region with the observed value – either for an individual year or even for a 20-30 year climatological period. The absolute value of modeled precipitation over a region is frequently biased or offset from the observed value due to both the limited spatial resolution of the model as well as the limited geographic coverage of the observations. This bias is removed through empirical-statistical downscaling before applying climate simulations to quantify impacts at the local to regional scale, and is not indicative of overall model reliability.

Model reliability is legitimately demonstrated when climate models are able to generate dynamical weather and precipitation patterns that: (1) occur due to known and observed processes; (2) are consistent with historical observations; (3) have shifted or changed (in terms of both temporal and/or spatial distribution) in a manner consistent with known physics and/or observed trends; and (4) project future changes that are consistent with known physics and/or observed trends. Valid evaluation standards for global climate model simulations are listed in Table 2.1.. Model projections are significant when their magnitude exceeds that of historical observed and internal model variability. Annex A1 describes opportunities for engineers and climate scientists to co-develop additional engineering-relevant evaluation standards.

Table 2.1. Valid performance evaluation standards for global climate model output.

Performance Attribute	Description	Rationale
Process Realism	Agreement with forcing mechanisms for precipitation	Do climate models recreate historical dynamical processes that bring dry and wet conditions to the region of interest?
Short-range Forecast	Agreement with observed long-term trend	Have climate models accurately forecasted observed trends over the last 20-30 years or more?
Internal Variability	Agreement with range of variability	Do climate models replicate the range of historical variability in the region over climate time scales of 20-30 years or more?
Model Variability	Agreement among models	Do future projections vary widely depending upon the climate model, or do they show consistent trends in the region of interest?
Signal Variability	Agreement or disagreement among different future scenarios	Do climate model projections of variables that basic physics indicates should differ depending on the amount of forcing applied to the system, such as temperature-related variables or heavy precipitation or sea level rise, vary by scenarios of future conditions? Do projections of other variables, such as mean annual or seasonal precipitation, that are not expected to differ broadly between future scenarios, diverge?
Signal-to-Noise	Ratio of mean to variability	Does the combination of model-simulated future trend and internal variability exceed differences in mean change between scenarios?

THE BOTTOM LINE: Global climate models are reliable for both historical simulations and future projections over climatological time scales of 20 to 30 years or more. They are intended to

reproduce the statistics of observed climate rather than track its day-to-day variability. Valid standards for model evaluation are based on their ability to reproduce the physics and dynamics of precipitation, not their bias or ability to reproduce specific historical events.

2.2. CMIP5 Simulations and Precipitation

The Coupled Model Intercomparison Project (CMIP) collects, standardizes, and archives global climate model simulations for use by the academic and stakeholder community. Each of the global models that provide output to CMIP has its own unique name, which is typically an acronym that reflects its provenance and the institution that created it, as well as the generation of the current model (e.g. HadCM3 stands for the U.K. Hadley Centre Climate Model version 3). Today, there are over 50 global climate models, each originating from a specific research institution in the U.S., Canada, the U.K., the E.U., China, Japan, and Australia. Collectively, it is correct to refer to the models that have submitted output to a CMIP experiment as "CMIP models". The Intergovernmental Panel on Climate Change uses CMIP output as the basis for its analyses and projections, but it is incorrect to refer to these models as "IPCC models" as they are neither created by nor archived by the IPCC.

CMIP Phase 3 (CMIP3) was the first to include both historical and transient (year-by-year) future simulations for a range of different scenarios. The most recent version of the archive, CMIP5, provides output from over 50 global climate models with spatial resolutions ranging from about 50 to 300 km (30 to 200 miles) per horizontal side. It is often the case that model ability to simulate regional precipitation patterns increases with its horizontal resolution or grid size; simulations for CMIP6 are currently underway, and are expected to include even higher-resolution simulations as fine as 25 km (15 miles). All CMIP archives provide output from a large ensemble of different climate models and future scenarios that enable researchers to quantify future climate change at global, continental, and broad regional scales.

How well do these models perform, relative to the evaluation standards described in Table 2.1.? Both 24-hour and 5-day precipitation from 12 CMIP3 models was evaluated by Kharin *et al.* (2005), using output from historical atmosphere-only simulations for the period 1979 to 1995 (see Annex A1 for more details on the difference between coupled versus atmosphere-only models). Calculating the 20-yr return period value of daily precipitation with a generalized extreme value distribution, and averaging the results over broad latitudinal regions (e.g., tropics, extratropics), they found that the majority of CMIP3 models underestimated the 20-yr return values of annual precipitation extremes, and their spatial variations. At the same time, they found that the spatial pattern of extreme precipitation rates in the mean model matches the observations reasonably well in the extratropical regions, but not in tropical regions.

CMIP3 simulations have also been used in formal detection and attribution studies (see Glossary) of extreme rainfall. For example, Zhang *et al.* (2007) used output from CMIP3 simulations to detect latitudinal changes in average precipitation that cannot be explained by natural climate variability or natural forcing, then expanded on their earlier work in Zhang *et al.* (2013) using output from CMIP5 experiments to estimate the human contribution to continental-scale change in 1-day and 5-day "extreme" or heavy precipitation. For North America, they concluded that human-induced climate change has increased annual maximum 1-day and 5-day precipitation by 3.3 percent and 3.8 percent, respectively, during the period 1951 to 2005. They also estimated that the 20-yr return period for extreme precipitation had decreased to 15 years for

1-day and 14 years for 5-day annual maximum precipitation. However, an analysis of trend in 1-day annual maximum precipitation in 15 CMIP5 models for the longer period 1901 to 2010 reveals the trend is underestimated (Krakauer and Fekete 2014, Asadieh and Krakauer 2015). Therefore, climate model reliability is sufficiently established to conclude that changes in both mean and extreme precipitation have already occurred, and – particularly for regions of the U.S. that have experienced the greatest changes, such as the Northeast and Midwest (Figure 2.1) – they are already affecting the reliability of engineering design precipitation metrics based on historical data.

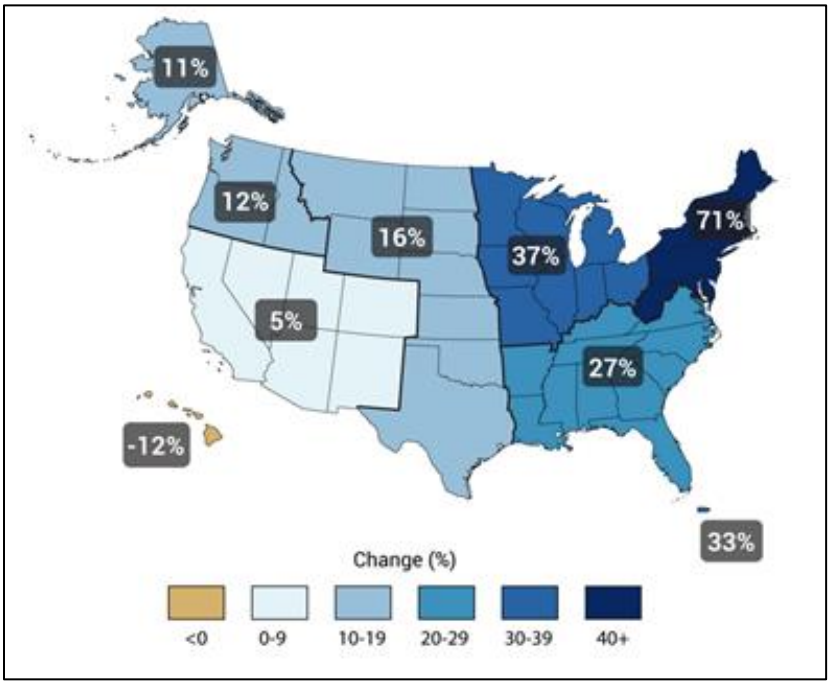

Figure 2.1. Percent increases in the amount of precipitation falling in very heavy events (defined as the heaviest 1% of all daily events) from 1958 to 2012 for each region of the continental United States. These trends are larger than natural variations for the Northeast, Midwest, Puerto Rico, Southeast, Great Plains, and Alaska. The trends are not larger than natural variations for the Southwest, Hawai'i, and the Northwest.(Source: Walsh *et al.* 2014)

The differences between CMIP3 versus CMIP5 simulations of extreme precipitation across the U.S. are minimal. For consistency and convenience, the international climate science community has developed a list of standard precipitation extremes summarized in Table 2.2 (Frich *et al.* 2002, Zhang *et al.* 2011). This list is not intended to be exhaustive; many more such indices can be developed from daily and sub-daily data. The list also illustrates how the types of precipitation events climate scientists consider to be 'extreme' are often much more frequent than what the hydrologic engineering community would call 'extreme.' Comparison of the Table 2.2 indices in CMIP3 versus CMIP5 shows that the model distributions overlap in every region of the United States (Kharin *et al.* 2013). Wuebbles *et al.* (2014) also compared the 5-year return value of 2-day precipitation and found no appreciable difference between CMIP3 and CMIP5 across the United States. For this reason, many climate scientists recommend using CMIP5 and CMIP3 simulations as a sort of "meta-ensemble" of simulations if a large sample size is required.

THE BOTTOM LINE: CMIP3 and CMIP5 archives provide a broad range of global climate model outputs that are comparable in terms of their ability to simulate extreme precipitation. Using CMIP simulations, climate scientists have been able to formally attribute observed increases in precipitation at higher latitudes, and increases in heavy precipitation at mid-latitudes, to human-induced climate change.

Table 2.2. Standard 'extreme' precipitation indices used by the international climate science community.

Indicator Name (ID)	Indicator Definition	Units
Max 1-day precipitation amount (RX1day)	Monthly maximum 1-day precipitation	mm
Max 5-day precipitation amount (RX5day)	Monthly maximum consecutive 5-day precipitation	mm
Simple Daily Intensity Index (SDII)	The ratio of annual total precipitation to the number of wet days (≥ 1 mm)	mm/day
Number of heavy precipitation days (R10)	Annual count when precipitation ≥ 10 mm	days
Number of very heavy precipitation days (R20)	Annual count when precipitation ≥ 20 mm	days
Consecutive dry days (CDD)	Maximum number of consecutive days when precipitation days < 1 mm	days
Consecutive wet days (CWD)	Maximum number of consecutive days when precipitation days >= 1 mm	days
Very wet days (R95p)	Annual total precipitation from days > 95th percentile	mm
Extremely wet days (R99p)	Annual total precipitation from days > 99th percentile	mm
Annual total wet-day precipitation	Annual total precipitation from days >= 1 mm	mm

2.3. Translating Global Model Output into Higher-Resolution, Localized Information

A recent Department of Defense report (Kotamarthi *et al.* 2016) gives an up-to-date and comprehensive review of downscaling and the use of high-resolution climate projections in quantifying impacts at the regional to local scale. This section provides a brief overview of the topic; more information is available in the full report and/or its accompanying webinar (see box on next page).

Global climate model output is typically generated at relatively coarse spatial scales ranging from 1 to 3 degrees of latitude and longitude. It is also subject to biases in the absolute value of precipitation as well as the shape of the probability distribution or density function. These biases are due to the GCMs' limited spatial resolution as well as uncertainty related to the physical representation of important processes, such as rainfall and cloud formation, that occur at spatial scales far smaller than the model is able to resolve. Analysis of CMIP3 model output finds that the value of 20-yr return and 30-yr interval for daily precipitation is more severely underestimated as grid spacing increases (Kharin *et al.* 2005, Wehner *et al.* 2010). For this reason, when using climate projections to quantify potential changes at the local to regional scale, global climate model output is typically downscaled, using a dynamical regional climate model (RCM) or an empirical-statistical downscaling model (ESDM).

To achieve the goal of reliably removing systematic errors from global climate model output, reliability of downscale models is evaluated differently than reliability of global climate models. The use of downscale models begins with the requirement that the global climate model being downscaled already produces reliable global climate simulation. Downscale methods must guard against introducing new errors, overfitting historical data, and sensitivity to non-stationarity (Table 2.3).

USE OF CLIMATE INFORMATION FOR DECISION-MAKING AND IMPACTS RESEARCH: A DOD REPORT ON THE STATE OF UNDERSTANDING (2016)

Useful and actionable climate information is often required over a range of scales to serve a variety of purposes. However, the provisioning of actionable climate information to decision-makers and practitioners—especially at spatial scales relevant to decision-making—is in its infancy. Although a vast amount of climate information is available at different spatial scales and temporal resolutions, corresponding information on its utility and appropriateness of use in a decision-making context is lacking.

This primer on the appropriate use of climate information for non-experts provides a summary of available climate information and a broad outline of the ways such information can be incorporated into vulnerability and impact assessments, climate resilience and preparedness considerations, and adaptation planning from a research perspective. It also includes a summary of the state of the science, our understanding of the appropriate use of that science in the context of decision-making, and a description of current and future research topics that clearly explain why climate is changing, how climate projections are generated, what types of climate impacts are studied, and how the results can be used in further analyses to inform planning, general decision-making, and impacts research.

Because the most appropriate climate inputs for any given application depend on the nature of both risk tolerance and associated vulnerabilities, this is not a prescriptive guidance document that outlines the "best" climate models, methods, or projections to use in any planning exercise. Instead, it conveys a basic understanding of climate change, global climate models, and future scenarios to place the use of high-resolution climate information into an appropriate context. It describes the available downscaling methods used to generate high-resolution climate projections at the local to regional scale, current understanding of their appropriate use (or non-use) in decision-making and impacts research, and recommendations as to appropriate use of downscaled model output for some regions with specific geographic or terrain features that constrain viable choices.

A webinar highlighting the main results of this report is available here, and the full report here.

RCMs are physically-based models of regional climate that cover a limited area of the world and are run at finer spatial and temporal scales than global models. In principle, they can provide output at each time step, typically 30 seconds to a few minutes. In practice, it is difficult to evaluate precipitation at sub-daily values, due to the lack of long-term observational datasets spanning multiple decades that would be required to accurately sample to obtain the range of natural variability. In addition to precipitation and temperature, they provide a host of other potentially useful variables as output, such as humidity, solar radiation, wind, etc. As a limited-resolution model, drawbacks are that they still require bias correction and they are extremely computationally demanding.

Table 2.3. Valid performance evaluation standards for downscaled global climate model output.

Performance Attribute	Description	Rationale
Climate Accuracy	Agreement with measurement distributions over a period of time.	Are RCMs and ESDMs able to recreate historical climate statistics?
Process Realism	Agreement with historical weather patterns and mechanisms for precipitation.	Do RCMs replicate weather processes?
Transferability	Agreement with measurement in regions separate from the model development region.	Do RCMs work well under climate conditions different from their development region? Are RCMs overfitting regional dynamics in their development region and performing poorly in other regions?
Within-sample versus out-of-sample accuracy	Agreement with measurement not used in model development.	Do ESDMs perform poorly on historical data outside the period of model development? Are ESDMs overfitting historical data and performing poorly on data outside the period of model development?
Sensitivity to non-stationarity	Agreement with future conditions substantially different than present.	Do ESDMs perform poorly when climate statistics have changed?

Since RCM simulations are technically and computationally demanding, most impacts analyses use existing, publicly available RCM simulations rather than generating new ones. Simulations from six regional climate models are currently available from the North American Regional Climate Change Assessment Project (NARCCAP) at horizontal resolution of 50 km, based on simulations from four CMIP3 global climate models for one mid-range future scenario (SRES A1B). NARCCAP output was originally not bias-corrected; correcting model biases using an ESDM was shown to reduce model error substantially in a similar European project called ENSEMBLES (Themeßl *et al.* 2012). A motivation for the NARCCAP dataset was to provide high-resolution climate change scenarios to study climate change impacts and adaptation (Mearns 2009). A report by Mearns *et al.* (2015) reviewed 30 impact studies using NARCCAP model output and found that NARCCAP model output was used because it has higher spatial and temporal (3 hr) resolution and provides 51 variables in addition to temperature and precipitation.

A major area in RCM research and development is improved simulation of sub-daily precipitation. At 50-km grid spacing, three-hourly precipitation results are inconsistent from model to model (Anderson *et al.* 2003; Cook *et al.* 2016; Annex A2). The same result was also found for extreme daily precipitation when Wehner (2013) used GEV to estimate 20-yr return interval value of season-dependent daily rainfall. This is related to RCM's inability to consistently relate convective precipitation to moisture flux divergence. The working hypothesis is that with finer grid spacing (4-km or less) the explicit simulation of convective rainstorms will result in consistency among models and will improve accuracy of spatial correlation and sub-daily rainfall. These efforts are highly experimental, involve very few simulations with a single model that may or may not be publicly accessible, and focus on specific regions. Results for U.K. show summer rainfall duration and hourly extremes in summer are improved substantially with higher resolution (Kendon *et al.* 2016). Similar simulations for the U.S. (Liu *et al.* 2016a)

show the models to better resolve inter-mountain west snowpack; results are still pending for warm-season rainfall through the rest of the United States.

ESDM downscaling can reduce – and in the case of a good ESDM, virtually eliminate -- biases and improve the accuracy of local climate information. In contrast to global climate model output, it is appropriate to compare the climatological mean absolute values from an ESDM for the historical period (Table 2.3). Comparing values over the same time period as the data used to train the ESDM quantifies the goodness of fit of the statistical model. Comparing values over an independent time period not used to train the model quantifies the extent to which the model is able to reproduce new or novel conditions. However, under no circumstances should ESDM output for a range of years encompassing both the training period and an independent period be compared with observations, because this is mixing apples and oranges and the results will be neither useful nor interpretable.

ESDMs use historical observations to remove the bias in global climate model output (and RCM output as well). They are computationally efficient, flexible, and able to process a large number of global climate scenarios in a limited amount of time. They are able to generate output at the scale of the observations, from a gridded dataset to an individual point source such as a weather station, and the absolute value of their output (e.g. seasonal precipitation, or the frequency of days per year with more than 2" of precipitation in 24 hours) will be virtually identical to that of the observations in the historical period, over climatological time scales. (As noted previously, global climate model output – whether downscaled or not – will never match the exact internal variability of the real climate system; this is not a flaw but rather an intentional design aspect of the models, to allow them to establish their own internally consistent patterns of natural variability.) ESDMs, however, can be sensitive to errors in the observational data, requiring extensive quality control and error-checking before the observations are used. They also assume that the relationship between local climate and large-scale weather patterns that can be resolved by global climate model output remains stationary both now and in the future (Mearns *et al.* 2015). This assumption is generally valid for more complex ESDM methods such as ARRM (Stoner *et al.* 2012), but is not true for simple methods such as the delta approach.

Two archives of empirical-statistical downscaled outputs are supported by federal agencies and used widely. The Downscaled CMIP3 and CMIP5 Climate and Hydrology Projections archive (http://gdo-dcp.ucllnl.org/downscaled_cmip_projections/) is maintained by several water agencies and climate research centers in the western United States. It is based on the Bias Correction Spatial Disaggregation (BCSD) method that applies an empirical quantile mapping approach to monthly global climate model outputs. This means that the output is accurate for seasonal and monthly precipitation, but not for sub-monthly indices (e.g. wettest week of the year, return period of the 1-in-10 wettest day). The USGS GeoData Portal (http://cida.usgs.gov/gdp/) is maintained by the USGS Center for Integrated Data and Analytics. It is based on the Asynchronous Regional Regression Model (ARRM1) method (Stoner *et al.* 2012) that applies a parametric quantile regression approach to daily global climate model outputs. This means the output is at least theoretically accurate to indices down to the individual day. A new version, ARRM2, has been developed that applies a non-parametric (i.e. allows for uncertainty in mapping observations to global climate model output) kernel density approach to daily global climate model output. Initial tests show significant improvement over ARRM1 and BCSD for both temperature and precipitation extremes at the tails of the distribution (Hayhoe, personal communication). Other statistical approaches used in publicly available datasets of

ESDM output include the constructed analogue method as used in the Bias Corrected Constructed Analogue (BCCA) and Localized Constructed Analogue (LOCA), where historical maps of weather data are used to construct a match to the pattern of a future weather map. The report referenced in the box above provides more information on specific downscaling methods and their reliability over various spatial and temporal scales, regions, and variables (Kotamarthi *et al.* 2016).

Evaluations of daily and sub-daily precipitation in these publicly accessible data archives are summarized in Annex A2. Downscaled daily precipitation must be evaluated carefully, at minimum performing evaluation set forth in Table 2.3. At present, an agency does not have the responsibility to ensure this evaluation has been completed and provide quality assurance of the projection data. This is in contrast to historical precipitation data for which NOAA ensures data accuracy, quality control, and quality assurance, and global climate projection data for which DOE provides data archival and quality assurance. Thus, a team of engineers and climate scientists often must work together to complete this step for downscaled daily precipitation. Sub-daily precipitation requires even larger amounts of historical data for evaluation compared to daily precipitation and, because of limited historical data availability, these methods have low reliability.

THE BOTTOM LINE: Global climate model output can be downscaled using regional climate or empirical-statistical downscaling models. Each approach has its own unique benefits and limitations that must be considered when deciding which to use for a given project. It is recommended that a team of engineers and climate scientists perform a careful assessment and evaluation before using daily projections. Very low reliance can be placed on available methods to generate sub-daily precipitation projections.

2.4. Selecting Global Climate Models

Selection of appropriate datasets, methods, and models can be complicated by the fact that climate projections are subject to important uncertainties arising from natural variability within the climate system, scientific or model uncertainty, and the future evolution of the human activities and emissions driving modern-day climate change (Figure 2.2). “The value for decision making of predictive information depends, to a large extent, on the signal-to-noise ratio of the prediction, i.e. how large is the expected change compared to the uncertainty in the prediction.” (Hawkins and Sutton 2011). CMIP3 was the first to address systematically these three sources of uncertainty in climate projections, by generating year-by-year projections from a broad range of GCMs and scenarios covering a range of plausible Representative Concentration Pathways from higher (RCP8.5, 6.0) to lower (RCP4.5, 2.6) (Moss *et al.* 2010). This framework has been adopted for the most recent CMIP5 and upcoming CMIP6 experiments.

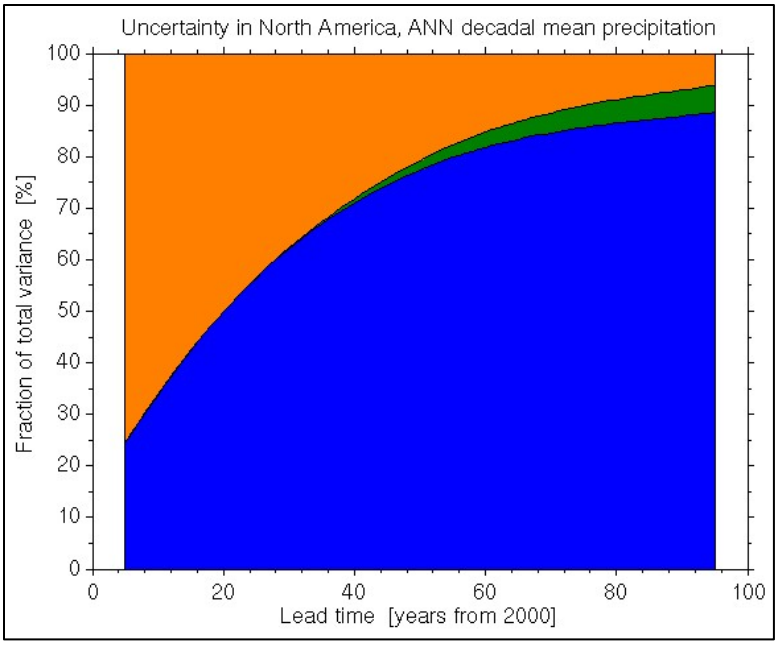

Figure 2.2. Proportion of the total uncertainty in future annual mean precipitation projections corresponding to the internal natural variability of the climate system (orange), scientific or model uncertainty (blue) and human or scenario uncertainty (green). Source: Hawkins and Sutton 2011.

Because of the uncertainties associated with global climate modeling, climate scientists do not provide confidence limits on future projections of climatic variables. Rather the approach is to use an ensemble of models and consider them all possible and equally credible outcomes of future climate despite the fact that models differ in terms of resolution, processes included, forcings and agreement with observations. Previous assessment reports have avoided weighting or ranking the models. However, there are known shortcomings in this approach. The following excerpts are from the Expert Meeting on Assessing and Combining Multi-Model Climate Projections (IPCC 2010):

- The reliability of projections might be improved if models are weighted according to some measure of skill and if their interdependencies are taken into account, or if only subsets of models are considered. Since there is little opportunity to verify climate forecasts on timescales of decades to centuries (except for a realization of the 20th century), the skill or performance of the models needs to be defined.
- Ensemble members may not represent estimates of the climate system behavior (trajectory) entirely independent of one another. This is likely true of members that simply represent different versions of the same model or use the same initial conditions. But even different models may share components and choices of parameterization of processes and may have been calibrated using the same datasets.

As stated above, the goal is not to try to identify a "most likely" scenario or a "best" GCM; rather, the goal is to use a selection of models and scenarios that capture both the spread of the model output (scientific or model uncertainty) as well as the possible range of future change (human or scenario uncertainty). To that end, conventional wisdom and scientific consensus dictates that impact assessments should include a range of climate models and a range of future scenarios (Clarke et al. 2012; see also Kotamarthi et al. 2016). FHWA pilot projects, including

the New Jersey Pilot (FHWA 2014b), the WSDOT Pilot (FHWA 2014c), and Gulf Coast 2 study (FHWA 2014d), all used a range of global climate models and scenarios in developing the information over a series of time periods. In New Jersey, GCMs were selected based on their ability to model precipitation for New Jersey. For the Gulf Coast, all GCMs were selected that had daily outputs and were well-documented for multiple generations in the scientific literature (i.e. they were not the first version of the model to be published, but rather had a long history of development and evaluation stretching back years and, in some cases, decades).

There is no standard method for selecting the GCMs to be used in a given assessment. In general, the scientific consensus tends to be that using more models is better than less; models should cover the range of accepted climate sensitivity, which ranges from 2 to 4.5ºC for a doubling of carbon dioxide in the atmosphere; and it is generally preferable to prioritize models with a long and well-documented history of development and evaluation in the peer-reviewed scientific literature. Table 9.5 in Flato et al. (2013) provides values of climate sensitivity for CMIP5 models, indicating which models are needed to capture the range of variability. Selection of the "best" models is to be avoided unless this selection is based on a comprehensive and often lengthy evaluation of model ability to reproduce specific dynamical features relevant to precipitation over a given region. Conversely, it should be established that excluded models are not able to simulate or reproduce those features and how they change over time when driven by anthropogenic forcing. However, it is reasonable to remove a model from consideration if extremely poor model performance indicates that the model cannot be trusted (Mendlik and Gobiet 2016). Lacking such clarity, the most defensible approach is to select models via the more basic criteria described above.

The Infrastructure and Climate Network (ICNet) provides an intercomparison tool prepared by Stoner and Hayhoe that includes a list of all CMIP3 and CMIP5 global climate models as well as summary information about the individual models (http://theicnet.org/?page_id=50). It describes the 25 modeling centers or groups that participated in the CMIP5 effort and submitted model output that is available for applications (http://cmip-pcmdi.llnl.gov/cmip5/docs/CMIP5_modeling_groups.pdf). Each group ran at least one model and numerous groups ran more than one model or model version. In total, there are 58 possible climate models that may potentially be used for climate adaptation. However, 12 of those models do not have output for any future scenarios. Of the remaining 46 models, 21 have output for all four scenarios, 8 are missing RCP6.0, 10 have only RCP4.5 and RCP8.5, five have only RCP4.5, and two have only RCP8.5. These numbers are reduced further when daily output is required. The ICNet has identified three types of models (http://theicnet.org/?page_id=50). The 28 Group 1 models are considered to be the most reliable. Models in this group represent the most recent versions of reliable, very well documented, long-established global climate models from modeling groups with decades of experience. Group 2 models and Group 3 models should be used with caution because they are either in development, entirely new, or from modeling groups with less experience.

If using multiple climate model simulations for an analysis, it is essential to always average across climate models as the very last step in the analysis; premature averaging will artificially dampen the variability and hence the extremes. Until recently, each model in a multi-model ensemble has been generally assumed to be independent, so when averaging the models, each is given a weighting factor of 1. The reality, however, is that GCMs build on previous generations and previous models, and are not independent from each other. As described by Knutti and

Sedlacek (2013) and Sanderson et al. (2015), many share both ideas and model components or code. For this reason, for the first time, the upcoming Fourth U.S. National Climate Assessment will use a weighting approach that assigns variable values to the output from multiple GCMs depending on their dependence or interdependence from each other.

THE BOTTOM LINE: There is no perfect model; always use a selection of several different GCMs, the more GCMs included, the better. Do not attempt to select a best model for the region of interest. This will likely bias the sample and not provide a reasonable estimate of the distribution of possible conditions.

2.5. Scenario Selection

The IPCC states, "There is no single most likely, "central", or "best-guess" scenario, either with respect to SRES scenarios or to the underlying scenario literature. Probabilities or likelihood are not assigned to individual SRES scenarios." (Davidson and Metz 2000) Although the older SRES scenarios have been replaced with the RCP scenarios, the same statement applies equally to them as well. For projects with lifetimes within the next two to three decades, scenario selection is less important. The dominant uncertainty for the near-term time scale is natural variability, compounded by scientific uncertainty. GCM simulations and even historical climate information from recent decades can be used, if observed trends are accounted for (Meyer et al. 2013), because uncertainty in hydrological model parameters and flood frequency estimates, for example, is even larger than uncertainty in climate model output (Kjeldsen et al. 2013).

Beyond two to three decades, future simulations should be used because uncertainty in flood frequency estimate and hydrological model parameters becomes less significant compared to uncertainty in future scenarios (Kjeldsen et al. 2013). When considering projected climate changes more than 20-30 years in the future, it is advisable to use a range of future scenarios to capture a reasonable range of uncertainty in human choice and behavior (Moss and Schneider 2000, Meyer et al. 2013). Regarding precipitation specifically, there is some research that shows that variability across models is more important than that from scenarios at midcentury and persists in all but the northern regions in the U.S until 2100 (Northrop and Chandler 2014, Anderson et al. 2013). After 2050, temperature projections diverge for different emission scenarios (Caltrans 2013, Meyer et al. 2013) even if the precipitation variability is still dominated by model-to-model differences. In the U.S., approximately 50 to 80 percent of the uncertainty in future temperatures is due to differences among emission scenarios (Hawkins and Sutton 2009). However, trends in mean seasonal precipitation continue to be dominated by model uncertainty rather than scenario uncertainty (Hawkins and Sutton 2011).

Confirming the importance of scenarios over longer-term analyses, the New Jersey pilot found that floodplain widths increased in 2050 and 2100 compared with the current 1-in-100-year flood plain under several future scenarios. In a European study, under four climate scenarios (A1B, E1, RCP8.5), by 2070-2100, change is plausible in several countries, but only for one or two scenarios (Nemry 2012).

For climate impact studies with time horizons past midcentury, a number of strategies are possible including using the higher emissions scenario to be conservative or using separate risk matrices for a range of possibility with a "lower emissions" scenario and a "higher emissions" scenario, or a range of emissions scenarios (Meyers 2012). Using a higher scenario quantifies the impacts that will be experienced if carbon emissions continue to rise; using a lower scenario

quantifies the benefits of carbon emission reductions and the minimum risks that will have to be adapted to, even under significant climate policy. In addition, when using multiple scenarios, never average across the scenarios. In this case, averaging will NOT improve the quality of the output because scenarios are entirely different possibilities of future development.

An alternative to selecting a transient pathway or scenario is instead to quantify projected impacts under a specific global mean temperature threshold, regardless of when that threshold may be reached or by what transient pathway. This approach is consistent with international targets, such as the Paris Agreement, that set a specific temperature target (regardless of when it may occur), as opposed to selecting a given pathway or scenario, that may be reached by different pathways. Using this approach enables quantification of the magnitude of impacts were that target to be realized. This approach is aligned with global targets (e.g., the Paris Agreement) that are not expressed in terms of a given RCP scenario; rather, they set a specific global temperature target. A National Research Council report (NAS 2011) states the primary justification for this approach is that "scientific research suggests that many key impacts can be quantified for given temperature increases." It finds the change per degree C of global warming is expected to result in several hydrological effects in the United States including a three to ten percent increase in rainfall from the heaviest 15 percent of daily rainfall and a five to ten percent change in streamflow in many river basins worldwide (NAS 2011, Swain and Hayhoe 2015).

There are multiple advantages of considering this approach for scenarios to inform future engineering design. First, the cost of adaptation is directly related to cost of greenhouse gas reduction. Though engineering design cost-benefit analysis may not consider the cost of greenhouse gas reduction, the relative public investment in adaptation and reduction is important to public financing. Second, adaptation and resilience planning can then be based on a future global temperature scenario that is consistent with global policy targets and for which the likelihood of reaching the temperature threshold can be determined. Third, as discussed at the very beginning of this section, it is virtually certain that the actual greenhouse gas emissions pathway will not follow any of the idealized RCP scenarios.

THE BOTTOM LINE: For applications with lifetimes past mid-century, it is important to use projections based on a range of future scenarios. For applications focusing on the next 20-30 years, there is no significant difference among scenarios and in some cases (depending on other associated uncertainties), even historical data can be used. Global mean temperature thresholds offer a promising way to increase the sample size of future projections for estimating extremes while providing information at the local to regional scale that is consistent with global policy targets such as the Paris Agreement.

2.6. Abrupt Climate Change and Surprises

While the transportation community has used the term abrupt climate change to differentiate discrete climate events such a hurricane or storms from longer-term incremental changes traditionally associated with global warming (Lindquist 2011), The CCSP (2008) definition of abrupt climate change is "A large-scale change in the climate system that takes place over a few decades or less, persists (or is anticipated to persist) for at least a few decades, and causes substantial disruptions in human and natural systems." However, Lindquist (2011) used the term abrupt climate change to differentiate discrete climate events such a hurricane or storms from longer-term incremental changes traditionally associated with global warming.

Based on the paleoclimatic record, four significant types of abrupt climate change have been identified that, if they were to recur, would be a significant risk to society: (1) rapid change in glaciers, ice sheets, and hence sea level; (2) widespread and sustained changes to the hydrologic cycle; (3) abrupt change in the northward flow of warm, salty water in the upper layers of the Atlantic Ocean associated with the Atlantic Meridional Overturning Circulation (AMOC); and (4) rapid release to the atmosphere of methane trapped in permafrost and on continental margins. The first two types are directly relevant to the hydrologic and hydraulic design of transportation infrastructure.

The likelihood of rapid ice melt and sea level rise depends on a number of physical factors. Large ice masses that are grounded below sea level (e.g., the West Antarctic Ice Sheet) have potential for rapid ice-sheet changes. If this potential is realized, projected sea level rise will likely increase substantially. The likelihood of widespread and sustained changes to the hydrologic cycle is already well documented in traditional climate change projections from GCMs. These indicate that, broadly, current wet areas are likely to get wetter and current dry areas are likely to get drier over periods of years to decades rather than gradually. To date, the focus of these abrupt changes has been on dry conditions/drought rather than wet conditions because floods tend to be more localized, in space and time, than droughts. However, large climate anomalies can result in major, regional flooding. There is considerable uncertainty regarding the likelihood of abrupt changes in the flood regime due to limitations in large-scale hydrological modeling, data sets for documenting past hydrological changes, and knowledge of the physical processes that generate floods.

While the likelihood of abrupt climate change is a subject of active research, little is known about specific effects on transportation and adaptation strategies if abrupt climate change were to occur. Although referring to ecosystems, Alley et al. (2003) indicate that abrupt climate changes are particularly harmful where the systems have long lifetimes or are relatively immobile. They also indicate that damage scales with the abruptness and unpredictability of the climate change. These findings are likely to be germane to transportation infrastructure. Infrastructure with 50 or 100-year design lifetimes are particularly vulnerable. However, assets with shorter lifetimes could have large impacts from abrupt climate change even though they may be relatively less sensitive to gradual hydrologic changes.

Abrupt climate change would likely require a “transformational adaption” approach (Kates et al. 2012) which include three classes: adaptations applied at a much large scale, adaptions that are new to a region or sector, and adaptations that transform places or shift locations. The Thames Estuary 2100 Plan (Environment Agency 2009) is an example of the first class. The Netherlands coastal defense and riverine flooding abatement (Deltacommissie 2008) is an example of the latter class.

THE BOTTOM LINE: Most global climate model simulations do not include the mechanisms responsible for many of the abrupt climate changes or “surprises” that have been observed in the paleoclimate record.

Chapter 3. Nonstationarity, Uncertainty, and Climate Inputs for Inland Hydrology Applications

This section of the literature review describes tools and strategies for incorporating nonstationarity, uncertainty, and climate inputs focused on inland hydrology applications.

3.1. Nonstationarity and Hydrologic Frequency Analysis

In the context of hydrologic analysis, the term **stationarity** refers to the assumption that the parameters of the probability distribution or distributions used to represent the probability structure of hydrologic events are constant. (Sample parameters, however, are random variables that approximate population parameters. Sample parameters change when additional observations are added to the sample.) The stationarity assumption is useful because it permits application of standard statistics tools to the analysis of hydrologic events. Analysts continue to use the stationarity assumption for the estimate of precipitation and runoff distributions, although that is beginning to change.

Hydrologic processes can be **nonstationary** for a number of reasons and engineers make determinations for nonstationary conditions as part of the design process. Urbanization, dam construction, stream diversion, and other human land-surface changes can create changes to flood risk. There is guidance on how to adjust for these changes, such as the index adjustment method and statistical detection methods for identifying nonhomogeneous data (McCuen et al. 2002). Barros et al. (2014) studied the effects of land use changes and river regulation on the stationarity of gauged data in the Southeast and Mid-Atlantic region of the United States, noting some changes and (more importantly) the need to maintain an adequate streamgaging network. Without the latter, identifying trends, including those resulting from climate change is more difficult if not impossible.

Recent research focused on the potential impact of climate change provides reason to doubt future utility of the stationary assumption (Milly et al. 2008). If hydrologic events are nonstationary, analysis of risk requires estimation of potential changes to population parameters for probability distributions as a function of time. There are few formal mechanics for such adjustments at this time, but Kilgore et al. (2016) provides description of selected approaches. However, adjustment of sample parameters can be informed by predictions of ensembles of climate models for the region of interest.

Several techniques for addressing nonstationarity are identified by Brewer et al. (2013). Obeysekera and Salas (2014) evaluated three methods – delta, bootstrap, and profile likelihood - for estimating confidence limits for nonstationary data. Salas and Obeysekera (2014) proposed methods for adapting the concepts of return period and risk in a nonstationary world. Read and Vogel (2015) extended the work of Obeyesekera and Salas (2014) to include an analysis and discussion of annual exceedance probability, return period, risk, and reliability for both stationary and nonstationary hydrologic processes. The results considered use of the log-Normal two-parameter distribution, but are extendible to the Gumbel distribution as well. Read and Vogel (2016a, 2016b) present use of hazard functions for evaluating risk and reliability of hydrologic estimates. The suggestion is that the traditional approach of risk communication and presentation (n-year return interval) be replaced with a reliability and/or hazard description.

There are many other recent papers that address the topic. The work is still in active development and no single analytical protocol has yet emerged as superior to the others.

3.2. Incorporating Climate Change into Hydrologic Analysis

Typical outputs from climate models, as discussed in previous sections, are typically limited to daily precipitation data on large spatial and time scales. For hydrologic analyses of large basins where those temporal and spatial scales are appropriate, the needed climate change data are available. However, many hydrologic analyses require finer temporal and spatial data, such as the analysis and design of hydraulic structures serving small watershed analyses, stormwater management facilities, and water quality facilities. Translating climate modeling outputs to these smaller scales is likely one of the most important challenges for engineers asked to address climate change in their designs.

Engineering analysis and design is generally focused on prediction of changes to watershed production of runoff. That production can be peak discharge rate or runoff volume, depending on the engineering problem to be solved. There are two broad classes of tools used for such predictions – statistical (either fitting of distributions to variables of interest or use of regression equations) and rainfall-runoff modeling. Fitting statistical models requires streamgauge data. Regional regression equations are determined based on statistical models of streamgauge data. Rainfall-runoff modeling is used where streamgauge data are not available, regression equations are not applicable, or if watershed conditions are expected to change and the changes are to be modeled for the engineering analysis/design. KCM (2015) provides an overview of literature through 2014 treating the use of hydrologic tools under climate change scenarios.

Meyer et al. (2014) completed a large research study intended to provide guidance to practicing engineers related to adapting to climate change. Hydrologic tools for incorporating climate change into engineering analysis/design depends on development of sound technical approaches to the problem and the type of analysis to be conducted.

3.2.1. Event-Based Versus Continuous Simulation Hydrologic Modeling

Among the many hydrologic and hydraulic models available, WinTR-20, WinTR-55 and HydroCAD are strictly event-based while HEC-HMS, P-8, SWMM, and EPA National Stormwater Calculator, may be used for event-based or continuous simulation analyses. Models such as HSPF and SWAT are exclusively continuous simulation models.

Metherall (2014) used WinTR-55 to evaluate the effect of changing climate on flood flows. This was done using the climate-adjusted precipitation data under future conditions. Climate adjusted IDF rainfall values for storm events corresponding to various return periods (2, 5, 10, and 25 years) were generated and used in WinTR-55. Using historical precipitation data at select climate stations in the Metro Vancouver area, a set of regression equations relating monthly precipitation and precipitation intensities at different durations were developed. The climate adjusted IDF curves were generated using the monthly precipitation data from Canadian Regional Climate Model, and applying the regression equations.

A customized version of long-term hydrologic impact assessment (L-THIA) modeling system was used to calculate the runoff and NPS pollutant loading for the entire state of Wisconsin, under various land use and climate change scenarios (Mednick et al. 2012). The statistically

downscaled GCM results with a cell size of approximately 5 x 7 miles were used for climate input. The application focused on impact assessment at the average conditions, as opposed to extreme events. This approach was taken considering the assessment by Fowler et al. (2007) that statistically downscaled climate projections are most appropriate for hydrologic modeling applications focused on average conditions.

Luo et al. (2013) used Soil and Water Assessment Tool (SWAT), a continuous simulation model, to evaluate hydrologic responses to climate change. They used climate simulations, both historical and projected, at a 1/8 degree (~12 km) spatial resolution, of daily precipitation, maximum and minimum temperatures, and wind speed from 2001 to 2099 from the Green Data Oasis (http://gdo-dcp.ucllnl.org) (Maurer et al. 2007). The data were downscaled from the native-scale outputs from climate models to a 1/8 degree grid using the bias correction and spatial disaggregation (BCSD) method (Wood et al. 2002, Wood et al. 2004).

Johnson et al. (2015) used SWAT to model the streamflow and water quality sensitivity to climate change and urban development in 20 watersheds, ranging in sizes between 15,000 to 70,000 km^2 across the U.S. NARCCAP climate model output were analyzed to obtain monthly change factors and was used in SWAT to modify precipitation, air temperature, relative humidity, surface downwelling shortwave radiation, and wind speed. Change factors were calculated as changes in NARCCAP model simulations for mid-21st Century (2041-2070) relative to baseline (1971-2000). Monthly change factors were then used to adjust 30 years of daily historical observations (approximately 1971-2000) at each location. Temperature and precipitation adjustments were made by applying monthly change factors to historical daily values. Projected changes in the proportion of precipitation volume occurring in larger events (i.e., event intensity) were represented by applying different change factors to events above and below the 70th percentile (based on daily depth).

HEC-HMS was applied to evaluate the hydrologic impacts of climate change by several investigators. Meenu et al. (2012) evaluated the impacts of possible future climate change scenarios on the hydrology of the catchment (watershed) area of the Tunga–Bhadra River, upstream of the Tungabhadra dam using statistically downscaled daily minimum and maximum temperature and daily precipitation for two emission scenarios. Shrestha (2014) assessed the potential impact of climate change on future water availability in Thailand. Kabiri et al. (2015) used downscaled climate simulations as input to the HEC-HMS model to evaluate the impact of climate change on runoff trends in the Klang Watershed in Malaysia.

Simonovic et al. (2016) present IDF_CC, which is a web based tool designed, developed, and implemented to allow local water professionals to develop estimates related to the impact of climate change on Intensity Duration Frequency (IDF) curves for almost any local rain monitoring station in Canada. The primary objective of the work was to standardize the IDF update process and make the results of current research on climate change impacts on IDF curves accessible to everyone. The tool is developed in the form of a decision support system (DSS) and represents an important step in increasing the capacity of Canadian water professionals to respond to the impacts of climate change.

3.2.2. Hydrologic Design of Small Watersheds

FHWA has summarized the results from 19 pilot projects supported by FHWA (FHWA 2016). A variety of findings were produced by those pilot projects. A significant finding for the current

project is that downscaled data from climate model projections are useful for "large watersheds" (defined as 100 square miles or more drainage area). For the Minnesota Pilot Project, analysts examined two small watersheds (19.6 and 13.9 square miles). Climate model outputs were downscaled and used to examine watershed and structure behavior for the existing condition and possible future conditions. The 24-hour event was used for analysis. Under the Gulf Coast 2 Pilot Project, watershed and structure hydrology/hydraulics for a 3.3 square mile basin were studied under existing and climate change conditions (USDOT 2014). Again, the 24-hour event was used.

Johnson and Weaver (2009) present a framework that explicitly incorporates the capabilities, tools, and methods needed to address the challenges associated with assessing climate change impacts on water and watershed systems. Rather than focusing on a single "most likely" outcome, planning for a range of outcomes will provide responses that are more robust to climate change. The framework is based on Ecological Risk Assessment (ERA), but does not exactly mimic the approach. A set of steps is presented that address linkages across spatial scales, temporal scales, and disciplines. Collectively, this series of steps make up a general strategy for using information about long-term climate change to conduct assessments of climate change impacts. The steps included in the framework are to define decision context, develop conceptual model, assess available climate data and model outputs, downscale global climate model outputs, select impact assessment models, conduct sensitivity analysis and scenario planning, and risk management (adaptation). This includes the use of empirical and mechanistic models to for simulating the biophysical processes linking climate drivers and assessment endpoints. Johnson and Weaver also described a case study for assessing the potential impacts of climate change on water quality within a 1927 km^2 watershed (the Monocacy River, Maryland) using the HSPF model. The projected simulations from seven GCMs for in temperature and precipitation for the mid-Atlantic region for the SRES A2 and B2 scenarios were obtained and statistically downscaled to adjust the historical hourly climate time-series.

Marshall and Randhir (2008) used the Soil Water Assessment Tool (SWAT) model to evaluate potential implications of increasing temperature on water quantity and quality at a regional scale in the Connecticut River Watershed of New England. Percent increases in temperature were modeled using the SRES mid-high (A2) and lower (B1) scenarios relative to historical simulations to estimate a range of possible temperature changes.

Dudula and Randhir (2016) simulated baseline watershed conditions using the HSPF (Hydrological Simulation Program Fortran) simulation model to examine the possible effects of changing climate on watershed processes. They also simulated the effects of adaptation and mitigation through specific best management strategies for various climatic scenarios. The study evaluated baseline, near-future climate (2035), and far-future climate (2065) conditions with and without BMPs using the lower RCP4.5 scenario compared with historic simulations using percent change.

Another tool available for water managers to assess and manage the impacts of climate variability and change is the BASINS Climate Assessment Tool (CAT), developed by EPA (U.S. EPA 2009). BASINS CAT was released with BASINS Version 4 and provides flexible capabilities for creating various weather scenarios to run Hydrologic Simulation Program FORTRAN (HSPF) watershed model. Climate change scenarios are created with BASINS CAT by modifying an arbitrary base period of historical temperature and precipitation data to reflect user-specified changes. BASINS CAT facilitates the application of one or more user-specified

operations, or adjustments, to that baseline time series. Users can adjust historical data using standard arithmetic operators applied monthly, seasonally, or over any other increment of time. A pre-existing, calibrated HSPF application, a WDM file containing HSPF input meteorological time series, and file(s) to which HSPF results are output are required for applying BASINS CAT.

3.2.3. Stormwater Management and Water Quality Analysis and Design

A fundamental challenge for incorporating climate change into stormwater management and water quality analyses and design is the mismatch of temporal and spatial scale between climate modeling outputs and hydrologic modeling inputs for these applications. Software application packages for incorporating climate change into stormwater management and water quality analyses include EPA's National Stormwater Calculator (U.S. EPA 2014a, U.S. EPA 2014b), Storm Water Management Model Climate Adjustment Tool (SWMM-CAT) (U.S. EPA 2014c), and the Stormwater Runoff Modeling System (SWARM) (Blair et al. 2014a, Blair et al. 2014b; Blair and Sanger 2016).

EPA's National Stormwater Calculator (U.S. EPA 2014a, U.S. EPA 2014b) is a simple tool for computing small site hydrology based on EPA SWMM for any location within the US. It can be used for estimating the stormwater runoff from a site under different development and control scenarios and provides a screening level analysis for sites less than few acres in size with uniform soil conditions. It also provides an ability to evaluate climate change scenarios using the climate data at a spatial scale of 0.5 degrees latitude and longitude from EPA's Climate Resilience Evaluation and Analysis Tool (CREAT). CREAT is a decision support tool to assist drinking water and wastewater utility owners in understanding, evaluating and addressing climate change risks using statistically-downscaled CMIP3 outputs (U.S. EPA 2016).

EPA also developed SWMM-CAT to provide climate assessment capabilities with SWMM simulations (U.S. EPA 2014c). SWMM is a dynamic rainfall-runoff-routing simulation model that has been used for several years for stormwater hydrological analysis. SWMM-CAT incorporates projected downscaled GCM output at a 0.5 degree latitude and longitude spatial scale into the regular SWMM model to analyze the impact of climate change on stormwater runoff and water quality. SWMM-CAT provides a set of location-specific monthly adjustment factors for climate time series that were derived from CMIP3 simulations.

The National Centers for Coastal Ocean Science (NCCOS) developed the Stormwater Runoff Modeling System (SWARM) to understand the impacts of development and climate change on stormwater runoff in small watersheds (less than 6500 ha). SWARM is a simple modeling system based on the U.S. Department of Agriculture Natural Resources Conservation Service curve number and unit hydrograph methods that permits an increase in precipitation by a user-specified percentage (Blair et al. 2014a, Blair et al. 2014b, Blair and Sanger 2016).

3.3. Sub-Daily Precipitation

Sub-daily precipitation data are commonly used for small watersheds, stormwater management and water quality, particularly in the form of IDF curves. Several techniques have been developed to establish these relations with historical data. Assuming stationarity in the relationship between various sub-daily parameters, the same techniques might be used with projected daily precipitation.

3.3.1. Historical Data

Daily (24-hour) precipitation is more readily available for estimating the frequency of design events than data on shorter duration precipitation (e.g. 1 hour). Bonner (1998) indicates there are 8,000 hourly accumulation precipitation stations and greater than 25,000 daily recording stations in the United States. There are even less sub-hourly recording stations that provide the short duration precipitation needed for estimating streamflow on small watersheds. For example, for Volume 2 of NOAA Atlas 14, Bonnin et al. (2004) used 2,846 daily precipitation stations, 994 hourly stations and 96 sub-hourly stations for the regional analysis in 14 states in or near the Ohio River Basin. The lack of hourly and sub-hourly precipitation data requires a linkage between daily precipitation data and the shorter durations.

As discussed previously in the section on climate modeling, projections of daily (24-hour) precipitation from downscaled GCM outputs is both more reliable and more commonly available than sub-daily precipitation (e.g. 3-hour). There is large uncertainty when estimating short duration precipitation from downscaled GCM output so these data are not as readily available. The Federal Highway Administration (FHWA) and other Federal agencies typically use projected daily precipitation that is available on the Downscaled CMIP3 and CMIP5 Climate and Hydrology Predictions (DCHP) web site (http://gdo-dcp.ucllnl.org/downscaled_cmip_projections/). Daily precipitation from the DCHP web site is useful for estimating streamflow for the larger watersheds (Anderson et al. 2015) but short duration precipitation data (1 hour or less) are needed when modeling smaller watersheds.

Synthetic rainfall distributions as developed by the Natural Resources Conservation Service (NRCS 2015) are one approach for linking daily rainfall to shorter duration events. The NRCS used data from TP-40 (U.S. Department of Commerce 1961) and Hydro-35 (U.S. Department of Commerce 1977) to develop the Type I, Type IA, Type II and Type III temporal distributions. These temporal distributions embed the ratios of 5-minute/24-hour through the 12-hour/24-hour values. These temporal distributions are used in event based hydrologic models like WinTR-20 and HEC-HMS. With the recent publication of NOAA Atlas 14 in most states, NRCS has developed new temporal distributions based on NOAA Atlas 14 using the ratios of 5-minute/24-hour through the 12-hour/24-hour values.

There are several approaches for disaggregating daily rainfall to obtain shorter duration rainfall for use in continuous hydrologic models. Choi et al. (2008) discuss a number of disaggregation methods and note that there are two broad categories: methods based on stochastic simulation and deterministic methods that utilize known weather patterns or measurements from nearby rainfall stations. Gutierrez-Magness and McCuen (2004) evaluated deterministic rainfall disaggregation methods for 74 stations near the Chesapeake Bay watershed in Maryland. Their methods included uniform distribution of daily rainfall over 24 hours, use of weather pattern methods, direct transfer of hourly data from one station to another location, and scaling transfer where the nondimensional intensity pattern at one station is used to disaggregate the daily rainfall at another station (Gutierrez-Magness and McCuen 2004). Socolofsky et al. (2001) describe a method that relies on measured hourly data in the same climatological regime as the daily data to be disaggregated and samples the measured hourly data directly. This method is applied to the Charles River watershed in Massachusetts where only daily data were available. Using the disaggregation technique, the model efficiency improved using the hourly rainfall data for estimating the annual runoff volume versus using the daily data. Choi et al. (2008) applied the method introduced by Socolofsky et al. (2001) to several rainfall stations in Texas. The

method was applied to estimate intensity-duration curves that captured the majority of intensities well and diverged by less than 17 percent from measured intensities for extreme runoff-generating events.

Stochastic simulation of rainfall is generally obtained by continuous stochastic rainfall models or through fractal random cascade models (Choi et al. 2008). Most stochastic rainfall models are based on the Bartlett-Lewis or Newman-Scott rectangular pulse models. These models utilize five to seven parameters to simulate rainfall. The advantage of these synthetic series is that they are of a continuous nature, able to be resampled at any desired aggregation level. Various fractal random cascade models make use of scale invariance of the rainfall process over a range of time scales. These stochastic models capture the variability between storms and within storms and require the fitting of scaling laws to apportion rainfall at different time scales. For all these simulation methods, two types of disaggregation are identified. In the first case, called downscaling, the model parameters are estimated for measured data at one time scale (e.g., daily) and used to obtain simulated data at a fine time scale (e.g., hourly). In the second case, the synthetic time series are used to reproduce measured daily rainfall totals by either sampling or conditioning the simulated rainfall (Glasbey et al. 1995; Koutsoyiannis and Onof 2001; Koutsoyiannis et al. 2003; Gyasi-Agyei 2005). While efficient at rainfall scale transformation (based on their ability to match measured rainfall statistics), each of these approaches uses multiple parameters to describe scaling laws, branching weights, and probability distributions (Choi et al. 2008).

3.3.2. Projected Data

NARCCAP (Mearns et al. 2007, updated 2014) remains one of the few sources for precipitation data with a sub-daily time scale (three hours). The data are available at a spatial resolution of 50 km and could be used in watershed modeling, however, additional watershed-specific analysis is required to ensure the data are reliable as discussed in Cook et al. (2016). These data are limited to the mid-high SRES A2 scenario. Moglen and Vidal (2014) used the 3-hr NARCCAP data and then extrapolated to shorter durations by fitting IDF curve shapes.

Dynamically downscaled data are available through the NA-CORDEX project (https://na-cordex.org/). For the North American continent, some datasets are listed (and presumably available for download) with hourly precipitation output (https://na-cordex.org/sub-daily-precipitation). It is possible these data might be usable for engineering purposes, but not without substantial additional investigation and validation.

Markus et al. (2016) outline a protocol for developing precipitation frequency estimates from climate model output. Their focus was on the 24-hour event and they applied L-moments to estimate distribution parameters. They note that uncertainty estimates from their results are greater than those using standard methods (such as NOAA Atlas 14).

The Minnesota Department of Transportation (MnDOT 2014) evaluated the impact of climate change on two small (less than 20 square miles) watersheds in Minnesota using WinTR-20. Precipitation frequency curves were developed using downscaled GCM output daily (24-hour) data from the DCHP web for current and future (2040, 2070, and 2100) conditions for 22 models. The median percent change was calculated and applied to the NOAA Atlas 14 analysis for current conditions to obtain future (2040, 2070, 2100) x-percent chance precipitation. These values were then used in the WinTR-20 model to determine the potential increases in the x-

percent chance discharges due to climate change. Use of the NRCS synthetic distributions provided estimates of flood discharges for small watersheds using the daily precipitation data from the DCHP web site.

Other investigators used various approaches to estimate the effects of climate change on small watershed design events and IDF curves. Zahmatkesh et al. (2014) uses a "change factor" to disaggregate 24-h precipitation to hourly data for SWMM modeling for urban stormwater analysis, but is not explicit about details. Kuo and Gan (2015) developed projected IDF curves with durations as short as 15 minutes, but leaves out the details of those computations. Luizzo and Feni (2015) performed detailed trend analyses of historical rainfall IDF relations as a basis for projecting IDF relations into the future. Their findings for the island of Sicily showed that some gauges showed upward trends, others showed downward trends, and the remainder showed no statistically significant trends.

FHWA (2014a) identified projections of sub-daily precipitation as one of the technical needs for improving our ability to design for climate change. In response to this need, Kilgore et al. (2016) developed recommendations for estimating projected precipitation data for use in hydrologic models. The recommendations included estimating the 24-hour projected precipitation for a given return period and future scenario using an ensemble of climate model simulations and adjusting that value for an area correction (based on the cell size of the climate data) and for an unconstrained 24-hour period (rather than the 24-hour calendar day). Kilgore et al. (2016) then recommended estimating shorter duration precipitation estimates from the 24-h duration based on the ratios in NOAA Atlas 14. While this latter recommendation relies on stationarity in these ratios, the recommendation was intended to fill a gap until better guidance can be developed.

The challenge of developing sub-daily precipitation for future scenarios has resulted in a range of approaches, each with their limitations. Kilgore et al. (2016) and many others have noted that other sources of change will affect projections of flow for small and large watersheds including changes in land use. Olsson et al. (2016) speculate that "future societal changes, such as population increase and urbanization, may have a stronger impact on future small-scale hydrological processes than climate change."

3.4. Confidence Limits and Uncertainty Bounds

Evaluation of model performance, as well as the input used to drive models, is the subject of confidence limits and uncertainty bounds. Confidence limits are a tool used by statisticians to associate a probability of an outcome being within a certain range with a specified degree of confidence, usually based on an assumption of normality in distribution (of the errors). The width of the confidence limit is an indication of the degree of uncertainty associated with a particular estimate (or quantile).

Uncertainty estimates arise as part of the analytical procedure being applied. Based on the literature reviewed, this technology continues to develop and might provide some useful tools for those sites that have streamgauge data for statistical analysis. It is not yet clear how those results will propagate to regional regression equation development.

Use of rainfall-runoff models, however, provides neither confidence limits nor uncertainty estimates as a result of model application. The primary input variable, precipitation, is treated as a known quantity (without a probability distribution). Error estimates for model parameters are not generally considered and model parameters are treated as constants, developed either by

estimation or by calibration using measured rainfall-runoff responses. Furthermore, no general methods for making estimates of uncertainty exist. Therefore, if confidence limits/uncertainty bounds are desired for estimates derived from rainfall-runoff modeling, then technology to compute such estimates will have to be developed. An example of an approach is provided by Chen et al. (2016), in which Monte-Carlo simulation was used to examine the uncertainty structure of a SWAT application for a watershed in China.

Many years ago, Eagleson (1978a-g) proposed a system for propagating uncertainty through the rainfall-runoff modeling process on an annual basis. It is possible that a similar approach could be developed for producing estimates of model output uncertainty. Farmer and Vogel (2016) make a case for treating hydrologic models as stochastic (probability) models. They describe how errors in hydrologic model output remain unknown and are generally not described.

As was described in the previous section on climate, there are several sources of uncertainty in projecting future climate. These sources include natural climatic variability, scientific or model uncertainty, and scenario uncertainty, all of which are difficult to estimate. There are not many examples of using confidence limits or uncertainty bounds in hydrologic analyses based on projected climate input. The most common approach seems to be to use the variation among the various GCMs as a basis for defining confidence limits. One such study is described below.

Anderson et al. (2015) analyzed the impact of climate change on six bridges in the Cedar and Skunk River Basins in Iowa. Anderson et al. (2015) used projected or future daily precipitation from the Downscaled CMIP3 and CMIP5 Climate and Hydrology Predictions (DCHP) web site (http://gdo-dcp.ucllnl.org/downscaled_cmip_projections/) from 9 different GCMs for three SRES scenarios : the higher A1FI (3 simulations), the mid-high A2 (9 simulations), and the mid-low A1B (7 simulations). These climate projections were used in a distributed watershed model to provide 19 estimates of flood discharges for the six bridges in the Cedar River and Skunk River Basins. Flood frequency curves were developed for two periods 1960-2009 and 1960-2059 using the median of the 19 projected model estimates. This approach was based on the assumption that the 19 model results were equally likely. The variation in the 19 frequency curves were used to define the upper and lower 95 confidence limits shown as the dotted lines in Figure 3.1 for one location in each watershed.

Kilgore et al. (2016) provides a framework for jointly considering uncertainty throughout the analytical process including the climate and hydrologic modeling activities so that cumulative decision making does not result in unintended conservative design estimates. They also provide recommendations for which confidence limits are appropriate considering the criticality of the infrastructure and its intended service life.

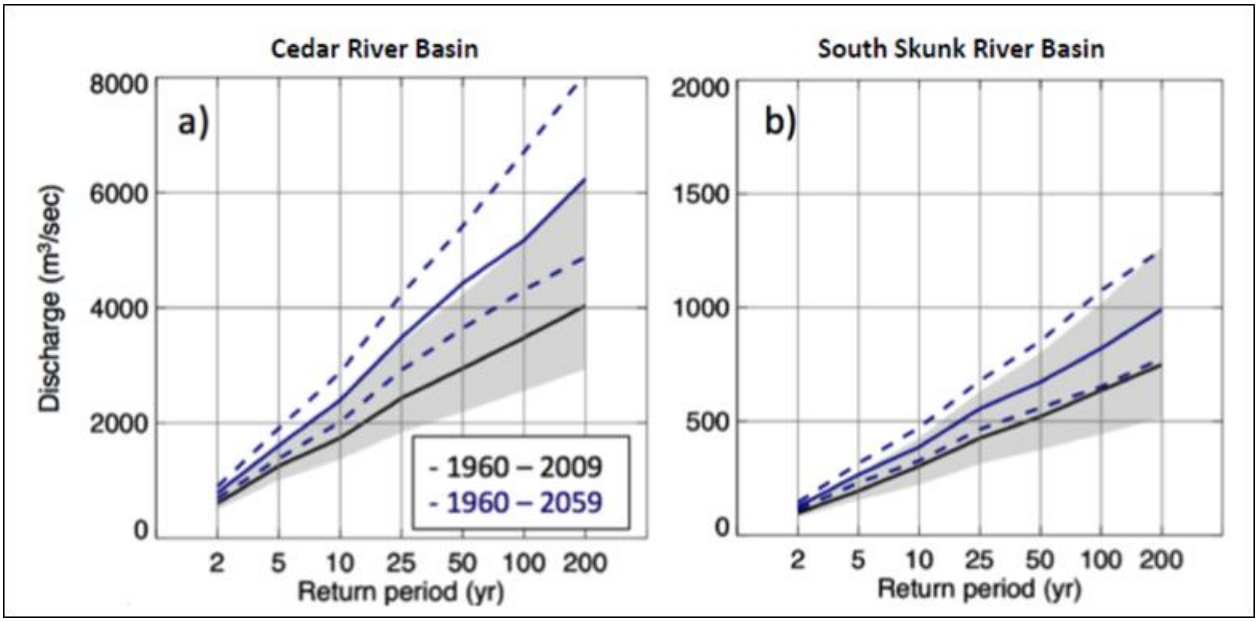

Figure 3.1. Frequency curves for the Cedar River and Skunk River in Iowa.

Chapter 4. Climate Changes to Coastal Processes Affecting Coastal Design Applications

In this section of the literature review, developments in understanding how climate change may affect coastal processes and coastal design is considered. The following subsections identify recent, published literature that describes some of the expected changes to coastal processes as a result of future climate change. The processes considered in this study include future rates of sea-level rise and their associated probabilities and/or uncertainties; the impacts of sea-level rise on groundwater levels and their potential contribution to flooding; possible changes in tropical cyclone (TC) and extratropical cyclone (ETC) intensity and frequency; watershed contributions to the total water level at the coast; methods for combining sea-level rise and coastal hazard information; and the potential changes in erosion and deposition as a result of future sea-level rise.

The synthesis of relevant literature provided hereafter should be considered as an extension of the literature review performed for HEC-25 Volume 2 (Douglass et al. 2014). As such, much of the literature identified in the following subsections was published within the past two or three years. In subject areas not addressed in HEC-25 Volume 2, the literature review is more broad.

4.1. Global Sea-Level Rise

In this section, the literature regarding historical and projected rates of sea-level rise is summarized. Scenario probabilities and selection is also addressed.

Historical Rates of Global Mean Sea Level Rise

One of the more certain impacts of atmospheric warming has been increasing sea levels. Previous studies have estimated the long term average rate of global mean sea level rise (GMSLR) between 1.6 mm/yr (1880-2000; Bindoff et al. 2007) and 1.7±0.2 mm/yr (1900-2009; Church and White, 2006). Church et al. (2004) estimated SLR for the latter half of the twentieth century (1950-2000) at 1.8±0.3 mm/yr. Recently, Hay et al. (2015) reevaluated GMSLR using tide gauge records combined with physics-based and model-derived distributions of the contributing signals and reported 1.2±0.2 mm/yr between 1901 to 1990 with a 90 percent confidence. Mitrovica et al. (2015) report that this range of estimates is consistent with the proper consideration of the effect of ice mass loss on the Earth's rotation, lending credence to estimates of historical and future GMSLR. Within the last couple of decades, sea level rise estimates using satellite altimetry indicate that the rate of SLR may be accelerating 3.1 mm/yr between 1993 and 2003 (Solomon 2007) and 3.2± 0.4 mm/yr between 1993 and 2009 (Church and White 2011). Hay et al. (2015) derived a similar estimate of 3.0 ±0.07 mm/yr from 1993 to 2014 using their methodology. The most recent satellite altimetry estimates of GMSL rate (1993 to mid-2014) range from 2.6±0.4 to 2.9 ± 0.4 mm/yr (Watson et al. 2015). Dangendorf et al. (2015) conclude with virtual certainty that at least 45 percent of the observed increase in GMSLR is anthropogenic in origin.

However, Ocana et al. (2016) demonstrate that some portion of the observed GMSLR trend could be caused by a combination of stochastic (random) variations within the coupled ocean-atmosphere-cryosphere system, which are not necessarily accounted for in the published estimates. Beenstock et al. (2015) point out that tide gauges are not randomly located, which can

lead to upward/downward bias in SLR estimates if tide gauges happen to be located where sea levels happen to be rising /falling. Their analysis of Permanent Service for Mean Sea Level tide gauge data from 1807 to 2010 found that tide gauge locations in 2000 were independent of SLR as measured by satellite altimetry, hence estimates of GMSLR from these gauges were unbiased. But, tide gauges placed during the 19th century were positively correlated with SLR, hence potentially resulting in an upward bias in GMSLR estimates.

4.1.1. Factors Contributing to Global Mean Sea Level Rise

Over the 20th and early 21st century, the two primary contributors to SLR have been the thermal expansion of seawater and the melting of land ice (glaciers and ice sheets). The warming oceans have accounted for 93 percent of the warming of the Earth's system since 1955 (Levitus et al. 2012). The long-term potential contribution of globally distributed glaciers to SLR (~0.6m) is small when compared to the potential contribution of continental-scale ice sheets on Greenland (~7m), West Antarctica (~5m), and East Antarctica (~53m) (Douglas et al. 2016). Mernild et al. (2014) reported that glaciers and ice caps contributed 0.51±0.16 mm/yr to GMSLR from 1979 to 2009 and 0.71±0.15 mm/yr from 1999 to 2009. The loss of mass from continental-scale ice sheets affects SLR in two ways: it adds water volume to the ocean, and it affects the sea surface elevation due to the gravitational pull of these massive ice sheets on the surrounding ocean waters. Woodward (1888) was the first to demonstrate the gravitational effect of ice sheets on global sea levels. Continental-scale ice sheets exert a gravitation pull on the surrounding water. As the ice sheet melts, the gravitational effect is reduced causing a migration of water away from the ice sheet. Within approximately 2000 km of the ice sheet, ocean levels fall despite the addition of melt water and beyond that distance, ocean levels increase at a rate greater than GMSLR. For North America, melting of the Greenland Ice Sheet (GrIS) would result in SLR rates less than 10 percent below GMSLR; melting of the Antarctic Ice Sheet (AIS) could result in an increase of more than 20 percent over GMSLR (Mitrovica et al. 2011). Mitrovica et al. (2009) also estimated that a collapse of the Western AIS (WAIS) would result in an approximately 37 percent far field increase over GMSLR, while Bamber et al. (2009) estimated a 25 percent far field increase from a WAIS collapse.

The mechanisms that result in ice sheet mass loss, as well as the timing and their relative contributions to GMSLR, are an area of very active and sometimes conflicting, research currently. Yan et al. (2014) projected that the Greenland Ice Sheet (GrIS) will contribute up to 16 cm to GMSLR by 2100 under RCP4.5, and up to 27 cm by 2100 under RCP8.5. Vasskog et al. (2015) estimated that the Greenland ice sheet is likely to roughly contribute 10 to 30 cm to GMSLR by 2100. Ritz et al. (2015) estimate that the Antarctic ice sheet will contribute up to 30 cm of equivalent sea-level rise by 2100 and 72 cm by 2200 (95% quantiles), and state that upper-bound estimates of 1 m by 2100 and 1.5 m by 2200 are implausible given our current understanding of the underlying physical mechanisms and triggers.

Hansen *et al*. (2016) present the results of a study that combined numerical climate simulations, paleoclimate data, and modern observations to investigate the effects of increasing ice melt from Antarctica and Greenland. Feedbacks related to differential ocean warming, ocean stratification and deep ocean ventilation could result in exponentially increasing mass loss from vulnerable ice sheets. Their modeling analysis projects that "continued high fossil fuel emissions this century are predicted to yield (1) cooling of the Southern Ocean, especially in the Western Hemisphere; (2) slowing of the Southern Ocean overturning circulation, warming of the ice shelves, and

growing ice sheet mass loss; (3) slowdown and eventual shutdown of the Atlantic overturning circulation with cooling of the North Atlantic region; (4) increasingly powerful storms; and (5) nonlinearly growing sea level rise, reaching several meters over a timescale of 50–150 years" (Hansen et al. 2016, p. 3762).

In addition, complete shutdown of the North Atlantic Overturning Circulation will occur within the next several decades if CO_2 emissions continue to grow as they have in the last several decades Hansen *et al*. (2016). In an investigation that coupled ice sheet and climate dynamics modeling, DeConto et al. (2016) estimated that Antarctica alone could contribute more than 1 m of sea-level rise by 2100 and more than 15 meters by 2500, if emissions continue unabated. Their models were calibrated to Pliocene and Last Interglacial sea-level estimates and applied to future scenarios. Golledge et al. (2015) found that the substantial contributions of Antarctic ice loss to GMSLR can only be prevented by limiting emissions to a pathway comparable to the lowest RCP2.6, which requires sharp, immediate reductions beginning in 2010 and negative carbon emissions – that is, net uptake of carbon dioxide - before 2100.

Terrestrial activities affect global SLR as well, although to a much smaller degree. The impoundment of terrestrial water behind dams was estimated to reduce SLR by 0.15±0.09 mm/yr between 1970 and 1990, while groundwater extraction was estimated to increase SLR by 0.57±0.09 mm/yr by 2000 (Wada et al. 2012). A reduction in dam building and an increase in groundwater extraction were estimated to contribute to global SLR by 0.25±0.09 mm/yr by 1990-2000 and 0.87±0.14 mm/yr by 2050 (ibid).

4.1.2. Local Factors in Sea Level Rise

How specific locations are affected by rising seas depends on factors in addition to GMSLR. For instance, Sallenger et al. (2012) identified the U.S. coastline north of Cape Hatteras, NC as a SLR "hot spot", with SLR rates 3-4 times faster than the global rate, likely due to an overall northward shift of the Gulf Stream during the twentieth century (Yin and Goddard 2013). A reduction in the strength of the Gulf Stream system is projected by many climate models for the 21st century (Yin, 2012; Yin and Goddard, 2013), mostly due to both the warming and freshening of the North Atlantic and a weakening of the Atlantic Meridional Overturning Circulation. Local variations in vertical land motion (tectonic uplift and down dropping, isostatic rebound and depression, land compaction, fluid extraction, etc.) either add to or reduce the effects of GMSLR. Kopp et al. (2015) found that 20th century relative SLR (the combination of GMSLR and local effects) along the coast of North Carolina was faster than during any other century over the last 2,900 years. Sea levels along the Eastern seaboard of the U.S. fluctuate annually around the increasing long-term trends. Goddard et al. (2015) report an unprecedented increase of 128 mm in sea level north of New York City during 2009-10 due to a 30 percent downturn in the Atlantic meridional overturning circulation and a significantly negative North Atlantic Oscillation index. These extreme variations are projected to increase in magnitude and frequency in the future, with consequences to coastal communities and infrastructure. Dagendorf et al. (2015) state that SLR estimates often ignore long-term persistence in local contributing factors and propose that slow, natural trends in volumetric processes may contribute as much as 1mm/yr, potentially leading to an overstatement of the anthropogenic influences on local SLR.

Moftakhari et al. 2015 report an increase in so-called nuisance flooding due to the ever decreasing height between high tide and flood stage from sea level rise. While not acutely

destructive like storm surge and wave action, nuisance flooding can create persistent disruptions to life and business and can lead to substantial economic losses due to road closures and accelerated infrastructure degradation.

Knott et al. (2016) found that the effects of sea-level rise on groundwater extend well over twice as far inland as surface-water inundation. Groundwater rise two mile inland was on the order of four feet for 6.6 feet of sea level-rise with specific values depending on local hydrogeology, the proximity to streams or wetlands, distance from the coast, and groundwater pumping.

4.1.3. Global Sea-Level Rise and Projected Probabilities

Projections of future, global eustatic sea-level rise are provided in numerous documents. Parris *et al.* (2012) reports, with a greater than 90 percent confidence, that global mean sea level rise will range from 0.2 m (0.7 ft) to 2.0 m (6.6 ft) by 2100. However, there are no widely accepted methods for assigning probabilities to future sea level rise estimates and probabilistic projections are simply not available at scales that are relevant for vulnerability assessment and adaptation planning (ibid). Furthermore, they state that, "coastal management decisions based solely on a most probable or likely outcome can lead to vulnerable assets resulting from inaction or maladaptation. Given the range of uncertainty in future global SLR, using multiple scenarios encourages experts and decision makers to consider multiple future conditions and to develop multiple response options."

The data in Figure 4.1 show the global mean sea levels and their likely ranges based on 21 CMIP5 models. For example, the expected mean global sea level for the period 2081 to 2100 is 0.63 m higher than the period 1986 to 2005 with a likely range of 0.45 to 0.82 m. Church et al. (2013) states that the calibrated uncertainty language in IPCC-AR5 means that there is approximately a 33 percent probability that sea-level rise by 2100 may fall outside of this range. According to the IPCC-AR5 studies, future rates of sea-level rise under all RCPs will very likely exceed the global average value of 2 mm/yr evaluated over the period 1971 to 2010. For example, the potential rate of rise for RCP8.5 could increase to as much as 8 to 16 mm/yr for the period 2081 to 2100 with what the report classifies as medium confidence. The IPCC-AR5 reports (IPCC 2013, IPCC 2014) provide additional statements regarding the likelihood and confidence of regional variability in future sea levels and potential contributions from the complete collapse of Greenland and Antarctic ice sheets.

The stability of massive ice sheets found in Greenland and Antarctica will no doubt play an important role in determining future global sea levels. Previously, Rignot et al. (2011) quantified the contributions of Greenland and Antarctica ice sheet melting to sea-level rise and noted acceleration over a preceding two-decade period. Those authors concluded that if mass loss continues at prevailing rates, the ice sheet contributions would dominate future sea-level rise and likely exceed accepted values by 2100. Recently, DeConto and Pollard (2016) have shown the potential for Antarctica to contribute more than 1 m of global mean sea level (GMSL) rise by the end of 2100 and more than 15 m by 2500. According to the authors, the onset of substantial ice-sheet retreat may occur as early as 2050 under the higher RCP8.5 scenario.

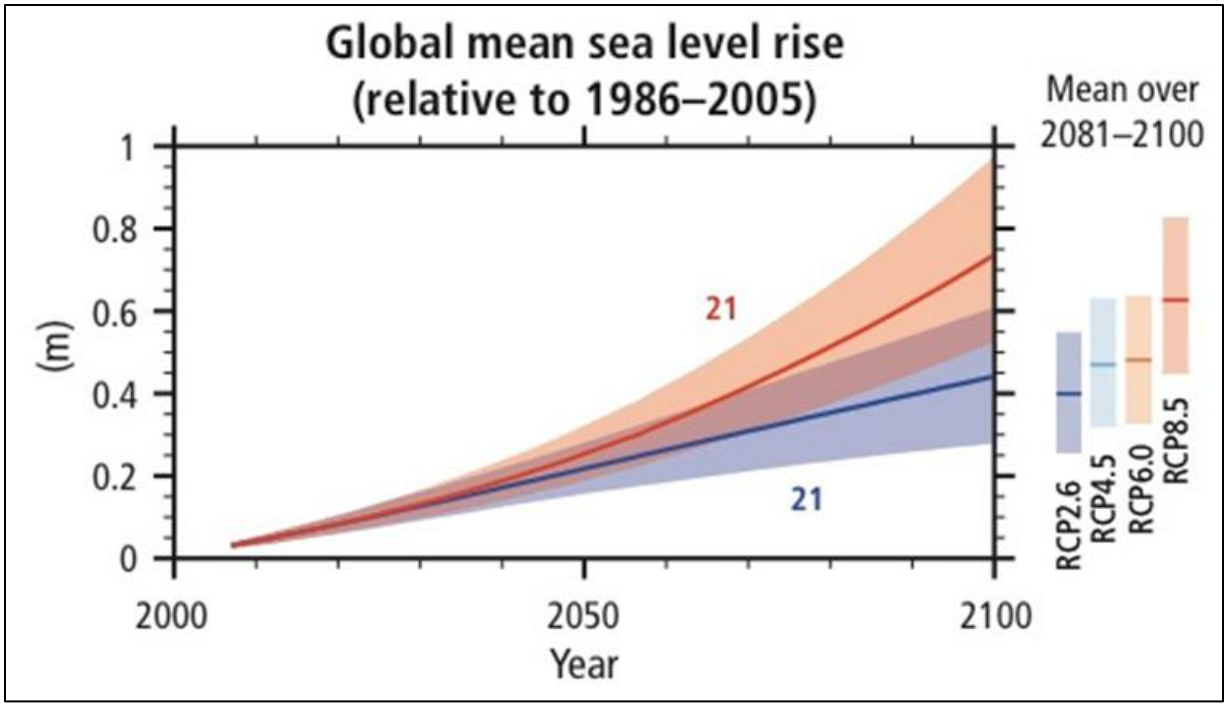

Source: Pachauri et al. 2014

Figure 4.1. Projected changes in global mean sea level and their associated averages and uncertainties for the period 2081-2100 (vertical bars).

As described in Church et al. (2013), the underlying uncertainties associated with the various contributions to future global mean sea level, including potential impacts of ice sheet collapse, make it impossible to assign detailed probabilities to the various RCP scenario projections. However, some have developed probability distributions using the uncertainty ranges presented in Church et al. (2013). For example, Houston (2013) developed normal distributions based on the uncertainties of the sea-level rise scenarios and their underlying assumptions. But those values were based on a set of older global sea-level rise projections presented in Solomon et al. (2007). More recently, Grinsted et al. (2015) derived scenario probabilities by drawing samples from the uncertainty distributions associated with the processes contributing to global sea-level rise through a Monte Carlo approach. Alternatively, Johansson et al. (2014) used ten published global sea level rise projections, and their associated probability or uncertainty ranges (e.g., 5% to 95%, 2.5% to 97.5%), to iteratively fit a three-parameter Weibull distribution such that the most likely "mean" value was coincident with the peak of the probability distribution (see Figure 4.2 for example).

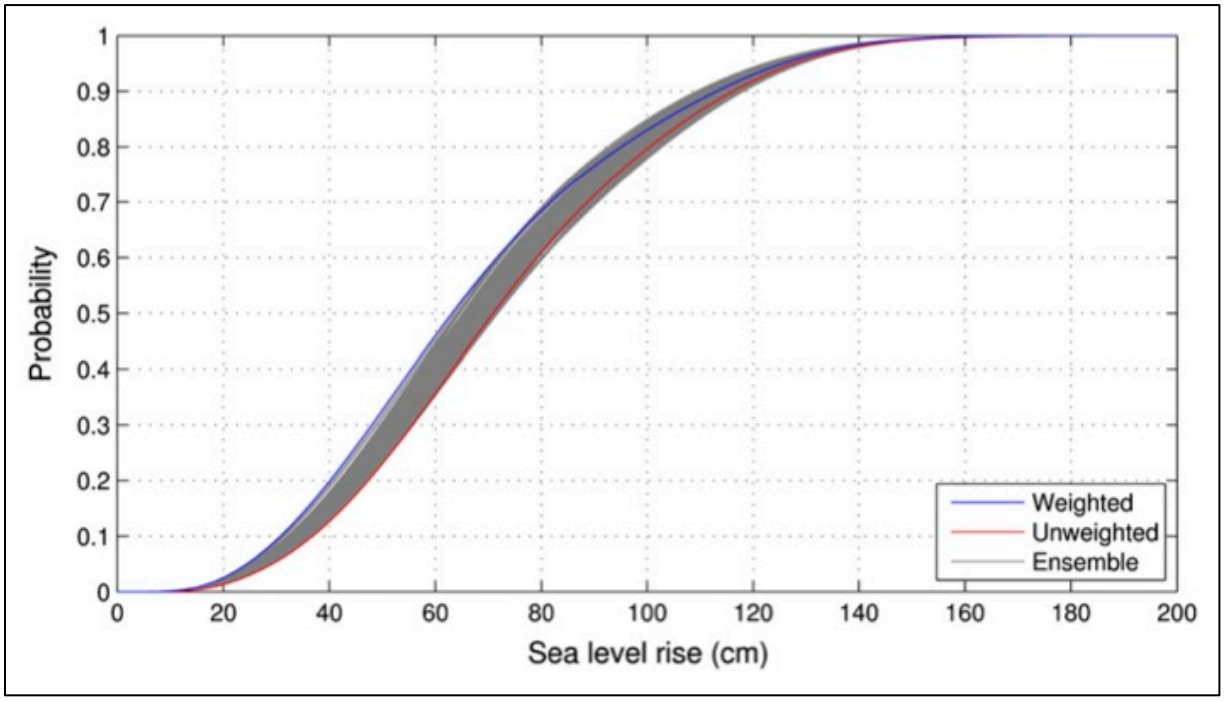

Source: Johansson et al. 2014

Figure 4.2. An ensemble of many combined cumulative probability distributions showing the effect of sea-level rise on the Gulf of Finland.

Other examples of sea-level rise probabilities are described in works by Horton et al. (2014) and Kopp et al. (2014), who largely rely on the results of a 90-person expert elicitation survey, and some process modeling, to estimate sea-level trends out to the year 2300.

Kopp et al. (2014) developed a global set of local SLR projections at decadal increments through 2100. This method combines the probability distributions of the major factors contributing to local SLR (vertical land movement, ice sheet fingerprint, ocean dynamics and global SLR) and generates a continuum of local SLR projections under three emissions scenarios (RCP8.5, 4.5 and 2.6). They state with 90 percent probability that GMSLR will be 0.5 to 1.2 m by 2100 under RCP8.5 and 0.4 to 0.9 m by 2100 under RCP4.5. Projections of local SLR generally sum the different sea-level contributions and often fail to formally propagate uncertainty into the analysis (Douglas et al. 2016).

4.1.4. Sea-level Rise Scenario Selection

There is a growing body of work related to the projection of future sea-levels under various climate scenarios. The most relevant of these works were highlighted previously. However, there are no specific publications in the primary literature that specifically address the selection of a particular climate and/or sea-level rise scenario for a given purpose. Instead, existing practical guidance tends to focus on scenario-based planning that is a function of risk and uncertainty. Such descriptions are found in USACE (2014) and Figure 4.3, along with general guidance for decision-making.

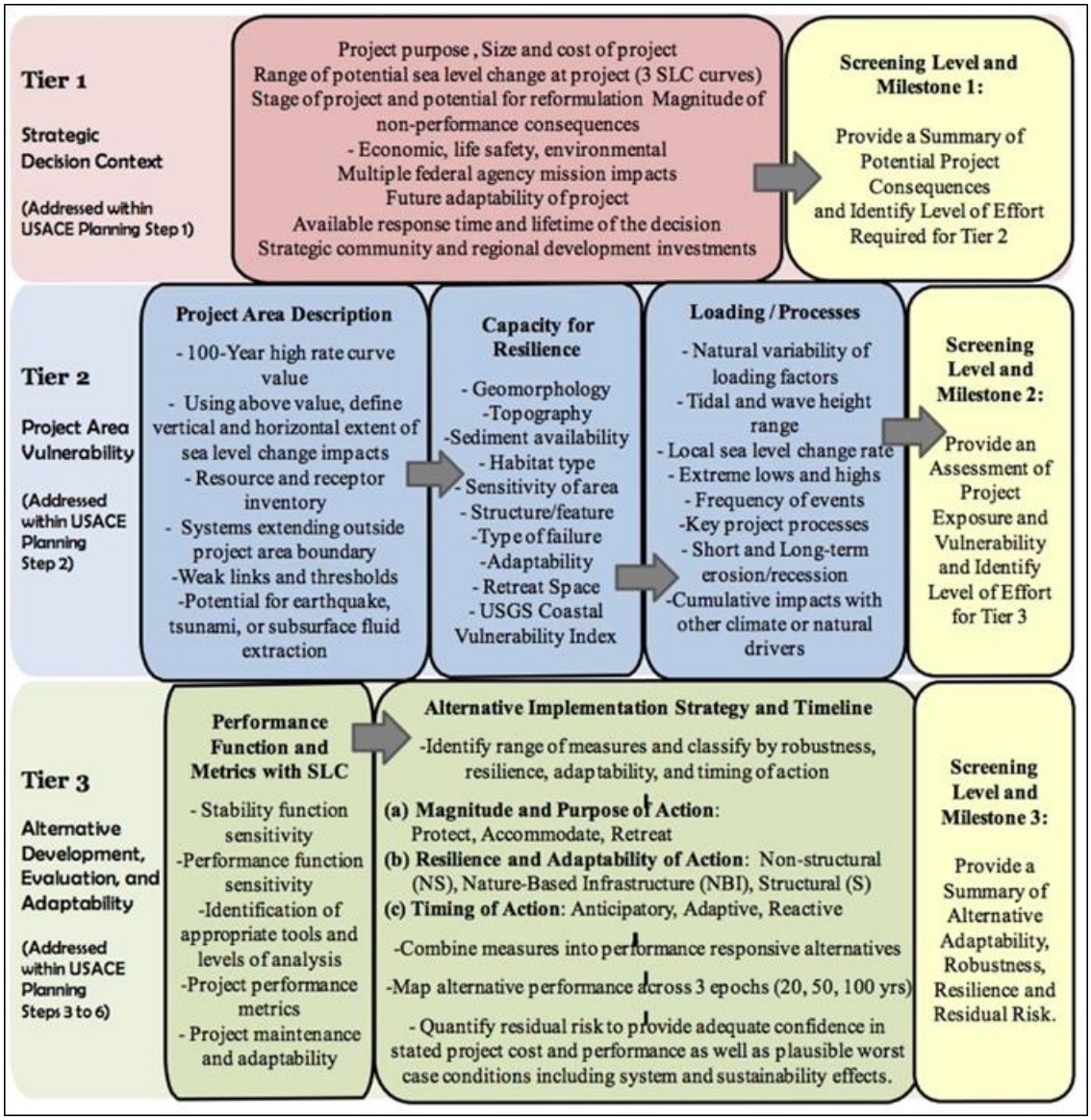

Source: USACE 2014

Figure 4.3. Screening analysis flowchart for consideration of sea-level rise.

The USACE document is heavily focused on the concept of risk and making risk-based decisions. The guidance provided therein views the problem of scenario selection as one of sensitivity and impacts. For example, they conclude that the selection of a sea-level rise (note that the document uses the more general term of sea-level change, or SLC) scenario is less important if your project is affected by all proposed rates of future sea-level rise. If, however, the project performance and/or impacts are substantially sensitive to different rates of sea-level rise, then USACE recommends that additional analysis be performed in order to capture all potential risks related to costs and impacts. It is worth noting that USACE suggests using the higher projection rates over a 100-year planning horizon for the purpose of vulnerability screening. This

is demonstrated in their screening tool flowchart provided in Figure 4.3. More information about screening-level assessments can be found in Garster *et al*. (2015).

4.2. Increasing Coastal Groundwater Levels

Much of the existing published literature pertaining to coastal groundwater levels and their relationship to sea-level rise falls into two broad categories: first, contributions of groundwater to the overall ocean budget and its sea-level positions; and second, the potential for seawater intrusion into coastal aquifers due to increasing head differences between the sea and groundwater table. However, within the last few years a number of studies have focused on the effects of sea-level rise on groundwater flow in coastal aquifers [e.g., Essink (1996); Masterson and Garabedian (2007); and Fordyce (2014)]; as well as the potential for groundwater inundation with rising sea levels [e.g., Bjerklie et al. (2012); Rotzoll and Fletcher (2012); Cooper et al. (2015); Kane et al. (2015); Manda et al. (2015); and Hoover et al. (2016)]. There are even some specific references describing the vulnerability of roads to sea-level rise and groundwater inundation (Roshani 2014 and Roshani et al. 2015).

With respect to coastal groundwater levels and their potential for inundation, the published literature presents a consistent view of the potential impacts: groundwater levels will rise at the same rate, and by amounts similar to, sea-level rise (see Figure 4.4). In coastal locations with considerable aquifer recharge, say through stormwater infiltration, the rise of the groundwater may be higher than that of local sea-level (Bjerklie et al. 2012). A recent study by Hoover et al. (2016) found that shallow aquifers with high hydraulic conductivities will be most vulnerable to sea-level rise and its effect on groundwater shoaling and emergence above the ground surface. Coastal areas with low elevations and high water tables, then, will likely see substantial inundation due to groundwater emergence. Studies by Rotzoll and Fletcher (2012) and Manda et al. (2015) found that the areal extent of groundwater inundation was at least equal to, or in some cases more than double, that of marine flooding by sea-level rise alone. Recent efforts to map inundation vulnerability have concluded that groundwater contributions play a significant role in estimating the total extent of flooding (Kane et al. 2015) as do the uncertainties resulting from future sea-level rise projections (Cooper et al. 2015).

Of relevance to this particular study, Roshani (2014), Roshani et al. (2015), and Knott et al. (2016) addressed the vulnerability of roadways to groundwater induced damages resulting from higher future sea levels. Roshani (2014) and Roshani et al. (2015) concluded that the primary damage mechanism for roads was related to degradation of the subgrade material with fatigue cracking controlling the pavement failure (Knott et al. 2016). Through modeling, Roshani (2014) and Roshani et al. (2015) found that increases in groundwater levels brought on by future sea-level rise lead to reductions in the resilient modulus of the subgrade material. However, impacts may be reduced in pavements with a thick asphalt concrete layer (Knott et al. 2016). Such reductions were found to occur more substantially in shallow water tables where subgrade material was located within the capillary zone (Roshani et al. 2015). While location specific, Roshani (2014) found that over 30 percent of the roads in their study area would be at high risk of failure by 2070 due to increasing groundwater levels brought on by sea-level rise. The most vulnerable roads are those where groundwater levels are currently near the top of the subgrade. Roads where groundwater levels are below 10 feet are unlikely to be vulnerable (Knott et al. 2016).

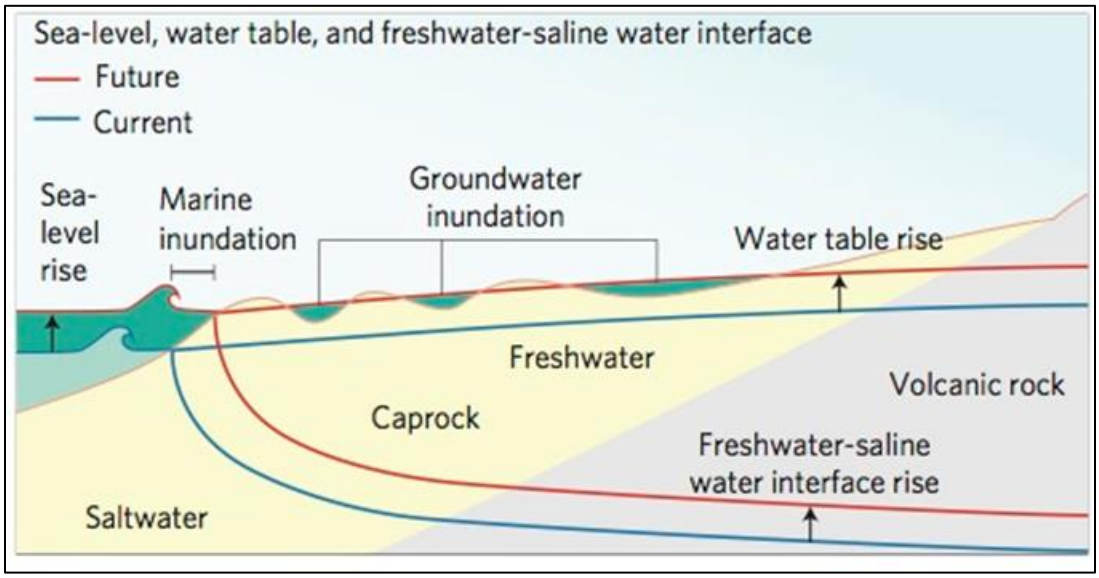

Source: Rotzoll and Fletcher (2012)

Figure 4.4. Schematic of marine and groundwater inundation due to sea-level rise in the southern Oahu aquifer.

4.3. Changes in Tropical and Extratropical Cyclones

The recent published literature, including the overall assessments provided in the IPCC-AR5 reports, seem to agree on the possible changes in tropical cyclones (TCs) and extratropical cyclones (ETCs) attributes resulting from future climate change. The body of literature tends to focus on TC and ETC intensity changes over time, modifications in their frequency of occurrence, changes in their intensity measures, and also their possible tracks.

The various IPCC reports, including the technical summary given by Stocker et al. (2013), the Synthesis Report, and the specific chapter on climate phenomenon by Christensen et al. (2013), are an excellent source of information regarding potential changes in TC and ETC behavior under future climate scenarios. The qualifying language used in those reports, however, is at times vague and non-committal in terms of expected changes. Other published literature, some of which is highlighted below, should be used when more quantitative descriptions are needed.

The IPCC reports conclude that basin-scale predictions of TC and ETC intensity and frequency are characterized by low confidence. The lack of confidence is largely related to the inability to account for interannual and interdecadal variability in storm characteristics. The reports do recognize the increase in TC activity, particularly in the North Atlantic, since 1970. However, they do not attribute the changes to a particular aspect of climate change and indicate low confidence that long-term changes in TC activity will be robust (Pachauri et al. 2014). The reports do place more confidence in the prediction of global TC characteristics. Stocker et al. (2013) suggest that it is likely that the global frequency of TCs will decrease or remain unchanged along with a likely increase in TC maximum wind speeds and precipitation rates.

Beyond the numerous IPCC-AR5 reports, there is a large body of primary literature related to future changes in TC and ETC characteristics. Comprehensive reviews are provided in Catto (2016) and Colle et al. (2015). Unlike the IPCC reports, many of these publications seek to describe the potential basin-scale TC and ETC behavior using higher resolution models. With some minor exceptions, the general findings about their intensity and frequency of occurrence are similar and will be more fully described below. There is less agreement and certainty regarding consistent future trends in storm track.

Almost unanimously, the published literature describes a global increase in TC intensity (~20 percent) with a corresponding decrease in frequency (~10 percent). Relevant information can be found in Knutson et al. (2010), Villarni and Vecchi (2013), Emanuel (2015), Knutson et al. (2015), Pfahl et al. (2015), and Walsh et al. (2016). A caveat is that the strongest (e.g., Category 4 and Category 5) storms may increase in frequency in the Pacific, particularly near Hawaii. This is supported by multiple publications, including the work of Holland and Bruyere (2014) who state that occurrence of global Category 4 and 5 TCs have increased at a rate of 40 percent in tandem with a decrease in Category 1 and 2 storms since 1975. However, the authors suggest that the occurrence of the strongest TCs may be saturating at a level of about 40 to 50 percent of total storm occurrence and that increased variability may attenuate even with future climate change. This may, or may not, result from a suppressive effect brought on by subsurface ocean cooling that appears to grow stronger with surface heating, as described in Huang et al. (2015).

Knutson et al. (2015) found fewer tropical cyclones globally in a warmer late-twenty-first-century climate, and an increase in average cyclone intensity, precipitation rates, and the number and occurrence days of very intense category 4 and 5 storms. Dwyer et al. (2015) found a longer TC season in the late 21st century when using CMIP5 model output but slightly shorter season with CMIP3 output. Kunkel et al. (2013) illustrate an apparent increasing trend in the Power Dissipation Index (PDI) of tropical cyclones in the North Atlantic since 1970, but state that this timeframe is too short to infer long-term trends in tropical storm activity. Hong et al. (2016) reported that a climate-regime shift in the Pacific during the middle to late 1990s resulted in interdecadal change in TC activity in the late 1990s.

Ranson et al. (2014) found strong but not conclusive evidence that damage from tropical storms and wind storms will increase with climate change. They claim that a global temperature increase of 2.5˚C would result in tropical storm damages increasing by 63 percent in the North Atlantic and 28 percent in the Western North Pacific tropical cyclones and in a 23 percent increase in damage from extratropical storms. Sobel et al. (2015) used the potential intensity (PI), an indicator of the maximum intensity achievable by a tropical cyclone in a given local environment, to investigate the effect of a warming climate on TC activity. They found that aerosol cooling reduced and hence canceled out, the increase in PI due to greenhouse gas driven warming. Without large reductions in greenhouse gas emissions, potential intensity will likely increasingly dominate over aerosol forcing, creating a potential for larger increases in tropical cyclone intensities. Guevara-Muara et al. (2015) found that aerosols from volcanic eruptions result in a consistent reduction in the number of TCs formed during the 3 years following major eruptions compared to the preceding 3 years, including after eruptions located at northern high latitudes, most likely due to decreasing local sea surface temperatures. Liu et al. (2016b) use 35 CMIP5 models to demonstrate the effect of sea surface temperatures (SST) on Tropical cyclone heat potential (TCHP) which can influence TC intensity and intensification. They project that as the upper ocean warms, TCHP will increase by 140 percent in the 21st century under the RCP4.5

particularly in the western Pacific, northwestern Indian and western tropical Atlantic oceans. The long and the short of it appears to be this: the complexity of the factors in hurricane genesis and intensification make predicting hurricane response to warming temperatures difficult in the short-term and highly uncertainty for the long-term.

To avoid the controversy over tropical cyclones in the historical record, Grinsted et al. (2012) developed a surge index from tide gauge records along the eastern and Gulf coasts of the U.S. and found that cyclones of all size ranges were more active during warm years than in cold years. They also reported a statistically significant trend in the frequency of large surge events since 1923. Grinsted et al. (2013) estimated that Katrina-magnitude events were two times more frequent in warm years than in cold years. Using statistically downscaled output from six climate models they report a two- to seven-fold increase in the frequency of Katrina magnitude events for a 1 °C rise in global temperature.

An extratropical cyclone (ETC) is a large-scale low pressure system that originates in the mid- and high latitudes; ETC make up the majority of cyclonic storms that impact the U.S. (Vose et al. 2014). There is a statistically significant increasing trend in both frequency and intensity of extratropical storm activity during the cold season in the Northern Hemisphere since 1950 (ibid). Vose et al (2014) also found evidence of a northward shift in extratropical storm tracks, which is consistent with the findings of Karl et al. (2009). Ranson et al. (2014) claim that a global temperature increase of 2.5˚C would result in a 23 percent increase in damage from extratropical storms. The mechanisms of extratropical cyclone generation are complex and not well understood and a warming climate affects these mechanisms differently; hence it is difficult if not impossible at this point to make conclusions about the effect of climate change on extratropical storms in the future. Given that extratropical storms make up the majority of storms that impact the U.S., especially along the coast, and given that sea level rise will allow storm surge and wave action to penetrate further inland, the impacts of and damage caused by even unchanging extratropical storm activity will likely increase in the future (Bosma et al. 2015).

With respect to ETC behavior, Stocker et al. (2013) find that it is unlikely that their global frequency will decrease by more than a few percent and that future changes in storms are likely small compared to natural interannual variability. However, there is some indication that there could be a weak poleward shift of ETC tracks accompanied by increases in winter precipitation. As noted in Christensen et al. (2013), and other publications mentioned below, there is some dependence of future ETC storm track on atmospheric blocking at higher latitudes owing to abnormally strong regions of high pressure. The degree to which blocking will interact with the poleward shift is not presently known.

The expected changes in ETC characteristics are in some cases similar to those of TCs mentioned previously: fewer storms and higher intensities. Catto (2016) provides a comprehensive review of numerous studies of ETC behavior and concludes that there is general agreement that ETC frequency may slightly decrease with a modest increase in precipitation intensity, without a clear increase in wind intensity. This is echoed in publications by Champion et al. (2011), Colle et al. (2015), and Marciano et al. (2015). Colle et al. (2015) conclude that ETC frequency may decrease by 6 percent to 33 percent depending on the season, whereas there will be a 10 percent to 40 percent increase in the number of (strong) storms with pressures less than 980 hPa. Interestingly, the literature almost unanimously points out the strong seasonal variability in future ETC trends of occurrence and intensity.

The potential changes in TC and ETC storm track lack the specificity and agreement found regarding their frequency and intensity. The current debate on storm track is centered on two major topics: poleward shift and atmospheric blocking. Studies by McDonald (2011), Kossin et al. (2014), Catto (2016), and Seiler and Zwiers (2016) all indicate the potential for a poleward shift in TC and/or ETC storm tracks over time. As explained in Kossin et al. (2014), the most likely explanation of a future poleward shift is related to expansion of the tropics resulting from increasing temperatures. The estimate of poleward shift provided therein is about 1 degree of latitude per decade, which agrees with the current expansion rate of the tropics.

The potential for a poleward shift in the Northern Hemisphere, particularly in the North Atlantic, would be mitigated by atmospheric blocking at high latitudes. For example, Mattingly et al. (2015) attribute the late westward track orientation of Hurricane Sandy (2012) to a phenomenon described as Greenland blocking, which was abnormally strong for that time of year (late October). It is unclear whether the blocking effect will have a distinct climate trend, but Mattingly et al. (2015) postulate that the blocking could strengthen if arctic warming continues at a faster rate than the rest of the Northern Hemisphere, as is presently occurring. This blocking effect is also described in Christensen et al. (2013).

While somewhat uncommon in the published literature, there are some statements regarding the rapid intensification (RI) of storms, particularly TCs. In a recent study, Lee et al. (2016) concluded that 79 percent of all storms experience RI at some point in their history. Emanuel (2016) suggest that RI immediately prior to landfall may increase with climate change by 2100, resulting in poor forecasting of storm intensity.

4.4. Watershed Contributions to Total Water Level at the Coast

There are relatively few descriptions of rainfall-runoff contributions to the total water level at the coast in the published literature. With only one exception, the available literature on this topic is exclusively based upon coupled modeling of storm surge and rainfall-runoff, or discharge, usually performed for a known storm event. For example, Blumberg et al. (2015), Klerk et al. (2015), McGuigan et al. (2015), and Torres et al. (2015) all used combinations of hydraulic and hydrodynamic models to simulate the flow and water levels associated with some known event. Their results all point to the importance of including the discharge that results from rainfall-runoff, but also underscore the local importance of the results due to topographic variability in watersheds and the time lag between a surge and rainfall event.

Some relevant conclusions can be drawn from the various model studies found. For instance, McGuigan et al. (2015) found the effect of combined discharge and storm surge, under a set of realistic conditions, on flooding to be significant and unique. Those authors concluded that the presence of surge resulted in higher flood levels upstream and that the combination of riverine and storm surge flooding just upstream from the estuary was substantially different than either component considered individually. Similar results were described in a study by van den Hurk et al. (2015).

In a model study by Torres et al. (2015), the peak flows from storm surge were found to dominate those from rainfall-runoff. However, their results showed that the rainfall-runoff contributes more than one-half of the total flood volume draining toward the coast due to a long-lasting persistence in the flood hydrograph well after the peak surge event (see Figure 4.5). As a result, hydraulic design that is concerned with flow volumes would be expected to be sensitive to

such effects (e.g., detention basins, routing reservoirs, stormwater wetlands, etc.), whereas design associated with peak flow (e.g., culvert, drain, etc.) would not be sensitive to the combined effect of rainfall-runoff and storm surge. Given the general agreement that future ETCs will be characterized by more (Colle *et al.* 2014, Marciano *et al*. 2015) and stronger precipitation (Catto 2016, Champion *et al*. 2011), the potential for routing larger volumes of stormwater runoff may also grow with climate change.

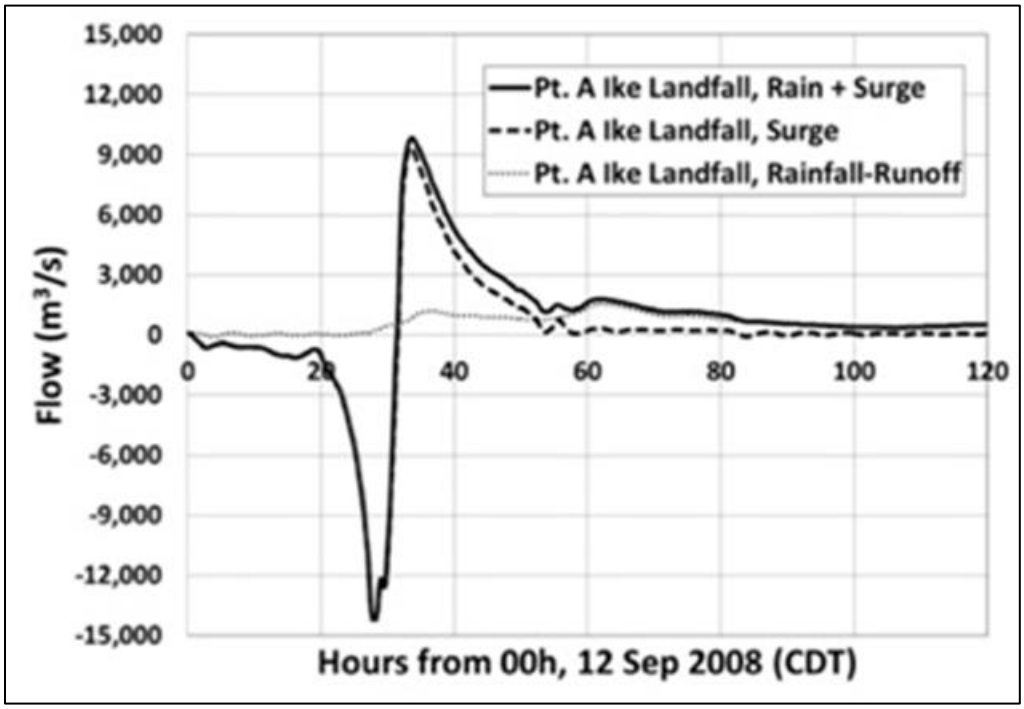

Source: Torres et al. (2015)

Figure 4.5. Time-series of discharge for hindcast simulations of Hurricane Ike accounting for rainfall-runoff, storm surge, and combinations thereof.

A number of the modeling studies presented above all referenced the need to consider the joint probabilities of rainfall-runoff and storm surge to account for the location-specific nature of the processes. One such example was found in the published literature. Wahl et al. (2015) describe the likelihood of joint occurrence of storm surge and rainfall for the contiguous US. The authors found that the risk of flooding from compounding rainfall-surge events is higher for the Atlantic and Gulf coasts than it is for the Pacific coast and that the number of such events has increased significantly over the past century. The authors conclude that changes in the joint distributions of surge and precipitation are likely to change with climate variability and may augment flood potential in some areas.

4.5. Climate Change and Historical Storm Surge and Wave Hazard Information

As noted in Hallegatte et al. (2011), future climate change may affect storm surge and/or waves in at least two different ways. First, the overall increase in mean sea level will allow storm surge

and waves to reach higher elevations and expand coastal inundation boundaries. Second, the potential for changes in TC and ETC frequency and intensity will lead to changes in the return period statistics of storm intensity measures, including central pressure, wind speed, rainfall, runoff, storm surge, and wave height. Most of the existing literature published in the past decade has focused on treatment of the former and only recently have studies considered the latter.

As a result of the USACE North Atlantic Coast Comprehensive Study (USACE 2015), and other related efforts, the USACE Engineering Research and Development Center (ERDC) maintains a web-based coastal hazards database. The database contains, among other things, annual exceedance probabilities (AEPs) for storm surge elevations and wave characteristics resulting from synthetic TC and ETC storm scenarios. These probabilistic surge and wave data are helpful, but only reflect the coastal flood and wave hazard under present-day sea levels.

Appropriate methodologies for adapting the surge and wave Annual Exceedance Probability (AEP) data to account for future sea-level rise would be useful in coastal hydraulic design. Currently there are no published works that specifically address modifications of the ERDC AEP data to account for climate change. However, there are some related works that describe potential solutions and these are identified below. There is an ongoing vulnerability assessment in Islesboro, Maine that may outline a more robust, statistical procedure in the near future (Pike and Dill 2016).

In the absence of existing methodologies that yield the joint probability of storm surge and sea level rise, or wave height and sea level rise, there are two common procedures for describing their combination: statically through a linear superposition of storm surge and sea-level rise; and dynamically through explicit hydrodynamic modeling of storm surge (and waves) on higher future sea levels. While there are many such examples, the reader is directed to Hallegatte et al. (2011) and Tebaldi et al. (2012) who used a static, linear combination of storm surge and sea-level rise for their analysis. They both argue that the uncertainty associated with future climate change and subsequent ranges of sea-level rise make it less important to consider any non-linear or dynamic coupling effects that may occur between storm surge and sea-level rise. An older study by Wu et al. (2002) used a similar linear combination methodology in their New Jersey flood study but acknowledged that the sea-level rise considered (60 cm) could have been inflated by as much as 50 percent in order to account for this non-linear coupling effect due to bathymetric sensitivity and wave contributions.

A number of recent studies have explicitly modeled the dynamic effect of sea-level rise (more importantly, relative sea-level rise) on storm surge and waves using hydrodynamic circulation and/or wave models. Examples of such studies include the works of Smith et al. (2010), Choate et al. (2012), Lin et al. (2012), Bilskie et al. (2014), and Irish et al. (2014). All of these studies show the non-linear effect of sea-level rise on storm surge and/or waves, whereby storm surge elevations and/or wave heights are not necessarily increased by an amount equivalent to the sea-level rise increment considered. For example, a 15-cm increase in mean sea level may produce surge elevations that are 45-cm, 60-cm, or higher as compared to present-day levels (see Figure 4.6). In some cases there may be damping effects on surge and waves due to an increase in water column depth with higher sea levels.

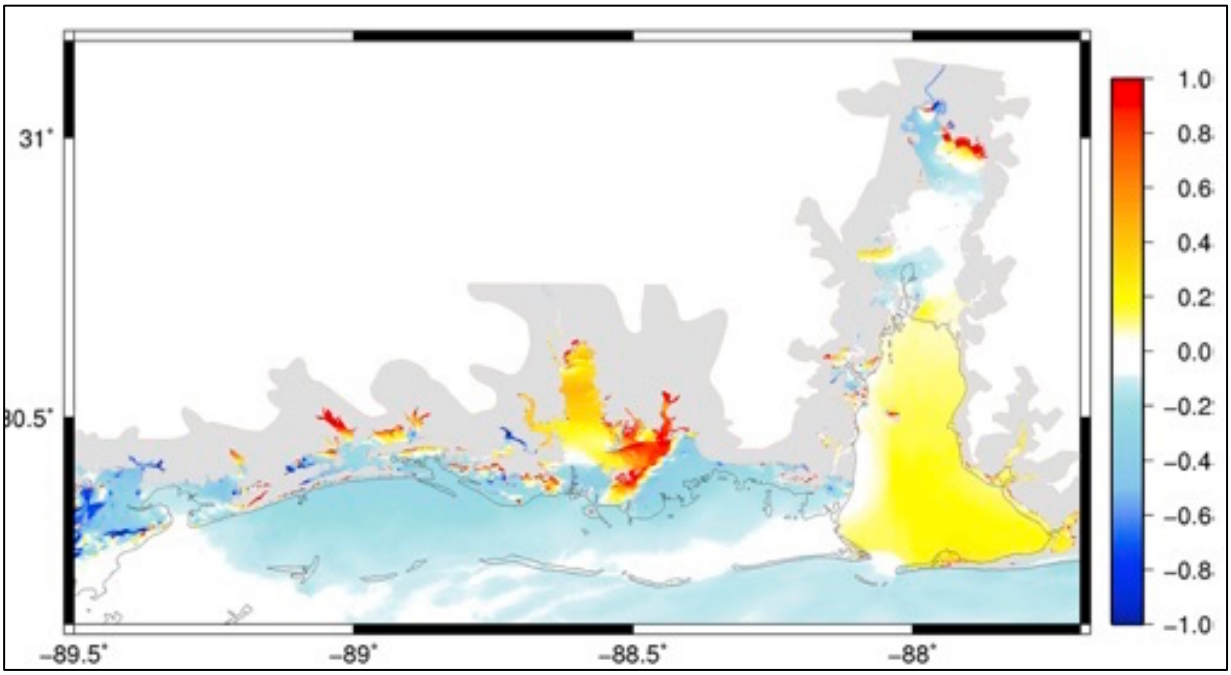

Source: Bilskie et al. (2014)

Figure 4.6. Non-linearity of storm surge due to a 15.2-cm sea-level rise for Hurricane Katrina in the northcentral Gulf coast. Values > (<) 0 show amplification (attenuation).

Methodologies for capturing the effects of future TC and ETC frequency and intensity, as well as potential uncertainties associated with future sea-level rise projections, on storm surge and waves are scarce. A recent study by Little et al. (2015) may provide a suitable methodology for filling this knowledge gap. In their study, Little et al. (2015) developed an index-based approach to explain the combined role of storm surge and sea-level rise which included the ability to account for future changes in TCs and ETCs. This was achieved through a probabilistic approach that incorporated changes in storm surge and covariance between the estimated power dissipation index (PDI) of future TCs and their associated sea-level rise scenarios (i.e., for various RCP scenarios). The investigators focused on five US locations scattered through the Gulf and Atlantic coasts. A Monte-Carlo sampling approach was used to examine their flood index changes for sea-level rise alone, as well as for combinations of future PDI and sea-level rise. The study concluded that strong correlation between future PDI and sea-level rise increases the tail of the coastal flood hazard probability distribution. This may suggest that simple linear combinations of sea-level rise and storm surge may greatly underestimate the coastal flood hazard for extreme (rare) events.

4.6. Climate Induced Changes to Coastal Morphology Including Erosion and Deposition

Climate change may impact coastal morphology in a number of different ways, but they generally fall into two broad categories: changes in fluvial processes and changes in coastal processes. With respect to the former, future changes in precipitation amounts and rates, as well

as the potential impacts of warmer temperatures on snowmelt runoff, may very well alter the fluvial processes that deliver sediment to coastal margins. The degree to which these processes will change is not well described in the available literature, but a comprehensive overview of the relevant fluvial processes, as well as their potential to be impacted by sea-level rise, is provided by Blum and Tornqvist (2000). Those authors illustrate the influences of climate change on continental interior rivers, their interaction with sea levels, and the subsequent potential for change in continental margin systems. Changes in discharge regimes, sediment supply, sediment storage, and sea-level rise are considered and described therein.

The role of sea-level rise in modifying critical coastal processes is described in Douglass et al. (2014). Subjects described there include the potential role of sea-level rise in modifying bluff erosion, intertidal marsh location, shoreline position, and barrier island behavior. Many studies, including that of Brooks and Spencer (2012) note the potential for increasing amounts of sediment to the coast as a result of bluff erosion and cliff retreat exacerbated by sea-level rise. Alternatively, some intertidal marshes have been successful in keeping pace with local sea-level rise when provided the opportunity to migrate (Raabe and Stumpf 2015). Much of the published literature shows that shorelines are, at the very least, mildly recessional under future sea-level rise scenarios. Finally, recent studies show the sensitivity of barrier islands to the rate of sea-level rise and that they are potentially most susceptible to width and/or height drowning (Lorenzo-Trueba and Ashton 2014). More information regarding barrier islands and shoreline position is provided below.

Some of the most prominent effects of sea-level rise on coastal morphology are described in USACE (2002) and Douglass et al. (2014), and include the response of beaches and barrier islands to sea-level rise. The methodology most commonly used to describe such changes is found in Bruun (1988). A number of assumptions ultimately limit the utility of the Bruun rule, but its simplicity is as helpful as it is illustrative: the beach profile adjusts to sea-level rise through erosion of the subaerial beach and a transfer of that material to the submerged profile, which ultimately increases in elevation by an amount equal to the sea-level rise considered.

But the Bruun rule ultimately suffers from a lack of physics and has been demonstrated, many times over, to be inaccurate (Cooper and Pilkey 2004). Indeed, a recent study by Houston (2016) demonstrates, with supporting data, that some beaches and shoreline position have naturally responded to previous rates of sea-level rise and have in many cases maintained their position within a range of standard error. However, some data certainly suggests that there is a significant positive correlation between sea-level rise and shoreline retreat (Leatherman et al. 2000), but it is often difficult to resolve the potential bias of seasonal weather events, major storms, and anthropogenic activities inherent in such comparisons.

More recently, Ranasinghe et al. (2012) described a fairly simple yet robust procedure for estimating coastal recession due to sea-level rise. Their Probabilistic Coastline Recession (PCR) model is a process-based model that provides probabilistic estimates of shoreline recession induced by sea-level rise. The model is relatively simple to develop, easy to apply, and is transferable to any coastline. Development of the storm time-series does require long-term measurements of tides and waves, but many such measurements exist along the US coastline and are provided by NOAA and other agencies.

Perhaps one of the complicating factors in studies of sea-level rise and its effects on coastline retreat and/or erosion is related to the local nature of such investigations. Indeed, a

comprehensive review of previous sea-level rise and shoreline change studies by Le Cozannet et al. (2014) determined that no general conclusions could be drawn relating sea-level rise and shoreline change on a global scale. That study concluded that the local characteristics were too variable to make uniform global descriptions of the relationship(s) between the two processes. Regardless, a study by Hinkel et al. (2013) quantifies the potential global impacts of sea-level rise on coastal margins while noting the possible uncertainties associated with such estimates. They concluded that global effects of sea-level rise and the erosion of sandy beaches would yield global land losses of 6000 – 17000 km^2 by 2100.

When the site-specific characteristics of relative sea-level rise and local geomorphology are considered, study results yield unique relationships between sea-level rise and shoreline retreat. For example, studies by Anderson et al. (2014) and Romine et al. (2016) demonstrate that coastal systems will respond to sea-level rise in different ways, but will typically show some erosional and/or recessional trends, particularly for low-gradient coastal systems (Anderson et al. 2014). However, Romine et al. (2016) point out that while some portions of a particular shoreline may be recessional, the local geomorphologic conditions may result in a proportional amount of accretion on adjacent shorelines. Such were the results for their study of carbonate bay-headland beach systems on the island of Oahu were erosion dominated the headlands while embayments were mostly characterized by accretion.

References

Alley, R.B., Marotzke, J., Nordhaus, W.D., Overpeck, J.T., Peteet, D.M., Pielke, R.A., Pierrehumbert, R., Rhines, P., Stocker, T., and Talley, L. 2003. Abrupt climate change. Science, 299, 2005-2010.

Anderson, C., R. Arritt, Z. Pan, E. Takle, W. Gutowski, F. Otieno, R. da Silva, D. Caya, J. Christensen, D. Lüthi, M. Gaertner, C. Gallardo, F. Giorgi, R. Laprise, S. Hong, C. Jones, H. Juang, J. Katzfey, J. McGregor, W. Lapenta, J. Larson, J. Taylor, G. Liston, R. Pielke and J. Roads. 2003. Hydrological Processes in Regional Climate Model Simulations of the Central United States Flood of June–July 1993. *Journal of Hydrometeorology*, 4(3), 584-598.

Anderson, C., D. Claman, and R. Mantilla. 2015. Iowa's Bridge and Highway Climate Change and Extreme Weather Vulnerability Assessment Pilot. Final Report HEPN-707, Institute for Transportation, Iowa State University, Ames, Iowa.

Anderson, J. B., Wallace, D. J., Simms, A. R., Rodriguez, A. B., and Milliken, K. T. 2014. "Variable response of coastal environments of the northwestern Gulf of Mexico to sea-level rise and climate change: Implications for future change." *Marine Geology*, 352, 348–366.

Asadieh, B. and Krakauer, N.Y., 2015. Global trends in extreme precipitation: climate models versus observations. Hydrology and Earth System Sciences, 19(2), pp.877-891.

Bamber, J.L., Riva, R.E.M., Vermeersen, L.L.A. & LeBrocq, A.M., 2009. Reassessment of the potential sea-level rise from a collapse of the West Antarctic Ice Sheet, Science, 324, 901–903.

Barros, A. P., Y. Duan, J. Brun, and M. A. Medina, Jr. 2014. "Flood Nonstationarity in the Southeast and Mid-Atlantic Regions of the United States," *Journal of Hydrologic Engineering*, 19(10).

Beenstock, M., D. Felsenstein, E. Frank, and Y. Reingewertz, 2015. Tide gauge location and the measurement of global sea level rise, Environmental and Ecological Statistics, 22 (1): 179-206, DOI: 10.1007/s10651-014-0293-4

Bilskie, M. V., Hagen, S. C., Medeiros, S. C., and Passeri, D. L. 2014. "Dynamics of sea level rise and coastal flooding on a changing landscape: BILSKIE ET AL." *Geophysical Research Letters*, 41(3), 927–934.

Bindoff, N.L., J. Willebrand, V. Artale, A, Cazenave, J. Gregory, S. Gulev, K. Hanawa, C. Le Quéré, S. Levitus, Y. Nojiri, C.K. Shum, L.D. Talley and A. Unnikrishnan, 2007: Observations: Oceanic Climate Change and Sea Level. In: Climate Change 2007: The Physical Science Basis. Contribution of Working Group I to the Fourth Assessment Report of the Intergovernmental Panel on Climate Change [Solomon, S., D. Qin, M. Manning, Z. Chen, M. Marquis, K.B. Averyt, M. Tignor and H.L. Miller (eds.)]. Cambridge University Press, Cambridge, United Kingdom and New York, NY, USA.

Bjerklie, D. M., Mullaney, J. R., Stone, J. R., Skinner, B. J., and Ramlow, M. A. 2012. *Preliminary investigation of the effects of sea-level rise on groundwater levels in New Haven, Connecticut*. Open-File Report, U.S. Geological Survey, 46.

Blair, A.; S. Lovelace; D. Sanger; A.F. Holland; L. Vandiver; S. White. 2014a. Exploring impacts of development and climate change on stormwater runoff. Hydrological Processes. 28(5): 2844-2854.

Blair, A., D. Sanger, D. White, A.F. Holland, L. Vandiver, C. Bowker, and S. White. 2014b. Quantifying and Simulating Stormwater Runoff in Watersheds. *Hydrological Processes*, 28(3): 559–569. DOI: 10.1002/hyp.9616.

Blair, A., and D. Sanger. 2016. Climate Change and Watershed Hydrology – Heavier Precipitation Influence on Stormwater Runoff. *Geosciences 2016*, 6, 34; doi:10.3390/geosciences6030034.

Blum, M. D., and Törnqvist, T. E. 2000. "Fluvial responses to climate and sea-level change: a review and look forward." *Sedimentology*, 47(s1), 2–48.

Blumberg, A. F., Georgas, N., Yin, L., Herrington, T. O., and Orton, P. M. 2015. "Street-Scale Modeling of Storm Surge Inundation along the New Jersey Hudson River Waterfront." *Journal of Atmospheric and Oceanic Technology*, 32(8), 1486–1497.

Bonner, W. D. 1998. Future of the national weather service cooperative observer network. National Research Council, National Academy Press, Washington, DC.

Bonnin, G., D. Martin, B. Lin, T. Parzybok, M. Yekta, and D. Riley. 2004. Precipitation-Frequency Atlas of the United State, NOAA Atlas 14, Volume 2 Version 3.0, U.S. Department of Commerce, National Oceanic and Atmospheric Administation, National Weather Service, Silver Spring, Maryland.

Brewer, M., T.C. Brown, C. McNutt and D. Raff (2013). Water Resources Sector Technical Input – Interim Report In Support of the U.S. Global Change Research Program 2014 National Climate Assessment. Institute for Water Resources Technical Report 2013-R-10. Washington, DC: US Army Corps of Engineers Institute for Water Resources

B.C. Ministry of Transportation and Infrastructure. 2014. *Developing Effective Dialogue between Practitioners of Climate Change Vulnerability-Risk Assessment: A Primer to Define Common Languages*, Pacific Climate Impacts Consortium, Vancouver, British Columbia.

Brooks, S. M., and Spencer, T. 2012. "Shoreline retreat and sediment release in response to accelerating sea level rise: Measuring and modelling cliffline dynamics on the Suffolk Coast, UK." *Global and Planetary Change*, 80-81, 165–179.

Bruun, P. 1988. "The Bruun Rule of Erosion by Sea-Level Rise: A Discussion of Large-Scale Two- and Three-Dimensional Usages." *Journal of Coastal Research*, 4, 627–648.

Caltrans. 2013. Addressing Climate Change Adaptation in Regional Transportation Plans: A Guide for California MPOs and RTPAs, California Department of Transportation.

Catto, J. L. 2016. "Extratropical cyclone classification and its use in climate studies: CLASSIFYING EXTRATROPICAL CYCLONES." *Reviews of Geophysics*, 54(2), 486–520.

Champion, A. J., Hodges, K. I., Bengtsson, L. O., Keenlyside, N. S., and Esch, M. 2011. "Impact of increasing resolution and a warmer climate on extreme weather from Northern Hemisphere extratropical cyclones: HIGH RESOLUTION GCM." *Tellus A*, 63(5), 893–906.

Chen, L., Y. Gong, and Z. Shen (2016). Structural uncertainty in watershed phosphorus modeling: Toward a stochastic framework. Journal of Hydrology, 537:36–44.

Choate, A., W. Jaglom, R. Miller, B. Rodehorst, P. Schultz, and C. Snow. 2012. *Impacts of Climate Change and Variability on Transportation Systems and Infrastructure: The Gulf Coast Study, Phase 2: Climate Variability and Change in Mobile, Alabama*: Final Report, Task 2. FHWA-HEP-12-053, 228 pp.

Choi, J., S. Socolofsky, and F. Olivera. 2008. Hourly Disaggregation of Daily Rainfall in Texas Using Measured Hourly Precipitation at Other Locations. *Journal of Hydrologic Engineering*, Vol. 13, No. 6, pp. 476-487.

Christensen, J. H., Kumar, K. K., Alrian, E., An, S.-I., Cavalcanti, I. F. A., de Castro, M., Dong, W., Goswami, P., Hall, A., Kanyanga, J. K., Kitoh, A., Kossin, J., Lau, N.-C., Renwick, J., Stephenson, D. B., Xie, S.-P., and Zhou, T. 2013. "Climate Phenomena and their Relevance for Future Regional Climate Change." *Climate Change 2013: The Physical Science Basis. Contribution of Working Group I to the Fifth Assessment Report of the Intergovernmental Panel on Climate Change*, Cambridge University Press, Cambridge, UK.

Church, J. A., N. J. White, R. Coleman and K. Lambeck, 2004. Estimates of regional distribution of sea level rise over the 1950-2000 period, J. Climate, DOI: http://dx.doi.org/10.1175/1520-0442(2004)017<2609:EOTRDO>2.0.CO;2.

Church, J. A. and N. J. White, 2006. A 20th century acceleration in global sea-level rise, Geophys. Res. Let, 33 (1), DOI: 10.1029/2005GL024826

Church, J. A. and N. J. White, 2011. Sea-Level Rise from the Late 19th to the Early 21st Century, Survey in Geophysics, 32 (4): 585–602

Church, J. A., Clark, P. U., Cazenave, A., Gregory, J. M., Jevrejeva, S., Levermann, A., Merrifield, M. A., Milne, G. A., Nerem, R. S., Nunn, P. D., and others. 2013. *Sea level change*. PM Cambridge University Press.

Clarke, I., C. Davies, S. Davies, J. Dora, C. Golightly, P. Hjerp, M. Kujawa, T. de Lannoy, A. Marrin, K. Medarova-Bergstrom, O. Mautone, Y. Mincheva, M. Wolfgang, A. Pauer, A. Payne, J. Sandor, M. Scatasta, M. Schiffler, and E. Tronnier. 2012. Guidelines for Project Managers: Making vulnerable investments climate resilient (Report for the European Commission), Acclimatise; European Commission Climate Action; COWI.

Clark, M.P., R.L. Wilby, E.D. Gutmann, J.A. Vano, S. Gangopadhyay, A.W. Wood, H.J. Fowler, C. Prudhommme, J.R. Arnold, and L.D. Brekke. 2016. "Characterizing Uncertainty of the Hydrologic Impacts of Climate Change." *Current Climate Change Reports*, Volume 2, Issue 2.

Climate Change Science Program and the Subcommittee on Global Change Research (CCSP). 2008. *Abrupt Climate Change*. A report by the U.S. Climate Change Science Program and the Subcommittee on Global Change Research. U.S. Geological Survey, Reston, Virginia.

Colle, B. A., Booth, J. F., and Chang, E. K. M. 2015. "A Review of Historical and Future Changes of Extratropical Cyclones and Associated Impacts Along the US East Coast." *Current Climate Change Reports*, 1(3), 125–143.

Cook, L.M., C.J. Anderson, and C. Samaras, 2016. A Framework for Incorporating Downscaled Climate Output into Existing Engineering Methods: Application to Precipitation Frequency Curves. *Journal of Infrastructure Systems* (under review).

Cooper, J. A. G., and Pilkey, O. H. 2004. "Sea-level rise and shoreline retreat: time to abandon the Bruun Rule." *Global and Planetary Change*, 43(3-4), 157–171.

Cooper, H. M., Zhang, C., and Selch, D. 2015. "Incorporating uncertainty of groundwater modeling in sea-level rise assessment: a case study in South Florida." *Climatic Change*, 129(1-2), 281–294.

Dangendorf, S., M. Marcos, A. Muller, E. Zorita, R. Riva, K. Berk and J. Jensen, 2015. Detecting anthropogenic footprints in sea level rise, Nature Communications, 6, art. 7849, DOI: 10.1038/ncomms8849

Davidson, O. and B. Metz. 2000. IPCC special report—Emissions scenarios: Summary for policy makers. In: Intergovernmental Panel on Climate Change. p. 11. Available online at: https://www.ipcc.ch/pdf/special-reports/spm/sres-en.pdf.

DeConto, R. M., and D. Pollard. 2016. "Contribution of Antarctica to past and future sea-level rise." *Nature*, 531(7596), 591–597.

Deltacommissie. 2008. Working Together with Water: A Living Land Builds for Its Future. In. The Hague: Delta Committee.

Douglas, E., P. Kirshen, R. Hannigan, R. Herst and A. Palardy, 2016. Climate Change and Sea Level Rise Projections for Boston, a report prepared by the Boston Research Advisory Group for Climate Ready Boston available on line at http://climateready.boston.gov/

Douglass, Scott L., Bret M. Webb, and Roger Kilgore (2014), "Highways in the Coastal Environment Volume 2," Hydraulic Engineering Circular 25 (HEC-25), October.

Dudula, John and Timothy Randhir. 2016. Modeling the influence of Climate Change on Watershed 1 Systems: Adaptation through Targeted Practices. *Journal of Hydrology*, Vol. 541: pp. 703-713.

Dwyer, J. G., S. J. Camargo, A. H. Sobel, M. Biasutti, K. A. Emanuel, G. A. Vecchi, M. Zhao and M. K. Tippett, 2015. Projected Twent-first century changes in the length of the tropical cyclone season, J. Climate, 28 (15): 6181-6192, DI 10.1175/JCLI-D-14-00686.1

Eagleson, P.S. Climate, soil, and vegetation: I. introduction to water balance dynamics. Water Resources Research, 14(5):705–712, 1978.

Eagleson, P.S. Climate, soil, and vegetation: II. the distribution of annual precipitation derived from observed storm sequences. Water Resources Research, 14(5):705–712, 1978.

Eagleson, P.S. Climate, soil, and vegetation: III. A simplified model of soil moisture movement in the liquid phase. Water Resources Research, 14(5):705–712, 1978.

Eagleson, P.S. Climate, soil, and vegetation: IV. the expected value of annual evapotranspiration. Water Resources Research, 14(5):705–712, 1978.

Eagleson, P.S. Climate, soil, and vegetation: V. A derived distribution of storm surface runoff. Water Resources Research, 14(5):705–712, 1978.

Eagleson, P.S. Climate, soil, and vegetation: VI. dynamics of the annual water balance. Water Resources Research, 14(5):705–712, 1978.

Eagleson, P.S. Climate, soil, and vegetation: VII. A derived distribution of annual water yield. Water Resources Research, 14(5):705–712, 1978.

Emanuel, K. 2015. "Effect of Upper-Ocean Evolution on Projected Trends in Tropical Cyclone Activity." *Journal of Climate*, 28(20), 8165–8170.

Emanuel, K. 2016. "Will Global Warming Make Hurricane Forecasting More Difficult?" *Bulletin of the American Meteorological Society*.

Environment Agency. 2009. Managing Flood Risk through London and the Thames Estuary In. London: Environment Agency.

Essink, G.O. 1996. *Impact of Sea Level Rise on Groundwater Flow Regimes: A Sensitivity Analysis for the Netherlands*. Delft University of Technology, 421.

Farmer, W. H. and Vogel, R. M. (2016). On the deterministic and stochastic use of hydrologic models. Water Resources Research, 52(7):5619–5633.

FHWA. 2014a. *Assessment of Key Gaps in the Integration of Climate Change Considerations into Transportation Engineering. Federal Highway Administration, FHWA-HEP-15-059.*

FHWA. 2014b. FHWA Climate Change Vulnerability Assessment Pilot Project: North Jersey Transportation Planning Authority. FHWA-HEP-14-005. pp. 4.

FHWA. 2014c. FHWA Climate Change Vulnerability Assessment Pilot Project: Washington State Department of Transportation. FHWA-HEP-14-004. pp. 4.

FHWA. 2014d. U.S. DOT Gulf Coast Study, Phase 2. FHWA-HEP-14-053. pp. 4.

FHWA. 2016. 2013–2015 climate resilience pilot program: Outcomes, lessons learned, and recommendations. Final report FHWA-HEP-16-079, Federal Highway Administration.

Fischback, J.R., R.J. Lempert, E. Molina-Perez, A.A. Tariq, M.L. Finucane, and F. Hoss. 2015.Managing Water Quality in the Face of Uncertainty: A Robust Decision Making Demonstration for EPA's National Water Program. Rand Corporation.

Flato, G., J. Marotzke, B. Abiodun, P. Braconnot, S.C. Chou, W. Collins, P. Cox, F. Driouech, S. Emori, V. Eyring, C. Forest, P. Gleckler, E. Guilyardi, C. Jakob, V. Kattsov, C. Reason and M. Rummukainen, 2013: Evaluation of Climate Models. In: Climate Change 2013: The Physical Science Basis. Contribution of Working Group I to the Fifth Assessment Report of the Intergovernmental Panel on Climate Change [Stocker, T.F., D. Qin, G.-K. Plattner, M. Tignor, S.K. Allen, J. Boschung, A. Nauels, Y. Xia, V. Bex and P.M. Midgley (eds.)]. Cambridge University Press, Cambridge, United Kingdom and New York, NY, USA

Fordyce, E. 2014. "Groundwater dynamics of a shallow coastal aquifer." University of Otago.

Fowler, H.J., S. Blenkinsopa, and C. Tebaldib. 2007. Linking climate change modelling to impacts studies: recent advances in downscaling techniques for hydrological modeling. *International Journal of Climatology* 27, pp.1547-1578.

Frich, P., Alexander, L. V., Della-Marta, P., Gleason, B., Haylock, M., Tank, A. M. G. K. and Peterson, T. 2002, "Observed coherent changes in climatic extremes during the second half of the twentieth century", *Clim. Res*. **19**, 193–212.

García, L.E., J.H. Matthews, D.J. Rodriquez, M. Wijnen, K.N. DiFrancesco, P. Ray. 2014. Beyond Downscaling: A Bottom-Up Approach to Climate Adaptation for Water Resources Management. AGWA Report 01, Washington, DC: World Bank Group.

Garster, J., Huber, M., and White, K. 2015. "US Army Corps of Engineers Screening-Level Assessment of Projects with Respect to Sea Level Change," Civil Works Technical Report, CWTS 2015-16, US Army Corps of Engineers: Washington, DC.

Glasbey, C., G. Cooper, and M. McGechan. 1995. Disaggregation of daily rainfall by conditional simulation from a point process model. *Journal of Hydrology*, 165(1-4), pp. 1-9.

Goddard, P. B., J. J. Yin, S. M. Griffies, and S. Q. Zhang, 2015. An extreme event of sea-level rise along the Northeast coast of North America in 2009-2010, Nature Communications, 6, art. 6346, DOI: 10.1038/ncomms7346.

Golledge, N. R., D. E. Kowalewski, T. R. Naish, R. H. Levy, C. J. Fogwill, and E. G. W. Gasson, 2015. The multi-millenial Antarctic commitment to future sea-level rise, Nature, 526 (7573): 421-+, DOI: 10.1038/nature15706

Grinsted, A., J. C. Moore and S. Jevrejeva, 2012. Homogeneous record of Atlantic hurricane surge threat since 1923, PNAS, vol. 109 | no. 48 | 19601–19605, doi: 10.1073/pnas.1209542109.

Grinsted, A., J.C. Moore, and S. Jevrejeva (2013) Projected Atlantic hurricane surge threat from rising temperatures, PNAS, 110, 14, 5369-5373. DOI: 10.1073/pnas.1209980110.

Grinsted, A., Jevrejeva, S., Riva, R., and Dahl-Jensen, D. 2015. "Sea level rise projections for northern Europe under RCP8.5." *Climate Research*, 64(1), 15–23.

Guevara-Murua, A., E. J. Hendy, A. C. Rust, and K. V. Cashman, 2015. Consistent decrease in North Atlantic cyclone frequency following major volcanic eruptions in the last three centuries, Geophys Res Letters, 42 (21): 9425-9432, DOI 10.1002/2015GL066154

Gutierrez-Magness, A. L., and R. H. McCuen. 2004. Accuracy evaluation of rainfall disaggregation methods. *Journal of Hydrologic Engineering,* Vol. 9, No. 2, pp. 71-78.

Gyasi-Agyei, Y. 2005. Stochastic disaggregation of daily rainfall into one-hour time scale. *Journal of Hydrology*, Vol. 309, pp. 178-190.

Haasnoot, M., H. Middelkoop, A. Offermans, E. van Beek, and W.P.A. van Deursen. 2012. "Exploring Pathways for Sustainable Water Management in River Deltas in a Changing Environment." *Climatic Change*.

Hallegatte, S., Ranger, N., Mestre, O., Dumas, P., Corfee-Morlot, J., Herweijer, C., and Wood, R. M. 2011. "Assessing climate change impacts, sea level rise and storm surge risk in port cities: a case study on Copenhagen." *Climatic Change*, 104(1), 113–137.

Hansen, J., M. Sato, P. Hearty, R. Ruedy, M. Kelley, V. Masson-Delmotte, G. Russell, G. Tselioudis, J. J. Cao, E. Rignot, I., Velicogna, B. Tormey, B. Donovan, E. Kandiano, K. von Schuckmann, P. Kharecha, A. N. Legrande, M. Bauer and K. W. Lo, 2016. Ice melt, sea level rise and superstorms: evidence from paleoclimate data, climate modeling and modern observations that 2 A degrees C global warming can be dangerous, Atmospheric Chemistry and Physics, 16 (6): 3761-3812.

Hawkins, E., and R. Sutton. 2009. "The Potential to Narrow Uncertainty in Regional Climate Predictions", Bull. Amer. Meteorol. Soc., 90, pp. 1095.

Hawkins, E. and Sutton, R., 2011. The potential to narrow uncertainty in projections of regional precipitation change. Climate Dynamics, 37(1-2), pp.407-418.

Hay, C. C., E. Morrow, R. E. Kopp and J. X. Mitrovica, 2015. Probabilistic reanalysis of twentieth-century sea-level rise, Nature, 517 (7535): 481-+, DOI: 10.1038/nature14093.

Hinkel, J., Nicholls, R. J., Tol, R. S. J., Wang, Z. B., Hamilton, J. M., Boot, G., Vafeidis, A. T., McFadden, L., Ganopolski, A., and Klein, R. J. T. 2013. "A global analysis of erosion of sandy beaches and sea-level rise: An application of DIVA." *Global and Planetary Change*, 111, 150–158.

Holland, G., and Bruyère, C. L. 2014. "Recent intense hurricane response to global climate change." *Climate Dynamics*, 42(3-4), 617–627.

Hong, C. C., Y. K. Wu and T. Li, 2016. Influence of climate regime shift on the interdecadal change in tropical cyclone activity over the Pacific Basin during the middle to late 1990s, Climate Dynamics, 47 (7-8): 2587-2600. DOI 10.1007/s00382-016-2986-x

Hoover, D. J., Odigie, K. O., Swarzenski, P. W., and Barnard, P. 2016. "Sea-level rise and coastal groundwater inundation and shoaling at select sites in California, USA." *Journal of Hydrology: Regional Studies*.

Horton, B. P., Rahmstorf, S., Engelhart, S. E., and Kemp, A. C. 2014. "Expert assessment of sea-level rise by AD 2100 and AD 2300." *Quaternary Science Reviews*, 84, 1–6.

Houston, J. R. 2013. "Global Sea Level Projections to 2100 Using Methodology of the Intergovernmental Panel on Climate Change." *Journal of Waterway, Port, Coastal, and Ocean Engineering*, 139(2), 82–87.

Houston, J. 2016. "Beach nourishment as an adaptation strategy for sea level rise: a Florida east coast perspective." *Shore & Beach*, 84(2), 3–12.

Huang, P., Lin, I.-I., Chou, C., and Huang, R.-H. 2015. "Change in ocean subsurface environment to suppress tropical cyclone intensification under global warming." *Nature Communications*, 6, 7188.

van den Hurk, B., van Meijgaard, E., de Valk, P., van Heeringen, K.-J., and Gooijer, J. 2015. "Analysis of a compounding surge and precipitation event in the Netherlands." *Environmental Research Letters*, 10(3), 035001.

IPCC. 2010. IPCC Expert Meeting on Assessing and Combining Multi Model Climate Projections. Meeting of the Working Group I (WG 1) – The Physical Science Basis at the National Center for Atmospheric Research, Mesa Laboratory, Boulder, Colorado, January 25-27, 2010.

IPCC. 2012: Managing the Risks of Extreme Events and Disasters to Advance Climate Change Adaptation. A Special Report of Working Groups I and II of the Intergovernmental Panel on Climate Change [Field, C.B., V. Barros, T.F. Stocker, D. Qin, D.J. Dokken, K.L. Ebi, M.D. Mastrandrea, K.J. Mach, G.-K. Plattner, S.K. Allen, M. Tignor, and P.M. Midgley (eds.)]. Cambridge University Press, Cambridge, UK, and New York, NY, USA, 582 pp.

IPCC. 2013: Annex III: Glossary [Planton, S. (ed.)]. In: Climate Change 2013: The Physical Science Basis. Contribution of Working Group I to the Fifth Assessment Report of the Intergovernmental Panel on Climate Change [Stocker, T.F., D. Qin, G.-K. Plattner, M. Tignor, S.K. Allen, J. Boschung, A. Nauels, Y. Xia, V. Bex and P.M. Midgley (eds.)]. Cambridge University Press, Cambridge, United Kingdom and New York, NY, USA.

IPCC, 2014: Climate Change 2014: Synthesis Report. Contribution of Working Groups I, II and III to the Fifth Assessment Report of the Intergovernmental Panel on Climate Change [Core Writing Team, R.K. Pachauri and L.A. Meyer (eds.)]. IPCC, Geneva, Switzerland, 151 pp.

Irish, J. L., Sleath, A., Cialone, M. A., Knutson, T. R., and Jensen, R. E. 2014. "Simulations of Hurricane Katrina 2005) under sea level and climate conditions for 1900." *Climatic Change*, 122(4), 635–649.

Johansson, M. M., Pellikka, H., Kahma, K. K., and Ruosteenoja, K. 2014. "Global sea level rise scenarios adapted to the Finnish coast." *Journal of Marine Systems*, 129, 35–46.

Johnson, T. E., and C. P.Weaver (2009), A framework for assessing climate change impacts on water and watershed systems, Environ. Manage. 43, 118–134.

Johnson, T., J. Butcher, D. Deb, M. Faizullabhoy, P. Hummel, J. Kittle, S. McGinnis, L.O. Mearns, D. Nover, A. Parker, S. Sarkar, R. Srinivasan, P. Tuppad, M. Warren, C. Weaver, and J. Witt, 2015. Modeling Streamflow and Water Quality Sensitivity to Climate Change and Urban Development in 20 U.S. Watersheds. Journal of the American Water Resources Association (JAWRA) 51(5): 1321-1341. DOI: 10.1111/1752-1688.12308.

Kabiri, R., Ramani Bai, V. and Chan, A. (2015). Assessment of hydrologic impacts of climate change on the runoff trend in Klang Watershed, Malaysia. *Environ Earth Sci* 73: 27. doi:10.1007/s12665-014-3392-5.

Kane, H. H., Fletcher, C. H., Frazer, L. N., and Barbee, M. M. 2015. "Critical elevation levels for flooding due to sea-level rise in Hawai'i." *Regional Environmental Change*, 15(8), 1679–1687.

Kates, R.W., Travis, W.R., and Wilbanks, T.J. 2012. Transformational adaptation when incremental adaptations to climate change are insufficient. Proceedings of the National Academy of Sciences, 109, pp. 7156-7161.

Kendon, E.J., Ban, N., Roberts, N.M., Fowler, H.J., Roberts, M.J., Chan, S.C., Evans, J.P., Fosser, G. and Wilkinson, J.M., 2016. Do convection-permitting regional climate models improve projections of future precipitation change?. Bulletin of the American Meteorological Society, (2016).

Kessler, R. 2011. Stormwater Strategies: Cities Prepare Aging Infrastructure for Climate Change. Environmental Health Perspectives volume 119 pages a514-a519.

Kharin, V.V., F.W. Zwiers, and X. Zhang. 2005: Intercomparison of near surface temperature and precipitation extremes in AMIP-2 simulations, reanalyses and observations. *Journal of Climate*, 18, 5201-5223.

Kharin, V., F. Zwiers, X. Zhang and M. Wehner. 2013. Change in temperature and precipitation extremes in the CMIP5 ensemble. *Climatic Change*, 119(2), 345-357.

Kilgore, R., G. Herrmann, W.O. Thomas, Jr., and D.B. Thompson. 2016. *Highways in the River Enviornment – Floodplains, Extreme Events, Risk, and Reslience.* Hydraulic Engineering Circular No. 17 (HEC-17), Federal Highway Administration, FHWA-HIF-16-018.

Kilgore Consulting and Management (KCM), 2015. Literature review, Task Order DTFH61-14-D-00044-T5009, HEC-17 Highways in the River Environment – Floodplains, Extreme Events, Risk, and Resilience, Federal Highway Administration, 42 pp.

Kirshen, P., L. Caputo, R.M. Vogel, P. Mathisen, A. Rosner, and T. Renaud. 2014. "Adapting Urban Infrastructure to Climate Change: A Drainage Case Study." *Journal of Water Resources Planning and Management.* ASCE.

Klerk, W. J., Winsemius, H. C., van Verseveld, W. J., Bakker, A. M. R., and Diermanse, F. L. M. 2015. "The co-incidence of storm surges and extreme discharges within the Rhine–Meuse Delta." *Environmental Research Letters*, 10(3), 035005.

Kjeldsen, T.R., Miller, J.D. and Packman, J.C., 2013. Modelling design flood hydrographs in catchments with mixed urban and rural land cover. *Hydrology Research*, 44 (6), pp. 1040-1057.

Knott, J., J.S. Daniel, J.M. Jacobs, P. Kirshen and M. Elshaer. 2016 . Assessing the Effects of Rising Groundwater from Sea-Level Rise on the Service Life of Pavements in Coastal Road Infrastructure. TRB Research Record: Journal of Transportation Research Board.Accepted pending revisions. To be resubmitted November, 2016.

Knutti, R. and J. Sedláček. 2013. Robustness and uncertainties in the new CMIP5 climate model projections. Nature Climate Change, 3(4), 369-373. http://onlinelibrary.wiley.com/doi/10.1002/grl.50256/full

Knutson, T. R., McBride, J. L., Chan, J., Emanuel, K., Holland, G., Landsea, C., Held, I., Kossin, J. P., Srivastava, A. K., and Sugi, M. 2010. "Tropical cyclones and climate change." *Nature Geoscience*, 3(3), 157–163.

Knutson, T. R., Sirutis, J. J., Zhao, M., Tuleya, R. E., Bender, M., Vecchi, G. A., Villarini, G., and Chavas, D. 2015. "Global Projections of Intense Tropical Cyclone Activity for the Late Twenty-First Century from Dynamical Downscaling of CMIP5/RCP4.5 Scenarios." *Journal of Climate*, 28(18), 7203–7224.

Kopp, R. E., Horton, R. M., Little, C. M., Mitrovica, J. X., Oppenheimer, M., Rasmussen, D. J., Strauss, B. H., and Tebaldi, C. 2014. "Probabilistic 21st and 22nd century sea-level projections at a global network of tide-gauge sites: KOPP ET AL." *Earth's Future*, 2(8), 383–406.

Kopp, R. E., B. P. Horton, A. C. Kemp, C. Tebaldi, 2015. Past and future sea-level rise along the coast of North Carolina, USA, Climatic Change, 132 (4): 693–707.

Kossin, J. P., Emanuel, K. A., and Vecchi, G. A. 2014. "The poleward migration of the location of tropical cyclone maximum intensity." *Nature*, 509(7500), 349–352.

Kotamarthi, R., C. Castro, K. Hayhoe, L. Mearns and D. Wuebbles. 2016. Use of Climate Information for Decision-Making and Impacts Research: State of our Understanding. U.S. Department of Defense Strategic Environmental Research and Development Program.

Koutsoyiannis, D., and C. Onof. 2001. Rainfall disaggregation using adjusting procedures on a Poisson cluster model. *Journal of Hydrology*, Vol. 246, pp. 109-122.

Koutsoyiannis, D., C. Onof, and H. Wheater. 2003. Multivariate rainfall disaggregation at a fine timescale. *Water Resources Research*, Vol. 39, No. 7, pp. 1-18.

Kuo, C-C and T.Y. Gan. 2015. "Risk of Excceding Extreme Design Storm Events Under Possible Impact of Climate Change." *Jornal of Hydrologic Engineering.* ASCE.

Krakauer, N.Y. and Fekete, B.M., 2014. Are climate model simulations useful for forecasting precipitation trends? Hindcast and synthetic-data experiments. Environmental Research Letters, 9(2), p.024009.

LaFontaine, J.H., L.E, Hay, R.J. Viger, R.S. Regan, and S.L. Markstrom. 2015. "Effects of Climate and Land Cover on Hydrology in the Southeastern U.S.: Potential Impacts on Watershed Planning." *Journal of the American Water Resources Association.*

Leatherman, S. P., Zhang, K., and Douglas, B. C. 2000. "Sea level rise shown to drive coastal erosion." *Eos, Transactions American Geophysical Union*, 81(6), 55–57.

Le Cozannet, G., Garcin, M., Yates, M., Idier, D., and Meyssignac, B. 2014. "Approaches to evaluate the recent impacts of sea-level rise on shoreline changes." *Earth-Science Reviews*, 138, 47–60.

Lee, C.-Y., Tippett, M. K., Sobel, A. H., and Camargo, S. J. 2016. "Rapid intensification and the bimodal distribution of tropical cyclone intensity." *Nature Communications*, 7, 10625.

Levitus, S., J.I. Antonov, T.P. Boyer, O.K. Baranova, H.E. Garcia, R.A. Locarnini, A.V. Mishonov, J.R. Reagan, D. Seidov, E.S. Yarosh and M.M. Zweng. 2012. World ocean heat content and thermosteric sea level change (0-2000 m), 1955-2010, GRL, 39, L10603, doi:10.1029/2012GL051106.

Lin, N., Emanuel, K., Oppenheimer, M., and Vanmarcke, E. 2012. "Physically based assessment of hurricane surge threat under climate change." *Nature Climate Change*, 2(6), 462–467.

Lindquist, E. 2011. Transportation Planning, Policy and Climate Change: Making the Long-Term Connection. In (p. 62). College Station, Texas: Texas Transportation Institute.

Little, C. M., Horton, R. M., Kopp, R. E., Oppenheimer, M., Vecchi, G. A., and Villarini, G. 2015. "Joint projections of US East Coast sea level and storm surge." *Nature Climate Change*, 5(12), 1114–1120.

Liu, C., Ikeda, K., Rasmussen, R., Barlage, M., Newman, A.J., Prein, A.F., Chen, F., Chen, L., Clark, M., Dai, A. and Dudhia, J., 2016a. Continental-scale convection-permitting modeling of the current and future climate of North America. *Climate Dynamics*, pp.1-25.

Liu, R., C. Chen and G. Wang, 2016b. Change of tropical cycle heat potential in response to global warming, Advances in Atmospheric Sciences, 23 (4): 504-510, DI 10.1007/s00376-015-5112-9

Liuzzo, L. and G. Freni. 2015. "Analysis of Extreme Rainfall Trends in Sicily for the Evaluation of Depth-Duration-Frequency Curves in Climate Change Scenarios." *Journal of Hydrologic Engineering.* ASCE.

Livneh et al 2013 http://journals.ametsoc.org/doi/pdf/10.1175/JCLI-D-12-00508.1

Lorenzo-Trueba, J., and Ashton, A. D. 2014. "Rollover, drowning, and discontinuous retreat: Distinct modes of barrier response to sea-level rise arising from a simple morphodynamic model." *Journal of Geophysical Research: Earth Surface*, 119(4), 779–801.

Luo Y, Ficklin DL, Liu X, and Zhang M (2013) Assessment of climate change impacts on hydrology and water quality with a watershed modeling approach. Science of the total Environment 450–451: 72–82. doi: 10.1016/j.scitotenv.2013.02.004

Manda, A. K., Sisco, M. S., Mallinson, D. J., and Griffin, M. T. 2015. "Relative role and extent of marine and groundwater inundation on a dune-dominated barrier island under sea-level rise scenarios: MARINE AND GROUNDWATER INUNDATION UNDER SEA-LEVEL RISE." *Hydrological Processes*, 29(8), 1894–1904.

Manning, M.R., M. Petit, D. Easterling, J. Murphy, A. Patwardhan, H-H. Rogner, R. Swart, and G. Yohe (eds.). 2004. IPCC Workshop on Describing Scientific Uncertainties in Climate Change to Support Analysis of Risk and of Options: Workshop Report. Intergovernmental Panel on Climate Change (IPCC), Geneva, Switzerland.

Marciano, C. G., Lackmann, G. M., and Robinson, W. A. 2015. "Changes in U.S. East Coast Cyclone Dynamics with Climate Change." *Journal of Climate*, 28(2), 468–484.

Markus, M., Angel, J., Byard, G., Zhang, C., Zaloudek, Z., and McConkey, S. (2016). Communicating the impacts of potential future climate change on the expected frequency of extreme rainfall events in Cook County, Illinois.

Marshall, Eric and Timothy Randhir. 2008. Effect of climate change on watershed system: a regional analysis. *Climatic Change.* August 2008, Vol. 89, Issue 3, pp. 263–280.

Masterson, J. P., and Garabedian, S. P. 2007. "Effects of Sea-Level Rise on Ground Water Flow in a Coastal Aquifer System." *Ground Water*, 45(2), 209–217.

Mastrandrea, M.D., C.B. Field, T.F. Stocker, O. Edenhofer, K.L. Ebi, D.J. Frame, H. Held, E. Kriegler, K.J. Mach, P.R. Matschoss, G.-K. Plattner, G.W. Yohe, and F.W. Zwiers. 2010. Guidance Note for Lead Authors of the IPCC Fifth Assessment Report on Consistent Treatment of Uncertainties. Intergovernmental Panel on Climate Change (IPCC). Available at <http://www.ipcc.ch>.

Mattingly, K. S., McLeod, J. T., Knox, J. A., Shepherd, J. M., and Mote, T. L. 2015. "A climatological assessment of Greenland blocking conditions associated with the track of Hurricane Sandy and historical North Atlantic hurricanes: GREENLAND BLOCKING AND NORTH ATLANTIC HURRICANES." *International Journal of Climatology*, 35(5), 746–760.

Maurer E.P., L.Brekke, T. Pruitt, and P.B. Duffy. 2007. Fine-resolution climate projections enhance regional climate change impact studies. *EOS* Trans Am Geophys Union 88(47).

McCuen, R.H., P.A. Johnson, and R.M. Ragan. 2002. "Highway Hydrology," Hydraulic Design Series 2 (HDS 2), Second Edition, FHWA-NHI-02-001.

McDonald, R. E. 2011. "Understanding the impact of climate change on Northern Hemisphere extra-tropical cyclones." *Climate Dynamics*, 37(7-8), 1399–1425.

McGuigan, K., Webster, T., and Collins, K. 2015. “A Flood Risk Assessment of the LaHave River Watershed, Canada Using GIS Techniques and an Unstructured Grid Combined River-Coastal Hydrodynamic Model.” *Journal of Marine Science and Engineering*, 3(3), 1093–1116.

Mearns, L.O., et al. 2007, updated 2014. The North American Regional Climate Change Assessment Program dataset, National Center for Atmospheric Research Earth System Grid data portal, Boulder, CO. Data downloaded 2016-10-26. [doi:10.5065/D6RN35ST]

Mearns, L.O., W.J. Gutowski, R. Jones, L.-Y. Leung, S. McGinnis, A.M.B. Nunes, and Y. Qian. 2009. "A regional climate change assessment program for North America." *EOS*, Vol. 90, No. 36, pp. 311-312

Mearns, L.O., Lettenmaier, D.P., and S. McGinnis. 2015. "Uses of Results of Regional Climate Model Experiments for Impacts and Adaptation Studies: The Example of NARCCAP", Current Climate Change Reports, 1, pp. 1-9.

Mednick, A. C., T. M. Possley Nelson, and D. J. Watermolen. (2012). Assessing Long-term Hydrological Impacts of Climate Change Across Wisconsin. The Wisconsin Department of Natural Resources. Madison, WI 53707.

Meehl, G. A., C. Covey, T. Delworth, M. Latif, B. McAvaney, J. F. B. Mitchell, R. J. Stouffer, and K. E. Taylor. 2007. “The WCRP CMIP3 multi-model dataset: A new era in climate change research”, *Bulletin of the American Meteorological Society,* 88, pp. 1383-1394.

Meenu, R., S. Rehana and P. P. Mujumdar. 2012. Assessment of hydrologic impacts of climate change in Tunga–Bhadra river basin, India with HEC-HMS and SDSM. *Hydrol. Process*. 27, pp. 1572–1589, DOI: 10.1002/hyp.9220.

Mendlik, T., and A. Gobiet. 2016. "Selecting climate simulations for impact studies based on multivariate patterns of climate change", Clim. Change, 135, pp. 381-393.

Mernild, S. H., G. E. Liston, and C. A. Hiemstra, 2014. Northern Hemisphere Glacier and Ice Cap Surface Mass Balance and Contribution to Sea Level Rise, J. Climate 27 (15): 6051-6072, DOI: 10.1175/JCLI-D-13-00669.1

Metherall, C. 2014. Assessing the value of green infrastructure networks to manage peak flows and support community resilience to climate change. Master’s Thesis. Royal Roads University.

Meyer, M., M. Flood, J. Keller, J. Lennon, G. McVoy, C. Dorney, K. Leonard, R. Hyman, and J. Smith. 2013. Climate Change, Extreme Weather Events, and the Highway System (vol 1), Transportation Research Board: National Cooperative Highway Research Program, Washington, DC.

Meyer, Michael, Michael Flood, Jake Keller, Justin Lennon, Gary McVoy, Chris Dorney, Ken Leonard, Robert Hyman, and Joel Smith (2014). “Volume 2: Climate Change, Extreme Weather Events, and the Highway System: Practitioner’s Guide and Research Report,” NCHRP Report 750.

Meyers, W. S. 2012. Rail Transportation Vulnerability and Resiliency to Impacts of Climate Change and Recommendations for Objective Measurement Methods, SYSTRA Inc.

Milly, P.C.D, J. Betancourt, M. Falkenmark, R.M. Hirsch, Z.W. Kundzewicz, D.P. Lettenmaier, and R.J. Stouffer. 2008. “Stationarity Is Dead: Whither Water Management?” *Science*, 319(5863): 573.

Minnesota Department of Transportation (MnDOT). 2014. MnDOT Flash Food Vulnerability and Adaption Assessment Pilot Project – Final Report. Prepared by Parsons Brinckerhoff and Catalysis.

Mishra, B.K. and S. Herath. 2014. “Assessment of Future Floods in the Bagmati River Basin of Nepal Using Bias-Corrected Daily GCM Precipitation.” *Journal of Hydrologic Engineering,* ASCE.

Mitrovica, J. X., N. Gomez, E. Morrow, C. Hay, K. Latychev and M. E. Tamisiea, 2011. On the robustness of predictions of sea level fingerprints, Geophys. J. Int. (2011) 187, 729–742.

Mitrovica, J.X., Gomez, N. & Clark, P.U., 2009. The sea-level fingerprint of West Antarctic collapse, Science, 323, 753.

Mitrovica, J. X., C. C. Hay, E. Morrow, R. E. Kopp, M. Dumberry and S. Stanley, 2015. Reconciling past changes in Earth's rotation with 20th century global sea-level rise: Resolving Munk's enigma, Science Advances, 1 (11): e1500679, DOI: 10.1126/sciadv.1500679

Moftakhari, H.R., A. AghaKouchak, B.F. Sanders, D. L. Feldman, W. Sweet, R. A. Matthew and A. Luke, 2015. Increased nuisance flooding along the coasts of the Unites States due to sea level rise: Past and future, Geophysical Research Letters, 42 (22): 9846-9852, DOI: 10.1002/2015GL066072.

Moglen, G.E. and G.E.R. Vidal. 2014. "Climate Change and Storm Water Infrastructure in the Mid-Atlantic Region: Design Mismatch Coming?" *Journal of Hydrologic Engineering.*

Moss, R., J.A. Edmonds, K.A. Hibbard, M.R. Manning, S.K. Rose, D.P. van Vuuren, T.R. Carter, S. Emori, M. Kainuma, T. Kram, G.A. Meehl, J. F. B. Mitchell, N. Nakicenovic, K. Riahi, S.J. Smith, R.J. Stouffer, A.M. Thomson, J.P. Weyant, and T.J. Wilbanks. 2010. The next generation of scenarios for climate change research and assessment. Nature, 463, 747-756.

Moss, R.H. and S. H. Schneider. 2000, 'Uncertainties in the IPCC TAR: Recommendations to Lead Authors for More Consistent Assessment and Reporting', in Pachuari, R., Tanaka, K. and Taniguchi, T. (eds.), Guidance Papers on the Cross Cutting Issues of the Third Assessment Report of the IPCC, Intergovernmental Panel on Climate Change, Geneva, pp. 33–51.

Natural Resources Conservation Service (NRCS). 2015. Chapter 4: Storm Rainfall Depth and Distribution, Part 630, National Engineering Handbook, Washington, DC.

National Academy of Sciences (NAS), 2011. Climate Stabilization Targets: Emissions, Concentrations, and Impacts over Decades to Millennia. Committee on Stabilization Targets for Atmospheric Greenhouse Gas Concentrations, National Academies Press, Washington D.C.

National Research Council (NRC). 2004. Adaptive Management for Water Resources Project Planning. Washington, DC: The National Academies.

Nemry, F. 2012. Impacts of Climate Change in Europe: A Focus on Road and Rail Transport Infrastructures, European Commission; Joint Research Centre.

Northrop, P. J., and R. E. Chandler. 2014. "Quantifying Sources of Uncertainty in Projections of Future Climate", Journal of Climate, 27, pp. 8793-8808.

Obeysekera and Salas (2014). "Quantifying the Uncertainty of Design Floods under Nonstationary Conditions," Journal of Hydrologic Engineering, ASCE, 19(7).

Ocana, V., E. Zorita, P. Heimbach, 2016. Stochastic secular trends in sea level rise, JOURNAL OF GEOPHYSICAL RESEARCH-OCEANS, 121 (4): 2183-2202.

Olsson, J.; Arheimer, B.; Borris, M.; Donnelly, C.; Foster, K.; Nikulin, G.; Persson, M.; Perttu, A.-M.; Uvo, C.B.; Viklander, M.; Yang, W. 2016. Hydrological Climate Change Impact Assessment at Small and Large Scales: Key Messages from Recent Progress in Sweden. *Climate* 2016, 4, 39.

Pachauri, R. K., Allen, M. R., Barros, V. R., Broome, J., Cramer, W., Christ, R., Church, J. A., Clarke, L., Dahe, Q., Dasgupta, P., and others. 2014. *Climate change 2014: synthesis Report. Contribution of working groups I, II and III to the fifth assessment report of the intergovernmental panel on climate change*. IPCC.

Parris, A., P. Bromirski, V. Burkett, D. Cayan, M. Culver, J. Hall, R. Horton, K. Knuuti, R. Moss, J. Obeysekera, A. Sallenger, and J. Weiss. 2012. Global Sea Level Rise Scenarios for the US National Climate Assessment. NOAA Tech Memo OAR CPO-1. 37 pp.

Pfahl, S., O'Gorman, P. A., and Singh, M. S. 2015. "Extratropical Cyclones in Idealized Simulations of Changed Climates." *Journal of Climate*, 28(23), 9373–9392.

Pike, L., and Dill, N. 2016. "The vulnerability to coastal flooding at two locations in Islesboro, ME." Long Branch, NJ, USA.

Raabe, E. A., and Stumpf, R. P. 2016. "Expansion of Tidal Marsh in Response to Sea-Level Rise: Gulf Coast of Florida, USA." *Estuaries and Coasts*, 39(1), 145–157.

Ranasinghe, R., Callaghan, D., and Stive, M. J. F. 2012. "Estimating coastal recession due to sea level rise: beyond the Bruun rule." *Climatic Change*, 110(3-4), 561–574.

Read, L.K. and R.M. Vogel (2015). "Reliability, Return Periods, and Risk Under Uncertainty," Water Resources Research, 51. DOI: 10.1002/2015WR017089.

Read, L.K. and R. M. Vogel, 2016a. Hazard function analysis for flood planning under nonstationarity. Water Resources Research, 52:4116–4131.

Read, L.K. and R. M. Vogel, 2016b. Hazard function analysis for nonstationary natural hazards. Natural Hazards Earth System Science, 16:915–925.

Reeder, T. and N. Ranger. 2011. How Do You Adapt in an Uncertain World" Lessons for the Thames Estuary 2100 Project. World Resources Report, Washington, DC.

Rignot, E., Velicogna, I., van den Broeke, M. R., Monaghan, A., and Lenaerts, J. T. M. 2011. "Acceleration of the contribution of the Greenland and Antarctic ice sheets to sea level rise: ACCELERATION OF ICE SHEET LOSS." *Geophysical Research Letters*, 38(5), n/a–n/a.

Ritz, C. T. L. Edwards, G. Durand, A. J. Payne, V. Peyaud, and R. C. A. Hindmarsh, 2015. Potential sea-level rise from Antarctic ice-sheet instability constrained by observations, Nature, 528 (7580): 115+-, **DOI:** 10.1038/nature16147.

Romine, B. M., Fletcher, C. H., Frazer, L. N., and Anderson, T. R. 2016. "Beach erosion under rising sea-level modulated by coastal geomorphology and sediment availability on carbonate reef-fringed island coasts." *Sedimentology*, V. Manville, ed.), 63(5), 1321–1332.

Roshani, A. 2014. "Road infrastructure vulnerability to groundwater table variation due to sea level rise."

Roshani, A., Mirfenderesk, H., Rajapakse, J., and Gallage, C. 2015. "Groundwater table response to sea level rise and its impact on pavement structure." *9th Annual International Conference of the International Institute for Infrastructure Renewal and Reconstruction 8-10 July 2013.*, Queensland University of Technology, 531–538.

Rosner, A., R.M. Vogel, and P.H. Kirshen. 2014. "A Risk-Based Approach to Flood Management Decisions in a Nonstationary World." *Water Resources Research*, 50, 1928-1942.

Rotzoll, K., and Fletcher, C. H. 2012. "Assessment of groundwater inundation as a consequence of sea-level rise." *Nature Climate Change*, 3(5), 477–481.

Salas and Obeysekera (2014). "Revisiting the Concepts of Return Period and Risk for Nonstationary Hydrologic Extreme Events," Journal of Hydrologic Engineering, ASCE, 19(3).

Sallenger, A.H., K.S. Doran, and P.A Howd, 2012. Hotspot of accelerated sea-level rise on the Atlantic coast of North America, *Nature Climate Change*, 2, 884–888 doi:10.1038/nclimate1597.

Selvanathan, S., M. Sreetharan, K. Rand, D. Smirnov, J. Choi, and M. Mampara. 2016. "Developing Peak Discharges for Future Flood Risk Studies Using IPCC's CMIP5 Climate Model Results and USGS WREG Program." *Journal of the American WaterResources Association.*

Seiler, C., and Zwiers, F. W. 2016. "How will climate change affect explosive cyclones in the extratropics of the Northern Hemisphere?" *Climate Dynamics*, 46(11-12), 3633–3644.

Simonovic, S.P, A. Schardong, D. Sandink, and R. Srivastav, 2016. A web-based tool for the development of Intensity Duration Frequency curves under changing climate. Environmental Modelling & Software. Volume 81, July 2016, Pages 136–153. http://dx.doi.org/10.1016/j.envsoft.2016.03.016.

Smith, J. M., Cialone, M. A., Wamsley, T. V., and McAlpin, T. O. 2010. "Potential impact of sea level rise on coastal surges in southeast Louisiana." *Ocean Engineering*, 37(1), 37–47.

Sobel, A. H., S. J. Camargo, T. M. Hall, C-Y Lee, M. K. Tippett and A. A. Wing, 2015. Human influences on tropical cyclone intensity, Science, 353 (6296): 242-246, DOI 10.1126/science.aaf6574

Socolofsky, S., E. Adams, and D. Entekhabi. 2001. Disaggreation of Daily Rainfall for Continuous Watershed Modeling. *Journal of Hydrologic Engineering*, Vol. 6, No. 4, pp. 300-309.

Solomon, S. (IPCC). 2007. *Climate change 2007: the physical science basis: contribution of Working Group I to the Fourth Assessment Report of the Intergovernmental Panel on Climate Change*. Cambridge University Press, Cambridge ; New York.

Shrestha, S (2014) Assessment of Water Availability under Climate Change Scenarios in Thailand. *J Earth Sci Clim Change* 5:184. doi: 10.4172/2157-7617.1000184.

Stocker, T. F., Qin, D., Plattner, G.-K., Alexander, L. V., Allen, S. K., Bindoff, N. L., Bréon, F.-M., Church, J. A., Cubasch, U., Emori, S., and others. 2013. "Technical summary." *Climate Change 2013: The Physical Science Basis. Contribution of Working Group I to the Fifth Assessment Report of the Intergovernmental Panel on Climate Change*, Cambridge University Press, 33–115.

Stoner, A., K. Hayhoe, X. Yang and D. Wuebbles. An asynchronous regional regression model for statistical downscaling of daily climate variables. *International Journal of Climatology*, doi: 10.1002/joc.3603.

Swain, S. and K. Hayhoe. Projected changes in drought and wet conditions over North America. *Climate Dynamics*, 44(9), 2737-2750.

Tebaldi, C., Strauss, B. H., and Zervas, C. E. 2012. "Modelling sea level rise impacts on storm surges along US coasts." *Environmental Research Letters*, 7(1), 014032.

Themeßl, M.J., A. Gobiet, and G. Heinrich. 2012. Empirical-statistical downscaling and error correction of regional climate models and its impact on the climate change signal. Climatic Change, 112(2), pp.449-468.

Torres, J. M., Bass, B., Irza, N., Fang, Z., Proft, J., Dawson, C., Kiani, M., and Bedient, P. 2015. "Characterizing the hydraulic interactions of hurricane storm surge and rainfall–runoff for the Houston–Galveston region." *Coastal Engineering*, 106, 7–19.

USACE. 2002. *Coastal Engineering Manual*. Engineering Manual, Department of the Army, U.S. Army Corps of Engineers, Washington, DC.

USACE. 2014. "Procedures to Evaluate Sea Level Change: Impacts, Responses, and Adaptation," ETL 1100-2-1, Department of the Army, U.S. Army Corps of Engineers, Washington, DC, 254, June 30, 2014.

USACE. 2015. *North Atlantic Coast comprehensive study: Resilient adaptation to increasing risk (main report)*. Final Report, U.S. Army Corps of Engineers, NY.

U.S. Department of Commerce, U.S. Weather Bureau. 1961. Rainfall Frequency Atlas of the United States for Durations from 30 Minutes to 24 Hours and Return Periods from 1 to 100 Years. Technical Paper NO. 40, Washington, DC.

U.S. Department of Commerce, National Oceanic and Atmospheric Administration. 1977. Five- to 60-Minute Precipitation Frequency for the Eastern and Central United States. NOAA Technical Memorandum NWS HYDRO-35. National Weather Service, Silver Spring, MD.

US DOT. 2014. "Engineering Assessments of Climate Change Impacts and Adaptation Measures (Task 3.2)," Impacts of Climate Change and Variability on Transportation Systems and Infrastructure – The Gulf Coast Study, Phase 2, FHWA-HEP-15-004, August.

U.S. EPA. 2009. BASINS 4.0 Climate Assessment Tool (CAT): Supporting Documentation and User's Manual. National Center for Environmental Assessment, Washington, DC; EPA/600/R-08/088F. Available from the National Technical Information Service, Springfield, VA, and online at http://www.epa.gov.

U.S. EPA 2010. Climate Change Vulnerability Assessments: A Review of Water Utility Practices, EPA 800-R-10-0001, Office of Water.

U.S. EPA. 2014a. National stormwater calculator. Cincinnati OH: National Risk Management Research Laboratory. Available at http://www2.epa.gov/water-research/national-stormwater-calculator.

U.S. EPA. 2014b. National stormwater calculator user's guide. (EPA/600/R-13/085c) Revised September 2014. Cincinnati, OH: National Risk Management Research Laboratory, 75pp. Available at http://nepis.epa.gov/Adobe/PDF/P100LOB2.pdf.

U.S. EPA. 2014c. SWMM-CAT user's guide. (EPA/600/R¬14/428). Cincinnati, OH: National Risk Management Research Laboratory. 16pp. Available at http://nepis.epa.gov/Exe/ZyPDF.cgi/P100KY8L.PDF?Dockey=P100KY8L.PDF.

U.S. EPA. 2016. Climate Resilience Evaluation and Awareness Tool, Version 3.0 Methodology Guide. https://www.epa.gov/sites/production/files/2016-05/documents/creat_3_0_methodology_guide_may_2016.pdf

van der Pol, T.D., S. Gabbert, H. Weikard, E.C. van Ierland, and E.M.T. Hendrix. 2016. "A Minimax Regret Analysis of Flood Risk Management Strategies Under Climate Change Uncertainty and Emerging Information." *Environmental and Resource Economics,* pp 1-23.

Vasskog, K., P. M. Langebroek, J. T. Andrews, J. E. O. Nilsen, and A. Nessie, 2015. The Greenland Ice Sheet during the last glacial cycle: Current ice loss and contributions to sea-level rise, Earth-Science Reviews, 150: 45-67, DOI**:** 10.1016/j.earscirev.2015.07.006

Villarini, G., and Vecchi, G. A. 2013. "Projected Increases in North Atlantic Tropical Cyclone Intensity from CMIP5 Models." *Journal of Climate*, 26(10), 3231–3240.

Wada, Y., L.P.H. van Beek, F.C. Sperna Weiland, B.F. Chao, Y-H Wu and M. F.P. Bierkens. 2012. Past and future contributions of global groundwater contributions to sea level rise, GRL, 39 (9), DOI: 10.1029/2012GL051230.

Wahl, T., Jain, S., Bender, J., Meyers, S. D., and Luther, M. E. 2015. "Increasing risk of compound flooding from storm surge and rainfall for major US cities." *Nature Climate Change*, 5(12), 1093–1097.

Walker, E.E., P. Harremoes,, J. Rotmans, J.P. van der Sluijs, M.B.A. van Asselt, P. Janssen, MlP. Krayer von Krauss, 2003. "Defining Uncertainty: A Conceptual Basis for Uncertainty Management in Model-Based Decision Support," *Integrated Assessment,* Volume 128, No. 2, pp. 282-289.

Walsh, J., D. Wuebbles, K. Hayhoe, J. Kossin, K. Kunkel, G. Stephens, P. Thorne, R. Vose, M. Wehner, J. Willis, D. Anderson, S. Doney, R. Feely, P. Hennon, V. Kharin, T. Knutson, F. Landerer, T. Lenton, J. Kennedy, and R. Somerville. 2014. Ch. 2: Our Changing Climate. *Climate Change Impacts in the United States: The Third National Climate Assessment*, J. M. Melillo, Terese (T.C.) Richmond, and G. W. Yohe, Eds., U.S. Global Change Research Program, 19-67. DOI:10.7930/J0KW5CXT.

Walsh, K. J. E., McBride, J. L., Klotzbach, P. J., Balachandran, S., Camargo, S. J., Holland, G., Knutson, T. R., Kossin, J. P., Lee, T., Sobel, A., and Sugi, M. 2016. "Tropical cyclones and climate change: Tropical cyclones and climate change." *Wiley Interdisciplinary Reviews: Climate Change*, 7(1), 65–89.

Watson, C. S., N. J. White, J. A. Church, M. A. King, R. J. Burgette, and B. Legresy, 2015. Unabated global mean sea-level rise over the satellite altimeter era, Nature Climate Change, 5 (6): 565.

Weaver, C.P., R.J. Lempert, C. Brown, J.A. Hall, D. Revell, and D. Sarewitz. 2013. "Improving the Contribution of Climate Model Information to Decision Making: The Value and Demands of Robust Decision Frameworks." *Climate Change*, Volume 4.

Wehner, M., R. Smith, G. Bala and P. Duffy. 2010. The effect of horizontal resolution on simulation of very extreme U.S. precipitation events in a global atmosphere model. *Climate Dynamics*, 34(2), 241-247.

Wehner, M. 2013. Very extreme seasonal precipitation in the NARCCAP ensemble: model performance and projections. *Climate Dynamics*, 40(1), 59-80.

Wood A.W., E.P. Maurer, A. Kumar, and D.P. Lettenmaier. 2002. Long-range experimental hydrologic forecasting for the eastern United States. *J Geophys Res* 107(D20): 4429.

Wood A.W., L.R. Leung, V. Sridhar, and D.P. Lettenmaier. 2004. Hydrologic implications of dynamical and statistical approaches to downscaling climate model outputs. *Climate Change* 62(1):189–216.

Woodward, R.S., 1888. On the form and position of mean sea level, US Geol. Surv. Bull., **48,** 87–170.

Wu, S.-Y., Yarnal, B., and Fisher, A. 2002. "Vulnerability of coastal communities to sea-level rise: a case study of Cape May County, New Jersey, USA." *Climate Research*, 22(3), 255–270.

Wuebbles, D., G. Meehl, K. Hayhoe, T. Karl, K. Kunkel, B. Santer, M. Wehner, B. Colle, E. Fischer, R. Fu, A. Goodman, E. Janssen, V. Kharin, H. Lee, W. Li, L. Long, S. Olsen, Z. Pan, A. Seth, J. Sheffield and L. Sun. 2014. CMIP5 Climate Model Analyses: Climate Extremes in the United States. *Bulletin of the American Meteorological Society*, 95, 571–583.

Yan, Q., H. J. Wang, O. M. Johannessen and Z. S. Zhang, 2014. Greenland ice sheet contribution to future global sea level rise based on CMIP5 models., Advances in Atmospheric Sciences, 31 (1): 8-16, **DOI:** 10.1007/s00376-013-3002-6

Yin, J. J. and P. B. Goddard, 2013. Oceanic control of sea level rise patterns along the East Coast of the United States, GRL, 40 (20): 5514-5520, **DOI:** 10.1002/2013GL057992

Yin, J., 2012. Century to multi-century sea level rise projections from CMIP5 models. Geophysical Research Letters, 39. doi:10.1029/2012GL052947.

Zahmatkesh, Z, M. Karamouz, E. Goharian, and S.J. Burian. 2014. "Analysis of the Effects of Climate Change on Urban Storm Water Runoff Using Statistically Downscaled Precipitation Data and a Change Factor Approach." *Journal of Hydrologic Engineering.*

Zhang, X., F. Zwiers, G. Hegerl, F.H. Lambert, N. Gillett, S. Solomon, P. Stott and T. Nozawa. 2007. Detection of human influence on twentieth-century precipitation trends. *Nature*, 448, 461-465.

Zhang, X., L. Alexander, G. C. Hegerl, P. Jones, A. K. Tank, T. C. Peterson, B. Trewin and F. W. Zwiers. 2011. Indices for monitoring changes in extremes based on daily temperature and precipitation data. *Wiley Interdisciplinary Reviews: Climate Change*, *2*(6), pp.851-870.

Zhang, X., H. Wan, F. Zwiers, G. Hegerl and S. Min. 2013. Attributing intensification of precipitation extremes to human influence. *Geophysical Research Letters*, 40(19), 5252–5257.

Annex A1: Collaborative Research Opportunity: Global Climate Model Datasets

Engineers often ask climate scientists how well climate models simulate weather. Climate scientists use a simulation framework to diagnose realism of historical weather as one step in establishing model reliability. The Atmospheric Model Intercomparison Project (AMIP) is one model evaluation step in the Coupled Model Intercomparis Project phase 6 design, having been a companion project with each previous phase. In AMIP simulations, only the atmosphere component of a global climate model is used. Instead of having an interactive ocean component, sea surface temperatures are set to observed values for each month. AMIP simulations by definition are only historical, and it is often assumed that they should reproduce observed, real world internal variability – i.e., if there is a heat wave in Chicago in 1995, then an AMIP simulation should also have a heat wave on the same dates in the same place. In reality, chaotic atmospheric processes and land interaction can create large dispersion in simulations, limiting the ability of climate models to replicate the historical sequence of weather.

AMIP simulations present engineers and climate scientists with a collaborative opportunity to evaluate climate model capability to replicate real world trends and events. If an AMIP poorly replicates the past, this means either the climate model is very poor or the internal variability is so large that the weather cannot be simulated with high precision. In either case, the result casts doubt on the ability to simulate a climate change signal. AMIP, therefore, provides a sort of minimum threshold test. The AMIP results demonstrate regions where AMIP cannot simulate the past well and this suggests the climate projections may not be able to diagnose a climate change signal. This and two other experimental climate model datasets not yet evaluated by engineers are available (Table 4.1).

Table 4.1. Global climate model collaborative research opportunities.

Dataset	Approach
Atmospheric Model Intercomparison Project	Models are given observed sea surface temperature, sea ice, and greenhouse gas concentration and evaluated for process realism.
Large Ensemble Experiment	Models are initialized from different starting conditions but given identical boundary conditions and evaluated for internal variability. This is essentially a small Monte Carlo approach containing no less than 40 simulations and provides a better estimate of extreme values.
Decadal Prediction Experiments	Models are used to forecast the next 10-30 yrs from present.

Annex A2: Summary of Evaluations of Downscaled Daily and Sub-Daily Precipitation.

Daily and sub-daily downscale precipitation is in the early stages of reliability evaluation. Most datasets are generated by individual scientists or science teams exploring a specific methodology for a specific region. Such experimental datasets are not suitable for widespread use.

A few archives have made available data from a small number of downscale approaches. Because of their accessibility, they have become widely used data for vulnerability assessment. Table 4.2 summarizes results from these studies. In general, they are incomplete evaluations of downscale data reliability, and the results should not be interpreted as simple error corrections that will make the data more reliable. In fact, only ARRM has been subjected to each category of performance evaluation in Table 2.3. We strongly recommend further research subjecting each dataset to the full performance evaluation described in Table 3 before extending their use beyond vulnerability assessments and pilot studies into the realm of engineering design criteria. Daily projections should be used with care; use of sub-daily projections is not recommended.

Table 4.2. Validity of available high-resolution climate projections.

Downscale Dataset	Summary of Evaluation
BCSD……....	(1) Values for 2-, 10-, 50-, and 100-yr return intervals for 1-, 2-, 3-, 4-, and 5-day precipitation using 1979 – 1999 calibration and 2001 – 2008 validation periods. (a) Similar results for each threshold. BCSD applied to monthly then disaggregated to daily is more accurate the BCSD applied to daily. Average error for 50-yr 1-day is -25% and +4% for BCSD applied to daily and monthly.
ARRM……....	(1) Values for 2-, 10-, 50-, and 100-yr return intervals for 1-, 2-, 3-, 4-, and 5-day precipitation using 1979 – 1999 calibration and 2001 – 2008 validation periods. (a) Similar results for each threshold. Average error for 50-yr 1-day is +6%. (2) Values for 75th, 95th, 99th, and 99.9th percentiles of daily precipitation during 1960 – 1999 with leave-one-year-out validation. (a) Errors small up to 99.9th percentile for which error is 0 – 20%.
BCCA……	(1) Values for 2-, 10-, 50-, and 100-yr return intervals for 1-, 2-, 3-, 4-, and 5-day precipitation using 1979 – 1999 calibration and 2001 – 2008 validation periods. (a) Similar results for each threshold. Average error for 50-yr 1-day is -40%.
LOCA……	(1) Values for 1-day annual maximum precipitation using 1970-2005 for calibration and 1940 – 1969 for testing (a) Error is +/- 20% in western United States but high correspondence to obs.
NARCCAP……..	(1) Values for 20-yr (P20) and 50-yr (P50) return interval for daily precipitation in spring, winter, summer, and fall for 1979 – 2004. (a) P20 and P50 error ranges 30 - 40%, -5 – 100%, 30 – 90% in winter, summer, and spring; smallest errors during fall in Hadley, Canadian models. (b) Spatial and temporal correspondence with measurements in the West but not central United States. (2) Intensity-Duration-Frequency curves for daily precipitation for 1979 - 2004.

	(a) Skewness, kurtosis parameters are poor from Great Lakes to Intermountain West. (b)Annual maximum precipitation overestimated in all models, ranging 25 – 200% with worst performance in Texas Plains, Florida, and southeast U. S. (3) Three-hourly precipitation during 1979 – 2006 for Allegheny County Pennsylvania. (a) Exceedance curves show close agreement with measurements for exceedance probability < 1%. For exceedance probability >1%, errors range -50% to +100% with three models having error +/- 5% (MM5I, HRM3, ECP2). (4) Three-hourly rainfall for simulations of 1993 June – July Midwest flood using thirteen regional climate models. Five models are predecessors of NARCCAP models. (a) Three-hourly rainfall exceeding 0.5" contributes smaller fraction to flood total rainfall in all models (10-30%) compared to station measurements (50%), except predecessors of NARCCAP models MM5I and ECP2. (b) Daily precipitation sequence poorly matches measurements.
	(1) Bias removed from European regional climate model with quantile mapping. (a) Bias remained for daily precipitation > 50 mm with range 10 – 30%
ENSEMBLES……..	

Appendix B. Detailed Information on ESDM and RCM Datasets

Table of Contents

Appendix B. Detailed Information on ESDM and RCM Datasets B-1

Table of Contents B-2

ARRM – Asynchronous Regional Regression Model – Gridded Output (Daily, U.S.) and Station Output (Daily, North/Central America) B-3
Dataset Details B-4

BCCA – Bias Correction-Constructed Analogs – Gridded Output (Daily, U.S.) B-5
Dataset Details B-5

BCSD – Bias Correction-Spatial Disaggregation – Gridded Output (Monthly, U.S.) B-7
Dataset Details B-7

LOCA – Localized Constructed Analogs – Gridded Output (Daily, U.S.) B-9
Dataset Details B-9

MACA v1 and v2 – Multivariate Adaptive Constructed Analogs – Gridded Output (Daily, U.S.) B-11
Dataset Details B-11

NEX-DCP30 – NEX Downscaled Climate Projections – Gridded Output (Monthly, U.S.) B-13
Dataset Details B-13

NEX-GDDP – NEX Global Daily Downscaled Projections – Gridded Output (Daily, Global) B-15
Dataset Details B-15

WorldClim version 1.4 – Gridded Output (Monthly, Global) B-17
Dataset Details B-17

NARCCAP – North American Regional Climate Change Assessment Program – Gridded Output (3-hourly, North America) B-19
Dataset Details B-19

NA-CORDEX – North American Coordinated Regional Climate Downscaling Experiment – Gridded Output (Daily, North America) B-20
Dataset Details B-20

These datasets are intended for use in scientific research only. Their use for other purposes, such as commercial applications, and engineering or design studies should only be considered after consultation with a qualified expert or based on credible written guidance.

ARRM – Asynchronous Regional Regression Model – Gridded Output (Daily, U.S.) and Station Output (Daily, North/Central America)

The asynchronous regional regression model (ARRM) method and dataset is an empirical statistical downscaling method that uses *parametric quantile regression* to determine relationships between two quantities that do not have temporal correspondence, but that are expected to have similar statistical properties such as mean and variance. The basic premise of asynchronous regression is to re-order a time series by rank, removing the time signature: an appropriate technique when working with observations and global climate model outputs at the same time, since there is no day-to-day correspondence between the two. In ARRM, daily values for each month are ranked and observed values plotted against modeled values separately for each month from 1960 to 2010. Each monthly relationship between observed and modeled values is quantified using piecewise linear regression, with breakpoints placed where the slope changes the most. This relationship is then used to bias-correct historical and future global climate model output. Additional steps such as pre-filtering the global climate model output fields using principal component analyses to remove low-level noise, spatial interpolation of the global model to the scale of the observations, and distinguishing between convective and large-scale precipitation further improves the relationship between observations and global model simulations.

The *advantages* of this dataset are that this method focuses on the details at the tails of the probability distribution (extreme values). It allows the shape of the distribution to change over time, including shifts in the mean, the variance, and even the skewness (symmetry) of the distribution. And it is the only dataset with both grid- and station-based values available, which allows for better resolution of extremes that tend to be smoothed out and diminished over a grid.

As with any empirical statistical downscaling method, ARRM assumes stationarity (i.e. that the derived relationship between observations and GCM output will continue to hold true in the future), and it also assumes that observations represent ground-truth, even though in reality observations may also contain errors and biases – although it does rely on a pre-existing gridded dataset with documented quality control, and conducts additional quality control for the station data prior to downscaling.

Some additional *disadvantages* of the gridded ARRM dataset are that, first, it is downscaled grid cell by grid cell, which can create discontinuities along grid cell boundaries. Discontinuities have mainly been observed in the precipitation dataset and for this reason, precipitation is analyzed in overlapping segments of 3x3 grid cells rather than individually. Second, for both grid and station values, at the tails of the distribution the slope of the line can be sensitive to outliers. This leads to a known bias towards over-estimating projected changes in extreme heat days beyond the 99th percentile of the distribution for locations within a few grid cells of ocean coastlines.

Disclaimer: Due to the known bias in extreme high temperatures along coastlines, this dataset is not recommended for projections of extreme heat in coastal locations.

Dataset Details

Dataset hosted by:	TTU Climate Science Center
Website:	https://www.depts.ttu.edu/csc/
Data Format:	NetCDF
CMIP Generation:	CMIP3
Available GCMs:	CCSM3, CGCM3-T47, CGCM3-T63, CNRM, CSIRO, ECHAM5, ECHO, GFDL2.0, GFDL2.1, GISS-AOM, HadCM3, HadGEM, MIROC-med, MIROC-hi, MRI-CGCM2, PCM
Future Scenarios:	SRES A1FI, A2, A1B, B1
Variables:	Daily maximum temperature, daily minimum temperature, daily total (convective + large-scale) precipitation
Time Period of Output:	1960-2099
Time Frequency:	Daily
Spatial Grid Coverage:	Continental U.S., southern Canada, northern Mexico (25.1875-52.5626N, 67.0325-124.6875W) Alaska (50.25-72.75N, 125.75-174.25W)
Resolution:	CONUS: 1/8th degree ~ 12 km Alaska: 0.5 degree ~ 55 km
Observational Training Dataset:	Maurer 1/8th degree Gridded Meteorological Data
Reference:	Stoner, A., K. Hayhoe, X. Yang and D. Wuebbles. 2013. An Asynchronous Regional Regression Model to Downscale Daily Temperature and Precipitation Climate Projections. International Journal of Climatology. DOI 10.1002/joc.3603.

BCCA – Bias Correction-Constructed Analogs – Gridded Output (Daily, U.S.)

The Bias Correction-Constructed Analogs (BCCA) method and dataset is an empirical statistical downscaling method that adjusts global climate model output in two steps. First, the GCM output is bias-corrected relative to observations by generating an empirical cumulative distribution function (CDF) for observations and for GCM simulations for each day of the year, from 1950 through 2005. It then compares the two CDFs at various probability thresholds to establish an *empirical quantile mapping* between the GCM data and the observations. This relationship is used to bias-correct historical and future global climate model output by looking up the probability quantile associated with the predicted climate values from the estimated GCM CDF and identifying the corresponding observed climate values at the same probability quantile in the observed CDF. Second, the entire domain is spatially downscaled by identifying a set of observed day-specific conditions at 2 degree resolution that approximate the bias-corrected GCM conditions for a given day from 1950 to 1999. The specific dates, appropriately weighted, that contribute to this "coarse resolution" whole-domain analog are then combined with the high-resolution versions of the day-specific observational dataset conditions in order to generate the final product.

Some *advantages* of this approach are that it is spatially coherent, with no discontinuities at grid cell boundaries. It mimics realistic large-scale weather patterns, and the use of constructed analogs allows for realistically sharp spatial gradients for daily temperature and precipitation.

As with any empirical statistical downscaling method, BCCA assumes stationarity (i.e. that the derived relationship between observations and GCM output will continue to hold true in the future), and it also assumes that observations represent ground-truth, even though in reality observations may also contain errors and biases – although it does rely on a pre-existing gridded dataset with documented quality control.

Some additional *disadvantages* are that the approach also must assume that the spatial patterns of temperature and precipitation across the U.S. that were observed from 1950 through 1999 will remain constant under future climate change. Also, this approach is restricted in that it only allows for weather patterns that have previously occurred. Finally, a dry bias has been identified in this dataset, affecting much of the contiguous U.S. Specifically, the downscaled GCM precipitation during the 20th century for some areas was up to 20% below observed climatology. This bias has been corrected with a simple bias-correction method as described in the Errata and FAQ on the website below. The corrected BCCA precipitation files are referred to as BCCAv2. No changes were made to the BCCA temperature files.

Disclaimer: Due to the known bias in average precipitation in many areas of the continuous U.S. and the simple correction that has been applied, extreme caution is recommended when using this dataset for projections of historical or future precipitation.

Dataset Details

Dataset hosted by:	Bureau of Reclamation, Climate Analytics Group, Climate Central, Lawrence Livermore National Laboratory, Santa Clara University, Scripps Institution of Oceanography, U.S. Army Corps of Engineers, and USGS
Website:	http://gdo-dcp.ucllnl.org
Data Format:	NetCDF, ASCII text
CMIP Generation:	CMIP3 and CMIP5

Available GCMs:	CMIP3: BCCR-BCM2.0, CCSM3, CGCM3-T47, CNRM-CM3, CSIRO-Mk3.0, ECHAM5, ECHO-G, GFDL-CM2.0, GFDL-CM2.1, GISS-ER, HadCM3, INM-CM3.0, IPSL-CM4, MIROC3.2-med, MRI-CGCM2.3.2, PCM CMIP5: ACCESS1-0, ACCESS1-3, BCC-CSM1-1, BCC-CSM1-1-M, BNU-ESM, CanESM2, CCSM4, CESM1-BGC, CESM1-CAM5, CMCC-CM, CNRM-CM5, CSIRO-Mk-3-6-0, EC-EARTH, FGOALS-g2, FGOALS-s2, FIO-ESM, GFDL-CM3, GFDL-ESM2G, GFDL-ESM2M, GISS-E2-H-CC, GISS-E2-R, GISS-E2-R-CC, HADGEM2-AO, HADGEM2-CC, HADGEM2-ES, INMCM4, IPSL-CM5A-LR, IPSL-CM5A-MR, IPSL-CM5B-LR, MIROC-ESM, MIROC-ESM-CHEM, MIROC5, MPI-ESM-LR, MPI-ESM-MR, MRI-CGCM3, NorESM1-M, NorESM1-ME
Future Scenarios:	CMIP3: SRES A2, A1B, B1 CMIP5: RCP2.6, RCP4.5, RCP6.0, RCP8.5
Variables:	Daily maximum temperature, daily minimum temperature, daily total precipitation
Time Period of Output:	CMIP3: 1961-2000, 2046-2065, 2081-2100 CMIP5: 1950-2099
Time Frequency:	Daily
Spatial Grid Coverage:	Continental U.S., southern Canada, northern Mexico (25.125-52.875N, 67-124.625W)
Resolution:	CMIP3: 1/8th degree ~ 12 km and 2 degrees ~ 222 km CMIP5: 1/8th degree ~ 12 km and 1 degree ~ 111 km
Observational Training Dataset:	Maurer 1/8th degree Gridded Meteorological Data
Reference:	Maurer, E. P., L. Brekke, T. Pruitt, and P. B. Duffy, 2007. 'Fine-resolution climate projections enhance regional climate change impact studies', Eos Trans. AGU, 88(47), 504. Reclamation, 2013. 'Downscaled CMIP3 and CMIP5 Climate and Hydrology Projections: Release of Downscaled CMIP5 Climate Projections, Comparison with preceding Information, and Summary of User Needs', prepared by the U.S. Department of the Interior, Bureau of Reclamation, Technical Services Center, Denver, Colorado. 47pp.

BCSD – Bias Correction-Spatial Disaggregation – Gridded Output (Monthly, U.S.)

The Bias Correction-Spatial Disaggregation (BCSD) method and dataset is an empirical statistical downscaling method that adjusts global climate model output in two steps. First, the GCM output is bias-corrected relative to observations by generating an empirical cumulative distribution function (CDF) for observations and for GCM simulations for each month of the year, from 1950 through 2005. It then compares the two CDFs at various probability thresholds to establish an *empirical quantile mapping* between the GCM data and the observations. This relationship is used to bias-correct historical and future global climate model output by looking up the probability quantile associated with the predicted climate values from the estimated GCM CDF and identifying the corresponding observed climate values at the same probability quantile in the observed CDF. Second, the bias-corrected GCM simulations are spatially disaggregated by combining the observed high-resolution climatology with the spatially disaggregated bias-corrected changes derived from the GCM relative to the same climatological period.

Some *advantages* of this dataset are that it allows for changes in the shape of the future probability distribution and it successfully reproduces observed means and non-extreme variability. It was originally developed for hydrological applications at the basin scale and has been widely used across a broad range of studies and applications.

As with any empirical statistical downscaling method, BCSD assumes stationarity (i.e. that the derived relationship between observations and GCM output will continue to hold true in the future), and it also assumes that observations represent ground-truth, even though in reality observations may also contain errors and biases – although it does rely on a pre-existing gridded dataset with documented quality control.

Some additional *disadvantages* are that it specifically assumes the processes determining how precipitation and temperature anomalies for any coarse GCM grid cell are distributed to fine $1/8^{th}$ degree grid within that coarser grid box will be the same in the future as they have been in the past. Furthermore, this methodology uses GCM monthly outputs only. This means that the frequency of wet and dry days will remain unchanged in the future.

Disclaimer: Due to the fact that this method uses only GCM monthly inputs, it is not recommended for application to projected changes extreme precipitation.

Dataset Details

Dataset hosted by:	Bureau of Reclamation, Climate Analytics Group, Climate Central, Lawrence Livermore National Laboratory, Santa Clara University, Scripps Institution of Oceanography, U.S. Army Corps of Engineers, and USGS
Website:	http://gdo-dcp.ucllnl.org
Data Format:	NetCDF, ASCII, CSV
CMIP Generation:	CMIP3 and CMIP5
Available GCMs:	CMIP3: BCCR-BCM2.0, CCSM3, CGCM3-T47, CNRM-CM3, CSIRO-Mk3.0, ECHAM5, ECHO-G, GFDL-CM2.0, GFDL-CM2.1, GISS-ER, HadCM3, INM-CM3.0, IPSL-CM4, MIROC3.2-med, MRI-CGCM2.3.2, PCM CMIP5: ACCESS1-0, ACCESS1-3, BCC-CSM1-1, BCC-CSM1-1-M, BNU-ESM, CanESM2, CCSM4, CESM1-BGC, CESM1-CAM5, CMCC-CM, CNRM-CM5, CSIRO-Mk-3-6-0, EC-EARTH, FGOALS-g2, FGOALS-s2, FIO-ESM, GFDL-CM3, GFDL-ESM2G, GFDL-ESM2M, GISS-E2-H-CC, GISS-E2-R, GISS-E2-R-CC, HADGEM2-AO, HADGEM2-CC, HADGEM2-ES, INMCM4, IPSL-CM5A-LR, IPSL-

	CM5A-MR, IPSL-CM5B-LR, MIROC-ESM, MIROC-ESM-CHEM, MIROC5, MPI-ESM-LR, MPI-ESM-MR, MRI-CGCM3, NorESM1-M, NorESM1-ME
Future Scenarios:	CMIP3: SRES A2, A1B, B1
	CMIP5: RCP2.6, RCP4.5, RCP6.0, RCP8.5
Variables:	Monthly mean maximum temperature, monthly mean minimum temperature, monthly total precipitation, streamflow
Time Period of Output:	CMIP3: 1961-2000, 2046-2065, 2081-2100
	CMIP5: 1950-2099
Time Frequency:	Monthly (climate), daily (streamflow, CMIP3 only)
Spatial Grid Coverage:	Continental U.S., southern Canada, northern Mexico (25.125-52.875N, 67-124.625W)
Resolution:	CMIP3: 1/8th degree ~ 12 km and 2 degrees ~ 222 km
	CMIP5: 1/8th degree ~ 12 km and 1 degree ~ 111 km
Observational Training Dataset:	Maurer 1/8th degree Gridded Meteorological Data
Reference:	Maurer, E. P., L. Brekke, T. Pruitt, and P. B. Duffy, 2007. 'Fine-resolution climate projections enhance regional climate change impact studies', Eos Trans. AGU, 88(47), 504.
	Reclamation, 2013. 'Downscaled CMIP3 and CMIP5 Climate and Hydrology Projections: Release of Downscaled CMIP5 Climate Projections, Comparison with preceding Information, and Summary of User Needs', prepared by the U.S. Department of the Interior, Bureau of Reclamation, Technical Services Center, Denver, Colorado. 47pp.

LOCA – Localized Constructed Analogs – Gridded Output (Daily, U.S.)

The LOcalized Constructed Analogs (LOCA) method and dataset is an empirical statistical downscaling method that uses a multiscale spatial matching scheme to select appropriate analog days for both historical and future GCM simulations from observations. First, a pool of candidate observed analog days is chosen by matching the GCM field for a given variable over the entire region to be downscaled to observed days over the same region that are positively correlated with the point being downscaled. This leads to a natural independence of the downscaling results to the extent of the domain being downscaled. Then, the one candidate analog day that best matches in the local area around the grid cell being downscaled is selected as the analog day to use for that location. Most grid cells are downscaled using only the single locally selected analog day, but locations whose neighboring cells identify a different analog day use a weighted combination of the center and adjacent analog days to reduce edge discontinuities. This is a significant improvement over previous constructed analog methods that used a weighted average of the same 30 analog days for the entire domain.

The bias correction step used for LOCA also represents a significant improvement over previous use of quantile mapping and cumulative distribution functions. As noted by Pierce et al. (2015), standard methods can alter the amount of change projected by a GCM by up to 2ºC for temperature and 30% for precipitation. Instead, LOCA uses an equidistant quantile mapping with an extension, referred to as PresRat, specifically aimed at preserving the change in precipitation projected by the original GCM. It also corrects for GCM biases in simulating variance as a function of frequency, including frequency-dependent bias corrections.

Some *advantages* of this dataset are that it does a better job than previous bias correction and constructed analog methods (BCCA, MACA) at maintaining both regional patterns of precipitation and the future climate changes predicted by reducing the averaging of historical information. Previous techniques typically used a weighted average of 30 similar historical days, while LOCA identifies the one best matching day. As noted above, it also includes several improvements and adjustments to the bias correction technique, to account for known issues in both the statistical techniques and the GCM simulations.

As with any empirical statistical downscaling method, LOCA assumes stationarity (i.e. that the derived relationship between observations and GCM output will continue to hold true in the future), and it also assumes that observations represent ground-truth, even though in reality observations may also contain errors and biases – although it does rely on a pre-existing gridded dataset with documented quality control.

Some *disadvantages* are that any form of constructed analogs specifically assumes stationarity in weather patterns, and only allows for weather patterns that have previously occurred in the historical record. LOCA reduces smoothing, but still has smoothing of grid cells along edges of point pools (30% of area). Furthermore, the method cannot preserve model-predicted mean precipitation change in very dry areas with insufficient precipitation days to bias correct.

Dataset Details

Dataset hosted by:	Center for Integrated Data Analytics
Website:	**https://gdo-dcp.ucllnl.org/downscaled_cmip_projections/dcpInterface.html**
Data Format:	NetCDF, ASCII, CSV

CMIP Generation:	CMIP5
Available GCMs:	ACCESS1-0, ACCESS1-3, BCC-CSM-1-M, CCSM4, CESM1-BGC, CESM1-CAM5, CMCC-CM, CMCC-CMS, CNRM-CM5, CSIRO-Mk3-6-0, CanESM2, EC-EARTH, FGOALS-g2, GFDL-CM3, GFDL-ESM2G, GFDL-ESM2M, GISS-E2-H, GISS-E2-R, HadGEM2-AO, HadGEM2-CC, HadGEM2-ES, IPSL-CM5A-LR, IPSL-CM5A-MR, MIROC5, MIROC-ESM, MIROC-ESM-CHEM, MPI-ESM-LR, MPI-ESM-MR, MRI-CGCM3, Nor-ESM1-M
Future Scenarios:	RCP4.5, RCP8.5
Variables:	Daily maximum and minimum temperature, daily total precipitation (more variables to come)
Time Period of Output:	1950-2100
Time Frequency:	Daily
Spatial Grid Coverage:	Continental U.S. (24-53N, 67-125W)
Resolution:	$1/16^{th}$ degree (~ 6 km)
Observational Training Dataset:	Livneh et al., 2013. ($1/16^{th}$ degree ~ 6 km resolution)
References:	Pierce, D.W., D.R. Cayan, and B.L. Thrasher, 2014. Statistical Downscaling using Localized Constructed Analogs (LOCA). *J. Hydrometeorology*, 15, 2558-2585. Pierce, D.W., D.R. Cayan, E.P. Maurer, J.T. Abatzoglou, and H.C. Hegewisch, 2015. Improved Bias Correction Techniques for Hydrological Simulations of Climate Change. *J. Hydrometeorology*, 16, 2421-2442.

MACA v1 and v2 – Multivariate Adaptive Constructed Analogs – Gridded Output (Daily, U.S.)

The Multivariate Adaptive Constructed Analogs (MACA) method and dataset is an empirical statistical downscaling method that pattern-matches anomaly fields (the differences in a given variable on a given day relative to the long-term climatology) and combines this with empirical quantile mapping to downscale daily GCM output. Using a 21-day moving window, it builds a daily GCM field ('target' pattern) by identifying the best predictor patterns from a library of observed patterns that fall within 45 days of the target date and combines the accompanying fine-scale observed patterns of the best matches to yield the downscaled field.

One important feature of the MACA method is that downscaling is performed jointly for temperature (maximum and minimum) and dew point temperature to improve coherence across downscaled fields. Analogs are identified separately for wind velocity and precipitation due to the inability to easily weight the influence of all variables in an analog search. Another important feature is that the analogs are adjusted to account for analogs that may emerge or disappear in the future. And finally, the empirical or non-parametric bias correction step that maps the CDF of the historical and future GCM output to the CDF of the observations is applied twice: first to the raw GCM output, and second to the spatially disaggregated or fine-scale GCM output after the constructed analogs step has been applied.

One key *advantage* of this dataset is that its multivariate approach improves the physical relationships between variables. This is advantageous compared to methods that treat variables independently.

As with any empirical statistical downscaling method, MACA assumes stationarity (i.e. that the derived relationship between observations and GCM output will continue to hold true in the future), and it also assumes that observations represent ground-truth, even though in reality observations may also contain errors and biases – although it does rely on a pre-existing gridded dataset with documented quality control.

Some *disadvantages* are that any form of constructed analogs specifically assumes some type of stationarity in weather patterns, even with MACA's "epoch adjustment" technique; although the magnitude of the variable is allowed to move beyond observed, it still only allows for weather patterns that have previously occurred in the historical record.

Some *disadvantages* are that the accuracy of this method degrades near the tails of the distribution, resulting in extremes that are generally under-estimated.

Dataset Details

Dataset hosted by:	University of Idaho, Northwest Knowledge Network
Website:	https://climate.northwestknowledge.net/MACA/
Data Format:	NetCDF
CMIP Generation:	CMIP5
Available GCMs:	BCC-CSM1-1, BCC-CSM1-1-M, BNU-ESM, CCSM4, CNRM-CM5, CSIRO-Mk3-6-0, CanESM2, GFDL-ESM2G, GFDL-ESM2M, HadGEM2-CC, HadGEM2-ES, INMCM4, IPSL-CM5A-LR, IPSL-CM5A-MR, IPSL-CM5B-LR, MIROC5, MIROC-ESM, MIROC-ESM-CHEM, MRI-CGCM3, Nor-ESM1-M
Future Scenarios:	RCP4.5, RCP8.5

Variables:	Daily maximum and minimum temperature, daily total precipitation, daily maximum and minimum relative humidity, daily average zonal and meridional wind, downward shortwave radiation flux at surface, specific humidity
Time Period of Output:	MACAv1: 1950-2100, MACAv2: 1950-2099
Time Frequency:	Daily, monthly
Spatial Grid Coverage:	Continental U.S.
Resolution:	METDATA version: 4 km, LIVNEH version: 1/16th degree ~ 6 km
Observational Training Dataset:	METDATA version: University of Idaho Gridded Surface Meteorological Data (METDATA, 4km resolution)
	LIVNEH version: Livneh et al., 2013. (1/16th degree resolution)
Reference:	Abatzoglou, J.T., and T.J. Brown (2011): A comparison of statistical downscaling methods suited for wildfire applications. Intl. J. Climatol., 32, 772-780.

NEX-DCP30 – NEX Downscaled Climate Projections – Gridded Output (Monthly, U.S.)

The NASA Earth Exchange (NEX) Downscaled Climate Projections dataset uses the Bias Correction-Spatial Disaggregation (BCSD) method described above. BCSD is an empirical statistical downscaling method that adjusts global climate model output in two steps. First, the GCM output is bias-corrected relative to observations by generating an empirical cumulative distribution function (CDF) for observations and for GCM simulations for each month of the year, from 1950 through 2010. It then compares the two CDFs at various probability thresholds to establish an *empirical quantile mapping* between the GCM data and the observations. This relationship is used to bias-correct historical and future global climate model output by looking up the probability quantile associated with the predicted climate values from the estimated GCM CDF and identifying the corresponding observed climate values at the same probability quantile in the observed CDF. Second, the bias-corrected GCM simulations are spatially disaggregated by interpolating the bias-corrected changes derived from the GCM to an extremely fine resolution grid of 30 arc-seconds or 0.008 degrees, based on.

Both the NEX-DCP30 and the BCSD datasets cover the U.S. They differ in their temporal and spatial resolution due to the observational data used as the basis for the bias correction. NEX is an extremely high-resolution dataset of monthly projections based on the PRISM system (Parameter-elevation Regressions on Independent Slopes Model; Daly et al. 1994). PRISM is a very high resolution observational dataset of temperature and precipitation from 1950 to 2010 that combines ground-based observations, a digital elevation model, and expert analysis of complex phenomena such as rain shadows that become important at high spatial resolutions.

Some *advantages* of this dataset are that it allows for changes in the shape of the future probability distribution and it successfully reproduces observed means and non-extreme variability. It was originally developed for hydrological applications at the basin scale and has been widely used across a broad range of studies and applications. Finally, the NEX dataset is the highest-resolution dataset of projections for the U.S.

As with any empirical statistical downscaling method, BCSD assumes stationarity (i.e. that the derived relationship between observations and GCM output will continue to hold true in the future), and it also assumes that observations represent ground-truth, even though in reality observations may also contain errors and biases – although it does rely on a pre-existing gridded dataset with documented quality control.

Some additional *disadvantages* are that it specifically assumes the processes determining how precipitation and temperature anomalies for any coarse GCM grid cell are distributed to the fine 0.008 degree grid within that coarser grid box will be the same in the future as they have been in the past. Furthermore, this methodology uses GCM monthly outputs only, which means that the frequency of wet and dry days will remain unchanged in the future, and it only provides monthly outputs.

Disclaimer: Due to the fact that this method uses only GCM monthly inputs and provides monthly outputs, it cannot be applied to study projected changes extreme precipitation.

Dataset Details

Dataset hosted by:	NCCS THREDDS
Website:	https://dataserver.nccs.nasa.gov/thredds/bypass/NEX-DCP30/catalog.html
Data Format:	NetCDF

CMIP Generation:	CMIP5
Available GCMs:	ACCESS1-0, BCC-CSM1-1, BCC-CSM1-1-M, BNU-ESM, CanESM2, CCSM4, CESM1-BGC, CESM1-CAM5, CMCC-CM, CNRM-CM5, CSIRO-Mk3-6-0, EC-EARTH, FGOALS-g2, FIO-ESM, GFDL-CM3, GFDL-ESM2G, GFDL-ESM2M, GISS-E2-H-CC, GISS-E2-H, GISS-E2-R-CC, HadGEM2-AO, HadGEM2-CC, HadGEM2-ES, INMCM4, IPSL-CM5A-LR, IPSL-CM5A-MR, IPSL-CM5B-LR, MIROC5, MIROC-ESM, MIROC-ESM-CHEM, MPI-ESM-LR, MPI-ESM-MR, MRI-CGCM3, Nor-ESM1-M
Future Scenarios:	RCP2.6, RCP4.5, RCP6.0, RCP8.5
Variables:	Maximum and minimum temperature, total precipitation
Time Period of Output:	1950-2099
Time Frequency:	Monthly
Spatial Grid Coverage:	CONUS
Resolution:	30 arc seconds (~ 800 m)
Observational Training Dataset:	Parameter-Elevation Regressions on Independent Slopes Model (PRISM) (30 arc seconds ~ 800 m resolution)
References:	Thrasher, B., Xiong, J., Wang, W., Melton, F., Michaelis, A., and R. Nemani, 2013. Downscaled Climate Projections Suitable for Resource Management. *Eos, Transactions American Geophysical Union*, 94, 321-323.

NEX-GDDP – NEX Global Daily Downscaled Projections – Gridded Output (Daily, Global)

The NASA Earth Exchange (NEX) Downscaled Climate Projections dataset uses the Bias Correction-Spatial Disaggregation (BCSD) method described above. BCSD is an empirical statistical downscaling method that adjusts global climate model output in two steps. First, the GCM output is bias-corrected relative to observations by generating an empirical cumulative distribution function (CDF) for observations and for GCM simulations for each month of the year, from 1950 through 2005. It then compares the two CDFs at various probability thresholds to establish an *empirical quantile mapping* between the GCM data and the observations. This relationship is used to bias-correct historical and future global climate model output by looking up the probability quantile associated with the predicted climate values from the estimated GCM CDF and identifying the corresponding observed climate values at the same probability quantile in the observed CDF. Second, the bias-corrected GCM simulations are spatially disaggregated by interpolating the bias-corrected changes derived from the GCM to the finer resolution grid of the 0.25-degree GMFD data.

The primary differences between the NEX-GDDP dataset and the BCSD dataset are the spatial extent and the observational data used as the basis for the bias correction. Both use monthly GCM simulations as input to produce daily output. However, NEX is a global dataset that uses Global Meteorological Forcing Dataset (GMFD) that combines reanalysis data with daily observations at a spatial resolution of 0.25 degrees.

Some *advantages* of this dataset are that it allows for changes in the shape of the future probability distribution and it successfully reproduces observed means and non-extreme variability. It was originally developed for hydrological applications at the basin scale and has been widely used across a broad range of studies and applications. Finally, the NEX dataset is the only global-scale dataset of daily temperature and precipitation projections currently available.

As with any empirical statistical downscaling method, BCSD assumes stationarity (i.e. that the derived relationship between observations and GCM output will continue to hold true in the future), and it also assumes that observations represent ground-truth, even though in reality observations may also contain errors and biases – although it does rely on a pre-existing gridded dataset with documented quality control.

Some additional *disadvantages* are that it specifically assumes the processes determining how precipitation and temperature anomalies for any coarse GCM grid cell are distributed to the fine 0.25 degree grid within that coarser grid box will be the same in the future as they have been in the past. Furthermore, this methodology uses GCM monthly outputs only, and samples the daily sequence from observations. This means that the frequency of wet and dry days will remain unchanged in the future. And finally, for the U.S., the spatial resolution of this dataset is relatively coarse compared to the others described above.

Disclaimer: Due to the fact that this method uses only GCM monthly inputs, it is not recommended for application to projected changes in extreme precipitation.

Dataset Details

Dataset hosted by: NCCS THREDDS

Website:	https://dataserver.nccs.nasa.gov/thredds/catalog/bypass/NEX-GDDP/catalog.html
Data Format:	NetCDF
CMIP Generation:	CMIP5
Available Downscaled GCMs:	ACCESS1-0, BCC-CSM1-1, BNU-ESM, CanESM2, CCSM4, CESM1-BGC, CNRM-CM5, CSIRO-Mk3-6-0, GFDL-CM3, GFDL-ESM2G, GFDL-ESM2M, INMCM4, IPSL-CM5A-LR, IPSL-CM5A-MR, MIROC5, MIROC-ESM, MIROC-ESM-CHEM, MPI-ESM-LR, MPI-ESM-MR, MRI-CGCM3, Nor-ESM1-M
Future Scenarios:	RCP4.5, RCP8.5
Variables:	Daily maximum and minimum temperature, daily total precipitation
Time Period of Output:	1950-2100
Time Frequency:	Daily
Spatial Grid Coverage:	Global
Resolution:	1/4th degree (~ 25 km)
Observational Training Dataset:	Global Meteorological Forcing Dataset (GMFD) (1/4th degree ~ 25 km resolution)
References:	Thrasher, B., Maurer, E. P., McKellar, C., & Duffy, P. B., 2012: Technical Note: Bias correcting climate model simulated daily temperature extremes with quantile mapping. *Hydrology and Earth System Sciences*, 16(9), 3309-3314.

WorldClim version 1.4 – Gridded Output (Monthly, Global)

The WorldClim Global Climate Data portal uses an extremely simple empirical statistical downscaling method known as the "delta method." For each month, it calculates the difference between future GCM temperature and precipitation values and the GCM-simulated values for the same month for a historical climatological period (here, 1960-1990). It then applies this difference, or "delta," to observed values for a high-resolution grid of 30 arc-seconds obtained by interpolating terrestrial weather station data. In addition to maximum and minimum temperature and precipitation, this method also calculates a suite of bioclimatic indicators relevant to ecosystem analyses for the climatological average of one historical and two future periods: 1960-1990, 2041-2060 and 2061-2080.

Some *advantages* of this dataset are that it is available at four different very high spatial resolutions, and covers the entire world. It was originally developed for macro-scale ecological applications and has been widely used across a broad range of studies and applications.

As with any empirical statistical downscaling method, the delta method assumes stationarity (i.e. that the derived relationship between observations and GCM output will continue to hold true in the future), and it also assumes that observations represent ground-truth, even though in reality observations may also contain errors and biases.

Some additional *disadvantages* of this method are that it specifically assumes that the shape of the distribution of monthly values will not change in the future—only the mean will shift. If the distribution becomes more skewed in one direction or the other, this means that the delta method will under-estimate the potential for more extreme monthly values. In addition, it only provides monthly outputs and a climatological average for two future time periods.

Disclaimer: Due to the fact that this method uses only GCM monthly inputs and provides monthly outputs, it cannot be applied to study projected changes in extreme precipitation; in addition, the simple delta method cannot be recommended due to its assumption that the shape of the distribution of monthly values remains unchanged.

Dataset Details

Dataset hosted by:	WorldClim
Website:	http://www.worldclim.org
Data Format:	TIF
CMIP Generation:	CMIP5
Available GCMs:	ACCESS1-0, BCC-CSM1-1, CCSM4, CESM1-CAM5, CNRM-CM5, GFDL-CM3, GFDL-ESM2G, GISS-E2-R, HadGEM2-AO, HadGEM2-CC, HadGEM2-ES, INMCM4, IPSL-CM5A-LR, MIROC5, MIROC-ESM, MIROC-ESM-CHEM, MPI-ESM-LR, MRI-CGCM3, Nor-ESM1-M
Future Scenarios:	RCP2.6, RCP4.5, RCP6.0, RCP8.5
Variables:	Maximum and minimum temperature, precipitation, BIOCLIM variables
Time Period of Output:	Three periods only (1960-1990, 2041-2060 and 2061-2080)
Time Frequency:	Monthly, climatological averages
Spatial Grid Coverage:	Global
Resolution:	10 min, 5 min, 1 min and 30 arc seconds (~ 800 m)

Observational Training Dataset:	Hijmans, R.J., Cameron, S., Parra, J., Jones, P. and Jarvis, A., 2005. Very high resolution interpolated climate surfaces for global land areas. *International Journal of Climatology*, 25: 1965-1978.
References:	Ibid.

NARCCAP – North American Regional Climate Change Assessment Program – Gridded Output (3-hourly, North America)

The North American Regional Climate Change Assessment Program (NARCCAP) hosts an archive of high-resolution regional climate model (RCM) outputs, referred to as dynamically downscaled projections. As with the empirical statistical downscaling methods and archives above, the primary purpose of NARCCAP is to allow scientists investigate uncertainties in regional scale projections of future climate and generate climate change scenarios for use in impacts research.

NARCCAP consists of the output from a set of RCMs driven by a set of GCMs over a domain covering the conterminous United States and most of Canada.

Some *advantages* of this dataset are that it contains 3-hourly data for all of North America and includes a large suite of surface and upper air variables not normally available in statistically downscaled products. Furthermore, it has a coherent spatial structure and interdependency between variables.

Some *disadvantages* are that the simulations only include one future mid-high scenario (SRES A2), only has 2 future 30-year periods as opposed to being continuous, uses a limited number of previous-generation CMIP3 GCMs as input, and has a spatial resolution which is still fairly coarse (50 km).

Dataset Details

Dataset hosted by:	Earth System Grid
Website:	https://www.earthsystemgrid.org/project/NARCCAP.html
Data Format:	NetCDF
CMIP Generation:	CMIP3
Available GCMs:	CCSM3, CGCM3, GFDL-CM2.1, HadCM3
Available RCMs:	CRCM, ECP2, HRM3, MM5I, RCM3, WRFG, ECPC, WRFP
Future Scenarios:	SRES A2
Variables:	42 different variables ranging from temperature-, precipitation-, humidity-, wind-related variables to cloud fraction, heat flux, surface runoff, and others
Time Period of Output:	1968-2000, 2038-2070
Time Frequency:	3-hourly
Spatial Grid Coverage:	North America
Resolution:	50 km
References:	Mearns, L.O., et al., 2007, updated 2014. *The North American Regional Climate Change Assessment Program dataset*, National Center for Atmospheric Research Earth System Grid data portal, Boulder, CO.

NA-CORDEX – North American Coordinated Regional Climate Downscaling Experiment – Gridded Output (Daily, North America)

The North American CORDEX (NA-CORDEX) Program also hosts a growing archive of high-resolution regional climate model (RCM) outputs, referred to as dynamically downscaled projections. NA-CORDEX is the North American branch of the International CORDEX Initiative, sponsored by the World Climate Research Program (WCRP). CORDEX is providing global coordination of regional climate downscaling for improved regional climate change adaptation and impact assessment.

Some *advantages* of this dataset are that it provides a long list of daily surface and upper air variables and has a coherent spatial structure and variable interdependency. Compared to NARCCAP, it uses a more recent set of CMIP5 GCM inputs and provides output for both a higher and a lower future scenario.

Some *disadvantages* are that the simulations still only include a limited number of GCMs, and the spatial resolution is still fairly coarse (25-50 km).

Dataset Details

Dataset hosted by:	Earth System Grid
Website:	https://www.earthsystemgrid.org/search/cordexsearch.html
Data Format:	NetCDF
CMIP Generation:	CMIP5
Available GCMs:	CanESM2, EC-EARTH, GFDL-ESM2M, HadGEM2-ES, MPI-ESM-LR, MPI-ESM-MR
Available RCMs:	CRCM5, RCA4, RegCM4, WRF, CanRCM4, HIRHAM5
Future Scenarios:	RCP4.5, RCP8.5
Variables:	30 different variables ranging from temperature-, precipitation-, humidity-, wind-related variables to cloud fraction, heat flux, surface runoff, and others (not all variables are available for all models)
Time Period of Output:	1950-2100
Time Frequency:	Daily, some models have sub-daily precipitation
Spatial Grid Coverage:	North America
Resolution:	25-50 km
References:	Giorgi, F., C. Jones, and G.R. Asrar, 2009. Addressing Climate Information Needs at the Regional Level: The CORDEX Framework. *World Meteorological Organization Bulletin*, 58, 175-183.

Appendix C. Continuous Simulation Watershed Models for Climate Change Studies

Table of Contents

Appendix C. Continuous Simulation Watershed Models for Climate Change Studies C-1

Table of Contents C-2

HSPF Model C-3

SWAT Model C-3

BASINS CAT Tool C-4

National Stormwater Calculator Tool C-5

HSPF Model

HSPF was developed in the mid-1970s by the United States Environmental Protection Agency (U.S. EPA) to model a broad range of hydrologic and water quality processes in the mixed agricultural and urban watersheds (Bicknell *et al.* 1997). HSPF is considered the most comprehensive and flexible model of watershed hydrology and water quality available. HSPF has been widely applied after becoming a part of USEPA's BASINS system for Total Maximum Daily Load (TMDL) analysis and development.

HSPF has been used to study climate change effects for multiple watersheds in the US (U.S. EPA 2013). The climatic input data for HSPF include hourly precipitation and temperature and daily Potential Evapotranspiration (PET), cloud cover, and wind speed. Meteorological time series for future climate scenarios can be created based on the climate projections using one of two extremely simplistic methods that are adequate for seasonal and annual means, but not adequate for extremes: a "change factor" or "delta change" method. With either approach, the observed (historical) local climate data time series observations are adjusted to reflect the changes in climate as simulated by GCMs. Monthly change factors for temperature and precipitation are calculated as the difference between projected average monthly values for a future period (e.g., 2041-2070) and a historical period (e.g., 1971-2000). These change factors are used to adjust historical time series of hourly precipitation and temperature to create projected time series.

There are several options for modifying precipitation records: 1) application of an empirical multiplier to all records that reflects a projected shift in total precipitation; 2) selective application a multiplier to specific seasons or months; 3) selective application of a multiplier to a range of months or years within the record; and 4) selective application of a multiplier to storm events of a specific size or intensity. The designer must determine the appropriate approach and multipliers based on an analysis of historical and projected information outside the HSPF modeling framework. Temperature records can be modified by adding or subtracting a constant (delta change) to all values in the record, or selective application to certain months or years within the record.

To account for changes in intensity, future scenarios can be created using the delta method by applying climate change adjustments separately to precipitation events within certain threshold values, such as greater than or equal to 80th percentile and events less than 80th percentile. However, evaluation of the delta method has shown that it displays a systematic dry bias beyond the 99^{th} percentile of the distribution over the continental U.S. (Hayhoe, *pers. comm*. 2017) The HSPF model is an example where the required climate change information has a high temporal resolution and also needs capture the changes in magnitude while maintaining the autocorrelation structure of the time series. The opportunity is to provide guidance on which methods are appropriate.

SWAT Model

SWAT is a physically based model and was developed by the United States Department of Agriculture (USDA) Agricultural Research Service (ARS) in the early 1990s for the prediction of the long-term impact of rural and agricultural management practices (such as detailed agricultural and planting, tillage, irrigation, fertilization, grazing and harvesting procedures) on

water, sediment and agricultural chemical yields in large, complex watersheds with varying soils, land use and management conditions (Neitsch *et al*. 2011).

SWAT is continuous simulation watershed model for analysis of both watershed hydrology and water quality. It is one of the most popular models in the world, especially for predominantly agricultural watersheds. The required SWAT model climatic input data include daily values of precipitation, minimum/maximum air temperatures, solar radiation, wind speed, relative humidity, and potential evapotranspiration. The SWAT model also comes with a built-in weather generator to develop climatic data for any watershed based on a set of statistical parameters.

Different methods can be used to address future climate changes in SWAT. These methods include simple percentage changes in precipitation and temperature, delta changes to the whole temperature time series, and a detailed change factor approach to modify precipitation and temperature for values above or below a threshold. In the simple method, the temperature changes over the period are projected by based on observed data, detrended to isolate natural variability, then scaled using a trend derived from climate model simulations.

Johnson *et al.* (2015) used SWAT to model the streamflow and water quality sensitivity to climate change and urban development in 20 watersheds across the U.S. ranging size from 15,000 to 70,000 km^2 using change factors. The climate model output is interpolated to each weather station used by the SWAT model. Projected monthly change statistics (change factors) at each weather station are calculated for total precipitation (%), precipitation above/below certain percentiles (%), air temperature (°C), relative humidity (°C), surface down-welling shortwave radiation (%), and wind speed (%). For the Johnson *et al.* (2015) study, change factors were calculated as changes in projected precipitation and temperature for a future period (2041-2070) relative to a baseline historical period (1971-2000) using data from the NARCCAP model simulations. Temperature and precipitation adjustments are made by applying monthly change factors to historical daily values. Projected changes in the proportion of precipitation volume occurring in larger events (i.e., event intensity) are represented by applying different change factors to events above and below the selected percentile (based on daily depth). The remaining weather inputs can be adjusted by modifying the monthly statistics used by the SWAT weather generator.

BASINS CAT Tool

BASINS Climate Assessment Tool (CAT) provides a scenario generation capability for creating meteorological time series reflecting any user-determined change in temperature and precipitation for use as input to the HSPF model (U.S. EPA 2009b). It does not provide additional hydrologic or water quality modeling capability beyond that provided in HSPF, but it provides a framework for easily modifying historical time series precipitation and temperature data to evaluate future conditions.

The adjusted (future conditions) records are stored within the same BASINS Watershed Data Management (WDM) file containing the original, historical weather records (Hummel, Kittle, and Gray 2001). Users can adjust historical weather data (stored in daily or hourly time step) using standard arithmetic operators applied monthly, seasonally, or over any other increments of time. In addition, adjustments to a climate variable can also be applied uniformly to all events, or be selectively applied only on those historical events that exceed (or fall below) a specified

threshold. The ability to selectively adjust only events within user-defined size classes allows future scenarios to be created reflecting these changes.

BASINS CAT facilitates analysis of three types of scenarios described by the IPCC Task Group on Data and Scenario Support for Impacts and Climate Analysis (TGICA): 1) synthetic scenarios, 2) analogue scenarios, and 3) scenarios based on outputs from climate models (IPCC-TGICA 2007). Synthetic scenarios describe techniques where particular climatic attributes are changed by given amount. For example, adjustments of baseline local temperatures by 1, 2, 3, and 4°C and baseline precipitation by 5, 10, 15 and 20 percent represent various magnitudes of future synthetic change. Analogue scenarios are constructed by identifying recorded (historical) climate regimes that may resemble future climate in another region. These records can be obtained from the past (temporal analogues) or from another region at the present (spatial analogues). Model-based scenarios can also be developed using downscaled GCM output.

Following are the options provided by BASINS CAT:

- Option 1: Modify historical precipitation records.
- Option 2: Modify historical air temperature records and regenerate evapotranspiration record.
- Option 3: Combine multiple adjustments of precipitation and temperature to create a future scenario.
- Option 4: Creating spatially variable climate change scenarios at multiple locations.

An example of a potential analysis is to evaluate the impact on watershed endpoints that results from combining the following adjustments to the historical records:

- 20 percent increase in summer (June through August) precipitation.
- 2-degree Celsius increase in air temperature during the cool season (November through April).
- 4-degree Celsius increase in air temperature during the warm season (May through October).

BASINS CAT provides the option to apply specified adjustment(s) to multiple meteorological datasets simultaneously, e.g., temperature time series data from multiple weather stations. This simple approach is justified when there is only limited knowledge of future climate change at fine spatial scales. BASINS CAT can also be used to create spatially variable future scenarios for different locations within a watershed by individually selecting and adjusting historical temperature and precipitation time series datasets from each location. This is particularly useful for large or topographically complex watersheds.

National Stormwater Calculator Tool

EPA's National Stormwater Calculator is a desktop application that estimates the annual amount of rainfall and frequency of runoff from a specific site anywhere in the United States (including Puerto Rico). Estimates are based on local soil conditions, land cover, and historic rainfall records. The Stormwater Calculator also provides an option to apply future climate change scenarios that modify the historical precipitation events and evaporation rates normally used by

the calculator. These scenarios are based on future outcomes produced by well-accepted GCMs from CMIP3. The Stormwater Calculator provides a framework for analysis that relies on the EPA SWMM model as its computational engine.

The Stormwater Calculator retrieves climate change scenario information on local precipitation and temperature from the EPA Climate Resilience and Analysis Tool (CREAT). (See later section on CREAT.). The tool facilitates modification of historical time series data to create future time series. Historical and future series are modeled with SWMM allowing assessment of climate change effects.

The Tool also facilitates consideration of the change in the size and frequency of intense precipitation events. CREAT considers this effect by fitting a GEV probability distribution to the collection of annual maximum 24-hour rainfall amounts over a 30-year period.

Appendix D. Flood Frequency Curves

Table of Contents

APPENDIX D. FLOOD FREQUENCY CURVES D-1

TABLE OF CONTENTS D-2

Sources of Flood Frequency Curves D-4
Statistical Analysis of Stream Gauge Data D-4
Regional Regression Equations D-4
Rainfall/Runoff Modeling D-5
Transposition of Gauge Data D-6

Flood Frequency Curve Shape D-7

Flood frequency curves (FFCs) are graphs or tables that represent the relation between flood magnitude (usually peak discharge and occasionally peak water surface elevation) and probability. When tabular, they are tables of ordered pairs of probability (e.g. annual exceedance probability or return period) and magnitude. Graphically, they are usually characterized as a smooth curve, with the ordinate being magnitude and the abscissa being some expression of probability. Historically, the curve is constructed by plotting probability and magnitude values from a table and connecting them (often manually/visually) with a smooth curve. Now, the frequency curve is determined analytically by assuming a theoretical frequency distribution. Often, probability is represented by a scale with divisions proportioned to the quantiles of some probability distribution, such as the normal or Gumbel (Extreme Value type I). A sample drawn from the distribution used would plot as a straight line.

The ordered pairs are most often chosen for convenience of probability. More-or-less standard values of probability are annual exceedances of 0.5, 0.2, 0.1, 0.04, 0.02, and 0.01 (2. 5, 10, 25, 50, and 100-yr return periods). Occasionally, probabilities greater than 0.5 or less than 0.01 are also used for specific purposes.

Figure 1 provides an example of a flood frequency curve. In this example, the abscissa scale is a normal probability scale and the ordinate scale is logarithmic. A straight line on this graph would represent a log-normally distributed quantity. Upward concavity, as shown here, would indicate *positive skew*, whereas downward concavity would indicate *negative skew*. Skew is a measure of asymmetry, and is an important component of the shape and growth characteristics of a FFC.

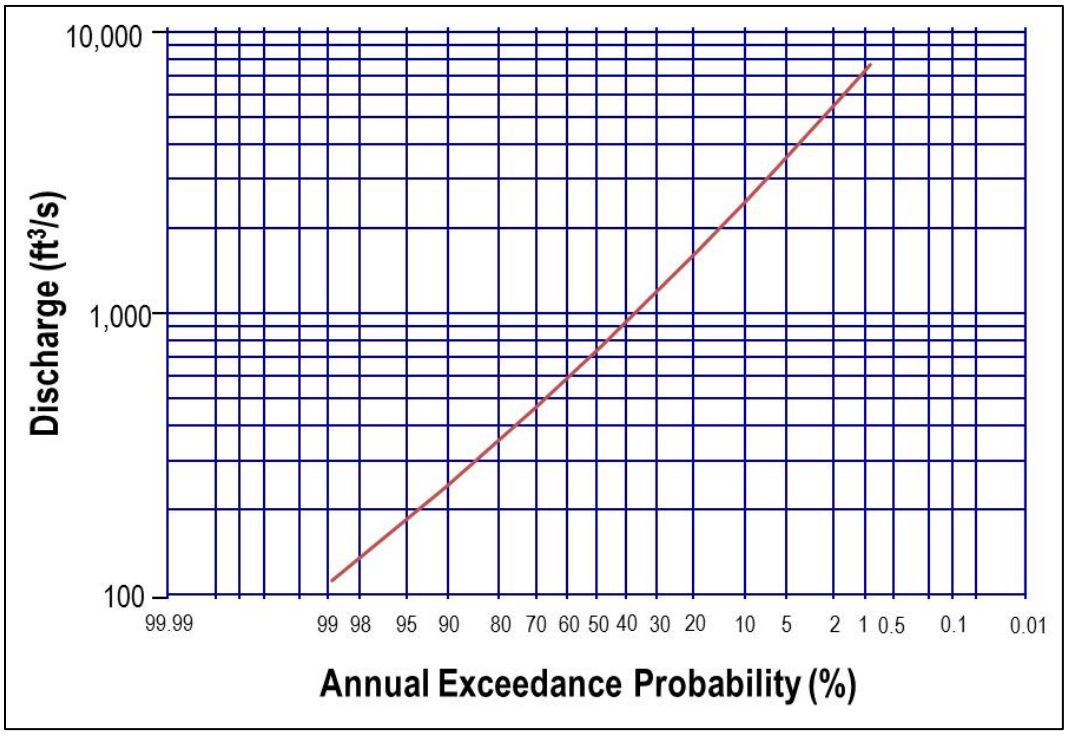

Figure 1. Example of a flood frequency curve.

Sources of Flood Frequency Curves

There are numerous methods for estimating the probability/magnitude relation for specific watersheds and constructing flood frequency curves, not all of which have potential for use in deriving FFCs for future scenarios. Among the most commonly used are the statistical analysis of stream gauge data, the construction and use of regional regression equations, and the mathematical modeling of rainfall/runoff processes. Each of the methods has advantages and disadvantages for general use and none are universally appropriate.

Statistical Analysis of Stream Gauge Data

The statistical analysis of stream gauge data generally best represents the flood frequency relation at any site where a stream gauge has a long record. A statistical distribution function is selected to represent the relationship (or is mandated by relevant policy), and parameters for the function are estimated from the data to "fit" the function to the data (approximate the "shape" of the data in probability/magnitude space). Distribution functions may be selected by information from the data itself (e.g. moment ratios or L-moment ratios), by agency policy, or by commonly accepted practice within a profession such as Bulletin 17B (IACWD 1982) and its successor Bulletin 17C (England *et al*. 2017). Magnitudes corresponding to the desired probabilities are obtained by evaluating the quantile (inverse) function of the selected distribution at the desired probabilities. The resulting "quantiles" can then be graphed to display a flood frequency curve. For each given watershed and stream gauge dataset, the result is a unique curve with a unique "shape."

There are different ways of estimating flood-frequency information from stream gauge data (Maidment 1993). Points of disagreement among practitioners arise from the selection of a distribution to represent a gauge dataset, the method of parameter estimation, and methods related to "outliers." Outliers are high or low values that may not have an appropriate place in a homogeneous dataset. Examples of outliers might be a discharge that results from a process other than the one resulting in the preponderance of values (base flow rather than direct runoff) or a value that does not represent the time interval of data collection (a value exceeding the 1000-year return period in a dataset of 20-year length). Each decision along such lines will result in a different "shape" for the flood frequency curve, yet at least some characteristics of those shapes should be similar to one another. However, to use these techniques, a gauge must be present, and have been present for long enough to provide a useful dataset. For the vast majority of watersheds on which the engineering community may need flood frequency estimates, gauges do not exist.

Regional Regression Equations

Regional regression equations are developed by fitting distributions to annual peak discharge datasets from many stream gauges thought to be within a reasonably homogeneous hydrologic/geographic "region." Regression analysis is then performed on each set of quantile values, with various "predictor variables" that are thought to exhibit correlated behavior or be physically related to flood magnitude (Ries, et al. 2007). The expected result is a suite of algebraic equations, one for each quantile, with expected peak discharge as the dependent variable, and predictor variables selected for their strength of correlation as the independent variables. In this process, each quantile described in a separate regression analysis; the "shape"

of each individual flood frequency curve is lost, because no connection is maintained between quantile groups with other quantile groups.

The technique of regression equations was developed for the specific purpose of estimating peak discharge associated with specific probabilities on ungauged watersheds. Regression equations capitalize on the similarity of shape among statistically derived flood frequency curves and on the correlated behavior of flood magnitude with physiographic, geographic, or climatic characteristics associated with watersheds. Examples of watershed characteristics are contributing area, main channel slope, watershed shape, and characteristic precipitation. Many other variables may be considered, and those that exhibit the strongest correlation are used in the regression analysis.

The principal advantage of regression equations is that they are applicable to a wide range of ungauged watersheds; the principal disadvantage is that their development requires many gauges of long record within a relatively homogeneous region. Additionally, the shape of the flood frequency curve resulting from regression equations is similar to an average value, which may only be truly appropriate for a subset of ungauged watersheds where the characteristics used as predictor variables are also close to the average of the values used in the regression. Regression equation estimates discharge quantiles are subject to large uncertainty in some areas of the US while in other areas they are considered reasonably accurate (standard errors of 30-40 percent) . Accuracy can only be assessed within the sample set of gauged watersheds used in the regression analysis; accuracy on ungauged watersheds can only be inferred. Values of the predictor variables for an ungauged watershed should be within the range of values of within the sample set of gauged watersheds used.

Rainfall/Runoff Modeling

Mathematical modeling of rainfall/runoff processes involve the simulation of (greatly simplified analogs to) the physical processes of rainfall on a watershed and the resulting movement through the watershed. Rainfall/runoff models assume that the physics of watershed processes are known and can be described mathematically to a useful degree. There are a multitude of particular techniques that can be used for each of the parts described (Maidment 1993, Chow *et al*. 1988).

The mathematical modeling of rainfall and the resulting runoff as it is typically performed by the profession for highway drainage design is connected to measured watershed runoff information only in very indirect ways. Other characteristics, some of them similar to the predictor variables in regression equations, are used to provide surrogate information. Contributing area, a characteristic time, geological information, land use information, vegetative cover, and urbanization are typical inputs to model the physical processes that result in flood flows from rainfall. Rainfall is separated into abstractions (rainfall that is “lost” to the runoff process) and “effective rainfall” (rainfall that escapes the watershed as runoff). The time-distributed response of the watershed to an input of effective rainfall is unique for every watershed. In the absence of contemporaneous data from rain gauges and stream gauges from the subject watershed, a response must be assumed from some generalized relationship. If such contemporaneous data does exist, techniques of estimation other than watershed modeling would normally be used for design estimation.

Rainfall/runoff modeling results in a single value of runoff for a single value of rainfall input. The variation of magnitude with probability is encapsulated within the variation of rainfall with

probability, that is, a rainfall frequency curve. Rainfall input for various probabilities (the same probabilities as for flood frequency) results in corresponding runoff. The shape of flood frequency curves that result from rainfall/runoff modeling closely mimic the shape of the rainfall frequency curves that they result from. They seldom bear much resemblance to curves developed from nearby stream gauges.

Transposition of Gauge Data

Another approach for estimating the FFC at ungauged watersheds is the transposition of gauge data from a similar gauged watershed. These techniques adapt (transpose) flood frequency curves from gauge locations to other, nearby sites that are thought to be reasonably similar to the gauge site. Transposition may be used from a gauged watershed to an ungauged watershed with similar characteristics or restricted to transposition from a gauge within a watershed to an ungauged location within the same watershed, but on the same stream. The following equation for the latter situation, known as the "drainage area ratio method," is presented in HDS 2 (McCuen *et al*. 2002):

$$Q_{d=}Q_g(\frac{A_d}{A_g})^C \quad \text{(D.1)}$$

where:

Q_d = *Discharge at the ungauged site.*

Q_g = *Discharge at the gauged site.*

A_d = *Contributing area at the ungauged (design) site.*

A_g = *Contributing area at the gauged site.*

C = *Transposition exponent.*

The value of the transposition exponent has historically been taken as the value of the exponent on drainage area taken from the applicable regression equation (McCuen *et al*. 2002). Usually, the value is related to the magnitude of rainfall in the region. In more arid regions like Texas, C is close to 0.5, while in very humid regions it is close to 0.8. Work by Asquith and Thompson (2008) in Texas found exponents close to 0.51 for the range return periods.

Sauer (1973) presented an alternative method of transposition, using a composite of gauge analysis results, regression equation estimates, and a weighting function. Because of the structure of Sauer's method, it is restricted to transposition from gauged watersheds to watersheds that do not vary from the gauged watershed contributing area by more than 50 percent. McCuen and Levy (2001) evaluated the drainage area ratio method and Sauer's method, finding that Sauer's method gave "slightly better results" than the drainage area ratio method. They also state that for transposition methods, "Currently, a major limitation is the lack of documentation on their accuracy and sensitivity."

Stream gauges for transposition should be selected carefully so that they are similar to the ungauged site of interest. Geographic proximity, stream nature (single main-channel, stream order), geology, topography, mean annual rainfall, and land use should all be considered. Transposition from several gauges (to one another and to the ungauged site) and comparison of

the results may be revealing. Estimates from different gauges may be weighted in some manner, e.g. inverse distance weighting, or inverse area weighting. Some representation of the distribution of flood ratios within a region or state may be developed for widespread use. The flood quantile discharges from statistical analysis used to develop regional regression equations are usually published in the USGS reports accompanying the deployment of regression equations (e.g. Asquith and Slade (1996), Asquith and Roussel (2009)). This information can easily be exploited to aid in the selection of stations for transposition.

Comparatively little evaluation or research has been published on transposition methods. Most publications and manuals that mention them recommend limiting their use to watersheds that are geographically proximate, and similar in contributing area. Little or no justification for these recommendations is given, other than a lack of research.

However, transposition of gauge data can be compared to regression analysis. Both techniques "pool" information to relate general behavior over a region to specific behavior at specific locations. In the presence of prior regression analyses and the FFCs and watershed characteristics published alongside of them as mentioned above, comparable proximate gauged watersheds (if they exist) can easily be identified for transposition. Multiple transpositions can be performed with relative ease, and the results compared. The advantage of transposition over regression equations is that the *shape of the FFC at each gauge is preserved and translated*.

Flood Frequency Curve Shape

Much research and discussion has occurred since the mid-20th century regarding the appropriate statistical distribution or distributions to describe the flood frequency relationship. Among the common choices are various forms of the log-normal, the Gumbel (type I extreme value), the GEV, and the Pearson Type III. When used with annual peak flood data, the chosen distribution is often assumed to apply to the logarithms of the data, rather than the untransformed data. Data often vary across several log cycles, and taking the logarithms of the discharges makes handling and graphing them more tractable. In addition, the logarithms plot in a curve that is closer to linear than the raw data values in natural units because the skew is closer to zero (more normally distributed).

Preference of distribution relates to two characteristics. One characteristic is the "fit" of the distribution to the data, that is, "how well does the fitted distribution follow the data?" The other is the "shape" of the distribution, which might be described as "curvature" and "slope." When discussing the slope and curvature of a distribution fitted to a dataset, the slope may be thought of as the "rate of rise" of discharge with diminishing probability of exceedance, and the curvature as a change in slope with diminishing probability of exceedance. Particularly when it is necessary to extrapolate the discharge/probability relationship far beyond the period of record of the dataset (e.g. to obtain a 100-year discharge estimate from 50 years of data), the curvature and slope of the chosen distribution has a great effect on the magnitude of discharge that is associated with a given probability.

To visualize shape and curvature in a dataset, and to visually compare data to the fitted distribution, it is necessary to assign probability to each data point in the dataset. This is commonly done using a ***plotting position formula*** - a simple formula that assigns a probability to each point based on position within the ordered dataset. Table 1 shows several popular plotting position formulae. Plotting position formulae assign a probability between 0 and 1 to each value

in the ranked sample set based solely on its position in the set; magnitude of the value has no influence at all. If the sample is ranked from largest to smallest, the corresponding probability is that of exceedance. The most frequently used is the Weibull; however, each has advantages (Cunnane 1978). Regardless of the formula used, a probability must be assigned to each value in a sample in order to plot them on a probability graph, and some assessment of shape can then be made. To use these formulae, i is the rank number of a value in the ranked sample, and n is the number of values in the sample.

Table 1. Plotting position formulae.

Name	Formula
Weibull	i/(n+1)
Blom	(i-0.375)/(n+0.25)
Cunnane	(i-0.4)/(n+0.2)
Gringorten	(i-0.44)/(n+0.12)

Numerous statistical methods are available to assess "goodness of fit" of statistical distributions to observed data. These tests could, in theory, aid in the selection of a distribution to a dataset. However, they are seldom used in flood frequency analysis with the exception of the L-moment methodology. More frequently, a distribution is specified by policy, agreement, or common acceptance within an agency, governmental entity, or common practice. Theoretically, optimizing goodness of fit is sacrificed for consistency and comparability among datasets, practitioners, and procedures. In specifying a distribution, curvature may well be constrained, as various distributions have characteristic bounds on shape. However, the slope of the fitted distribution must approximate the slope of the dataset, or the distribution diverges from the data rapidly.

Datasets that are of sufficient length to match or exceed frequently desired ARI values (50-100 years, or 250 years in the case of scour analysis) are quite rare or non-existent. For that reason, extrapolation beyond the length of available data is the norm, rather than the exception, in transportation engineering hydrologic design. The shape, both slope and curvature, of a FFC exert great influence on the magnitude of the discharge/probability relation in extrapolated values. Particularly considering that such analyses occur on logarithms of discharge, small changes in slope and/or curvature of a FFC invariably have large influences on discharge estimates. It is essential that information regarding shape of FFCs obtained from gauged sites be preserved and exploited at ungauged sites.

The index flood method is a method for estimating design discharges at ungauged sites based on flood frequency analysis of historical data at gauged sites. Since the advent of USGS Regional Regression Equations, it has seen little use in the United States, but it is still popular in many other areas of the world.